

THE DYNAMICS AND
THERMODYNAMICS OF

**COMPRESSIBLE
FLUID FLOW**

Volume I

ASCHER H. SHAPIRO

*The Dynamics and Thermodynamics of
COMPRESSIBLE FLUID FLOW*

VOLUME I

BEGINNING WITH A BRIEF REVIEW of the foundation concepts of fluid dynamics and thermodynamics and an introduction to the concepts of compressible flow, this volume treats one-dimensional gas dynamics, including flow in nozzles and diffusers, normal shocks, frictional flows and flows with heat transfer or energy release; the differential equations governing the two- and three-dimensional motion of a nonviscous compressible fluid; analytical methods and experimental results for subsonic, two- and three-dimensional flows; two-dimensional supersonic flows from the theoretical and practical points of view; and, in Appendices, the theory of characteristic curves and sets of numerical tables of compressible-flow functions.

VOLUME II

IN THIS VOLUME are treated three-dimensional supersonic flows past wings and bodies of revolution; hypersonic flows; flows containing both subsonic and supersonic regions; transonic flows; unsteady flows in one dimension, including continuous wave motion and moving shocks; theoretical and experimental surveys of friction and heat transfer in laminar and turbulent boundary layers for external and internal flows; and the interaction between boundary layers and shock waves.

**The Dynamics
and Thermodynamics of
COMPRESSIBLE FLUID
FLOW**

By

ASCHER H. SHAPIRO

*Professor of Mechanical Engineering
Massachusetts Institute of Technology*

IN TWO VOLUMES

VOLUME I

THE RONALD PRESS COMPANY ✓ NEW YORK

Copyright, 1953, by
THE RONALD PRESS COMPANY

All Rights Reserved

The text of this publication or any part
thereof may not be reproduced in any
manner whatsoever without permission in
writing from the publisher.

2

TO THE MEMORY OF MY FATHER,
BERNARD SHAPIRO

PREFACE

During the past two decades a rapid growth of interest in the motion of compressible fluids has accompanied developments in high-speed flight, jet engines, rockets, ballistics, combustion, gas turbines, ram jets and other novel propulsive mechanisms, heat transfer at high speeds, and blast-wave phenomena. My purpose in writing this book is to make available to students, engineers, and applied physicists a work on compressible fluid motion which would be suitable as an introductory text in the subject as well as a reference work for some of its more advanced phases. The choice of subject matter has not been dictated by any particular field of engineering, but rather includes topics of interest to aeronautical engineers, mechanical engineers, chemical engineers, applied mechanicians, and applied physicists.

In selecting material from the vast literature of the field the basic objective has been to make the book of practical value for engineering purposes. To achieve this aim, I have followed the philosophy that the most practical approach to the subject of compressible fluid mechanics is one which combines theoretical analysis, clear physical reasoning, and empirical results, each leaning on the other for mutual support and advancement, and the whole being greater than the sum of the parts.

The analytical developments of this book comprise two types of treatments: those leading to design methods and those leading to exemplary methods. The design methods are direct and rapid, and easily applied to a variety of problems. Therefore, they are suited for use in the engineering office. The discussions of these design methods are detailed and illustrative examples are often given. The exemplary methods, on the other hand, comprise those theoretical analyses which are time consuming, which generally require mathematical invention, and which are not easily applied to a variety of problems. Such methods are primarily of value for yielding detailed answers to a small number of typical problems. Although they are not in themselves suitable for the engineering office, the examples which they permit to be worked out often provide important information about the behavior of fluids in typical situations. Thus they serve as guides to the designer in solving the many complex problems where even the so-called design methods are not sufficient. The treatment of exemplary methods in this book usually consists of a brief outline of the method, together with a presentation of those results obtained by the method which illuminate significant questions concern-

ing fluid motion and which help to form the vital "feel" so desired by designers.

In keeping with the spirit of the several foregoing remarks, all the important results of the book have been reduced to the form of convenient charts and tables. Unless otherwise specified, the charts and tables are for a perfect gas with a ratio of specific heats (k) of 1.4.

In those parts of the book dealing with fundamentals, emphasis is placed on the introduction of new concepts in an unambiguous manner, on securing a clear physical understanding before the undertaking of an analysis, on the rigorous application of physical laws, and on showing fruitful avenues of approach in analytical thinking. The remaining part of the work proceeds at a more rapid pace befitting the technical maturity of advanced students and professionals.

The work is organized in eight parts. Part I sets forth the basic concepts and principles of fluid dynamics and thermodynamics from which the remainder of the book proceeds and also introduces some fundamental concepts peculiar to compressible flows. In Part II is a discussion of problems accessible by the most simple picture of fluid motion—the one-dimensional analysis. Part III constitutes a summary of the basic ideas and concepts necessary for the succeeding chapters on two- and three-dimensional flow. Parts IV, V, and VI then present in order comprehensive surveys of subsonic flows, of supersonic flows (including hypersonic flow), and of mixed subsonic-supersonic flows. In Part VII is an exposition of unsteady one-dimensional flows. Part VIII is an examination of the viscous and heat conduction effects in laminar and turbulent boundary layers, and of the interaction between shock waves and boundary layers. For those readers not already familiar with it, the mathematical theory of characteristic curves is briefly developed in Appendix A. Appendix B is a collection of tables which facilitate the numerical solution of problems.

The "References and Selected Bibliography" at the end of each chapter will, it is hoped, be a helpful guide for further study of the voluminous subject. Apart from specific references cited in each chapter, the lists include general references appropriate to the subject matter of each chapter. The choice of references has been based primarily on clarity, on completeness, and on the desirability of an English text, rather than on historical priority.

My first acknowledgment is to Professor Joseph H. Keenan, to whom I owe my first interest in the subject, and who, as teacher, friend, and colleague, has been a source of inspiration and encouragement.

In an intangible yet real way I am indebted to my students, who have made teaching a satisfying experience, and to my friends and colleagues

at the Massachusetts Institute of Technology who contributed the climate of constructive criticism so conducive to creative effort.

Many individuals and organizations have been cooperative in supplying me with helpful material and I hope that I have not failed to acknowledge any of these at the appropriate place in the text. The National Advisory Committee for Aeronautics and the M.I.T. Gas Turbine Laboratory have been especially helpful along these lines.

I was fortunate in being able to place responsibility for the important work of the drawings in the competent hands of Mr. Percy H. Lund, who, with Miss Prudence Santoro, has been most cooperative in this regard.

For help with the final revision and checking of the manuscript I wish to give thanks to Dr. Bruce D. Gavril and Dr. Ralph A. Burton.

Finally, but by no means least, I must express a word of appreciation to Sylvia, and to young Peter, Mardi, and Bunny, who, one and all, made it possible for me to escape from the office into the somewhat less trying atmosphere of the home, and there to carry this work forward to its completion.

ASCHER H. SHAPIRO

Arlington, Mass.

April 4, 1953

C O N T E N T S

V O L U M E I

Part I. Background

CHAPTER	PAGE
1 FOUNDATIONS OF FLUID DYNAMICS	3
Properties of the Continuum. Systems and Control Volumes. Conservation of Mass. Momentum Theorem. Theorem of Moment of Momentum. Units and Dimensions.	
2 FOUNDATIONS OF THERMODYNAMICS	23
The First Law of Thermodynamics. The Second Law of Thermodynamics. Thermodynamic Properties of the Continuum. The First Law for a Control Volume. The Second Law for a Control Volume. The Perfect Gas.	
3 INTRODUCTORY CONCEPTS TO COMPRESSIBLE FLOW	45
The Velocity of Sound. Physical Differences Between Incompressible, Subsonic, and Supersonic Flows. The Mach Number and Mach Angle. Similarity Parameters. Domain of the Continuum. Classification of Compressible Flows. Optical Methods of Investigation.	

Part II. One-Dimensional Flow

4 ISENTROPIC FLOW	73
General Features of Isentropic Flow. Adiabatic Flow of a Perfect Gas. Isentropic Flow of a Perfect Gas. Working Charts and Tables for Isentropic Flow. Choking in Isentropic Flow. Operation of Nozzles Under Varying Pressure Ratios. Special Relations for Low Mach Numbers. Deviations from Perfect Gas Laws. Performance of Real Nozzles. Some Applications of Isentropic Flow.	
5 NORMAL SHOCK WAVES	112
Governing Relations of the Normal Shock. Normal Shock in a Perfect Gas. Working Formulas, Curves, and Tables. Weak Shock Waves. Formation of Shock Waves. Thickness of Shock Waves. Normal Shocks in Ducts. Moving Shock Waves. Operating Characteristics of Converging-Diverging Nozzle. One-Dimensional Supersonic Diffusers. Supersonic Pitot Tube.	

CHAPTER	CONTENTS	PAGE
6	FLOW IN CONSTANT-AREA DUCTS WITH FRICTION	159
	Adiabatic, Constant-Area Flow of a Perfect Gas. Performance of Long Ducts at Various Pressure Ratios. Isothermal Flow in Long Ducts. Experimental Friction Coefficients.	
7	FLOW IN DUCTS WITH HEATING OR COOLING	190
	Simple-Heating Relations for a Perfect Gas. Choking Effects in Simple T_0 -Change. Shock Waves with Changes in Stagnation Temperature. The Recovery Factor. The Coefficient of Heat Transfer.	
8	GENERALIZED ONE-DIMENSIONAL CONTINUOUS FLOW	219
	Physical Equations and Definitions. Working Equations and Tables of Influence Coefficients. Flow with Constant Specific Heat and Molecular Weight. General Features of Flow Patterns. General Method of Solution. Simple Types of Flow. Example of Combined Friction and Area Change. Examples of Combined Friction and Heat Transfer. Special Conditions at the Sonic Point.	

Part III. Introduction to Flow in Two and Three Dimensions

9	THE EQUATIONS OF MOTION FOR STEADY, IRROTATIONAL FLOW	265
	The Physical Significance of Irrotational Motion. Euler's Equations of Motion. Kelvin's Theorem. The Connection Between the Rotation and the Thermodynamic Properties of the Flow. The Equation of Continuity. The Laws of Thermodynamics. Differential Equations in Terms of the Velocity Potential. Differential Equations in Terms of the Stream Function. Relations Between the Velocity Potential and the Stream Function.	

Part IV. Subsonic Flow

10	TWO-DIMENSIONAL, SUBSONIC FLOW WITH SMALL PERTURBATIONS	303
	Linearization of the Potential Equation. Linearization of the Pressure Coefficient. Flow Past a Wave-Shaped Wall. Goert's Rule. The Prandtl-Glauert Rule. Experimental Results for Thin Profiles. Wind Tunnel Corrections. Flow Inside Two-Dimensional Passages.	
11	HODOGRAPH METHOD FOR TWO-DIMENSIONAL, SUBSONIC FLOW	336
	Derivation of the Hodograph Equations. The Tangent-Gas Approximation. The Karman-Tsien Pressure Correction Formula. Calculation of Profile Shape Correction. Extension of Karman-Tsien Method. Miscellaneous Examples.	

CHAPTER	CONTENTS	PAGE
12	MISCELLANEOUS METHODS AND RESULTS FOR TWO-DIMENSIONAL, SUBSONIC FLOW	364
	The Rayleigh-Janzen Method of Expansion in Series of the Mach Number. The Prandtl-Glauert Method of Expansion in Series of a Shape Parameter. Relaxation Method. Some Measured Effects of Compressibility in Subsonic Flow. The Streamline Curvature Method.	
13	THREE-DIMENSIONAL, SUBSONIC FLOW	393
	Goert's Rule for Uniform Flow with Small Perturbations. Flow Past Ellipsoids. Bodies of Revolution. Spheres. Wings of Finite Span. Sweptback Wings. Sweptback Wings of Finite Span.	

Part V. Supersonic Flow

14	TWO-DIMENSIONAL, SUPERSONIC FLOW WITH SMALL PERTURBATIONS	427
	Linearization of the Equations. The General Solution for Linearized Supersonic Flow. Geometrical Interpretation of the General Solution. Flow Past a Wave-Shaped Wall. Supersonic Airfoils. Reflection and Interaction of Waves.	
15	METHOD OF CHARACTERISTICS FOR TWO-DIMENSIONAL, SUPERSONIC FLOW	462
	Flow with Waves of One Family by Extension of Linear Theory. Flow with Waves of Both Families by Extension of Linear Theory. Application of Theory of Characteristics. Simple Waves by Theory of Characteristics. Field Method Versus Lattice-Point Method. Unit Processes. Graphical Versus Numerical Method. Some Special Features of Supersonic Flow. Applications of Method of Characteristics. Design of Supersonic Wind Tunnel Nozzles. Adiabatic, Nonviscous Flow with Rotation.	
16	OBLIQUE SHOCKS	529
	Oblique Shock Equations. Shock Geometry. Shock Polars. Some Special Aspects of Oblique Shocks. Very Weak Shocks. Reflection and Interaction of Shocks. Curved Shocks. Explicit Solutions by Series Expansions. Examples of Two-Dimensional Flows Containing Shocks. Two-Dimensional Profiles. Interaction of Shock Waves with Boundary Layer.	

Appendix

A	THEORY OF CHARACTERISTICS	595
	The Characteristic Curves. Method of Constructing Characteristic Curves. Simple Waves.	
B	TABLES OF COMPRESSIBLE-FLOW FUNCTIONS	610
	INDEX	635

VOLUME II

Part V. Supersonic Flow (Continued)

CHAPTER

17 AXIALLY SYMMETRIC SUPERSONIC FLOW

Exact Solution for Flow Past a Cone. Linear Theory for Slender Bodies of Revolution. Method of Characteristics. Miscellaneous Experimental Results.

18 SUPERSONIC FLOW PAST WINGS OF FINITE SPAN

Preliminary Considerations of Finite Wings. Sweptback Wings. Similarity Rule for Supersonic Wings. The Method of Supersonic Source and Doublet Distributions. The Method of Conical Fields. Typical Theoretical Results for Finite Wings. Comparison of Theory with Experiment.

19 HYPERSONIC FLOW

Similarity Laws for Hypersonic Flow. Oblique Shock Relations for Hypersonic Flow. Simple-Wave Expansion Relations for Hypersonic Flow. Hypersonic Performance of Two-Dimensional Profiles. Hypersonic Performance of Bodies of Revolution. Experimental Results.

Part VI. Mixed Flow

20 THE HODOGRAPH METHOD FOR MIXED SUBSONIC-SUPERSONIC FLOW

Equations of the Hodograph Method. Source-Vortex Flow. Compressible Flow with 180° Turn. The Limit Line. Solution of Hodograph Equations by Hypergeometric Functions.

21 TRANSONIC FLOW

The Transonic Similarity Law. Applications of the Transonic Similarity Law. Flow in Throat of Converging-Diverging Nozzle. Relaxation Method. Transonic Flow Past a Wavy Wall. Flow at Mach Number Unity. Slopes of Force Coefficients at $M_\infty = 1$. Transonic Flow Past Wedge Nose.

22 DRAG AND LIFT AT TRANSONIC SPEEDS

Experimental Validity of Transonic Similarity Law. Characteristics of Wing Profiles. Characteristics of Wings. Transonic Drag of Bodies of Revolution. Detached Shocks. Theoretical Consideration of Transonic Flow Without Shocks. Interaction Between Boundary Layer and Shock Wave.

Part VII. Unsteady Motion in One Dimension

CHAPTER

23 UNSTEADY WAVE MOTION OF SMALL AMPLITUDE

Equations of Motion. Waves of Small Amplitude. Simplified Physical Analysis of Pressure Pulse. Characteristic Curves. Application of Theory. Development of Wave Form. Effects of Gradual Changes in Area.

24 UNSTEADY, ONE-DIMENSIONAL, CONTINUOUS FLOW

Extension of Linearized Theory. Method of Characteristics. Simple Waves. Waves of Both Families. Unit Operations and Boundary Conditions. Unsteady, One-Dimensional Flow. Remarks on Details of Working Out the Method of Characteristics. Some Examples.

25 UNSTEADY, ONE-DIMENSIONAL SHOCK WAVES

Analysis in Terms of Stationary Shock Formulas. Analysis of Moving Shocks. The Shock Tube—Riemann's Problem. Weak Shock Waves. Modified Calculation Procedure for Weak Shocks. End Conditions and Interaction Effects for Strong Shocks. Comparison Between Experimental and Theoretical Results.

Part VIII. Flow of Real Gases with Viscosity and Heat Conductivity

26 THE LAMINAR BOUNDARY LAYER

Differential Equations of the Laminar Boundary Layer. Flow With Prandtl Number Unity. Flow With Arbitrary Prandtl Number. Integral Equations of the Laminar Boundary Layer. Laminar Boundary Layer for Axi-Symmetric Flow. Experimental Results for Laminar Boundary Layers. Stability of the Laminar Boundary Layer.

27 THE TURBULENT BOUNDARY LAYER

Differential Equations of the Turbulent Boundary Layer. Integral Equations of the Turbulent Boundary Layer. Analyses of Recovery Factor, Skin Friction, and Heat Transfer for Turbulent Flow Past a Flat Plate with Turbulent Prandtl Number of Unity. Theoretical and Experimental Results for Skin Friction on Flat Plates. Recovery Factor for Turbulent Flow. Turbulent Boundary Layer on Bodies of Revolution.

28 BOUNDARY LAYERS IN TUBES AND IN THE PRESENCE OF SHOCK WAVES

Flow in Tubes. Shock-Boundary Layer Interactions in Supersonic Flow. Shock-Boundary Layer Interactions in Transonic Flow. Normal Shocks in Ducts. Boundary-Layer Separation Produced by Shock Waves.

INDEX FOR VOLUMES I AND II

PART I
BACKGROUND

Chapter 1

FOUNDATIONS OF FLUID DYNAMICS

1.1. Introductory Remarks

An engineering science like fluid dynamics rests on foundations comprising both theory and experiment. With fluid dynamics, progress has been especially dependent upon an intimate cross-fertilization between the analytical and empirical branches; the experimental results being most fruitfully interpreted in terms of theoretical reasoning, and the analyses in turn suggesting critical and illuminating experiments which further amplify and strengthen the theory.

The analytical branch of a science is constructed from concepts, definitions, and the statements of physical laws. The latter are in terms of the concepts and definitions and are in conformity with experimental observations. All analyses concerning the motion of compressible fluids must necessarily begin, either directly or indirectly, with the statements of the four basic physical laws governing such motions. These laws, which are independent of the nature of the particular fluid, are

- (i) the law of conservation of mass
- (ii) Newton's second law of motion
- (iii) the first law of thermodynamics
- (iv) the second law of thermodynamics

In addition to these fundamental principles, it is usually necessary to bring into an analysis certain subsidiary laws relating to the particular fluid or class of fluids in question. Examples are the equation of state of a perfect gas, the proportionality law between shear stress and rate of shear deformation in a Newtonian fluid, the Fourier law of heat conduction, etc.

In this book emphasis is placed on the manner in which important conclusions spring from analyses growing out of the four basic laws mentioned above. For this reason the first two chapters are devoted to a review of these principles and the associated concepts and definitions. In this way the general point of view and phraseology of the book will be established.

Definition of a Fluid. The rigorous classification of substances in various ways is usually thwarted because certain substances behave so

anomalously as to defy being neatly placed in a pigeonhole. For our present purpose, we wish principally to distinguish between the numerous common substances we call fluids and such other substances as solids and plastics.

We shall define a *fluid* as a substance which *deforms continuously under the action of shearing forces*. When shearing forces are applied to a solid, the latter undergoes a certain deformation which does not change so long as the applied forces are maintained constant. A fluid, however, whether viscous or nonviscous, exhibits relative motion between its elementary parts so long as shearing forces are applied. Thus we say that "a fluid cannot withstand shearing stresses."

An important corollary which follows from the definition of a fluid is the observation that if there is no relative motion within the fluid, i.e., if fluid particles are not deformed, then there can be no shear stresses acting on such particles.

LIQUIDS VS. GASES. The usual methods of attempting to distinguish rigorously between a liquid and a gas, both of which are fluids, are futile and indeed not of any practical use. That this is so may be seen by considering that a mass of "water" at 1 atm and 100°C in a glass cylinder closed by a piston may, by suitable heat transfers and motions of the piston, be transformed to a mass of "steam" at 1 atm and 100°C, without a meniscus once being observed! For most practical purposes the words "liquid" and "gas" are of value insofar as the former denotes a fluid which generally exhibits only small percentage changes in density.

The subject matter of this book relates for the most part to highly compressible fluids, and so we shall generally speak of gases.

The Concept of a Continuum. Matter, while seemingly continuous, is composed of myriads of molecules in constant motion and collision. The most fundamental approach in analyzing the motion of matter in the aggregate is, therefore, to set down the laws of motion for each individual molecule and to trace the history of each molecule, or of statistical groups of molecules, subsequent to some initial state of affairs. This approach, which usually goes under the name of kinetic theory or statistical mechanics, has obvious merits, but, on the other hand, is often too cumbersome for practical calculations.

In most engineering problems our primary interest lies not in the motions of molecules, but rather in the gross behavior of the fluid thought of as a continuous material. Although the postulate of a continuous fluid is nothing but a convenient fiction, it is fortunately a valid approach to many practical problems where only macroscopic or phenomenological information is of interest. The treatment of fluids as continua may be said to be valid whenever the smallest volume of fluid of interest contains so many molecules as to make statistical averages meaningful.

The great simplification afforded by the concept of a continuum is that instead of dealing with instantaneous states of innumerable molecules, we deal instead with certain macroscopic properties describing the gross behavior of the substance. In the motion of compressible fluids the relevant properties are density, pressure, shear stress, velocity, coefficient of viscosity, temperature, internal energy, entropy, and coefficient of thermal conductivity. These are defined in Arts. 1.3 and 2.4.

This book concerns the motion of compressible fluids which may be treated as continua. To avoid the impression that the methods and results of this book are universally valid, it seems well at this point to mention that the macroscopic approach fails whenever the mean free path of the molecules is of comparable size with the smallest significant dimension of the problem. Thus, whenever we deal with highly rarefied gases (as in rocket flight at extreme altitudes, high vacuum technology, or electronic tubes), the continuum approach of classical fluid mechanics and thermodynamics must be abandoned in favor of the microscopic approach of kinetic theory.

NOMENCLATURE

<i>a</i>	acceleration	<i>u</i>	component of velocity in <i>x</i> -direction
<i>A</i>	area	<i>v</i>	component of velocity in <i>y</i> -direction
A	area vector	U	volume
<i>F</i>	force	<i>V</i>	speed
F	force vector	V	velocity
<i>g</i>	magnitude of body force per unit mass	<i>w</i>	mass rate of flow
<i>g₀</i>	constant of proportionality in Newton's second law	<i>x, y, z</i>	Cartesian coordinates
<i>m</i>	mass	<i>γ</i>	angle
M	moment of a force, or torque	<i>μ</i>	coefficient of viscosity
<i>p</i>	normal force per unit area, or pressure	<i>ρ</i>	mass density at a point
<i>r</i>	magnitude of radius vector	<i>r</i>	tangential force per unit area, or shear stress
r	radius vector		
<i>t</i>	time		

1.2. Properties of the Continuum

We discuss here those continuum properties relevant to the laws of motion.

Density at a Point. Consider the mass of fluid dm in a volume $δV$ surrounding the point *P* in a continuous fluid (Fig. 1.1a). The ratio $dm/δV$ is called the average mass density of the fluid within the volume

δV . Now suppose that at first δV is rather large, and that it is subsequently shrunk about the point P . Then a plot of $\delta m/\delta V$ versus δV would be typified by Fig. 1.1b. At first the average density tends to approach an asymptote as the volume encloses fluid more and more homogeneous in nature. However, when δV becomes so small as to contain relatively few molecules, the average density fluctuates substantially with time as molecules pass into and out of the volume, and so it is impossible to speak of a definite value for $\delta m/\delta V$. We may then

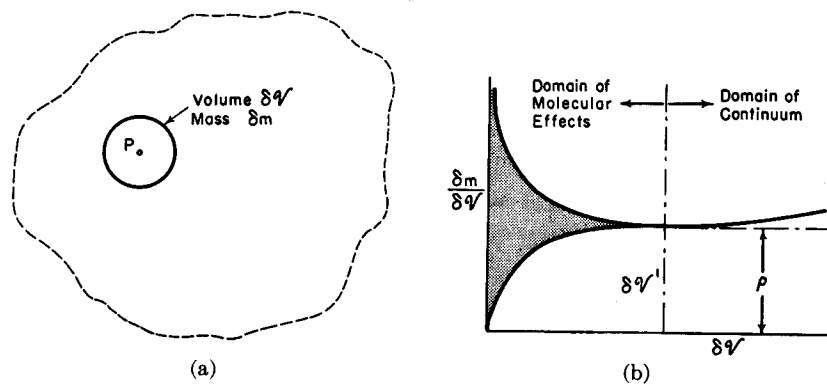


FIG. 1.1. Definition of density at a point.

imagine the smallest volume which can be regarded as continuous to $\delta V'$, and then define the *density at a point* as

$$\rho \equiv \lim_{\delta V \rightarrow \delta V'} \frac{\delta m}{\delta V} \quad (1.1)$$

This definition illuminates the idea of a continuum and shows the true nature of a continuum property "at a point" as a fictitious but highly useful concept.

Fluid Velocity at a Point. The fluid velocity at a point is quite independent of the instantaneous velocity of the molecule nearest that point. Rather we consider the motion of the center of gravity of the volume $\delta V'$ (Fig. 1.1b) instantaneously surrounding that point, and define the *fluid velocity at the point P* as the instantaneous velocity of this center of gravity. Thus the fluid velocity at a point is the instantaneous velocity of the fluid particle which at that moment is passing through the point. By *fluid particle* we mean here a small mass of fluid of fixed identity and of size comparable with $\delta V'$.

Whereas density at a point is a scalar quantity, fluid velocity at a point is a vector. After the introduction of a coordinate system, it is therefore possible to resolve the vector velocity into three scalar components.

STREAMLINES. At any instant, every point of a fluid continuum has a corresponding fluid velocity vector. The curves which are everywhere tangent to the velocity vector are known as the *instantaneous streamlines* of the flow, and comprise one of the most common and most useful graphical representations of the flow. When we speak of the flow pattern, we often mean the streamline picture.

In unsteady flows the streamline pattern changes from instant to instant. When the flow is steady, however, the streamlines are constant in time and represent also the path lines, or the trajectories of fluid particles.

STREAM TUBE. Consider an elementary area δA normal to the velocity vector at some point. The streamlines passing through the circumference of δA form a surface which is called a *stream tube*. Since there is no velocity component normal to the streamline, the walls of a stream tube may be thought of as being impervious to flow.

Stress at a Point. Consider a plane passing in a given direction through point P of the continuous medium of Fig. 1.2, and imagine a

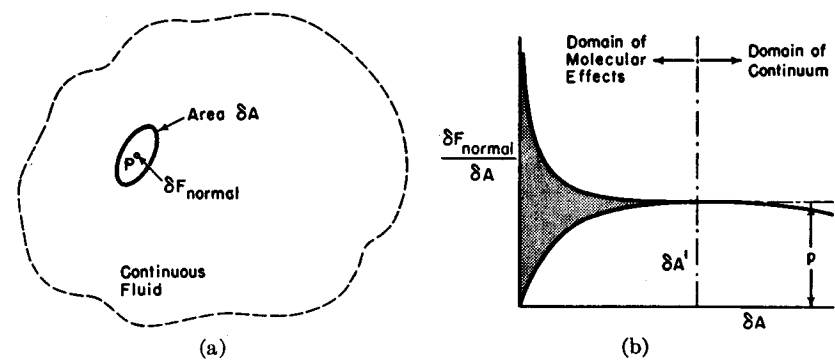


FIG. 1.2. Definition of normal stress at a point.

circular area δA in this plane surrounding P . It is a matter of experience that the fluid on one side of this surface exerts a force on the fluid on the other side; and, by the third law of Newton, the fluid on the latter side exerts an equal but opposite force on the fluid on the first side. Such forces are called *surface forces*.

NORMAL STRESS. The surface force acting on the area δA may be resolved into a component normal to δA and a component lying in the plane of δA . Considering first the normal force component, and referring to Fig. 1.2b, we define the *fluid pressure* at the point P in the given direction as the limit of the normal component of force per unit area:

$$p \equiv \lim_{\delta A \rightarrow \delta A'} \frac{\delta F_{\text{normal}}}{\delta A} \quad (1.2)$$

SHEAR STRESS. Similarly, the *shear stress* τ is defined in terms of the limit of the tangential component of force per unit area acting on δA :

$$\tau = \lim_{\delta A \rightarrow \delta A'} \frac{\delta F_{\text{tangential}}}{\delta A} \quad (1.3)$$

Both the pressure and the shear stress are, of course, vector quantities. The area $\delta A'$ and volume $\delta V'$, it should be noted, have comparable dimensions.

HYDROSTATIC PRESSURE. We now raise the question whether at the point P the pressure, or normal stress, depends upon the orientation of the plane δA .

To answer this question, let us first consider an inviscid fluid, that is, a fluid in which no viscous stresses (tangential or shear stresses) exist even though there is relative motion within the fluid. Suppose for mathematical simplicity that only two dimensions are considered, and let us then investigate the dynamics of an infinitesimally small triangular piece of fluid of unit depth surrounding P in Fig. 1.3. Then, since shear stresses are assumed absent, only normal stresses, or pressures, act on the three faces. The forces exerted by the fluid outside the triangle on the fluid within the triangle are shown in the sketch, where p_x denotes the pressure at

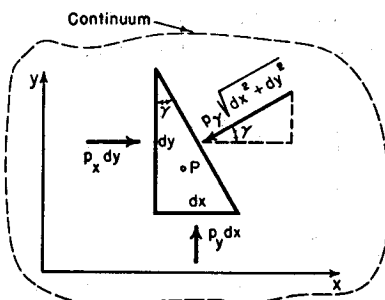


FIG. 1.3. Normal stress forces acting at a point.

point P in the x -direction, p_y denotes the pressure at point P in the y -direction, and p_γ denotes the pressure at point P in the γ -direction. Let g_x and g_y be the components of body force (e.g., gravity force) acting on the fluid per unit mass. Now we may write Newton's second law in the x -direction, as follows:

$$\Sigma F_x = ma_x$$

$$p_x dy - p_\gamma \sqrt{dx^2 + dy^2} \cos \gamma + g_x \rho \frac{dx dy}{2} = \rho \frac{dx dy}{2} a_x$$

where a_x is the acceleration in the x -direction. From the geometry of the triangle, we see that

$$\sqrt{dx^2 + dy^2} \cos \gamma = dy$$

and then, noting that $dx dy$ is negligible compared with dy , we obtain the result that $p_x = p_\gamma$.

By similarly applying Newton's second law in the y -direction, we get $p_y = p_\gamma$. Thus we have finally that

$$p_x = p_y = p_\gamma$$

and, since the direction γ was chosen without prejudice, we conclude that *in an inviscid fluid, whether in motion or not, the fluid pressure at a point is the same in all directions*. Such a condition is termed a *hydrostatic state of stress*.

Consider next a viscous fluid at rest. Shear stresses are again absent because of the lack of relative motion, and a similar analysis yields the same result of a hydrostatic state of stress.

STATE OF STRESS IN VISCOUS FLUID. Turning next to the general case of a viscous fluid in motion, shearing stresses must be inserted in Fig. 1.3. By writing the laws of motion, it is soon found that p_x , p_y , and p_γ are all different, and indeed the state of stress is similar to that existing in a solid, as described graphically by Mohr's circle of stress.

In this case, which is in fact the situation usually obtaining in practice, it is meaningless to speak of the pressure at a point, but rather it is necessary to speak in terms of six stress components at a point.⁽¹⁾ Nevertheless, we often do speak of the pressure at a point in viscous fluids, and this is justified by the fact that in such cases (specifically, when the Reynolds Number is large compared with unity) the shear stresses are small compared with the normal stresses, and consequently the variation of normal stress with orientation is correspondingly small.

Coefficient of Viscosity. In all real fluids, experimental observations indicate that a shearing deformation is always accompanied by a shearing stress. Most common engineering fluids are Newtonian in nature, which means that the shearing stress is proportional to the rate of shearing deformation.

Consider in two dimensions a fluid particle of fixed identity which at some instant of time t is rectangular and which at the same t has one corner at point P in space (Fig. 1.4). Let the shear stresses acting on the two faces passing through P be denoted by τ_{xy} and τ_{yx} .

As in the analysis connected with Fig. 1.3, the inertia forces and body forces are of higher order than the surface forces. Then, applying Newton's second law for moments of forces, it follows that $\tau_{xy} = \tau_{yx}$.

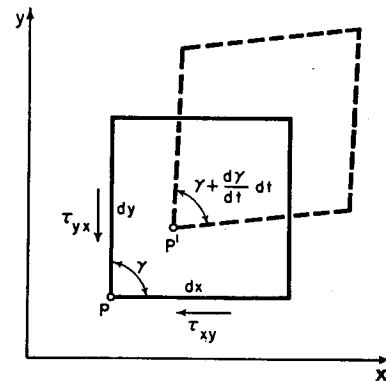


FIG. 1.4. Shear deformation in a fluid.

After a time interval dt , the particle has moved to the position shown by the dashed lines, and the corner at P has moved to P' . Furthermore, the included angle at P has changed by the amount $d\gamma$. A *Newtonian fluid* is now defined as one exhibiting the proportionality

$$\tau_{xy} \sim \frac{d\gamma}{dt}$$

The constant of proportionality is called the *coefficient of viscosity*, μ and is defined by

$$\tau_{xy} = \tau_{yx} = \mu \frac{d\gamma}{dt} \quad (1.4)$$

In Chapter 9 a study of the kinematics of two-dimensional motion yields an expression for $d\gamma/dt$ leading to

$$\tau_{xy} = \tau_{yx} = \mu \left(\frac{\partial u}{\partial y} + \frac{\partial v}{\partial x} \right) \quad (1.5)$$

where u and v are the respective velocity components in the x - and y -directions.

PERFECT FLUIDS. A *perfect fluid* is defined as one having a zero coefficient of viscosity, which means physically that shear stresses are absent despite shearing deformations in the fluid. No real fluids are inviscid, but the concept of a perfect fluid is useful inasmuch as it provides a simple model which at the same time approximates real fluids in many situations.

An *inviscid fluid* differs from a viscous fluid in one other important respect. All real, and hence viscous, fluids stick to solid boundaries with which they are in contact; that is, at solid boundaries the fluid has the same velocity as the boundary. A perfect fluid, however, may glide past solid boundaries with complete freedom.

BOUNDARY LAYER. Since many real engineering fluids have small viscosity, but nevertheless stick to solid boundaries, the concept of a boundary layer has proved immensely useful. According to this concept, viscous forces in the fluid may be ignored in comparison with inertia forces at some distance from the boundary. In a thin *boundary layer* near the solid boundary, however, shear forces must necessarily be significant because of the large shearing deformations resulting from the fluid's being at rest at the solid boundary. This division of the field of flow into two distinct parts is often of great practical service in making problems simple enough for analytical treatment.

Mathematical Description of Continuum. There are two possible viewpoints in describing the motion of fluids. First, there is the *method*

of *Lagrange*, usually used in the dynamics of discrete particles, wherein the history of individual fluid particles is described; that is, at each instant of time the location, density, state of stress, etc., are specified for a certain fluid particle of fixed identity.

The *method of Euler*, on the other hand, focuses attention on a fixed point of space, and specifies at each instant of time the density, pressure, etc., of the fluid particle which happens to occupy that point at that instant.

In most problems of fluid motion Euler's description proves far more convenient, and it is the viewpoint adopted in this book.

Treating the density as a typical continuum property defined at a point, we say in the Eulerian method that the density is a function of location and time. Mathematically, with x , y , z as Cartesian coordinates, we indicate this by writing

$$\rho = \rho(x, y, z, t) \quad (1.6)$$

Then for arbitrary increments in x , y , z , and t , the corresponding increment in ρ may be written in terms of the partial differential quotients:

$$d\rho = \frac{\partial \rho}{\partial x} dx + \frac{\partial \rho}{\partial y} dy + \frac{\partial \rho}{\partial z} dz + \frac{\partial \rho}{\partial t} dt \quad (1.7)$$

Relations like Eqs. 1.6 and 1.7 may be written for all continuum properties thus far defined.

STEADY FLOW. Many engineering problems refer to a steady condition of operation. Specifically we define *steady flow* as a condition where at each point of space there is no variation of any property with respect to time. Using the density for illustration, we may then write

$$\rho = \rho(x, y, z)$$

$$\partial \rho / \partial t = 0$$

1.3. Systems and Control Volumes

The System. The four basic principles listed in Art. 1.1 are always stated in the first instance in terms of a "system." A *system*, which is sometimes called a *free body* or *isolated body*, is defined as an arbitrary collection of matter of *fixed identity*. Everything external to the system is called the *surroundings*. The *boundary of a system* is defined as the imaginary surface which separates the system from its surroundings.

Through the use of the system concept one focuses attention on the body or substance of immediate interest and then observes interactions between the system and the surroundings.

To illustrate, consider Newton's second law, $F = ma$. Here F is the resultant vector force exerted by all the surroundings *on the system*; m is the mass of *the system*; and a is the vector acceleration experienced by the center of mass of the system.

The first step in applying the laws of conservation of mass, conservation of momentum, conservation of energy, and the second law of thermodynamics in their elementary forms is necessarily the definition of a system. Without this step it is useless to speak of such things as force, mass, heat, work, etc., for these terms are ambiguous until the system is specifically and rigorously defined.

To begin an analysis in terms of a system is never incorrect, but sometimes it is an inconvenient starting point when dealing with fluids. Fluids are extremely mobile, and it is therefore difficult to identify the boundaries of a fluid system for any appreciable length of time. This is particularly true in the interior of turbomachines, where complex processes occur and where different particles of fluid passing through the machine experience different histories. With fluids in motion it is, therefore, simpler to think in terms of a given volume of space through which fluid flows than it is to think in terms of a particular mass of fluid of fixed identity.

The Control Volume. With this in mind, we define a *control volume* as an arbitrary volume, *fixed in space*, and through which fluid flows. The identity of the fluid occupying the control volume changes from instant to instant. The surface which bounds the control volume is called the *control surface*; it is always a closed surface, but may be either singly or multiply connected. For some purposes, useful results are obtained by considering infinitesimal control volumes; for others, by considering control volumes of finite size.

To make practical use of the control volume concept, it is first necessary to cast the four basic principles into a form where they apply to the control volume rather than to the system. Then these forms may be used as starting points for analysis. The reformulation of the physical laws into control volume form is effected in Arts. 1.4, 1.5, 2.5, and 2.6.

1.4. Conservation of Mass

The principle of conservation of mass, when referred to a system of fixed identity, simply states that the mass of the system is constant. This statement is a concise summary of experimental observation, relativity and nuclear effects being of course absent.

Consider an arbitrary control volume through which fluid streams (Fig. 1.5a). We wish to derive the form of the law of conservation of mass as it applies to this control volume. However, in order to apply

the law, we must begin with a system of fixed identity, and so we define our system as the fluid which at some instant t occupies the control volume.

Next, we consider what happens during the succeeding time interval dt . By definition, the control volume remains fixed in space, but the

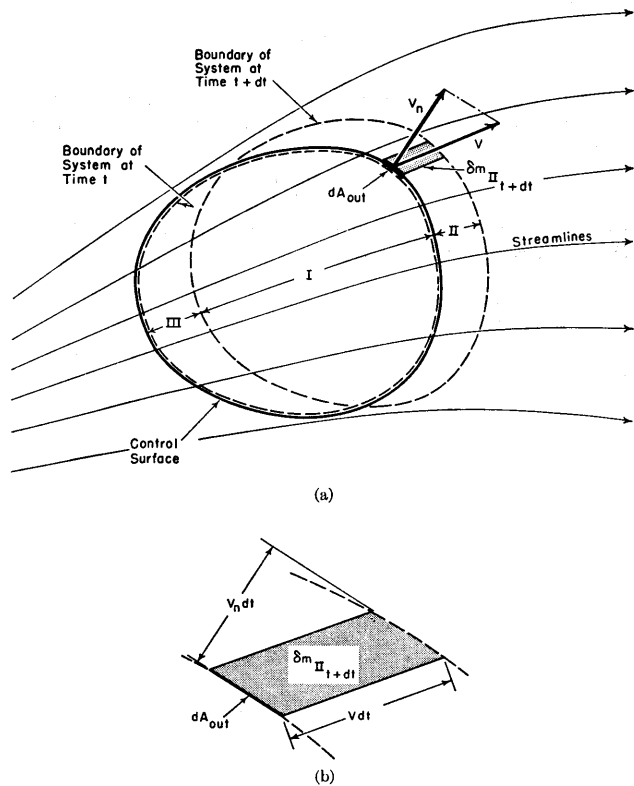


FIG. 1.5. Flow through a control volume.

system moves in the general direction of the streamlines. The two positions of the system are shown in Fig. 1.5a by dashed lines.

For convenience in analysis, we consider three regions of space, denoted by I, II, III in Fig. 1.5a. At time t the system occupies spaces

I and III, and at time $t + dt$ it occupies spaces I and II. Thus, since the mass of the system is conserved, we write

$$m_{I_t} + m_{III_t} = m_{I_{t+dt}} + m_{II_{t+dt}}$$

where m_{I_t} means the mass of fluid in space I at time t , and so on. A simple rearrangement then gives

$$\frac{m_{I_{t+dt}} - m_{I_t}}{dt} = \frac{m_{III_t} - m_{II_{t+dt}}}{dt}$$

The first term represents the time rate of change of mass within space I. But, as dt goes to zero, space I coincides with the control volume, and so, in the limit,

$$\frac{m_{I_{t+dt}} - m_{I_t}}{dt} \rightarrow \frac{\partial}{\partial t} (m_{c.v.})$$

where $m_{c.v.}$ denotes the instantaneous mass within the control volume.

The third term may be written

$$\frac{m_{II_{t+dt}}}{dt} = \frac{\Sigma \delta m_{II_{t+dt}}}{dt} = \sum \frac{\delta m_{II_{t+dt}}}{dt} = \int dw_{out}$$

where $\delta m_{II_{t+dt}}$ represents the amount of mass crossing the elementary surface dA_{out} during the time dt . The ratio $\delta m_{II_{t+dt}}/dt$ is called the outgoing flux of mass across the area dA_{out} , or the mass rate of flow, and is denoted for convenience by dw_{out} . The integral sign in $\int dw_{out}$ signifies that the mass rate of flow is to be summed up for all elements of control surface area dA_{out} through which fluid leaves the control volume.

Similar reasoning yields

$$\frac{m_{III_t}}{dt} = \int dw_{in}$$

and so the conservation law may now be expressed as

$$\frac{\partial}{\partial t} (m_{c.v.}) = \int dw_{in} - \int dw_{out} \quad (1.8)$$

which states that the rate of accumulation of mass within the control volume is equal to the excess of the incoming rate of flow over the outgoing rate of flow.

Continuity Equation. For detailed computations, we note that at any instant

$$m_{c.v.} = \int \delta m_{c.v.} = \int_{c.v.} \rho dV$$

where dV is an element of control volume, ρ is the local mass density

of that element, and the integral is to be taken over the entire control volume. Furthermore,

$$\frac{\partial m_{c.v.}}{\partial t} = \frac{\partial}{\partial t} \int_{c.v.} \rho dV = \int_{c.v.} \frac{\partial \rho}{\partial t} dV$$

With the help of Fig. 1.5b, we may express the mass rate of flow in the form

$$dw_{out} = \frac{\delta m_{II_{t+dt}}}{dt} = \frac{\rho (dA_{out})(V_n dt)}{dt} = \rho V_n dA_{out}$$

where ρ is the local instantaneous mass density in the neighborhood of dA_{out} and V_n is the corresponding local instantaneous component of velocity normal to dA_{out} .

With the foregoing expressions, Eq. 1.8 may now be written

$$\int_{c.v.} \frac{\partial \rho}{\partial t} dV = \int \rho V_n dA_{in} - \int \rho V_n dA_{out} \quad (1.9)$$

a form which is usually called the *equation of continuity*, since it is based on the assumption of a continuous medium. In vector form it is written

$$\int_{c.v.} \frac{\partial \rho}{\partial t} dV = - \oint_{c.s.} \rho \mathbf{V} \cdot d\mathbf{A} \quad (1.10)$$

where the last integral is a surface integral summed up over the entire control surface.

Steady Flow. When the flow is steady, the identity of the fluid within the control volume changes continuously, but the total mass remains constant. Or, mathematically, $\partial \rho / \partial t$ is zero for each element of control volume. Then Eq. 1.9 states that the incoming and outgoing mass rates of flow are identical:

$$\int \rho V_n dA_{in} = \int \rho V_n dA_{out} \quad (1.11)$$

It is interesting to observe that the same result applies to incompressible, unsteady flows.

One-Dimensional Steady Flow. Consider the steady flow through a duct or stream tube (Fig. 1.6) and assume the flow to be one-dimensional. Then since ρ and V are constant over each cross section, Eq. 1.11 yields

$$\rho_1 V_1 A_1 = \rho_2 V_2 A_2 \quad (1.12)$$

where A_1 represents the cross-sec-

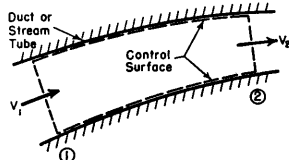


FIG. 1.6. One-dimensional flow.

tional area at section 1, measured in a plane normal to the axis of the tube. This equation is of great practical utility for simplified calculations.

1.5. Momentum Theorem

The fundamental principle of dynamics is Newton's second law of motion. Following the approach used in Art. 1.4, we now derive the form of this law appropriate to a control volume.

Fig. 1.7 shows the arbitrary control volume, together with the position of the system at times t and $t + dt$, the system being defined as the mate-

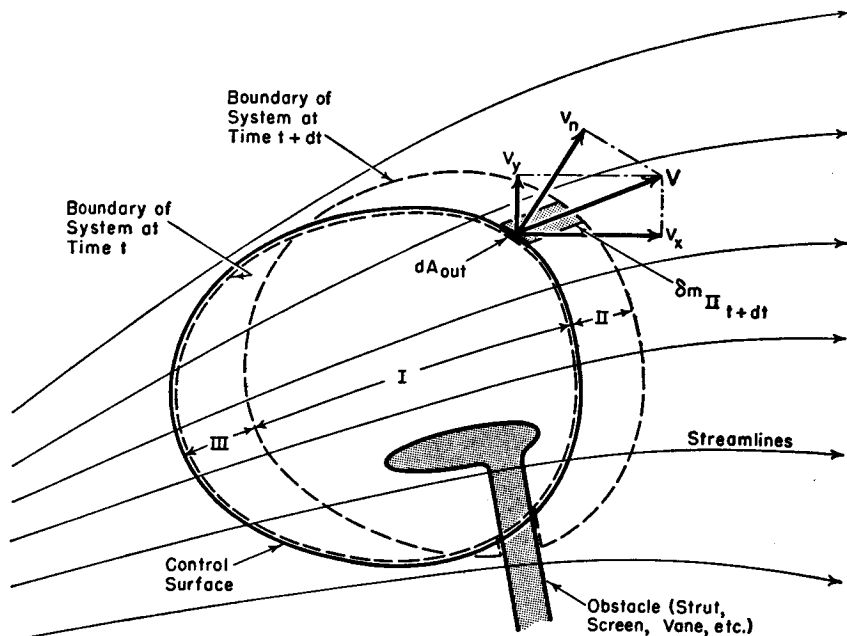


FIG. 1.7. Flow through a control volume.

rial occupying the control volume at time t . For the sake of generality there is also shown protruding into the control volume some sort of obstacle, such as a strut, screen, flameholder, guide vane, or turbo-machine blade. For the control volume chosen, that part of the obstacle lying within the control volume is part of the system whose motion during the time dt is being studied.

Newton's second law is a vector relation. Considering the x -direction, we write, for the system

$$\Sigma F_x = \frac{d}{dt} (mV_x)$$

where the left-hand side represents the algebraic sum of the x -forces

acting on the system during the time interval dt , and the right-hand side represents the time rate of change of the total x -momentum of the system. The right-hand side may, however, be expressed as

$$\frac{d}{dt} (mV_x) = \frac{(mV_x)_{I_{t+dt}} + (mV_x)_{II_{t+dt}} - (mV_x)_{I_t} - (mV_x)_{III_t}}{dt}$$

The combination of terms

$$\frac{(mV_x)_{I_{t+dt}} - (mV_x)_{I_t}}{dt}$$

represents the time rate of change of x -momentum within space I. In the limit as dt goes to zero, space I coincides with the control volume, and so the term in question becomes the time rate of change of x -momentum within the control volume.

We now form the expression

$$\frac{(mV_x)_{II_{t+dt}}}{dt} = \frac{\Sigma V_x \delta m_{II_{t+dt}}}{dt} = \sum V_x \frac{\delta m_{II_{t+dt}}}{dt} = \int V_x dw_{out}$$

and note that a similar expression applies to the incoming flow. The term $\int V_x dw$ which appears here is called the *flux of x -momentum*.

Now, with the expressions developed above, the dynamic relation may be written

$$\Sigma F_x = \frac{\partial}{\partial t} (mV_x)_{c.v.} + \int V_x dw_{out} - \int V_x dw_{in} \quad (1.13)$$

In the limit, as dt vanishes, we note that ΣF_x becomes the algebraic net x -force acting instantaneously on the fluid within the control volume. Eq. 1.13 is usually called the momentum theorem and states that the net force acting instantaneously on the fluid within the control volume is equal to the time rate of change of momentum within the control volume plus the excess of outgoing momentum flux over incoming momentum flux.

Working Form of Momentum Theorem. A useful working form of the momentum theorem is obtained by observing that

$$\frac{\partial}{\partial t} (mV_x)_{c.v.} = \frac{\partial}{\partial t} \int_{c.v.} \rho V_x dV = \int_{c.v.} \frac{\partial}{\partial t} (\rho V_x) dV$$

where ρ and V_x are the local density and x -velocity, respectively, of the fluid element of volume dV within the control volume. Then, using the expression for dw developed in Art. 1.4, the momentum theorem is written

$$\Sigma F_x = \int_{c.v.} \frac{\partial}{\partial t} (\rho V_x) dV + \int \rho V_n V_x dA_{out} - \int \rho V_n V_x dA_{in} \quad (1.14)$$

Two similar relations apply to the y - and z -directions. By using vector notation, the momentum theorem for a control volume may be represented by a single equation,

$$\Sigma \mathbf{F} = \frac{\partial}{\partial t} \int_{c.v.} \rho \mathbf{V} dV + \oint_{c.s.} \rho (\mathbf{V} \cdot d\mathbf{A}) \mathbf{V} \quad (1.15)$$

which is the fundamental principle in the dynamics of fluid motion.

Discussion of Forces. The term $\Sigma \mathbf{F}$ in Eq. 1.15 (or ΣF_x in Eq. 1.14 for the x -direction) is the algebraic sum of all forces exerted by the surroundings on the material instantaneously occupying the control volume. Here it is well to recall that forces may be divided into two classes, (i) body forces, and (ii) surface forces.

BODY FORCES. Body forces are forces which are proportional either to the volume or mass of the body, and comprise those forces involving action at a distance. Such forces arise from force fields, and include such examples as the force of gravitational attraction, magnetic forces, and electrodynamic forces. For accelerating coordinate systems, inertia forces such as centrifugal and Coriolis forces would also be included.

SURFACE FORCES. Surface forces are those forces which are exerted at the control surface by the material outside the control volume on the material inside the control volume. Such forces are exerted in the form of surface stresses. Often it is useful to divide surface forces into two types: (i) those arising from normal stresses, or pressures, acting on the control surface, and (ii) those arising from shear stresses, or viscous stresses, acting on the control surface. Where interfaces between phases are involved, surface tensions also form a special type surface force, but they are not of interest for our present purpose.

Referring to Fig. 1.7, the force acting on the surface of intersection between the obstacle and control surface must be included in $\Sigma \mathbf{F}$, and generally involves shear stresses and either tensile or compressive stresses in the metal. However, the fluid pressures and shear stresses acting on the part of the obstacle within the control volume do not enter into $\Sigma \mathbf{F}$ because the surfaces on which they act do not form part of the control surface.

Moving Reference Systems. The acceleration term appearing in the law of motion is the acceleration with reference to the fixed stars. In most engineering problems, the acceleration of the earth's surface with respect to the fixed stars is negligibly small. In practice, therefore, we usually evaluate Newton's law with reference to the earth's surface as a coordinate system.

If, on the other hand, we employ an accelerating coordinate system, as for example the rotor of a turbomachine, Newton's law in its usual

form is not valid since there must be inserted additional terms to take account of the centrifugal and Coriolis accelerations. Since the momentum theorem derives from the law of motion, a similar conclusion applies, namely that in Eq. 1.15 the velocities must be measured with respect to the earth, or with reference to a coordinate system moving at constant velocity with respect to the earth.

1.6. Theorem of Moment of Momentum

In dynamics useful information is often obtained by employing Newton's law of motion in the form where it applies to the moments of the forces. This form of the law is especially valuable for the analysis of turbomachines, where we may be more concerned with moments of forces (or torques) than with the forces themselves.

For a system, the sum of the moments of the external forces is equal to the time rate of change of moment of momentum. In vector notation this is written

$$\Sigma \mathbf{F} \times \mathbf{r} = \frac{d}{dt} (\Sigma m \mathbf{V} \times \mathbf{r})$$

where \mathbf{r} is the radius vector from an arbitrary origin of moments. In Cartesian notation, and referring to Fig. 1.8, this is written

$$M_z = \Sigma r F_t = \frac{d}{dt} (\Sigma m r V_t)$$

where r is the radius in the xy -plane to the element of mass m , F_t is the component normal to r of the vector force projected in the xy -plane, V_t is the component normal to r of the vector velocity projected in the xy -plane, and M_z is the net moment of forces about the z -axis.

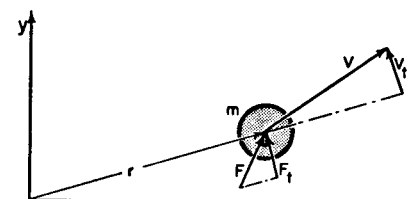


FIG. 1.8. Illustrating Newton's second law for moments.

Working Form of Theorem of Moment of Momentum. By following the methods employed in Arts. 1.4 and 1.5 for converting from a system to a control volume, the *theorem of moment of momentum* may be derived for a control volume. In vector form, it is written

$$\Sigma \mathbf{F} \times \mathbf{r} = \int_{c.v.} \frac{\partial}{\partial t} (\rho \mathbf{V} \times \mathbf{r}) dV + \oint_{c.s.} (\rho \mathbf{V} \cdot d\mathbf{A}) \mathbf{V} \times \mathbf{r} \quad (1.16)$$

In Cartesian form, and considering moments about, say, the z -axis, Eq. 1.16 is written as

$$\Sigma r F_t = \int_{c.v.} \frac{\partial}{\partial t} (\rho r V_t) dV + \int \rho r V_n V_t dA_{out} - \int \rho r V_n V_t dA_{in} \quad (1.17)$$

which states that the algebraic sum of the moments is equal to the time rate of change of moment of momentum within the control volume plus the excess of outgoing flux of moment of momentum over the corresponding incoming flux.

The remarks in Art. 1.5 concerning forces are evidently applicable also to the moments of the forces.

1.7. Units and Dimensions

It seems in order at this point to explain the system of dimensions in use throughout the book.

Newton's dynamic formulation is stated in terms of four completely independent physical quantities: force, mass, length, and time. Before the statement of the law of motion, the units in which these quantities could be measured were totally unrelated, and so Newton could state his law only as a proportionality, $F \sim ma$, or

$$F = \frac{1}{g_0} ma$$

where g_0 is an experimentally determined constant whose magnitude depends only upon the units of measure of the four primary quantities.

However, once the proportionality law is known, it is evidently possible to redefine one of the units of measure in terms of the other three, thus reducing by one the number of primary quantities.

These ideas are illustrated by the following tabulation of three systems of units in engineering use

Mass	Length	Time	Force	g_0
lbm	ft	sec	lbf	$32.174 \frac{\text{lbm ft}}{\text{lbf sec}^2}$
lbm	ft	sec	poundal	$1 \frac{\text{lbm ft}}{\text{poundal sec}^2}$
slug	ft	sec	lbf	$1 \frac{\text{slug ft}}{\text{lbf sec}^2}$

The last system, which is the one employed in this book, is one where g_0 has the numerical magnitude unity, and thus one for which unit force gives unit mass unit acceleration. For such a system of units, we may eliminate g_0 from the mathematical statement of the law, which is tantamount to eliminating one of the primary units of measure and defining it instead in terms of the remaining three. Thus, writing as we do,

$$F = ma$$

we imply that

$$1 \text{ lbf} \equiv 1 \frac{\text{slug ft}}{\text{sec}^2}; \text{ or } 1 \text{ slug} \equiv 1 \frac{\text{lbf sec}^2}{\text{ft}}$$

Since we usually employ the slug as mass unit for numerical calculations, but often refer to results in terms of pound masses, it is convenient to remember that

$$1 \text{ slug} \equiv 32.174 \text{ lbm}$$

REFERENCES AND SELECTED BIBLIOGRAPHY

1. LAMB, H. *Hydrodynamics*. 6th ed. New York: Dover Press, 1945.
2. PRANDTL, L., and TIEFJENS, O. G. *Fundamentals of Hydro- and Aeromechanics*. New York: McGraw-Hill Book Co., Inc., 1934.
3. HUNSAKER, J. C., and RIGHTMIRE, B. G. *Engineering Applications of Fluid Mechanics*. New York: McGraw-Hill Book Co., Inc., 1947.

PROBLEMS

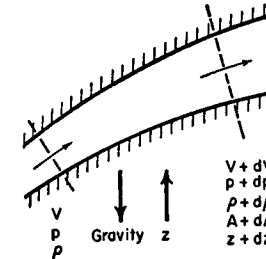
1.1. Consider the frictionless, steady flow of a compressible fluid in an infinitesimal stream tube.

(a) Demonstrate by the continuity and momentum theorems that

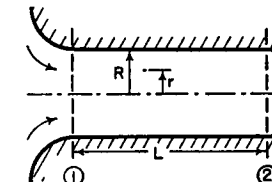
$$\frac{dp}{\rho} + \frac{dA}{A} + \frac{dV}{V} = 0$$

$$dp + \rho V dV + \rho g dz = 0$$

(b) Determine the integrated forms of these equations for an *incompressible* fluid.



PROB. 1.1.



PROB. 1.2.

1.2. An incompressible fluid flows in a pipe of radius R . At the inlet, section 1, the velocity is uniform over the cross section, with a value V_1 . At section 2, where the flow is laminar and fully developed, the velocity varies with radius according to the relation

$$V = V_{\max} \left(1 - \frac{r^2}{R^2}\right)$$

(a) Demonstrate that $V/V_{\max} = \frac{1}{2}$.

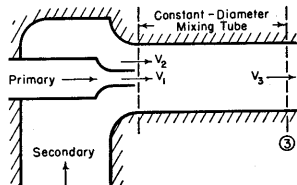
(b) If τ_w is the average wall shearing stress retarding the flow between sections 1 and 2, find the pressure drop $(p_1 - p_2)$ in terms of V_{\max} , ρ , L , r and τ_w .

1.3. The sketch shows a jet pump (ejector or injector) in which a primary stream of high velocity liquid at section 1 entrains a secondary stream of the same liquid at low velocity at section 2. At the end of the constant-diameter mixing-tube, i.e., at section 3, the streams are thoroughly mixed and uniform in velocity, as the result of friction between the streams.

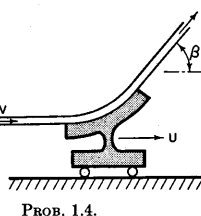
For the purpose of this analysis, assume that at sections 1 and 2 both streams have the same static pressure and that shearing stresses at the walls of the mixing tube are negligible.

Assuming that $A_1 = 0.1 \text{ ft}^2$, $A_3 = 1 \text{ ft}^2$, $V_1 = 100 \text{ ft/sec}$, $V_2 = 10 \text{ ft/sec}$, and $\rho = 64.4 \text{ lbm/ft}^3$

- Calculate V_3 (ft/sec).
- Calculate $p_3 - p_1$ (lbf/in²).



PROB. 1.3.



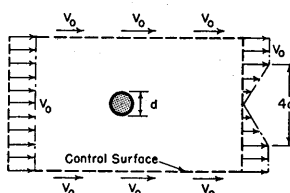
PROB. 1.4.

1.4. The sketch shows a vane with a turning angle β which moves with a steady speed U . The vane receives a jet which leaves a fixed nozzle with speed V .

(a) Assuming that the vane is mounted on rails as shown in the sketch, show that the work done against the restraining force is a maximum when $U/V = \frac{1}{3}$.

(b) Assuming that there are a large number of such vanes attached to a rotating wheel moving with peripheral speed U , show that the work delivered to the wheel is a maximum when $U/V = \frac{1}{2}$.

1.5. In an experiment to determine drag, a circular cylinder of diameter d



PROB. 1.5.

was immersed in a steady, two-dimensional, incompressible flow. Measurements of velocity and pressure were made at the boundaries of the control surface shown. The pressure was found to be uniform over the entire control surface. The x -component of velocity at the control surface boundary was approximately as indicated by the sketch.

From the measured data, calculate the drag coefficient of the cylinder, based on the projected area and on the free stream dynamic head, $\frac{1}{2}\rho V_0^2$.

$$C_D = \frac{\text{Drag Force per Unit Length}}{\frac{1}{2}\rho V_0^2 d}$$

Chapter 2

FOUNDATIONS OF THERMODYNAMICS

2.1. Introductory Remarks

In Art. 1.1 it was pointed out that the four fundamental principles governing the motion of compressible fluids are the law of conservation of mass, Newton's laws of motion, and the two laws of thermodynamics. The basic concepts, definitions, and analytical statements relating to the first two of these four principles were reviewed in Chapter 1, and we now proceed to a similar brief review of the foundations of thermodynamics. It is not the intent here to treat this subject with the fullness and detail found in well-known thermodynamics textbooks,^(1,2) but rather to set out the general point of view, method of procedure, and necessary relations employed in this book, insofar as thermodynamics is concerned.

Much of the preliminary discussion contained in Arts. 1.1 and 1.2 is relevant also to thermodynamics. The definition of a fluid, the concept of a continuum, and the definition of a continuum property "at a point" are implicit in classical thermodynamics. Likewise, the definitions of the system and of the control volume given in Art. 1.3, together with the remarks concerning their relative utility, remain applicable.

NOMENCLATURE

A	area	q	vector heat flux per unit area
c_p	specific heat at constant pressure	Q	rate of heat transfer
c_v	specific heat at constant volume	R	gas constant
e	internal energy per unit mass	\mathcal{R}	universal gas constant
E	internal energy of a system in general	s	entropy per unit mass
g	local acceleration of gravity	S	entropy
h	enthalpy per unit mass	T	absolute temperature
k	ratio of specific heats	u	same as U , except for a unit mass
m	mass	U	that part of the internal energy of a system independent of motion, gravity, electricity, capillarity, and magnetism
p	pressure	v	specific volume
Φ	power	V	volume
q, Q	heat		
q_x	heat transfer per unit time per unit area in the x -direction		

NOMENCLATURE—Continued

V	speed	η	thermal efficiency
w	mass rate of flow	λ	coefficient of thermal conductivity
W	work; molecular weight		
z	elevation above given datum	ρ	density

2.2. The First Law of Thermodynamics

In this article we shall outline the structure of the First Law as it relates to a system of fixed identity, and in Art. 2.5 we shall develop the appropriate form of the First Law for a control volume.

Definitions and Concepts. STATE. The *state* of a system is its *condition* or *configuration*, described in sufficient detail so that one state may be distinguished from all other states.

PROPERTY. A *property* of a system is any *observable characteristic* of a system. The properties we shall deal with are all measurable in terms of numbers and units of measurement and include such physical quantities as location, speed, direction, pressure, density, etc. A listing of a sufficient number of independent properties constitutes a complete definition of the state of a system.

PROCESS. A *process* is a *change of state* and is described in part by the series of states passed through by the system. Often, but not always, some sort of *interaction* between the system and surroundings occurs during a process; the specification of this interaction completes the description of the process.

CYCLE. A *cycle* is a process wherein the initial and final states of the system are identical. For this to be true it is only necessary that the initial and final states have identical values of all respective properties.

EQUALITY OF TEMPERATURE. It is a common fact of experience that when two bodies, one of which "feels hot" to the touch, the second of which "feels cold," are brought together, some sort of interaction occurs, as evidenced by the changes in properties which occur in both. After some time, however, no further changes are observed, and we then say that the two bodies are equal in temperature. Formally, we define *equality of temperature* between two bodies by saying that this equality exists when no interaction occurs upon the two bodies being brought into communication with each other.

TEMPERATURE. The concept of inequality of temperature derives by implication from the concept of equality of temperature. Furthermore

since we distinguish inequality of temperature by observing changes of properties of the two bodies concerned, it follows that an arbitrary scale of temperature may be defined in terms of some convenient property of a standard body called a thermometer. A simple and familiar temperature scale, for example, is the length of a mercury thread in a glass column, with numerical values established by a precisely defined, but nonetheless arbitrary, system of markings on the glass.

THE ZERO TH LAW OF THERMODYNAMICS. Further thought concerning the possible utility of a thermometer as defined above reveals that the practical applications of thermometry hinge on the assumption that two bodies respectively equal in temperature to a third body must also be equal in temperature to each other. Fortunately, this assumption is amply verified by innumerable experiments. It is sometimes called the *Zeroth Law of Thermodynamics*.

EQUAL-TEMPERATURE PROCESS. The definition of equality of temperature is based on the cognizance of some sort of interaction between a system and its surroundings which occurs when equality of temperature does not prevail. Later we shall identify this type of interaction as *heat*. For the present, however, we observe only that if a process occurs in which the system and surroundings are at each step equal in temperature, then the particular type of interaction associated with temperature inequality is absent from the process. This in no way implies that the temperature of the system need be constant during the process.

The use of constant-temperature baths and of evacuated jackets (such as Dewar flasks) are common laboratory techniques for effecting *equal-temperature processes*.

Work. The laws of thermodynamics deal with interactions between a system and its surroundings as they respectively pass through equilibrium states. These interactions may be divided into two classes: (i) work and (ii) heat interactions.

In mechanics *work* is defined as an effect produced by a system on its surroundings when the system moves the surroundings in the direction of a force exerted by the system on its surroundings. The magnitude of the effect is measured by the product of the distance moved and the component of force in the direction of motion.

Thermodynamics deals with phenomena considerably more complex than does mechanics, and so it is necessary to generalize the foregoing definition of work.

RECOGNITION OF WORK DONE. We say that work is done by a system on its surroundings if some other process can be found in which the system passes through the same series of states as in the original process,

but in which the sole effect in the surroundings is the rise of a weight.

This means that "motion of a force through a distance" is not essential to a work interaction. Instead, it is only necessary that there be some alternative surroundings which might engage in the process in such a way that the motion of a force through a distance would be the only effect external to the system.

To illustrate, suppose a storage battery, which we consider as the system, discharges while lighting an electric light bulb. If the bulb were replaced by an electric motor having very large conductors and a pulley on which is wound a string suspending a weight, then the storage battery could pass through the same series of states with no net outside effect except the rise of the weight. By the criterion for a work interaction, it follows that the storage battery did work in the original process.

MEASUREMENT OF WORK. The amount of work done by a system is measured by the number of standard weights which may be raised from one prescribed level to another in the alternative surroundings previously used for the recognition of work.

For example, the amount of work in ft-lb is the same as the number of pound masses which can be raised from a certain location on the earth to an elevation one foot higher.

When the system does work *on* the surroundings, it is conventional to call the work positive.

WORK RECEIVED. Thus far we have spoken only of work *done* by a system. To complete the definition of work, we say that if a system does work *on* the surroundings, then the surroundings receive work of the same amount from the system. To recognize work received by a system, it is then necessary to interchange temporarily the system and surroundings.

When work is received by a system, the magnitude of the work is taken to be negative.

With these conventions it follows that if a work interaction occurs between bodies *A* and *B*, then $W_A = -W_B$, where W_A denotes the work done by body *A* and W_B denotes the work done by body *B*. This rule is analogous to Newton's third law for forces: action and reaction are equal.

The First Law. The principal experimental foundations of the First Law are the remarkable investigations of Joule,⁽³⁾ who carried out processes from a given initial state to a given final state by a variety of processes, some involving electrical work and others involving mechanical work with various mechanical arrangements. These different processes involving several different kinds of work were, moreover,

carried out on a variety of systems, comprising several pure substances, mixtures, and substances undergoing chemical reaction. The nature of the experiments were such that the processes were carried out with substantial temperature equality between the system and surroundings.

These experiments revealed that, for a given system passing from a given initial state to a given final state by different equal-temperature processes, the amount of work done was the same for all such processes. This result has such important practical implications that it is called the First Law of Thermodynamics, and may be stated formally as follows:

The amount of work done by any system in going from one state to another does not depend on the course of states passed through by the system nor on the manner of work interaction, so long as the system and surroundings are equal in temperature at each step of the process.

INTERNAL ENERGY. From this law follows the important corollary that the amount of work done during an equal-temperature process depends only on the end states of the process and not on the intermediate series of states. Since the work in an equal-temperature process depends on the end states, this suggests that we define a new *property* or *state function*, the decrease in which represents the work during an equal-temperature process, namely,

$$E_1 - E_2 = (W_{e.t.})_{1 \rightarrow 2} \quad (2.1)$$

where E is the newly defined property, and $(W_{e.t.})_{1 \rightarrow 2}$ denotes the work done by the system during an equal-temperature process while going from state 1 to state 2.

Thus, assuming that for a given system an arbitrary value of E is assigned to some specified reference state, corresponding values of E at all other states may be found by measuring the work in equal-temperature processes and applying Eq. 2.1.

The property E defined by Eq. 2.1 is usually called the *energy* or the *internal energy* of the system.

Heat. When temperature equality does not prevail during a process, some type of interaction occurs which is different in nature from the work interaction, and the work done is not equal to the decrease in the property E . The type of interaction owing to temperature inequality is called a *heat interaction*, and the amount of heat is measured by the difference between the work done during the actual process and the work which would be done during an equal-temperature process between the same end states. Thus, denoting the heat "received" by Q , and the actual work done by W , we define

$$Q = W - W_{e.t.} \quad (2.2)$$

But $W_{e.t.}$ is given by the decrease in the property E , according to Eq. 2.1, and so we have

$$Q = E_2 - E_1 + W \quad (2.3)$$

Although Eq. 2.3 is nothing but a definition, it is often called the First Law of Thermodynamics. This is in fact an acceptable statement if one adds that E is a property defined by Eq. 2.1.

In differential form for a small change of state, Eq. 2.3 is written

$$\delta Q = dE + \delta W \quad (2.4)$$

where the symbols δQ and δW represent small amounts of quantities which are not properties, whereas dE denotes an increment of a property.

It is a matter of experience that when δQ as defined by Eq. 2.4 is positive, the system is at a lower temperature (on all conventional thermometric scales) than the surroundings, and vice versa. This observation is, in fact, connected with the Second Law of Thermodynamics. When δQ is positive we say that heat is "received by the system," or that heat is "transferred to the system."

It may be demonstrated that when heat is defined by Eq. 2.3, the heat for the system is equal in magnitude to and opposite in sign to the heat for the surroundings. Thus, if bodies A and B exchange heat only with each other, then $Q_A = -Q_B$, which, again, is like Newton's third law of motion.

JOULE'S CONSTANT. Thermodynamics as we now know it was preceded by calorimetry, which was based on the caloric theory of heat. We find in the literature independent definitions of work and heat (for example, the ft-lb and the Btu) together with the Joulean "mechanical equivalent of heat."

Within the framework of the First Law as stated here, however, and entirely in accord with Joule's interpretation, we may regard the Btu as a measure of the change in E , and define it as the change in E of a pound mass of water between a state at 1 atm and 59.5°F and a state at 1 atm and 60.5°F. Taking this as the definition of the Btu, experiments substantially like Joule's, but more precise, may be interpreted according to Eq. 2.1 to mean that

$$1 \text{ Btu} \equiv 778.2 \text{ ft lbf}$$

The First Law for a Cycle. Since E is a property, the net change in E for a cyclic process is exactly zero, and so from Eq. 2.4 it follows that

$$\oint \delta Q = \oint \delta W \quad (2.5)$$

which states that the algebraic net heat received by the system during a

cycle is equal to the algebraic net work done by the system during the cycle.

Adiabatic Process. It is a matter of experience that when barriers, called heat insulators, are placed between a system and surroundings at different temperatures, the heat Q reckoned from Eq. 2.3 becomes very small, and it is not difficult to extrapolate in one's mind to the condition where the insulation is so effective as to make the heat zero. Such a process is said to be *adiabatic*. Since Q is also zero in an equal-temperature process, it follows that an equal-temperature process is also an adiabatic process.

2.3. The Second Law of Thermodynamics

In this Article we shall briefly outline the structure of the Second Law, following closely the detailed development of Keenan.⁽¹⁾

Heat Engines. A heat engine is defined as a system of fixed identity which undergoes a cyclic process during which there are work and heat interactions with the surroundings. The most familiar example of a heat engine is the steam power plant, and the closed-cycle gas turbine is another. Neither open-cycle gas turbines nor internal combustion engines, on the other hand, are heat engines according to this definition.

THERMAL EFFICIENCY OF HEAT ENGINES. That part of the surroundings from which the system receives heat during the cycle is called a *source of heat*, and the amount of heat is denoted by q_1 . Similarly, q_2 represents the amount of heat rejected by the system to the *sink* during the cycle. The First Law for a cyclic process, Eq. 2.5, requires that the net work of the engine during a complete cycle be given by

$$W_{\text{eng}} = q_1 - q_2 \quad (2.6)$$

The useful output of an engine is the mechanical work, W_{eng} , whereas the factor most closely connected with the cost of operation is the heat received, q_1 . Consequently, the *thermal efficiency* of an engine is taken to be

$$\eta = \frac{W_{\text{eng}}}{q_1} = \frac{q_1 - q_2}{q_1} = 1 - \frac{q_2}{q_1} \quad (2.7)$$

PERPETUAL MOTION OF THE SECOND KIND. A heat engine having a thermal efficiency of 100 per cent is called a *perpetual motion machine of the second kind*. It may be demonstrated that, if such a machine could be constructed, it would be possible to obtain mechanical power without the use of any fuel whatsoever, the heat q_1 being taken either from the atmosphere, or, better still, from some low-temperature body which it is desired to refrigerate.

The Second Law of Thermodynamics. Experience teaches that perpetual motion of the second kind, although greatly to be desired, is impossible to achieve. This statement has such important practical implications that it is called the Second Law of Thermodynamics, which may now be stated as follows:

No system can pass through a complete cycle of states and deliver positive work to the surroundings while exchanging heat with only a single source of heat at uniform temperature.

The confidence placed in this law derives not alone from the failure of efforts to construct perpetual motion machines of the second kind, but even more from innumerable experiments which serve only to confirm the many corollaries and consequences which stem from the Second Law.

Reversibility and Irreversibility. Our personal experiences that natural events tend to proceed in one direction only, that is, that real processes are irreversible, are intimately connected with the Second Law.

REVERSIBILITY. We say that a process is reversible if it is possible for the effects of the process to be entirely effaced—that is, if there exists some known way by which the system and all parts of the surroundings can be restored to their respective initial states. A reversible process “does not make history,” for it may be completely undone, and in this sense it is equivalent to the absence of a process.

No real processes are reversible, but often real processes can be refined to the point where they approximate reversible processes. For this reason the reversible process is a useful standard of comparison against which real processes may be evaluated.

IRREVERSIBILITY. The definition of an irreversible process is implicit in the definition of a reversible process. That is, we say that a process is irreversible if there is no known way by means of which the system and all parts of the surroundings can be restored to their respective initial states.

For the types of phenomena of interest in this book, the irreversibilities can always be traced to three basic causes: (i) viscosity, (ii) heat conduction, and (iii) mass diffusion. Note that all these are phenomenological manifestations of molecular actions.

The connection between irreversibility and the Second Law stems from the proposition that *if a way were found to undo any irreversible process it would then be possible to construct a perpetual motion machine of the second kind.*

For example, suppose that in Fig. 2.1a the heat passes by conduction through the metal bar from the high-temperature reservoir T_1 to the

low-temperature reservoir T_2 . If this process could be undone, then heat q_1 would be transferred to reservoir T_1 while the same amount of heat was lost from reservoir T_2 . However, by operating a heat engine as shown in Fig. 2.1b, the cyclically operating system enclosed by the dashed lines becomes a perpetual motion machine of the second kind, inasmuch as it delivers positive work W_{eng} to the surroundings while receiving heat $q_1 - q_2$ from the single uniform-temperature source T_2 .

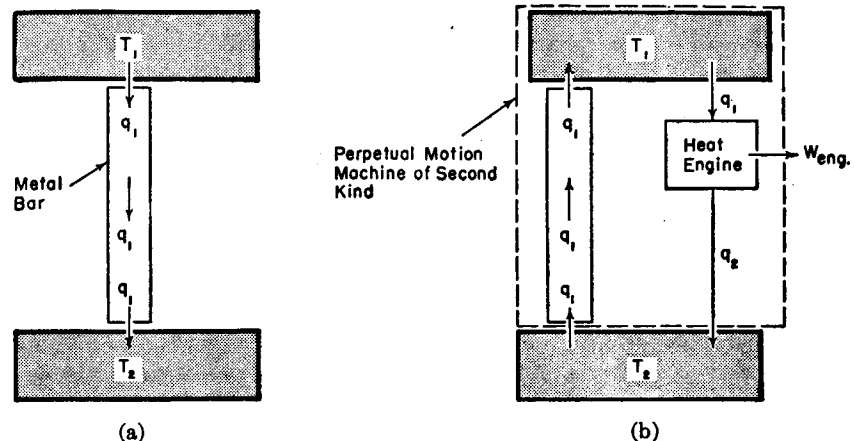


FIG. 2.1. Conduction of heat from low temperature to high temperature permits perpetual motion of second kind.

Thus we have proved that our oft perceived observation of the irreversibility of heat conduction from a high-temperature to a low-temperature body is in fact a logical consequence of the Second Law. The proposition stated above may be similarly proved for irreversible processes in general, and this suggests an alternative definition of irreversibility:

A process is irreversible if the undoing of all the effects of the process would make possible the construction of a perpetual motion machine of the second kind.

Corollaries of the Second Law. The following corollaries of the Second Law, comprising the most important results for its practical utilization, stem by logical processes from its statement. Again we follow closely the development of Keenan.⁽¹⁾

COROLLARY 1. No heat engine operating between two heat reservoirs of fixed and uniform temperature can have a greater thermal efficiency than a reversible heat engine which operates between the same two reservoirs, for it can be shown that otherwise perpetual motion of the second kind would be possible.

Here it is well to remark that a reversible engine is reversible in each element of its cycle, so that the reversal of a reversible engine leads to the reversal of the net cyclic work and heat interchanges with the surroundings. Friction must be absent from reversible engines, and they can exchange heat with the surroundings only when the temperature difference between the working fluid and the surroundings is vanishingly small.

COROLLARY 2. From Corollary 1 it follows that all reversible heat engines operating between the same two reservoirs of fixed and uniform temperature have the same thermal efficiency.

COROLLARY 3. THE ABSOLUTE TEMPERATURE SCALE. From Corollary 2 it may be shown that a temperature scale defined in terms of the efficiency of a reversible engine operating between two reservoirs of fixed and uniform temperature depends only on the temperatures of these reservoirs and not on the nature of the engine nor of the thermometric fluid.

Thus, by using a reversible engine as a thermometer, it is possible to avoid a basic difficulty of thermometers constructed as outlined in Art. 2.2—namely, that different thermometers agree only at one or two fixed points but generally differ at all other points.

The *Kelvin scale of absolute temperature* is defined by

$$\frac{q_1}{q_2} = \frac{T_1}{T_2} \quad (2.8)$$

where T_1 is the temperature of the reservoir supplying the heat q_1 to the engine, and T_2 is the temperature of the reservoir receiving the heat q_2 rejected from the engine.

The ice point (0°C , 32°F) has a temperature of 273.2 on the Kelvin, or absolute centigrade scale; and a temperature of 491.7 on the Rankine, or absolute Fahrenheit scale. In this book absolute temperatures will be reported on the Rankine scale (e.g., 530°R). The Rankine temperature is obtained from the Fahrenheit temperature by adding 459.7, often rounded off as 460, to the latter.

It follows further from Corollary 3 that it is impossible for systems to have zero or negative absolute temperature.

COROLLARY 4. THE INEQUALITY OF CLAUSIUS. It may be shown that when a system passes through a complete cycle, perpetual motion of the second kind is possible unless

$$\oint \frac{\delta Q}{T} \leq 0 \quad (2.9)$$

where δQ is a small amount of heat received at a part of the boundary

of the system during an elementary part of the cycle, and T is the corresponding absolute temperature at that part of the boundary. The integral is to be summed for all parts of the boundary and over the entire cycle.

COROLLARY 5. THE ENTROPY. From Corollary 4 it may be shown that, in a cycle made up of reversible steps,

$$\oint \left(\frac{\delta Q}{T} \right)_{\text{rev}} = 0 \quad (2.10)$$

From this it follows that in going from a given state 1 to a given state 2 by two different processes, both of which are reversible, the integral of $\delta Q/T$ will be the same for both processes. More generally, we may say that the $\int (\delta Q/T)_{\text{rev}}$ depends only on the end states and not on the intermediate series of states. The quantity $\delta Q/T$ for a reversible infinitesimal process is, therefore, an exact differential, and is the differential of a thermodynamic property. This property, which is called the *entropy*, is defined by

$$dS \equiv \left(\frac{\delta Q}{T} \right)_{\text{rev}} \quad (2.11)$$

and is most useful for practical calculations.

Thus, just as the First Law led to the definition of a new property (the internal energy), so the Second Law also leads to the definition of a property—the entropy.

Although the entropy is defined in terms of reversible processes and can only be reckoned from Eq. 2.11 with the aid of imaginary reversible processes, this in no way diminishes its utility for irreversible processes, inasmuch as it is a property having a particular value (with respect to some reference condition) for each equilibrium state of a system. It will be recalled that a similar situation exists for the internal energy, which although defined only for equal temperature processes, has meaning nonetheless for processes which are not at equal temperature.

For reversible processes the heat received by a system in passing from state 1 to state 2 is given, according to Eq. 2.11, by

$$Q_{\text{rev}} = \int T dS \quad (2.12)$$

and this may be represented by the area under the curve representing the process on a thermodynamic diagram of temperature versus entropy (Fig. 2.2).

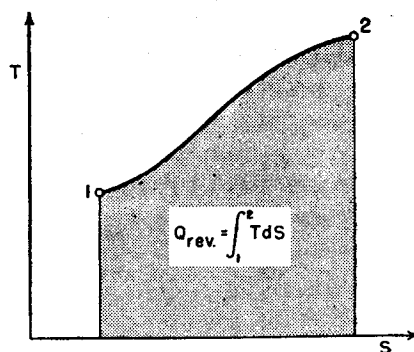


FIG. 2.2. Reversible heat transfer on temperature-entropy diagram.

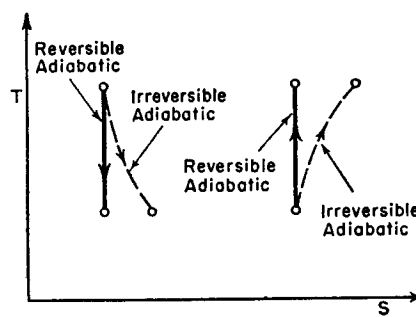


FIG. 2.3. Reversible and irreversible adiabatics.

COROLLARY 6. THE SECOND LAW IN ANALYTICAL FORM. From Corollaries 4 and 5, together with the definition of the entropy, it may be shown that, in general, for an infinitesimal process of any system,

$$dS \geq \frac{\delta Q}{T} \quad (2.13)$$

where δQ and T have the same meaning as in Eq. 2.9. This relation is the most convenient analytical form of the Second Law.

When a system is isolated from all heat exchange with the surroundings, Eq. 2.13 shows that

$$(dS)_{\text{adiabatic}} \geq 0 \quad (2.14)$$

which is the well known *principle of the increase of entropy*.

Since the entropy is defined by Eq. 2.11, it follows that the equality sign necessarily applies in Eqs. 2.13 and 2.14 for reversible processes. Furthermore, it may be shown that the inequality sign always applies to irreversible processes.

Fig. 2.3 illustrates the paths of reversible and irreversible adiabatics on the temperature-entropy diagram.

RELATION BETWEEN FIRST AND SECOND LAW PROPERTIES FOR A PURE SUBSTANCE. A system whose chemical composition during a given process is both homogeneous and invariable is called a pure substance. For a pure substance defined in this way, and in the absence of electrical, magnetic, and capillary forces, it may be shown that

$$dS = \frac{dU + p dV}{T} \quad (2.15)$$

where V is the volume of the system and U is that part of the internal

energy E which is independent of the system's motion and of gravitational, electrical, magnetic, and capillary forces.

Eq. 2.15 refers to changes in properties between equilibrium states of a system and is, therefore, the most practical way of measuring changes in entropy, since the change in U can be evaluated from measurements of work in processes which are not necessarily reversible.

2.4. Thermodynamic Properties of the Continuum

The continuum properties density and pressure, defined in the preceding chapter, are important also in thermodynamics. In addition, we have in this chapter introduced several additional properties more uniquely related to thermodynamics, namely, the *temperature*, the *internal energy*, and the *entropy*.

Regarding the latter two, it is convenient to work with the "specific" values of the properties, i.e., the values per unit mass. Hence we define

$$e \equiv E/m$$

$$s \equiv S/m$$

where e is the specific internal energy, or internal energy per unit mass, E is the internal energy for the entire system, m is the mass of the system, and so on. Small letters denote values per unit mass, and capital letters represent values for the entire system. The specific volume is the volume per unit mass and is, therefore, the inverse of the density,

$$v \equiv V/m = 1/\rho$$

The values of such properties as e , s , v , etc., "at a point," or for a fluid particle, are defined according to the train of thought illustrated by Fig. 1.1.

The Internal Energy U for a Pure Substance. Capillary, electrical, and magnetic forces are absent or negligible in most engineering problems involving fluids, but the system may undergo accelerations and may be subject to gravitational forces. In addition, the system may undergo other changes in state owing to heat transfers or to motions of the boundary against external forces, these changes being made manifest by changes in pressure, density, and temperature.

Often it is convenient to employ an expression for e which separates the effects mentioned above. Since e is a property, it may be evaluated for any chosen process between a selected pair of end states. Let us select a simple process comprising three steps: (i) an equal-temperature change of speed of the system in which there are no changes in p , ρ , and z , where z denotes elevation above the earth's surface, (ii) an equal-temperature change of elevation of the system in which there are no

changes in p , ρ , and V , where V denotes the speed of the system, and (iii) a process involving changes in p , ρ , and T , but no changes in z and V .

For the first step, it follows from Eq. 2.1 and Newton's second law that $e_2 - e_1 = (V_2^2 - V_1^2)/2$, the right-hand side usually being called the increase in kinetic energy.

For the second step, it follows again from Eq. 2.1 and Newton's second law that $e_2 - e_1 = g(z_2 - z_1)$ where g is the local acceleration of gravity. The right-hand side is usually called the increase in potential energy.

For the third step, by definition, we set $e_2 - e_1 = u_2 - u_1$, in which the right-hand side is the change of internal energy of a pure substance in the absence of changes in speed and of body and capillary forces.

For the entire process, therefore, we have

$$e_2 - e_1 = u_2 - u_1 + \frac{V_2^2 - V_1^2}{2} + g(z_2 - z_1) \quad (2.16)$$

The Enthalpy. In most flow problems the terms u and pv appear as a sum, and so it is convenient to define a shorthand symbol for this sum, called the enthalpy:

$$h \equiv u + pv \equiv u + \frac{p}{\rho} \quad (2.17)$$

Specific Heats. Two "specific heats" are in common use, namely, c_p and c_v . As will be seen from their definitions, the word "heat" in their titles is a misnomer carried over from caloric theory:

$$c_p \equiv \left(\frac{\partial h}{\partial T} \right)_p; \quad c_v \equiv \left(\frac{\partial u}{\partial T} \right)_v \quad (2.18)$$

Coefficient of Thermal Conductivity. Fourier's law of heat conduction states that the heat flux per unit area in a given direction is proportional to the temperature gradient in the same direction, the factor of proportionality depending only on the units of measurement and on the local thermodynamic state. The proportionality constant is called the *coefficient of thermal conductivity* λ , and is defined by

$$q_x \equiv -\lambda \frac{\partial T}{\partial x} \quad (2.19a)$$

where q_x is the heat transfer per unit time per unit area in the x -direction, and $\partial T/\partial x$ is the temperature gradient in the x -direction. The minus sign is inserted as the heat always flows from high to low temperatures.

In vector language, λ is defined by

$$\mathbf{q} = -\lambda \nabla T \quad (2.19b)$$

where \mathbf{q} is the vector heat flux per unit area, and ∇T is the vector gradient of the temperature.

Units and Dimensions. We shall adopt as standard units the ft, sec, lbf, slug, and degree Rankine. The units of some typical thermodynamic quantities are then as follows:

Q	ft lbf
u	ft lbf/slug
c_p	ft lbf/slug R
s	ft lbf/slug R
λ	lbf/sec R

2.5. The First Law for a Control Volume

Just as it was desirable to put the law of conservation of mass and Newton's second law of motion into forms applicable to the flow through

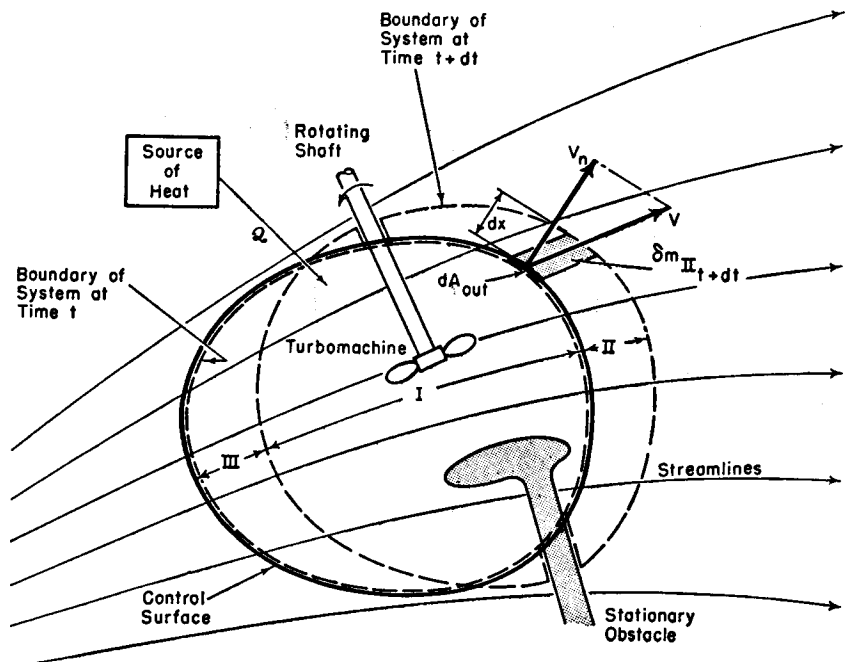


FIG. 2.4. Flow through control volume.

a control volume, so now it is desirable to do the same for the two laws of thermodynamics. In this article we shall do so for the First Law, following identically the pattern of procedure employed in Chapter 1.

Consider the flow through the control volume of Fig. 2.4, with the system defined as the material occupying the control volume at time t . We consider what happens during the time interval dt . Passing through the control surface are a stationary strut and a rotating shaft attached to a turbomachine, perhaps a compressor or turbine.

Eq. 2.4 may here be written, for the system, as

$$\frac{\delta Q}{dt} = \frac{dE}{dt} + \frac{\delta W}{dt}$$

in terms of the *rate* of heat transfer, etc. Now we put the three terms of this expression into more convenient form.

Rate of Heat Transfer. If \mathcal{Q} is the rate of heat transfer (ft lbf/sec) through the control surface from the surroundings, then, as the interval dt becomes vanishingly small, we may write

$$\frac{\delta Q}{dt} = \mathcal{Q}$$

Rate of Change of E . Referring to Fig. 2.4, we write

$$\begin{aligned} \frac{dE}{dt} &= \frac{(E_{I_{t+dt}} + E_{II_{t+dt}}) - (E_{I_t} + E_{III_t})}{dt} \\ &= \frac{E_{I_{t+dt}} - E_{I_t}}{dt} + \frac{\int e \delta m_{II_{t+dt}}}{dt} - \frac{\int e \delta m_{III_t}}{dt} \end{aligned}$$

Since space I coincides with the control volume as dt vanishes, this becomes

$$\frac{dE}{dt} = \left(\frac{\partial E}{\partial t} \right)_{c.v.} + \int e dw_{out} - \int e dw_{in}$$

Rate of Work Done. Omitting from our considerations capillary, magnetic, and electrical forces, the work done during the process is the result of normal and shear stresses at the moving boundaries of the system.

WORK DONE BY NORMAL STRESSES. Taking the normal stress at the boundary of the system as the hydrostatic pressure, the work done by the system owing to normal forces at an element of area dA_{out} is $p dA_{out} dx$, where dx is the component of distance moved normal to dA_{out} . But $dA_{out} dx$ is the volume of the mass element $\delta m_{II_{t+dt}}$, which volume may be written as $v \delta m_{II_{t+dt}}$. The total rate of work done by normal stresses during the process may now be set down, with the aid of the foregoing, as

$$\left(\frac{\delta W}{dt} \right)_{normal} = \frac{\int pv \delta m_{II_{t+dt}}}{dt} - \frac{\int pv \delta m_{III_t}}{dt} = \int pv dw_{out} - \int pv dw_{in}$$

WORK DONE BY SHEAR STRESSES. This work may be conveniently divided into two categories: (i) the work done by the part of the shaft inside the system on the part outside the system, owing to the torque in

the rotating shaft resulting from the shear stresses in the plane cut by the boundary of the system; (ii) the shear work done at the boundaries of the system on adjacent fluid which is in motion. These are respectively denoted by $\mathcal{P}_{\text{shaft}}$ and $\mathcal{P}_{\text{shear}}$, the power delivered by means of a rotating shaft and the power delivered by other shear forces. Note that shearing forces at the strut do not contribute to $\mathcal{P}_{\text{shear}}$, since the strut is not in motion. Likewise, if the control surface coincides with the stationary wall of a duct or machine casing, $\mathcal{P}_{\text{shear}}$ is zero at such points even though there may be appreciable shear stresses. On the other hand, $\mathcal{P}_{\text{shear}}$ plays an important role for a control surface lying within the viscous boundary layer.

In the limit, as dt vanishes, $\mathcal{P}_{\text{shaft}}$ and $\mathcal{P}_{\text{shear}}$ of course refer to the material instantaneously occupying the control volume.

The First Law. Combining the expressions developed above, and using the expression for e given by Eq. 2.16 and the expression for h given by Eq. 2.17, we finally obtain the following expression applicable to the control volume:

$$\begin{aligned} \mathcal{Q} &= \left(\frac{\partial E}{\partial t} \right)_{c.v.} + \mathcal{P}_{\text{shaft}} + \mathcal{P}_{\text{shear}} + \int \left(h + \frac{V^2}{2} + gz \right) dw_{out} \\ &\quad - \int \left(h + \frac{V^2}{2} + gz \right) dw_{in} \end{aligned} \quad (2.20)$$

where the integrals involve such terms as the "flux of enthalpy," "flux of kinetic energy," etc.

We may rewrite Eq. 2.20 somewhat more compactly with the help of vector notation:

$$\mathcal{Q} = \mathcal{P}_{\text{shaft}} + \mathcal{P}_{\text{shear}} + \int_{c.v.} \frac{\partial}{\partial t} (e\rho) dV + \oint_{c.s.} \left(h + \frac{V^2}{2} + gz \right) \rho \mathbf{V} \cdot d\mathbf{A} \quad (2.21)$$

Steady-Flow Energy Equation. In many practical engineering problems, the flow is steady and may also be regarded as one-dimensional. If the control surface also coincides with the inner casing of a machine, $\mathcal{P}_{\text{shear}}$ is zero. Eq. 2.21 is then simplified greatly. Let section 1 represent the incoming flow through the control surface (Fig. 2.5), and section 2 the outgoing flow. The mass flow w is then alike at both sections, and so it is convenient to define $Q \equiv \mathcal{Q}/w$ as the heat received per unit mass of fluid passing through, and $W_x \equiv \mathcal{P}_{\text{shaft}}/w$ as the shaft work delivered per unit mass of fluid passing through.

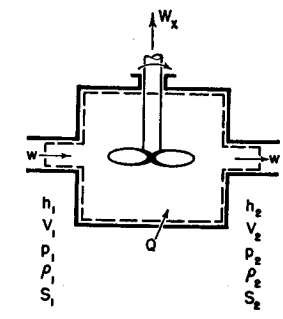


FIG. 2.5. One-dimensional flow.

With these assumptions, Eq. 2.21 is reduced to the form

$$Q = W_x + h_2 - h_1 + \frac{V_2^2 - V_1^2}{2} + g(z_2 - z_1) \quad (2.22)$$

which is the familiar form found in most textbooks on engineering thermodynamics.

Nonequilibrium States. Thermodynamics deals with equilibrium states of a system, so that in this respect the science would be more appropriately named "thermostatics." How, then, can we apply the usual methods of thermodynamics to flow problems where fluid particles are undergoing changes of state at a finite rate, and so cannot be passing through equilibrium states? Investigations of this point reveal that in most practical problems, even when supersonic speeds are involved, the departure from thermodynamic equilibrium is negligibly small, and we are, therefore, justified in proceeding in the present manner.

On the other hand, it should be realized that there are a few problems, notably the flow through a shock wave, wherein the departure from thermodynamic equilibrium is very great.

2.6. The Second Law for a Control Volume

Employing the same control volume, the same system, and the same process as in Fig. 2.4, Eq. 2.13 may be put into either of the following forms applicable to the flow through a control volume:

$$\oint_{c.s.} \frac{dQ}{T} \leq \left(\frac{\partial S}{\partial t} \right)_{c.v.} + \int s dw_{out} - \int s dw_{in} \quad (2.23a)$$

$$\oint_{c.s.} \frac{dQ}{T} \leq \int_{c.v.} \frac{\partial}{\partial t} (s\rho) dV + \oint_{c.s.} s\rho \mathbf{V} \cdot d\mathbf{A} \quad (2.23b)$$

where dQ is the incoming rate of heat transfer through an elementary area dA of the control surface, and T is the corresponding temperature of the control surface at that point.

For steady, one-dimensional flow (Fig. 2.5), Eq. 2.23 reduces to

$$w(s_2 - s_1) \geq \oint_{c.s.} \frac{dQ}{T} \quad (2.24)$$

and, if heat transfers across the control surface are negligible, there results

$$s_2 \geq s_1 \quad (2.25)$$

2.7. The Perfect Gas

For most problems in gas dynamics, the assumption of the perfect gas laws is sufficiently in accord with the properties of real gases as to be acceptable. We shall therefore set down here for later reference the special thermodynamic relations which apply to a perfect gas.

Equation of State. The definition of a perfect gas is in two parts, the first of which is the pressure-density-temperature relation, or equation of state, given by

$$pv = \frac{p}{\rho} = RT = \frac{R}{W} T \quad (2.26)$$

where T is the absolute temperature, R is the gas constant of the particular gas, R is the universal gas constant, and W is the molecular weight. In the usual engineering units,

$$R = 1545.4 \frac{\text{ft lbf}}{\text{R lbm-mole}} = (1545.4)(32.174) \frac{\text{ft lbf}}{\text{R slug-mole}}$$

Real gases appear to obey Eq. 2.26 exactly at zero pressure or at infinite temperature. For temperatures not low compared with the critical temperature, Eq. 2.26 is an accurate approximation to real gases provided that the pressure is low compared with the critical pressure.

Internal Energy and Enthalpy Changes. From well-known thermodynamic relations it may be shown that for any pure substance obeying Eq. 2.26 it is also true that

$$(\partial u / \partial v)_T = 0$$

which is equivalent to saying that the internal energy of a perfect gas does not depend on density, and hence depends on temperature alone.

Since we are dealing with a pure substance, we may write with the aid of the foregoing result,

$$u = u(v, T)$$

$$du = \left(\frac{\partial u}{\partial v} \right)_T dv + \left(\frac{\partial u}{\partial T} \right)_v dT$$

$$du = 0 \cdot dv + c_v dT = c_v dT \quad (2.27a)$$

so that the change in internal energy between any pair of end states is given by

$$u_2 - u_1 = \int_{T_1}^{T_2} c_v dT \quad (2.27b)$$

From the definition of the enthalpy it follows that h is also a function of temperature only, inasmuch as both u and pv are functions only of temperature. Hence

$$(\partial h / \partial p)_T = 0$$

$$dh = \left(\frac{\partial h}{\partial p} \right)_T dp + \left(\frac{\partial h}{\partial T} \right)_p dT = 0 \cdot dp + c_p dT = c_p dT \quad (2.28a)$$

and

$$h_2 - h_1 = \int_{T_1}^{T_2} c_p dT \quad (2.28b)$$

Gas Constants. When a substance obeys the perfect gas law there is a simple relation between c_p , c_v , and R . From the definitions of c_p and h , the perfect gas law, and the knowledge that h depends on T alone, we form

$$c_p \equiv \left(\frac{\partial h}{\partial T} \right)_p = \frac{dh}{dT} = \frac{d}{dT} (u + pv) = \frac{du}{dT} + \frac{d}{dT} RT = c_v + R \quad (2.29)$$

The ratio of specific heats, k , plays an important role in isentropic processes. It is defined by

$$k = c_p / c_v \quad (2.30)$$

Of the four quantities c_p , c_v , R , and k , only two are algebraically independent. With Eqs. 2.29 and 2.30, we may derive, for example,

$$c_p = \frac{k}{k-1} R; \quad c_v = \frac{R}{k-1}; \quad \text{etc.}$$

For the most simple molecular model, the kinetic theory of gases shows that

$$k = \frac{n+2}{n}$$

where n is the number of degrees of freedom of the molecule. Thus, monatomic gases have $n = 3$, $k = \frac{5}{3}$. Diatomic gases such as oxygen, nitrogen, etc., have $n = 5$, $k = \frac{7}{5}$. Extremely complex molecules, such as freon and gaseous compounds of uranium have large values of n and consequently values of k only slightly larger than unity.

Gas with Constant Specific Heats. The second part of the definition of a perfect gas is that c_v , which has already been shown to be dependent on T only, is assumed to be constant. This restriction is not so good an approximation to real gases as is the equation of state, and so sometimes we speak of a "semi-perfect gas," that is, one for which $pv = RT$ but having specific heats variable with temperature.

Considering now a perfect gas, it follows from Eq. 2.29 that c_p is also a constant, and then Eqs. 2.27 and 2.28 yield

$$u_2 - u_1 = c_v(T_2 - T_1) \quad (2.31a)$$

$$h_2 - h_1 = c_p(T_2 - T_1) \quad (2.31b)$$

Changes of Entropy. Applying the special relations of a perfect gas to the general relation between s , u , and v , we get

$$ds = \frac{du}{T} + \frac{p \, dv}{T} = c_v \frac{dT}{T} + R \frac{dv}{v}$$

and, upon integration,

$$s_2 - s_1 = c_v \ln \frac{T_2}{T_1} + R \ln \frac{v_2}{v_1} = c_v \ln \left(\frac{T_2}{T_1} \right) \left(\frac{v_2}{v_1} \right)^{k-1} \quad (2.32a)$$

Alternatively, we may eliminate either T or v from this expression with the aid of $pv = RT$, and so obtain

$$s_2 - s_1 = c_v \ln \frac{p_2}{p_1} + c_p \ln \frac{v_2}{v_1} = c_v \ln \left(\frac{p_2}{p_1} \right) \left(\frac{v_2}{v_1} \right)^k \quad (2.32b)$$

$$s_2 - s_1 = c_p \ln \frac{T_2}{T_1} - R \ln \frac{p_2}{p_1} = c_v \ln \left(\frac{T_2}{T_1} \right)^k \left(\frac{p_2}{p_1} \right)^{-(k-1)} \quad (2.32c)$$

allowing the entropy change to be simply calculated in terms of the end properties.

The Isentropic. Often the isentropic process is taken as a model or as a limit for real adiabatic processes. If the entropy is constant at each step of the process, it follows from Eqs. 2.32 that T and v , p and v , and T and p are connected with each other during the process by the following laws:

$$Tv^{k-1} = \text{const.}$$

$$pv^k = p/\rho^k = \text{const.}$$

$$T^{\frac{k}{k-1}}/p = \text{const.}$$

For isentropic flow processes the enthalpy change is important. It is calculated in terms of the initial temperature and the pressure ratio as follows:

$$(\Delta h)_s = c_p(T_2 - T_1)_s = c_p T_1 \left[\left(\frac{T_2}{T_1} \right)_s - 1 \right] = c_p T_1 \left[\left(\frac{p_2}{p_1} \right)^{\frac{k-1}{k}} - 1 \right] \quad (2.33)$$

REFERENCES AND SELECTED BIBLIOGRAPHY

1. KEENAN, J. H. *Thermodynamics*. New York: John Wiley & Sons, Inc., 1941.
2. ZEMANSKY, M. W. *Heat and Thermodynamics*. New York: McGraw-Hill Book Co., Inc., 1937.
3. JOULE, J. P. *The Scientific Papers of James Prescott Joule*. (Phys-Soc. of London.) London: Taylor & Francis, 1884.

Chapter 3

INTRODUCTORY CONCEPTS TO COMPRESSIBLE FLOW

3.1. The Velocity of Sound

The term *compressible flow* implies variations in density throughout the field of flow. These variations are, in many cases, the result principally of pressure changes from one point to another. The rate of change of density with respect to pressure is, therefore, an important parameter in the analysis of compressible flow, and, as we shall see, it is closely connected with the velocity of propagation of small pressure disturbances, i.e., with the velocity of sound.

NOMENCLATURE

<i>a</i>	mean molecular velocity	<i>T</i>	absolute temperature
<i>A</i>	area	<i>V</i>	velocity
<i>c</i>	velocity of sound	<i>w</i>	mass rate of flow
<i>c_p</i>	specific heat at constant pressure	<i>W</i>	molecular weight
<i>k</i>	ratio of specific heats	α	Mach angle
<i>l</i>	mean free molecular path	β	bulk modulus of compression
<i>L</i>	length	δ	boundary layer thickness
<i>M</i>	Mach Number	λ	coefficient of thermal conductivity
<i>p</i>	pressure	μ	coefficient of viscosity
<i>R</i>	gas constant	ρ	density
<i>R</i>	universal gas constant		
<i>s</i>	entropy per unit mass		

Velocity of Propagation of a Plane Pressure Pulse. Let us calculate the *velocity of sound* for a plane, infinitesimal pressure wave proceeding along a pipe of uniform cross section. Such a wave might have been initiated, for example, by a slight inward motion of a piston at the left-hand end of the pipe.

In Fig. 3.1a the wave front is assumed to propagate steadily to the right with a velocity *c*. The fluid through which the wave front has passed is at a pressure *p* + *dp*, has a density ρ + $d\rho$, and moves to the right with a velocity *dV*. The fluid on the right, into which the wave front is moving, has a pressure *p* and a density ρ , and is motionless.

To simplify the analysis, we reduce the process to one of steady motion by imagining that the observer travels with the steady speed of the wave

front. Fig. 3.1b shows the appearance of the process to such an observer who is moving to the right with the velocity c . Fluid flows steadily from right to left, and, as it passes through the wave front, the velocity is reduced from c to $(c - dV)$. At the same time, the pressure rises from p to $p + dp$, and the density from ρ to $\rho + d\rho$.

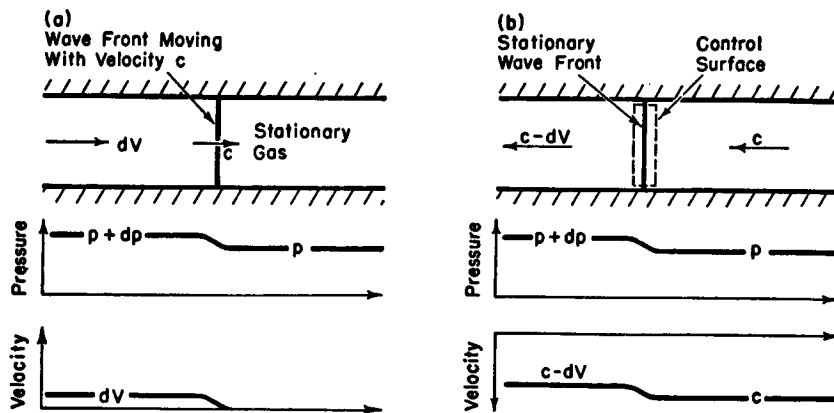


FIG. 3.1. Propagation of an infinitesimal pressure pulse.

- (a) Observer at rest.
- (b) Observer moving with wave front, which is equivalent to superposing a leftward velocity c on the flow of part (a).

MOMENTUM EQUATION. Considering a stationary control surface surrounding the stationary wave front of Fig. 3.1b, the shear forces on this control volume are negligibly small compared with the pressure forces. The momentum equation may be written, therefore, as

$$A[p - (p + dp)] = w[(c - dV) - c]$$

where A is the cross-sectional area. Simplifying, and noting that from the continuity equation,

$$w = \rho A c,$$

we get

$$dp = \rho c dV \quad (3.1)$$

This equation, it might be noted, is Euler's equation for a steady motion (note that dV is the decrease in velocity in the direction of motion).

CONTINUITY EQUATION. The continuity equation is then written for the fluid on both sides of the wave front. Noting that the area is unchanged, we get,

$$\rho c = (\rho + d\rho)(c - dV)$$

which reduces to

$$\frac{dp}{\rho} = \frac{dV}{c} \quad (3.2)$$

Combination of Eq. 3.1 with Eq. 3.2 then yields

$$c^2 = (\partial p / \partial \rho)_s; \quad \text{or} \quad c = \sqrt{(\partial p / \partial \rho)_s} \quad (3.3)$$

The ratio $dp/d\rho$ is written in Eq. 3.3 as a partial derivative at constant entropy because the variations in pressure and temperature are vanishingly small, and consequently, the process is nearly reversible. Moreover, the comparative rapidity of the process, together with the smallness of the temperature variations, makes the process nearly adiabatic. In the limit, for an infinitesimal wave, the process may be considered both reversible and adiabatic, and, therefore, isentropic.

Identical results for the velocity of propagation of a small disturbance are obtained for a cylindrical wave spreading from a line source and for a spherical wave spreading from a point source.

Velocity of Sound in a Perfect Gas. For a perfect gas the relation between pressure and density in an isentropic process is given by

$$p/\rho^k = \text{constant} \quad (3.4)$$

Putting this into logarithmic form, differentiating, and noting that $p = \rho RT$ for a perfect gas, we obtain

$$\ln p - k \ln \rho = \text{constant}$$

$$\frac{dp}{p} = k \frac{d\rho}{\rho}; \quad \left(\frac{\partial p}{\partial \rho} \right) = kp/\rho = kRT$$

Thus, we get for the velocity of sound in a perfect gas,

$$c = \sqrt{kp/\rho} = \sqrt{kRT} = \sqrt{kRT/W} \quad (3.5)$$

where W is the molecular weight.

EFFECT OF MOLECULAR WEIGHT. Since k varies only between narrow limits, we see that, in general, gases with small molecular weights have large sound velocities and vice versa. At normal atmospheric temperature, the speed of sound in air is of the order of 1100 ft/sec; in hydrogen, of the order of 4200 ft/sec; and in freon refrigerating gases or uranium hexafluoride, of the order of 300 ft/sec.

An interesting conclusion concerning turbomachinery can be drawn from these figures. To avoid excessive stresses, the tip speeds of rotors in turbomachines must not exceed a figure in the neighborhood of 1000 to 1500 ft/sec. It is also a matter of experience that losses in efficiency mount rapidly as the flow velocity relative to the blades approaches the sonic velocity. Thus, in air compressors, the limiting design factor on rotative speed may be either stress considerations or compressibility considerations. In hydrogen compressors, on the other hand, the compress-

ibility limitation is never a factor. At the opposite end of the scale, compressibility effects represent the principal limiting factor on the rotative speed for freon and uranium hexafluoride compressors.

Velocity of Sound in Air. In the case of air at normal pressure and temperature, Eq. 3.5 becomes

$$c = 49.02\sqrt{T} \quad (3.6)$$

where c is in ft/sec and T is in degrees R, or degrees F abs.

VELOCITY OF SHOCK WAVE. A wave of finite strength, usually called a shock wave, always propagates with a greater velocity than that indicated in Eq. 3.3, the velocity of propagation increasing with the wave strength. Shock waves are discussed in Chapter 5 and in Volume II, Chapter 25.

Velocity of Sound in Incompressible Fluid. Since an incompressible fluid is one which, by definition, cannot experience changes in density, Eq. 3.3 shows that the speed of sound is infinite in such a fluid. Pressure pulses emitted anywhere in the fluid are thus felt simultaneously at all other points.

No fluids are truly incompressible, although liquids show little change in density. The speed of sound in common liquids is of the order of 5000 ft/sec, which is enormously in excess of fluid velocities which can be produced in a liquid.

Often we speak of the "incompressible flow of a gas," in the sense that the fractional changes in density are so small as to be negligible.

Realms of Fluid Motion. Some of the different fields of fluid motion may now be classified as follows:

ACOUSTICS. The fluid velocities are extremely small compared with the velocity of sound, but the fractional variations in pressure, temperature, and density are of significant magnitude.

INCOMPRESSIBLE FLUID MECHANICS. The fluid velocities are small compared with the velocity of sound, and the fractional variation in density is insignificant; however, the fractional variations in pressure and temperature may be very large. It will be shown later that the error produced by neglecting compressibility in the computation of pressure variations is of the order of one-fourth the square of the ratio of the stream velocity to the sound velocity. Consequently, this ratio may be as great as 0.2 (corresponding to a velocity of about 200 ft/sec for air at normal atmospheric temperature) before the computed error in the pressure variation exceeds one per cent. For many problems in the flow of gases, therefore, the flow may with little error be treated as incompressible.

COMPRESSIBLE FLUID MOTION. The velocities are appreciable compared with the velocity of sound, and the fractional variations in pressure, temperature, and density are all of significant magnitude. This realm, often called *Gas Dynamics*, is the principal subject of this book. The science of Ballistics is a special branch of Gas Dynamics, pertaining to the free flight of projectiles at velocities greater than that of sound. Although the term *Gas Dynamics* is used, it is well to remember that the science of thermodynamics plays a role equally important to that of the science of dynamics in the motion of compressible fluids.

3.2. Physical Differences Between Incompressible, Subsonic, and Supersonic Flows

The influence of compressibility of the medium can lead to marked qualitative differences between the physical natures of incompressible and compressible flows. And, in compressible flows, there are astonishing differences in flow pattern and general behavior, depending on whether the fluid velocity is greater or less than the local speed of sound. Indeed, it is safe to say that one's "instincts" or past experience with subsonic flows are completely useless when dealing with supersonic flows and are apt to lead to false conclusions.

Pressure Field Created by a Moving Point Disturbance. To illustrate this in a simple way, it is useful to adopt momentarily a point of view which is somewhat oversimplified yet at the same time brings out the salient physical phenomena. When a body moves through a fluid, or when a fluid flows past a body or within the walls of a duct, each element of solid surface tends to divert the fluid from the course which it might otherwise take. For example, in the case of a projectile moving through air, each element of the projectile's surface area pushes the neighboring air out of the way, and this local disturbance creates a pressure pulse which propagates into the exterior air, much as the impulsive motion of the piston in Fig. 3.1 results in the propagation of a pressure wave down the duct. At any instant of time, therefore, the pressure perturbation at a point away from the projectile will be some sort of sum (not necessarily linear) of those pressure pulses which were initiated earlier at each element of projectile surface and which have arrived at the point in question after spreading spherically from the individual points of emission.

Following this line of thought, let us consider the pressure field created by the most elementary type of a moving disturbance—namely, a point source of disturbance moving at uniform linear speed through a compressible medium. At each instant of time the point source may be imagined to emit an infinitesimal pressure wave which spreads spherically from the point of emission with the speed of sound *relative to the*

fluid. The pressure pattern which exists at any instant is then found by superposition of all the pressure pulses which were previously emitted.

Fig. 3.2 shows several pressure pulse patterns for different values of the speed of the source compared with the speed of sound in the fluid.

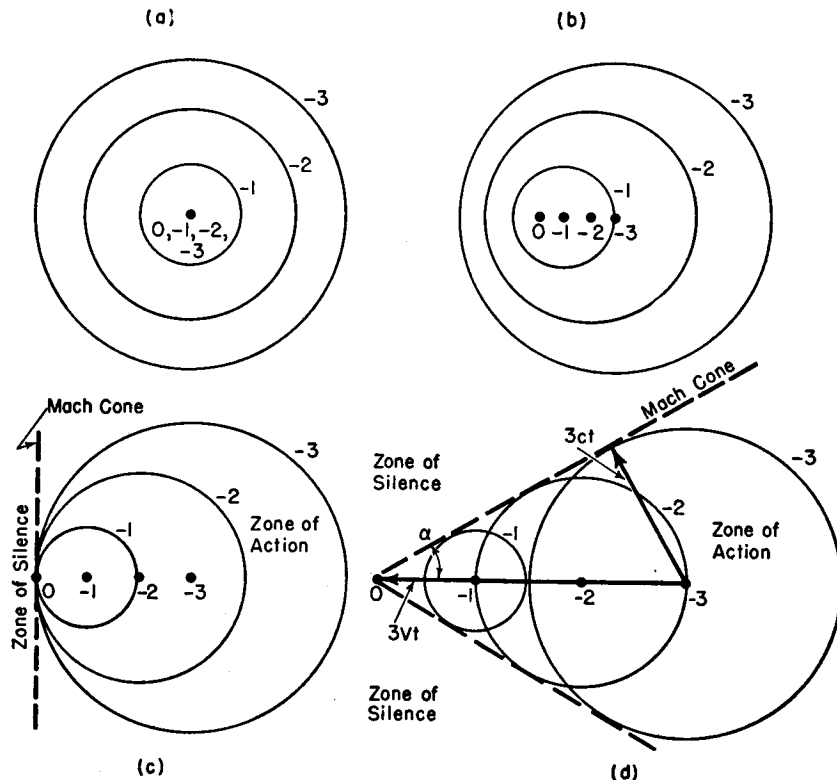


FIG. 3.2. Pressure field produced by a point source of disturbance moving at uniform speed leftwards.

- Incompressible fluid ($V/c = 0$).
- Subsonic motion ($V/c = \frac{1}{2}$).
- Transonic motion ($V/c = 1$).
- Supersonic motion, illustrating Karman's three rules of supersonic flow ($V/c = 2$).

In each pattern the point 0 represents the present location of the disturbance, the point -1 represents the location one unit of time previously, and so on. For each of these previous locations there is drawn a concentric circle showing the distance to which the corresponding wave has spread. For example, to find the present location of the wave which was emitted at time -3 , a circle is drawn with -3 as a center and with a radius $3ct$, where t is the unit of time. The distance between point -3 and point 0 is then given by $3Vt$ where V is the velocity of the point disturbance with respect to the medium.

INCOMPRESSIBLE FLOW. When the medium is incompressible (Fig. 3.2a), or when the speed of the moving point disturbance is small compared with the speed of sound, the pressure pulse spreads uniformly in all directions.

SUBSONIC FLOW. When the source moves at subsonic speeds, Fig. 3.2b, the pressure disturbance is felt in all directions and at all points in space (neglecting dissipation due to viscosity), but the pressure pattern is no longer symmetrical.

SUPERSONIC FLOW. For supersonic speeds Fig. 3.2d indicates that the phenomena are entirely different from those at subsonic speeds. All the pressure disturbances are included in a cone which has the point source at its apex, and the effect of the disturbance is not felt upstream of the source of disturbance. The cone within which the disturbances are confined is called the Mach cone. Fig. 3.2c shows the pressure pattern at the boundary between subsonic and supersonic flow, that is, for the case where the stream velocity is identical with the sonic velocity; here the wave front is a plane.

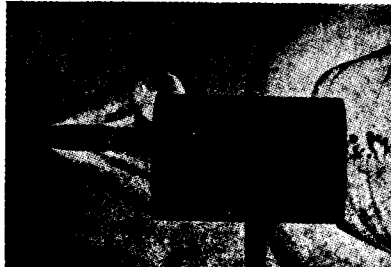
Karman's Rules of Supersonic Flow. Fig. 3.2d illustrates the three rules of supersonic flow proposed by von Karman.⁽¹⁾ These rules apply exactly only for small disturbances, but are usually qualitatively applicable for large disturbances.

THE RULE OF FORBIDDEN SIGNALS. The effect of pressure changes produced by a body moving at a speed faster than sound cannot reach points ahead of the body.

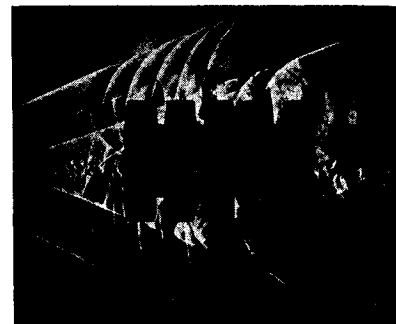
THE ZONE OF ACTION AND THE ZONE OF SILENCE. A stationary point source in a supersonic stream produces effects only on points that lie on or inside the Mach cone extending downstream from the point source. Conversely, the pressure and velocity at an arbitrary point of the stream can be influenced only by disturbances acting at points that lie on or inside a cone extending upstream from the point considered and having the same vertex angle as the Mach cone.

THE RULE OF CONCENTRATED ACTION. The proximity of the circles representing the different pressure impulses in Fig. 3.2 is a measure of the intensity of the pressure disturbance at each point in the field of flow. Thus, for the stationary source, the intensity of the disturbance is symmetrical about the source. For the subsonic source, the intensity is unsymmetrical. In the case of the supersonic source, we have the rule of concentrated action: the pressure disturbance is largely concentrated in the neighborhood of the Mach cone that forms the outer limit of the zone of action.

These rules explain why a projectile or rocket moving at supersonic speed cannot be heard until the wave attached to the nose of the body



(a)



(b)

FIG. 3.3. Shadowgraph of supersonic bullet passing through cylindrical tube, showing Mach cone and spherically spreading wave fronts (after Ackeret).

- (a) Single tube.
- (b) Several short tubes in series, showing individual wavelets which passed through the open space between the tubes.

passes over the ear of the observer; and why, when the latter does occur, the noise is concentrated in a "crack."

Configurations like those of Fig. 3.2 may easily be observed in the form of gravity waves on a free water surface when a sharp-pointed object is drawn through the water at varying speeds. The bow wave of a surface ship resembles the Mach cone of Fig. 3.2d.

Patterns like those of Fig. 3.2 can be made visible in gas flows by means of shadow, schlieren, or interferometer techniques, which are optical methods for demonstrating density variations in a gas. Fig. 3.3a, for example, is a shadowgraph of a bullet which has just passed through a cylindrical tube while traveling at supersonic speed. Fig. 3.3b is a schlieren photograph of a similar arrangement, except that slots are cut in the tube to allow only a selected number of wavelets to pass out of the tube into the field of view.

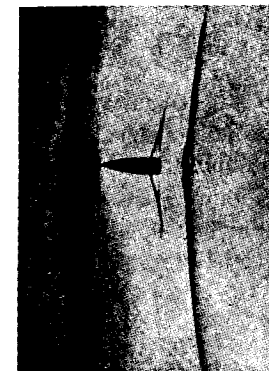
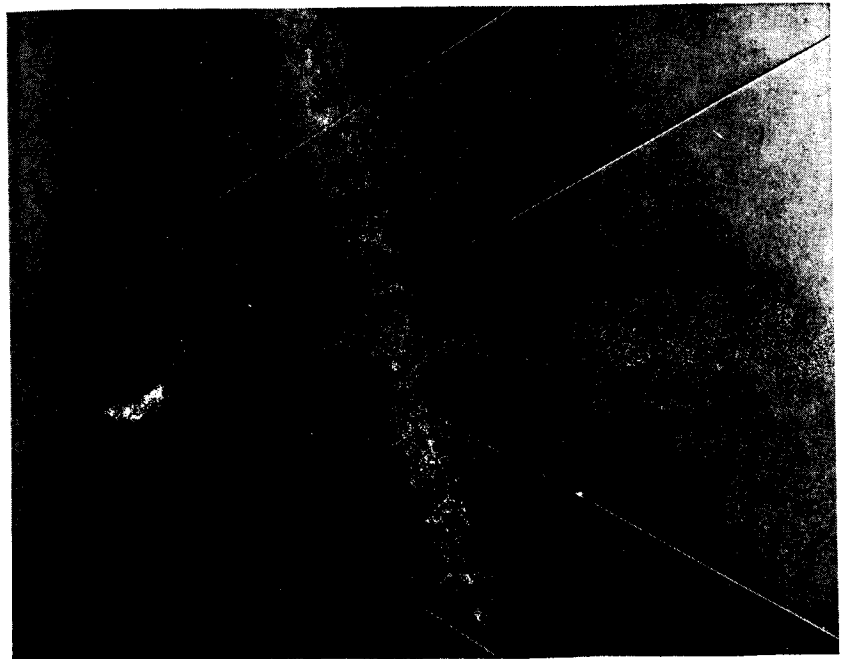
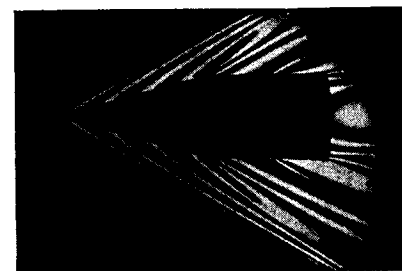


FIG. 3.4. Schlieren photograph of bullet traveling at near the speed of sound (after Ackeret).

Fig. 3.4 shows a bullet traveling at nearly the speed of sound and having a wave front similar to that of Fig. 3.2c. At low subsonic speeds, corresponding to Fig. 3.2b, no wave front appears.



(a)



(b)

FIG. 3.5. Cone-cylinder projectile traveling at supersonic speed (Ballistic Research Laboratory, Aberdeen).

- (a) Schlieren photograph.
- (b) Interferometer photograph.

The Mach cones produced in a supersonic wind tunnel by the nose, fins, and tail of a model of a guided missile are shown in Fig. 3.6.

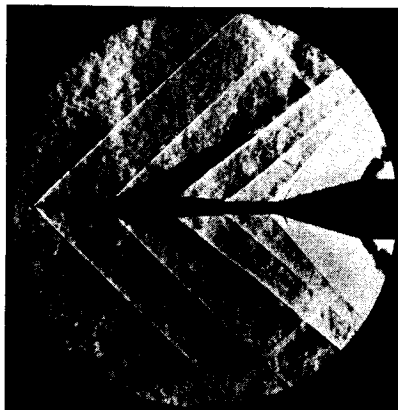


FIG. 3.6. Schlieren photograph of a model of a guided missile in a supersonic wind tunnel. Mach cones from nose, fins, and tail are visible (NACA).

3.3. The Mach Number and Mach Angle

In the preceding article it was shown that the nature of the flow pattern depends on the comparative magnitudes of the stream velocity and the sonic velocity. The ratio of these two velocities is called the *Mach Number*. Thus,

$$M = V/c \quad (3.7)$$

The speed of sound in Eq. 3.7 is to be taken at the local temperature and pressure of the stream, and, of course, it varies from point to point in the flow field.

The semi-angle of the Mach cone (Fig. 3.2d) is related to the Mach Number by

$$\sin \alpha = 1/M \quad (3.8)$$

Note that the *Mach angle* is imaginary for subsonic flow.

We have found the Mach Number to be a criterion of the type of flow pattern. Later it will be shown that it is also a parameter which almost always appears in the equations of motion. In the next article we shall see that it is a dimensionless parameter important for model testing.

3.4. Similarity Parameters

Consider a prototype flow pattern and a model which is geometrically similar (as regards solid boundaries) to the prototype. We inquire as to the conditions which must be met in order that the flow pattern for the model be similar to that for the prototype.

Let L be a characteristic length for the prototype, and let $f_L L$ be the corresponding characteristic length for the model, where f_L is the scale factor for length. Similarly, we can summarize the other properties of the prototype flow and model flow as follows:

Prototype	Model
V	$f_V V$
ρ	$f_\rho \rho$
p	$f_p p$
L	$f_L L$
c	$f_c c$
M	$f_M M$
k	$f_k k$

Ignoring viscosity for the present, Euler's equation of motion must be satisfied for both the prototype and model. Thus:

$$dp = -\rho V dV$$

and

$$d(f_p p) = -(f_\rho \rho)(f_V V) d(f_V V)$$

Since the scale factors are constant, both of these equations can be satisfied only if

$$f_p = f_A f_V^2 \quad (3.9a)$$

From Eq. 3.5 we obtain in similar fashion

$$c = \sqrt{kp/\rho}$$

and

$$f_c c = \sqrt{f_k f_p / f_\rho} \sqrt{kp/\rho}$$

so that

$$f_c = \sqrt{f_k f_p / f_\rho} \quad (3.9b)$$

Likewise, from Eq. 3.7, we have:

$$M = V/c$$

and

$$f_M M = f_V V / f_c c$$

so that

$$f_M = f_V / f_c \quad (3.9c)$$

Combining Eqs. 3.9a, 3.9b, and 3.9c, we finally get:

$$f_M = 1 / \sqrt{f_k}$$

By examining the energy equation, taking into account the further effects of viscous work and heat conductivity, it may be shown that the ratio of specific heats, k , must be the same for both model and prototype, i.e., $f_k = 1$. Thus, we conclude that

$$f_M = 1$$

or the Mach Number must be the same for the model and prototype if the flows are to be similar.

When viscosity is present, a similar analysis applied to the inertia and viscous terms in the Navier-Stokes equation leads to the criterion that the Reynolds Number must be the same for similarity in flow patterns.

Dimensionless Groups Governing Compressible Flows. By considering all the physical equations which govern the flow, namely, the Navier-Stokes equation, the continuity equation, the energy equation, and the equation of state, it is possible to arrive at four dimensionless parameters which must be the same in order for two flow patterns to be similar. These are

- (i) The Mach Number
- (ii) The Reynolds Number
- (iii) The ratio of specific heats, k
- (iv) The Prandtl Number, $c_p \mu / \lambda$, where c_p denotes the specific heat at constant pressure, μ the coefficient of viscosity, and λ the thermal conductivity.

POTENTIAL FLOW OUTSIDE BOUNDARY LAYER. For those regions of the flow outside the boundary layer, where viscous effects and heat conduction effects are relatively unimportant, it is usually necessary that only M and k be alike in order to have similarity. Of the two, similarity in M is by far the more important, since k has a relatively weak influence on the flow pattern.

BOUNDARY-LAYER FLOW. In the boundary layer or in the interior of shock waves, viscous and heat conduction effects are all-important, and so the Reynolds Number and Prandtl Number must be included in the similarity conditions. Fortunately, the Prandtl Number is nearly the same for all gases and varies only slowly with temperature.

3.5. Domain of the Continuum

The concept of the continuum has already been discussed in Chapter 1, where it was pointed out that the criterion for continuum mechanics is that the mean free molecular path be small compared with the smallest significant body dimension.

In order to determine when this condition is valid, let us consider a steady flow and make some approximate calculations of an order-of-magnitude nature.

Now kinetic theory ⁽²⁾ shows that, in respect to orders of magnitude,

$$\mu \cong \rho a l$$

and

$$a \cong c$$

where a is the mean molecular velocity and l is the mean free molecular path.

Using the foregoing relations, we now express the Reynolds Number of the body as

$$\text{Rey} \equiv \frac{\rho V L}{\mu} \equiv \frac{\rho a l}{\mu} \cdot \frac{V}{c} \cdot \frac{c}{a} \cdot \frac{L}{l} \cong \frac{V}{c} \cdot \frac{L}{l}$$

where L is a characteristic body dimension on which Rey is based. This relation may be rearranged to give

$$\frac{L}{l} \cong \frac{\text{Rey}}{M} \quad (3.10)$$

thus showing that the ratio of Reynolds Number to Mach Number is a dimensionless parameter indicative of whether or not a given problem is amenable to the continuum hypothesis. It is seen that the continuum concept is likely to fail either at very high Mach Numbers or at extremely low Reynolds Numbers.

Rules for determining the validity of the continuum concept in terms of Rey and M cannot be stated generally since they depend on the particular type of problem. However, we may illustrate the approach to this problem by supposing that, in a given problem, the smallest significant body dimension is of the order of the boundary-layer thickness, δ . If the Reynolds Number is large compared with unity, and if the boundary-layer flow is also laminar, then the boundary-layer relations for a flat plate show that

$$\frac{\delta}{L} \cong \frac{1}{\sqrt{\text{Rey}}}$$

which, when combined with Eq. 3.10, yields

$$\frac{\delta}{l} \cong \frac{\sqrt{\text{Rey}}}{M}$$

For this case Tsien ⁽³⁾ suggests that the realm of continuum gas dynamics be limited to instances where the boundary-layer thickness is at least 100 times the mean free path. That is,

$$\sqrt{\text{Rey}}/M > 100$$

Fig. 3.7 shows the Reynolds Number per unit length as a function of flight Mach Number for various altitudes, based on the standard atmosphere.

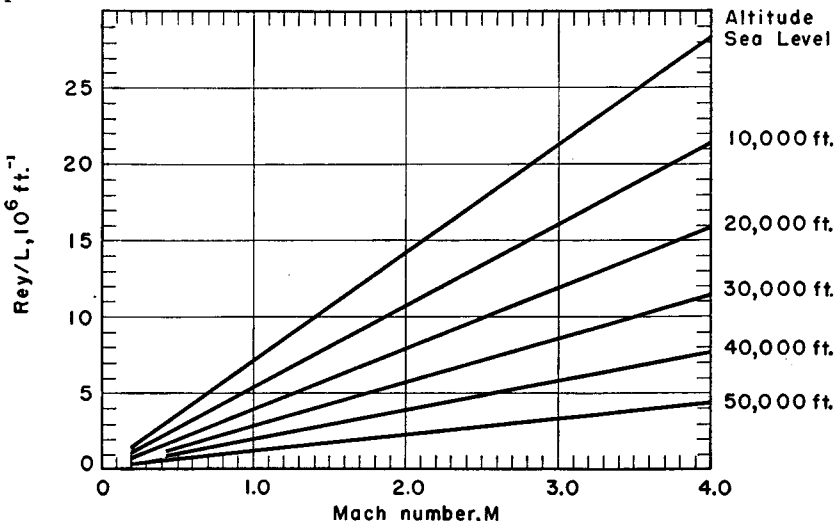


FIG. 3.7. Reynolds Number per foot versus Mach Number, based on standard atmosphere (NACA Tech. Note, No. 1428).

3.6. Classification of Compressible Flows

When dealing with problems of steady motion, it is sometimes convenient to subdivide the subsonic and supersonic categories in classifying different types of flow.

The Adiabatic, Steady-Flow Ellipse. Consider a stream tube in which the flow does not exchange heat with the fluid in neighboring stream tubes. The steady-flow energy equation for the flow in such a tube is then

$$\frac{V^2}{2} + h = \text{constant}$$

Now, for a perfect gas, $\Delta h = c_p \Delta T$, and $T = c^2/kR$. Introducing these, together with the relations between the gas constants, the energy equation may be written as

$$V^2 + \frac{2}{k-1} c^2 = \text{constant} = \frac{2}{k-1} c_0^2 = V_{\max}^2 \quad (3.11)$$

where c_0 is the speed of sound at the stagnation condition (where V is zero) and V_{\max} is the maximum possible velocity in the fluid (where the absolute temperature is zero).

According to Eq. 3.11, the possible states in the stream tube are represented in a diagram of c versus V by the *steady-flow ellipse* (Fig. 3.8). Different parts of this ellipse represent schematically different realms of compressible flow having significantly different physical characteristics.

Incompressible Flow. The velocity is small compared with the sonic speed. Changes in c are very small compared with changes in V .

Subsonic Compressible Flow. The velocity and sonic speed are of comparable magnitudes, but the former is less than the latter. Changes in Mach Number occur primarily because of changes in V , and only secondarily through changes in c .

Transonic Flow. The *difference* between V and c is small compared with either V or c . Changes in V and c are of comparable magnitude.

Supersonic Flow. The velocity and sonic speed are of comparable magnitude, but the former is larger than the latter. Changes in Mach Number take place through substantial variations in both V and c .

Hypersonic Flow. The velocity is very large compared with the sonic speed. Changes in velocity are very small, and thus variations in Mach Number are almost exclusively the result of changes in c .

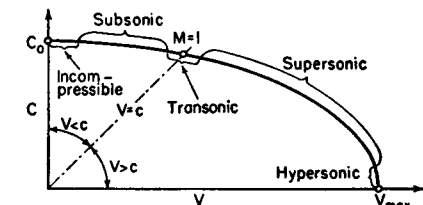


FIG. 3.8. Steady-flow adiabatic ellipse, showing realms of compressible flow.

3.7. Optical Methods of Investigation

Apart from the conventional methods of experimentally investigating flow patterns by means of pressure and velocity surveys, compressible gas flows lend themselves particularly well to optical methods of investigation.

Comparison of Methods. Fundamentally, the optical methods in common use (the interferometer, the schlieren, and the shadowgraph) depend on one of two physical phenomena: (i) the speed of light depends on the index of refraction of the medium through which it passes, and the index of refraction of a gas in turn depends upon its density; and, as a consequence of this first phenomenon, (ii) light passing through a density gradient in a gas (and therefore through a gradient in index of refraction) is deflected in the same manner as though it were passing through a prism. In a high-speed gas flow the density changes are sufficiently large to make these phenomena sizable enough for optical observation.

The interferometer, based on phenomenon (i), measures directly changes of density, and is primarily suited for quantitative determination of the density field.

The schlieren method, based on phenomenon (ii), measures density gradients. Although it is theoretically adaptable to quantitative use, it is inferior to the interferometer in this respect, and its greatest utility is in giving an easily interpretable picture of the flow field together with a rough picture of the density variations in the flow.

The shadowgraph method, also based on phenomenon (ii), measures the second derivative of the density (i.e., the first derivative of the density gradient). Therefore it makes visible only those parts of the flow where the density gradients change very rapidly, and it has found its greatest utility in the study of shock waves.

Of the three methods mentioned, the interferometer yields the most information, and the shadowgraph the least. On the other hand, the interferometer is the most costly and the most difficult to operate, whereas the shadowgraph is the least costly and the easiest to operate. Each method therefore has its own useful niche in experimental work, and the choice of method depends on the nature of the investigation.

In order to assist the reader in the interpretation of photographs taken by the three methods, the basic principles of operation will be outlined, without attention to the numerous optical and mechanical refinements required. Details of these refinements may be found in References 4 to 12.

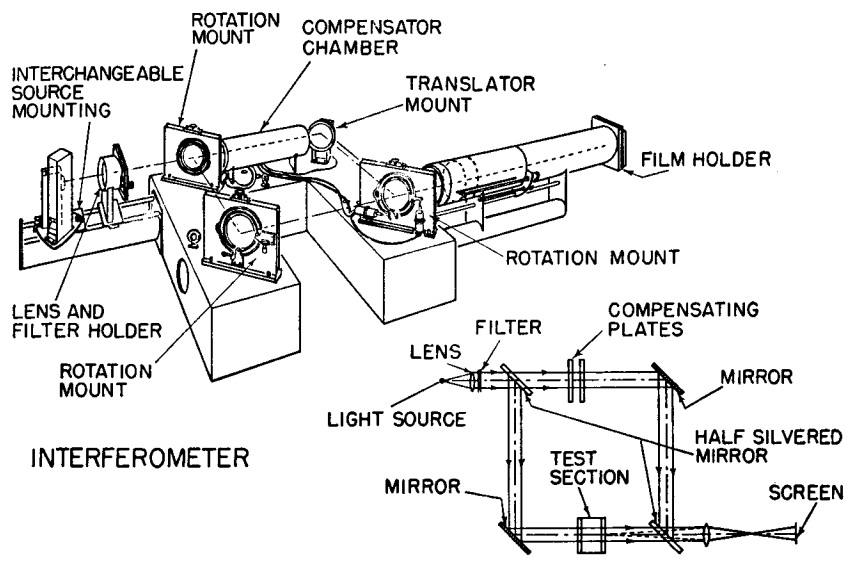
The Interferometer. Fig. 3.9 shows the essential parts of the Mach-Zehnder interferometer, the type which seems to be the most useful for gas-flow investigations.

FORMATION OF INTERFERENCE PATTERNS. Referring to Fig. 3.9, light from the source first passes through a collimating lens which renders the light parallel, and then passes through a monochromatic filter. It then passes through the first "splitting plate," which is a plane half-silvered mirror that passes half the light and reflects half the light. The light which is reflected is changed back to its original direction by the lower mirror and then passes through the test section. The light which passes through the first splitting plate passes through a pair of glass compensating plates which duplicate in thickness and quality the glass side walls of the test section, and is then directed to the lower splitting plate by means of the upper mirror. The two beams which divided at the upper splitting plate are recombined at the lower splitting plate and are then focussed by a lens system on either a ground glass screen or on a photographic plate.

We shall assume for this discussion that the flow in the test section is normal to the paper and that the flow is two-dimensional in planes nor-

mal to the paper and normal to the light beam. Thus, except for slight refraction effects, each ray of light passing through the test section traverses gas of constant density.

The chief difference between the two beams of light in Fig. 3.9 is that the lower beam has passed through the test section. Since the different rays of the lower beam are retarded by different amounts as they pass through portions of the test section of different density, these rays will



SCHEMATIC DIAGRAM - INTERFEROMETER

FIG. 3.9. Mach-Zehnder type of interferometer (M.I.T. Gas Turbine Laboratory).

have various phase differences with the corresponding rays of the upper beam when they are recombined, and thus an interference pattern will be formed at the screen.

INFINITE-FRINGE INTERFEROGRAM. Suppose to begin with that all the mirrors and splitting plates are exactly parallel and in line, that there is no flow, and that the air in the test section has exactly the same density as the reference air of the upper light beam. Then the two light beams will be exactly in phase when they recombine, and the screen will appear uniformly bright. Now imagine that the pressure in the test section is uniformly and gradually increased. Since the entire lower light beam is thus retarded by the same amount, the screen will remain uniform in light intensity, but will gradually darken as the test-section density is increased. After the density has reached the point where the lower beam is out of phase with the upper by one-half wave length, the

screen will be uniformly dark. Further increases of density will produce a lightening of the screen until, with a phase difference of one wave length, the screen will again be at maximum brightness. As the density continues to increase, the cycle of darkening and brightening will be repeated.

With the same mirror geometry as before, consider now the situation with flow through the test section. The optics are the same as above, except that the screen is no longer uniform in brightness, but has on it contours of brightness. These contours represent contours of constant

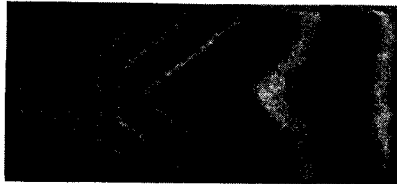


FIG. 3.10. Infinite-fringe interferogram of flow through supersonic nozzle (M.I.T. Gas Turbine Laboratory).

are loci of points where there is complete interference, and represent contours of constant density.

QUANTITATIVE EVALUATION. The change in density from one dark band to the next in an interferogram like that of Fig. 3.10 may be evaluated in the following manner. On the dark bands the light waves passing through the test section are out of phase with those which pass through the room air in the compensating chamber by $\frac{1}{2}, \frac{1}{2}, \frac{1}{2}, \dots$ room-air wave lengths. Therefore, the light beams passing through adjacent dark bands of the test section are out of phase by *one* room-air wave length. Hence, if *a* represents the fluid lying in one dark band, and *b* the fluid in an adjacent dark band, the difference in time for a light beam to pass through *a* as compared with that to pass through *b* is given by

$$t_b - t_a = \frac{\lambda_{\text{room}}}{V_{\text{room}}} \quad (3.12)$$

where λ and V denote respectively the wave length of the light and the speed of light. This difference in traversal time is also related to the difference in speed of light in the test section. Thus,

$$t_b - t_a = \frac{L}{V_b} - \frac{L}{V_a} \quad (3.13)$$

where L is the length of test section along the light direction, and V_b and V_a denote respectively the speeds of light in fluid *b* and *a*.

Now the frequency f of a given monochromatic light is constant. Therefore,

$$f = \frac{V}{\lambda} = \frac{V_{\text{room}}}{\lambda_{\text{room}}} = \frac{V_a}{\lambda_a} = \frac{V_b}{\lambda_b} = \frac{V_{\text{vacuo}}}{\lambda_{\text{vacuo}}} \quad (3.14)$$

The velocity of light in a given medium is related to the velocity of light in vacuo through the index of refraction n , defined by

$$n \equiv V_{\text{vacuo}}/V; \quad n_a \equiv V_{\text{vacuo}}/V_a; \quad n_b \equiv V_{\text{vacuo}}/V_b \quad (3.15)$$

Eliminating $t_b - t_a$ from Eqs. 3.12 and 3.13, and introducing Eqs. 3.14 and 3.15, we may obtain for the difference in index of refraction between adjacent bands

$$n_b - n_a = \lambda_{\text{vacuo}}/L \quad (3.16)$$

It remains to connect the index of refraction with the gas density. This is done through the empirical Gladstone-Dale equation, which states that

$$\frac{n-1}{\rho} = K_{\text{G-D}} \quad (3.17)$$

where $K_{\text{G-D}}$, the Gladstone-Dale constant, is constant for a given gas. Eliminating n in Eq. 3.16 in favor of ρ by means of Eq. 3.17, we obtain finally

$$\rho_b - \rho_a = \frac{\lambda_{\text{vacuo}}}{LK_{\text{G-D}}} \quad (3.18)$$

The right-hand side of this equation is easily computed from the dimension of the test section, the color of the monochromatic light employed, and the value of $K_{\text{G-D}}$ for air. Referring again to Fig. 3.10, the density in the low-speed flow upstream of the throat is found by measuring the temperature and pressure in this low-speed region. With this as a reference, the density on each dark band in the nozzle may be computed from Eq. 3.18, although the accuracy of this procedure using the infinite-fringe interferogram is not high unless the optical components are extraordinarily accurate.

FRINGE-DISPLACEMENT METHOD. For a more accurate quantitative evaluation, the method described above is modified as now described.

Let us return to the situation where room air is in the test section of Fig. 3.9. If the second splitting plate is rotated through a small angle with respect to the first splitting plate, two "coherent" beams of light which were in phase at the first splitter will, through the change in lengths of light paths, be out of phase at the screen. If the splitters are rotated about axes normal to the paper, there will be formed on the screen successive light and dark fringes, uniformly spaced, with each fringe lying parallel to the axis of rotation (see, for example, Fig. 3.11a).

The spacing of successive dark fringes may be shown to be equal to $\lambda_{\text{room}}/2\delta$, where δ is the difference in angles of rotation between the two splitters, and thus the number of fringes in the flow field is controlled by adjusting the geometry of the optical elements.

Now suppose that the air density in the test section is uniformly increased. This will produce a uniform displacement of all the wave fronts passing through the test section. This displacement in turn will cause

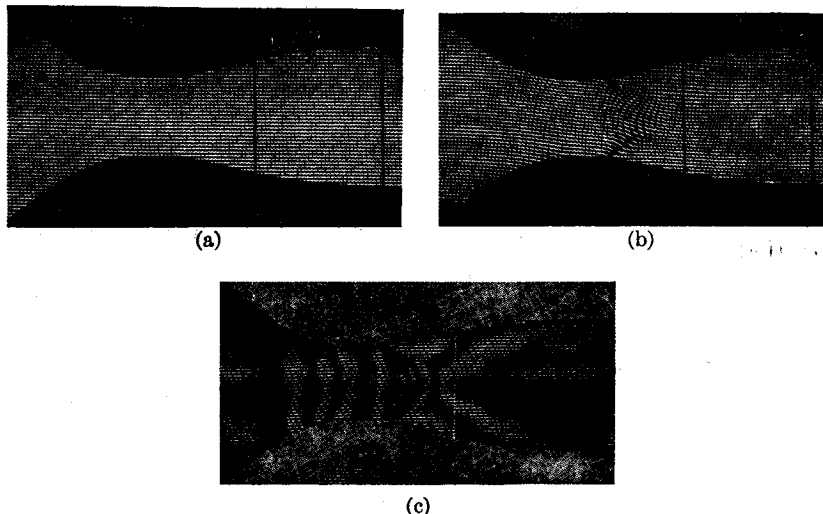


FIG. 3.11. Fringe-shift interferograms for supersonic nozzle (M.I.T. Gas Turbine Laboratory).

- (a) No flow.
- (b) Supersonic flow in test section.
- (c) Superposition of (a) and (b).

the interference bands on the screen to shift in a direction normal to the bands, although the bands will remain parallel and uniformly spaced. The *fringe shift* is a measure of the change in density in the test section. By an analysis similar to that given previously, it may be shown that

$$\rho_2 - \rho_1 = \frac{\lambda_{\text{vacuo}}}{L K_{G-D}} \left(\frac{l}{d} \right) \quad (3.19)$$

where ρ_2 is the density in the test section, ρ_1 is the density at the initial reference condition, d is the distance between dark fringes in the reference condition, and l is the distance shifted by a dark fringe in passing from condition 1 to condition 2.

When there is flow in the test section, with corresponding nonuniform density changes, similar fringe shifts will occur, but, as they are no longer uniform, the resultant fringes will be curved (Fig. 3.11b). Eq. 3.19 may

then be applied at each point in the flow. If both a flow and a no-flow photograph are taken, Eq. 3.19 may be used to determine at each point the density change referred to the no-flow density. Or, from the flow photograph alone, Eq. 3.19 may be used for finding the density differences between two points of the flow.

SUPERPOSITION METHOD. If the no-flow negative (Fig. 3.11a) is superimposed on the flow negative (Fig. 3.11b), the light passing through the combination produces the light pattern of Fig. 3.11c. This is a particularly convenient way of determining the contours of constant density, for a consideration of the geometry of the two fringe patterns shows that the fuzzy dark bands of Fig. 3.11c are lines of constant fringe shift, and, therefore, that they are lines of constant density. Indeed, the pattern of Fig. 3.11c is like that of Fig. 3.10, and Eq. 3.18 may be applied to either.

The Schlieren Method. Fig. 3.12 shows one of the numerous types of schlieren (striae) arrangements. Light from a uniformly illuminated line

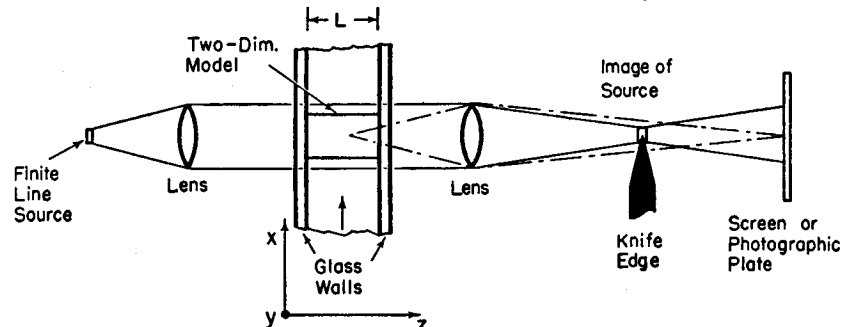


FIG. 3.12. Schlieren system.

source of small but finite width is collimated by the first lens and then passes through the test section. It is then brought to a focus by the second lens and projected on the screen. At the focal point, where there exists an image of the source, there is introduced a knife-edge which cuts off part of the light. With no flow in the test section the knife-edge is usually adjusted so as to intercept about half the light, and the screen is uniformly illuminated by the portion of the light escaping the knife-edge. When the flow is established in the test section (assumed here, for simplicity, to be two-dimensional, with each light ray passing through a path of constant air density) any light ray passing through a region in which there is a density gradient normal to the light direction will be deflected as though it had passed through a prism. Therefore, depending on the orientation of the knife-edge with respect to the density gradient, and on the sign of the density gradient, more or less of

the light passing through each part of the test section will escape the knife-edge and illuminate the screen.

Thus the schlieren system makes density gradients visible in terms of intensity of illumination. A photographic plate at the viewing screen records density gradients in the test section as different shades of gray.

THEORY OF LIGHT DEFLECTION. Let us assume that the flow in the test section is parallel and in the x,y -plane, and that the light passes through the test section in the z -direction.

Since the speed of a wave front of light varies inversely with the index of refraction n of the medium through which the light travels, it follows that a given wave front will rotate as it passes through a gradient in n . Accordingly, the normal to the wave front will follow a curved path; since this normal is what we mean by the light ray, the latter is refracted as it passes through the density gradient. Noting that n is nearly unity for gases, it may be shown that

$$\frac{1}{R} = \text{gradient } n$$

where R is the radius of curvature of the light ray. The total angular deflection ϵ of the ray in passing through the test section of width L is therefore given by

$$\epsilon = \frac{L}{R} = L \text{ grad } n$$

Resolving this into Cartesian components, and taking note of Eq. 3.17, we get for the angular deflections of the light in the x - and y -directions

$$\epsilon_x = L \frac{\partial n}{\partial x} = L K_{G-D} \frac{\partial \rho}{\partial x} \quad (3.20a)$$

$$\epsilon_y = L \frac{\partial n}{\partial y} = L K_{G-D} \frac{\partial \rho}{\partial y} \quad (3.20b)$$

If the knife-edge is aligned in the y -direction (i.e., normal to the flow), as in Fig. 3.12, only deflections ϵ_x will influence the light passing the knife-edge. Hence density gradients in the x -direction will be made visible, but gradients in the y -direction will not be visible. Similarly, if the knife-edge is parallel to x , only gradients in the y -direction will become visible.

In interpreting a schlieren photograph of a two-dimensional flow, it is convenient to imagine that the photograph represents a plan view of a relief map of the flow field in which the vertical elevation is the gas density. If the map is illuminated by glancing side light nearly parallel to x , the pattern of shadows and brightness will correspond to a schlieren

photograph with knife-edge in the y -direction. Similarly, illumination in the y -direction corresponds to placing the schlieren knife-edge parallel to the x -direction.

Figs. 3.13a and 3.13b are schlieren photographs of the supersonic nozzle of Figs. 3.10 and 3.11, and show the different effects obtainable



(a)



(b)

FIG. 3.13. Schlieren photographs of flow through nozzle of Figs. 3.10 and 3.11 (M.I.T. Gas Turbine Laboratory).

- (a) Knife-edge horizontal.
(b) Knife-edge vertical.

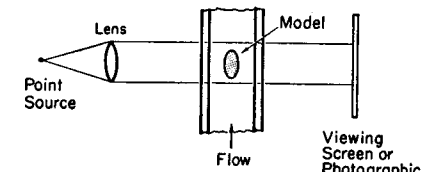
with different orientations of the knife-edge. In Fig. 3.13a (knife-edge horizontal) light areas on the upper half correspond to dark areas on the lower half, and vice versa; the boundary layers on the walls are clearly visible, since with this knife-edge orientation the density gradients normal to the flow are made visible. In Fig. 3.13b (knife-edge vertical) the upper and lower halves look alike; the boundary layers are not visible except on the inclined walls of the nozzle.

The Shadowgraph. A shadow system (Fig. 3.14) comprises simply a small, bright source, a collimating lens, and a viewing screen or photographic plate. If the source is far from the test section the collimating lens is unnecessary.

Assume at first that the test section has stagnant air in it and that the intensity of illumination on the screen is uniform. When flow is established in the test section the light beam will be refracted wherever there is a density gradient. However, if the density gradient were constant, every light ray would be deflected by the same amount, and there would be no change in illumination on the screen. Only if there is a *gradient in density gradient* will there be any tendency for the light rays to diverge or converge. From this it is evident that variations in illumination of the screen are proportional to the second derivative of the density gradient, i.e., to the term

$$\frac{\partial^2 \rho}{\partial x^2} + \frac{\partial^2 \rho}{\partial y^2}$$

FIG. 3.14. Shadowgraph system.



assuming two-dimensional flow in the x,y -plane.

The shadowgraph is therefore suited to flows with rapidly varying density gradients, and is insensitive to flows with gently varying gradients. It is especially convenient and simple for making shock waves visible.

Fig. 3.15a is a typical shadowgraph of a detached shock wave. Across such a shock the density increases from one side to the other in an S-shaped curve. Hence the rate of change of density gradient is positive on the upstream side of the shock and is negative on the downstream

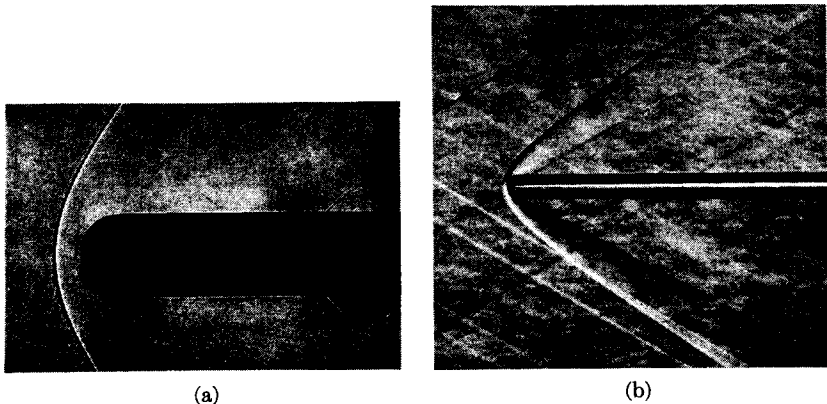


FIG. 3.15. Detached shock in front of blunt body (Ordnance Aerophysics Laboratory).

- (a) Shadowgraph.
- (b) Schlieren, knife-edge horizontal.

side. In the shadow picture the shock therefore shows as a dark line followed by a bright line. For comparison, Fig. 3.15b shows a schlieren photograph of a similar shock.

REFERENCES AND SELECTED BIBLIOGRAPHY

1. VON KÁRMÁN, TH. Supersonic Aerodynamics—Principles and Applications, *Jour. Aero. Sci.*, Vol. 14, No. 7 (1947), p. 373.
2. JEANS, SIR JAMES. *An Introduction to the Kinetic Theory of Gases*. Cambridge: Cambridge University Press, 1946.
3. TSIEN, H. S. Superaerodynamics, Mechanics of Rarefied Gases, *Jour. Aero. Sci.*, Vol. 13, No. 2 (1946), p. 653.
4. SCHARDIN, H. Das Toeplersche Schlierenverfahren, *Forschungsheft V.D.I.*, 367, Ausgabe B, Band 5 (July-August, 1934).
5. ZOBEL, TH. Development and Construction of an Interferometer for Optical Measurements of Density Fields, *NACA Tech. Memo.*, No. 1184 (1947).
6. BARNES, N. F., and BELLINGER, S. L. Schlieren and Shadowgraph Equipment for Air Flow Analysis, *Jour. Opt. Soc. Amer.*, Vol. 35, No. 8 (1945), p. 497.
7. LADENBURG, R., WINCKLER, J., and VAN VOORHIS, C. C. Interferometric Studies of Faster Than Sound Phenomena, *Phys. Rev.*, Vol. 73, No. 11 (1948), p. 1359.
8. ASHKENAS, H. I., and BRYSON, A. E. Design and Performance of a Simple Interferometer for Wind-Tunnel Measurements, *Jour. Aero. Sci.*, Vol. 18, No. 2 (1951), p. 82.

9. DEFRADE, L. A., BARRY, F. W., and BAILEY, D. Z. A Portable Mach-Zehnder Interferometer, *Meteor Report*, No. 51, M. I. T., Cambridge, Mass. (1950).
10. SCHARDIN, H. Theorie und Anwendung des Mach-Zehnderschen Interferenz-Refraktometers, *Zeitschrift für Instrumentenkunde*, Vol. 53 (1933), pp. 396, 424. Also see R.A.E. Translation, No. 79.
11. LIEPMANN, H. W., and PUCKETT, A. E. *Introduction to Aerodynamics of a Compressible Fluid*. New York: John Wiley & Sons, Inc., 1947.
12. PANKHURST, R. C., and HOLDER, D. W. *Wind-Tunnel Technique*. London: Sir Isaac Pitman & Sons, 1952.

PROBLEMS

- 3.1. The compressibility of a liquid is usually expressed in terms of the bulk modulus of compression,

$$\beta = \rho \frac{dp}{d\rho}$$

Show that

$$c = \sqrt{\beta/\rho}$$

- 3.2. Calculate the velocity of sound at 70°F in the following media:

- (a) Air, (b) hydrogen, (c) uranium hexafluoride, (d) mercury vapor, (e) water vapor, (f) liquid water at 14.7 psia.

- 3.3. To what pressure must liquid water be compressed in order that it leave a nozzle at atmospheric pressure with a jet velocity equal to the sonic velocity? Assume a constant bulk modulus of compression of 300,000 psi.

- 3.4. Plot and compare curves of the sonic velocity in air versus absolute temperature (a semi-log plot is suggested) using

- (a) a value of k of 1.4 for all temperatures, and (b) the actual value of k for each temperature.

- 3.5. A projectile in flight carries with it a more or less conical-shaped shock front. From physical reasoning it appears that at great distances from the projectile this shock wave becomes truly conical and changes in velocity and density across the shock become vanishingly small.

Photographs of a bullet in flight show that at a great distance from the bullet the total included angle of the cone is 50.3°. The pressure and temperature of the undisturbed air are 14.62 psia and 73°F, respectively.

Calculate the velocity of the bullet, in ft/sec, and the Mach Number of the bullet relative to the undisturbed air.

- 3.6. Show that, for a perfect gas, the fractional change in pressure across a small pressure pulse is given by

$$\frac{dp}{p} = k \frac{dV}{c}$$

and that the fractional change in absolute temperature is given by

$$\frac{dT}{T} = (k - 1) \frac{dV}{c}$$

3.7. (a) Demonstrate that a compression wave (i.e., a pressure pulse which increases the density of the fluid over which it passes) which moves rightward imparts a rightward velocity to the fluid.

(b) Derive similar rules for a rightward-moving rarefaction wave and for leftward-moving compression and rarefaction waves.

(c) The rightward-moving compression wave of Fig. 3.1a strikes a stationary wall closing the right-hand end of the duct. Demonstrate that it is necessary for a reflected wave to travel leftward, and determine whether the reflected wave is a compression or rarefaction. Compare the pressure change across the incident wave with that across the reflected wave.

3.8. A compression pulse changes the velocity of the fluid over which it passes by 10 ft/sec. Calculate the pressure rise (psi) across the pulse for (a) water, and (b) air at 14.7 psia and 70°F.

PART II

ONE-DIMENSIONAL FLOW

Chapter 4

ISENTROPIC FLOW

4.1. Introductory Remarks

The one-dimensional, steady-flow treatment of isentropic flow finds important applications in two kinds of problems, namely, (i) flow in ducts and (ii) flow in stream tubes.

Flow in Ducts. The flow in pipes and ducts is very often adiabatic. When the duct is short, as it is in nozzles and diffusers, the frictional effects are comparatively small, and the flow may as a first approximation be considered reversible, and, therefore, isentropic. Furthermore, since the function of nozzles and diffusers is to accelerate or decelerate a stream as efficiently as possible, the isentropic process provides a useful standard of comparison for actual nozzles and diffusers.

Flow in a Stream Tube. In virtually all problems involving flow around bodies, and in many involving flow through passages, there are elementary stream tubes which lie entirely outside the boundary layer. Viscous and heat conduction effects for such stream tubes, it appears from experiment, are negligible. Hence the equations of isentropic flow may be considered exact, unless discontinuities such as shock waves appear.

The One-Dimensional Approximation. By a one-dimensional flow we mean a flow in which all fluid properties are uniform over any cross section of the duct. Or, more strictly, we mean a flow in which the rate of change of fluid properties normal to the streamline direction is negligibly small compared with the rate of change along the streamline.

No approximation whatsoever is involved in the case of a stream tube, for the flow through an infinitesimal stream tube is, in the limit, exactly one-dimensional.

When applying the one-dimensional assumption to the flow in ducts, where it is well known that the properties vary over each cross section, we in effect deal with certain kinds of average properties for each cross section. The errors in predicting the rate of change of properties along the duct axis may be expected to be small then, if

- (i) The fractional rate of change of area with respect to distance along the axis is small ($dA/A dx \ll 1$).

- (ii) The radius of curvature of the duct axis is large compared with the passage diameter.
- (iii) The shapes of the velocity and temperature profiles are approximately unchanged from section to section along the axis of the duct.

The great virtue of the one-dimensional approximation is the marvelous simplicity it affords, leading as it does to rapid calculation methods for a great variety of practical engineering problems. Indeed, the information resulting from the one-dimensional point of view is, when carefully interpreted, so useful and so reliable that this method is one of the most powerful tools in the armory of the engineer.

At the same time, it is well to remember that the one-dimensional approach, by its very nature, supplies information only as to the way in which the average fluid properties over the duct cross section vary with distance along the axis of the duct, and is completely silent as to the variation of properties normal to the streamlines. For many practical problems the latter is of the essence, and then the one-dimensional treatment must be supplemented by a two- or even three-dimensional analysis.

NOMENCLATURE

A	cross-sectional area	s	entropy per unit mass
c	speed of sound	T	absolute temperature
c_p	specific heat at constant pressure	\mathcal{J}	thrust
c_v	specific heat at constant volume	V	velocity
C_p	pressure coefficient	w	mass rate of flow
C_w	nozzle discharge coefficient	W	molecular weight
F	impulse function	η	nozzle efficiency
G	mass velocity, w/A	μ	viscosity
h	enthalpy per unit mass	ρ	density
k	ratio of specific heats	$(\)_0$	signifies stagnation state
M	Mach Number	$(\)^*$	signifies state at which the Mach Number is unity; does not apply to M^*
M^*	dimensionless speed, V/c^*	$(\)_\infty$	signifies free stream conditions
p	pressure		
R	gas constant		
\mathcal{R}	universal gas constant		

4.2. General Features of Isentropic Flow

Let us first consider the isentropic flow of any fluid whatsoever through a passage of varying cross section (Fig. 4.1). All possible states lie on a line of constant entropy, as shown in Fig. 4.2. One state on this isentropic corresponds to zero velocity. The pressure at this state, p_0 , is

usually called the *isentropic stagnation pressure*, and is sometimes called the *total pressure*. The *value of the stagnation enthalpy*, h_0 , is independent of whether or not entropy changes occur, since it has the same value for all states which are reachable from it adiabatically.

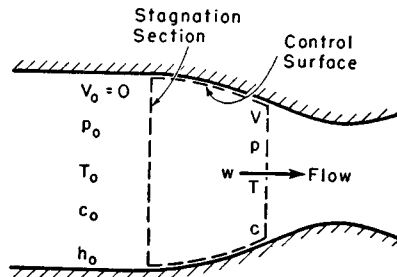


FIG. 4.1. Flow between stagnation section and any other section.

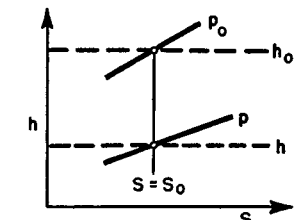


FIG. 4.2. Isentropic acceleration or deceleration on Mollier chart, showing stagnation enthalpy and isentropic stagnation pressure.

Governing Physical Equations. The following physical equations may be written for a control surface extending between the stagnation section and any other section in the channel:

First Law of Thermodynamics.

$$h_0 = h + \frac{V^2}{2} \quad (4.1a)$$

Second Law of Thermodynamics.

$$s = s_0 \quad (4.1b)$$

Equation of Continuity.

$$G = w/A = \rho V \quad (4.1c)$$

Equation of State. This may be expressed in the form of charts, tables, or algebraic equations. We may write implicitly that

$$h = h(s, p) \quad (4.1d)$$

$$\rho = \rho(s, p)$$

Definition of Mach Number.

$$M = V/c = V/\sqrt{(\partial p/\partial \rho)_s} \quad (4.1e)$$

Performance Curves. For a given stagnation condition, i.e., for fixed values of s_0 and p_0 , Eqs. 4.1 may be used for constructing the performance curves shown in Fig. 4.3. For example, suppose an arbitrary value of p less than p_0 is selected. Then the corresponding values of h and ρ

may be found from Eq. 4.1d, inasmuch as s is known from Eq. 4.1b; the corresponding value of V may next be found from Eq. 4.1a; and, finally, the corresponding values of w/A and M may be reckoned from Eqs. 4.1c and 4.1e.

The curves shown in Fig. 4.3 are typical of gases and vapors but are somewhat different for liquids and liquid-vapor mixtures.

Critical Pressure Ratio. The most interesting feature of Fig. 4.3 is the maximum in the curve of flow per unit area, which indicates that an accelerating stream starting from rest must first decrease in cross section and then subsequently increase in cross section. The pressure ratio, p/p_0 , where the flow per unit area is a maximum, is called the *critical pressure ratio*, and has a value, for all real gases and vapors, of approximately one-half.

Pressure ratios greater than the critical correspond to subsonic flow, and pressure ratios less than the critical correspond to supersonic flow. This will now be demonstrated in a completely general manner.

Distinction Between Subsonic and Supersonic Flow. We first write the steady-flow energy equation in differential form for two cross sections infinitesimally distant from each other. Thus

$$dh = -d(V^2/2) = -V dV \quad (4.2a)$$

From the thermodynamic relation, $T ds = dh - dp/\rho$, and the condition of constant entropy, we have

$$dh = dp/\rho \quad (4.2b)$$

so that

$$dp = -\rho V dV \quad (4.2c)$$

This will be recognized as Euler's equation of motion for an inviscid fluid. This is not surprising, as the kinetic-energy term in the steady-flow energy equation was originally obtained with the help of Newton's second law of motion.

Next we introduce the equation of continuity in logarithmic differential form,

$$d(\ln \rho A V) = 0; \quad \text{or} \quad d(\ln \rho) + d(\ln A) + d(\ln V) = 0$$

giving

$$\frac{dp}{\rho} + \frac{dA}{A} + \frac{dV}{V} = 0 \quad (4.2d)$$

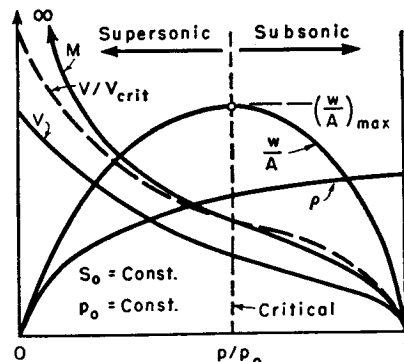


FIG. 4.3. Typical variation of flow properties in isentropic flow.

Substituting Eq. 4.2c into Eq. 4.2d and rearranging, we get

$$\frac{dA}{A} = \frac{dp}{\rho} \left(\frac{1}{V^2} - \frac{dp}{dp} \right)$$

Since the process is isentropic,

so that

$$\frac{dA}{A} = \frac{dp}{\rho V^2} \left(1 - \frac{V^2}{c^2} \right) = \frac{1 - M^2}{\rho V^2} dp \quad (4.2e)$$

Now, from Eq. 4.2c, which is the dynamic equation for a frictionless fluid, it is seen that the pressure always decreases in an accelerating flow, and increases in a decelerating flow. In other words,

$$\frac{dV}{dp} < 0$$

Using this result in conjunction with Eq. 4.2e, we arrive at the following conclusions of practical significance:

(i) *For subsonic speeds ($M < 1$)*,

$$\frac{dA}{dp} > 0; \quad \frac{dA}{dV} < 0$$

(ii) *For supersonic speeds ($M > 1$)*,

$$\frac{dA}{dp} < 0; \quad \frac{dA}{dV} > 0$$

(iii) *For sonic speeds ($M = 1$)*,

$$\frac{dA}{dp} = 0; \quad \frac{dA}{dV} = 0$$

Thus, we have the astonishing result that the effects of an area change, say an increase in area, are exactly opposite for subsonic and supersonic flow.

The possible types of flow, according to this tabulation, are summarized schematically in Fig. 4.4.

At Mach Number unity the area goes through a minimum. This important conclusion is valid irrespective of the type of fluid considered, whether gaseous or liquid.

In constructing the curves of Fig. 4.3, the equation of state, Eq. 4.1d, was employed. Since the equation of state for real gases and vapors can seldom be put into simple algebraic form, the curves of Fig. 4.3 cannot, in general, be formulated analytically, but instead are found through

direct computation. If, on the other hand, it is assumed that the perfect gas laws are valid, analytical results are obtainable, and the numerical computation of problems is greatly simplified. For many engineering gases, particularly air at moderate pressures and temperatures, the deviations from the perfect gas laws are negligible; hence, most calculations are based on these simple relations.

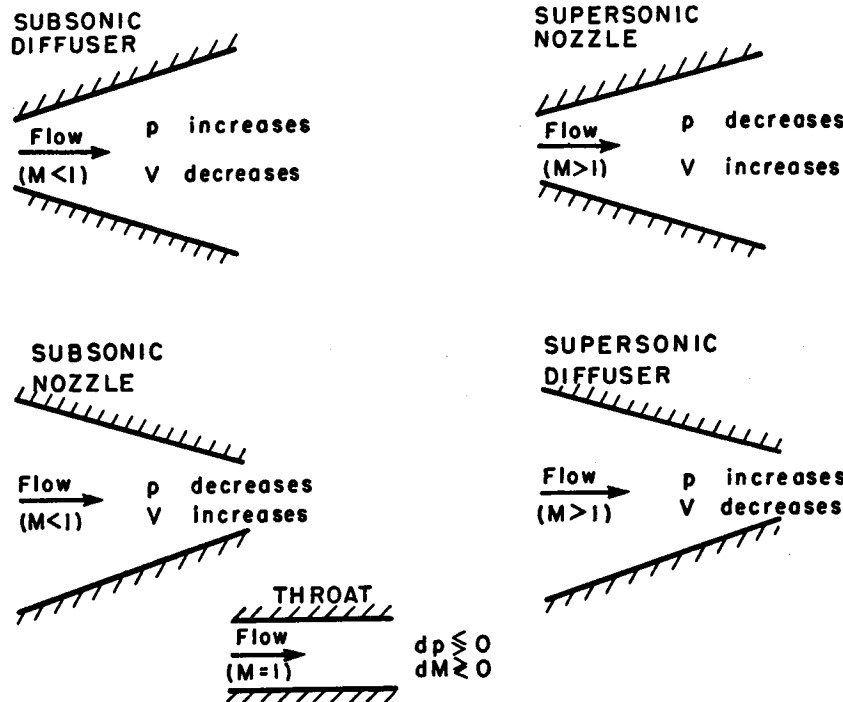


FIG. 4.4. Effects of area change on pressure and velocity in subsonic and supersonic flow.

4.3. Adiabatic Flow of a Perfect Gas

Before restricting the discussion to isentropic flow, certain relations obtainable from the energy equation alone will be derived. These relations are valid for any adiabatic flow of a perfect gas, whether reversible or not.

For a perfect gas we have

$$\Delta h = c_p \Delta T \quad (4.3a)$$

$$c_p - c_v = R \quad (4.3b)$$

$$c_p/c_v = k \quad (4.3c)$$

$$c_p = \frac{k}{k-1} R \quad (4.3d)$$

Using Eq. 4.3a and 4.3d, the steady-flow energy equation (Eq. 4.1a) becomes

$$V = \sqrt{2c_p(T_0 - T)} = \sqrt{\frac{2k}{k-1} R(T_0 - T)} \quad (4.4)$$

From this we see that for a fixed *stagnation temperature* T_0 , (sometimes called *total temperature*), all states with the same temperature have the same velocity. Referring to the temperature-entropy diagram of Fig. 4.5, lines of constant velocity are horizontal, and the vertical distance between T_0 and T is proportional to the square of the velocity.

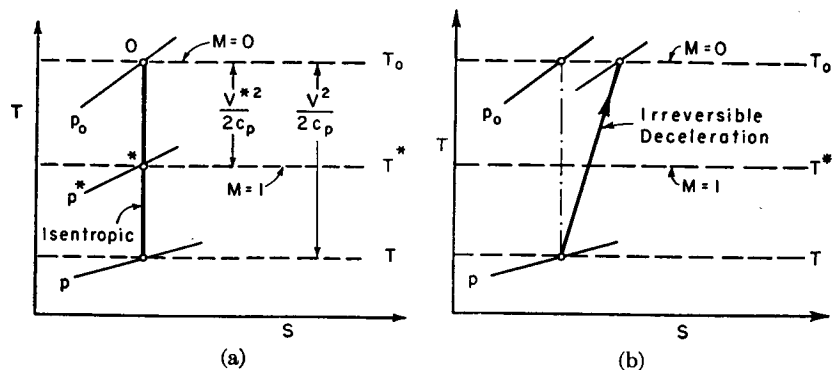


FIG. 4.5. Flow processes on temperature-entropy diagram.

- (a) Isentropic acceleration or deceleration.
- (b) Irreversible adiabatic deceleration.

Three Reference Speeds. Since negative temperatures on the absolute scale are not attainable, it is evident from Eq. 4.4 that there is a maximum velocity corresponding to a given stagnation temperature. This maximum velocity, which is often used for reference purposes, is given by

$$V_{\max} = \sqrt{\frac{2k}{k-1} RT_0} \quad (4.5a)$$

Another useful reference velocity is the speed of sound at the stagnation temperature,

$$c_0 = \sqrt{kRT_0} \quad (4.5b)$$

Still a third convenient reference velocity is the critical speed, i.e., the velocity at Mach Number unity. Using an asterisk to denote conditions at $M = 1$, we have, by definition,

$$V^* \equiv c^*$$

or, using Eq. 4.4 and the equation for the sound speed in a perfect gas,

$$\sqrt{\frac{2k}{k-1} R(T_0 - T^*)} = \sqrt{kRT^*}$$

which gives, after rearrangement

$$\frac{T^*}{T_0} = \frac{2}{k+1}$$

Substituting this value of T^* for T in Eq. 4.4, we get

$$V^* = c^* = \sqrt{\frac{2k}{k+1} RT_0} \quad (4.5c)$$

Now, using Eqs. 4.5, we get the following relations between the three reference velocities, together with the numerical values for $k = 1.4$:

$$\frac{c^*}{c_0} = \sqrt{\frac{2}{k+1}} = 0.913 \quad (4.6a)$$

$$\frac{V_{\max}}{c_0} = \sqrt{\frac{2}{k-1}} = 2.24 \quad (4.6b)$$

$$\frac{V_{\max}}{c^*} = \sqrt{\frac{k+1}{k-1}} = 2.45 \quad (4.6c)$$

Stagnation-Temperature Ratio. Eq. 4.4 may be written

$$\frac{T_0}{T} = 1 + \frac{V^2}{2c_p T} = 1 + \frac{V^2}{kRT} \frac{kR}{2c_p}$$

Since $c_p = kR/(k-1)$ and $c^2 = kRT$, this takes the simple and convenient form

$$\frac{T_0}{T} = 1 + \frac{k-1}{2} \frac{V^2}{c^2} = 1 + \frac{k-1}{2} M^2 \quad (4.7)$$

which shows that the *stagnation-temperature ratio* depends only on the gas constant k and Mach Number M .

The Energy Equation in Kinematic Form. The energy equation for adiabatic flow of a perfect gas is

$$V^2 + 2c_p T = \text{constant}$$

Moreover, for a perfect gas,

$$c_p T \equiv \frac{c_p}{kR} kRT = \frac{1}{k-1} c^2$$

Combining these relations, and evaluating the constant at the three reference conditions of (i) zero speed, (ii) zero temperature, and (iii) sonic speed, we obtain three alternate and useful forms of the energy equation involving only the local velocity, local sound speed, and k :

$$V^2 + \frac{2}{k-1} c^2 = \frac{2}{k-1} c_0^2 = V_{\max}^2 = \frac{k+1}{k-1} c^{*2} \quad (4.8)$$

Note that Eqs. 4.5 through 4.7 may be obtained rather easily from Eq. 4.8.

The Dimensionless Velocity M^* . As a dimensionless parameter the Mach Number is very convenient, but it has two disadvantages: (i) it is not proportional to the velocity alone and, (ii) at high speeds it tends towards infinity. Often, therefore, it is useful to work with a dimensionless velocity obtained through dividing the flow velocity V by one of the three reference velocities of Eq. 4.8. Generally the most useful of these ratios is defined by

$$M^* \equiv V/c^* \equiv V/V^*$$

It should be noted immediately that although in general the asterisk denotes the value of a property at Mach Number unity, this convention is not followed in the definition of M^* . The latter is *not* the value of M at the local sonic condition, but is rather defined as given above.

There is a unique relation between M and M^* for adiabatic flow. From the definitions of M^* and M ,

$$M^{*2} \equiv \frac{V^2}{c^{*2}} = \frac{V^2}{c^2} \frac{c^2}{c^{*2}} = M^2 \frac{c^2}{c^{*2}}$$

Furthermore, the first and last parts of Eq. 4.8 may be divided by c^{*2} to give

$$\frac{V^2}{c^{*2}} + \frac{2}{k-1} \frac{c^2}{c^{*2}} = \frac{k+1}{k-1}$$

Eliminating c^2/c^{*2} from this pair of equations, and rearranging, we get the useful formulas

$$M^{*2} = \frac{\frac{k+1}{2} M^2}{1 + \frac{k-1}{2} M^2} \quad (4.9)$$

and

$$M^2 = \frac{\frac{2}{k+1} M^{*2}}{1 - \frac{k-1}{k+1} M^{*2}} \quad (4.10)$$

The value of M^* is a simple index of when the flow is subsonic and when supersonic, for we find from Eqs. 4.9 and 4.10 that

when $M < 1$, then $M^* < 1$

when $M > 1$, then $M^* > 1$

when $M = 1$, then $M^* = 1$

when $M = 0$, then $M^* = 0$

$$\text{when } M = \infty, \text{ then } M^* = \sqrt{\frac{k+1}{k-1}}$$

Fig. 4.3 illustrates the relative magnitudes of M and M^* in subsonic and supersonic flow.

Flow per Unit Area. Next we will derive a useful relation between the flow per unit area, stagnation temperature, static pressure and Mach Number. Starting with the equation of continuity, we make the following rearrangements:

$$\begin{aligned} \frac{w}{A} = \rho V = \frac{p}{RT} V &= \frac{pV}{\sqrt{kRT}} \sqrt{\frac{k}{R}} \sqrt{\frac{T_0}{T}} \frac{1}{\sqrt{T_0}} \\ &= \sqrt{\frac{k}{R}} \frac{p}{\sqrt{T_0}} M \sqrt{1 + \frac{k-1}{2} M^2} \end{aligned}$$

This is best arranged in the form of a mass flow parameter involving T_0 , p , and the molecular weight W . The parameter itself then depends only on k and M according to the relation

$$\begin{aligned} \frac{w}{A} \frac{\sqrt{T_0}}{p} \frac{1}{\sqrt{W}} &= \sqrt{\frac{k}{R}} M \sqrt{1 + \frac{k-1}{2} M^2} \quad (4.11) \end{aligned}$$

The parameter is plotted in Fig. 4.6 for $k = 1.4$. With this chart it is easy to solve the common problem of computing the local Mach Number from given values of w , A , T_0 , and p .

FIG. 4.6. Mass flow parameter versus M and M^* . Units: w (slug/sec); A (ft²); T_0 (deg. Rankine); p (lbf/ft²); W (lb/lb mol, or slug/slug mol).

4.4. Isentropic Flow of a Perfect Gas

All the relations of the preceding section are valid for both isentropic and nonisentropic flows. Referring to Fig. 4.5, they are applicable to any sort of change in the vertical (T) coordinate, irrespective of changes in the horizontal (s) coordinate, provided that all states have the same stagnation temperature.

We now further restrict the analysis to the isentropic case. All states along the channel or stream tube lie on a line of constant entropy and have the same stagnation temperature. The state of zero velocity is called the *isentropic stagnation state*, and the state with $M = 1$ is called the *critical state*. All states with the same entropy and the same stagnation temperature have the same isentropic stagnation state and the same critical state. When a stream with a given pressure, temperature, and velocity (Fig. 4.5b) is decelerated to zero velocity, the final pressure will be less than the isentropic stagnation pressure if the deceleration is irreversible, but the final temperature will be equal to the adiabatic stagnation temperature for either reversible or irreversible deceleration.

The relations between pressure, temperature, and density for an isentropic process of a perfect gas are

$$\frac{p}{p_0} = \left(\frac{\rho}{\rho_0} \right)^k; \quad \frac{T}{T_0} = \left(\frac{p}{p_0} \right)^{\frac{k-1}{k}} \quad (4.12)$$

Also, the pressure-temperature density relation of a perfect gas is

$$\frac{p}{\rho T} = \frac{p_0}{\rho_0 T_0} = R \quad (4.13)$$

Temperature, Pressure, and Density Ratios as Functions of Mach Number. Substitution of Eqs. 4.12 into Eq. 4.7 now yields the important relations

$$\frac{T_0}{T} = 1 + \frac{k-1}{2} M^2 \quad (4.14a)$$

$$\frac{p_0}{p} = \left(1 + \frac{k-1}{2} M^2 \right)^{\frac{k}{k-1}} \quad (4.14b)$$

$$\frac{\rho_0}{\rho} = \left(1 + \frac{k-1}{2} M^2 \right)^{\frac{1}{k-1}} \quad (4.14c)$$

The particular values of the temperature, pressure, and density ratios at the critical state (i.e., at the minimum area) are found by setting

$M = 1$ in the above expressions. The resulting formulas, together with the numerical values for $k = 1.4$, are as follows:

$$\frac{T^*}{T_0} = \frac{c^*^2}{c_0^2} = \frac{2}{k+1} = 0.8333 \quad (4.15a)$$

$$\frac{p^*}{p_0} = \left(\frac{2}{k+1} \right)^{\frac{1}{k-1}} = 0.5283 \quad (4.15b)$$

$$\frac{\rho^*}{\rho_0} = \left(\frac{2}{k+1} \right)^{\frac{1}{k-1}} = 0.6339 \quad (4.15c)$$

Thus, the temperature at the throat is only about 17 per cent less than the stagnation temperature, whereas the throat pressure is only about half the isentropic stagnation pressure.

The critical pressure ratio, p^*/p_0 , is of the same order of magnitude for all gases. It varies almost linearly with k from 0.6065 for $k = 1$ to 0.4867 for $k = 1.67$.

Mass Flow Relations in Terms of Mach Number. From Eqs. 4.14 and 4.10 it is clear that either T/T_0 , p/p_0 , ρ/ρ_0 , M or M^* may be taken as an independent parameter, and that the remaining quantities would then depend uniquely on the value of the chosen independent parameter. By and large, the variable M has been found to be the most convenient choice as far as simplicity of practical calculations is concerned. We shall, therefore, follow the practice in this and succeeding chapters of deriving all the working formulas in terms of M as the independent variable.

To find a convenient formula for the mass flow per unit area in terms of M , we eliminate p in the equation preceding Eq. 4.11 by means of the isentropic law (Eq. 4.14b). Thus we obtain

$$\frac{w}{A} = \sqrt{\frac{k}{R} \frac{p_0}{\sqrt{T_0}}} \frac{M}{\left(1 + \frac{k-1}{2} M^2 \right)^{\frac{k+1}{2(k-1)}}} \quad (4.16)$$

This shows that, for a given Mach Number, the flow is proportional to the stagnation pressure and inversely proportional to the square root of the stagnation temperature. For this reason, flow test data on compressors and turbines, or indeed on any flow passage which operates over a wide range of pressure and temperature levels, are usually plotted with $w\sqrt{T_0}/p_0$ as the flow variable. In this way the results of a given test become applicable to operation at levels of temperature and pressure different from the original test conditions.

Now it is evident that if M were eliminated from Eq. 4.16 with the help of Eq. 4.14b, we would have w/A in terms of k , R , p_0 , T_0 , and p/p_0 . The resulting expression is then the algebraic formula, for a perfect gas, corresponding to the curve of w/A versus p/p_0 in Fig. 4.3.

MAXIMUM FLOW PER UNIT AREA. To find the condition of maximum flow per unit area, we could compute the derivative $d(w/A)/d(p/p_0)$ and set this derivative equal to zero. From this we would find that the critical pressure ratio is given by Eq. 4.15b.

An equivalent procedure would be to differentiate Eq. 4.16 with respect to M and set this derivative equal to zero. At this condition, we would find that $M = 1$.

However, neither of these procedures is necessary inasmuch as we have proved quite generally in Art. 4.2 that the cross-sectional area for isentropic flow passes through a minimum at Mach Number unity. Therefore, to find $(w/A)_{\max}$, we need only set $M = 1$ in Eq. 4.16.

Thus we find

$$\left(\frac{w}{A} \right)_{\max} = \frac{w}{A^*} = \sqrt{\frac{k}{R} \left(\frac{2}{k+1} \right)^{\frac{k+1}{k-1}} \frac{p_0}{\sqrt{T_0}}} \quad (4.17)$$

For a given gas, therefore, the maximum flow per unit area depends only on the ratio $p_0/\sqrt{T_0}$. For given values of the stagnation pressure and stagnation temperature and for a passage with a given minimum area, Eq. 4.17 shows that the maximum flow which can be passed is relatively large for gases of high molecular weight and relatively small for gases of low molecular weight. Doubling the pressure level doubles the maximum flow, whereas doubling the absolute temperature level reduces the maximum flow by about 29 per cent.

FLIEGNER'S FORMULA. Using the values $k = 1.4$ and $R = 53.3$ ft lbf/lbm[°]R, corresponding to air, we obtain from Eq. 4.17

$$\frac{w}{A^*} \frac{\sqrt{T_0}}{p_0} = 0.532 \quad (4.18)$$

for air, where w is in lbm/sec, A^* in ft², T_0 in [°]R, and p_0 in lbf/ft².

This formula, which we have derived on purely analytical grounds, was discovered empirically by Fliegner nearly a century ago at a time when the theoretical considerations outlined here were scarcely understood! Fliegner's experiments, which were conducted on a simple converging nozzle, gave a value of the constant within about 1 per cent of the value in Eq. 4.18.

THE AREA RATIO. Just as we have found it convenient to work with the dimensionless ratios p/p_0 , etc., so it is convenient to introduce a

dimensionless area ratio. Obviously the appropriate reference area is A^* , and so we compute from Eqs. 4.16 and 4.17 the formula

$$\frac{A}{A^*} = \frac{w/A^*}{w/A} = \frac{1}{M} \left[\left(\frac{2}{k+1} \right) \left(1 + \frac{k-1}{2} M^2 \right) \right]^{\frac{k+1}{2(k-1)}} \quad (4.19)$$

The area ratio is always greater than unity, and for any given value of A/A^* there always correspond two values of M —one for subsonic flow, and the other for supersonic flow.

The Impulse Function. For problems involving jet propulsion it is sometimes convenient to employ a quantity called the impulse function, defined by

$$F \equiv pA + \rho A V^2 \quad (4.20)$$

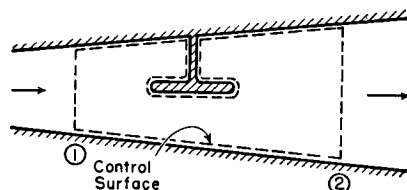


FIG. 4.7. Illustrating use of impulse function.

Applying the momentum equation to the flow through the control surface of Fig. 4.7, it is seen that

$$3 + p_1 A_1 - p_2 A_2 = \rho_2 A_2 V_2^2 - \rho_1 A_1 V_1^2$$

or

$$3 = (p_2 A_2 + \rho_2 A_2 V_2^2) - (p_1 A_1 + \rho_1 A_1 V_1^2) = F_2 - F_1 \quad (4.21)$$

where 3 is the net "thrust" produced by the stream between sections 1 and 2. The term thrust, as used here, is defined as the net force exerted by the stream on the internal solid surfaces which the fluid wets, acting in the direction opposite to the direction of flow. It includes the forces due to pressure and viscous stresses on the duct walls as well as the total drag of any stationary obstacles in the stream. This is true whether the flow is adiabatic or nonadiabatic, and whether the flow is reversible or irreversible.

For a perfect gas,

$$\rho V^2 \equiv \frac{p}{RT} V^2 \equiv \frac{p}{kRT} kV^2 = kpM^2$$

and so

$$F = pA(1 + kM^2) \quad (4.22)$$

For isentropic flow, a dimensionless impulse function is formed by writing

$$\frac{F}{p_0 A^*} = \frac{p}{p_0} \frac{A}{A^*} (1 + kM^2) \quad (4.23)$$

where p/p_0 and A/A^* are functions of M given respectively by Eqs. 4.14b and 4.19.

Another way of forming a dimensionless impulse function is by evaluating F^* at $M = 1$, and setting

$$\frac{F}{F^*} = \frac{p}{p^*} \cdot \frac{A}{A^*} \cdot \frac{1 + kM^2}{1 + k} = \frac{p}{p_0} \cdot \frac{p_0}{p^*} \cdot \frac{A}{A^*} \cdot \frac{1 + kM^2}{1 + k}$$

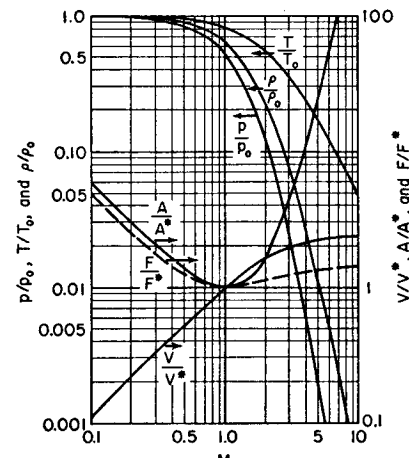
substituting p/p_0 , p_0/p^* , and A/A^* from Eqs. 4.14b, 4.15b, and 4.19, respectively, there is obtained after simplification,

$$\frac{F}{F^*} = \frac{1 + kM^2}{M \sqrt{2(k+1) \left(1 + \frac{k-1}{2} M^2 \right)}} \quad (4.24)$$

4.5. Working Charts and Tables for Isentropic Flow

Since the formulas thus far derived lead to tedious numerical calculations, often of a trial-and-error nature, practical computations are greatly facilitated by working charts and tables

Chart for Isentropic Flow. Fig. 4.8 represents in graphical form the various dimensionless ratios for isentropic flow with M as independent variable. Since changes of fluid properties in isentropic flow are brought about through changes in cross-sectional area, the key curve on this chart is that of A/A^* . The effects of changes in area on other properties may easily be found by tracing the curve of A/A^* , keeping in mind that A^* , p_0 , F^* , etc. are all constant reference values for a given problem. For example, an increase in area at subsonic speed produces a decrease in velocity, an increase in F , and increases in p , T , and ρ .



It may be seen from Fig. 4.8 that up to a Mach Number of about 0.3 (corresponding to about 300 ft/sec for air at normal conditions), changes in density are almost negligible for engineering calculations. This explains why in so many instances air is treated as though it were an incompressible fluid.

FIG. 4.8. Working chart for isentropic flow, with $k = 1.4$.

Working Tables. For accurate or extensive calculations, Table B.2 lists the various isentropic flow functions for $k = 1.4$, with Mach Number as independent argument.

Illustrative Example. The use of the compressible flow functions is best explained by an example.

PROBLEM. A supersonic wind-tunnel nozzle is to be designed for $M = 2$, with a throat section 1 sq ft in area. The supply pressure and temperature at the nozzle inlet, where the velocity is negligible, are 10 psia and 100°F, respectively. The preliminary design is to be based on the assumptions that the flow is isentropic, with $k = 1.4$, and that the flow is one-dimensional at the throat and test section. It is desired to compute the mass flow, the test-section area, and the fluid properties at the throat and test section.

SOLUTION. Table B.2 is to be used. First we work out the reference stagnation properties. We are given $p_0 = 10$ psia and $T_0 = 459.7 + 100 = 559.7^{\circ}\text{R}$. From these we compute

$$p_0 = \frac{p_0}{RT_0} = \frac{10(144)}{53.3(559.7)} = 0.0483 \text{ lbm/ft}^3$$

$$c_0 = 49.1\sqrt{T_0} = 49.1\sqrt{559.7} = 1162 \text{ ft/sec}$$

Next, we find the properties at the throat by selecting values from Table B.2 at $M = 1$:

$$p^*/p_0 = 0.528; \quad \therefore p^* = 10(0.528) = 5.28 \text{ psia}$$

$$T^*/T_0 = 0.833; \quad \therefore T^* = 0.833(559.7) = 466^{\circ}\text{R}$$

$$\rho^*/p_0 = 0.634; \quad \therefore \rho^* = 0.634(0.0483) = 0.0306 \text{ lbm/ft}^3$$

$$c^*/c_0 = \sqrt{T^*/T_0} = 0.913; \quad \therefore c^* = V^* = 0.913(1162) = 1060 \text{ ft/sec}$$

Entering Table B.2 at $M = 2$, we now calculate properties in the test section:

$$M^* = V/c^* = 1.6330; \quad \therefore V = 1.633(1060) = 1731 \text{ ft/sec}$$

$$p/p_0 = 0.1278; \quad \therefore p = 0.1278(10) = 1.278 \text{ psia}$$

$$\rho/\rho_0 = 0.2300; \quad \therefore \rho = 0.2300(0.0483) = 0.01110 \text{ lbm/ft}^3$$

$$T/T_0 = 0.556; \quad \therefore T = 0.556(559.7) = 311^{\circ}\text{R}$$

$$A/A^* = 1.6875; \quad \therefore A = 1.6875(1) = 1.6875 \text{ ft}^2$$

Finally, we compute the mass flow from Eq. 4.18:

$$w = \frac{0.532p_0A^*}{\sqrt{T_0}} = \frac{0.532(10)(144)(1)}{\sqrt{559.7}} = 32.4 \text{ lbm/sec}$$

Alternatively, the mass flow may be computed from the continuity equation at the throat or test section. For example,

$$w = \rho^*A^*V^* = 0.0306(1)(1060) = 32.4 \text{ lbm/sec}$$

4.6. Choking in Isentropic Flow

The fact that the curve of mass flow per unit area has a maximum is connected with an interesting and important effect called choking.

Let us consider two sections of a stream tube having a ratio of areas A_2/A_1 , and let us specify all flow properties at section 1, such as p_1 , T_1 , M_1 , etc. From the tables or graphs we can then solve for the properties at section 2, except as discussed later. For example, corresponding to M_1 we may find in the tables $(p/p_0)_1$, $(T/T_0)_1$, and $(A/A^*)_1$. Then, since A^* is constant during the process, we may write

$$\frac{A_2}{A_1} = \frac{(A/A^*)_2}{(A/A^*)_1}$$

and so we may compute $(A/A^*)_2$. Returning to the tables, we then obtain at this value of $(A/A^*)_2$ the corresponding values of M_2 , $(p/p_0)_2$, $(T/T_0)_2$, etc. Since p_0 and T_0 are constant, this allows us to compute p_2 and T_2 from

$$\frac{p_2}{p_1} = \frac{(p/p_0)_2}{(p/p_0)_1}; \quad \frac{T_2}{T_1} = \frac{(T/T_0)_2}{(T/T_0)_1}$$

Now, let us consider a passage with a given area ratio A_2/A_1 and compute in the manner outlined above the values of M_2 corresponding to several values of M_1 . The results may then be plotted as in Fig. 4.9. Examination of this chart indicates two peculiarities:

(i) For a given initial Mach Number M_1 and a given area ratio A_2/A_1 , there are either two solutions for the final state M_2 or none at all. When there are two solutions, one of the two is subsonic and the other is supersonic. Which one of the two occurs depends in part on whether a throat intervenes between sections 1 and 2, for we have demonstrated that in order to go from supersonic speed to subsonic speed, or vice versa, it is necessary for the flow to pass through a throat at $M = 1$. For example, if M_1 is subsonic and the passage is converging, then M_2 must also be subsonic. On the other hand, if M_1 is subsonic and the passage is converging-diverging (i.e., has a minimum area between sections 1 and 2) the flow at section 2

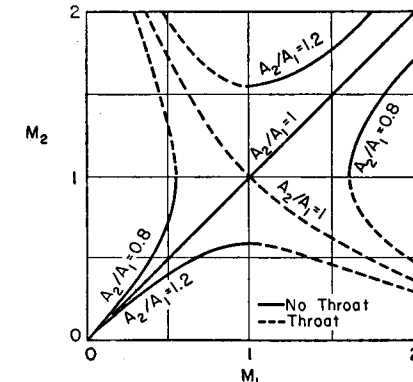


FIG. 4.9. Typical curves of M_2 versus M_1 for fixed values of area ratio A_2/A_1 .

may be either subsonic, as in a conventional venturi, or supersonic, as in a supersonic nozzle; which of these two situations prevails depends on the pressures imposed at the inlet and exit of the passage, as discussed more fully in Art. 4.7.

(ii) When, for selected values of M_1 and A_2/A_1 , there is no solution in Fig. 4.9, the solution is imaginary in the mathematical sense. This occurs only when A_2 is smaller than A_1 . Physically, this result signifies that for given conditions at section 1, there is a maximum contraction which is possible; this maximum contraction corresponds to sonic velocity at section 2. Or, put quite simply, if conditions at section 1 are specified, the mass flow is accordingly determined, and there is then a minimum cross-sectional area required to pass this flow. This phenomenon is called choking, and may be summarized by saying that for a given area reduction, there is in subsonic flow a maximum initial Mach Number which can be maintained steadily; and in supersonic flow a minimum initial Mach Number which can be maintained steadily. At either of these limiting conditions, the flow at section 2 is sonic, and is said to be choked.

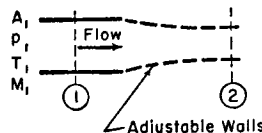


FIG. 4.10. Illustrates choking of flow.

Fig. 4.10. Illustrates choking of flow.

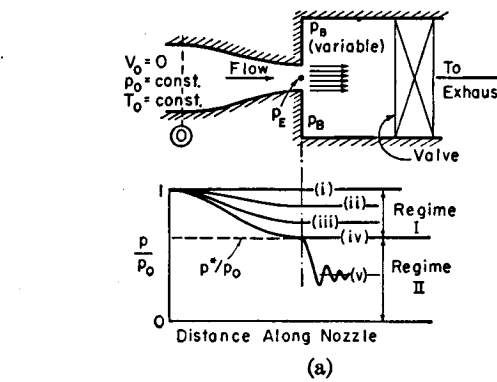
To illustrate further the phenomenon of choking, let us suppose that at a section 1 in a duct there is a subsonic flow with certain values of M_1 , p_1 , T_1 , and A_1 . These parameters fix the flow rate, w . Let us imagine further that, at a section 2 downstream, the walls are flexible; thus the area A_2 is adjustable, as shown in Fig. 4.10. If A_2 is equal to A_1 , all conditions at section 2 will be identical with the corresponding conditions at section 1. A slight reduction in A_2 will produce certain effects at section 2, which, according to Fig. 4.8, will comprise an increase in M_2 , a decrease in p_2 , and a decrease in T_2 . This slight reduction in A_2 without a change in conditions at section 1 must, therefore, be accompanied by a reduction in the back pressure, p_2 , according to the requirements of Fig. 4.8. Further reductions in A_2 may be made in the same way until the value of M_2 reaches unity.

After this point has been reached, there is no way of reducing the area further without a simultaneous change in the steady-state conditions at section 1. If, for example, the pressure and temperature at section 1 are maintained constant, a reduction in A_2/A_1 beyond its limiting value will, after a transient period of wave propagation, result in a reduced steady-state M_1 , which in turn means that the flow rate will be decreased. The maximum possible value of M_1 (which will correspond to the maximum possible flow rate) is obtained when $M_2 = 1$. To obtain this limiting flow, the back pressure, p_2 , must of course be adjusted accordingly. Fig. 4.8 shows that any area reduction whatsoever may be made if the initial Mach Number is sufficiently low or sufficiently high.

4.7. Operation of Nozzles Under Varying Pressure Ratios

The phenomenon of choking discussed above may be manifested in several different ways. To illustrate still another aspect of choking, let us discuss the practical problem of nozzles operating under varying pressure ratios.

Converging Nozzles. Suppose, for the sake of concreteness, that a converging passage (Fig. 4.11a) with a large entrance area at section 0



(a)

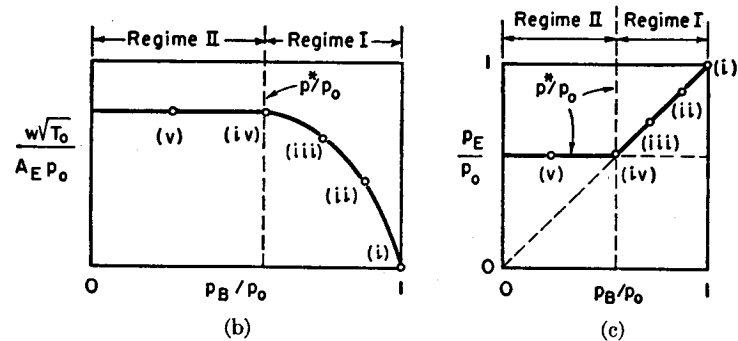


FIG. 4.11. Operation of converging nozzle at various back pressures.

discharges into a region where the back pressure, p_B , is controllable by means of a valve. The values of p_0 and T_0 will be maintained constant, and the experiment will involve variations in p_B . If p_E denotes the pressure in the exit plane of the nozzle, we inquire as to the effects of variations in back pressure on the distribution of pressure in the passage, on the flow rate, and on the exit-plane pressure. These effects are portrayed graphically in Figs. 4.11a, b, and c, respectively.

To begin with, suppose that $p_B/p_0 = 1$, shown as condition (i) in Fig. 4.11a. The pressure is then constant through the nozzle, and there is no flow.

If p_B is now reduced to a value slightly less than p_0 , as shown by condition (ii), there will be flow with a constantly decreasing pressure through the nozzle. Because the exit flow is subsonic, the exit-plane pressure p_E must be the same as the back pressure p_B , except for minor secondary circulation effects in the exhaust space. That this must be so can be seen by supposing for a moment that p_E is substantially larger than p_B . If this were so the stream would expand laterally upon leaving the nozzle; however, such an area increase at subsonic speeds causes the stream pressure to rise even further. Since the back pressure is, by definition, the pressure which the stream ultimately achieves in the exhaust space, it follows that p_E cannot be larger than p_B . A similar argument leads to the conclusion that p_E cannot be substantially less than p_B .

A further reduction in p_B to condition (iii) acts to increase the flow rate and to change the pressure distribution, but there is no qualitative change in performance.

Similar considerations apply until condition (iv) is reached, at which point p_B/p_0 equals the critical pressure ratio and the value of M_E equals unity.

Further reductions in p_B/p_0 , say to condition (v), cannot produce further changes in conditions within the nozzle, for the value of p_E/p_0 cannot be made less than the critical pressure ratio unless there is a throat upstream of the exit section (it is assumed here that the stream fills the passage). Consequently, at condition (v), the pressure distribution within the nozzle, the value of p_E/p_0 , and the flow rate, are all identical with the corresponding quantities for condition (iv). The pressure distribution outside the nozzle cannot be predicted on one-dimensional grounds, and for the present is shown in Fig. 4.11a as a wavy curve.

To summarize the preceding discussion, the two different types of flow will be denoted as regime I and regime II. These regimes may be compared as follows:

Regime I

$$p_B/p_0 > p^*/p_0$$

$$p_E/p_0 \cong p_B/p_0$$

$$M_E < 1$$

$$\frac{w\sqrt{T_0}}{A_E p_0} \text{ dependent on } p_B/p_0 \quad \frac{w\sqrt{T_0}}{A_E p_0} \text{ independent of } p_B/p_0$$

Regime II

$$p_B/p_0 < p^*/p_0$$

$$p_E/p_0 = p^*/p_0$$

$$M_E = 1$$

In regime I the values of p_E and p_B are virtually identical. Hence, except for a constant multiplier, the flow curve in regime I of Fig. 4.11b is identical with the curve of w/A in the subsonic part of Fig. 4.3.

A simple converging nozzle of the type discussed often serves as a flow nozzle. It is particularly useful when p_B/p_0 is less than the critical pressure ratio, for then the flow rate is given by Eq. 4.18, and measurements of only p_0 , T_0 , and A_E are necessary for computation of the flow rate.

For accurate measurements, the effects of boundary layer and of departures from one-dimensionality require that the nozzle be calibrated. Discharge coefficients for rounded-entrance nozzles are usually of the order 0.98 to 0.99, except for very low Reynolds Numbers where they may be considerably less.

The converging nozzle may occasionally be used to advantage as a simple flow regulator because of the fact that the flow rate is independent of back pressure when the latter is less than about half the supply pressure.

Converging-Diverging Nozzles. Consider an experiment similar to the one described above, except that a converging-diverging nozzle is to be used (Fig. 4.12).

With p_B less than p_0 by only a small amount, the flow is similar to that through a venturi passage, and it may be treated approximately as incompressible. The corresponding pressure distribution is shown by curves (i) and (ii) in Fig. 4.12.

When p_B/p_0 is reduced to the value corresponding to curve (iii), the Mach Number at the throat is unity, and no further reductions in p_T/p_0 are possible if the stream fills the passage.

We consider next the operation when the flow is entirely supersonic, corresponding to curve (iv). The value of p_B/p_0 for curve (iv) corresponds exactly to the area ratio of the nozzle, A_E/A_T , as given by the isentropic tables (in this case $A_T = A^*$, since $M_T = 1$). This is often called the "design" pressure ratio of the nozzle.

No flow pattern fulfilling the conditions of isentropic and one-dimensional flow can be found which will correspond to values of p_B/p_0 between those of curves (iii) and (iv) in Fig. 4.12. One method of finding solutions for these boundary conditions is to suppose that irreversible

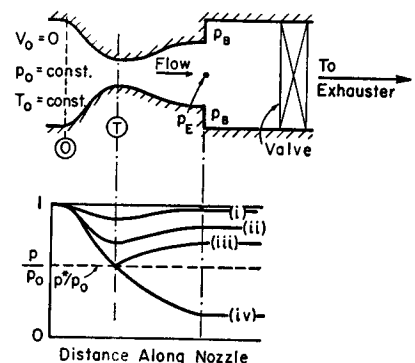


FIG. 4.12. Operation of converging-diverging nozzle at various back pressures.

discontinuities involving entropy increases occur somewhere within the passage. The analysis of such discontinuities, called shock fronts, is the subject of Chapter 5. A complete discussion of the converging-diverging nozzle will, therefore, be postponed until the shock wave analysis has been presented.

4.8. Special Relations for Low Mach Numbers

In many flow problems the Mach Numbers are comparatively small, but compressibility effects cannot be entirely ignored. Using binomial expansions, the formulas of the preceding articles may be put into simple algebraic forms which are accurate and convenient for such cases.

Correction to Incompressible Pitot-Tube Formula. For example, suppose that it is desired to examine the error incurred in the computation of pressure variations when the gas is assumed incompressible. From Eqs. 4.8 and 4.14b, we find that

$$\frac{p}{p_0} = \left[1 - \frac{k-1}{2} \left(\frac{V}{c_0} \right)^2 \right]^{\frac{1}{k-1}}$$

Expanding the right-hand side of this expression by the binomial theorem and rearranging, we get, if only terms up to $(V/c_0)^4$ are included,

$$\frac{p_0 - p}{\frac{1}{2} \rho_0 V^2} = 1 - \frac{1}{4} \left(\frac{V}{c_0} \right)^2 + \dots \quad (4.25)$$

If the fluid were taken as incompressible, the right-hand side of Eq. 4.25 would reduce to unity, and the equation would be identical with Bernoulli's theorem. The departure from unity is then a measure of the error incurred in ignoring compressibility. This error in the calculation of pressure changes is shown in the following table for several values of V/c_0 :

V/c_0	$\frac{p_0 - p}{\frac{1}{2} \rho_0 V^2} - 1$
0	0
0.1	-0.0025
0.2	-0.01
0.3	-0.0225
0.4	-0.04
0.5	-0.0625

Suppose that the incompressible formula were used for interpreting the reading of a pitot tube, based on the density at the stagnation pressure; at what air speed would this formula be in error by 1 per cent?

in this case p is the static pressure and p_0 is the pressure measured at the mouth of the tube. If V is in error by 1 per cent, then V^2 is in error by 2 per cent. Hence we set

$$\frac{1}{4} \left(\frac{V}{c_0} \right)^2 = 0.02; \text{ from which } \frac{V}{c_0} \leqq 0.28$$

The latter figure corresponds to an air speed at normal temperatures of about 300 ft/sec. At higher speeds the error increases quite rapidly.

Isentropic Formulas in Powers of Mach Number. Expanding Eqs. 4.9, 4.14, 4.16, and 4.19 in powers of M^2 by means of the binomial theorem, the following convenient formulas for low-speed isentropic flow, valid up to orders of M^4 , may be found:

$$M^* = \sqrt{\frac{k+1}{2}} M \left(1 - \frac{k-1}{4} M^2 + \dots \right) \quad (4.26)$$

$$\frac{p_0 - p}{p} = \frac{k M^2}{2} \left(1 + \frac{M^2}{4} + \dots \right) \quad (4.27)$$

$$\frac{\rho_0 - \rho}{\rho} = \frac{M^2}{2} \left(1 - \frac{k M^2}{4} + \dots \right) \quad (4.28)$$

$$\frac{w}{A} = \sqrt{\frac{k}{R} \frac{p_0}{\sqrt{T_0}}} M \left(1 + \frac{k-1}{4} M^2 + \dots \right) \quad (4.29)$$

$$\frac{A}{A^*} = \left(\frac{2}{k+1} \right)^{\frac{k+1}{2(k-1)}} \left[\frac{1}{M} + \frac{k+1}{4} M + \frac{(3-k)(k+1)}{32} M^3 + \dots \right] \quad (4.30)$$

4.9. Deviations from Perfect Gas Laws

Thus far all the isentropic formulas have been based on the two assumptions of a perfect gas, namely, (i) $p = \rho RT$, and (ii) $c_v = \text{constant}$. In practice, either of these assumptions may be weak to some extent. For example, if the process occurs at very high temperatures but at moderate pressures, as in the case of ram jets, there may be appreciable variations in specific heat. On the other hand, if the process occurs at moderate temperatures, but is carried out at an extremely high pressure level, as in hypersonic wind tunnels, there may be significant deviations from the law $p = \rho RT$.

These two effects have been studied ⁽¹⁾ for the isentropic flow of air. Since the analysis is a lengthy one, only the main results of practical significance are summarized here.

Effect of Variable Specific Heat when $p = \rho RT$. The equation of state of a perfect gas is retained at first, but the specific heat is expressed from quantum mechanics as

$$\frac{c_v}{R} = \frac{5}{2} + \left(\frac{\theta}{T}\right)^2 \frac{e^{\theta/T}}{(e^{\theta/T} - 1)^2}$$

where $\theta = 5526^\circ\text{R}$ for air. The results are embodied in Fig. 4.13, in which are shown the per cent errors in the pressure, temperature, and density ratios incurred through use of constant rather than variable specific heats. At stagnation temperatures of 1000°R or less, the error is seen to be small for engineering purposes; but, at temperatures greater than 2000°R , the error can be substantial, especially at supersonic Mach Numbers.

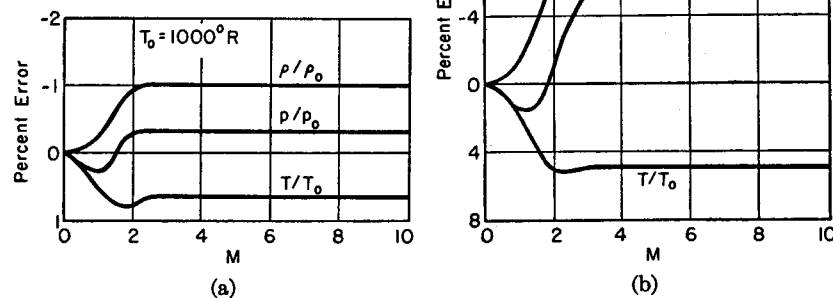


FIG. 4.13. Error incurred through assumption of constant specific heats for air, with $p = \rho RT$ (after Donaldson).

(a) $T_0 = 1000^\circ\text{R}$.

(b) $T_0 = 2000^\circ\text{R}$.

Effect of Deviations from Perfect-Gas Equation of State. Based on the use of constant specific heats but the van der Waals equation of state for air, the isentropic pressure ratio and area ratio are plotted versus M in Fig. 4.14 for several stagnation pressures. It is seen that the deviations from results obtained with the perfect-gas equation of state are negligible up to about 50 atmospheres, but are appreciable at 200 atmospheres and above.

Combined Effect of Variations in Specific Heat and Deviations from Perfect-Gas Equation of State. The simultaneous effects on pressure ratio and area ratio of both high temperature level (i.e., variations in specific heat) and high pressure level (i.e., deviations from $p = \rho RT$) are illustrated in Fig. 4.15. There is an interesting anomaly here in that the effects of pressure level are in one direction at low pressures and in the other direction at high pressures.

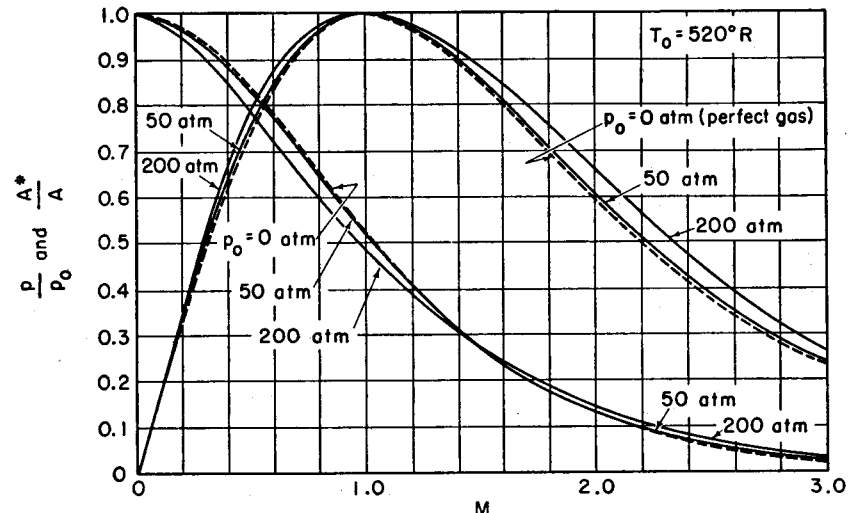


FIG. 4.14. Effect of pressure level on isentropic flow functions, using van der Waals equation for air (after Donaldson).

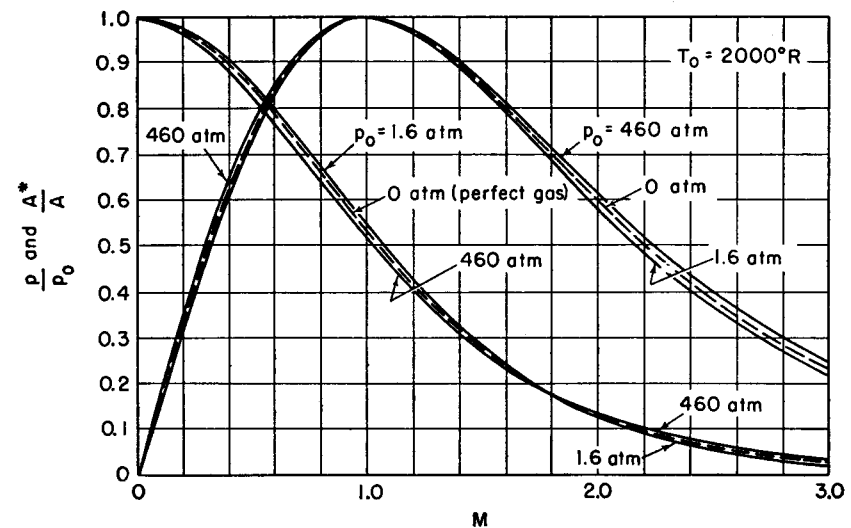


FIG. 4.15. Simultaneous effects of high pressure and high temperature on pressure ratio and area ratio (after Donaldson).

4.10. Performance of Real Nozzles

Because of frictional effects, the performance of real nozzles differs slightly from that computed with the isentropic flow relations. Since the departures from isentropic flow are usually small, the usual design procedure is based on the use of the isentropic flow formulas modified by two types of empirically determined coefficients—the nozzle efficiency and the coefficient of discharge.

Nozzle Efficiency. The term nozzle efficiency is employed primarily in turbine design where it is important to estimate accurately the

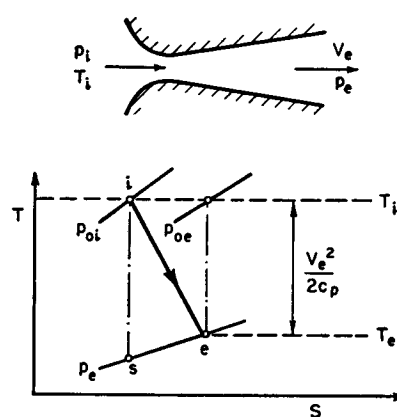


FIG. 4.16. Illustrating definition of nozzle efficiency.

steady-flow energy equation the efficiency may be written

$$\eta = \frac{V_e^2/2}{c_p(T_i - T_s)} \quad (4.31)$$

This may be rearranged further to give

$$\eta = \frac{\frac{V_e^2}{2} \frac{kR}{c_p T_i}}{1 - \frac{T_s}{T_i}} = \frac{\frac{k-1}{2} \frac{V_e^2}{c_i^2}}{1 - \left(\frac{p_e}{p_i}\right)^{\frac{k-1}{k}}} \quad (4.32)$$

which is convenient for reckoning the exit velocity when the efficiency, pressure ratio, and stagnation temperature are all known.

Occasionally the term "velocity coefficient" is used, denoting the square root of the nozzle efficiency.

Frictional effects in nozzles are usually confined to thin boundary layers on the walls. Since the boundary layer thickness depends primarily on the Reynolds Number (based on some equivalent nozzle length) and on the pressure-distance curve in the nozzle, no simple expression for nozzle efficiency can be given which is applicable to all nozzles. In general, the nozzle efficiency becomes nearly unity for extremely large nozzles because the boundary layer thickness is so small compared with the size of the passage. With very small nozzles, however, the boundary layer may nearly fill the passage, and then the nozzle efficiency may drop drastically.

When well-designed nozzles with straight axes are operated at their design pressure ratio and at high Reynolds Numbers, they are found to have efficiencies ranging from 94 to 99 per cent, and even higher for sizable wind tunnel nozzles.

Well-designed turbine nozzles with curved axes have efficiencies of the order of 90 to 95 per cent when operated with suitable pressure ratios at high Reynolds Numbers.

Nozzle Discharge Coefficient. The nozzle discharge coefficient, C_w , is defined as the ratio of the actual nozzle flow to the flow calculated from the isentropic laws for the initial and final pressures of the actual nozzle.

$$C_w = \frac{w}{\text{Isentropic Flow Rate}}$$

If the over-all pressure ratio of the nozzle is such that the velocity at the minimum section is subsonic, then the "isentropic flow" is reckoned in terms of the exit conditions of the nozzle. However, if the pressure ratio is such that sonic velocity prevails at the minimum section, then the "isentropic flow" is reckoned by using the formula for choking flow at the throat. These specifications apply to both converging and converging-diverging passages.

The remarks made previously concerning the factors influencing nozzle efficiency pertain also to the discharge coefficient.

For well-designed nozzles with straight axes having "pipe" Reynolds Numbers measured at the minimum area of 10^6 or more, the discharge coefficient is of the order of 0.99, but it may be considerably less for low Reynolds Numbers.

Neither the discharge coefficient nor the velocity coefficient of rounded-entrance nozzles suitably designed for the operating pressure ratio are significantly dependent upon the leaving Mach Number.

Sharp-Edged Orifice Meter. The deviation from unity of the discharge coefficient for a sharp-edged orifice meter is due primarily to the contraction (*vena contracta*) in the stream following the orifice. The contraction in turn is due to three-dimensional effects. The coefficient of contraction increases substantially as the result of compressibility effects (Fig. 4.17). It should be noted that the isentropic flow on which the discharge coefficient is based is reckoned as though a rounded-entrance converging nozzle, having the same exit area as the orifice, were supplied with gas at stagnation pressure p_1 and discharged to a region having the pressure p_2 .

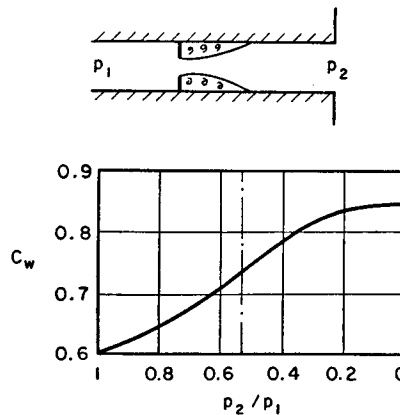


FIG. 4.17. Discharge coefficient of sharp-edged orifice meters with zero velocity of approach (after J. A. Perry).

4.11. Some Applications of Isentropic Flow

Thrust of Rocket Motor. Consider a rocket motor (Fig. 4.18a) which generates gas steadily at p_0 and T_0 . The nozzle has a throat area A_t , an exit area A_e , and discharges to an atmosphere at pressure p_a . Experimental data verify that the isentropic flow equations predict, within a few per cent, the thrust produced by such a rocket.

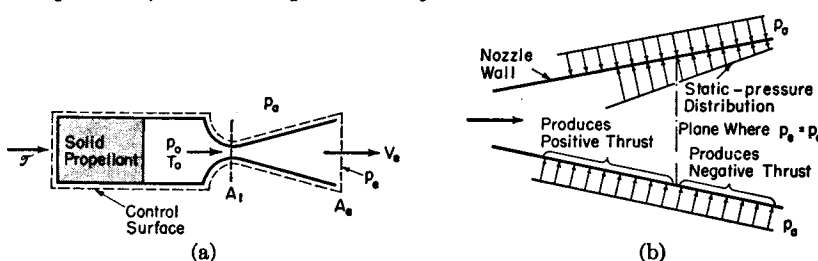


FIG. 4.18. Isentropic flow in rocket motor.

- (a) Diagrammatic sketch.
- (b) Pressure distributions on internal and external surfaces of diverging portion of nozzle.

Since rocket motors generate gas at about 500 psia and operate in atmospheres at 14.7 psia or less, a converging-diverging nozzle is usually used. Except under operating conditions far from the design point, sonic conditions occur at the throat, and the flow to the nozzle exit is shock-free. We shall assume these conditions for the present analysis.

In the following chapter, however, it is pointed out that a nozzle having a given area ratio and operating at certain ratios of back pressure to supply pressure cannot be isentropic because shocks are present. Such cases are not covered by the equations about to be derived.

Under the assumed conditions, the pressure ratio p_e/p_0 is fixed by the area ratio, and so the exit-plane pressure in general differs from the surrounding atmospheric pressure. Applying the momentum equation to the control volume of Fig. 4.18a, we find the thrust \mathcal{J} to be given by

$$\mathcal{J} = wV_e + A_e(p_e - p_a)$$

which is then put into dimensionless form through division by p_0A_t :

$$\frac{\mathcal{J}}{p_0A_t} = \frac{w}{p_0A_t} V_e + \frac{A_e}{A_t} \left(\frac{p_e}{p_0} - \frac{p_a}{p_0} \right)$$

From Eq. 4.17, for choking flow,

$$\frac{w}{A_t p_0} = \sqrt{\frac{k}{R}} \left(\frac{2}{k+1} \right)^{\frac{k+1}{k-1}} \frac{1}{\sqrt{T_0}}$$

and, from the energy equation and isentropic law,

$$\begin{aligned} V_e &= \sqrt{2c_p(T_0 - T_e)} = \sqrt{2c_p T_0} \sqrt{1 - \frac{T_e}{T_0}} \\ &= \sqrt{2c_p T_0} \sqrt{1 - \left(\frac{p_e}{p_0} \right)^{\frac{k-1}{k}}} \end{aligned}$$

Substituting these into the thrust equation, and rearranging, there results

$$\frac{\mathcal{J}}{p_0A_t} = k \sqrt{\frac{2}{k-1} \left(\frac{2}{k+1} \right)^{\frac{k+1}{k-1}}} \sqrt{1 - \left(\frac{p_e}{p_0} \right)^{\frac{k-1}{k}}} + \frac{A_e}{A_t} \left(\frac{p_e}{p_0} - \frac{p_a}{p_0} \right) \quad (4.33)$$

Since the pressure ratio p_e/p_0 depends only on the area ratio, Eq. 4.33 indicates that the thrust for a nozzle of given size and geometry depends only on p_0 and the ratio p_a/p_0 , and is independent of the temperature T_0 .

EFFECT OF AREA RATIO. We now ask, for given values of A_t , p_0 , and p_a , what exit area should be used in order to obtain maximum thrust? By applying the calculus to Eq. 4.33 it may be shown after a laborious calculation that \mathcal{J} is a maximum when the area ratio is chosen in such a way as to make the pressure in the exit plane exactly equal to p_a . How-

ever, this result may more easily be obtained with the simplest of physical reasoning. The net thrust on the rocket is the resultant of static pressures acting on all the surfaces of the motor. Suppose, as in Fig. 4.18b, that there is a certain exit area for which $p_e = p_a$. If the nozzle is continued beyond this point, the pressure in the nozzle will drop further, and the added piece of divergent nozzle will have negative thrust

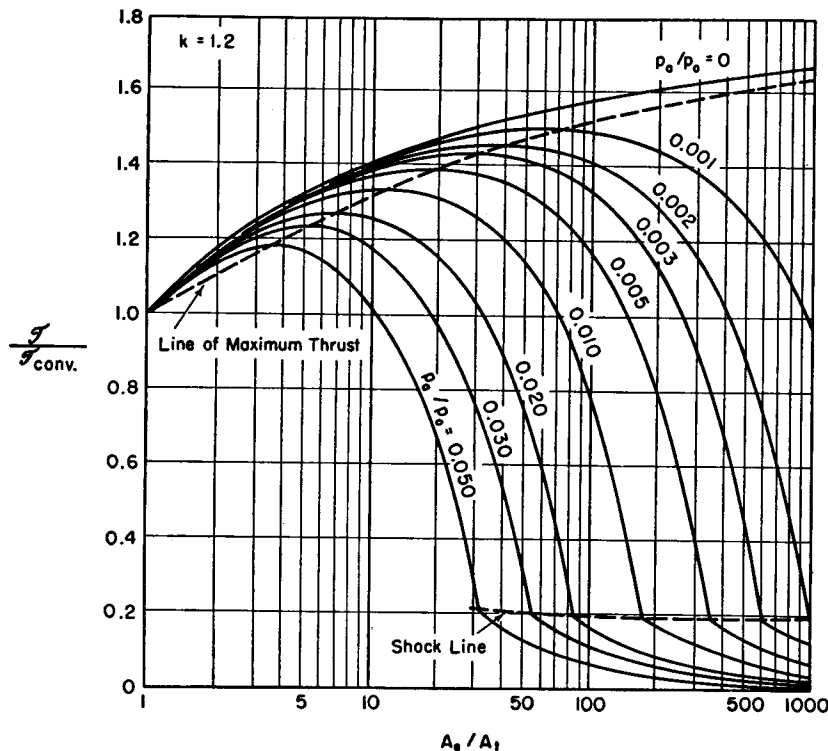


FIG. 4.19. Performance characteristics of rocket nozzle, $k = 1.2$ (after Malina).

because the internal pressure on this added piece is less than the external pressure. By similar reasoning, it follows that cutting off a piece of nozzle upstream of the plane where $p_e = p_a$ would also act to reduce the thrust. Hence we conclude that the thrust is a maximum when $p_e = p_a$. Applying this criterion to Eq. 4.33, we get

$$\frac{J_{\max}}{p_0 A_t} = k \sqrt{\frac{2}{k-1} \left(\frac{2}{k+1} \right)^{\frac{k+1}{k-1}}} \sqrt{1 - \left(\frac{p_a}{p_0} \right)^{\frac{k-1}{k}}} \quad (4.34)$$

If the nozzle were a simple converging nozzle, A_e would equal A_t , and p_e/p_0 would be the critical pressure ratio. Making these substitutions

in Eq. 4.33 and simplifying, there is obtained

$$\frac{J_{\text{conv}}}{p_0 A_t} = 2 \left(\frac{2}{k+1} \right)^{\frac{1}{k-1}} - \frac{p_a}{p_0} \quad (4.35)$$

To illustrate the effect of area ratio on nozzle thrust, we form the ratio

$$\frac{J}{J_{\text{conv}}} = \frac{J/p_0 A_t}{J_{\text{conv}}/p_0 A_t} = \frac{k \sqrt{\frac{2}{k-1} \left(\frac{2}{k+1} \right)^{\frac{k+1}{k-1}} \left(1 - \frac{p_e}{p_0} \right)^{\frac{k-1}{k}}} + \frac{A_e}{A_t} \left(\frac{p_e}{p_0} - \frac{p_a}{p_0} \right)}{2 \left(\frac{2}{k+1} \right)^{\frac{1}{k-1}} - \frac{p_a}{p_0}} \quad (4.36)$$

This ratio is plotted against area ratio in Fig. 4.19 for various values of p_e/p_0 , with $k = 1.2$ (typical value for rocket gas). It is seen that the curves are quite flat near their maxima, so that the area ratio need not be exactly adjusted in order to obtain substantially maximum thrust. In practice, rocket nozzles are usually designed with p_e greater than p_a , since this reduces the size of the nozzle without materially reducing the thrust.

Reynolds Number for Supersonic Wind Tunnel. Fig. 4.20 shows a supersonic wind tunnel with a test section having a Mach Number M_1

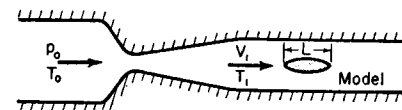


FIG. 4.20. Supersonic wind tunnel.

and in which is inserted a model of length L . We shall derive a convenient relation for the Reynolds Number of the model, based on fluid properties in the test section and on the length L . With the aid of the perfect gas laws and the isentropic flow relations, we form the expression

$$\begin{aligned} \frac{\text{Rey}}{p_0 L} &= \frac{\rho_1 V_1 L / \mu_1}{p_0 L} = \frac{\rho_1 V_1 p_1}{\mu_1 p_1 p_0} = \frac{V_1}{\mu_1 R T_1} \sqrt{\frac{k T_0}{k T_0 p_0}} \\ &= \frac{M_1 \sqrt{\frac{k}{R}}}{\mu_1 \sqrt{T_0}} \frac{\sqrt{1 + \frac{k-1}{2} M_1^2}}{\left(1 + \frac{k-1}{2} M_1^2 \right)^{\frac{k}{k-1}}} = \frac{\sqrt{k/R}}{\mu_1 \sqrt{T_0}} \frac{M_1}{\left(1 + \frac{k-1}{2} M_1^2 \right)^{\frac{k+1}{2(k-1)}}} \end{aligned} \quad (4.37)$$

Now T_1 , and accordingly the viscosity μ_1 , are determined by the values of T_0 and M_1 . Thus the Reynolds Number per unit length and per unit stagnation pressure depends, for a given gas, only on the test-section Mach Number and on the stagnation temperature. A convenient chart representing this relation for air flow is shown in Fig. 4.21.

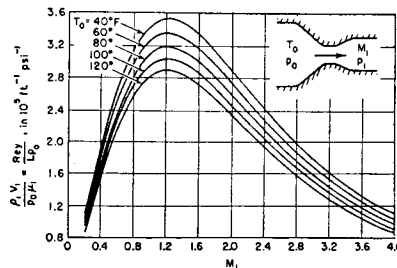


FIG. 4.21. Reynolds Number for supersonic wind tunnel (*NACA Tech. Note*, No. 1428).

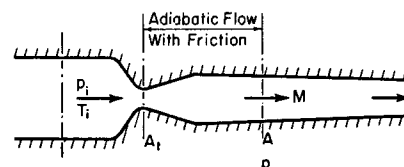


FIG. 4.22. Flow in duct with friction.

Supersonic Flow in Duct with Friction. When a duct is supplied with a supersonic flow by a converging-diverging nozzle, and when the flow in the duct is adiabatic but not frictionless, a useful expression may be obtained for determining the local Mach Number in terms of the local area and static pressure. The nomenclature is shown in Fig. 4.22.

Since the nozzle throat is choked, the mass flow through the system is given by Eq. 4.17 when modified by the discharge coefficient C_w :

$$\frac{w}{A_t} = C_w \sqrt{\frac{k}{R}} \left(\frac{2}{k+1} \right)^{\frac{k+1}{k-1}} \frac{p_i}{\sqrt{T_i}}$$

Furthermore, Eq. 4.11 yields

$$\frac{w}{A} = \sqrt{\frac{k}{R}} \frac{p}{\sqrt{T_i}} M \sqrt{1 + \frac{k-1}{2} M^2}$$

Dividing one of these by the other, it may be shown by direct comparison that

$$C_w \frac{A_t/A}{p/p_i} = \frac{(A^*/A)_{isen}}{(p/p_0)_{isen}} \quad (4.38)$$

where $(A^*/A)_{isen}$ is the function of k and M given by Eq. 4.19, and $(p/p_0)_{isen}$ is the function of k and M given by Eq. 4.14b.

Since the type of problem discussed here arises frequently in experimental work, the quantity on the right-hand side of Eq. 4.38 is listed in the isentropic flow tables. Given the areas A_t and A and the measured

pressures p_i and p , together with the discharge coefficient C_w , the local Mach Number M may be found from these tables by a quick computation. An illustrative example is given in Chapter 6.

Eq. 4.38 typifies a technique which we shall find useful from time to time—namely, to use the tabulated functions of k and M in Appendix B not only for the particular types of flow underlying the construction of the tables, but for such other problems where identical functions of k and M appear.

REFERENCES AND SELECTED BIBLIOGRAPHY

1. DONALDSON, C. duP. Note on the Importance of Imperfect-Gas Effects and Variation of Heat Capacities on the Isentropic Flow of Gases, *NACA R.M.*, No. L8J14 (1948).

PROBLEMS

4.1. Consider the reversible adiabatic flow of steam through a passage of variable cross section. At the section where the velocity is zero the pressure and temperature are $p_0 = 50$ psia and $T_0 = 800^\circ\text{F}$. Denoting the pressure at any other point in the stream by p , plot against p/p_0 the values of specific volume (ft^3/lb), velocity (ft/sec), and mass velocity ($\text{lb}/\text{ft}^2 \text{ sec}$), for the following conditions:

- (a) The properties of steam are taken from the Steam Tables of Keenan and Keyes.
- (b) The steam is considered as a perfect gas, with a value of 1.3 for k .
- (c) The steam is considered as incompressible with a density equal to the density corresponding to p_0 and T_0 .

In the above calculations choose for the lowest value of p/p_0 the value of p which corresponds to the first appearance of moisture in part (a).

4.2. Consider the reversible, adiabatic flow of a perfect gas. Plot the values of p^*/p_0 , T^*/T_0 , ρ^*/ρ_0 , c^*/c_0 , V_{\max}/c^* , and V_{\max}/c_0 , all versus k , for values of the latter between 1 and 2.

4.3. An airplane flies at an altitude of 40,000 ft (temperature = -67.0°F , pressure = 2.72 psia) with a speed of 400 mph. Neglecting frictional effects,

- (a) Calculate the critical velocity of the air relative to the aircraft.
- (b) Calculate the maximum possible velocity of the air relative to the aircraft.

4.4. Sketch a curve of pressure (p/p^*) versus velocity (V/V^*) for isentropic flow, paying special attention to zero or infinite slopes, direction of curvature, and points of inflection. Indicate the values of p/p^* and V/V^* at their maximum and minimum points, at points of zero or infinite slope, and at points of inflection. What is the physical significance of the tangent to the curve of p/p^* versus V/V^* ?

4.5. A stream of air flows in a duct of 4 inches diameter at a rate of 2.20 lb/sec. The stagnation temperature is 100°F. At one section of the duct the static pressure is 6 psia.

Calculate the Mach Number, velocity, and stagnation pressure at this section.

4.6. A perfect gas ($k = 1.4$, $R = 100 \text{ ft lbf/lbm}^\circ\text{R}$) is supplied to a converging nozzle at low velocity and at 100 psia and 540°F. The nozzle discharges to atmospheric pressure, 14.7 psia. Assuming frictionless adiabatic flow, and a mass rate of flow of 1 lbm/sec, calculate

- The pressure in the exit plane, in psia
- The velocity in the exit plane, in ft/sec
- The cross-sectional area of the exit plane, in square feet

4.7. Show that for isentropic flow of a perfect gas, the pressure, temperature, and density, when made dimensionless with respect to the corresponding critical values, are given by

$$\frac{p}{p^*} = \left[\frac{k+1}{2 \left(1 + \frac{k-1}{2} M^2 \right)} \right]^{\frac{k}{k-1}}$$

$$\frac{T}{T^*} = \frac{k+1}{2 \left(1 + \frac{k-1}{2} M^2 \right)}$$

$$\frac{\rho}{\rho^*} = \left[\frac{k+1}{2 \left(1 + \frac{k-1}{2} M^2 \right)} \right]^{\frac{1}{k-1}}$$

4.8. Derive simplified, approximate versions of the isentropic flow relations for a perfect gas valid at Mach Numbers large compared with unity.

4.9. A pitot-static tube records a static pressure of 5.20 psig and a difference between impact pressure and static pressure of 19.42 inches of mercury. The barometer reads 29.73 inches Hg, and the stagnation temperature of the air stream is 80°F. Compute the air velocity, (a) assuming the air incompressible, and (b) assuming the air compressible.

4.10. A stream of air flowing in a duct is at a pressure of 20 psia, has a Mach Number of 0.6, and flows at a rate of 0.5 lb/sec. The cross-sectional area of the duct is one square inch.

- Compute the stagnation temperature of the stream in degrees F.
- What is the maximum percentage reduction in area which could be introduced without reducing the flow rate of the stream?
- For the maximum area reduction of part (b), find the velocity and pressure at the minimum area, assuming no friction and no heat transfer.

4.11. A converging nozzle with an exit area of one square inch is supplied with air at low velocity and at a pressure and temperature of 100 psia and 200°F, respectively.

Plot the mass rate of flow through the nozzle versus back pressure, assuming the flow to be isentropic.

4.12. A rocket combustion chamber is supplied with 24 lb/sec of hydrogen and 76 lb/sec of oxygen. Before entering the nozzle all the oxygen is consumed, the pressure is 23 atmospheres, and the temperature is 4960°F. Neglecting dissociation and friction, find the throat area of the nozzle required. Assume $k = 1.25$.

4.13. At a certain point in a stream tube, air flows with a velocity of 500 ft/sec and has a pressure and temperature of 10 psia and 40°F, respectively.

(a) Calculate the following quantities at a point further downstream in the stream tube where the cross-sectional area is 15 per cent smaller than at the upstream section: the stagnation pressure and temperature, the stream pressure and temperature, the velocity, the Mach Number, and the value of M^* .

(b) Compute the maximum possible reduction in area of the stream tube. For the section with the minimum area, compute the quantities listed in part (a).

4.14. When a body is placed in a stream which at infinite distance upstream is in uniform flow with free-stream conditions V_∞ , p_∞ , M_∞ , etc., the local pressures in the neighborhood of the body are usually reported in terms of the dimensionless pressure coefficient, C_p :

$$C_p \equiv \frac{p - p_\infty}{\frac{1}{2} \rho_\infty V_\infty^2}$$

(a) Show that the value of the pressure coefficient corresponding to the appearance of the critical velocity is given by

$$C_p^* = \frac{\left[\frac{2 + (k-1)M_\infty^2}{k+1} \right]^{\frac{k}{k-1}} - 1}{\frac{k}{2} M_\infty^2}$$

(b) Plot $\log(-C_p^*)$ versus $\log M_\infty$ for $k = 1.4$ and for values of M_∞ between 0.1 and 1.0.

(c) Suppose that an airplane is flying at sea level with a velocity of 500 mph. What is the maximum pressure coefficient which may be attained on the wings without the speed becoming anywhere supersonic?

4.15. Pressure coefficients, lift coefficients, drag coefficients, etc., of airfoils which are in a free stream with conditions p_∞ , M_∞ , etc., are usually expressed in terms of the dynamic head of the free stream. Thus

$$C_p \equiv \frac{p - p_\infty}{\frac{1}{2} \rho_\infty V_\infty^2}; \quad C_L \equiv \frac{L/A}{\frac{1}{2} \rho_\infty V_\infty^2}; \quad \text{etc.}$$

Alternate definitions for compressible flow, not usually employed, are as follows:

$$C_p' \equiv \frac{p - p_\infty}{p_0 - p_\infty}; \quad C_L' \equiv \frac{L/A}{p_0 - p_\infty}; \quad \text{etc.}$$

where p_0 is the isentropic stagnation pressure corresponding to p_∞ and M_∞ .

Derive an expression for C_p'/C_p in terms of M_∞ and k . Plot C_p'/C_p versus M_∞ for $k = 1.4$ and for values of M_∞ between 0 and ∞ .

4.16. (a) Show, for a source-type flow (either two- or three-dimensional) of a compressible fluid, that either supersonic or subsonic flow may subsist, but that both types may not exist together.

(b) Show that for a finite flow rate from the source there is a minimum radius within which a source-type flow pattern is impossible. What is the Mach Number at this minimum radius? Find expressions for r/r_{\min} as functions of M and k for the line source (two-dimensional) and the point source (three-dimensional), where r is the radius at M and r_{\min} is the minimum radius.

(c) For the four possible types of flow outside the minimum radius, depending on whether the flow is outwards (source) or inwards (sink) and on whether it is subsonic or supersonic, specify the directions of the pressure gradient and of the fluid acceleration.

4.17. Consider the vortex motion of a perfect gas in which all streamlines have the same entropy and the same stagnation-enthalpy. The equation of this motion is $Vr = \Gamma/2\pi$, where V is the tangential velocity, r is the radius of the streamline, and Γ is a constant called the circulation.

(a) Show that there is a minimum radius inside of which the vortex motion may not exist, and that this radius is given by

$$r_{\min} = \frac{\Gamma}{2\pi c^*} \sqrt{\frac{k-1}{k+1}}$$

(b) Show that the field of flow outside the minimum radius includes all Mach Numbers from zero to infinity, and that the radius corresponding to the critical velocity is given by

$$r^* = r_{\min} \sqrt{\frac{k+1}{k-1}}$$

4.18. From schlieren photographs of the flow of air through a converging-diverging nozzle it is found that the average Mach angle over the exit cross section is 40° . The measured static pressure at the exit cross section is 0.198 atm, while the pressure upstream of the nozzle, where the velocity is small, is 1.000 atm.

Calculate the ratio of the average exit kinetic energy per unit mass of the stream to the exit kinetic energy corresponding to isentropic expansion to the measured exit pressure,

- (a) Using the assumption that air is a perfect gas, with $k = 1.4$
- (b) Using the Air Tables of Keenan and Kaye and a measured value for the stagnation temperature, T_0 , of 2400°F abs

4.19. During a reaction-stand test of a turbojet engine, measurements indicate a thrust of 1845 lb when the flow rate is 30 lb/sec. The temperature at the entrance to the thrust nozzle, where the velocity is 300 ft/sec, is 1400°F . The nozzle has no diverging section, so that the stream reaches atmospheric pressure, 14.7 psia, somewhere outside the nozzle.

Assuming no heat loss from the gas, that the direction of the air stream entering the engine is at right angles to the direction of thrust, and that the nozzle is frictionless, estimate the pressure in the exit plane of the nozzle.

4.20. Derive the following expressions for isentropic flow with the pressure ratio p/p_0 as a parameter:

$$V = \sqrt{\frac{2kR}{k-1}} \sqrt{T_0} \sqrt{1 - (p/p_0)^{\frac{k-1}{k}}}$$

$$M^2 = \frac{2}{k-1} \left[(p_0/p)^{\frac{k-1}{k}} - 1 \right]$$

$$M^{*2} = \frac{k+1}{k-1} \left[1 - (p/p_0)^{\frac{k-1}{k}} \right]$$

$$\frac{w}{A} \frac{\sqrt{T_0}}{p_0} = (p/p_0)^{\frac{1}{k}} \sqrt{1 - (p/p_0)^{\frac{k-1}{k}}} \sqrt{\frac{2k}{R(k-1)}}$$

$$\frac{A^*}{A} = \sqrt{\frac{2}{k-1} \left(\frac{k+1}{2} \right)^{\frac{k+1}{k-1}} \cdot (p/p_0)^{\frac{1}{k}} \sqrt{1 - (p/p_0)^{\frac{k-1}{k}}}}$$

4.21. Derive relations between M and V/c_0 and between M and V/V_{\max} , for adiabatic flow of a perfect gas.

4.22. Derive a relation between M^* and the mass flow parameter

$$\frac{w}{A} \frac{\sqrt{T_0}}{p} \frac{1}{\sqrt{W}}$$

applicable to adiabatic flow of a perfect gas.

4.23. By expanding Eq. 4.11 in a power series of M with the aid of the binomial theorem, show that for low Mach Numbers the mass flow parameter may be approximated by

$$\frac{w}{A} \frac{\sqrt{T_0}}{p} \frac{1}{\sqrt{W}} = \sqrt{\frac{k}{\mathcal{R}}} \left(M + \frac{k-1}{4} M^3 + \dots \right)$$

4.24. Derive Eqs. 4.14 without use of the steady-flow energy equation, by employing Euler's equation for frictionless flow, $dp = -\rho V dV$, and the perfect gas relations $p = \rho RT$, $c^2 = kRT$, and $p/\rho^k = \text{constant}$.

4.25. Consider a perfect gas flowing in a *constant-area* duct *adiabatically* and without friction. Changes in state come about as the result of changes in elevation in the earth's gravity field. The z -direction is away from the center of the earth, and hence gravity acts in the negative z -direction.

(a) Starting from first principles, determine by analysis the direction of change (increase or decrease) of the Mach Number, gas speed, sound speed, density, pressure, stagnation temperature, and isentropic stagnation pressure, all for a *positive increase in z* ,

- (i) For *subsonic* speeds
- (ii) For *supersonic* speeds

- (b) Is choking possible for this type of flow? Justify your answer.
 (c) Considering frictionless, adiabatic gas flows for aircraft, fluid machinery, and ventilating systems, would you expect gravity effects to be significant for
- Speeds negligible compared with the speed of sound?
 - Subsonic speeds of the order of Mach Number 0.5?
 - Speeds very close to the local speed of sound?
 - Supersonic speeds of the order of Mach Number 2.0?
 - Supersonic speeds of the order of Mach Number 10.0?

In analyzing this problem it is suggested that the governing equations be written in differential form.

4.26. Consider a nozzle with an efficiency η between the inlet and any station downstream.

(a) Derive the expression

$$\frac{p}{p_0} = \left[1 - \frac{1}{\eta} \frac{\frac{k-1}{2} M^2}{1 + \frac{k-1}{2} M^2} \right]^{\frac{k}{k-1}}$$

(b) Derive a corresponding expression for

$$\frac{w}{A} \frac{\sqrt{T_0}}{p_0}$$

(c) Show that Mach Number unity does not occur at the minimum area, and find the Mach Number at the throat.

4.27. Consider a supersonic nozzle constructed with a ratio of exit to throat area of 2.0. The nozzle is supplied with air at low speed at 100 psia and 140°F. The over-all nozzle efficiency from inlet to exit is 90 per cent, but the flow is isentropic to the throat.

Calculate the pressure, velocity, and Mach Number at exit, and compare with the corresponding values for isentropic flow.

4.28. A tank having a volume of 100 ft³ is initially filled with air at 100 psia and 140°F. Suddenly the air is allowed to escape to the atmosphere (14.7 psia) through a frictionless converging nozzle of one-inch diameter. It is agreed to assume that the flow is quasi-steady, i.e., that the steady flow equations may be applied to the nozzle at any instant of time. Furthermore, the tank is to be considered as insulated perfectly against heat conduction and as having no heat capacity.

Plot the pressure in the tank versus elapsed time.

4.29. A supersonic nozzle with a throat area of 1 sq in. discharges air into a duct having a cross-sectional area of 2 sq in. The supply pressure is 100 psia, and the nozzle has a discharge coefficient of 0.98. At one section of the duct the pressure is 14.2 psia. Calculate the Mach Number and isentropic stagnation pressure at this section.

4.30. Consider the isentropic flow of a highly compressible liquid having a pressure-density relation given by

$$\beta = \rho \left(\frac{\partial p}{\partial \rho} \right)_s$$

where β is a constant.

(a) Show that

$$p_0 - p^* = \beta \ln 2$$

where p_0 is the stagnation pressure and p^* is the critical pressure.

(b) Derive expressions for p/p_0 and A/A^* in terms of M and β .

4.31. A large main is connected to an evacuated tank with a volume of 10 ft³ by means of a rounded-entrance, converging nozzle having a diameter of 0.01 in. Initially, a diaphragm over the orifice seals the tank from the main. The air in the main is at 100 psia and 70°F. The diaphragm is suddenly broken and air rushes into the tank. Estimate the time required for the pressure in the tank to reach 25 psia, based on the following assumptions:

- The flow is quasi-static.
- There is no heat conduction from the tank to the air.
- The pressure and temperature in the main are constant.

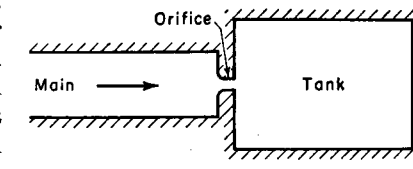
Under what circumstances will these assumptions lead to accurate results?

4.32. Show that the coefficient of contraction for a Borda re-entrant orifice is given by

$$\frac{1}{kM^2} \left[\left(1 + \frac{k-1}{2} M^2 \right)^{\frac{k}{k-1}} - 1 \right]$$

where M is the Mach Number of the jet.

Note that the coefficient goes from 0.50 at $M = 0$ to approximately 0.64 at $M = 1$, and that the percentage change is of the same order of magnitude as that for ordinary sharp-edged orifices.



PROB. 4.31.

Chapter 5

NORMAL SHOCK WAVES

5.1. Introductory Remarks

It was shown in Chapter 4 that for certain combinations of initial and final pressures there are no completely isentropic solutions to the problem of one-dimensional flow through a converging-diverging passage. In order to find solutions fitting these boundary conditions, some new phenomenon must be introduced. A clue to the nature of this phenomenon is given by schlieren (striation) photographs of the flow in nozzles and around projectiles. These photographs show that at supersonic speeds there sometimes occur very rapid changes in the velocity and pressure of the stream.

In a real fluid discontinuities in fluid properties cannot exist for finite periods of time, for viscous, heat conduction, and mass diffusion effects tend to smooth out such discontinuities. However, photographs of supersonic projectiles (Figs. 3.5 and 3.6) show "conical shock waves" which are so thin that the changes in pressure and velocity which occur across the wave are effected in an extraordinarily short distance. Further evidence is adduced in Fig. 5.1, showing a *normal shock wave* in a supersonic wind tunnel. Here the pressure increases across the shock by five-fold, and the velocity decreases by a factor of three; yet the changes occur in a distance too small to be measured on a photographic plate. Indeed, theoretical calculations and experimental measurements show that the thickness of a normal shock is of the order of 10^{-5} inches and is comparable with the mean free path of the molecules.

For practically all engineering calculations we are concerned primarily with the net changes in fluid properties across the shock, and have no interest in the complex viscous and heat conduction phenomena in the interior of the shock wave. It is profitable, therefore, to ignore the interior details of the shock wave, and to employ a simplified model, namely, a pure discontinuity.

We therefore focus our attention on the relations between the stream properties on the two sides of such a discontinuity, and on the question of whether all such discontinuities are possible. Although experiments show that these discontinuities are often oblique to the direction of flow (as in Fig. 3.5) we will consider now only one-dimensional motion, i.e.,

only discontinuities normal to the direction of flow (as in Fig. 5.1). *Oblique discontinuities* will be treated in Chapter 16.

² Additional material relevant to the subject matter of the present chapter may be found in Volume II, Chapters 25 and 28.

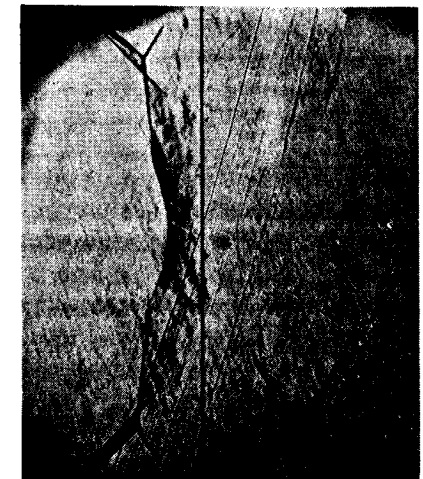


FIG. 5.1. Schlieren photograph of "normal shock" in supersonic wind tunnel at $M \approx 2$, with flow from left to right. The straight vertical line is a reference wire outside the tunnel, and the light parallel lines are defects in the glass walls of the tunnel. The shock itself is not quite straight. At each end of the normal shock is a pair of forked oblique shocks which arise from the interaction of the normal shock with the boundary layers on the walls of the tunnel (M.I.T. Gas Turbine Laboratory).

NOMENCLATURE

A	area	w	mass rate of flow
c	speed of sound	x, y	Cartesian coordinates
c_p	specific heat at constant pressure	β	bulk modulus of compression
h	enthalpy per unit mass	δ	shock thickness
k	ratio of specific heats	η_D	diffuser efficiency
l	mean free molecular path	μ	coefficient of viscosity
M	Mach Number	ρ	density
M^*	V/c^*	$(\)_0$	signifies stagnation state
p	pressure	$(\)^*$	signifies state at which $M = 1$
P	strength of a shock wave	$(\)_\infty$	signifies free-stream conditions
Q	heat	$(\)_x$	signifies conditions upstream of normal shock
R	gas constant	$(\)_y$	signifies conditions downstream of normal shock
s	entropy per unit mass	$(\)_w$	signifies a quantity associated with a pressure wave
t	time		
T	absolute temperature		
v	specific volume		
V	velocity		

5.2. Governing Relations of the Normal Shock

Physical Equations. Suppose that conditions on the upstream and downstream sides of the discontinuity are denoted respectively by subscripts x and y (Fig. 5.2). Then, since there is no heat transfer across the control surface, the steady-flow energy equation may be written in the form

$$h_x + \frac{V_x^2}{2} = h_y + \frac{V_y^2}{} = h_0 \quad (5.1)$$

where h_0 is the stagnation enthalpy on both sides of the shock.

The cross-sectional areas must be the same on both sides of the discontinuity. From the equation of continuity, therefore,

$$\frac{w}{A} = \rho_x V_x = \rho_y V_y \quad (5.2)$$

Application of the momentum theorem to the flow through the discontinuity yields

$$p_x - p_y = \frac{w}{A} (V_y - V_x) \quad (5.3)$$

Combination of Eqs. 5.2 and 5.3 then gives

$$p_x + \rho_x V_x^2 = p_y + \rho_y V_y^2 \quad (5.4)$$

The equation of state of the fluid may be written implicitly in the form

$$h = h(s, \rho) \quad (5.5a)$$

$$s = s(p, \rho) \quad (5.5b)$$

The Fanno Line. Let us fix all conditions at section x and inquire as to the conditions at section y .

The energy equation (Eq. 5.1), the continuity equation (Eq. 5.2), and the equations of state (Eq. 5.5) together define a locus of states passing through point x , a locus which in the h - s diagram of Fig. 5.3 is called the *Fanno line*.

For example, if a particular value of V_y is chosen, then ρ_y may be computed from Eq. 5.2, h_y may be computed from Eq. 5.1, and s_y may be found from Eq. 5.5a. By repeating this calculation for vari-

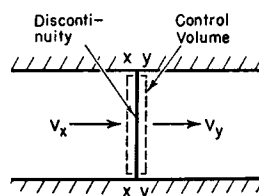


Fig. 5.2. Control surface around a normal discontinuity.

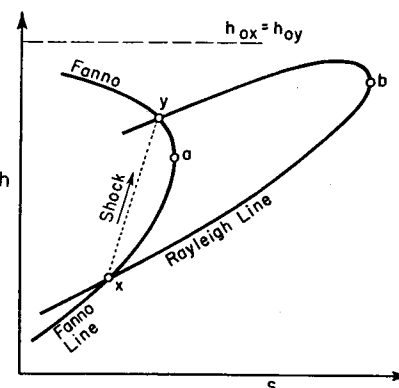


Fig. 5.3. Fanno line and Rayleigh line.

Art. 5.2 GOVERNING RELATIONS OF THE NORMAL SHOCK

ous values of V_y , the Fanno line may easily be constructed. Since the momentum equation has not yet been introduced, the Fanno line represents states with the same flow per unit area and the same stagnation enthalpy, but not necessarily with the same value of the impulse function. Thus, in general, frictional effects are required to pass continuously along the Fanno line from state x to any other state on the line.

The Rayleigh Line. We next consider the locus of states passing through point x which are defined by the momentum equation (Eq. 5.4), the continuity equation (Eq. 5.2), and the equation of state (Eq. 5.5). To compute this locus, we first select a particular value of V_y ; then ρ_y may be computed from Eq. 5.2, p_y may be computed from Eq. 5.4, and s_y may be found from Eq. 5.5. By repeating these calculations for various values of V_y , the locus of possible states reachable from state x , while satisfying Eqs. 5.4, 5.2 and 5.5, may be plotted on the diagram. The resulting curve is called the *Rayleigh line*. Since states on the Rayleigh line have, in general, different stagnation enthalpies, they are reachable from each other by continuous changes along the Rayleigh line only through heat transfer effects.

At this point it is well to state that the introduction of the Rayleigh and Fanno lines in the present discussion is not meant to imply that the shock process occurs along either or both of these curves. Rather they are introduced because they help to explain graphically certain peculiar features of normal shocks, and also because we shall later find them of use in discussing a number of other one-dimensional flow processes.

The normal shock itself must satisfy Eqs. 5.1, 5.2, 5.4, and 5.5 simultaneously. For a given state x , therefore, the end state of the normal shock must lie on both the Fanno line and Rayleigh line passing through x . Hence the intersection of the two lines at point y represents the conditions at the downstream side of the discontinuity corresponding to the prescribed conditions at section x .

Consider now an infinitesimal process in the neighborhood of the point of maximum entropy (point a) on the Fanno line. For such a process, Eq. 5.1 becomes

$$dh + d(V^2/2) = 0$$

or

$$dh + V dV = 0 \quad (5.6)$$

Similarly, the continuity equation becomes

$$d(\rho V) = 0$$

or

$$\rho dV + V d\rho = 0 \quad (5.7)$$

From the thermodynamic relation

$$T ds = dh - dp/\rho$$

we see that at point a ,

$$dh = dp/\rho \quad (5.8)$$

Combining Eqs. 5.6, 5.7, and 5.8, and noting that there is no entropy change for the infinitesimal process under consideration, we arrive at

$$V = \sqrt{(\partial p/\partial \rho)_s} \quad (5.9)$$

The right-hand side represents the local sound velocity; consequently, we conclude that the Mach Number is unity at point a .

In similar fashion it may be demonstrated that $M = 1$ at the point of maximum entropy, point b , on the Rayleigh line. It may also be shown that the upper branches of the Fanno and Rayleigh lines represent subsonic speeds, and the lower branches supersonic speeds.

Direction of Shock Wave. The analysis thus far given places no restriction on the direction of the process, that is, whether from x to y , or from y to x . For all fluids thus far investigated, however, point y on Fig. 5.3 lies to the right of point x . According to the Second Law of Thermodynamics, the entropy may not decrease during an adiabatic change. Hence, only the change from x to y is possible. In other words, the normal discontinuity always involves a change from supersonic to subsonic speed with a consequent pressure rise, and never the reverse. This conclusion will, in the following article, be demonstrated rigorously for a perfect gas.

5.3. Normal Shock in a Perfect Gas

For a given fluid and for a given state x upstream of the shock, Eqs. 5.1, 5.2, 5.4, and 5.5 suffice to permit the calculation of fluid properties at state y . However, simple relations connecting the properties on the two sides of the shock cannot be derived unless a simple equation of state in algebraic form is employed. We turn now, therefore, to the special case of a perfect gas.

Governing Equations. The energy equation, Eq. 5.1, may be written in the case of a perfect gas as

$$c_p T_x + \frac{V_x^2}{2} = c_p T_y + \frac{V_y^2}{2} = c_p T_0 \quad (5.10a)$$

or

$$T_{0x} = T_{0y} \quad (5.10b)$$

Consequently, all the adiabatic formulas of Art. 4.3 are applicable to states x and y . Furthermore, states x and y have the same adiabatic

values of T^* and therefore the same adiabatic values of c^* and of c_0 . Using the adiabatic relation between T_0 , T , and M , Eq. 5.10b takes the form

$$\frac{T_y}{T_x} = \frac{1 + \frac{k-1}{2} M_x^2}{1 + \frac{k-1}{2} M_y^2} \quad (5.11)$$

From the continuity expression, Eq. 5.2, and the relation $p = \rho RT$, we get

$$\frac{T_y}{T_x} = \frac{p_y \rho_x}{p_x \rho_y} = \frac{p_y}{p_x} \frac{V_y}{V_x}$$

This equation is now modified by introducing the definition of M and the formula for the sound speed in a perfect gas:

$$\frac{T_y}{T_x} = \frac{p_y}{p_x} \frac{M_y c_y}{M_x c_x} = \frac{p_y}{p_x} \frac{M_y}{M_x} \sqrt{\frac{T_y}{T_x}}$$

from which it follows that

$$\frac{T_y}{T_x} = \left(\frac{p_y}{p_x} \right)^2 \left(\frac{M_y}{M_x} \right)^2 \quad (5.12)$$

Combining Eqs. 5.11 and 5.12, we find the equation of the Fanno line in terms of p and M ,

$$\frac{p_y}{p_x} = \frac{M_x}{M_y} \frac{\sqrt{1 + \frac{k-1}{2} M_x^2}}{\sqrt{1 + \frac{k-1}{2} M_y^2}} \quad (5.13)$$

For a perfect gas, $\rho V^2 = kpM^2$. Hence the combined momentum and continuity relation, Eq. 5.4, yields the following form of the Rayleigh line equation in terms of p and M :

$$\frac{p_y}{p_x} = \frac{1 + kM_x^2}{1 + kM_y^2} \quad (5.14)$$

Finally, after eliminating p_y/p_x from Eqs. 5.13 and 5.14, we get a relation between M_x and M_y ,

$$\frac{M_x \sqrt{1 + \frac{k-1}{2} M_x^2}}{1 + kM_x^2} = \frac{M_y \sqrt{1 + \frac{k-1}{2} M_y^2}}{1 + kM_y^2} \quad (5.15)$$

Working Formulas. Upon squaring and algebraic rearrangement, Eq. 5.15 may be solved explicitly for M_y . Two solutions are obtained, namely,

$$M_y = M_x \quad (5.16a)$$

and

$$M_y^2 = \frac{\frac{M_x^2}{k-1} + \frac{2}{k-1}}{\frac{2k}{k-1} M_x^2 - 1} \quad (5.16b)$$

The first of these solutions is trivial since it expresses the obvious fact that conditions may be identical at sections x and y . Inspection of Eqs. 5.11 and 5.13 shows that, for the trivial solution, $p_y = p_x$ and $T_y = T_x$. The second solution indicates the connection which must subsist between the states on the two sides of the discontinuity. In the subsequent discussion attention is given to the discontinuity solution.

Substituting for M_y and M_x from Eq. 4.10 gives the following simple relation between M_x^* and M_y^* known as *Prandtl's equation*:

$$M_x^* M_y^* = 1 \quad (5.17a)$$

or, since $c_x^* = c_y^*$,

$$V_x^* V_y^* = c^*{}^2 \quad (5.17b)$$

From this it is evident that if the flow at x is supersonic, the flow at y must be subsonic, and vice versa.

To find the ratio of pressures fore and aft of the shock, we substitute Eq. 5.16b into Eq. 5.14, and thus obtain

$$\frac{p_y}{p_x} = \frac{2k}{k+1} M_x^2 - \frac{k-1}{k+1} \quad (5.18a)$$

An alternative form is

$$\frac{p_y - p_x}{\frac{1}{2} \rho_x V_x^2} = \frac{2}{k+1} \left(1 - \frac{1}{M_x^2}\right) \quad (5.18b)$$

Substituting the value of M_y^2 from Eq. 5.16b into Eq. 5.11, we get for the temperature ratio,

$$\frac{T_y}{T_x} = \frac{\left(1 + \frac{k-1}{2} M_x^2\right) \left(\frac{2k}{k-1} M_x^2 - 1\right)}{\frac{(k+1)^2}{2(k-1)} M_x^2} \quad (5.19)$$

The density ratio may be found in terms of M_x from Eqs. 5.18a and 5.19, and the perfect gas law,

$$\frac{\rho_y}{\rho_x} = \frac{p_y}{p_x} \sqrt{\frac{T_y}{T_x}} \quad (5.20)$$

and the velocity ratio follows from Eq. 5.2,

$$\frac{V_y}{V_x} = \frac{\rho_x}{\rho_y}$$

The ratio of stagnation pressures is a measure of the irreversibility in the shock process. It may be found by observing that

$$\frac{p_{0y}}{p_{0x}} = \frac{p_{0y}}{p_y} \frac{p_y}{p_x} \frac{p_x}{p_{0x}}$$

Now p_y/p_x is given by Eq. 5.18a, and p_{0y}/p_y and p_x/p_{0x} may be found from Eq. 4.14b. Using Eq. 5.16b for the value of M_y , we get, after algebraic simplification,

$$\frac{p_{0y}}{p_{0x}} = \left[\frac{\frac{k+1}{2} M_x^2}{1 + \frac{k-1}{2} M_x^2} \right]^{\frac{k}{k-1}} \sqrt{\left[\frac{2k}{k+1} M_x^2 - \frac{k-1}{k+1} \right]^{\frac{1}{k-1}}} \quad (5.21)$$

To evaluate the entropy change across the shock, we employ the perfect-gas formula,

$$s_y - s_x = c_p \ln \frac{T_y}{T_x} - R \ln \frac{p_y}{p_x} = c_p \ln \frac{T_y/T_x}{(p_y/p_x)^{\frac{k-1}{k}}} \quad (5.22)$$

Also, since

$$\frac{T_0}{T} = 1 + \frac{k-1}{2} M^2$$

and

$$\frac{p_0}{p} = \left(1 + \frac{k-1}{2} M^2\right)^{\frac{k}{k-1}}$$

we get an alternative expression for the entropy change in terms of stagnation temperatures and isentropic stagnation pressures,

$$s_y - s_x = c_p \ln \frac{T_{0y}/T_{0x}}{(p_{0y}/p_{0x})^{\frac{k-1}{k}}} \quad (5.23)$$

In the present case, $T_{0y} = T_{0x}$, so that

$$\frac{s_y - s_x}{R} = - \ln \frac{p_{0y}}{p_{0x}}$$

or, after substituting the value of p_{0y}/p_{0x} given in Eq. 5.21,

$$\frac{s_y - s_x}{R} = \frac{k}{k-1} \ln \left[\frac{2}{(k+1)M_x^2} + \frac{k-1}{k+1} \right] + \frac{1}{k-1} \ln \left[\frac{2k}{k+1} M_x^2 - \frac{k-1}{k+1} \right] \quad (5.24)$$

Impossibility of a Rarefaction Shock. Careful study of Eq. 5.24 indicates that for gases with $1 < k < 1.67$ the entropy change is always positive when M_x is greater than unity, and is always negative when M_x

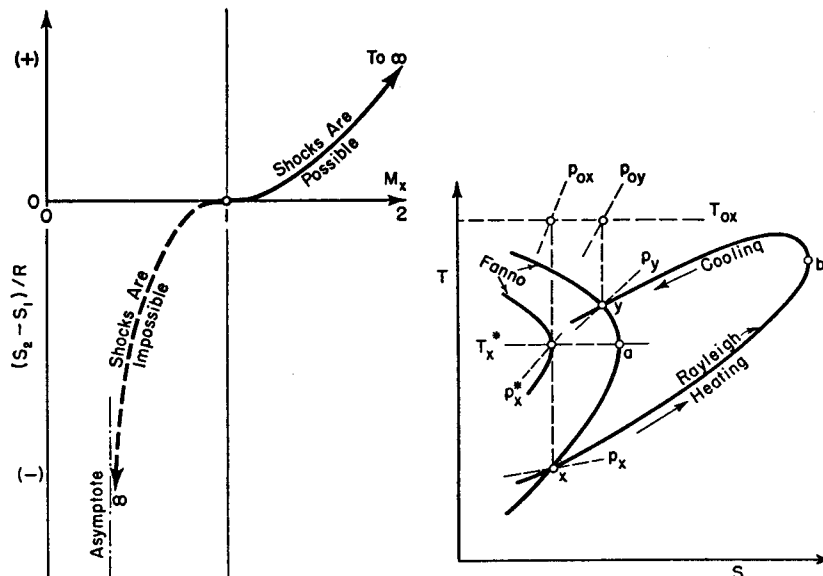


FIG. 5.4. Entropy change across normal discontinuity.

FIG. 5.5. Illustrating the impossibility of a rarefaction shock.

is less than unity. The general form of Eq. 5.24 is shown graphically in Fig. 5.4. It is thus proven rigorously that for a perfect gas only the shock from supersonic to subsonic speed is possible.

The irreversibility of the normal shock for perfect gases can also be demonstrated with the help of the temperature-entropy diagram, Fig. 5.5. Since, for a perfect gas, the enthalpy is a linear function of temperature, the Fanno and Rayleigh curves of Fig. 5.5 are similar to the corresponding curves of Fig. 5.3. Continuous processes which follow

the Rayleigh line involve reversible heat transfer. Imagine that state y is reached reversibly from state x by adding heat at constant area along the Rayleigh line from x to b and then rejecting heat from b to y . Since the process is reversible, the area under the curve on the T - s diagram represents the net heat transfer, i.e.,

$$Q_{\text{rev}} = \int T \, ds$$

Now, since the stagnation temperatures are the same at x and y , the net heat transfer for the process considered must be zero, and, consequently, the net area under the curve xyb must be zero. The heating from x to b is at low temperatures, and the cooling from b to y is at high temperatures. Hence state y must have a greater entropy than state x .

Since s_y must exceed s_x , the equation preceding Eq. 5.24 leads to the important conclusion that there is always a decrease in isentropic stagnation pressure across a shock wave.

The Rankine-Hugoniot Relation. An interesting relation connecting the pressure ratio and density ratio is known as the *Rankine-Hugoniot equation*. Substituting the value of M_y^2 from Eq. 5.16b into Eq. 5.11, we obtain, after algebraic rearrangement,

$$\frac{T_y}{T_x} = \frac{\frac{p_y}{p_x} \left[1 + \left(\frac{k-1}{k+1} \right) \frac{p_y}{p_x} \right]}{\frac{p_y}{p_x} + \frac{k-1}{k+1}} \quad (5.25)$$

Then, using Eq. 5.20, we find that

$$\frac{\rho_y}{\rho_x} = \frac{\left(\frac{k+1}{k-1} \right) \frac{p_y}{p_x} + 1}{\frac{p_y}{p_x} + \frac{k+1}{k-1}} \quad (5.26)$$

or, solving for p_y/p_x ,

$$\frac{p_y}{p_x} = \frac{\left(\frac{k+1}{k-1} \right) \frac{p_y}{p_x} - 1}{\frac{k+1}{k-1} - \frac{\rho_y}{\rho_x}} \quad (5.27)$$

This relation is plotted in Fig. 5.6, together with the isentropic relation between pressure and density ($p \propto \rho^k$). It is seen that for diatomic gases the density can at most increase by a factor of six, whereas the

pressure ratio may reach infinity. The curves indicate another important feature, namely that *weak shocks are nearly isentropic*; by "weak shock" we mean a shock in which the percentage rise in pressure is small.

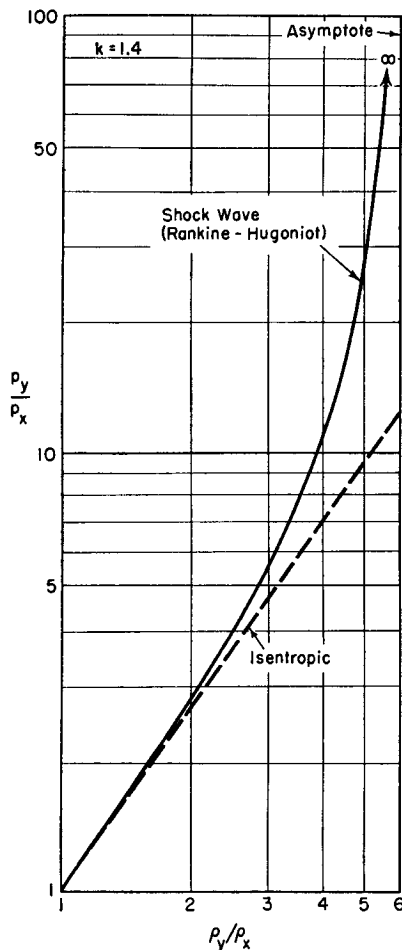


FIG. 5.6. The Rankine-Hugoniot curve, for $k = 1.4$.

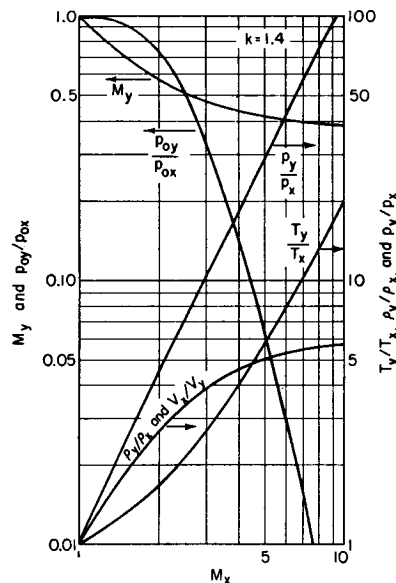


FIG. 5.7. Working curves for normal shock, for $k = 1.4$.

5.4. Working Formulas, Curves, and Tables

As in the case of isentropic flow, it is convenient to regard the Mach Number M_x as the foremost parameter of the normal shock equations. Then, for any chosen value of M_x , the corresponding values of M_y , p_y/p_x , T_y/T_x , ρ_y/ρ_x , V_y/V_x , and p_{0y}/p_{0x} are easily computed from the equations of Art. 5.3.

Fig. 5.7 gives the important shock relations in graphical form for a gas with $k = 1.4$.

To facilitate extensive or accurate numerical calculations, the normal shock functions are tabulated in Table B.3 for $k = 1.4$.

Illustrative Example. The use of the tables is best explained by means of a sample problem.

PROBLEM. A stream of air with a Mach Number of 2, pressure of 10 psia, and temperature of 30°F passes through a normal shock. Calculate the final velocity and stagnation pressure.

SOLUTION. We are given

$$M_x = 2; \quad p_x = 10 \text{ psia}; \quad T_x = 489.7^\circ\text{R}$$

From Table B.2 (isentropic flow) we find, at $M_x = 2$

$$\left(\frac{p_x}{p_{0x}}\right) = 0.1278; \quad \therefore \quad p_{0x} = \frac{10}{0.1278} = 78.4 \text{ psia}$$

Also, since

$$c_x = 49.1\sqrt{T_x} = 49.1\sqrt{489.7} = 1087 \text{ ft/sec}$$

it follows that

$$V_x = M_x c_x = 2(1087) = 2174 \text{ ft/sec}$$

Now, from Table B.3, at $M_x = 2.00$,

$$V_z/V_y = 2.667; \quad p_{0y}/p_{0x} = 0.7209$$

whence

$$V_y = 2174/2.667 = 815 \text{ ft/sec}$$

$$p_{0y} = (78.4)(0.7209) = 56.5 \text{ psia}$$

5.5. Weak Shock Waves

Certain important features of shock waves may be illuminated by working out special relations for shocks of small strength.

Strength of Shock Wave. Let us define the *strength of a shock wave* as the ratio of the pressure increase to the initial pressure, i.e.,

$$P = \frac{p_y - p_x}{p_x} = \frac{p_y}{p_x} - 1 \quad (5.28)$$

Rearrangement of Eq. 5.18a yields

$$P = \frac{2k}{k+1} (M_x^2 - 1) \quad (5.29)$$

Also, from the Rankine-Hugoniot relation, Eq. 5.27,

$$P = \frac{\frac{2k}{k-1} \left(\frac{\rho_y}{\rho_x} - 1 \right)}{\frac{2}{k-1} - \left(\frac{\rho_y}{\rho_x} - 1 \right)} \quad (5.30)$$

From Eq. 5.29 it appears that the term $(M_x^2 - 1)$ is directly proportional to the shock strength. If the shock is relatively weak, Eq. 5.30 indicates that the ratio of density increase to initial density,

$$\left(\frac{\rho_y}{\rho_x} - 1 \right)$$

is also approximately proportional to the shock strength. Hence $(M_x^2 - 1)$ and the percentage increase in density may be chosen as alternative measures of shock strength.

Shock of Vanishing Strength. Suppose that the shock strength approaches zero. Then, from Eq. 5.29, the value of M_x approaches unity. Furthermore, from Eqs. 5.16b and 5.30, M_y approaches unity, and the density change across the shock approaches zero. A shock of infinitesimal strength is therefore identical with a sound wave. Since M_x is unity for such a shock, it follows that a very weak pressure disturbance travels with the speed of sound with respect to the fluid in which it is propagating. This same conclusion was reached in Chapter 3. An infinitesimal plane pressure wave is, therefore, the limiting case of a normal shock. The shock itself travels with a speed greater than the speed of sound in the fluid into which it is propagating, the ratio of the two speeds being M_x .

Irreversibility of Weak Shock. It is of interest to examine the irreversibility associated with a weak shock of finite strength. The irreversibility will be measured in terms of the entropy increase in passing through the shock.

Rearrangement of Eq. 5.26 yields

$$\frac{\rho_y}{\rho_x} = \frac{1 + \frac{k+1}{2k} P}{1 + \frac{k-1}{2k} P}$$

Now, from Eq. 2.32b,

$$\frac{s_y - s_x}{c_v} = \ln \left[\left(\frac{\rho_y}{\rho_x} - 1 \right) + 1 \right] - k \ln \frac{\rho_y}{\rho_x}$$

Inserting the previous expression for ρ_y/ρ_x , we find

$$\frac{s_y - s_x}{c_v} = \ln (1 + P) - k \ln \left(1 + \frac{k+1}{2k} P \right) + k \ln \left(1 + \frac{k-1}{2k} P \right) \quad (5.31)$$

Now, for weak shocks, each of the terms on the right-hand side of Eq. 5.31 is of the form

$$\ln (1 + \epsilon)$$

where ϵ is much smaller than unity. We therefore employ for each term the series expansion

$$\ln (1 + \epsilon) = \epsilon - \frac{\epsilon^2}{2} + \frac{\epsilon^3}{3} - \frac{\epsilon^4}{4} + \dots$$

Carrying out these operations and simplifying, we find that the first-order and second-order terms in the shock strength vanish, leaving

$$\frac{s_y - s_x}{c_v} = \frac{k^2 - 1}{12k^2} P^3 - \frac{k^2 - 1}{8k^2} P^4 + \dots \quad (5.32a)$$

or

$$\frac{s_y - s_x}{R} = \frac{k+1}{12k^2} P^3 - \frac{k+1}{8k^2} P^4 + \dots \quad (5.32b)$$

In terms of $(M_x^2 - 1)$, we find by substituting Eq. 5.29 into Eq. 5.32b that the entropy increase is given by

$$\frac{s_y - s_x}{R} = \frac{2}{3} \frac{k}{(k+1)^2} (M_x^2 - 1)^3 - \frac{2k^2}{(k+1)^2} (M_x^2 - 1)^4 + \dots \quad (5.33)$$

Thus, for weak shocks, the entropy increase is of the third order with respect to the shock strength. As a first approximation, therefore, the irreversibility connected with weak shocks may be ignored, and the isentropic relation between pressure and density may be used for connecting the states on both sides of the shock.

This result explains why in Fig. 5.6 the isentropic curve and Rankine-Hugoniot curve have the same slope and the same radius of curvature at the lower left-hand corner of the chart. It explains also why in Fig. 5.7 there is scarcely any loss in stagnation pressure across the shock for initial Mach Numbers less than about 1.25.

5.6. Formation of Shock Waves

We have seen from the Second Law of Thermodynamics that a compression shock involves an entropy increase (or a loss in stagnation pressure), and that rarefaction shocks are impossible. Two questions come naturally to mind: (i) what are the mechanical reasons underlying

the appearance in nature of compression shocks and the impossibility of rarefaction shocks? and (ii) what are the dissipative phenomena in a shock leading to an entropy increase? The first of these questions is answered in this article, and the second in Art. 5.7.

To explain in the simplest manner the physical mechanism leading to compression shocks, we shall adopt the point of view of Art. 3.2. There we regarded each element of surface bounding a fluid stream as pushing the neighboring fluid out of its way and thereby propagating a pressure pulse into the fluid. It is also necessary to point out that a steady-state flow is always arrived at through a series of transient flows which asymptotically approach the steady-state condition after a long period of time. Therefore, in order to explain the existence of shock waves in a duct or attached to a moving body, it is necessary to examine the way in which the steady-state condition is achieved from a condition of no motion.

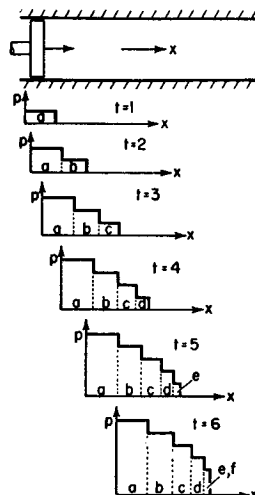


FIG. 5.8. Wave fronts formed at successive times as piston accelerates rightward by a series of equally spaced impulses.

each pair of impulsive accelerations. Each successive pressure wave produced follows the laws derived in Art. 3.2.

In Fig. 5.8 the pressure distribution in the duct is shown schematically at various times after the beginning of motion. The position of the vertical axis on each chart indicates the instantaneous location of the piston. After the first impulsive acceleration of the piston, i.e., at $t = 1$, the pressure wave (shown as a vertical front) has moved down the duct a short distance and influenced the mass of gas labeled "a." The gas mass "a" is therefore at a slightly increased pressure and is moving to the right with the velocity of the piston. Between $t = 1$ and $t = 2$, the mass "a" receives a further increase in pressure and velocity from the second acceleration of the piston, and the original wave travels along the duct and imparts a pressure and velocity pulse to mass "b." This process continues as each of the pressure waves travels downstream and as fresh waves are initiated by successive piston accelerations.

Now each of these pressure waves travels with the *local* speed of sound *relative* to the fluid through which it is passing. But the masses nearer the piston have forward motions greater than those further from the piston. Moreover, since the process is isentropic, the masses nearer the piston have greater sound velocities by virtue of the higher temperatures associated with their greater pressures. Consequently, the pressure waves nearer the piston tend to overtake those further from the piston. For example, referring to $t = 3$, the wave in mass "a" travels faster than the wave in mass "b," because "a" is moving faster to the right and also because the velocity of sound in "a" is greater than the velocity of sound in "b."

The net result of this process is that the wave profile becomes steeper and steeper, until, at $t = 6$, the pressure gradient becomes infinite. Thus, at $t = 6$, a small compression shock has been formed, a shock which grows in strength as the process continues.

A similar analysis applied to a leftward motion of the piston, i.e., for an expansion wave, indicates that expansion waves become less steep with the passage of time. Thus, because of the nonlinearity of finite wave motion, compression waves become steeper and ultimately form a discontinuity, while expansion waves spread out and thus are unable to support a discontinuity.

These results are summarized in Fig. 5.9, showing successive appearances of a wave form of constant total pressure change, corresponding

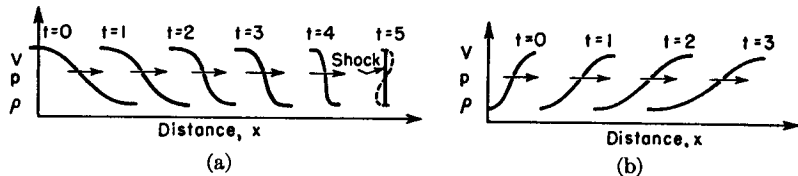


FIG. 5.9. Development of wave form of constant strength.

- (a) Compression wave.
(b) Expansion wave.

to the case where the piston accelerates to a constant speed and then moves at constant velocity; this is analogous to the case of a projectile starting from rest and accelerating to a constant final speed. The wave form at a given instant is defined as the curve of some fluid property (say p , ρ , or V) plotted against distance x .

STEEPENING OF COMPRESSION WAVES. The compression wave, Fig. 5.9a, becomes ever steeper as it propagates rightward, until, between $t = 4$ and $t = 5$, it tends to become infinitely steep at some point. The present analysis then ceases to be valid because viscous and heat conduction effects are no longer negligible in the face of such extraordinary gradients in velocity and temperature. Indeed, if the isentropic analysis

were continued to $t = 5$, the wave would "topple over" to the form shown by the dashed line; this is physically absurd, as it means that at the same time and location the fluid has simultaneously three different values of pressure, velocity, and density. Viscous and heat conduction effects intervene soon after $t = 4$ and act to produce a stationary shock wave of unchanging form.

SPREADING OF RAREFACTION WAVES. The rarefaction wave, Fig. 5.9b, becomes ever less steep as it propagates rightward, and so no discontinuity effects are observed. Indeed, if a rarefaction shock were momentarily established, the dynamic effects outlined here would cause the shock to decay immediately into a continuous expansion wave.

THE SURF ANALOGY. A similar phenomenon may be seen at ocean beaches. As an incoming gravity wave approaches the shore, the front part of the wave (corresponding to compression) is seen to steepen, and

the rear part (corresponding to rarefaction) is seen to spread out. In this case, however, the geometry of the flow permits the forward part to tumble over, as in Fig. 5.9a, $t = 5$; this tumbling over produces the well-known ocean "breakers."

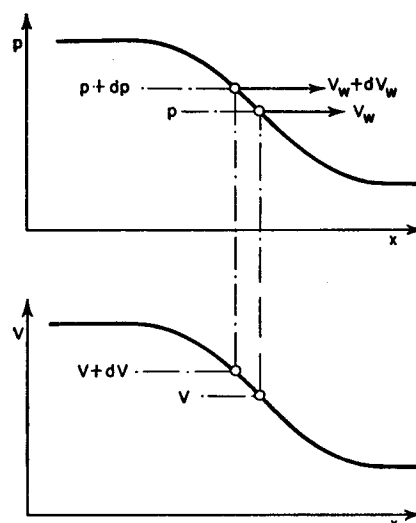


FIG. 5.10. Illustrates analysis on development of wave form.

magnitude by dV , dp , $d\rho$, dc , etc. The respective parts of the wave passing through these same points differ in wave speed by the amount dV_w . Since a finite wave may be thought of as a succession of infinitesimal pressure pulses, each element of the wave may be analyzed as in Art. 3.2. As long as the velocity and temperature gradients are moderate, experience confirms the assumption that longitudinal viscous and heat conduction effects are negligible. Consequently each elementary part of the wave travels at the *local* speed of sound with respect to the fluid in which it is propagating. The propagation velocity of a

part of the wave with respect to fixed coordinates is, therefore,

$$V_w = V + c$$

and the propagation velocity of an adjacent part of the wave is

$$V_w + dV_w = (V + dV) + (c + dc)$$

whence it follows that

$$dV_w = dV + dc \quad (5.34a)$$

We are interested in whether adjacent parts of the wave travel at the same or different speeds. Therefore we form the ratio

$$\frac{dV_w}{dp} = \frac{dV}{dp} + \frac{dc}{dp} \quad (5.34b)$$

From the analysis of Art. 3.2 we obtain, for a rightward-moving wave,

$$\frac{dV}{dp} = \frac{1}{\rho c} \quad (5.35)$$

Furthermore, since each particle of fluid undergoes isentropic changes, and we assume that the entire fluid was originally at rest with uniform pressure and temperature, the increments in pressure and density between adjacent fluid particles obey the relation

$$c^2 = \frac{dp}{d\rho}$$

Differentiating with respect to p , we have

$$2c \frac{dc}{dp} = \frac{d}{dp} \left(\frac{dp}{d\rho} \right) = \left(\frac{dp}{d\rho} \right) \frac{d}{dp} \left(\frac{dp}{d\rho} \right) \quad (5.36)$$

Substituting Eqs. 5.35 and 5.36 into Eq. 5.34b, we obtain

$$\frac{dV_w}{dp} = \frac{1}{\rho c} \left[1 + \frac{\rho}{2} \frac{d}{dp} \left(\frac{dp}{d\rho} \right) \right]_s \quad (5.37a)$$

By definition, $\rho = 1/v$, where v is the specific volume. Hence

$$\frac{d}{dp} = \frac{dv}{dp} \frac{d}{dv} = -\frac{1}{\rho^2} \frac{d}{dv} = -v^2 \frac{d}{dv}$$

Applying this transformation to Eq. 5.37a, we obtain

$$\frac{dV_w}{dp} = -\frac{v^2}{2c} \frac{(d^2p/dv^2)_s}{(dp/dv)_s} \quad (5.37b)$$

For a fluid to be thermodynamically stable (i.e., if it is not to collapse or expand catastrophically), $(dp/dv)_s$ must be negative. Hence, the isentrope must have a negative slope on the pressure-volume diagram. Consequently, the sign of dV_w/dp depends exclusively on the sign of $(d^2p/dv^2)_s$, that is, on whether the isentrope on the pressure-volume diagram is concave upwards or concave downwards.

CRITERIA FOR CHANGE IN WAVE SHAPE. Now, if dV_w/dp is positive, the higher-pressure parts of the wave overtake the lower-pressure parts, and a compression wave steepens as it progresses; similarly, a rarefaction wave becomes less steep. But if dV_w/dp is negative, a compression wave becomes less steep and a rarefaction wave steepens into a compression shock. From these considerations we arrive at the following criteria:

- (i) Compression waves steepen and expansion waves flatten when $(d^2p/dv^2)_s > 0$ (5.38a)

- (ii) Compression waves flatten and expansion waves steepen when $(d^2p/dv^2)_s < 0$ (5.38b)

The shapes of the isentropes corresponding to these two criteria are illustrated in Fig. 5.11.

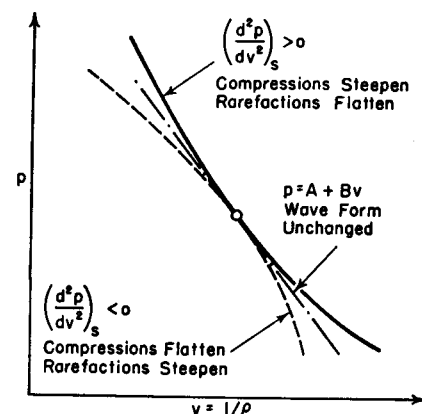


FIG. 5.11. Criteria for steepening or flattening of compression and rarefaction waves in terms of curvature of p - v isentrope.

GAS WITH UNCHANGING WAVE SHAPE. When the isentropic pressure-density relation has a special form, waves of finite amplitude propagate through the gas with unchanged shape. According to Eq. 5.38, this occurs when

$$\left(\frac{d^2p}{dv^2}\right)_s = 0$$

Integrating twice, we obtain

$$p = A + Bv$$

as the unique isentropic relation for unchanging wave shape, where A and B are constants. This p - v isentrope is a straight line on the p - v diagram of Fig. 5.11 and marks the dividing line in curvature between gases in which compression waves steepen and gases in which they flatten.

PERFECT GAS. In a perfect gas, pv^k is constant during an isentropic process. By differentiating twice it is found that

$$\left(\frac{d^2p}{dv^2}\right)_s = \frac{k(k+1)p}{v^2}$$

Since k is positive for all known gases, it follows from Eq. 5.38a that in a perfect gas compression waves steepen and rarefaction waves flatten.

LIQUIDS. The isentropic relation for liquids may usually be represented at moderate pressures by

$$v \left(\frac{dp}{dv}\right)_s = -\beta$$

where β is positive and nearly constant. Differentiating, we get

$$\left(\frac{d^2p}{dv^2}\right)_s = \frac{\beta}{v^2}$$

Comparing this with Eq. 5.38a, we conclude that, in liquids obeying the law of constant β , compression waves steepen and expansion waves flatten.

OTHER FLUIDS. No example has yet been adduced of a real fluid obeying Eq. 5.38b. However, there seems to be no basic principle forbidding the existence of such a fluid. Possibly certain fluids in the neighborhood of the critical pressure and temperature can exhibit stationary rarefaction shocks.

5.7. Thickness of Shock Waves

We now turn to the question of how dissipative effects account for the entropy increase in a shock wave.

In the foregoing article we saw that, in the absence of viscosity and heat conduction, compression waves tend to become infinitely steep. The analysis underlying this result was based on a form of the equation of motion containing only pressure and inertia forces. However, as the wave becomes very steep, viscous stresses must inevitably become appreciable, no matter how small the coefficient of viscosity. Moreover, heat conduction effects must inevitably become substantial, no matter how small the coefficient of thermal conductivity, and so a particle of fluid undergoes nonadiabatic effects.

Since viscous and heat conduction effects tend to wipe out discontinuities in velocity and temperature, they tend also to resist the steepening of a compression wave. From this it follows that the thickness of a shock wave is in part controlled by viscous and heat conduction effects.

In short, when a compression wave has reached a stationary form, the spreading influences of viscosity and heat conduction just balance the steepening influence of pressure and inertia forces.

Order-of-Magnitude Considerations. The ideas outlined above lead to a simple estimate of the order of magnitude of the shock thickness. In a shock of stationary form, the pressure, viscous, and inertia terms in the equation of motion must all be of comparable magnitude.

Physical considerations dictate that the stationary shock have a form like that of Fig. 5.12. The velocity curve approaches the end values V_x and V_y asymptotically, and so the thickness is actually infinite. However, virtually the entire change in velocity occurs in a very short distance. It is convenient, therefore, to define a characteristic shock thickness δ as shown by the sketch, or,

$$\delta = \frac{V_x - V_y}{(dV/dx)_{\max}}$$

Now, since the longitudinal viscous stress must be of the same order of magnitude as the inertia stress,

$$\frac{4}{3} \mu^* \frac{d}{dx} \left(\frac{dV}{dx} \right) \cong \rho^* V^* \frac{dV}{dx}$$

or, evaluating the derivatives in order-of-magnitude fashion, and assuming $\frac{4}{3} \cong 1$

$$\mu^* \frac{(V_x - V_y)/\delta}{\delta} \cong \rho^* V^* \frac{V_x - V_y}{\delta}$$

from which we get

$$\text{Rey}_{\text{shock}} \equiv \frac{\rho^* V^* \delta}{\mu^*} \cong 1$$

which says that the Reynolds Number of the shock, based on the thickness δ and on the fluid properties at T^* is of the order of magnitude of unity.

By introducing certain further relations from the kinetic theory of gases, it may be shown that, in respect to order of magnitude,

$$\frac{\delta}{l^*} \cong \frac{5}{8} \text{Rey}$$

where l is the mean free molecular path. Thus it follows that the shock thickness is of the order of the mean free path. Thermodynamic equilib-

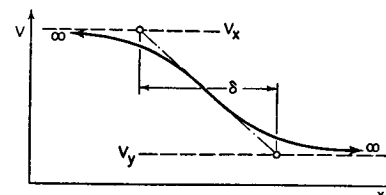


FIG. 5.12. Definition of shock thickness.

rium does not prevail within a shock, therefore, and the analysis of a shock from continuum considerations at best gives approximate results for the shock structure. Kinetic theory or even quantum mechanics may be necessary for an adequate analysis.

Shock Thickness in Perfect Gas. The structure of the shock wave may be investigated more fully by solving the exact Navier-Stokes equation and the exact energy equation for such a dissipative, one-dimensional region. The results of such studies are more accurate than the order-of-magnitude result reached above but are nonetheless subject to the same weakness of being based on the assumption of a continuum.

A formula showing a shock thickness Reynolds Number as a function of Mach Number, Prandtl Number, specific-heat ratio, and viscosity-temperature variation has been derived by Shapiro and Kline.⁽¹⁾ It has the form

$$\frac{\rho_x c_x \delta}{\mu_x} = \frac{D}{(k+1)M_x^*} \cdot \frac{M_x^* + 1}{M_x^* - 1} \left[\left(\frac{k+1}{2} \right) \left(1 - \frac{k-1}{k+1} M_x^{*2} \right) \right]^{1-n} \left[1 \pm \sqrt{1 + \frac{8k(k+1)}{3Pr^*} \frac{1}{D^2} \frac{(M_x^* - 1)^2}{M_x^*}} \right] \quad (5.39a)$$

where

$$D = \frac{4}{3} + \frac{2k}{Pr^*} - \frac{k+1}{2Pr^*} \frac{M_x^{*2} + 1}{M_x^*} \quad (5.39b)$$

and where n is the exponent in a viscosity-temperature relationship of the form $\mu \sim T^n$ (from kinetic theory, $n = \frac{1}{2}$ for perfect gases; for air, experimental values yield $n = 0.768$ at ordinary temperatures). The symbol Pr^* denotes the value of the Prandtl Number at the temperature T^* . When D is positive, the plus sign in Eq. 5.39a is used; when D is negative, the minus sign.

VERY WEAK SHOCKS. When M_x^* approaches unity, Eq. 5.39a may be approximated by

$$\left(\frac{\rho_x c_x \delta}{\mu_x} \right)_{M_x^* \rightarrow 1} \cong \frac{4}{k+1} \left(\frac{4}{3} + \frac{k-1}{Pr^*} \right) \frac{1}{M_x^* - 1} \quad (5.39c)$$

Hence the thickness of weak shocks is inversely proportional to the strength of the shock if we choose the strength to be measured by $(M_x^* - 1)$. Even for extremely weak shocks, however, the shock thickness at normal pressure and temperature is extremely small compared with the dimensions of physical objects, as may be seen from Fig. 5.14.

TABLE OF SHOCK THICKNESSES. Using constants corresponding to air ($k = 1.4$, $Pr^* = \frac{3}{4}$, and $n = 0.768$), Eqs. 5.39a and b yield the values shown in the following table for the shock thickness parameter.

Also shown are order-of-magnitude values for the ratio of shock thickness to the mean free molecular path at state x .

M_x^*	M_x	$\rho_x c_x \delta / \mu_x$	δ / l_x
1.36	1.5	8.0	4
1.63	2	4.6	2
1.96	3	3.1	2
2.14	4	2.9	2
2.24	5	2.9	2
2.30	6	2.9	2
2.33	7	3.0	2
2.36	8	3.1	2
2.38	9	3.3	2
2.39	10	3.4	2
2.45	∞	∞	∞

In the range where measurements of shock thickness have been made (up to about $M_x = 1.5$), Eq. 5.39a is in excellent agreement with experi-

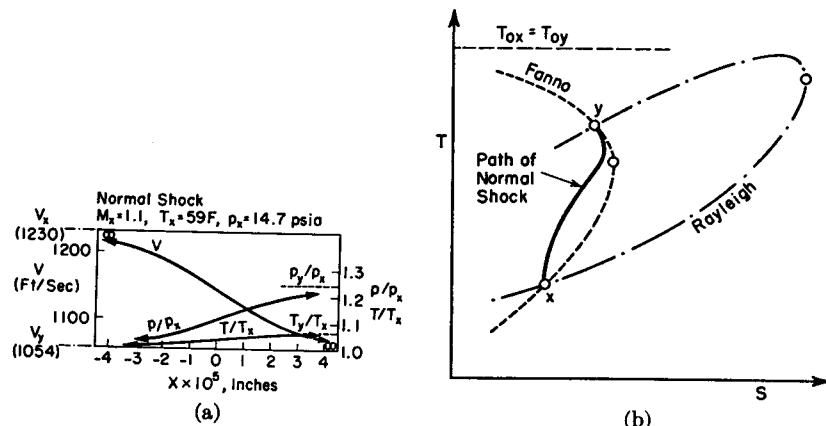
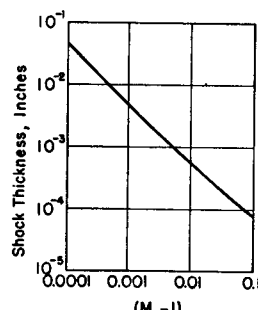


FIG. 5.13. Variation of fluid properties in a normal shock.

mental observation for monatomic gases such as argon, and underestimates the shock thickness by about 25% for diatomic gases like nitrogen.

Fig. 5.13a shows typical velocity, temperature, and pressure distributions in a weak shock wave. The corresponding course of thermodynamic states is shown in the temperature-entropy diagram of Fig. 5.13b, which indicates that entropy decreases occur near the end of the wave. The thickness of a compression shock at normal atmospheric pressure and temperature (Fig. 5.14) is extraordinarily small, thus justifying the treatment of the shock as a discontinuity for most practical computations.

FIG. 5.14. Thickness of a normal shock at standard atmospheric pressure and temperature.



5.8. Normal Shocks in Ducts

When the pressures at the entrance and exit of a duct in which a gas flows supersonically are adjusted so that a compression shock appears in the duct, the latter is found to be radically different from a plane discontinuity. This difference arises as the result of an interaction between the shock wave and the boundary layer on the walls of the duct.

The phenomenon in its details is most complicated, but the outstanding physical features can be readily explained. The normal shock in the core of the stream imposes an extraordinarily large adverse pressure gradient on the stream as a whole. As the boundary layer flow has been retarded by wall friction, however, it does not have sufficient momentum to negotiate this adverse pressure gradient. Consequently, apart from the thickening of the boundary layer produced by the adverse pressure gradient, there is often a back flow in the boundary layer near the shock. This back flow produces a separation of the stream from the walls.

The boundary layer effects described above lead to oblique shock waves in the pattern, and consequently the flow is far from one-dimensional.

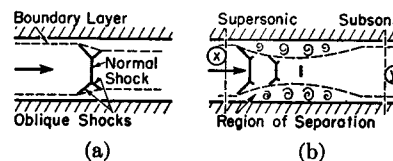


FIG. 5.15. Typical shock-boundary layer interactions in a duct.

(a) Thin boundary layer and weak shock.
(b) Thick boundary layer and strong shock.

Typical Experimental Results. Typical flow patterns are shown in Fig. 5.15. When the shock is weak and the boundary layer thin, as might be the case slightly downstream of the throats of supersonic



FIG. 5.16. Schlieren photographs of compression shock in a duct, with flow from left to right (M.I.T. Gas Turbine Laboratory).

(a) Moderately thick boundary layer. The light, diamond-shaped regions represent regions of acceleration.
(b) Very thick boundary layer.

nozzles, the normal shock extends over most of the stream and a thickening of the boundary layer occurs (Fig. 5.15a). When the shock is strong and the boundary layer thick, as in long ducts fed by supersonic nozzles, back flow and separation occur (Fig. 5.15b). The main stream

separates from the walls, alternately passes through a series of accelerations and shocks, and, finally, after reaching subsonic speeds, diverges and fills the passage again.



FIG. 5.17. Schlieren photographs showing the effect of boundary-layer removal on the compression shock in a duct, with flow from left to right (after A. Weise).

(a) Boundary layer present.

(b) Boundary layer removed through suction slits.

Typical schlieren photographs of these phenomena are shown in Figs. 5.1 and 5.16. That the boundary layer is indeed responsible for the complex flow pattern with repeated shocks is seen from the schlieren photographs of Fig. 5.17, where it is evident that the simple normal shock can be made to occur by removing the boundary layer from the walls of the passage. This figure also indicates the possibility of eliminating complex and lengthy shock patterns by means of boundary layer suction.

Fig. 5.18 illustrates a typical static pressure distribution measured at the wall of a duct containing a compression shock.⁽²⁾ In the particular case shown, for which the Mach Number at the beginning of the shock was 2.8, about ten diameters of duct were required for the pressure rise to be attained. In other tests of similar nature the length of the "shock" was found to vary between 14 diameters for a Mach Number of 4.2, and 9 diameters for a Mach Number of 1.8. These figures are doubtless a function of the Reynolds Number and of the boundary-layer thickness. Measurements of the maximum pressure rise for the steeply

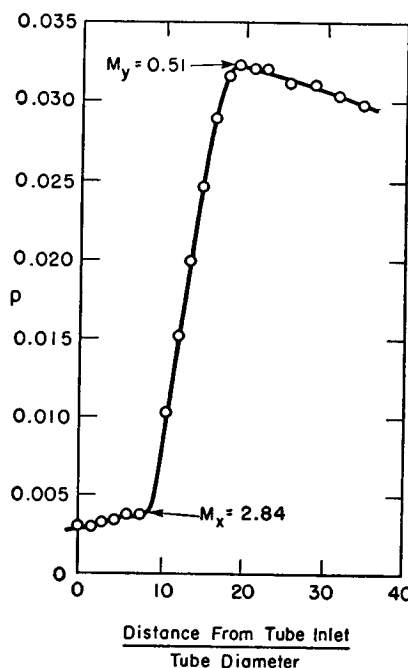


FIG. 5.18. Measured static pressure distribution at the wall of a duct containing a compression shock like that of Fig. 5.16b (after E. G. Newberg, Jr.).

doubtless a function of the Reynolds Number and of the boundary-layer thickness. Measurements of the maximum pressure rise for the steeply

ascending portions of the pressure-distance curves indicated that the measured value of p_y/p_x was about 6 per cent less than the value corresponding to the normal shock equations and the measured value of M_x . This agreement is good, considering the fact that at neither section x nor section y is the flow strictly one-dimensional. The good agreement between the measured and calculated pressure rises is explained by the fact that the wall shearing forces in the region of separation in Fig. 5.15b are extremely small, and hence the normal shock equations are approximately applicable between sections x and y . From this we reach the important conclusion that, although the compression shock in a duct is far from a plane discontinuity, the normal shock equations are a good guide to the changes in fluid properties across such a shock region. It is important to remember, however, that a substantial distance is required for the net change in state to be effected.

Additional information on shocks in ducts is presented in Volume II, Chapter 28.

5.9. Moving Shock Waves

In a number of practical problems, such as those relating to explosion waves, the V-1 "buzz bomb" engine, and the Comprex, it is necessary to deal with compression shocks which are not stationary. If in such cases the shock wave travels at constant speed, the problem may be reduced to that of a stationary shock merely by employing a moving coordinate system relative to which the shock is at rest; the shock relations already derived are then applicable to the fluid properties in this moving coordinate system. The same result is true to a very good approximation even when the shock strength is changing with time or when the shock speed is not constant; this is so because the shock thickness is minute, from which it follows that the time rates of change of mass, momentum, and energy within a control surface surrounding the shock are negligible compared with the changes in the respective fluxes of these quantities passing through the control surface.

Transformation of Moving Shock to Stationary Shock. To illustrate the general approach by which the stationary shock relations can be made applicable to a moving shock, consider a moving shock wave such as might have been created by an explosion in a gas at rest (Fig. 5.19b). By superposing on the pattern of Fig. 5.19b a uniform velocity to the right, the stationary shock pattern of Fig. 5.19a is obtained. In Fig. 5.19a, gas approaches the shock with the speed V_x and pressure p_x , and with the supersonic Mach Number M_x . It leaves the shock with a higher pressure, lower speed, and with a subsonic Mach Number. In the case of the moving shock, the gas over which the shock has passed is at a higher pressure than the undisturbed gas. The gas over which the

shock has passed travels leftward with the speed $V_x - V_y$, and, since this is less than the shock speed V_x , a particle of high-pressure gas falls farther and farther behind the shock front.

Let us define the Mach Number of the moving shock wave as the ratio of the speed of the wave to the speed of sound in the stationary gas. This ratio is identical with the value of M_x for the stationary discontinuity. Now, since for a wave of finite strength M_x is greater than unity,

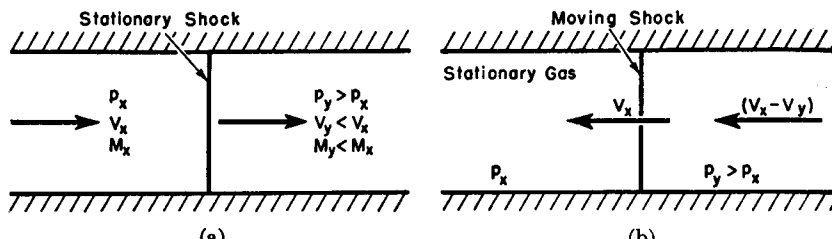


FIG. 5.19. Transformation of coordinate system.

- (a) Gas flowing through stationary shock.
- (b) Shock moving into stationary gas.

it follows that such waves travel faster than the speed of sound in the undisturbed medium. Only in the case of a wave of infinitesimal strength does the wave propagate with the speed of sound.

Transformation Formulas. The equations of Art. 5.3 are, of course, valid only in terms of Fig. 5.19a, i.e., only for quantities measured by an observer who travels with the discontinuity. In order to obtain equations which are applicable to quantities seen by an observer at rest with respect to the low-pressure gas, all quantities containing a velocity term must be modified in accord with the change in coordinate system.

Suppose we signify with primes those quantities measured by an observer who is at rest with respect to the gas toward which the discontinuity moves. Then we may write

$$p'_x = p_x; \quad p'_y = p_y \quad (5.40a, 5.40b)$$

$$T'_x = T_x; \quad T'_y = T_y \quad (5.41a, 5.41b)$$

$$M_x = V_x/c_x; \quad M'_x = 0 \quad (5.42a, 5.42b)$$

$$M_y = V_y/c_y; \quad M'_y = \frac{V_x - V_y}{c_y} = \frac{c_x}{c_y} M_x - M_y \quad (5.43a, 5.43b)$$

$$T'_{0x} = T_x \left(1 + \frac{k-1}{2} M_x^2 \right); \quad T'_{0x'} = T_x \quad (5.44a, 5.44b)$$

$$T_{0y} = T_y \left(1 + \frac{k-1}{2} M_y^2 \right); \quad T'_{0y'} = T_y \left[1 + \frac{k-1}{2} (M_y')^2 \right] \quad (5.45a, 5.45b)$$

$$p'_{0x} = p_x \left(1 + \frac{k-1}{2} M_x^2 \right)^{\frac{k}{k-1}}; \quad p'_{0x'} = p_x \quad (5.46a, 5.46b)$$

$$p'_{0y} = p_y \left(1 + \frac{k-1}{2} M_y^2 \right)^{\frac{k}{k-1}}; \quad p'_{0y'} = p_y \left[1 + \frac{k-1}{2} (M_y')^2 \right]^{\frac{k}{k-1}} \quad (5.47a, 5.47b)$$

Through the use of these transformations and the equations of Art. 5.3, the shock relations may be worked out for the observer of Fig. 5.19b.

It is worthy of note that the change in stagnation temperature is dependent on the observer's motion, as indicated by the following expressions:

$$\begin{aligned} \Delta T_0 &= T_{0y} - T_{0x} \\ &= T_y - T_x + \frac{V_y^2 - V_x^2}{2c_p} \\ \Delta T'_0 &= T'_{0y'} - T'_{0x'} \\ &= T_y - T_x + \frac{(V_x - V_y)^2}{2c_p} \end{aligned}$$

and, since $\Delta T_0 = 0$, we find that

$$\Delta T'_0 = \frac{V_x(V_x - V_y)}{c_p}$$

Similar transformation relations may be worked out for the case where the flow in a pipe is suddenly brought to rest at one end, thus initiating a shock wave which propagates back through the pipe. The corresponding physical situation is pictured (with some poetic license) in Fig. 5.20.



FIG. 5.20. Metaphorical shock propagating into a flowing medium which has been suddenly brought to rest. (Reprinted courtesy R. Courant and K. O. Friedrichs, *Supersonic Flow and Shock Waves*, Interscience Publishers, New York, copyright 1948.)

5.10. Operating Characteristics of Converging-Diverging Nozzle

We return now to the problem of the operating characteristics of converging-diverging nozzles under varying pressure ratios, discussed previously in Art. 4.7.

Simplified Theoretical Analysis. Fig. 5.21a shows the experimental arrangement considered for purposes of discussion. Figs. 5.21b, c, and d show the characteristics computed on the basis of frictionless flow, but admitting the possibility of normal shocks. The measured characteristics are in general agreement with those illustrated here and differ chiefly because of boundary-layer effects.

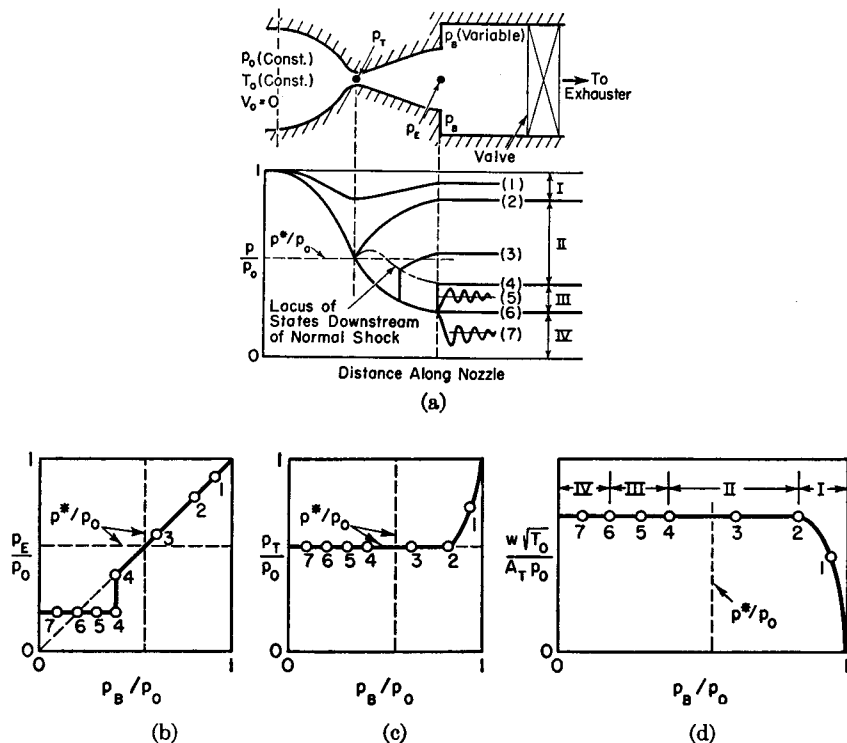


FIG. 5.21. Performance of converging-diverging nozzle with various ratios of back pressure to supply pressure.

- (a) Curves of pressure versus distance along nozzle axis.
- (b) Exit-plane pressure versus back pressure.
- (c) Throat pressure versus back pressure.
- (d) Mass flow parameter versus ratio of back pressure to supply pressure.

Four different regimes are possible. In regime I the flow is entirely subsonic, and the passage behaves like a conventional venturi tube. The flow rate is sensitive to changes in back pressure.

At condition 2, which forms the dividing line between regimes I and II, the Mach Number at the throat is unity. As regime II is entered, a normal shock appears downstream of the throat, and the process aft of the shock comprises subsonic deceleration. As the back pressure is lowered, the shock moves down the nozzle until, at condition 4, it appears

in the exit plane of the nozzle. In regime II, as in regime I, the exit-plane pressure p_e is virtually identical with the back pressure p_b . On the other hand, the flow rate in regime II is constant and is unaffected by the back pressure. This is in accord with the fact that throughout regime II all stream properties at the throat section are constant.

In regime III, as for condition 5, the flow within the entire nozzle is supersonic, and the pressure in the exit plane is lower than the back pressure. The compression which subsequently occurs outside the nozzle involves oblique shock waves which cannot be treated on one-dimensional grounds.

Condition 6 is termed the design condition for the nozzle under supersonic conditions, since the exit-plane pressure is then identical with the back pressure. A reduction in the back pressure below that corresponding to condition 6 has no effect whatsoever on the flow pattern within the nozzle. In regime IV the expansion from the exit-plane pressure to the back pressure occurs outside the nozzle in the form of oblique expansion waves which also cannot be studied by a one-dimensional analysis.

In both regimes III and IV the flow pattern within the nozzle is independent of back pressure, and corresponds to the flow pattern for the design condition. Adjustments to the back pressure are made outside the nozzle.

For subsonic flow, there are an infinite number of possible pressure-distance curves. For the supersonic region of flow, however, the pressure-distance curve is unique. To put it differently, in subsonic flow the pressure ratio does not depend solely on the area ratio; in supersonic flow the pressure ratio does depend solely on the area ratio.

Only over a narrow range of back-pressure ratios, namely, the range covered by regime I, does the flow rate depend on the back pressure. For regimes II, III, and IV, the flow rate is independent of back pressure, and, since $M = 1$ at the throat, may be computed from Eq. 4.17.

Experimental Results. Fig. 5.22 shows schlieren photographs of the flow through a converging-diverging nozzle. Figs. 5.22a, b, and c correspond to regime II and show a normal shock advancing down the nozzle as the back pressure is lowered. In Figs. 5.22a and 5.22b the shock is weak and the boundary layer thin, and there is a single and substantially normal shock. In Fig. 5.22c the shock is fairly strong and there is boundary-layer separation with a repeated shock pattern. With sufficiently low back pressure (regimes III and IV) the shock moves out of the nozzle, and the flow in the passage is entirely supersonic, as in Fig. 5.22d.

Measured pressure distributions on the nozzle axis are shown in Fig. 5.23. They are seen to agree generally with the simple model of Fig. 5.21a, the chief difference being a gradual rather than a steep rise in

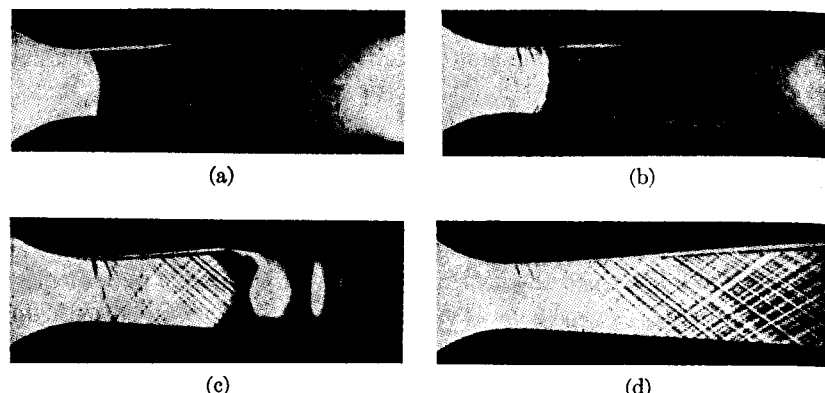


FIG. 5.22. Schlieren photographs of flow through converging-diverging nozzle, with flow from left to right (after Prandtl).

- (a) Weak shock just downstream of throat.
- (b) Shock further downstream than in (a).
- (c) Strong shock accompanied by flow separation.
- (d) Back pressure low enough to permit purely supersonic flow in passage. Inclined lines are Mach wavelets generated by slight roughness on the walls.

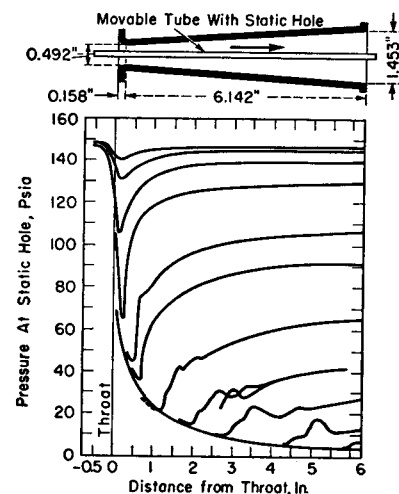


FIG. 5.23. Experimentally determined curves of static pressure on axis versus distance along axis for converging-diverging nozzle (after Stodola).

pressure across the shock. This difference is caused by boundary-layer thickening and separation.

Flow patterns in the exit jet for regimes III and IV are illustrated by the schlieren photographs of Fig. 5.24. Analytical studies of the oblique waves seen in these pictures are presented in Chapters 14, 15, and 16.

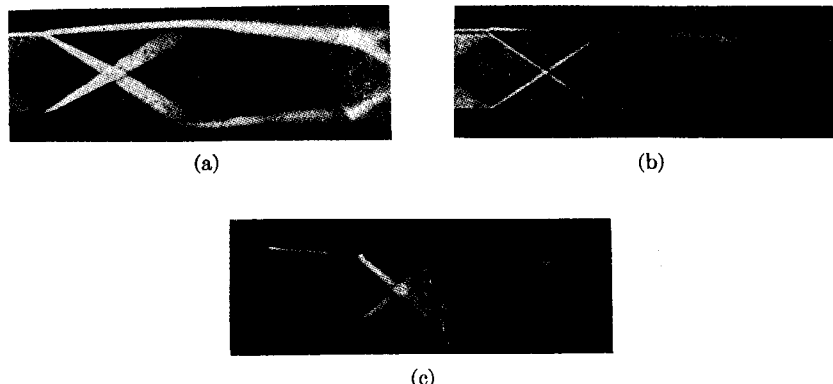


FIG. 5.24. Schlieren photographs of flow at exit of converging-diverging nozzle, with flow from left to right (after Prandtl).

- (a) Pressure in exit plane greater than back pressure (regime IV).
- (b) Pressure in exit plane equal to back pressure (condition 6).
- (c) Pressure in exit plane less than back pressure (regime III).

5.11. One-Dimensional Supersonic Diffusers

Diffusers, or passages which decelerate a stream to low velocity, are important elements in such different devices as compressors, wind tunnels, and ram jets. The supersonic diffuser offers certain unusual problems not met with in the design of subsonic diffusers.

Special Problems of Supersonic Diffusers. At first thought it might appear that a supersonic diffuser could be designed as though it were the reverse of a converging-diverging nozzle. Two difficulties arise, however. First, if the diffuser is in a closed system and is preceded by a supersonic nozzle, frictional effects between the nozzle and the diffuser require that the diffuser throat be somewhat larger than the nozzle throat. If the diffuser throat is made slightly too small, supersonic flow will not be attained in the nozzle; and, if the diffuser throat is made slightly too large, there will necessarily be a shock somewhere within the diffuser. Indeed, even if the two throats did match perfectly, it appears that the combined system would be unstable and that flow oscillations would occur.

A second and more serious difficulty arises. Most flow systems start from rest and accelerate to the operating velocity. During the starting period normal shock waves pass through the system. Across a normal shock there is no change in flow rate or in stagnation temperature. According to Eq. 4.17, therefore, the product $A_x^* p_{0x}$ must equal the product $A_y^* p_{0y}$. As the stagnation pressure is reduced by a normal shock, it follows that there is a corresponding increase in the minimum area through which the flow can be made to pass. The design problems raised by this aspect of the process will be discussed for two applications, namely, wind tunnel diffusers and propulsion engine diffusers.

Supersonic Wind Tunnel Diffusers. In order to focus attention on the essential features of the problem, it will be assumed that the flow is isentropic, except for entropy increases which occur across normal shocks. We shall assume also that the flow is quasi-steady during the period of starting the flow.

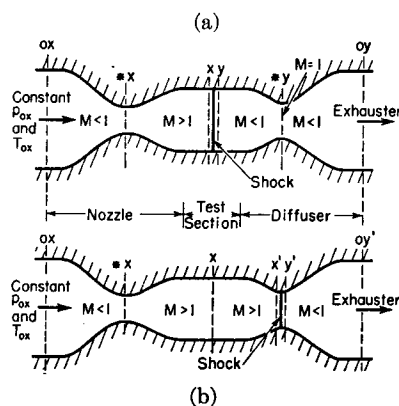


FIG. 5.25. Starting of supersonic wind tunnel diffuser.

- (a) Most unfavorable starting condition.
- (b) Best operating condition.

5.10. During this period, the nozzle throat is passing the maximum possible flow, and, since $A^* p_0$ is constant across the shock, it follows that the flow can pass through the diffuser throat only if the latter is larger than the nozzle throat. The worst condition in this respect occurs when the shock is moving through the test section (Fig. 5.25a) inasmuch as the shock then occurs at the maximum possible Mach Number and, consequently, produces the largest loss in stagnation pressure. The minimum area of the diffuser throat is therefore given by

$$\frac{A_{\text{min. diff. throat}}}{A_{\text{nozzle throat}}} = \frac{A_y^*}{A_x^*} = \frac{p_{0x}}{p_{0y}} \quad (5.48)$$

where p_{0y}/p_{0x} is the stagnation pressure ratio for a shock at the test-

section Mach Number. The limiting contraction ratio A_x/A_y^* for the diffuser is accordingly given by

$$\frac{A_x}{A_y^*} = \frac{A_x}{A_x^*} \frac{A_x^*}{A_y^*} = \frac{A_x}{A_x^*} \frac{p_{0y}}{p_{0x}}$$

The area ratio A_x/A_x^* is given in terms of M_x by the isentropic formula, Eq. 4.19, and the ratio p_{0y}/p_{0x} is given in terms of M_x by the shock formula, Eq. 5.21. Hence A_x/A_y^* depends only on the test-section Mach Number. This area ratio is plotted versus M_x in Fig. 5.26, together with a curve showing the area contraction which would be possible if the stream at M_x could be diffused without a shock.

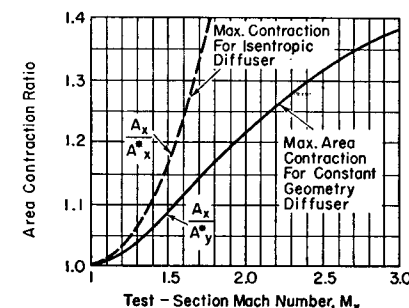


FIG. 5.26. Maximum area contraction for which supersonic wind tunnel diffuser of fixed geometry will permit supersonic flow to be established in test section.

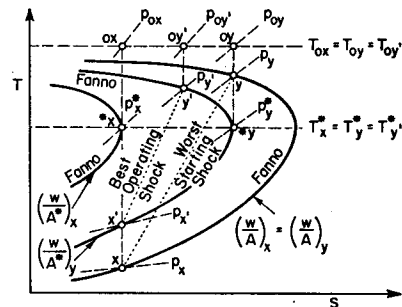


FIG. 5.27. Starting operation of supersonic wind tunnel diffuser illustrated on temperature-entropy diagram.

With the limiting diffuser throat area corresponding to Eq. 5.48, the diffuser is barely able to "swallow" the flow during starting, and the flow at the diffuser throat is exactly sonic when the shock is in the test section. If the diffuser throat is slightly smaller than that required by Eq. 5.48, a normal shock will stand in the diverging portion of the nozzle, and subsonic flow will exist in the test section. Should the diffuser throat be considerably smaller than that given by Eq. 5.48 the flow will be subsonic throughout the entire system, except possibly downstream of the diffuser throat.

The worst starting shock is illustrated in the T - s diagram of Fig. 5.27. In interpreting this diagram it is well to remember that all states on the same Fanno line have a common stagnation temperature and flow per unit area. A change in cross-sectional area has associated with it a shift from one Fanno line to another. It is clear from this diagram that during the "starting" condition there is a large loss in stagnation pressure and a consequent increase in the area required to pass the flow. The path of states during the most unfavorable starting condition (i.e., while the shock is in the test section) is from $0x$ to x to y to $*y$ to $0y$.

OPERATING CONDITIONS. Assuming now that the diffuser is large enough for supersonic flow to be established in the test section, a sufficient lowering of the exhaust pressure will cause the shock to move through the test section and to be swallowed by the diffuser throat. The position at which the shock comes to rest depends on the manner in which the operating characteristic of the exhauster is matched to the pressure-flow characteristic of the remainder of the system. For best efficiency, the system and exhauster should be matched so that the equilibrium position of the shock is in the diffuser throat, as the shock will then occur at the minimum possible Mach Number in the diffuser. This best operating condition is shown in Fig. 5.25b. The corresponding path of states in Fig. 5.27 is from $0x$ to x to x' to y' to $0y'$. The stagnation pressure loss for best operation is less than for starting up because of the lower Mach Number at which the shock occurs. Hence the pressure ratio required of the exhauster is determined by the starting condition rather than by the operating condition. A comparison of the two limiting stagnation pressure ratios is shown in Fig. 5.28. The lower curve represents also the operating condition of a diffuser having no contraction whatsoever, i.e., a normal shock followed by isentropic subsonic diffusion. For low test-section Mach Numbers it is evident that the normal shock is so efficient as hardly to justify the use of a converging-diverging diffuser.

In practice the shock is maintained slightly downstream of the diffuser throat during operation. This is done because with a fixed exhaust pressure the shock is unstable in the converging portion of the diffuser. For example, if the shock were maintained exactly at the minimum area, a slight disturbance might make it move temporarily into the converging section. But this would augment the loss in stagnation pressure, and, if the exhaust pressure were fixed, transient waves would cause the shock to move further upstream. This would make the situation still worse, and the shock would move upstream progressively until it came to rest in the diverging part of the nozzle at a point where the stagnation pressure loss in the system matched the exhaust pressure of the system. In order again to obtain supersonic flow in the test

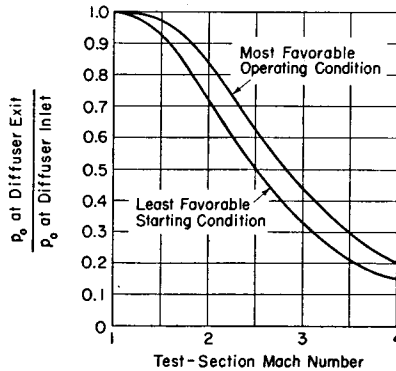


Fig. 5.28. Stagnation pressure loss for supersonic wind tunnel diffuser of fixed geometry. Curve marked "least favorable starting condition" shows also the stagnation pressure loss for a diffuser comprising a normal shock followed by isentropic subsonic diffusion.

sents also the operating condition of a diffuser having no contraction whatsoever, i.e., a normal shock followed by isentropic subsonic diffusion. For low test-section Mach Numbers it is evident that the normal shock is so efficient as hardly to justify the use of a converging-diverging diffuser.

In practice the shock is maintained slightly downstream of the diffuser throat during operation. This is done because with a fixed exhaust pressure the shock is unstable in the converging portion of the diffuser. For example, if the shock were maintained exactly at the minimum area, a slight disturbance might make it move temporarily into the converging section. But this would augment the loss in stagnation pressure, and, if the exhaust pressure were fixed, transient waves would cause the shock to move further upstream. This would make the situation still worse, and the shock would move upstream progressively until it came to rest in the diverging part of the nozzle at a point where the stagnation pressure loss in the system matched the exhaust pressure of the system. In order again to obtain supersonic flow in the test

section, it would be necessary to lower the exhaust pressure to the minimum value required for starting, as determined from Fig. 5.28.

To insure that a supersonic diffuser of fixed geometry will start, the throat area must be made slightly larger than the theoretical minimum value to account for inaccurate estimates of the effects of friction, of the departures from one-dimensionality, and so forth.

ADDITIONAL CONSIDERATIONS. Thus, because practical reasons require that the best design be compromised by an enlargement of the throat and by an operating condition with the shock at a Mach Number greater than the minimum in the passage, the practically attainable efficiencies of such diffusers fall somewhat short of the values which seem possible in principle.

Experimental investigations confirm in a general way the theoretical considerations outlined here, although there are modifications owing to viscous effects. Wall friction of course produces slight additional losses in stagnation pressure. The chief effect of viscosity, however, is to make the shock occur in a length of several passage diameters, rather than abruptly; unless this feature is taken into account in the design, the diffuser efficiency may be considerably lower than anticipated.⁽⁴⁾

Some of the diffuser problems outlined here may be avoided by such means as (i) variable-geometry diffusers, (ii) variable-geometry diffusers in conjunction with variable-geometry nozzles, (iii) driving the shock through the diffuser throat by means of a large-amplitude pressure pulse, and (iv) taking advantage of effects which are not one-dimensional.

Supersonic Inlets. Let us now consider the inlets of air-breathing propulsion engines such as turbojets and ram jets when these operate at supersonic speeds. Such engines always reach their operating speed by being accelerated from lower speeds, and so we must investigate operation of the supersonic inlet during starting. Here again, for simplicity, we shall treat the flow as quasi-static and shall ignore all losses except those occurring in normal shocks.

SWALLOWING OF SHOCK. Fig. 5.29a shows a converging-diverging supersonic inlet having an inlet area A_1 and minimum area A_2 . If no

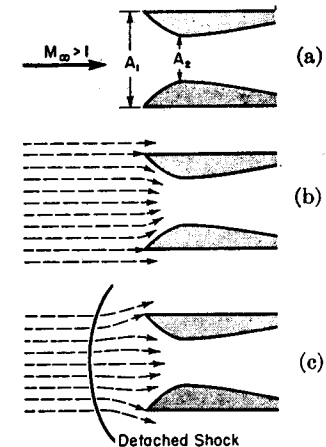


Fig. 5.29. Supersonic inlet.

- Nomenclature.
- No detached shock, with all the free stream flow corresponding to the area A_1 entering the inlet.
- Detached shock, with spill-over.

shock stands ahead of the inlet when the latter travels at supersonic speeds, there is no possibility of the air flow being diverted before reaching the inlet, and all the free-stream flow corresponding to the cross-sectional area A_1 enters the engine (Fig. 5.29b). Should the inlet not be able to pass this amount of flow, a detached shock stands ahead of the inlet (Fig. 5.29c), as then the flow behind the shock is subsonic and may spill over the inlet lip of the diffuser. Fig. 5.30 is a schlieren photograph illustrating this phenomenon.

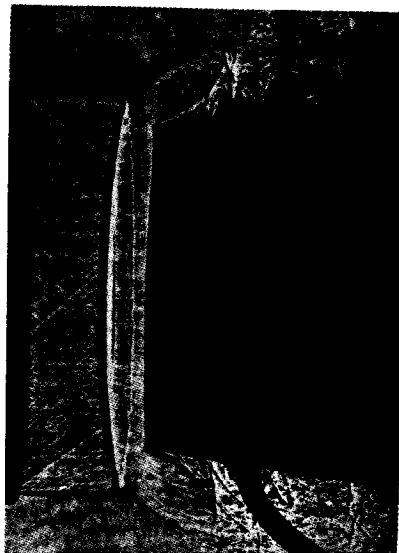


FIG. 5.30. Schlieren photograph of supersonic inlet fed by supersonic free jet. The streamlines were made visible by means of a time exposure. The detached normal shock permits some of the flow to spill over the inlet lip (Department of the Navy, U.S.A.).

The lower curve of Fig. 5.31 shows the maximum contraction possible when there is no shock whatsoever, and comes directly from the isentropic relations. The upper curve shows the maximum contraction possible for the special case where a detached normal shock hangs on the inlet lip, thus forcing all the air through the engine but with a reduced stagnation pressure. The ordinates of these curves are the reciprocals of the corresponding ordinates of Fig. 5.26.

CONSTANT-GEOMETRY INLET. Consider now a fixed-geometry inlet designed to operate at the speed $M_{\infty a}$, and having the area ratio $(A_2/A_1)_a$. Fig. 5.32 shows various stages during starting. In Fig. 5.32a, the speed is too low for the flow to be swallowed, and a detached shock is present (point *b* of Fig. 5.31). When the speed is slightly less than the design speed (Fig. 5.32b), the shock hangs on the inlet lip. A slight increase in speed causes the shock to move into the inlet, provided of course that the exhaust pressure is sufficiently low. The equilibrium position of the shock depends on the way in which the performance characteristics of

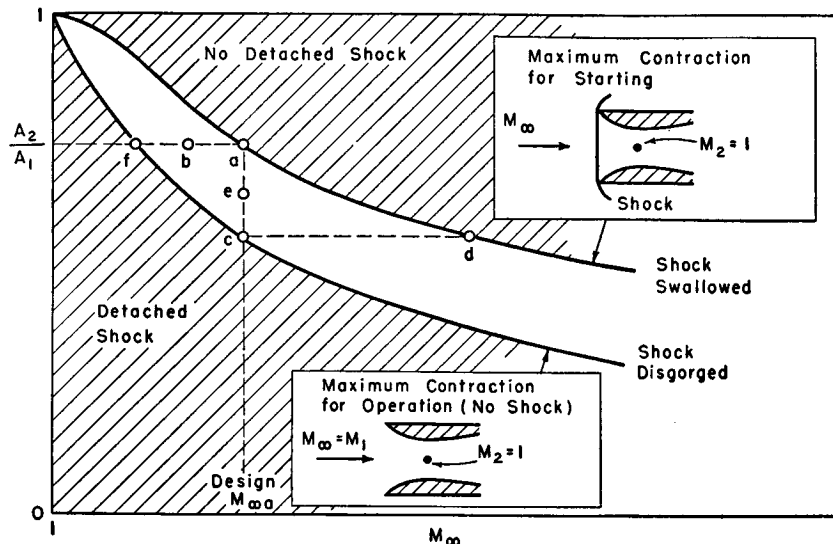


FIG. 5.31. Limiting contraction ratio versus free-stream Mach Number.

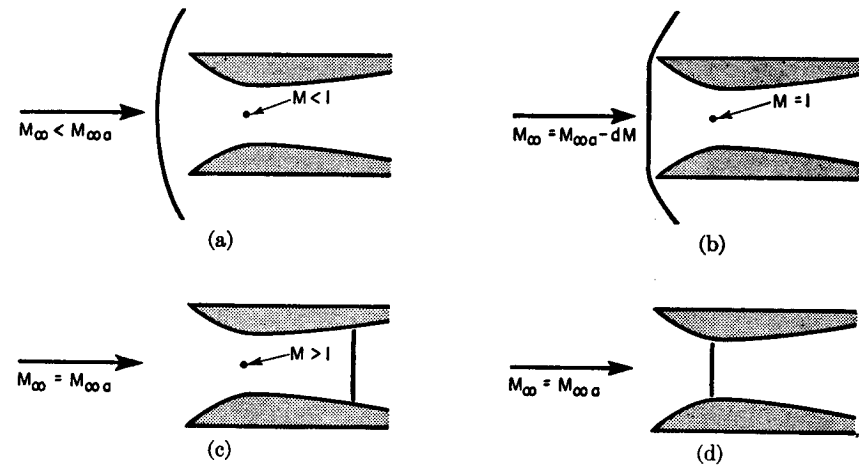


FIG. 5.32. Starting of fixed-geometry supersonic inlet, designed for free-stream Mach Number $M_{\infty a}$, and having contraction ratio $(A_2/A_1)_a$.

the inlet are matched to the performance characteristics of the remainder of the engine. In Fig. 5.32c the shock is too far downstream for good efficiency, and in Fig. 5.32d it is in the farthest upstream position for which the flow is stable. A slight disturbance in the flow pattern of Fig. 5.32d would cause the shock to be disgorged.

Such a diffuser has an interesting hysteresis effect. Assuming that the exhaust pressure is sufficiently low, the shock will not be swallowed during acceleration until the speed $M_{\infty a}$ (Fig. 5.31) is reached. Once swallowed, however, the shock will not be disgorged upon deceleration until the speed $M_{\infty f}$ (Fig. 5.31) is reached.

OVERSPEEDING OF CONSTANT-GEOMETRY INLET. It is possible to eliminate altogether the operating shock of a supersonic fixed-geometry inlet if the engine may be overspeeded. Fig. 5.33 shows various stages

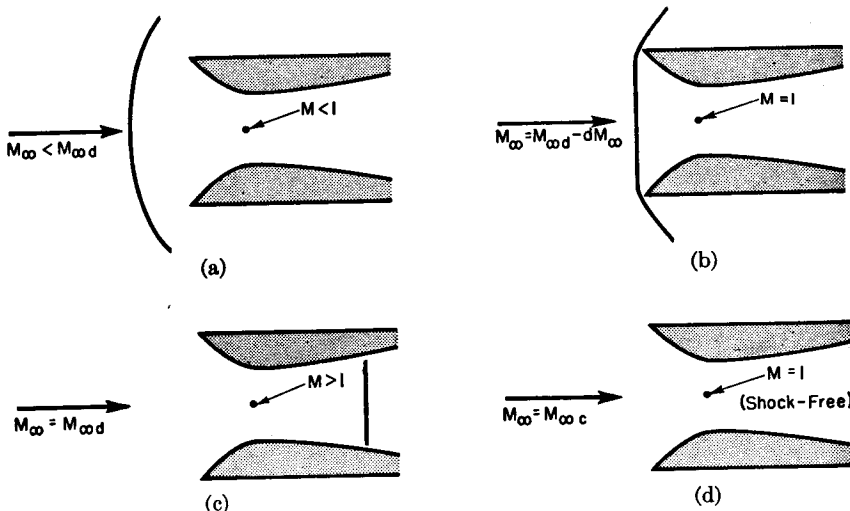


FIG. 5.33. Overspeed starting of fixed-geometry supersonic inlet, designed for free-stream Mach Number $M_{\infty a}$, and having contraction ratio $(A_2/A_1)_c$.

in the acceleration period of an inlet designed for the speed $M_{\infty a}$ and having in Fig. 5.31 a contraction ratio $(A_2/A_1)_c$. By overspeeding the engine to the speed $M_{\infty d}$ (Fig. 5.31), the shock is swallowed, and then the engine may be decelerated at most to $M_{\infty a}$ before the shock is disgorged.

VARIABLE-GEOMETRY INLET. The operating shock may also be eliminated through the use of a variable-geometry diffuser. Suppose that such a diffuser is operating at the speed $M_{\infty a}$ of Fig. 5.31. If the throat area is too small, corresponding perhaps to point *c* of Fig. 5.31, a detached shock stands ahead of the inlet (Fig. 5.34a). By increasing the throat area, the shock is brought closer to the inlet. When point *a* of

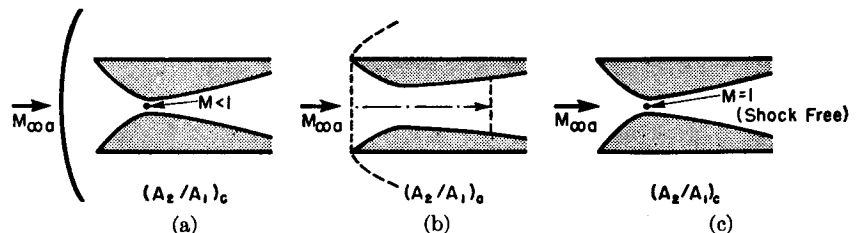


FIG. 5.34. Starting of variable-geometry supersonic inlet, designed for free-stream Mach Number $M_{\infty a}$.

Fig. 5.31 is reached, the shock reaches the inlet lip and may be swallowed (Fig. 5.34b). Subsequently, the throat area may be reduced without disgorging the shock until point *c* of Fig. 5.31 is reached, and, if the exhaust pressure is properly adjusted, the diffuser is then free of shocks (Fig. 5.34c).

Diffuser Efficiency. The most common definition of diffuser efficiency is parallel to the definition employed for compressor efficiency. Referring to Fig. 5.35, and assuming that the velocity leaving the diffuser is negligible, we define

$$\eta_D = \frac{(\Delta h)_s}{V_1^2/2} = \frac{h_3 - h_1}{h_2 - h_1} \quad (5.49)$$

where state 1 is the actual state entering the diffuser, 2 is the actual state leaving the diffuser, and 3 is a fictitious state at the actual leaving pressure but at the entering entropy.

For a perfect gas Eq. 5.49 becomes

$$\eta_D = \frac{T_3 - T_1}{T_2 - T_1} = \frac{T_1 \left(\frac{T_3}{T_1} - 1 \right)}{V_1^2/2c_p}$$

and, since

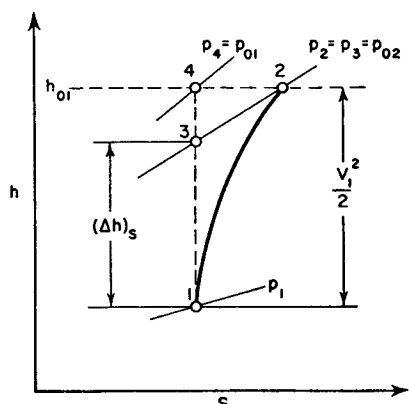
$$T_3/T_1 = (p_2/p_1)^{\frac{k-1}{k}}$$

and

we get

$$\eta_D = \frac{(p_2/p_1)^{\frac{k-1}{k}} - 1}{\frac{k-1}{2} M_1^2} \quad (5.50)$$

FIG. 5.35. Illustrates definition of diffuser efficiency.



The efficiency is uniquely related to the stagnation pressure ratio for a given inlet Mach Number. To demonstrate this, we write

$$\frac{p_2}{p_1} = \frac{p_{01}}{p_1} \cdot \frac{p_2}{p_{01}} = \frac{p_{01}}{p_1} \cdot \frac{p_{02}}{p_{01}}$$

Employing the isentropic relation for p_{01}/p_1 , and substituting into Eq. 5.50, we get after rearrangement,

$$\eta_D = \frac{\left(1 + \frac{k-1}{2} M_1^2\right) \left(\frac{p_{02}}{p_{01}}\right)^{\frac{k-1}{k}} - 1}{\frac{k-1}{2} M_1^2} \quad (5.51)$$

Corresponding to the two curves of Fig. 5.28, there are plotted in Fig. 5.36, with the aid of Eq. 5.51, the maximum efficiencies for fixed-geometry diffusers and normal shock diffusers.

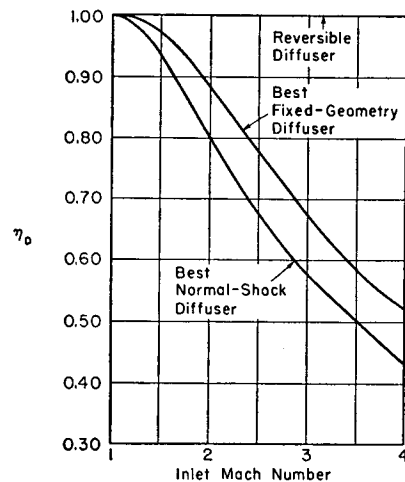
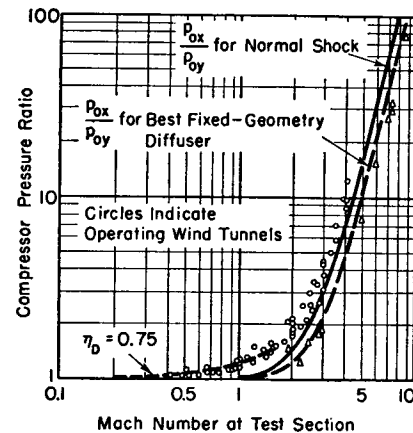


FIG. 5.36. Maximum efficiency of one-dimensional supersonic diffusers.



Wind Tunnel Performance. In Fig. 5.37 are plotted the compressor pressure ratios for a number of operating wind tunnels. This chart shows that subsonic tunnels correspond roughly to a diffuser efficiency of 75 per cent. It is evident that the principal loss in supersonic wind tunnels is caused by the shock in the diffuser and that the maximum gain in supersonic wind tunnel economy, at least from the point of view of machinery installation, is to be had by improving the performance of supersonic diffusers.

5.12. Supersonic Pitot Tube

The pitot tube has long been an important instrument for measuring the velocities of subsonic streams. When used with supersonic streams, modifications must be made in the interpretation of the measured data.

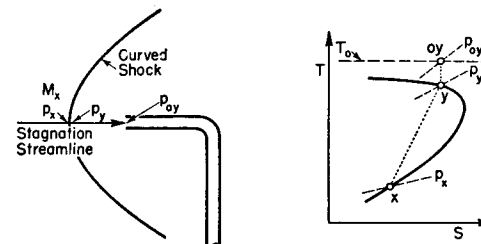


FIG. 5.38. Supersonic pitot tube.

Rayleigh Supersonic Pitot-Tube Formula. Photographs reveal that when an impact tube is placed in a supersonic stream, a curved shock wave stands ahead of the mouth of the tube, as shown in Fig. 5.38. The Mach Number of the undisturbed stream ahead of the shock wave may be found from measured data if the following assumptions are made:

(a) The shock wave is locally normal to the stagnation streamline at the point where the latter crosses it. This condition will, by symmetry requirements, be true when the tube is placed parallel to a uniform stream.

(b) Particles following the stagnation streamline are brought to rest isentropically in the subsonic region aft of the shock.

These assumptions are illustrated graphically on the $T-s$ diagram of Fig. 5.38. We write

$$\frac{p_{0y}}{p_x} = \frac{p_{0y}}{p_y} \cdot \frac{p_y}{p_x}$$

Now, p_{0y}/p_y may be expressed in terms of M_x by using Eqs. 4.14b and 5.16b; and p_y/p_x is given in

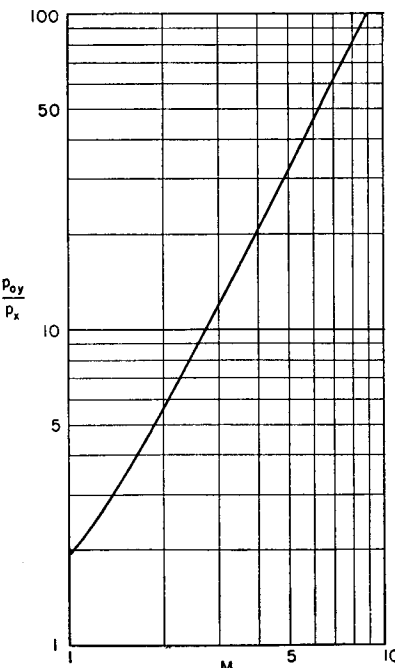


FIG. 5.39. Plot of Rayleigh supersonic pitot-tube formula for $k = 1.4$.

terms of M_x by Eq. 5.18a. Introducing these expressions, we get the Rayleigh pitot-tube formula:

$$\frac{p_{0y}}{p_x} = \left(\frac{k+1}{2} M_x^2 \right)^{\frac{k}{k-1}} / \left(\frac{2k}{k+1} M_x^2 - \frac{k-1}{k+1} \right)^{\frac{1}{k-1}} \quad (5.52)$$

Fig. 5.39 shows this relation for a gas with $k = 1.4$. The ratio p_{0y}/p_x is also tabulated in Table B.3.

Subsonic Pitot Tube. For subsonic flow, there is no shock (unless M_x is close to unity), and Eq. 5.52 is not applicable. Instead, the customary isentropic relation, Eq. 4.14b, is used for relating the Mach Number, the static pressure, and the isentropic stagnation pressure.

Measurement of Static Pressure. In using Eq. 5.52, the static pressure p_x must be measured upstream of the shock wave. If the stream is in a wind tunnel, this might be done with a static pressure tap in the wall of the tunnel.

Pitot tubes often have a static tap built into the side wall of the probe. In supersonic flow this tap does not give an easily interpretable measurement. However, experimental data indicate that if the static tap is placed some ten tube diameters aft of the nose, the static pressure at the tap is a close approximation to the static pressure upstream of the shock.

REFERENCES AND SELECTED BIBLIOGRAPHY

1. SHAPIRO, A. H., and KLINE, S. J. *On the Thickness of Normal Shock Waves in Air*. Istanbul, Turkey: Eighth International Congress on Theoretical and Applied Mechanics, 1952.
2. NEWBERG, E. G., JR. Measurements of Diffuser Efficiency of Supersonic Pressure Shocks. S.M. thesis, Dept. of Mech. Eng., Mass. Inst. of Tech. (1946).
3. KANTROWITZ, A., and DONALDSON, COLEMAN DUP. Preliminary Investigation of Supersonic Diffusers, *NACA, ARR No. L5D20* (1945).
4. NEUMANN, E. P., and LUSTWERK, F. High-Efficiency Supersonic Diffusers, *Jour. Aero. Sci.*, Vol. 51, No. 6 (1951), p. 369.

PROBLEMS

5.1. Air flows steadily through a pipe of constant cross-sectional area and at a certain section has properties $p_x = 10$ psia, $T_x = 1240^\circ\text{F}$, and $V_x = 3000$ ft/sec.

(a) Plot the Fanno and Rayleigh lines corresponding to point x on the p - v , T - v , and T - s diagrams. Find from these diagrams the pressure, temperature, and velocity downstream of a normal shock occurring at condition x .

(b) Compare your results with the corresponding results found from the shock tables.

5.2. Show that for a very weak shock in air,

$$\frac{p_{0x} - p_{0y}}{p_{0x}} \cong 1.3(M_x - 1)^3$$

5.3. Derive simple approximate formulas for very weak shocks, expressing $(1 - M_y)$, $(p_y - p_x)/p_x$, $(T_y - T_x)/T_x$, $(V_y - V_x)/V_x$, and $(p_{0x} - p_{0y})/p_{0x}$ all in terms of $(M_x - 1)$.

5.4. (a) Find the limiting forms of the normal shock equations for a perfect gas with $k = 1$. (b) Find simple asymptotic forms of the normal shock equations for a perfect gas when the Mach Number approaching the shock is very large compared with unity.

5.5. (a) Show that the equation of the Fanno line for a perfect gas is

$$\frac{s - s_a}{c_p} = \ln \left(\frac{2}{k-1} \right)^{\frac{k-1}{2k}} \left(\frac{T}{T_a} \right)^{\frac{1}{k}} \left(\frac{k+1}{2} - \frac{T}{T_a} \right)^{\frac{k-1}{2k}}$$

where s_a and T_a denote respectively the entropy and temperature at the point of maximum entropy on the Fanno line.

(b) Show that the equation of the Rayleigh line for a perfect gas is

$$\frac{s - s_b}{c_p} = \ln \frac{T}{T_b} \left[\frac{2}{(k+1) - \sqrt{(k+1)^2 - 4k \frac{T}{T_b}}} \right]^{\frac{k-1}{k}}$$

where s_b and T_b are respectively the entropy and temperature at the point of maximum entropy on the Rayleigh line. Demonstrate that there is a point of maximum temperature on the Rayleigh line and find a relation connecting the entropy and temperature at this point with s_b and T_b .

5.6. Consider a normal shock in a fluid (not a perfect gas) whose density depends only on the pressure according to the relation

$$\rho \frac{dp}{d\rho} = \beta$$

where β is a positive constant.

(a) Show that the inlet and exit Mach Numbers are related by

$$M_x^2 - M_y^2 = \ln \frac{M_x^2}{M_y^2}$$

(b) Find expressions for $(p_y - p_x)$ and V_y/V_x in terms of M_x and β .

5.7. Show that the local Mach Number is unity at the point of maximum entropy on the Rayleigh line.

5.8. Demonstrate with the help of the Rayleigh line that in the case of a perfect gas the existence of an expansion shock wave would permit the construction of a perpetual motion machine of the second kind.

5.9. Consider a pipe in which air at 70°F and 10 psia flows uniformly with a speed of 400 ft/sec. The end of the pipe is suddenly closed by a valve, and a shock wave propagates back into the pipe. Compute the speed of the wave and the pressure and temperature of the air which has been brought to rest.

5.10. A shock moves into stationary gas according to the sketch of Fig. 5.19b. Derive a formula for the speed of the high-pressure gas in terms of the properties of the low-pressure gas and the strength of the wave. It is suggested that this be put in the form of a relation between $(V_x - V_y)/c_x$ and M_x .

5.11. Suppose that a blast wave, which might have been initiated by an atomic bomb explosion, is traveling through air at standard atmospheric conditions with a speed of 200,000 ft/sec.

Estimate the changes in pressure (atm), temperature ($^{\circ}\text{F}$), stagnation pressure (atm), stagnation temperature ($^{\circ}\text{F}$), and velocity (ft/sec), produced by the wave with respect to an observer who is stationary with respect to the undisturbed air.

5.12. A particular converging-diverging nozzle is designed for a Mach Number of 2 on the basis of reversible, adiabatic flow. When the ratio of exhaust-region pressure, p_e , to supply-region pressure p_0 , is raised considerably above the design value, a normal compression shock appears in the nozzle. The pressures before and after the shock will be denoted by p_x and p_y , respectively.

Assuming reversible, adiabatic flow both upstream and downstream of the shock, plot p_x/p_0 and p_y/p_0 against p_e/p_0 for the range in which the shock lies between the throat and the exit plane. The shock may be considered as being infinitesimal in thickness, and the fluid may be taken as a perfect gas with $k = 1.4$.

Compare the curve of p_y/p_0 with a curve representing the isentropic pressure ratio at the same location in the nozzle for the limiting case of subsonic operation, that is, for the case where the Mach Number is unity at the throat and the flow in the diverging section is subsonic.

5.13. A rocket nozzle which is intended to operate at an altitude of 100,000 ft has an area ratio of 5.16. At launching, however, the rocket exhausts to normal atmospheric pressure, 14.7 psia. The rocket gases are generated at 400 psia and have $k = 1.3$. Assuming frictionless, adiabatic flow in the nozzle, find the ratio of the rocket thrust at launching to the thrust at 100,000 ft.

5.14. A fixed-geometry, convergent-divergent wind tunnel diffuser is to be designed for Mach Number 2. Assuming no friction, compare the maximum possible efficiency and the minimum possible per cent loss in stagnation pressure during operation for the following cases:

- The best possible design is employed.
- The design is conservative, with a throat area 5 per cent larger than that required for starting, and with the shock located during operation at an area 5 per cent greater than the throat area.
- The converging portion is eliminated, and the process comprises a normal shock followed by reversible subsonic compression.

5.15. Consider a fixed-geometry, converging-diverging wind tunnel diffuser in which the minimum area is 15 per cent smaller than the entrance area, and in which the efficiency for subsonic deceleration to zero velocity is 90 per cent. Frictional effects upstream of the shock are negligible.

(a) Plot the maximum possible efficiency and the minimum possible per cent loss in stagnation pressure versus the approach Mach Number. What is the minimum value of the latter for starting purposes?

(b) Assume that during operation, because of conservative design, the shock stands downstream of the throat at a point where the area is 10 per cent larger than the throat area. Plot the efficiency and the per cent loss in stagnation pressure versus the approach Mach Number.

5.16. A ram jet aircraft is to fly at 40,000 ft altitude with a speed of 2000 mph.

(a) Design the best fixed-geometry, convergent-divergent diffuser for this aircraft, and compute for it the maximum efficiency and the least per cent loss in stagnation pressure.

(b) Suppose that it were possible to overspeed the aircraft to 2400 mph. Design the best convergent-divergent diffuser which could then be used, and find for it the maximum efficiency and the least per cent loss in stagnation pressure at the operating speed of 2000 mph.

5.17. A supersonic wind tunnel is to be designed for a Mach Number of 2 with a test section one square foot in area. The general arrangement of the tunnel will be as follows:

Air will be taken from the atmosphere (14.7 psia, 70°F) and will be accelerated to a Mach Number of 2 in a converging-diverging nozzle. From the test section the air will be diffused to substantially zero velocity in a diffuser and will then be discharged to the atmosphere by a compressor.

The design of the tunnel and compressor will be based on the following assumptions: (1) The nozzle is frictionless to the throat, while the over-all efficiency ($\Delta h/\Delta h_s$) of the nozzle, from entrance to exit, is 95 per cent. (2) Although an attempt will be made to diffuse the supersonic stream through a throat, for purposes of design the assumptions will be made that the stream with $M = 2$ passes through a normal shock and that the subsonic stream is then diffused with an efficiency ($\Delta h_s/\Delta h$) of 80 per cent. The conservative nature of this assumption will tend to balance the fact that no account is taken of losses in the test section. (3) The compressor has an efficiency, $\Delta h_c/\Delta h$, based on the reversible adiabatic work of compression, of 82 per cent.

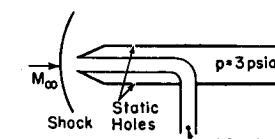
(a) Make a sketch of this tunnel, showing the cross-sectional areas at various sections.

(b) Indicate on the sketch the pressure (psia) and temperature ($^{\circ}\text{F}$) at the test section, at the entrance to the compressor, and at the exit of the compressor.

(c) Specify the diameter of the nozzle throat.

(d) Specify, for the compressor, the pressure ratio, the volume rate of flow at inlet (cfm), and the horsepower required for operation.

5.18. A certain pitot tube is used for measuring the Mach Number M_{∞} of a supersonic air stream, and the pressures shown in the sketch are recorded. It is known that for the particular tube employed, the pressure coefficient (referred to free-stream conditions) at the static holes is 0.1. Estimate the free-stream Mach Number.



PROB. 5.18.

5.19. When an impact tube with a blunt nose is placed in a supersonic stream, a curved shock front stands at some distance in front of the tube. An impact-tube traverse in a wind tunnel gives values of 2.34 psia and 10.02 psia for the static pressure upstream of the shock and the pressure at the mouth of the tube, respectively. Estimate the Mach Number of the tunnel.

5.20. Explain why entropy decreases occur as a fluid particle nears the end of its passage through a shock wave.

5.21. (a) Consider a rightward moving wave in a perfect gas. Show that, as one follows a part of the wave corresponding to a particular fluid velocity and pressure, the time rate of change of wave steepness is given by

$$\frac{d}{dt} \left(\frac{\partial V}{\partial x} \right) = - \frac{k+1}{2} \left(\frac{\partial V}{\partial x} \right)^2$$

(b) Show that the time required for a given part of the wave to acquire infinite slope is given by

$$t = - \frac{2}{k+1} / \frac{\partial V}{\partial x}$$

where $\partial V/\partial x$ is the wave steepness at $t = 0$.

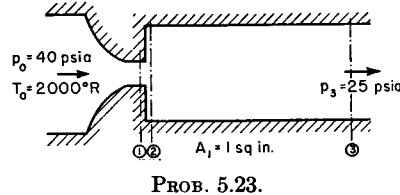
5.22. Consider a plane progressive sound wave in air at 70°F and 14.7 psia. The wave has a frequency of 10,000 cycles per second and an intensity level of 120 decibels. Neglecting damping of the wave, show that the wave tends to become saw-toothed in form. Using the results of Problem 5.21, calculate the time and distance required for the wave to develop into a series of shocks separated by rarefactions.

5.23. Air flows through a frictionless, converging nozzle (see sketch) into a sudden enlargement. At section 3 the flow is substantially uniform and parallel, and between sections 2 and 3 wall friction is negligible.

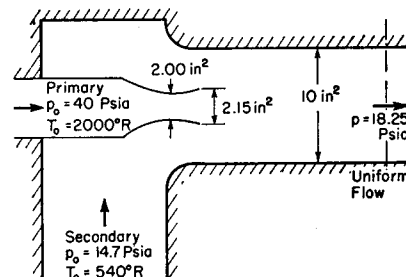
Calculate the pressure acting on the annular surface of section 2 and the mass rate of flow, assuming that $A_3/A_1 = 2.33$.

Hints: (i) If the nozzle is choked, the pressure on the annular face of section 2 may be less than p_1 ; but if the nozzle is unchoked, then p_2 must equal p_1 .

(ii) Apply the momentum, energy, and continuity equations between sections 2 and 3.



PROB. 5.23.



PROB. 5.24.

5.24. A jet pump (see sketch) uses a high-pressure stream of air to pump a second stream of atmospheric air to a pressure of 18.25 psia. The mixing tube of this particular pump has constant cross-sectional area. As a first approximation, all irreversibilities except those associated with viscous mixing are to be ignored.

Calculate the mass rates of flow of primary air and secondary air.

Chapter 6

FLOW IN CONSTANT-AREA DUCTS WITH FRICTION

6.1. Introductory Remarks

The flow of compressible gases in ducts of constant area is of importance in many engineering fields, including stationary power plants, aircraft propulsion engines, high-vacuum technology, transport of fluids in chemical process plants, transport of natural gas in long pipe lines, and various types of flow machinery. It is the purpose of this chapter to discuss such flows from a simple one-dimensional point of view.

We shall here consider flows in which wall friction is the chief factor bringing about changes in fluid properties, and we shall assume that no special attempt is made to transfer heat to or from the stream. When the ducts are reasonably short, therefore, the flow is approximately adiabatic. When the ducts are extremely long, however, as in the case of natural-gas pipe lines, there is sufficient area for heat transfer to make the flow nonadiabatic and approximately isothermal. Both of these limiting cases will be investigated in this chapter. More general cases of compressible flow with heat transfer are treated in Chapters 7 and 8.

Additional material relevant to the subject matter of the present chapter may be found in Volume II, Chapters 24, 26, 27, and 28.

NOMENCLATURE

<i>A</i>	area	<i>L</i>	duct length
<i>c</i>	velocity of sound	<i>L</i> _{max}	maximum duct length for continuous flow
<i>c_p</i>	specific heat at constant pressure	<i>M</i>	Mach Number
<i>D</i>	hydraulic diameter	<i>p</i>	pressure
<i>f</i>	coefficient of friction	<i>Q</i>	heat
<i>f̄</i>	length mean coefficient of friction	<i>R</i>	gas constant
<i>F</i>	impulse function	<i>s</i>	entropy per unit mass
<i>G</i>	mass velocity, ρV	<i>T</i>	absolute temperature
<i>h</i>	enthalpy per unit mass	<i>V</i>	velocity
<i>k</i>	ratio of specific heats	<i>w</i>	mass rate of flow
		<i>x</i>	Cartesian coordinate

NOMENCLATURE—Continued

ρ	density	$(\cdot)^*$ signifies state at which $M = 1/\sqrt{k}$ in isothermal flow
τ_w	wall shearing stress	$(\cdot)_0$ signifies stagnation state
$(\cdot)^*$	signifies state at which $M = 1$ for adiabatic, constant-area flow with friction	

Preliminary Considerations of Adiabatic Flow. We now make the assumptions that (i) the flow is one-dimensional, (ii) the flow is steady, (iii) there is neither external heat exchange nor external shaft work, (iv) differences in elevation produce negligible changes compared with frictional effects, and (v) the duct is of constant area.

GOVERNING PHYSICAL LAWS. The energy equation of steady flow may be written

$$h + \frac{V^2}{2} = h_0 \quad (6.1)$$

where h and V are respectively the corresponding values of the enthalpy and velocity at an arbitrary section of the duct, and h_0 (the *stagnation enthalpy*) has a constant value for all sections of the duct. Physically, h_0 is the enthalpy at the section where the velocity is zero.

The equation of continuity is written

$$\frac{w}{A} = \rho V \equiv G \quad (6.2)$$

where ρ is the density at the section where V and h are measured, and G (the *mass velocity*) has a constant value for all sections of the duct.

Combining Eqs. 6.1 and 6.2, we get the equation of the Fanno line in terms of the enthalpy and density:

$$h = h_0 - \frac{G^2}{2\rho^2} \quad (6.3)$$

Since h_0 and G are constants for a given flow, Eq. 6.3 defines a relation between the local enthalpy and the local density. This relation is shown graphically in Fig. 6.1 for a single value of h_0 and for several values of G . All possible states of the fluid for a given adiabatic, constant-area flow lie on one of these lines.

THE FANNO LINE. For a pure substance, $s = s(h, \rho)$, i.e., the entropy is determined by the enthalpy and density. The curves of Fig. 6.1 may thus be transferred to the enthalpy-entropy diagram, giving the

familiar *Fanno curves* of Fig. 6.2. For all substances thus far investigated, the Fanno curves have the general shape shown in Fig. 6.2.

It was shown in Art. 5.2 that the upper branch of each Fanno curve corresponds to subsonic flow, that the lower branch corresponds to supersonic flow, and that the Mach Number is unity at the point of maximum entropy on each Fanno curve.

SECOND-LAW LIMITATIONS. Since the flow is adiabatic, the Second Law of Thermodynamics tells us that the entropy may increase but

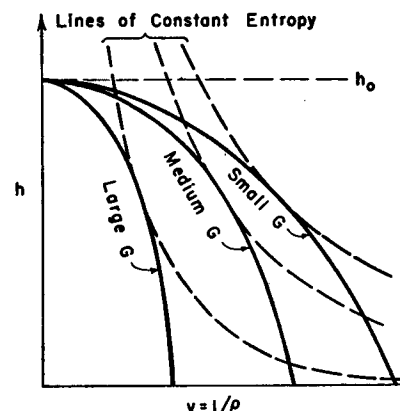


FIG. 6.1. Fanno lines on h - v diagram. Solid lines have the same stagnation enthalpy but different flows per unit area. Dashed lines are isentropes.

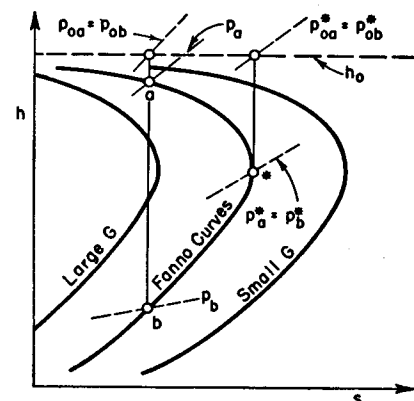


FIG. 6.2. Fanno lines on h - s diagram. The three curves shown have the same stagnation enthalpy but different flows per unit area.

may not decrease. Thus, the path of states along any one of the Fanno curves must be toward the right.

Consequently, if the flow at some point in the duct is subsonic (point a of Fig. 6.2), the effects of friction will be to increase the velocity and Mach Number and to decrease the enthalpy and pressure of the stream. If, on the other hand, the flow is initially supersonic (point b of Fig. 6.2), the effects of friction will be to decrease the velocity and Mach Number and to increase the enthalpy and pressure of the stream. A subsonic flow may therefore never become supersonic, and a supersonic flow may never become subsonic, unless a discontinuity is present. Thus we observe that, as in the case of isentropic flow, the qualitative character of the flow is markedly influenced by whether the flow is subsonic or supersonic.

The limiting pressure, beyond which the entropy would suffer a decrease, occurs at Mach Number unity and is denoted by p^* . The asterisk here denotes the state where $M = 1$ for the particular process under consideration, namely, adiabatic flow at constant area. Thus, referring

to state a as an example, the value of p_a^* will be different for an isentropic flow as compared with the value for an adiabatic, constant-area flow.

Fig. 6.2 indicates that the isentropic stagnation pressure is reduced as a result of friction, irrespective of whether the flow is subsonic or supersonic.

CHOKING DUE TO FRICTION. Consider a situation in which the stagnation enthalpy, flow per unit area, and length of duct are such that Mach Number unity is reached at the end of the duct. If the duct length is increased, it is evident from the foregoing considerations that some sort of adjustment in the flow is necessary. When the flow is subsonic, this adjustment is in the form of a reduction in the flow rate, that is, the flow is *choked*. When the flow is supersonic, the adjustment at first involves the appearance of shock waves, and, for sufficiently large increases in duct length, involves ultimately a choking of the flow. This will be discussed more fully in Arts. 6.2 and 6.3.

6.2. Adiabatic, Constant-Area Flow of a Perfect Gas

If it is assumed that the fluid is a perfect gas, the analytical treatment is greatly simplified, and, moreover, it becomes possible to draw broad conclusions which would otherwise not be apparent.

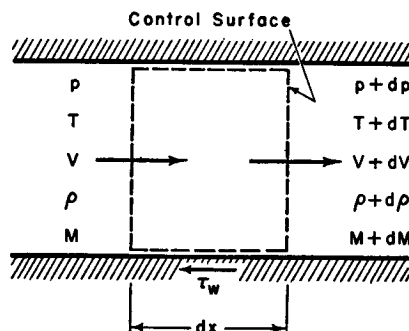


FIG. 6.3. Control surface for analysis of adiabatic, constant-area flow.

Our purpose is to find in analytical form the variations in all stream properties along the length of a duct of constant area. Naturally, the rate of change of properties depends upon the amount of friction, so that the momentum equation must be introduced into the analysis. In Chapter 4 the isentropic relations were derived by writing the various physical relations for two sections a finite distance apart. To illustrate another method of approach, we shall carry out the present analysis in differential form, employing the infinitesimal control volume of Fig. 6.3.

Governing Physical Equations and Definitions. PERFECT-GAS EQUATION. Starting with the perfect-gas relation,

$$p = \rho RT$$

we take logarithmic differentials, and thus obtain

$$\frac{dp}{p} = \frac{d\rho}{\rho} + \frac{dT}{T} \quad (6.4)$$

DEFINITION OF MACH NUMBER. From the expression for the Mach Number in a perfect gas, $M^2 = V^2/kRT$, we get by logarithmic differentiation,

$$\frac{dM^2}{M^2} = \frac{dV^2}{V^2} - \frac{dT}{T} \quad (6.5)$$

STEADY-FLOW ENERGY EQUATION. The energy equation of steady flow is written for a perfect gas in the form

$$c_p dT + d\left(\frac{V^2}{2}\right) = 0$$

Dividing through by $c_p T$, and using the definition of the Mach Number, this becomes

$$\frac{dT}{T} + \frac{k-1}{2} M^2 \frac{dV^2}{V^2} = 0 \quad (6.6)$$

CONSERVATION OF MASS. The continuity equation is

$$G = w/A = \rho V$$

or, since G is a constant,

$$\frac{d\rho}{\rho} + \frac{1}{2} \frac{dV^2}{V^2} = 0 \quad (6.7)$$

MOMENTUM EQUATION. Referring to Fig. 6.3, the momentum equation is written

$$-A dp - \tau_w dA_w = w dV$$

where A is the cross-sectional area, τ_w is the shearing stress exerted on the stream by the walls, and dA_w is the wetted wall area over which τ_w acts.

DEFINITION OF FRICTION COEFFICIENT. The drag coefficient, or the *coefficient of friction* as it is usually called for flow in ducts, is defined as the ratio of the wall shearing stress to the dynamic head of the stream. Thus,

$$f = \frac{\tau_w}{\rho V^2/2}$$

The hydraulic diameter is defined as four times the ratio of cross-sectional area to wetted perimeter,

$$D \equiv \frac{4A}{dA_w/dx} = 4 \frac{A}{dA_w} dx$$

We now introduce the latter two expressions and the continuity equation into the momentum equation, and thus obtain

$$-dp - 4f \frac{\rho V^2}{2} \frac{dx}{D} = \frac{w}{A} dV = \rho V^2 \frac{dV}{V}$$

Next, we divide through by p , and, upon noting that $\rho V^2 = kpM^2$, obtain

$$\frac{dp}{p} + \frac{kM^2}{2} 4f \frac{dx}{D} + \frac{kM^2}{2} \frac{dV^2}{V^2} = 0 \quad (6.8)$$

ISENTROPIC STAGNATION PRESSURE. We retain our previous definition of the *isentropic stagnation pressure* corresponding to a given state as that pressure which would be attained if the stream were isentropically decelerated from the given state to the state of zero velocity. Then, from Eq. 4.14b,

$$p_0 = p \left(1 + \frac{k-1}{2} M^2 \right)^{\frac{k}{k-1}}$$

or, in differential form,

$$\frac{dp_0}{p_0} = \frac{dp}{p} + \frac{kM^2/2}{1 + \frac{k-1}{2} M^2} \frac{dM^2}{M^2} \quad (6.9)$$

IMPULSE FUNCTION. From the definition of the *impulse function*,

$$F \equiv pA + \rho AV^2 = pA(1 + kM^2)$$

we get, after noting that the area is constant,

$$\frac{dF}{F} = \frac{dp}{p} + \frac{kM^2}{1 + kM^2} \frac{dM^2}{M^2} \quad (6.10)$$

Effects of Wall Friction on Fluid Properties. At this point we notice that we have seven simultaneous, linear algebraic equations, namely, Eqs. 6.4, 6.5, 6.6, 6.7, 6.8, 6.9, and 6.10, which relate eight differential variables: dp/p , $d\rho/\rho$, dT/T , dM^2/M^2 , dV^2/V^2 , dp_0/p_0 , dF/F , and $4f dx/D$. The physical phenomenon causing changes in state is viscous friction. Hence we select the variable $4f dx/D$ as independent. The remaining seven variables may consequently be found in terms of $4f dx/D$ with the aid of the seven equations. The usual methods for

solving simultaneous equations are used. For example, the term dT/T may be eliminated from Eqs. 6.4 and 6.6, yielding

$$\frac{dp}{p} = \frac{d\rho}{\rho} - \frac{k-1}{2} M^2 \frac{dV^2}{V^2}$$

Next, $d\rho/\rho$ is eliminated from this expression with the help of Eq. 6.7, thus giving

$$\frac{dp}{p} = - \frac{1 + (k-1)M^2}{2} \frac{dV^2}{V^2}$$

Finally, we use this relation for eliminating dV^2/V^2 from Eq. 6.8, and obtain, following algebraic rearrangement,

$$\frac{dp}{p} = - \frac{kM^2[1 + (k-1)M^2]}{2(1-M^2)} 4f \frac{dx}{D} \quad (6.11)$$

Using similar methods, the formulas which follow are obtained:

$$\frac{dM^2}{M^2} = \frac{kM^2 \left(1 + \frac{k-1}{2} M^2 \right)}{1 - M^2} 4f \frac{dx}{D} \quad (6.12)$$

$$\frac{dV}{V} = \frac{kM^2}{2(1-M^2)} 4f \frac{dx}{D} \quad (6.13)$$

$$\frac{dT}{T} = \frac{1}{2} \frac{dc}{c} = - \frac{k(k-1)M^4}{2(1-M^2)} 4f \frac{dx}{D} \quad (6.14)$$

$$\frac{d\rho}{\rho} = - \frac{kM^2}{2(1-M^2)} 4f \frac{dx}{D} \quad (6.15)$$

$$\frac{dp_0}{p_0} = - \frac{kM^2}{2} 4f \frac{dx}{D} \quad (6.16)$$

$$\frac{dF}{F} = - \frac{kM^2}{2(1+kM^2)} 4f \frac{dx}{D} \quad (6.17)$$

SECOND LAW OF THERMODYNAMICS. Since the flow is adiabatic, the stagnation temperature is constant. From Eq. 5.23, therefore, the entropy change is

$$\frac{ds}{c_p} = - \frac{k-1}{k} \frac{dp_0}{p_0} \quad (6.18)$$

or, using Eq. 6.16,

$$\frac{ds}{c_p} = \frac{(k-1)M^2}{2} 4f \frac{dx}{D} \quad (6.19)$$

By convention, dx is positive in the direction of flow. The Second Law of Thermodynamics states that the entropy may not decrease in an adiabatic process, whence we conclude from Eq. 6.19 that the friction coefficient f must always be a positive number. In formulating Eq. 6.8 it was assumed that the shearing stress acted on the stream in a direction opposite to the direction of flow. Since f must always be positive, we conclude that the shearing stress must always act in the direction assumed.

It appears from Eqs. 6.16 and 6.17 that both the isentropic stagnation pressure and the impulse function must decrease when friction is present. This is true for either subsonic or supersonic flow. Wall friction therefore reduces the effectiveness of all types of flow machinery and also reduces the thrust obtainable from jet propulsion devices.

SUMMARY OF FRICTIONAL EFFECTS. The directions of changes in the remaining stream properties, according to Eqs. 6.11 through 6.15, depend on whether the Mach Number is greater or less than unity, since the term $(1 - M^2)$ appears in the denominator of each of these equations. We may summarize the various changes as follows:

	Subsonic	Supersonic
Pressure, p	decreases	increases
Mach Number, M	increases	decreases
Velocity, V	increases	decreases
Temperature, T	decreases	increases
Density, ρ	decreases	increases
Stagnation Pressure, p_0	decreases	decreases
Impulse function, F	decreases	decreases

We see that the Mach Number always tends toward unity. Continuous transitions either from subsonic to supersonic flow, or from supersonic to subsonic flow, are consequently impossible. For given conditions at an initial section of the duct, therefore, the maximum possible duct length which can be employed without altering these given initial conditions and without introducing discontinuities is that length for which the exit Mach Number is exactly unity.

It is at first surprising to see that friction has the net effect of accelerating a subsonic stream, and perhaps even astonishing to observe that friction causes a rise in pressure at supersonic speeds.

Working Formulas. Our next step is to integrate the previously given differential equations in order to obtain formulas suitable for practical

computations. We shall use the Mach Number as the independent variable for this purpose.

Eq. 6.12 is rearranged to read

$$\int_0^{L_{\max}} 4f \frac{dx}{D} = \int_{M_1}^1 \frac{1 - M^2}{kM^4 \left(1 + \frac{k-1}{2} M^2\right)} dM^2$$

where the limits of integration are taken as (i) the section where the Mach Number is M_1 , and where x is arbitrarily set equal to zero, and (ii) the section where the Mach Number is unity, and x is the maximum possible length of duct, L_{\max} .

Carrying out the integration, we obtain

$$4\bar{f} \frac{L_{\max}}{D} = \frac{1 - M^2}{kM^2} + \frac{k+1}{2k} \ln \frac{(k+1)M^2}{2 \left(1 + \frac{k-1}{2} M^2\right)} \quad (6.20)$$

where \bar{f} is the mean friction coefficient with respect to length, defined by

$$\bar{f} = \frac{1}{L_{\max}} \int_0^{L_{\max}} f dx$$

Eq. 6.20 gives the maximum value of $4\bar{f}L/D$ corresponding to any initial Mach Number M_1 .

Since $4\bar{f}L_{\max}/D$ is a function only of M_1 , the length of duct L required for the flow to pass from a given initial Mach Number M_1 to a given final Mach Number M_2 is found from the expression

$$4\bar{f} \frac{L}{D} = \left(4\bar{f} \frac{L_{\max}}{D}\right)_{M_1} - \left(4\bar{f} \frac{L_{\max}}{D}\right)_{M_2} \quad (6.21)$$

To illustrate how the local stream properties are found in terms of the local Mach Number, we shall take the pressure as an example. First, we note that Eqs. 6.11 and 6.12 may be combined to give

$$\frac{dp/p}{dM^2/M^2} = - \frac{1 + (k-1)M^2}{2 \left(1 + \frac{k-1}{2} M^2\right)}$$

or,

$$\frac{dp}{p} = - \frac{1 + (k-1)M^2}{2M^2 \left(1 + \frac{k-1}{2} M^2\right)} dM^2$$

Denoting the pressure at $M = 1$ by the symbol p^* , we integrate between the section where $M = M$, $p = p$, and the section where $M = 1$, $p = p^*$, and thus obtain

$$\frac{p}{p^*} = \frac{1}{M} \sqrt{\frac{k+1}{2\left(1 + \frac{k-1}{2}M^2\right)}} \quad (6.22)$$

By similar methods we get the relations which follow:

$$\frac{V}{V^*} = M \sqrt{\frac{k+1}{2\left(1 + \frac{k-1}{2}M^2\right)}} \quad (6.23)$$

$$\frac{T}{T^*} = \frac{c^2}{c^{*2}} = \frac{k+1}{2\left(1 + \frac{k-1}{2}M^2\right)} \quad (6.24)$$

$$\frac{\rho}{\rho^*} = \frac{V^*}{V} = \frac{1}{M} \sqrt{\frac{2\left(1 + \frac{k-1}{2}M^2\right)}{k+1}} \quad (6.25)$$

$$\frac{p_0}{p_0^*} = \frac{1}{M} \sqrt{\left[2\left(1 + \frac{k-1}{2}M^2\right)\right]^{\frac{k+1}{k-1}}} \quad (6.26)$$

$$\frac{F}{F^*} = \frac{1 + kM^2}{M \sqrt{2(k+1)\left(1 + \frac{k-1}{2}M^2\right)}} \quad (6.27)$$

$$\frac{s - s^*}{c_p} = \ln M^2 \sqrt{\left[\frac{k+1}{2M^2\left(1 + \frac{k-1}{2}M^2\right)}\right]^{\frac{k+1}{k}}} \quad (6.28)$$

The quantities marked with an asterisk in these expressions, such as p^* , V^* , etc., represent the values of the stream properties at the section in the duct where $M = 1$. Since they are constants for a given adiabatic, constant-area flow, they may be regarded as convenient reference values for normalizing the equations. In order to find the change in some

stream property, say the pressure, between the sections where the Mach Numbers are M_1 and M_2 , respectively, we set

$$\frac{p_2}{p_1} = \frac{(p/p^*)_{M_2}}{(p/p^*)_{M_1}}$$

where $(p/p^*)_{M_2}$ is the value of the right-hand side of Eq. 6.22 corresponding to M_2 , and so forth.

Graphical Representation of Working Formulas. The formulas of Eqs. 6.20 to 6.27 are represented graphically in Figs. 6.4 and 6.5, from which general orders of magnitude and rates of change may be found with ease. On this chart the curve of $4fL_{\max}/D$ is the key to direction of change, inasmuch as $4fL_{\max}/D$ must always decrease.

Working Tables. For extensive or accurate numerical calculations, the important dimensionless ratios are tabulated in Table B.4, with Mach Number as the argument.

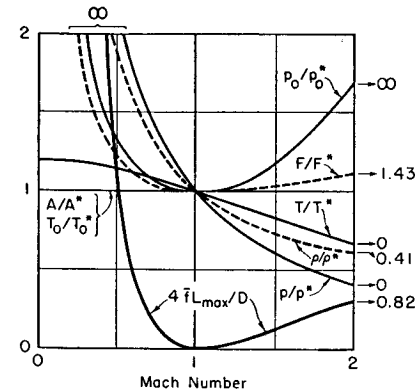


FIG. 6.4. Variation of fluid properties on Fanno line, $k = 1.4$.

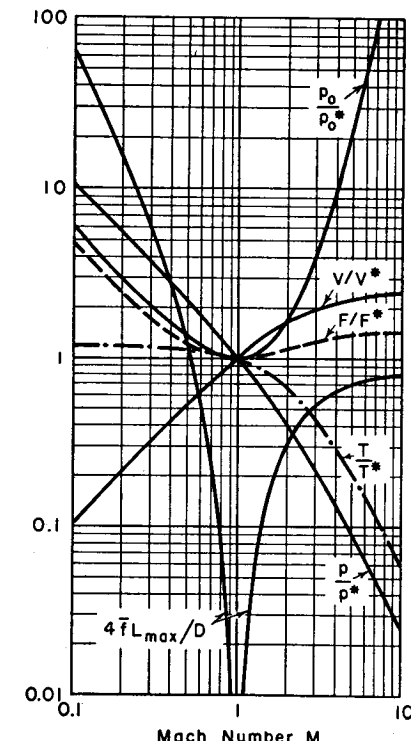


FIG. 6.5. Variation of fluid properties on Fanno line, $k = 1.4$.

Illustrative Example.

PROBLEM. With an experimental rig comprising a converging-diverging nozzle attached to a smooth, round tube, the following data were obtained with the aim of measuring friction coefficients for the supersonic flow of air:

Pressure upstream of nozzle = 516 cm Hg abs

Temperature upstream of nozzle = 107.3°F

Throat diameter = 0.2416 inches
 Diameter of nozzle exit and of tube = 0.5009 inches
 Pressure of stream at a point 1.75 diameters from tube inlet
 = 18.25 cm Hg abs
 Pressure of stream at a point 29.60 diameters from tube inlet
 = 37.1 cm Hg abs

It is desired to calculate the average friction coefficients between the sections where $x/D = 1.75$ and $x/D = 29.60$. It will be assumed that the flow to the throat of the nozzle is isentropic, and that the flow in the entire system is adiabatic.

SOLUTION. Since the flow to the throat is isentropic and the entire flow is adiabatic, the column labeled $(p/p_0)(A/A^*)$ in Table B.2 may be used, as explained in Chapter 4, for finding the Mach Number at any section.

$$(A/A^*)_1 = (0.5009/0.2416)^2 = 4.2986$$

$$(p/p_0)_1 = 18.25/516 = 0.03537$$

$$(p/p_0)_1(A/A^*)_1 = (0.03537)(4.2986) = 0.1520$$

From Table B.2, then, $M_1 = 2.524$

Using this value of M_1 , we get, from Table B.4,

$$(p/p^*)_1 = 0.2878$$

$$(4fL_{\max}/D)_1 = 0.4371$$

Now, since

$$\frac{p_2}{p_1} = \frac{(p/p^*)_2}{(p/p^*)_1}$$

we obtain

$$(p/p^*)_2 = \frac{37.1}{18.25} (0.2878) = 0.5850$$

Entering Table B.4 with this value of $(p/p^*)_2$, we find that

$$M_2 = 1.542$$

$$(4fL_{\max}/D)_2 = 0.1512$$

Therefore,

$$4f \frac{\Delta L}{D} = 0.4371 - 0.1512 = 0.2859$$

and, since

$$\Delta L/D = 29.60 - 1.75 = 27.85$$

the average friction coefficient is

$$\bar{f} = \frac{0.2859}{4(27.85)} = 0.0257$$

Limiting Duct Length for Supersonic Speeds. Frictional effects are very serious at high Mach Numbers. To illustrate, the following table

shows the maximum length-diameter ratio for several initial Mach Numbers, assuming that $f = 0.0025$:

M_{\max}/D	0	.25	.50	.75	1	1.5	2	3	∞
	∞	850	110	12	0	14	31	52	82

An interesting fact revealed by this table is that for purely supersonic flow, no matter how great the initial Mach Number, the total length of duct is limited to about 82 diameters for a friction coefficient of 0.0025. Apart from this, the large losses in stagnation pressure which are incurred at supersonic speeds make it desirable to avoid long runs of duct in which the flow is supersonic. For example, with an initial Mach Number of 3.0 and a friction coefficient of 0.0025, the Mach Number is reduced to 2.0 in 21 duct diameters, and at the same time the isentropic stagnation pressure is reduced to about 40 per cent of the initial value.

Choking Due to Friction. If the value of $4fL/D$ between two sections is fixed, then for each initial Mach Number M_1 there will correspond a certain final Mach Number M_2 which may be easily found from Fig. 6.5. Illustrative curves of M_2 versus M_1 constructed in this way are shown in Fig. 6.6 for values of $4fL/D$ of 0 and 0.1.

For the limiting case where $4fL/D$ is equal to zero, there is of course a trivial solution for which $M_1 = M_2$ and there are no changes in any stream properties. On the other hand, a shock might occur in zero length. The corresponding initial and final Mach Numbers for a shock may be found from Figs. 6.4 and 6.5 by connecting the two branches of the F/F^* curve with a horizontal line, since the normal shock conditions of constant area, constant stagnation temperature, and constant impulse function are then satisfied. In Fig. 6.6 the curved line labeled $4fL/D = 0$ represents, therefore, a normal shock. The portion of this line for which M_1 is less than unity is imaginary, since it corresponds to an expansion shock.

When there are no shocks present, the relative magnitudes of M_1 and M_2 for a fixed length of duct are illustrated in Fig. 6.6 by the solid curves labelled $4fL/D = 0.1$. If the flow is initially supersonic, i.e., if $M_1 > 1$, there is a possibility of shocks occurring in the given length of duct. The relation between M_1 and M_2 will then depend on the location of the

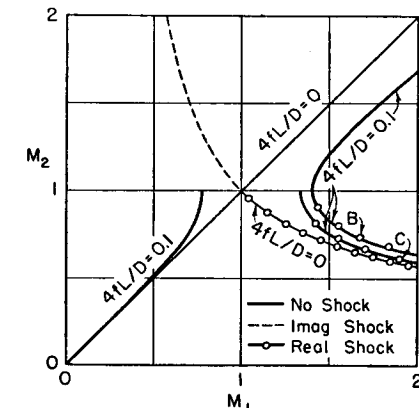


FIG. 6.6. Illustrates choking due to an increase in $4fL/D$.

shock. In Fig. 6.6 the curves labeled *B* and *C* represent the two extreme locations: *B* referring to a normal shock at the exit of the duct, and *C* referring to a normal shock at the inlet to the duct.

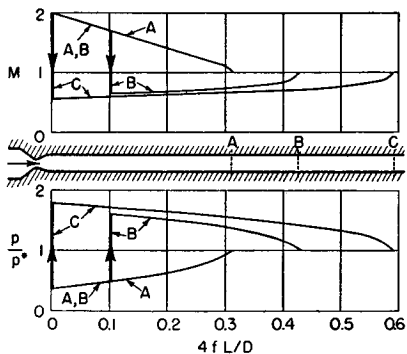
It is clear from Fig. 6.6 that for any initial Mach Number there is a maximum value of $4fL/D$ for which a solution is possible, and that $M_2 = 1$ at this condition. From a different point of view, for a given value of $4fL/D$ there is in subsonic flow a maximum initial Mach Number for which a solution is possible, and in supersonic flow a minimum initial Mach Number for which a solution may be found. It is pertinent to ask, therefore, what happens when the duct length initially has its maximum value for a given M_1 and the duct length is subsequently increased. In answering this question we shall suppose that the back pressure to which the duct exhausts is maintained as low as necessary, so that any diminutions in the flow are due exclusively to limiting effects produced by friction.

SUBSONIC FLOW. An increase in the value of $4fL/D$ over its maximum value will act to decrease M_1 until a steady-state solution again becomes possible with $M_2 = 1$. This results in a reduction in the flow rate, i.e., the flow is "choked" by friction.

SUPersonic FLOW. An increase in the value of $4fL/D$ over its maximum value at first produces a shock in the duct which moves upstream as the duct length is increased. In

other words, for a fixed M_1 and a variable $4fL/D$, the value of M_2 remains at unity, but the flow pattern in the duct moves from a condition corresponding to curve *B* in Fig. 6.6 toward a condition corresponding to curve *C*. After the shock reaches the duct inlet, a further increase in duct length causes the shock to move into the nozzle which feeds the duct. This causes the Mach Number at the inlet to the duct to become subsonic. Further increases in duct length cause the shock to move farther into the nozzle, which in the duct inlet. Finally, the shock vanishes in the throat, and further increases in length produce reductions in flow rate.

Fig. 6.7 shows the course of states in a duct of varying length with an initial Mach Number of 2. Length *A* represents the maximum length



turn reduces the Mach Number at the duct inlet. Finally, the shock vanishes in the throat, and further increases in length produce reductions in flow rate.

Fig. 6.7 shows the course of states in a duct of varying length with an initial Mach Number of 2. Length *A* represents the maximum length

without a shock. When the length is increased to *B*, a shock stands in the passage. Finally, when the length is increased to *C*, the shock stands at the inlet of the duct length, and the flow in the entire duct is subsonic.

6.3. Performance of Long Ducts at Various Pressure Ratios

To illustrate an important aspect of choking, let us investigate how the adiabatic flow in a duct varies with the ratio of back pressure to supply pressure. We must distinguish between two cases: (i) that in which the duct is fed by a converging nozzle, and (ii) that in which it is fed by a converging-diverging nozzle.

Duct Fed by Converging Nozzle. First we shall consider the case of a duct fed by a frictionless, converging nozzle. Referring to Fig. 6.8a, suppose that the supply pressure, p_{0I} , and the supply temperature, T_0 , are fixed, and that the back pressure, p_B , is variable. Conditions at the duct inlet are denoted by the subscript *I*, and at the duct exit by the subscript *E*. Four conditions of operation, namely, *a*, *b*, *c*, and *d*, are shown in Figs. 6.8b through 6.8f. The states at the inlet for these conditions are represented by the symbols *a'*, *b'*, *c'*, and *d'*, and the corresponding states at the exit by *a''*, *b''*, *c''*, and *d''*.

In condition *a* the back pressure is slightly less than the supply pressure. There are small pressure drops through the supply nozzle and duct. The stream leaving the duct is subsonic, and is therefore at a pressure equal to the back pressure.

A reduction in back pressure to condition *b* acts to increase the flow rate and the pressure drops in the nozzle and duct. The leaving stream is at a higher Mach Number than for condition *a*, but is still subsonic. Thus, conditions *a* and *b* are qualitatively equivalent.

No qualitative changes are observed until the back pressure is reduced to the value corresponding to condition *c*, at which point the exit Mach Number is unity. Further reductions in back pressure cannot produce further increases in flow rate, because M_E cannot become greater than unity. Thus the flow pattern within the duct for condition *d* is identical with that for condition *c*, and the flow is choked. The expansion to the back pressure for condition *d* involves oblique expansion waves in the stream leaving the duct.

Based on these considerations, and using the isentropic flow equations for the nozzle together with the relations derived in this chapter for adiabatic flow in a duct, Fig. 6.9a shows the flow passed by ducts of various length with various ratios of exhaust pressure to supply pressure. When this ratio is sufficiently low, the flow is choked; then Fig. 6.9b shows the ratio of the maximum flow which can be passed by the nozzle—

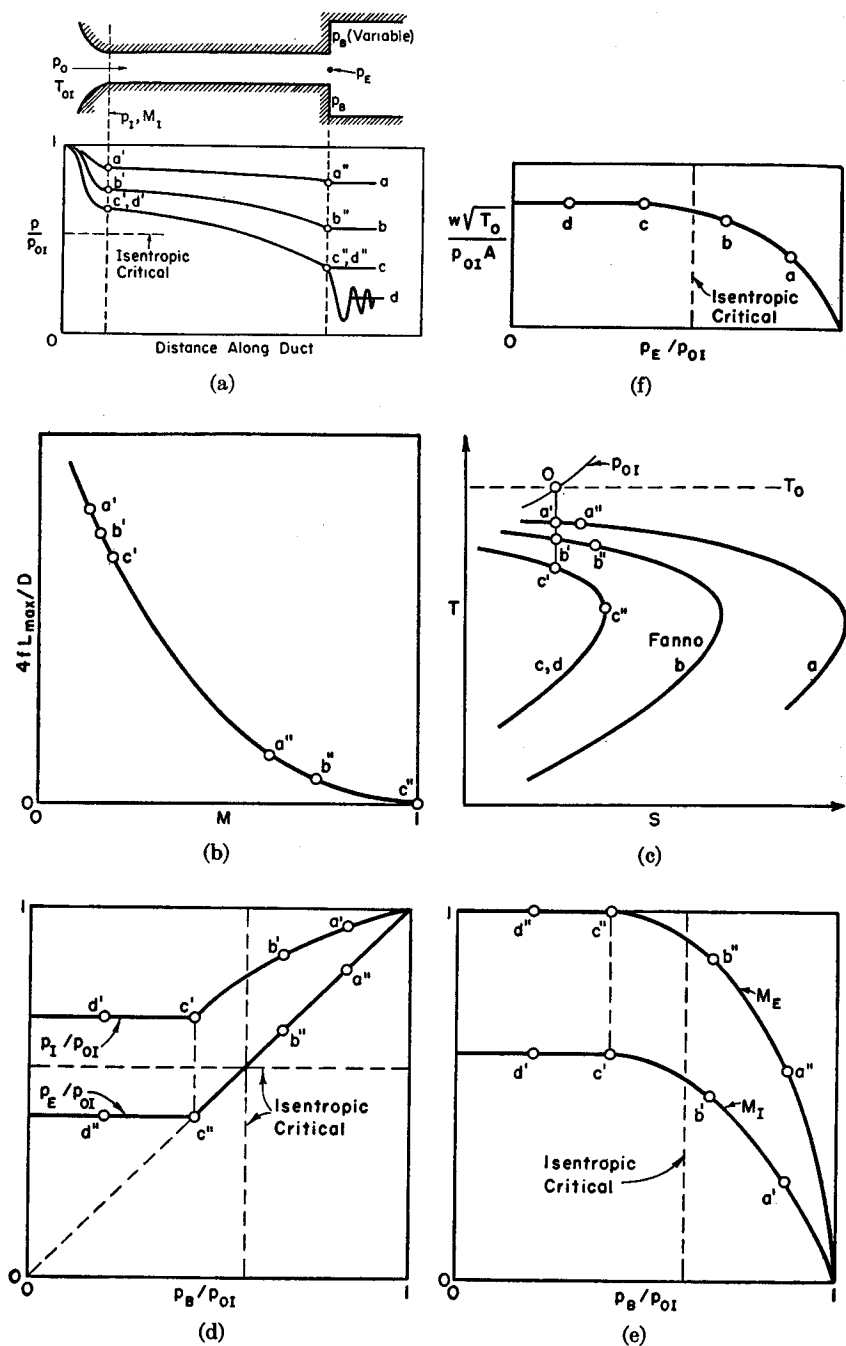
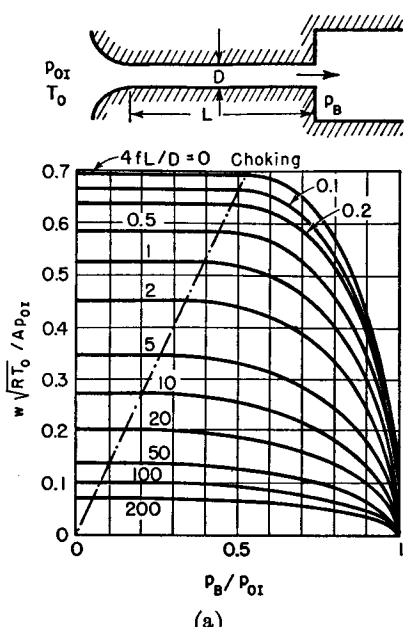


FIG. 6.8. Performance of duct fed by converging nozzle.

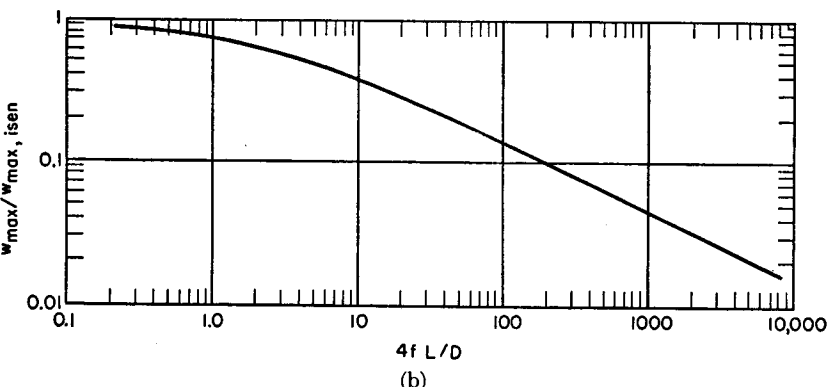
duct combination to the maximum flow which can be passed by the nozzle alone.

Duct Fed by Converging-Diverging Nozzle. Let us consider next the case of a long duct which is fed by a frictionless converging-diverging nozzle. Referring to Fig. 6.10, we shall suppose the supply pressure p_{0I} and supply temperature T_0 to be held constant, and that the back pressure, p_B , is variable. The pressure at the inlet of the duct will be denoted by p_I , and at the exit by p_E .

The operation of the system of Fig. 6.10 under a varying back pressure is considerably more complex than is that of Fig. 6.8, chiefly



(a)



4fL/D

(b)

FIG. 6.9. Flow passed by long adiabatic duct fed by isentropic converging nozzle ($k = 1.4$).

- Dimensionless flow parameter versus ratio of exhaust pressure to supply pressure.
- Ratio of choking flow to choking flow through nozzle alone, as function of $4fL/D$.

because the converging-diverging nozzle of fixed area ratio allows of only one Mach Number greater than unity at the duct inlet. We shall confine our attention to the case where there are no shocks in the nozzle, since the flow characteristics of the nozzle alone have been discussed in Art. 5.10, and the characteristics of subsonic flow in a long duct have just been examined.

Since the nozzle is without shocks, the pressure and Mach Number at section I are fixed by the area ratio of the nozzle. To the Mach Number M_I corresponds a particular value of $4fL_{\max}/D$ according to Eq. 6.20. We therefore divide the types of flow into two main classes, depending

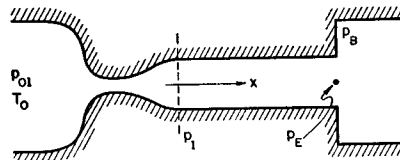


FIG. 6.10. Duct fed by isentropic converging-diverging nozzle.

on whether the actual length of duct gives a value of $4fL/D$ greater or less than the maximum allowable value. For convenience in classification, the pressure at the duct exit for *shockless flow* is denoted by $p_{E'}$, regardless of whether shockless flow can in fact occur. The pressure corresponding to Mach Number unity is denoted by p^* . We may now define the classes of flow as follows:

CLASS (1). The duct length is less than the maximum possible length, so that $p_{E'} < p^*$ and $L < L_{\max}$ (Fig. 6.11).

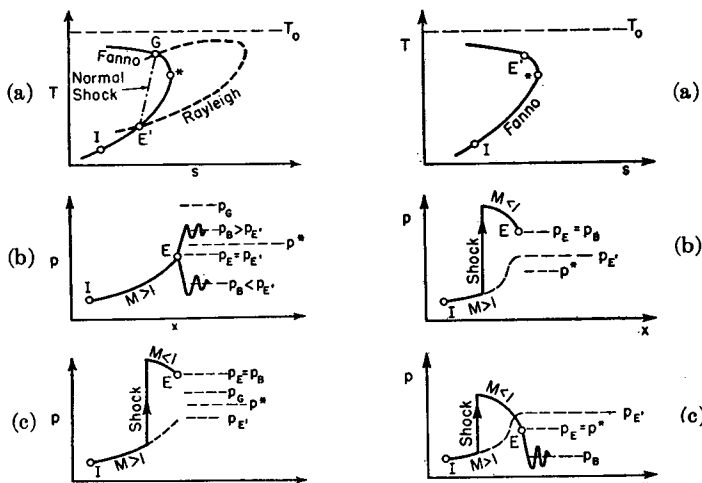


FIG. 6.11. Operation of system of Fig. 6.10 when $p_{E'} < p^*$ and $L < L_{\max}$.

CLASS (2). The duct length is greater than the maximum possible length, so that $p_{e'}$ > p^* and $L > L_{\max}$ (Fig. 6.12).

The value of p^* is a function only of M_I and p_I . The value of $p_{E'}$, on the other hand, depends on M_I , p_I , and $4fL/D$.

We shall now discuss the several types of flow in each class.

CLASS (1a): $p_{E'} < p^*$, and $p_B < p_{E'}$ (Fig. 6.11b). The duct length is less than the maximum, and the back pressure is lower than the exit pressure for shockless flow.

A shock cannot be present, for, if it were, the flow at the tube exit would in general be subsonic. But, as the exit pressure would therefore have to be identical with the back pressure, the entropy would decrease adiabatically near the end of the tube.

Accordingly, we conclude that the flow in the tube is shockless. The actual exit pressure, p_E , is then determined completely by the magnitudes of p_I , M_I , and $4fL/D$. In other words, $p_E = p_{E'}$, and the exit flow is supersonic.

The stream leaves the tube at a pressure higher than the back pressure, and the adjustment to the back pressure occurs downstream of the duct exit in the form of oblique expansion waves.

CLASS (1b): $p_{E'}$ < p^* , and $p_G > p_B > p_{E'}$ (Fig. 6.11b). The duct length is less than the maximum, and the back pressure is, within limits, greater than the exit pressure for shockless flow.

If the back pressure, p_B , is not too much greater than the pressure $p_{E'}$, there will be no shocks in the duct, and the flow pattern in the duct will be identical with that for Class (1a). The adjustment of the stream to the back pressure will then occur outside the duct in the form of oblique shock waves.

After the back pressure is raised to the value corresponding to the pressure p_G downstream of a normal shock in the duct exit, further increases in back pressure cause a normal shock to appear in the duct.

CLASS (1c): $p_{E'} < p^*$, and $p_B > p_G$ (Fig. 6.11c). The duct length is less than the maximum, but the back pressure is so high that the stream cannot leave the duct in supersonic flow (with the pressure $p_{E'}$) and adjust itself to the back pressure.

Instead, a normal shock stands in the duct, with subsonic flow in the part of the duct downstream of the shock. As the flow at the duct exit is subsonic, the actual exit pressure p_E must be identical with the back pressure p_B . This condition, namely, that $p_E = p_B$, determines the location of the shock.

An increase in back pressure causes the shock to move upstream. Ultimately it moves into the diverging portion of the nozzle, and, after the shock disappears into the throat, further increases in back pressure produce a reduction in flow rate.

CLASS (2a): $p_{E'} > p^*$, and $p_B > p^*$ (Fig. 6.12b). Shockless flow to the exit (shown by the dashed curve in Fig. 6.12b) would involve a decrease of entropy. Consequently, a shock stands in the duct. Since

$p_B > p^*$, the flow at the duct exit must be subsonic, and, therefore, the exit pressure p_E must be identical with the back pressure p_B . This condition, namely, that $p_E = p_B$, determines the location of the shock in the tube.

Increases in the back pressure cause the shock to move upstream and ultimately to vanish in the throat of the nozzle.

Class (2b): $p_E > p^*$, and $p_B < p^*$ (Fig. 6.12c). As in the case of Class (2a), the duct length is so great that it is impossible for the flow to be supersonic in the entire length of duct. Accordingly, a shock is present.

The flow at the duct exit cannot be supersonic, for the flow downstream of the shock is subsonic and can, therefore, not become supersonic except through area change or heat transfer.

Furthermore, the flow at the duct exit cannot be subsonic, with a pressure greater than p^* , for on leaving the duct it would diverge on account of the exit pressure being greater than the back pressure, and the pressure increase produced by this divergence would make it impossible for the stream ever to adjust itself to the back pressure.

The sole remaining possibility is that the stream leaves the duct at Mach Number unity, or, in other words, that $p_E = p^*$. The adjustment of the stream to the back pressure then occurs outside the duct in the form of oblique expansion waves. As long as the back pressure is less than p^* , therefore, there is only one location in the duct at which the shock may stand.

Finally, it should be mentioned that the flow patterns of Figs. 6.10 and 6.11 are idealized in that the shocks are shown as discontinuities. Because of boundary-layer effects, the transition from supersonic to subsonic flow is more likely to be extended over a considerable distance, as explained in Chapter 5.

6.4. Isothermal Flow in Long Ducts

As pointed out earlier, isothermal flow with friction is of interest in connection with pipe lines for transporting gas over long distances. Although the Mach Numbers for such flows are usually quite low, there are substantial changes in pressure owing to the great lengths over which friction acts, and so the flow may not be treated as incompressible.

Governing Physical Equations and Definitions. The analysis is parallel to that for adiabatic flow, except that the energy equation now includes changes in stagnation temperature. For a perfect gas the energy equation may be written

$$dQ = c_p dT + d \frac{V^2}{2} = c_p dT_0 \quad (6.29)$$

where T_0 is the local adiabatic stagnation temperature, i.e., the temperature which the local stream would acquire if brought to rest adiabatically. The change in T_0 is a direct measure of the amount and direction of heat transfer.

In Chapter 4 we derived the relation

$$T_0 = T \left(1 + \frac{k-1}{2} M^2 \right)$$

Taking logarithmic differentials and noting that $dT = 0$, we get

$$\frac{dT_0}{T_0} = \frac{(k-1)M^2}{2 \left(1 + \frac{k-1}{2} M^2 \right)} \frac{dM^2}{M^2} \quad (6.30)$$

For isothermal flow, the equation of state of a perfect gas becomes

$$dp/p = d\rho/\rho \quad (6.31)$$

Similarly, Eq. 6.5 becomes

$$dM^2/M^2 = 2 dV/V \quad (6.32)$$

Eqs. 6.7, 6.8 and 6.9 are valid as they stand for isothermal flow.

Qualitative Effects of Friction Under Isothermal Conditions. Solving the simultaneous equations, Eqs. 6.30, 6.31, 6.32, 6.7, 6.8, and 6.9, with $4f dx/D$ as the independent variable, we get

$$\frac{dp}{p} = \frac{d\rho}{\rho} = - \frac{dV}{V} = - \frac{1}{2} \frac{dM^2}{M^2} = - \frac{kM^2}{2(1-kM^2)} 4f \frac{dx}{D} \quad (6.33)$$

$$\frac{dp_0}{p_0} = \frac{kM^2 \left(1 - \frac{k+1}{2} M^2 \right)}{2(kM^2 - 1) \left(1 + \frac{k-1}{2} M^2 \right)} 4f \frac{dx}{D} \quad (6.34)$$

$$\frac{dT_0}{T_0} = \frac{k(k-1)M^4}{2(1-kM^2) \left(1 + \frac{k-1}{2} M^2 \right)} 4f \frac{dx}{D} \quad (6.35)$$

From these equations it is seen that the direction of change depends not on whether the flow is subsonic or supersonic, but principally on whether kM^2 is greater or less than unity. Noting that $4f dx/D$ is always

positive, the directions of change are summarized for gases with $k > 1$ in the table which follows.

	$M < 1/\sqrt{k}$ (Subsonic)	$M > 1/\sqrt{k}$ (Subsonic or Supersonic)
Pressure	decreases	increases
Density	decreases	increases
Velocity	increases	decreases
Mach Number	increases	decreases
Stagnation temperature	increases	decreases
Stagnation pressure	decreases	$\begin{cases} \text{increases for } M < \sqrt{2/(k+1)} \\ \text{decreases for } M > \sqrt{2/(k+1)} \end{cases}$

It is seen that the Mach Number always tends towards $1/\sqrt{k}$. This value therefore represents a limit for continuous isothermal flow, in the same way that $M = 1$ represents a limit for continuous adiabatic flow. When M is less than $1/\sqrt{k}$, heat is added to the stream; when M exceeds $1/\sqrt{k}$, heat is rejected from the stream.

Working Formulas. Eq. 6.33 may be rearranged to give

$$\int_0^{L_{\max}} 4f \frac{dx}{D} = \int_{M^2}^{1/k} \frac{1 - kM^2}{kM^4} dM^2$$

where the lower limit of integration is taken at $x = 0$, $M = M_0$, and the upper limit is taken at $M = 1/\sqrt{k}$, beyond which the continuous isothermal flow may not proceed. Integration yields

$$4f \frac{L_{\max}}{D} = \frac{1 - kM^2}{kM^2} + \ln kM^2 \quad (6.36)$$

Now $M^2 = V^2/kRT$, and T is constant. Denoting properties at $M = 1/\sqrt{k}$ by such symbols as V^{*t} , p^{*t} , etc., we may write, therefore,

$$\frac{M^2}{V^2} = \frac{1/k}{(V^{*t})^2}$$

from which

$$\frac{V}{V^{*t}} = \sqrt{k} \mathbb{M} \quad (6.37)$$

From the equation of continuity,

$$\rho V = \rho^{*t} V^{*t}; \quad \therefore \quad \frac{\rho}{\rho^{*t}} = \frac{1}{\sqrt{k} M} \quad (6.38)$$

The perfect-gas relation yields

$$\frac{p}{p^{*t}} = \frac{\rho}{\rho^{*t}} = \frac{1}{\sqrt{k} M} \quad (6.39)$$

Art. 6.4 ISOTHERMAL FLOW IN LONG DUCTS

$$\begin{aligned} \frac{p_0}{p_0^{*t}} &= \frac{p}{p^{*t}} \frac{\left(1 + \frac{k-1}{2} M^2\right)^{\frac{k}{k-1}}}{\left(1 + \frac{k-1}{2} \frac{1}{k}\right)^{\frac{k}{k-1}}} \\ &= \frac{1}{\sqrt{k}} \left(\frac{2k}{3k-1}\right)^{\frac{k}{k-1}} \frac{\left(1 + \frac{k-1}{2} M^2\right)^{\frac{k}{k-1}}}{M} \end{aligned} \quad (6.40)$$

Finally, the formula for stagnation temperature yields

$$\frac{T_0}{T_0^{*t}} = \frac{T}{T^{*t}} \frac{1 + \frac{k-1}{2} M^2}{1 + \frac{k-1}{2} \frac{1}{k}} = \frac{2k}{3k-1} \left(1 + \frac{k-1}{2} M^2 \right) \quad (6.41)$$

Working Charts. The formulas of Eqs. 6.36 to 6.41 are represented graphically in Fig. 6.13. The procedure for employing the working formulas and chart for computations is similar to that for adiabatic pipe flow.

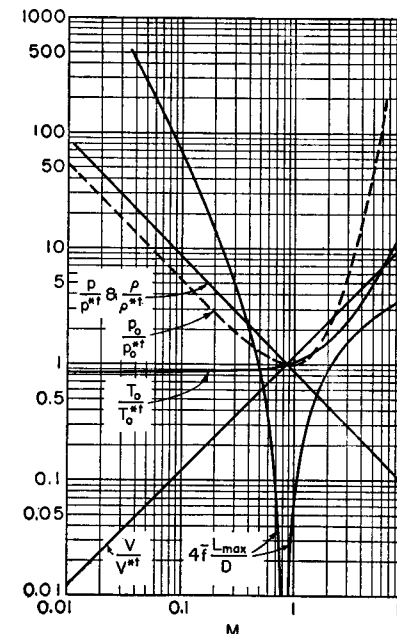


FIG. 6.13. Working chart for isothermal flow in ducts $k = 1.4$

Relations for Low Mach Numbers. In long commercial pipe lines the Mach Numbers employed are so low that the loss in stagnation pressure is virtually identical with the loss in static pressure. For such cases it is useful to have a direct relation connecting p_2/p_1 , $4fL/D$, and M_1 , where subscripts 1 and 2 refer respectively to the inlet and exit conditions for a pipe of length L . From Eq. 6.36,

$$4f \frac{L}{D} = \left(4f \frac{L_{\max}}{D} \right)_1 - \left(4f \frac{L_{\max}}{D} \right)_2$$

$$= \frac{1 - kM_1^2}{kM_1^2} - \frac{1 - kM_2^2}{kM_2^2} + \ln \frac{M_1^2}{M_2^2}$$

Also, from Eq. 6.39,

$$\frac{p_1}{p_2} = \frac{M_2}{M_1}; \quad \therefore \quad M_2 = M_1 \frac{p_1}{p_2}$$

Substituting this value of M_2 into the previous equation, and rearranging, we obtain

$$4f \frac{L}{D} = \frac{1 - \left(\frac{p_2}{p_1} \right)^2}{kM_1^2} - \ln \left(\frac{p_1}{p_2} \right)^2 \quad (6.42)$$

Fig. 6.14 is a convenient nomograph representing this relation. From Eq. 6.39 and the fact that M_2 cannot exceed $1/\sqrt{k}$, it follows that

$$\left(\frac{p_2}{p_1} \right)^2 > kM_1^2$$

Hence, although for given values of M_1 and $4fL/D$ there are two solutions for p_2/p_1 , only the left-hand intersection may be used. The right-hand intersection implies negative values of f and involves a violation of the Second Law of Thermodynamics. A tangent-type intersection indicates choking flow, and, when there is no intersection at all, L exceeds L_{\max} .

When the per cent pressure drop is fairly small, it is convenient to expand the right-hand side of Eq. 6.42 in a power series of the fractional pressure drop, $(p_1 - p_2)/p_1$. Carrying out this expansion, and retaining terms up to the second power of this variable, we obtain the following useful approximation applicable to low pressure drops:

$$4f \frac{L}{D} \cong \frac{2}{kM_1^2} \left(\frac{p_1 - p_2}{p_1} \right) \left[(1 - kM_1^2) - \left(\frac{1 + kM_1^2}{2} \right) \left(\frac{p_1 - p_2}{p_1} \right)^2 \right] \quad (6.43a)$$

The conventional pressure-drop formula for incompressible flow is similar to Eq. 6.43a except that the square bracket on the right-hand side has the value unity. From this we see that the error incurred through assuming the fluid incompressible is negligible only when both kM_1^2 and $(p_1 - p_2)/p_1$ are both negligible compared with unity.

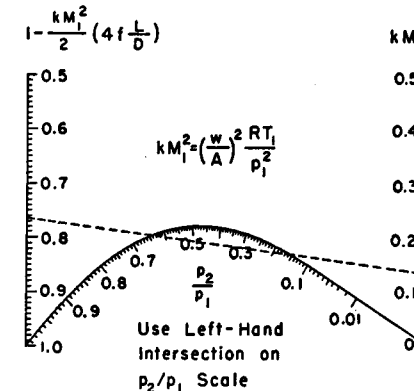


FIG. 6.14. Nomograph for determining static pressure drop for isothermal flow in duct of length L . Subscripts 1 and 2 refer respectively to inlet and exit conditions. *Example:* If $k = 1.4$, $M_1 = 0.313$, and $4fL/D = 3.43$, then left-hand ordinate is 0.765 and right-hand ordinate is 0.137; using left-hand intersection, $p_2/p_1 = 0.638$. (After G. W. Thomson, *Ind. and Eng. Chem.*, Vol. 34, No. 12, July, 1942, p. 1485.)

Eq. 6.43a is a quadratic in the fractional pressure drop, and may be solved explicitly for the latter in the convenient form

$$\frac{p_1 - p_2}{p_1} = \frac{1 - kM_1^2}{1 + kM_1^2} - \sqrt{\frac{(1 - kM_1^2)^2}{(1 + kM_1^2)^2} - \frac{kM_1^2}{1 + kM_1^2} \left(4f \frac{L}{D} \right)} \quad (6.43b)$$

In employing Eqs. 6.42 and 6.43 it is convenient to remember that

$$kM_1^2 = \left(\frac{w}{A} \right)^2 \frac{RT_1}{p_1^2} \quad (6.44)$$

Choking Effects. Since, for a given value of M_1 , there is a maximum length for continuous isothermal flow, it follows that choking effects may occur in similar fashion to those for adiabatic pipe flow.

It should be kept in mind, however, that when a subsonic isothermal flow approaches the limiting Mach Number, all fluid properties change rapidly with distance. Unless heat is transferred purposefully, therefore, the flow process under these circumstances is likely to be more nearly adiabatic rather than isothermal. At $M = 1/\sqrt{k}$, Eqs. 6.35 and 6.29 indicate the need for infinite heat transfer per unit length; thus this limit is artificial and not physically real.

6.5. Experimental Friction Coefficients

Subsonic Flow. Keenan and Neumann⁽¹⁾ measured friction coefficients for turbulent flow in smooth pipes over a range of Mach Numbers between zero and nearly unity (Volume II, Chapter 28).

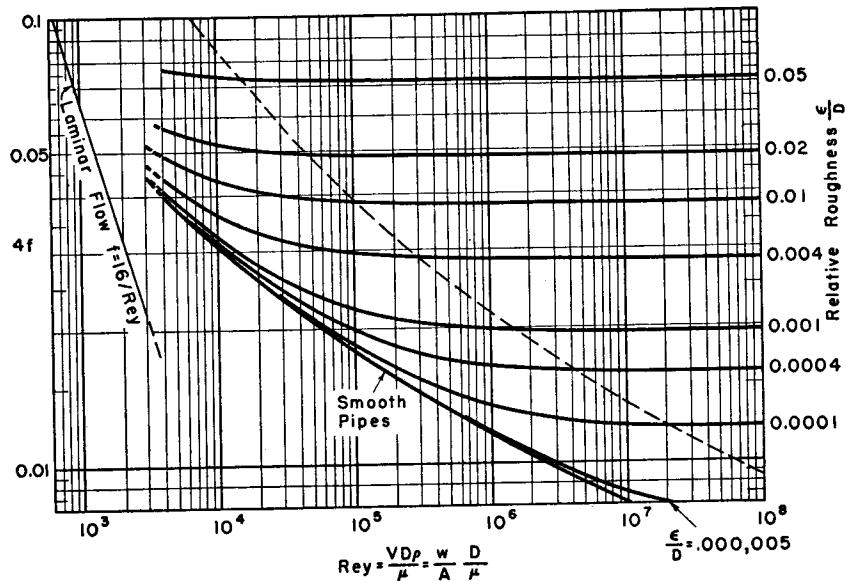


FIG. 6.15. Friction coefficient versus pipe Reynolds number for incompressible, fully developed flow. Roughness of pipe is measured by ϵ , and has typical values as follows (after Moody):

Pipe	ϵ , ft
Drawn tubing	0.000005
Commercial steel	0.00015
Asphalted cast iron	0.0004
Galvanized iron	0.0005
Cast iron	0.00085
Concrete	0.001-0.01
Riveted steel	0.003-0.03

For a fully developed velocity profile, i.e., at distances from the duct inlet greater than about 50 diameters, no significant effect of Mach Number was observed. In other words, the relation between friction coefficient and pipe Reynolds Number for subsonic flow at any Mach Number was found to agree with the well-known Karman-Nikuradse formula for incompressible flow:

$$\frac{1}{\sqrt{4f}} = -0.8 + 2 \log_{10} [\text{Rey} \sqrt{4f}] \quad (6.45)$$

where Rey is the pipe Reynolds Number based on diameter.

For ready reference, the incompressible friction coefficient is plotted versus Rey in Fig. 6.15 for both smooth pipes and for rough pipes, in a form developed by Moody.⁽²⁾

SHORT PIPES. Near the duct inlet the one-dimensional analysis is misleading, for the changes in velocity profile which occur there have associated with them changes of momentum flux of appreciable magnitude. In the region of changing velocity profile, therefore, the symbol f in Eq. 6.8 represents an "apparent friction coefficient," since it includes momentum-flux effects as well as the effects of shearing stress.

The measurements of Reference 3 indicate that near the inlet the flow is similar to that on a flat plate, inasmuch as the boundary-layer thickness is a small fraction of the pipe diameter. The Reynolds Number based on distance from the inlet is more significant than the pipe Reynolds Number, and the boundary layer is laminar up to a length Reynolds Number of about $5(10)^5$. For short pipes the average apparent friction coefficient may be substantially in excess of that shown in Fig. 6.15.

Supersonic Flow. The foregoing remarks concerning flow in short ducts apply with special force to supersonic flow, since the maximum possible length of duct for supersonic flow is so small that a fully developed flow can never be established. Here it might be stated parenthetically that at high Mach Numbers, fully developed flow could not be realized even in very long ducts, since all fluid properties change rapidly along the length of duct.

The complexities thus introduced are discussed in some detail in Chapter 28. Here we shall simply point out that the local apparent friction coefficient is influenced by (i) Mach Number, (ii) whether the local boundary layer is laminar or turbulent, (iii) changes in momentum flux associated with changes in velocity profile owing to the regular development of either a laminar or turbulent boundary layer, (iv) changes in momentum flux shortly after transition because of a fairly rapid change from a laminar velocity profile to a turbulent velocity profile, and (v) changes in momentum flux occurring after the boundary layer fills the pipe because of continuous alterations in the "fully developed velocity profile."

It is evident from these considerations that the local apparent friction coefficient is likely to be significantly dependent upon several factors, including Mach Number, pipe Reynolds Number, length Reynolds Number, initial thickness of boundary layer, and initial degree of turbulence. Consequently the experimental data^(1,4) are most notable for the scatter displayed, with no simple correlation seemingly possible; under certain conditions the local apparent friction coefficient may even be negative. To obtain a more coherent correlation of the data, it is necessary to take account of two-dimensional effects because the one-

dimensional model of the flow omits certain essential features. Of course this complicates considerably the otherwise simple calculations.

EXPERIMENTAL RESULTS. To assist in making order-of-magnitude estimates, the results of Keenan and Neumann⁽¹⁾ may be summarized as follows:

For tubes between 10 and 50 tube diameters in length, the average apparent friction coefficient for the entire tube length was found to vary between 0.002 and 0.003. The Mach Number range was from about 1.2 to 3, and the range of pipe Reynolds Numbers from 25,000 to 700,000. The corresponding range of friction coefficients for fully developed incompressible flow is from about 0.003 to 0.0065. The measured apparent friction coefficients for supersonic flow were therefore only about half as great as the coefficients commonly employed for incompressible flow.

Additional details on friction coefficients for compressible flow in ducts are presented in Volume II, Chapter 28.

REFERENCES AND SELECTED BIBLIOGRAPHY

1. KEENAN, J. H., and NEUMANN, E. P. Measurements of Friction in a Pipe for Subsonic and Supersonic Flow of Air, *Jour. App. Mech.*, Vol. 13, No. 2 (1946), p. A-91.
2. MOODY, L. F. Friction Factors for Pipe Flow, *Trans. A.S.M.E.*, Vol. 66 (1948), p. 671.
3. SHAPIRO, A. H., and SMITH, R. D. Friction Coefficients in the Inlet Length of Smooth Round Tubes, *NACA Tech. Note*, No. 1785 (1948).
4. KAYE, J., KEENAN, J. H., and SHOULBERG, R. H. Measurement of Recovery Factors and Friction Coefficients for Supersonic Flow of Air in a Tube, *Proceedings of the General Discussion on Heat Transfer*, London: The Institution of Mechanical Engineers, September, 1951.

PROBLEMS

6.1. A stream of air flows in an insulated tube of constant area having a cross-sectional area of 1 sq ft. At a section 1 the pressure is 10 psia, the temperature is 40°F, and the mass velocity is 29.6 lb/sec ft². The pressure in the space to which the tube exhausts is so low that a "choking" condition prevails, i.e., alterations in the pressure of the exhaust region have no effect on the flow through the tube.

(a) Calculate the Mach Number at section 1.

(b) Calculate the Mach Number, temperature, and pressure at the exit of the tube.

(c) Calculate the total force in the axial direction which must be exerted to hold stationary the section of the duct between section 1 and the exit.

6.2. A perfect gas flows in an insulated pipe. Show that the pressure at the choking condition is given by

$$p^* = \frac{w}{A} \sqrt{\frac{R}{k}} \sqrt{\frac{2T_0}{k+1}}$$

6.3. (a) Estimate the maximum flow rate of air (lbm/sec) which can flow through the passage shown, assuming that the friction coefficient of the duct is 0.005. (b) For what range of back pressures will this maximum flow rate be achieved?

6.4. Consider a long, round insulated tube fed with air by a frictionless nozzle. The critical pressure ratio of this system is defined as the ratio of the minimum possible pressure at the duct exit to the nozzle supply pressure. Plot this critical pressure ratio versus the duct $4fL/D$ for values of the latter from 0 to 10.

6.5. Air enters an insulated tube of 1-inch diameter through a converging-diverging nozzle with a throat diameter of 0.400 inches. The pressure and temperature in the low-velocity region at the nozzle entrance are 100 psia and 140°F, respectively. The flow through the nozzle may be assumed frictionless, and the average friction coefficient in the duct may be taken as 0.0025.

(a) Plot the pressure, temperature, Mach Number, and isentropic stagnation pressure as a function of distance from the tube inlet, assuming shockless flow to the exit. Determine the maximum length of duct for these conditions.

(b) Suppose that the tube is 40 inches long. Plot, versus the back pressure in the space to which the duct discharges, the following quantities: mass rate of flow, pressure and Mach Number at the duct exit, pressure and Mach Number at the duct inlet, and location of shock.

(c) Repeat part (b) for a tube 90 inches long.

6.6. An isentropic nozzle having an area ratio of 2.00 discharges air into an insulated pipe of length L and diameter D . The nozzle is supplied at 100 psia and 70°F, and the duct discharges into a space where the pressure is 40 psia. Calculate the $4fL/D$ of the pipe and the mass flow per unit area in the pipe (lbm/sec ft²) for the cases where a normal shock stands:

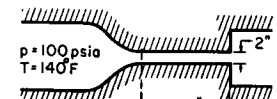
- In the nozzle throat
- In the nozzle exit plane
- In the duct exit plane

6.7. (a) Demonstrate that for incompressible flow of a perfect gas in a pipe the fractional pressure drop is given by

$$\frac{p_1 - p_2}{p_1} = \frac{kM_1^2}{2} 4f \frac{L}{D}$$

(b) Derive the corresponding expression for the fractional loss in stagnation pressure.

6.8. Natural gas (molecular weight 18, $k = 1.3$) is to be pumped through a pipe of 36 inches I.D. connecting two compressor stations forty miles apart. At the upstream station the pressure is not to exceed 90 psig and at the downstream station it is to be at least 10 psig. Calculate the maximum allowable rate of flow (cubic feet per day at 70°F and 1 atm), assuming that there is sufficient heat transfer through the pipe wall to maintain the gas at 70°F.



PROB. 6.3.

6.9. A converging nozzle supplied with air at 100 psia and 70°F discharges into a duct 10 inches in diameter and 1000 ft long. Assuming the flow in the nozzle isentropic and the flow in the duct isothermal,

(a) Plot the mass rate of air flow (lb/sec) versus the exhaust pressure (psia) in the space to which the duct discharges.

(b) What is the maximum mass rate of flow?

(c) What is the rate of heat transfer (Btu/hr) to the duct for the maximum flow rate?

(d) What is the inlet Mach Number to the duct at the maximum flow rate?

6.10. Consider isothermal flow through a frictionless nozzle supplied with a gas at low velocity, pressure p_i , and temperature T_i .

(a) Derive relations for p/p_i , ρ/ρ_i , V/V^{*t} , T_0/T_{0i} , p_0/p_{0i} , and A/A^{*t} , all in terms of the local Mach Number M , where T_0 and p_0 are respectively the isentropic stagnation temperature and pressure, and V^{*t} and A^{*t} are respectively the velocity and cross-sectional area at the section where w/A is a maximum.

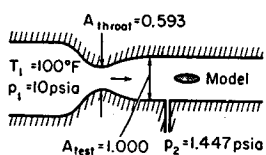
(b) Show that at the minimum area the Mach Number is $1/\sqrt{k}$ and the pressure ratio is $p^{*t}/p_i = 1/\sqrt{e} = 1/\sqrt{2.718\cdots}$.

(c) In what way are the results of parts (a) and (b) identical with what would be found from the isentropic-flow relations by setting $k = 1$? Investigate the reasons for the similarities and dissimilarities.

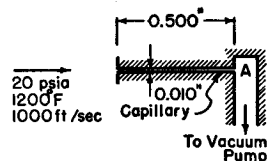
6.11. Derive a formula relating $(T ds - dQ)$ to $4f dx/D$ for the isothermal pipe flow of a perfect gas. From this show that the friction coefficient f must always be positive.

6.12. The measurements shown on the sketch are made in a certain wind tunnel where it is known that the boundary layers on the walls of the test section are very thin.

In interpreting test data on the model, what would you consider the free-stream Mach Number for the model? Defend your conclusion.



PROB. 6.12.



PROB. 6.13.

the gas has properties $k = 1.4$ and $R = 53.3 \text{ ft lbf/lbm F}$. The viscosity of the gas may be taken as $2.6(10)^{-5} \text{ lbm/ft sec}$. Since the flow in the capillary is likely to be laminar, the friction coefficient is given by the Poisseeulle formula:

$$f = 16/\text{Rey}$$

(a) Estimate the maximum rate at which gas may be sampled, in pounds per second.

(b) How much vacuum must the pump develop, in inches Hg, in order to realize the maximum flow rate?

(c) What is the pressure at the inlet of the capillary at the condition of maximum flow?

6.14. Consider the steady, laminar seepage of a perfect gas through a long, fine capillary tube of diameter D and length L . Because of its very great length and small diameter, the resistance to flow is very large, and consequently the fluid velocities are so small that changes in fluid momentum and kinetic energy are negligible. At the same time, the pressure drop is so large that there are great variations in fluid density.

Show that the pressure drop is given by "d'Arcy's formula,"

$$p_1^2 - p_2^2 = \frac{256\mu}{\pi D^4} wRT_1 L$$

where μ is the coefficient of viscosity.

Hint: Demonstrate first that the Hagen-Poisseeulle law for laminar flow is approximately valid for each increment of length.

6.13. It is proposed to measure the chemical composition of the gases approaching the nozzle of a turbojet engine by withdrawing a sample of gas through a capillary tube 0.500 inches in length and 0.010 inches in internal diameter. The capillary will be attached to a much larger tube at A , as shown in the sketch, and the gas will be pumped to the chemical apparatus by a vacuum pump. One of the practical questions is whether or not the time required to draw a sample of reasonable size is excessive, and it is therefore desired to estimate the maximum rate at which gas can be drawn through the capillary.

The stream in which the probe is placed is at 20 psia and 1200°F, and flows at a speed of 1000 ft/sec. For purposes of estimating, it may be assumed that

Chapter 7

FLOW IN DUCTS WITH HEATING
OR COOLING

7.1. Introductory Remarks

From a one-dimensional point of view, the three most common factors tending to produce continuous changes in the state of a flowing stream are (i) changes in cross-sectional area, (ii) wall friction, and (iii) energy effects such as external heat exchange, combustion, or moisture condensation. In Chapter 4 we studied the effects of area change with frictional and energy effects absent; the corresponding process, which we have called isentropic flow, might aptly be termed *Simple Area Change*. In Chapter 6 we studied the effects of wall friction in the absence of area change and energy effects; the corresponding process is described by the Fanno curve and may aptly be termed *Simple Friction*.

In this chapter attention is focused on a process involving changes in the stagnation enthalpy or stagnation temperature of a gas stream which flows at constant area and without frictional effects. This process will be called *Simple T_0 -Change*.

Such a process is difficult to achieve in practice. If the stagnation temperature is raised or lowered through external heat exchange, the connection between the mechanisms of friction and of heat transfer assure that frictional effects will be present. Similarly, if the stagnation temperature changes because of combustion, there will be a change in chemical composition. To cite still a third example, a reduction in stagnation temperature through evaporation of a liquid into the gas stream means that both the mass rate of gas flow and the chemical composition will change.

Despite these objections, many important conclusions of practical significance may be drawn by analyzing the process of *Simple T_0 -Change*. These conclusions can be expected to have a high degree of validity when the departures from the assumptions of the model are small. For example, when the heating or cooling is through external heat exchange, frictional effects per unit length of duct will be relatively unimportant compared to heating effects per unit length of duct in those cases where the temperature differential between the duct wall and the moving stream is large. In the combustion of hydrocarbons with air, the fuel-air

ratio is small; consequently, effects owing to change in chemical composition are small compared with the effects owing to changes in stagnation temperature.

Additional material relevant to the subject matter of the present chapter may be found in Volume II, Chapters 25, 26, 27, and 28.

NOMENCLATURE

A	area	\mathcal{R}	recovery factor
c	speed of sound	s	entropy per unit mass
c_p	specific heat at constant pressure	T	absolute temperature
D	pipe diameter	T_{aw}	adiabatic wall temperature
F	impulse function	T_w	wall temperature
G	mass velocity	V	velocity
h	enthalpy per unit mass	w	mass rate of flow
h_{fg}	latent heat per unit mass		
ΔH	heat of reaction at constant temperature and pressure per unit mass of mixture	λ	coefficient of thermal conductivity
\mathcal{h}	heat transfer coefficient	μ	coefficient of viscosity
k	ratio of specific heats	ρ	density
M	Mach Number	()*	signifies state at which $M = 1$ for process of simple T_0 -Change
p	pressure	() ₀	signifies isentropic stagnation state.
q	rate of heat transfer per unit wetted area		
Q	heat		
R	gas constant		

Governing Physical Equations. Using the assumptions of constant area and no friction, the momentum equation may be written

$$p + \rho V^2 = \frac{F}{A} = \text{constant} \quad (7.1)$$

The equation of continuity is

$$\rho V = \frac{w}{A} = G = \text{constant} \quad (7.2)$$

Combining these, we have

$$p + \frac{G^2}{\rho} = \frac{F}{A} \quad (7.3)$$

The Rayleigh Line. For fixed values of the flow per unit area and the impulse function per unit area, Eq. 7.3 defines a unique relation between the pressure and the density, a relation which we have previously called the *Rayleigh line*. Since both the enthalpy and entropy are functions of

pressure and density, it follows that Eq. 7.3 may be used for representing the Rayleigh line on the enthalpy-entropy diagram, as in Fig. 7.1.

Writing Eq. 7.3 in differential form and introducing Eq. 7.2, we get

$$\frac{dp}{d\rho} = \frac{G^2}{\rho^2} = V^2$$

or,

$$V = \sqrt{dp/d\rho}$$

FIG. 7.1. Rayleigh curve for Simple T_0 -Change.

Now, $\sqrt{dp/d\rho}$ represents the local velocity of sound only for a special circumstance, namely, when the infinitesimal variation of pressure with density is such that there is no change of entropy. This condition is fulfilled at the point of maximum entropy on the Rayleigh line (Fig. 7.1). This point is marked with an asterisk to denote that it is the state of Mach Number unity for the *process of Simple T_0 -Change*. The words *process of Simple T_0 -Change* are italicized here because, beginning with state 1 on Fig. 7.1, Mach Number unity might be reached in several ways (isentropically, adiabatically at

FIG. 7.1. Rayleigh curve for Simple T_0 -Change.

for simple heating that the asterisk point of Fig. 7.1 will correspond to Mach Number unity.

Second Law of Thermodynamics. All fluids thus far investigated have Rayleigh curves of the general form shown in Fig. 7.1.

The branch of the Rayleigh curve above the point of maximum entropy generally corresponds to subsonic flow, whereas that below corresponds to supersonic flow. Since the process of simple heating is thermodynamically reversible, heat addition must correspond to an entropy increase and heat rejection must correspond to an entropy decrease. At subsonic speeds, therefore, the Mach Number is increased by heating and decreased by cooling. At supersonic speeds, on the other hand, the Mach Number is decreased by heating and increased by cooling. Thus, heat addition is like friction in that it always tends to make the Mach Number approach unity. Cooling causes the Mach Number to change always in the direction away from a Mach Number of unity.

For heat addition at either subsonic or supersonic speeds, the amount of heat input cannot be greater than that for which the leaving Mach

Number is unity. If the heat addition is too great, the flow will be choked, that is, the initial Mach Number will be reduced to a magnitude which is consistent with the specified amount of heat input.

These phenomena will be investigated in detail in the articles which follow.

7.2. Simple-Heating Relations for a Perfect Gas

As in the preceding chapters, we shall pay special attention to the flow of a perfect gas. The inaccuracies which are thus introduced are in most cases more than justified by the resulting simplicity.

Governing Physical Equations and Definitions. Consider the flow through the control surface of Fig. 7.2. We shall write the physical

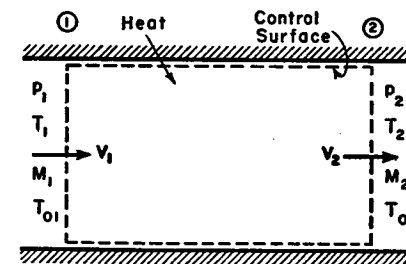


FIG. 7.2. Control surface for analysis of Simple T_0 -Change.

equations governing the flow in such a way as to obtain relations between the ratios of corresponding stream properties at sections 1 and 2 a finite distance apart.

CONSERVATION OF MASS. The continuity equation for constant area is

$$\frac{\rho_2}{\rho_1} = \frac{V_1}{V_2} \quad (7.4)$$

MOMENTUM THEOREM. The momentum equation, in the absence of frictional forces, is

$$p_1 - p_2 = \frac{w}{A} (V_2 - V_1)$$

Using the continuity equation, $w/A = \rho V$, and noting that for a perfect gas $\rho V^2 = kpM^2$, this may be arranged to give

$$\frac{p_2}{p_1} = \frac{1 + kM_1^2}{1 + kM_2^2} \quad (7.5)$$

PERFECT-GAS LAW. From the pressure-density-temperature relation of a perfect gas we get

$$\frac{p_2}{n_1} = \frac{\rho_2}{\rho_1} \frac{T_2}{T_1} \quad (7.6)$$

MACH NUMBER. Using the definition of the Mach Number and the formula for the sound velocity in a perfect gas, we find

$$\frac{M_2}{M_1} = \frac{V_2 c_1}{V_1 c_2} = \frac{V_2}{V_1} \sqrt{\frac{T_1}{T_2}} \quad (7.7)$$

IMPULSE FUNCTION. From the definition of the impulse function,

$$\frac{F_2}{F_1} = \frac{p_2(1 + kM_2^2)}{p_1(1 + kM_1^2)}$$

and Eq. 7.5, we get

$$F_2/F_1 = 1 \quad (7.8)$$

ISENTROPIC STAGNATION PRESSURE. The definition of the isentropic stagnation pressure, Eq. 4.14b, gives

$$\frac{p_{02}}{p_{01}} = \frac{p_2}{p_1} \frac{\left(1 + \frac{k-1}{2} M_2^2\right)^{\frac{k}{k-1}}}{\left(1 + \frac{k-1}{2} M_1^2\right)^{\frac{k}{k-1}}} \quad (7.9)$$

ENTROPY CHANGE. The entropy change may be found from Eq. 2.32c. Thus,

$$\frac{s_2 - s_1}{c_p} = \ln \frac{T_2/T_1}{(p_2/p_1)^{\frac{k-1}{k}}} \quad (7.10)$$

STAGNATION TEMPERATURE. The considerations thus far put forward merely serve to establish the relations between different points on the Rayleigh line. From a physical viewpoint the changes in stream properties are due primarily to changes in stagnation temperature. Or, to put it differently, the rate of change of stream properties along the Rayleigh line is a function of the rate of change of stagnation temperature.

The stagnation temperature corresponding to a given state is that temperature which the stream would assume if it were adiabatically decelerated to zero velocity. From the energy equation, then,

$$T_0 = T + \frac{V^2}{2c_p} = T \left(1 + \frac{V^2}{2c_p T}\right) = T \left(1 + \frac{k-1}{2} M^2\right)$$

Or,

$$\frac{T_{02}}{T_{01}} = \frac{T_2}{T_1} \frac{1 + \frac{k-1}{2} M_2^2}{1 + \frac{k-1}{2} M_1^2} \quad (7.11)$$

When the process involves heat exchange, the change in stagnation temperature is a direct measure of the amount of heat transfer. For, from the energy equation,

$$Q = c_p(T_2 - T_1) + \frac{V_2^2 - V_1^2}{2} = c_p(T_{02} - T_{01}) \quad (7.12)$$

When the process involves combustion or evaporation, it is usually possible to devise an approximately equivalent process of Simple T_0 -Change. In such cases the initial and final stagnation temperatures would be made respectively identical for the real process and for the equivalent process.

Eqs. 7.4 through 7.11 may be combined and rearranged algebraically to give the ratios of stream properties at sections 1 and 2 in terms of the Mach Numbers at these sections. For example, Eqs. 7.4 and 7.5 may be inserted into Eq. 7.6, giving

$$\frac{T_2}{T_1} = \frac{1 + kM_1^2}{1 + kM_2^2} \frac{V_2}{V_1}$$

Then using the value of V_2/V_1 from Eq. 7.7, we obtain

$$\frac{T_2}{T_1} = \frac{M_2^2 (1 + kM_1^2)^2}{M_1^2 (1 + kM_2^2)^2} \quad (7.13)$$

Elimination of T_2/T_1 from Eqs. 7.11 and 7.13 next yields

$$\frac{T_{02}}{T_{01}} = \frac{M_2^2 (1 + kM_1^2)^2}{M_1^2 (1 + kM_2^2)^2} \frac{\left(1 + \frac{k-1}{2} M_2^2\right)}{\left(1 + \frac{k-1}{2} M_1^2\right)} \quad (7.14)$$

Working Formulas. Similarly, expressions for ρ_2/ρ_1 , V_2/V_1 , etc., all in terms of M_1 and M_2 , may be found. In the interest of constructing simple and useful tables and charts, however, it is convenient to normalize the equations by setting the Mach Number equal to unity at one of the sections. Let us suppose that the Mach Number is unity at section 1, and that section 2 is any other section of the duct. Section 1 will be denoted by an asterisk, and section 2 will be without subscript. We therefore write

$$M_1 = 1, \quad p_1 = p^*, \quad T_1 = T^*, \quad T_{01} = T_0^*, \quad \text{etc.}$$

and

$$M_2 = M, \quad p_2 = p, \quad T_2 = T, \quad T_{02} = T_0, \quad \text{etc.}$$

Equation 7.13 then becomes

$$\frac{T}{T^*} = \frac{(k+1)^2 M^2}{(1+kM^2)^2} \quad (7.15)$$

and Eq. 7.14 becomes

$$\frac{T_0}{T_0^*} = \frac{2(k+1)M^2 \left(1 + \frac{k-1}{2} M^2\right)}{(1+kM^2)^2} \quad (7.16)$$

Similarly, we obtain the following formulas:

$$\frac{V}{V^*} = \frac{\rho^*}{\rho} = \frac{(k+1)M^2}{1+kM^2} \quad (7.17)$$

$$\frac{p}{p^*} = \frac{k+1}{1+kM^2} \quad (7.18)$$

$$\frac{p_0}{p_0^*} = \frac{k+1}{1+kM^2} \left[\frac{2 \left(1 + \frac{k-1}{2} M^2\right)}{k+1} \right]^{\frac{k}{k-1}} \quad (7.19)$$

$$\frac{s - s^*}{c_p} = \ln M^2 \left(\frac{k+1}{1+kM^2} \right)^{\frac{k+1}{k}} \quad (7.20)$$

Using these normalized expressions, the ratios of properties at two sections where the Mach Numbers are M_1 and M_2 are given by expressions of the type

$$\frac{T_{02}}{T_{01}} = \frac{(T_0/T_0^*)_{M_2}}{(T_0/T_0^*)_{M_1}} \quad (7.21)$$

where $(T_0/T_0^*)_{M_2}$ is found from Eq. 7.16, and so forth.

Working Charts and Tables. To facilitate calculations, it is well to have the working formulas given above in graphical or tabular form.

Fig. 7.3 is a graphical form of the Simple T_0 -Change formulas, with Mach Number as the independent variable.

The corresponding functions are also tabulated in Table B.5.

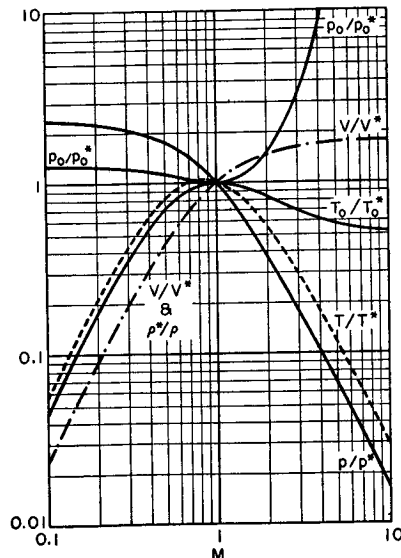


FIG. 7.3. Working chart for Simple T_0 -Change, $k = 1.4$.

Illustrative Example.

PROBLEM. A gaseous mixture of air and fuel enters a ram-jet combustion chamber with a velocity of 200 ft/sec, at a temperature of 120°F, and at a pressure of 5 psia. The heat of reaction ΔH of the mixture for the particular fuel-air ratio employed is 500 Btu per pound of mixture. It is desired to find the stream properties at the exit of the combustion chamber. It will be assumed that friction is negligible, that the cross-sectional area is constant, and that the properties of both the reactants and the products are equivalent to air in respect to molecular weight and specific heat.

SOLUTION. We begin by computing additional properties at the inlet, which will be called section 1. The sound velocity c_1 is

$$c_1 = \sqrt{kRT_1} = \sqrt{(1.4)(53.35)(32.174)(579.7)} \\ = 1180.3 \text{ ft/sec}$$

and

$$M_1 = V_1/c_1 = 200/1180.3 = 0.16945$$

The stagnation temperature and isentropic stagnation pressure at section 1 are found for this value of M_1 from Table B.2. Thus,

$$\left(\frac{p}{p_0}\right)_1 = 0.9801; \quad p_{01} = \frac{5}{0.9801} = 5.102 \text{ psia}$$

$$\left(\frac{T}{T_0}\right)_1 = 0.99429; \quad T_{01} = \frac{579.7}{0.99429} = 583.0^\circ\text{R}$$

To analyze the changes in the combustion process, we first find from Table B.5 the ratios of stream properties to the corresponding properties at $M = 1$. For $M_1 = 0.16945$, we find

$$(T_0/T_0^*)_1 = 0.128 \quad (p/p^*)_1 = 2.308$$

$$(T/T^*)_1 = 0.153 \quad (p_0/p_0^*)_1 = 1.2435$$

$$(V/V^*)_1 = 0.0663$$

The stagnation-temperature rise for the equivalent process of Simple T_0 -Change is given by

$$T_{02} - T_{01} = \Delta H/c_p$$

Now, $\Delta H = 500 \text{ Btu/lb}$, and

$$c_p = \frac{k}{k-1} R = \frac{1.4}{0.4} \frac{53.35}{778.3} = 0.23991 \text{ Btu/lb}^\circ\text{F}$$

so that

$$T_{02} - T_{01} = \frac{500}{0.23991} = 2084.1^\circ\text{F}$$

$$T_{02} = 2084.1 + 583.0 = 2667.1^\circ\text{R}$$

$$T_{02}/T_{01} = 2667.1/583.0 = 4.5748$$

The properties at section 2 are found with the help of the T_{02}/T_{01} ratio. We first compute

$$\left(\frac{T_0}{T_0^*}\right)_2 = \left(\frac{T_0}{T_0^*}\right)_1 \left(\frac{T_{02}}{T_{01}}\right) = (0.128)(4.5748) = 0.5856$$

With this value of $(T_0/T_0^*)_2$, we again enter Table B.5 and find that

$$\begin{aligned} M_2 &= 0.4329 & (p/p^*)_2 &= 1.9012 \\ (T/T^*)_2 &= 0.677 & (p_0/p_0^*)_2 &= 1.1425 \\ (V/V^*)_2 &= 0.3563 \end{aligned}$$

Finally, we obtain the remaining properties at section 2 with the relations

$$T_2 = T_1 \frac{(T/T^*)_2}{(T/T^*)_1} = 579.7 \frac{0.677}{0.153} = 2560^\circ\text{R}$$

$$p_2 = p_1 \frac{(p/p^*)_2}{(p/p^*)_1} = 5 \frac{1.9012}{2.308} = 4.119 \text{ psia}$$

$$p_{02} = p_{01} \frac{(p_0/p_0^*)_2}{(p_0/p_0^*)_1} = 5.102 \frac{1.1425}{1.2435} = 4.688 \text{ psia}$$

$$V_2 = V_1 \frac{(V/V^*)_2}{(V/V^*)_1} = 200 \frac{0.3563}{0.0663} = 1075 \text{ ft/sec}$$

It is also of interest to find the maximum heat of reaction for which flow with the specified initial conditions may be maintained. Choking will occur when the exit Mach Number is unity. Hence, denoting the choking condition by subscript 3,

$$T_{03} = T_{01} \frac{(T_0/T_0^*)_3}{(T_0/T_0^*)_1} = 583.0 \frac{1}{0.128} = 4550^\circ\text{R}$$

and

$$\begin{aligned} (\Delta H)_{\max} &= c_p(T_{03} - T_{01}) \\ &= (0.2399)(4550 - 583) \\ &= 952 \text{ Btu/lb} \end{aligned}$$

After the fuel-air ratio has been increased to the value corresponding to this maximum heat of reaction, further enrichment of the mixture will produce a reduction in mass rate of flow and a consequent reduction in the initial Mach Number.

Effects of Changes in T_0 . The effects of changes in T_0 on the remaining stream properties may be found from differential relations of the type derived in the previous chapter. Such differential relations are derived as part of a more general analysis in the next chapter and so are not presented here.

However, the desired information may also be found from Fig. 7.3, at least for the special value of $k = 1.4$. The key curve on this chart is that of T_0/T_0^* , for it is directly connected with the magnitude and

direction of heat transfer. For example, if the speed is supersonic and the stagnation temperature is increased, the curve of T_0/T_0^* shows that the Mach Number must decrease. From the curve of T/T^* we then see that the temperature will increase, and, from the curve of p_0/p_0^* , that the isentropic stagnation pressure will decrease. The directions of these and other changes may be summarized as follows:

	Heating $M < 1$	Heating $M > 1$	Cooling $M < 1$	Cooling $M > 1$
T_0	increases	increases	decreases	decreases
M	increases	decreases	decreases	increases
T	Note (1)	increases	Note (2)	decreases
p	decreases	increases	increases	decreases
p_0	decreases	decreases	increases	increases
V	increases	decreases	decreases	increases

Note (1): increases for $M < 1/\sqrt{k}$, and decreases for $M > 1/\sqrt{k}$

Note (2): decreases for $M < 1/\sqrt{k}$, and increases for $M > 1/\sqrt{k}$

Heating always acts to reduce the stagnation pressure, irrespective of whether the speed is subsonic or supersonic. This has obvious practical implications for heat exchangers, combustion chambers, etc. Increases in stagnation pressure, on the other hand, may be obtained at either subsonic or supersonic speeds by a cooling process which reduces the stagnation temperature; in practice this is difficult because other effects are always present which tend to reduce the stagnation pressure.

The value of T/T^* goes through a maximum at $M = 1/\sqrt{k}$, corresponding to point g on Fig. 7.1. In the case of air, therefore, for values of M between 0.85 and 1, heat addition acts to *reduce* the stream temperature and heat rejection acts to *increase* the stream temperature!

Choice of End State. A horizontal line connecting the two branches of the T_0/T_0^* curve of Fig. 7.3 defines a pair of end states having the same flow per unit area, the same value of the impulse function, and the same stagnation temperature. Accordingly they are the corresponding states on the two sides of a normal shock.

When the initial state is supersonic (point 1 on Fig. 7.4a), the final state may be either supersonic (state $2'$) or subsonic (state $2''$). The latter condition corresponds to the combination of simple heating and a normal compression shock. Identical results are obtained for (i) simple heating from 1 to $2'$, followed by a normal shock to $2''$; (ii) a normal shock from 1 to 4, followed by simple heating at subsonic speeds from 4 to $2''$; and (iii) simple heating at supersonic speeds from 1 to a state between 1 and $2'$, followed by a normal shock, and concluding with simple heating at subsonic speeds to state $2''$.

When the initial state is subsonic (point 1 on Fig. 7.4b), the final state may be only subsonic (state $2'$), for supersonic speeds could only be

attained through a violation of the Second Law of Thermodynamics in the form of a normal expansion shock from state $2'$ to state $2''$. This conclusion is valid, of course, only when the heat transfer is in one direction only. Otherwise a subsonic stream could be accelerated to Mach Number unity by heating from states 1 to 3 in Fig. 7.4b, after which the speed could be made supersonic by cooling from states 3 to $2''$.

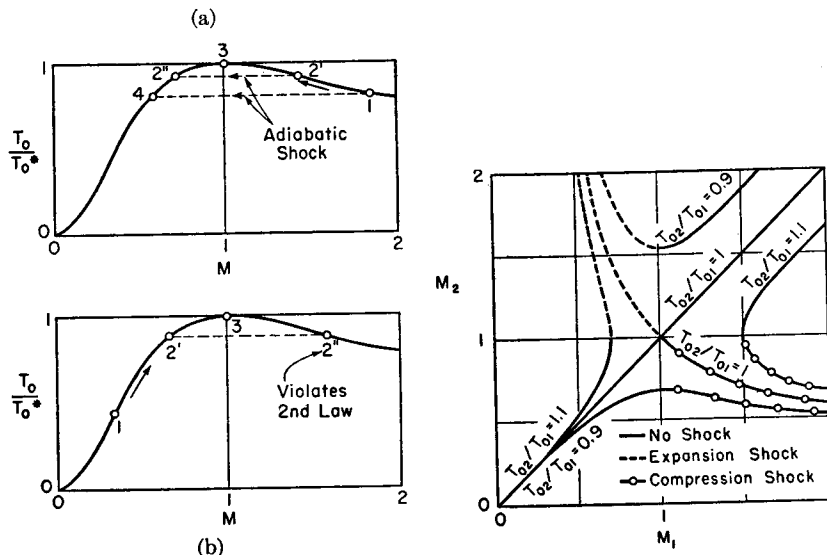


FIG. 7.4. Illustrates possible end states for Simple T_0 -Change.

- (a) Initial flow supersonic.
- (b) Initial flow subsonic.

Fig. 7.5 shows illustrative curves of M_2 versus M_1 for fixed values of T_{02}/T_{01} . When $T_{02}/T_{01} = 1$, one of the two curves is for the trivial case in which no change of state occurs, and the other of the two curves represents an adiabatic normal shock. For a value of T_{02}/T_{01} such as 1.1, corresponding to heat addition, there is a branch corresponding to an initially subsonic flow and a branch corresponding to an initially supersonic flow. On each such branch there are two values of M_2 for each value of M_1 . For initial states which are supersonic the entire curve of M_2 versus M_1 represents physically possible solutions. For initially subsonic states, however, only that part of the curve is valid in which the final Mach Number is less than unity. The remaining part of the curve implies the existence of a rarefaction shock. Similar considerations apply to cooling curves, such as the curves labeled $T_{02}/T_{01} = 0.9$.

7.3. Choking Effects in Simple T_0 -Change

Rise in Stagnation Temperature. It is evident from Figs. 7.3 and 7.5 that if the process involves a rise in stagnation temperature, there is for each initial Mach Number a maximum possible ratio of stagnation temperatures for which a solution is possible. In the limiting case where the stagnation-temperature ratio of the process is at its maximum allowable value, the leaving Mach Number is exactly unity. From another viewpoint, if the initial stagnation temperature as well as the stagnation temperature rise are fixed, there is in subsonic flow a maximum allowable initial Mach Number and in supersonic flow a minimum allowable initial Mach Number for which steady flow is possible.

Fall in Stagnation Temperature. When the process involves cooling, no limitations on the stagnation-temperature ratio exist, provided that the initial Mach Number is less than unity. For initially supersonic speeds, however, and when no discontinuity in the form of a shock is present, there is a maximum allowable reduction in stagnation-temperature ratio corresponding to any given initial Mach Number. With this minimum stagnation-temperature ratio the leaving Mach Number is infinite; this condition corresponds to zero stream temperature at exit and to a leaving kinetic energy which is equal to the leaving value of $c_p T_0$.

Problems involving a rise in stagnation temperature are more common than those involving a reduction. Our attention will, therefore, be focused on problems of this type.!

Subsonic Flow. Considering subsonic flow first, let us suppose that the stream flows with an initial Mach Number M_1 and that the imposed increase of T_0 yields a value of T_{02}/T_{01} which is greater than the maximum value read from Fig. 7.3. It is clear that some sort of readjustment in the flow pattern is necessary if the specified stagnation-temperature rise is to occur. This readjustment is brought about by a series of transient effects characterized by pressure waves propagating in both directions along the duct. When the flow finally reaches a steady condition, we say that the flow is *choked*; that is, the initial Mach Number, and hence the flow rate, is reduced sufficiently to permit the specified amount of heating to occur. Assuming that the back pressure on the duct is low enough, the choking will reduce the initial Mach Number to the point where the leaving velocity is exactly sonic.

The above considerations may best be illustrated by a practical example. Suppose that a ram-jet combustion chamber of uniform cross-sectional area and without friction is at first operating cold (that is, without combustion) with an air velocity of about 500 ft/sec

corresponding to $M = 0.5$ and $T_0 = 500^\circ\text{R}$. Suppose also that it is desired to burn enough fuel to raise the stagnation temperature to 2000°R , corresponding to a four-fold increase in T_0 . From Fig. 7.3, however, we see that, with an initial M of 0.5, the value of T_0 (or of T_0/T_0^*) may be increased by only about 45 per cent. When combustion begins, therefore, the flow is choked until in steady flow the leaving Mach Number is unity. We therefore set $M_2 = 1$, and write

$$\frac{(T_0/T_0^*)_2}{(T_0/T_0^*)_1} = \frac{T_{02}}{T_{01}} = 4$$

Since $M_2 = 1$, it follows that

$$(T_0/T_0^*)_1 = 0.25$$

The corresponding value of M_1 is found from Fig. 7.3 as 0.246, which means that the maximum possible air speed at the inlet to the combustion region is about 250 ft/sec. Fig. 7.3 also yields $(p_0/p_0^*)_1 = 1.219$, so that

$$\frac{p_{02}}{p_{01}} = \frac{(p_0/p_0^*)_2}{(p_0/p_0^*)_1} = \frac{1}{1.219} = 0.82$$

The above results are significant because the assumed stagnation temperatures are in the range of interest for both ram-jet propulsion and for gas turbines. We see that the entering velocity is limited by choking effects to about 250 ft/sec. This represents a restriction on the capacity of high-output combustors over and above the limitation imposed by the maximum velocity for which a stable flame may be maintained. It is also noteworthy that with the maximum entering speed a loss in stagnation pressure of at least 18 per cent is inevitable, entirely apart from the losses caused by friction.

Supersonic Flow. Let us now consider heat transfer to a supersonic stream flowing in a duct which is fed by a converging-diverging nozzle. If the stagnation-temperature rise is too great to allow of a solution with the specified initial Mach Number, an adiabatic shock somewhere in the heating region would not provide an adequate form of readjustment, since there is no change in stagnation temperature across an adiabatic shock. For example, if the state at the duct inlet is represented by point 1 in Fig. 7.4a, the maximum allowable ratio of final to initial stagnation temperature is given by $(T_0/T_0^*)_3/(T_0/T_0^*)_1$. The occurrence of a normal shock in the region of heating, say from 2' to 2'', does not alter the magnitude of the maximum stagnation temperature, namely, that corresponding to state 3. The adjustment of the flow must, therefore, occur in the nozzle which feeds the duct. A normal shock in the diverging section of the nozzle will act to reduce the Mach

Number at the duct inlet below the value corresponding to state 4; this allows a greater stagnation-temperature ratio for the heating process without any accompanying reduction in flow rate.

For very large increases in stagnation temperature, however, the flow in the nozzle would have to be entirely subsonic, and the flow at the duct exit would at most be exactly sonic. This would represent a choking condition for the combined nozzle-duct system inasmuch as the flow rate would, for a fixed stagnation-temperature ratio, be insensitive to variations in back pressure as long as the exit velocity was sonic.

7.4. Shock Waves with Changes in Stagnation Temperature

The adiabatic normal shock wave discussed in Chapter 5 is only a special type of quasi-discontinuity. Other types of discontinuities occur in nature. These involve such effects as chemical reaction, evaporation or condensation, as well as the associated effects of changes in the mass rate of gas flow, changes in chemical composition, and changes in specific heat and molecular weight.

We shall consider here two illustrative examples of discontinuities involving changes in stagnation temperature, namely, (i) the moisture condensation shock, and (ii) explosion waves in combustible mixtures. We shall restrict the analysis to the assumptions of the process of Simple T_0 -Change. In other words, the changes in chemical composition, specific heat, molecular weight, and mass flow of gas phase will be ignored, and primary attention will be focused on the changes in stagnation temperature.

The analysis of Art. 7.2 may be used for these discontinuities because no restriction was made there as to whether the change from section 1 to section 2 is continuous or discontinuous.

Moisture Condensation Shocks. The problem of *moisture condensation shocks* first received attention in connection with the flow through the nozzles of steam turbines. In many cases the supply pressure, supply temperature, and pressure ratio for such nozzles are such that at some point in the nozzle the saturation condition is reached, and a wet mixture of saturated vapor and saturated liquid might be expected upon further expansion of the stream. Experiments show, however, that the precipitation of moisture is delayed beyond the point where saturation is reached. The phenomenon is called *supersaturation*, and, during the period when the vapor pressure is greater than the saturation pressure corresponding to the temperature, it involves the existence of states of metastable equilibrium. The point of precipitation probably is connected with the appearance of nuclei, perhaps comprising foreign particles or accidentally formed groups of steam molecules. On the

Mollier (enthalpy-entropy) diagram the line of precipitation states, called the Wilson line, has been found by experiment to lie about 60 Btu/lb below the line of saturation states.

The precipitation of moisture is quite sudden, as the state of the fluid jumps quickly towards a state of stable equilibrium, and may in the first instance be treated as a discontinuity (Fig. 7.6). In steam nozzles it is observed to occur only in the diverging portion of the nozzle.



FIG. 7.6. Schlieren photographs (flow left to right) of moisture condensation shock in air. The moisture shock is immediately downstream of the throat; as it is not quite normal near the wall, there is a reflected expansion wave at each wall. Further downstream of the moisture shock is an adiabatic normal shock with attendant boundary-layer separation (M.I.T. Gas Turbine Lab.).

- (a) Schlieren knife-edge vertical.
(b) Schlieren knife-edge horizontal.

SUPersonic WIND TUNNELS. Moisture condensation shocks in supersonic wind tunnels present a serious problem because the sudden condensation of the supersaturated water vapor contained in the air stream not only alters the anticipated Mach Number and pressure, but, and of more importance, gives rise to nonuniformities in the direction and velocity of flow at the nozzle exit. These nonuniformities occur because moisture condensation shocks are not strictly normal but rather assume various shapes depending on the nozzle contour and on the degree of supersaturation. The moisture condensation shock in wind tunnels is observed only in the diverging portion of the nozzle. In experiments¹ it was found that the water vapor does not precipitate until the temperature of the stream is about 110°F below the temperature at which saturation is first reached. As the specific heat of steam at low pressures and temperatures is about 0.45 Btu/lb F, this means that the line of condensation is about 50 Btu/lb below the saturation line, a figure which is in moderately good agreement with the Wilson-line figure of about 60 Btu/lb for steam nozzles.

SIMPLIFIED ANALYSIS. Within the assumptions of the process of Simple T_0 -Change, the energy equation for the condensation shock may be written

$$wc_p(T_{02} - T_{01}) = w_L h_{fg} \quad (7.22)$$

where w denotes the mass rate of flow of the main gas stream, c_p the specific heat at constant pressure of the main gas stream, T_{01} and T_{02} the respective stagnation temperatures upstream and downstream of

the shock, w_L the mass rate of flow of condensing liquid, and h_{fg} the latent heat per unit mass of condensing liquid.

Eq. 7.22 may be rearranged to give

$$\frac{T_{02}}{T_{01}} = 1 + \frac{w_L}{w} \frac{h_{fg}}{c_p T_{01}} \quad (7.23)$$

The simplified model of the moisture condensation shock is now taken to be a process of Simple T_0 -Change with the stagnation-temperature ratio of Eq. 7.23. Referring to Fig. 7.4a, if the state before the shock were represented by point 1, the state after the moisture shock might be either $2'$ or $2''$, depending on the back pressure of the nozzle. For supersonic nozzles with low back pressures the downstream side of the shock would be represented by state $2'$, and would correspond to supersonic flow. It is evident from Figs. 7.4a and 7.3 that moisture condensation shocks tend to reduce the Mach Number and increase the pressure at the nozzle exit.

It is to be noted that the droplets formed during condensation are exceedingly small. Because of the associated effects of surface tension, the equilibrium relation between vapor pressure and temperature will depend upon the radius of the droplet, and the term h_{fg} in Eqs. 7.22 and 7.23 must be thought of as an equivalent latent heat which takes into account the surface energy of the droplets. Little data are available concerning the size of droplets initially formed, and virtually no data are available concerning the rate of growth of the droplets.

CHOKING. Thermal choking may play a role in moisture condensation shocks. For instance, suppose that the condensation begins at state 1 in Fig. 7.4a. With an assumed droplet size, we may compute the value of T_{02}/T_{01} , corresponding to conditions after equilibrium is established between vapor and liquid. If this ratio is greater than the value of $(T_0/T_0^*)_3/(T_0/T_0^*)_1$ in Fig. 7.4a, it is clear that the assumed solution is not possible. There seem to be two possible alternatives. First, it may be that thermodynamic equilibrium is established after the shock, but that thermal choking sets an upper limit to the size of droplets which may be formed. Second, it may be that the size of droplets formed is governed by an independent physical mechanism; in this case thermodynamic equilibrium would not be established after the shock, and the amount of water vapor condensed would be such as to yield a Mach Number of unity downstream of the shock. The Mach Number would remain at unity as further expansion permitted additional condensation until equilibrium was finally reached, whereupon the Mach Number would once again increase. Further experimental data are necessary to determine which, if either, of the above alternatives best describes the course of events, or whether steady flow is impossible and an oscillatory flow occurs.

Explosion Waves in Combustible Mixtures. A problem of practical importance in connection with combustion chamber design, bomb explosions, and detonation in internal combustion engines, concerns the manner in which an explosion wave travels through a combustible mixture. The significant quantities of interest include the speed of the wave relative to the unburned gas, the motion of the burned gas through which the wave has already passed, and the increases in pressure and temperature through the wave.

We shall consider here only steady explosion waves, which might be defined as waves in which the flow on both sides of the wave is steady with respect to an observer who moves with the wave front. However, the results are applicable also to unsteady waves provided that the thickness of the discontinuity zone is extremely small. This is usually the case in practice. The assumptions of simple heating will be adhered to, so that no notice will be given the changes in chemical composition, molecular weight, and specific heat.

Let us consider the case where the unburned gas is motionless with respect to the earth, so that an ordinary observer sees the wave advancing into the unburned gas, and the process appears to be unsteady. However, steady-state conditions will prevail with respect to a second observer who moves with the wave front. The equations of Section 7.2 would then be valid for this second observer. In order to obtain relations for the changes in stream properties for the observer at rest with respect to the unburned gas, transformation formulas like those of Art. 5.9 must be employed.

SIMPLIFIED ANALYSIS. Writing the energy equation for the steady flow viewed by the observer moving with the wave, we find that, within the assumptions of the process of simple heating,

$$T_{02} - T_{01} = \frac{\Delta H}{c_p} \quad (7.24)$$

where ΔH is the heat of reaction at constant pressure and temperature per unit mass of mixture, and c_p is the specific heat at constant pressure. In order to make use of the convenient tables and charts of Simple T_0 -Change, we put this expression in the form

$$\frac{\Delta H}{c_p T_1} = \frac{T_{02} - T_{01}}{T_1} = \frac{T_{02} - T_{01}}{T_{01}} \cdot \frac{T_{01}}{T_1} = \left(1 + \frac{k-1}{2} M_1^2\right) \left(\frac{T_{02}}{T_{01}} - 1\right) \quad (7.25)$$

$$\frac{\Delta H}{c_p T_1} = \left(1 + \frac{k-1}{2} M_1^2\right) \left[\frac{(T_0/T_0^*)_2}{(T_0/T_0^*)_1} - 1\right] \quad (7.26)$$

The left-hand side is determined by the nature of the chemical reaction

and by the properties of the unburned gas. Assuming that these are known in a given case, and remembering that T_0/T_0^* depends only on M and k , it follows that Eq. 7.26 is a relation between M_1 and M_2 . Fig. 7.7 shows illustrative curves of M_2 versus M_1 for several values of $\Delta H/c_p T_1$ in the range corresponding to hydrocarbon explosions; also shown are curves of constant p_2/p_1 .

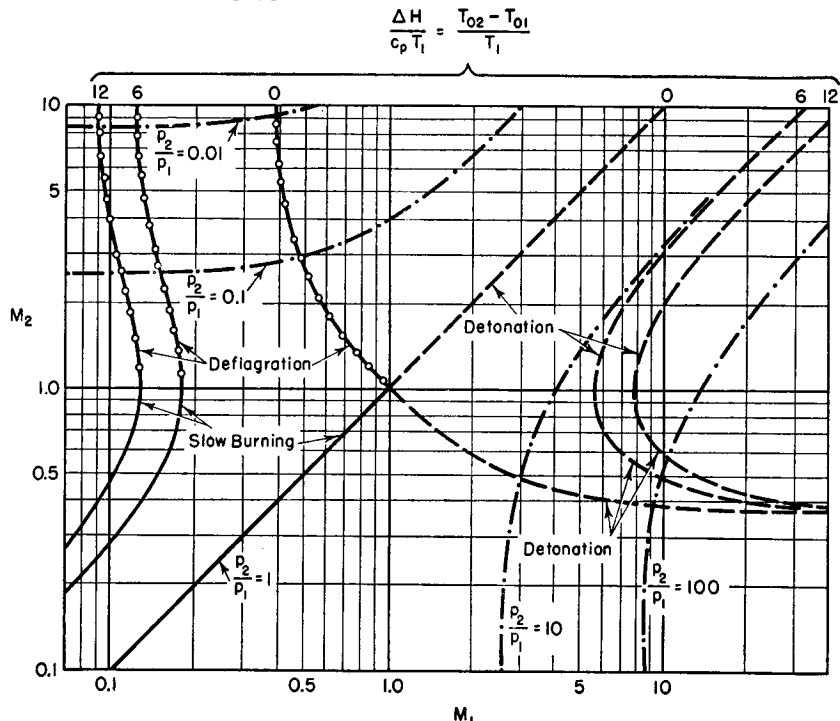


FIG. 7.7. Curves of M_2 versus M_1 for values of the parameter $\Delta H/c_p T_1$ in the usual range of hydrocarbon explosions. Dot-dash curves indicate values of p_2/p_1 ($k = 1.4$).

FLAME PROPAGATION SPEED. The Mach Number M_1 is the ratio of the speed of the wave relative to the unburned gas to the speed of sound in the unburned gas. Hence the leaving Mach Number M_2 seen by the observer moving with the wave front depends, according to Eq. 7.26, on the speed with which the flame front propagates into the unburned gas.

This flame propagation speed depends on such factors as the conduction of heat and the diffusion of mass through the combustion zone. The detailed consideration of these factors is beyond the scope of this book. We shall discuss here only the different classes of explosion waves resulting from different flame propagation speeds; in this respect the most distinctive criterion will be seen to be whether the speed of the flame front is subsonic or supersonic relative to the unburned gas, i.e., whether M_1 is less than or greater than unity.

It will be found most convenient to think in terms of the steady-state process viewed by an observer traveling with the wave, but the *results will be expressed for an observer at rest with respect to the unburned gas*. Fig. 7.3 may be employed for determining the velocity and pressure changes in the steady-state frame of reference. The various configurations discussed below are illustrated in Figs. 7.7 and 7.8.

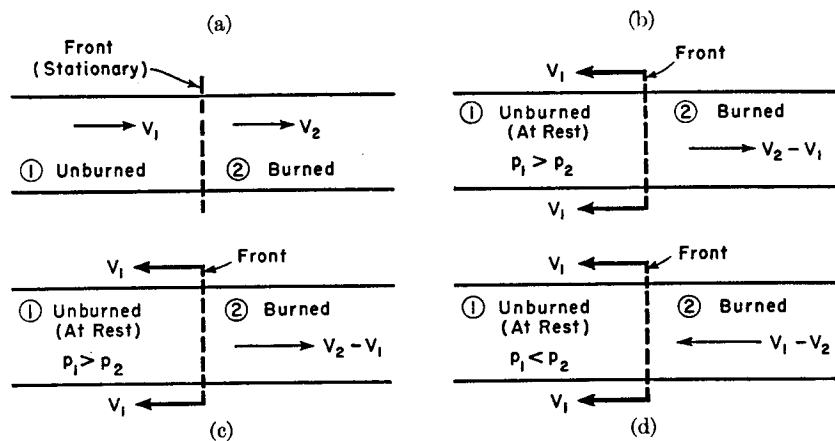


FIG. 7.8. Illustrates explosion waves (compare with Fig. 7.7).

(a) Process seen by observer in moving reference frame with respect to which the wave front is stationary. In (b), (c), and (d) the observer sees the unburned gas at rest and the wave front moving leftward with speed V_1 .

(b) Slow burning, corresponding to process $1 \rightarrow 2'$ of Fig. 7.4b; $V_1 < c_1$; $V_2 < c_2$; $V_2 > V_1$; burned gas flows away from unburned gas and pressure drops during burning.

(c) Deflagration, corresponding to process $1 \rightarrow 2''$ of Fig. 7.4b; $V_1 < c_1$; $V_2 > c_2$; $V_2 > V_1$; burned gas flows away from unburned gas and pressure drops during burning.

(d) Detonation, corresponding either to process $1 \rightarrow 2'$ or process $1 \rightarrow 2''$ of Fig. 7.4a; $V_1 > c_1$; $V_2 \leq c_2$; $V_2 < V_1$; burned gas flows toward unburned gas and pressure rises during burning.

SLOW BURNING. This corresponds to a process from state 1 to state $2'$ in Fig. 7.4b. The speed of the flame front is subsonic relative to the unburned gas, and the burned gas flows away from the unburned gas. The pressure drops as the front passes the observer.

DEFLAGRATION. This corresponds to a process from state 1 to state $2''$ in Fig. 7.4b. The speed of the flame front is subsonic relative to the unburned gas, and the burned gas flows away from the unburned gas. The pressure drops as the flame front passes the observer. Although these effects are qualitatively the same as in slow burning, the magnitudes of the changes in velocity and pressure are very much greater than for slow burning. For the assumptions of simple heating, a stationary deflagration constitutes a violation of the Second Law of Thermo-

dynamics, but it is not clear whether this is also the case for processes involving chemical reaction.

DETONATION. This corresponds to a process from state 1 to either state $2'$ or $2''$ in Fig. 7.4a. The speed of the flame front is supersonic relative to the unburned gas, and the burned gas flows toward the unburned gas. There is a great pressure rise as the flame front passes the observer. Relative to the front, the flow of the burned gas may be either subsonic or supersonic.

Assuming that an explosion occurs in a specified combustible mixture, what will be the steady-state speed of the front relative to the unburned gas? That is, what will be the value of M_1 , the ratio of the above-named speed to the speed of sound in the unburned gas? As explained previously, the equations of continuity, momentum, and energy allow of an infinite number of steady-state wave speeds M_1 (see Fig. 7.7). To each of these values of M_1 there correspond either two values of M_2 or none at all. The latter situation implies that a phenomenon similar to thermal choking defines an upper limit to the value of M_1 for subsonic wave speeds, and a lower limit to the value of M_1 for supersonic wave speeds. In both these limiting cases the value of M_2 is unity.

The values of M_1 and M_2 which will occur in a given instance depend not only on the conservation principles of continuity, momentum, and energy, but also on the kinetics of the chemical reaction and on the boundary conditions in space and time, insofar as the latter influence the formation of the steady-state wave front. Without going into detail, the following facts may be stated.

(i) In slow combustion the speed of the steady-state flame front must be identical with the speed of propagation of the flame relative to the unburned gas. The speed of flame propagation depends on such factors as the nature of the chemical reaction, the temperature of the unburned gas, the degree of turbulence, and the size of the apparatus in which the process is carried out. It is to be noted that steady-state slow combustion is impossible if the flame speed is greater than the value corresponding to the maximum value of M_1 indicated by Eqs. 7.14 and 7.26. In such instances it appears that the process, after passing through a transient phase, becomes one of detonation.

(ii) All detonation experiments thus far performed have yielded steady-state wave speeds of magnitudes such as to make the speed of the burned gas exactly sonic with respect to the wave front. Stated differently, the observed values of M_1 correspond to the solution of Eqs. 7.14 and 7.26 for M_2 exactly equal to unity (point 3 of Fig. 7.4a), and represent the minimum possible steady-state detonation speeds in each experiment. This experimental result may be partially rationalized through considerations of the stability of a detonation wave and

of the mechanism by which a wave starting from rest ultimately reaches the stage of detonation.^(2,3) The enormous flame propagation speeds in a detonation wave are possible because the detonation is a combination of an adiabatic compression shock and a subsequent slow burning. The shock precedes the flame zone and raises the temperature and pressure of the unburned gas to such high values that the kinetics of the chemical reaction are augmented to the point where the flame zone propagates rapidly enough to keep pace with the shock front.

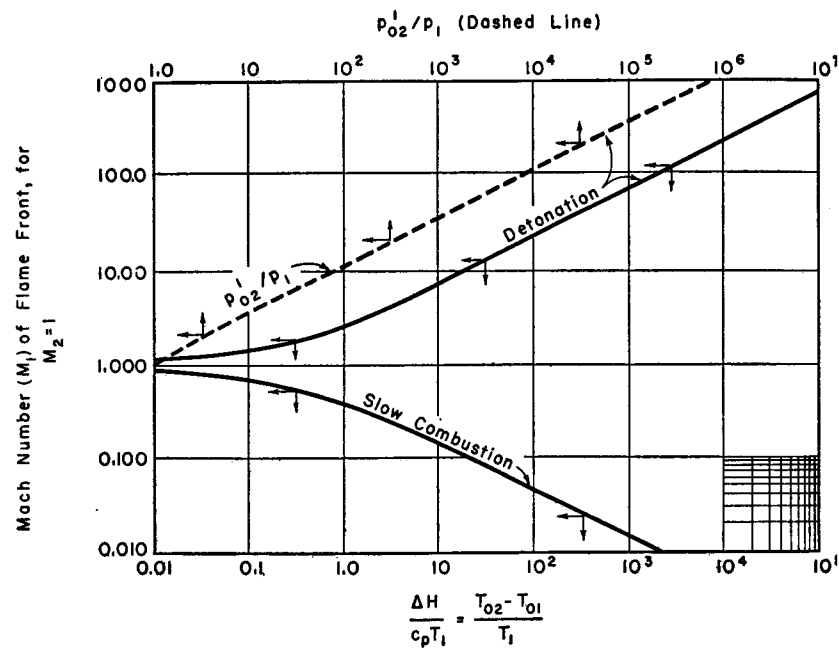


FIG. 7.9. Thermally-choked combustion waves ($M_2 = 1$), for $k = 1.4$. Solid curves show maximum flame speed M_1 for slow combustion, and minimum flame speed M_1 for detonation. The latter is the detonation Mach Number always observed in experiments. Dashed curve shows for detonation with $M_2 = 1$ the stagnation pressure ratio for an observer at rest with respect to the unburned gas.

THE CHAPMAN-JOUQUET RULE. The observed fact that $M_2 = 1$ for a detonation wave is often called the *Rule of Chapman and Jouguet*. In order to find the corresponding detonation speed M_1 , we set $(T_0/T_0^*)_1$ equal to unity, and substitute for $(T_0/T_0^*)_1$ in Eq. 7.26 the value given by Eq. 7.16. Carrying out these operations, and simplifying, we obtain

$$\left(\frac{T_{02} - T_{01}}{T_1} \right)_{M_2=1} = \left(\frac{\Delta H}{c_p T_1} \right)_{M_2=1} = \frac{(1 - M_1^2)^2}{2(k + 1)M_1} \quad (7.27)$$

The two values of M_1 which may be found from this equation correspond to the maximum flame-front speed for slow combustion and the

minimum speed for detonation. These speeds are plotted in Fig. 7.9 as a function of the energy parameter $\Delta H/c_p T_1$.

One measure of the potentialities for damage of a steady detonation wave is the rise in stagnation pressure experienced by an obstacle over which the wave passes. Denoting by p_{02}' the stagnation pressure of the burned gas in a coordinate system where the unburned gas is at rest, it may be shown that

$$\left(\frac{p_{02}'}{p_1} \right)_{M_2=1} = \frac{1 + kM_1^2}{k + 1} \left[1 + \frac{k - 1}{2} \left(\frac{M_1^2 - 1}{1 + kM_1^2} \right)^2 \right]^{\frac{k}{k-1}} \quad (7.28)$$

This ratio is also plotted in Fig. 7.9 for a Chapman-Jouguet detonation. In the usual hydrocarbon detonation, T_1 is about 520°R , $\Delta T_0/T_1$ is about 6, and the speed of sound is about 1000 ft/sec. From Fig. 7.9 it may be seen that the flame-front speed is then about 5500 ft/sec and the stagnation pressure increases to about 25 atmospheres. The temperature after an adiabatic shock traveling at 5500 ft/sec is found from the adiabatic normal shock tables to be about 3000°F ; thus, as indicated previously, there is considerable preheating effect available for increasing the flame speed to values necessary for detonation.

The temperatures in an atomic explosion are said to be measured in millions of degrees. If $\Delta T_0/T_1$ is assumed to equal 10^4 for such an explosion, Fig. 7.9 indicates a wave speed of the order of magnitude of 200,000 ft/sec and a stagnation pressure of the order of magnitude of 40,000 atmospheres!

7.5. The Recovery Factor

When a fluid flows through a pipe having an insulated wall, the temperature at the wall (called the adiabatic wall temperature, T_{aw}) is neither the average stagnation temperature T_0 nor the average static temperature T of the stream. In a gas flow the adiabatic wall temperature usually lies between T and T_0 . The factors influencing T_{aw} and theoretical methods for predicting its value are discussed in detail in Volume II, Chapters 27, 28, and 29. For the present we shall introduce some elementary considerations and shall summarize some experimental results of value for practical computations of pipe flow.

Physical Mechanism of Frictional Heating. The temperature assumed by an insulated wall, past which flows a high-speed gas stream, is controlled by complex phenomena in the boundary layer. Fluid layers far from the wall deliver viscous shear work to layers near the wall. The consequent temperature rise of the inner layer is necessarily accompanied by heat conduction through the fluid away from the wall,

thus tending to limit the temperature rise. After these effects have been brought into balance everywhere in the fluid, the wall is at the equilibrium temperature T_{aw} . The temperature distribution in the boundary layer is then as shown by the solid curve of Fig. 7.10. Corresponding curves for a hot wall and a cold wall are also shown; it should be noted that whether heat flows into or out of the wall depends on the direction of the temperature gradient in the gas at the gas-solid boundary.

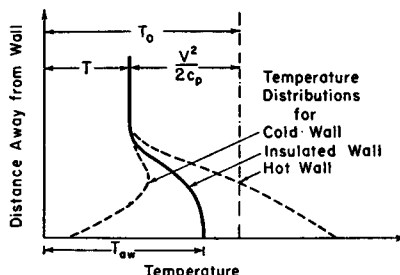


FIG. 7.10. Illustrates definition of adiabatic wall temperature.

The Recovery Factor. The magnitude of T_{aw} relative to the one-dimensional mean values of T and T_0 is usually expressed by the so-called *recovery factor* \mathfrak{R} , which is defined by

$$\mathfrak{R} = \frac{T_{aw} - T}{T_0 - T} = \frac{T_{aw} - T}{V^2/2c_p} \quad (7.29)$$

This may also be expressed as

$$\mathfrak{R} = \frac{\frac{T_{aw}}{T} - 1}{\frac{V^2/2c_p}{T}} = \frac{\frac{T_{aw}}{T} - 1}{\frac{k-1}{2} M^2}$$

so that

$$\frac{T_{aw}}{T} = 1 + \mathfrak{R} \frac{k-1}{2} M^2 \quad (7.30)$$

In Volume II, Chapter 28 it is pointed out that various experiments have yielded values of the recovery factor for subsonic pipe flow between 0.87 and 0.91; and for supersonic pipe flow between 0.83 and 0.90.

7.6. The Coefficient of Heat Transfer

Definition of the Film Coefficient. The *film coefficient of heat transfer* \mathfrak{C} for incompressible pipe flow is ordinarily based on the difference between the wall temperature and the mean stream temperature. For high-speed compressible flow, however, it is more appropriate to base \mathfrak{C} on the difference between the actual wall temperature, T_w , and the adiabatic wall temperature, T_{aw} . With any other method of defining \mathfrak{C} it would be possible for \mathfrak{C} to have both negative and positive values.

Moreover, it is shown in Volume II, Chapters 26, 27, and 28 (cf. Fig. 28.4) that the value of \mathfrak{C} defined in terms of $(T_{aw} - T_w)$ is the only one leading to an experimental correlation which is independent of the rate of heat transfer. Accordingly, we define \mathfrak{C} by

$$q = \mathfrak{C}(T_w - T_{aw}) \quad (7.31)$$

where q is the rate of heat flow per unit wetted area. Substituting for T_{aw} with the aid of Eq. 7.30, the heat transfer equation becomes

$$q = \mathfrak{C} \left[T_w - \left(1 + \mathfrak{R} \frac{k-1}{2} M^2 \right) T \right] \quad (7.32)$$

Summary of Experimental Results. Experimental results for subsonic pipe flow are discussed in Volume II, Chapter 28. They may be summarized as follows:

- (i) Between $M = 0$ and $M = 1$ the curve of Nusselt Number $\mathfrak{C}D/\lambda$ versus Reynolds Number $VD\rho/\mu$ is substantially independent of Mach Number.
- (ii) Between $M = 0$ and $M = 1$ the Reynolds analogy between friction and heat transfer is substantially independent of Mach Number.
- (iii) For turbulent flow up to Reynolds Numbers of 400,000 the heat-transfer data are correlated by the equation

$$\frac{\mathfrak{C}D}{\lambda} = 0.0364 \left[\left(\frac{\rho VD}{\mu} \right) \left(\frac{c_p \mu}{\lambda} \right) \right]^{0.75} \quad (7.33)$$

For theoretical considerations concerning the coefficient \mathfrak{C} in laminar and turbulent flows the reader is referred to Volume II, Chapters 26 and 27.

REFERENCES AND SELECTED BIBLIOGRAPHY

1. SIMONS, W. W., and BOWEN, J. S. Investigation of the Condensation Shock in Air by Use of the Schlieren Method, S.M. Thesis, Dept. of Naval Arch., Mass. Inst. of Tech., Cambridge, Mass. (1946).
2. SHAPIRO, A. H., and HAWTHORNE, W. R. The Mechanics and Thermodynamics of Steady, One-Dimensional Gas Flow, *Jour. App. Mech., Trans. A.S.M.E.*, Vol. 14, No. 4 (1947), p. 317.
3. COURANT, R., and FRIEDRICHHS, K. O. *Supersonic Flow and Shock Waves*. New York: Interscience Publishers, Inc., 1948.

7.1. (a) Fuel is to be burned in a stream of air moving with a Mach Number of 2.0, a temperature of -160°F , and a pressure of 10 psia in a duct of constant area. Estimate the maximum possible rise in stagnation temperature, and the corresponding final values of the temperature, pressure, and stagnation pressure.

(b) If the supersonic stream of part (a) were to pass through a normal shock before fuel was burned, estimate the maximum possible rise in the temperature,

and the corresponding final values of the temperature, pressure, and stagnation pressure.

7.2. Make log-log plots of M_2 versus M_1 , p_2/p_1 versus M_1 , T_2/T_1 versus M_1 , and p_{02}/p_{01} versus M_1 , for fixed values of T_{02}/T_{01} of 1.2 (heating) and 0.8 (cooling). Note that there are two branches on each plot for each value of T_{02}/T_{01} . Use solid lines to indicate which portion of each branch is physically possible and dashed lines to indicate which portions involve violations of the Second Law of Thermodynamics.

7.3. Derive the asymptotic forms of the Simple T_0 -Change formulas for:

- (a) Very low Mach Numbers
- (b) Very high Mach Numbers

7.4. Show that, in Simple T_0 -Change at Mach Numbers less than about 0.2, changes in density are produced almost exclusively by changes in temperature. Based on this observation, and considering two sections 1 and 2, demonstrate that at very low Mach Numbers,

$$p_{02} - p_{01} \cong \frac{R}{p_{01}} \left(\frac{w}{A} \right)^2 (T_{01} - T_{02})$$

7.5. Fuel is injected and burned in air moving down a straight pipe of uniform diameter. If the constant-pressure heat of reaction of the fuel is 19,000 Btu/lb, the stagnation temperature of the air at inlet is 900°R , and the burned gas stream discharges from the duct into a region where the pressure is 15 psia, plot the isentropic stagnation pressure at the duct inlet section against the Mach Number of the air at the inlet section for fuel-air ratios of 0.02 and 0.04. To simplify the computations, it is agreed to neglect friction, the change in the mass rate of flow, the change in chemical composition, and to assume that there is no diffuser at the exit of the duct.

7.6. Air is brought into a tube through a converging-diverging nozzle designed for a Mach Number of 2, and has initially a stagnation temperature of 500°R and a stagnation pressure of 100 psia. The air is to be cooled by some mechanism not involving friction.

(a) Assuming that there are no shocks, compute the maximum possible amount of heat rejection per pound of air passing through the duct. Find, for this limiting condition, the final temperature, pressure, and stagnation pressure.

(b) Investigate the types of flow patterns which might exist in the nozzle-duct system if the amount of cooling is greater than that computed for part (a).

7.7. A wind tunnel nozzle for a Mach Number of 2 is to be supplied with air at 30 psia and 80°F . It is desired to estimate the maximum relative humidity at the nozzle entrance for each of the following conditions:

- (a) At no point in the nozzle is a condition of saturated water vapor reached.
- (b) Precipitation of water vapor occurs at no point in the nozzle. It will be assumed for this purpose that condensation does not occur until the stream temperature is 110°F below the temperature at which saturation is first reached.
- (c) The amount of water vapor is such that the Mach Number just downstream of the moisture condensation shock is exactly unity, assuming that

thermodynamic equilibrium with droplets of "infinite" size is attained. As in part (b), it will be assumed that condensation does not occur until the stream temperature is 110°F below the temperature at which saturation is first reached. For this case, compute the Mach Number, pressure, temperature, stagnation pressure, and stagnation temperature at the nozzle exit and compare with the corresponding values for flow without moisture condensation shocks.

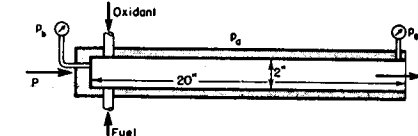
7.8. The sketch shows a tube rocket motor, comprising a long tube which is fed with liquid fuel and liquid oxidant at one end, with hot gases leaving the open end.

In one test of such a motor, the measured thrust, P , was 676 lb; the pressure on the back face of the motor, p_b , was 265 psia; and atmospheric pressure, p_a , was 15 psia.

With the fuel-oxidant combination used, the gases are characterized by $k = 1.3$ and $R = 30 \text{ ft lbf/lbm F}$.

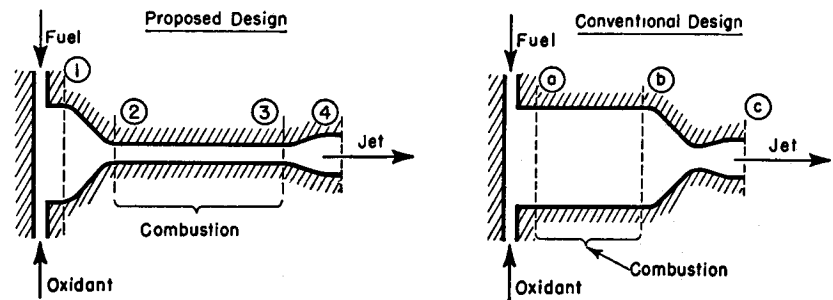
Because of uncertainties as to whether combustion is completed and as to the degree of dissociation, the stagnation temperature of the leaving gases is not known, but it is suspected to be between 3000°F and 5000°F .

- (a) What is the pressure p_e in the exit plane, in psia?
- (b) What is the average shearing stress acting on the inside walls of the motor, in psi?



PROB. 7.8.

7.9. It has been suggested that the combustion in rocket motors should be carried out at high speed in a tube of constant cross-section, as indicated in the sketch. It is desired to compare the specific thrust (thrust force per unit mass rate of flow, in lbf sec/slug) of such a rocket motor with the specific thrust of the conventional motor, also shown in the sketch.



PROB. 7.9.

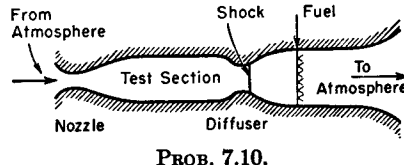
To simplify the calculations it will be assumed that friction is negligible, that the jet leaves the nozzle at the pressure of the ambient atmosphere (say 5 psia), that the fuel and oxidant are supplied as gases, and that both rockets are supplied at the same pressure ($p_{01} = p_{0a} = 500 \text{ psia}$). Also, all processes will be considered adiabatic, except that the combustion will be replaced by an equiva-

lent process of Simple T_0 -Change, with $T_{01} = T_{0a} = 500^{\circ}\text{R}$, and $T_{03} = T_{0b} = 5000^{\circ}\text{R}$. As an approximation, take $k = 1.4$ and use a molecular weight of 20.

For the proposed design assume that the velocity is negligible at section 1, that all combustion occurs between 2 and 3, and that the Mach Number is unity at section 3. For the conventional design assume negligible velocity at a and complete combustion between a and b .

Calculate for both motors the specific impulse (lbf sec/slug) and the throat area per unit of thrust (sq ft/lbf) under the assumed conditions.

7.10. It has been proposed that a supersonic wind tunnel be operated by a ram-jet device, as indicated by the accompanying sketch.



PROB. 7.10.

Do you consider this scheme feasible? Justify your conclusion by suitable arguments. Would your conclusion be altered if the fuel were burned in the supersonic stream following the test section?

7.11. Consider a steady-state explosion wave traveling in a hydrocarbon-air mixture for which the constant-pressure heat of reaction is 1200 Btu per lb of mixture. The inflammable mixture is at rest and at a temperature of 70°F and a pressure of 1 atmosphere. For the two limiting cases in which (i) the wave speed is the maximum for slow combustion, and (ii) the wave speed is the minimum for detonation, compute the following quantities of interest:

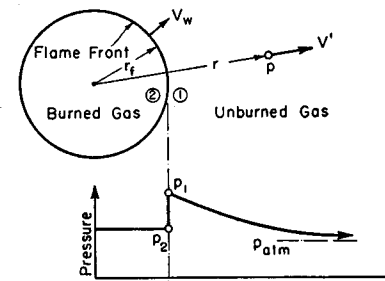
- The speed of the wave front and of the burned gas
- The pressure of the burned gas
- The temperature of the burned gas
- The isentropic stagnation pressure of the burned gas referred to an observer at rest with respect to the unburned gas
- The stagnation temperature of the burned gas referred to an observer at rest with respect to the unburned gas
- In the case of detonation waves, it is probable that the large flame speeds necessary to support the wave are obtained with the help of the preheating effect caused by an approximately adiabatic shock which precedes slightly the flame front proper. Compute, therefore, the temperature behind an adiabatic shock which travels at the speed of the detonation wave.

7.12. Verify Equation 7.28.

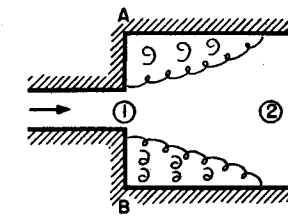
7.13. The sketch shows a slow combustion wave propagating spherically from a point ignition source into a combustible mixture. The velocity of the flame front is V_w , and instantaneously it is at the radius r_f . On the two sides of this front the pressures are p_1 (unburned gas) and p_2 (burned gas), and the

corresponding densities are ρ_1 and ρ_2 . At any radius r the pressure is p and the velocity is V' . At $r = \infty$, the pressure is p_{atm} .

The speed of propagation V_w is extremely low (i.e., a few feet per second). It is, therefore, permissible to assume that the fractional variations in pressure are so small that the density can be taken as constant except across the flame front, where there is a large temperature change.



PROB. 7.13.



PROB. 7.14.

Show that the curve of p versus r is as shown in the sketch and that outside the flame front it is represented by

$$\frac{p - p_{\text{atm}}}{\frac{1}{2}\rho_1 V_w^2} = \left(1 - \frac{\rho_2}{\rho_1}\right) \left(\frac{\rho_2}{\rho_1} + 3\right) + 4 \left(1 - \frac{\rho_2}{\rho_1}\right) \left(\frac{r_f}{r} - 1\right) - \left(1 - \frac{\rho_2}{\rho_1}\right)^2 \left[\left(\frac{r_f}{r}\right)^4 - 1\right]$$

Show also that

$$\frac{p_1 - p_2}{\frac{1}{2}\rho_1 V_w^2} = 2 \frac{\rho_2}{\rho_1} \left(1 - \frac{\rho_2}{\rho_1}\right); \quad \frac{p_2 - p_{\text{atm}}}{\frac{1}{2}\rho_1 V_w^2} = \left(1 - \frac{\rho_2}{\rho_1}\right) \left(3 - \frac{\rho_2}{\rho_1}\right)$$

Investigate these results for endothermic and exothermic reactions.

7.14. Consider the flow of a combustible gas mixture through a sudden expansion in a pipe (see sketch). Combustion occurs between section 1 at the exit of the small pipe and section 2 in the large pipe where the flow is uniform and there is no longer any turbulence. Wall friction between sections 1 and 2 is assumed to be negligible. The flow at section 1 is supplied from a converging nozzle and has stagnation properties p_{01} and T_{01} . If M_1 is subsonic, the pressure on the annular boundary AB is equal to p_1 . If $M_1 = 1$, however, the pressure on this annular boundary may be less than p_1 . The heat of reaction is denoted by ΔH , and the area ratio A_2/A_1 by α .

(a) When M_1 is subsonic, show that the leaving Mach Number is determined by

$$\frac{M_2^2 \left(1 + \frac{k-1}{2} M_2^2\right)}{(1 + kM_2^2)^2} = \left(1 + \frac{\Delta H}{c_p T_{01}}\right) \frac{M_1^2 \left(1 + \frac{k-1}{2} M_1^2\right)}{(\alpha + kM_1^2)^2}$$

- (b) When M_1 is subsonic, $\Delta H/c_p T_{01} = 0$, and $\alpha = \infty$, show that

$$\frac{p_{01}}{p_{02}} = \left(1 + \frac{k-1}{2} M_1^2\right)^{\frac{k}{k-1}}$$

and comment on the significance of this.

- (c) Derive appropriate relations for the case where M_2 is exactly unity.

7.15. Air with a stagnation temperature of 70°F is supplied to an insulated pipe at Mach Number 3 by means of a converging-diverging nozzle. Assuming a recovery factor of 0.85, estimate the wall temperature of the pipe.

7.16. A ram jet flies at sea level with a speed of 1500 miles per hour. At one point in the inlet duct the Mach Number is 0.5. Estimate the adiabatic wall temperature at that section.

Chapter 8

GENERALIZED ONE-DIMENSIONAL CONTINUOUS FLOW

8.1. Introductory Remarks

Analyses were presented in the previous chapters for simple types of flow, that is, for flow processes in which only a single independent parameter was allowed to change. For example, in Chapter 4 the effects of area change alone were considered; in Chapter 6 the effects of friction alone were considered; and in Chapter 7 the effects of changes in stagnation temperature alone were considered.

In most practical problems these effects occur simultaneously, and, in addition, there may be present such other phenomena as chemical reaction, change of phase, injection or withdrawal of gases, and changes in molecular weight and specific heat. As examples in which simultaneous effects are present, we may cite rocket nozzles, ram jets, combustion chambers for gas turbines and turbojet engines, injectors and ejectors, moisture condensation shocks, moving flame fronts, detonation waves, heat exchangers, and gas-cooled nuclear reactors.

The phenomena which we shall take into account in our analysis include:

- (i) Area change
- (ii) Wall friction
- (iii) Drag of internal bodies
- (iv) External heat exchange
- (v) Chemical reaction
- (vi) Change of phase, e.g., evaporation or condensation of water or fuel
- (vii) Mixing of gases which are injected into the main stream
- (viii) Changes in molecular weight and specific heat occasioned by combustion, evaporation, gas injection, etc.

The assumptions made are as follows:

- (i) The flow is one-dimensional and steady.
- (ii) Changes in stream properties are continuous.
- (iii) The gas is semiperfect, i.e., it obeys Boyle's and Charles' laws and has a specific heat which varies only with temperature and composition.

The method of analysis follows closely that of Shapiro and Haw-thorne.⁽¹⁾

Additional material relevant to the subject matter of the present chapter may be found in Chapters 4, 5, 6, 7, and in Volume II, Chapters 26, 27, and 28.

NOMENCLATURE

<i>A</i>	area	<i>s</i>	entropy per unit mass (single phase)
<i>A_w</i>	wetted area of pipe wall	\bar{s}	total entropy per unit mass of gas stream
<i>c</i>	speed of sound	<i>T</i>	absolute temperature
<i>c_p</i>	specific heat at constant pressure	<i>T_{aw}</i>	adiabatic wall temperature
<i>D</i>	mean hydraulic diameter	<i>T_w</i>	temperature of pipe wall
<i>e</i>	base of natural logarithms, 2.718	<i>V</i>	velocity
<i>f</i>	coefficient of friction	<i>V'</i>	forward component of velocity of injected fluid
<i>F</i>	impulse function	<i>w</i>	mass rate of flow of gas stream
<i>F_{T₀}, F_f, etc.</i>	influence coefficient defined by Eqs. 8.49	<i>W</i>	molecular weight
\bar{F}_{T_0}	mean influence coefficient evaluated at $(M_1 + M_2)/2$	<i>W_x</i>	work
<i>h</i>	enthalpy per unit mass	<i>X</i>	drag force
<i>h_{pr}</i>	constant-pressure heat of reaction per unit mass, positive when exothermic	<i>x</i>	Cartesian coordinate
<i>H</i>	energy term defined by Eq. 8.15	<i>y</i>	V'/V ; also see Eq. 8.22c
\mathcal{H}	heat transfer coefficient	<i>ρ</i>	density
<i>k</i>	ratio of specific heats	τ_w	wall shearing stress
<i>L</i>	length	ξ	x/L
<i>M</i>	Mach Number	$(\cdot)_0$	signifies stagnation state
<i>p</i>	pressure	$(\cdot)^*$	signifies state at which $M = 1$
<i>Q</i>	net heat per unit mass of gas	$(\cdot)_g$	signifies injected gas dw_g
<i>R</i>	gas constant	$(\cdot)_L$	signifies evaporated liquid dw_L entering control volume
\mathfrak{R}	universal gas constant; recovery factor		

8.2. Physical Equations and Definitions

Consider the flow in a duct between two sections an infinitesimal distance dx apart (Fig. 8.1). In this element of duct length gas is injected into the stream at the mass rate of flow dw_g , liquid evaporates

into the stream at the mass rate of flow dw_L , heat in the amount dQ is added to the stream from external sources, and shaft work, shearing work, or electrical work is delivered by the stream to external bodies in the amount dW_x .

The various physical equations and definitions will be expressed in logarithmic differential form. It will be seen that this procedure allows easy separation of the physical variables.

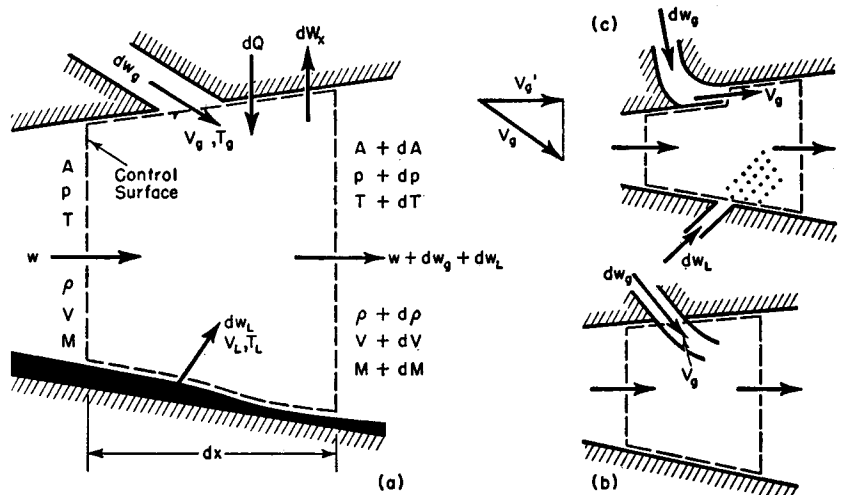


FIG. 8.1. Control surfaces defined for several methods of gas injection and liquid evaporation.

Equation of State. The pressure-density-temperature relation is

$$p = \rho \mathfrak{R} T / W \quad (8.1)$$

Taking logarithms, we get

$$\log p = \log \rho + \log \mathfrak{R} + \log T - \log W$$

Then, taking the differential of each side, we have

$$\frac{dp}{p} = \frac{d\rho}{\rho} + \frac{dT}{T} - \frac{dW}{W} \quad (8.2)$$

Sound Velocity. The expression for the sound velocity in a semi-perfect gas is

$$c^2 = k \mathfrak{R} T / W \quad (8.3)$$

or

$$\frac{dc}{c} = \frac{1}{2} \left(\frac{dk}{k} + \frac{dT}{T} - \frac{dW}{W} \right) \quad (8.4)$$

Definition of Mach Number. From the definition of the Mach Number and Eq. 8.3, we find that

$$M^2 = V^2/c^2 = V^2 W/k\mathcal{R}T \quad (8.5)$$

or

$$\frac{dM^2}{M^2} = \frac{dV^2}{V^2} + \frac{dW}{W} - \frac{dk}{k} - \frac{dT}{T} \quad (8.6)$$

Equation of Continuity. Fig. 8.1 shows several methods by which the injected gas and liquid may be brought into the main stream. Also shown are the corresponding control surfaces employed for purposes of analysis. Any liquid travelling through the duct, whether it be in the form of droplets, filaments, or sheets, is considered to lie outside the control volume. Accordingly, liquid which travels through the length dx without evaporating neither enters nor leaves the control volume. The infinitesimal flow dw_L which evaporates in the length is considered to be liquid which enters the control volume at the liquid-gas interface and which leaves as a gas with the main gas stream.

The injected gas flow dw_g is assumed to be injected continuously along the length of the duct, i.e., dw_g/dx is assumed to be finite or zero. This may be thought of as a simple model of real injection processes.

It is assumed further that the injected streams dw_L and dw_g are mixed perfectly with the main stream at the downstream boundary of the control volume.

The mass flow of the main gas stream may be expressed as

$$w = \rho A V \quad (8.7)$$

or

$$\frac{dw}{w} = \frac{dp}{\rho} + \frac{dA}{A} + \frac{dV}{V} \quad (8.8)$$

In this expression dw denotes the total increase of mass flow in the main stream and includes both injected gas and evaporated gas. The equation of continuity is, therefore,

$$dw = dw_L + dw_g$$

If vapor is condensed, dw_L is negative. It is important to note also that dA refers to the change in cross-sectional area occupied by the main gas stream and does not include the cross-sectional area of the injected streams before mixing. Nor does it include that part of the cross section of the pipe occupied by liquid, although usually the volume of liquid may in fact be neglected in comparison with the volume of gas.

Energy Equation. Only the liquid crossing the control-surface boundary and evaporating within the control surface is taken into account in evaluating the flux of enthalpy. Changes in temperature of the liquid

traveling along with the stream are taken to be the result of external heat exchange to or from the main stream. As the flows dw_L and dw_g , thoroughly mixed with the main stream, pass out of the control surface, they are assumed to be at the temperature of the latter.

The energy equation for the flow through the control surface of Fig. 8.1 may be written, assuming gravity effects to be negligible, as

$$\begin{aligned} w(dQ - dW_x) = & [w(h + dh) + h_{gT} dw_g + h_V dw_L] \\ & - [wh + h_g dw_g + h_L dw_L] \\ & + (w + dw_g + dw_L) \left(\frac{V^2}{2} + d \frac{V^2}{2} \right) \\ & - \left[w \frac{V^2}{2} + \frac{V_g^2}{2} dw_g + \frac{V_L^2}{2} dw_L \right] \end{aligned} \quad (8.9)$$

In this expression dQ is the net heat added to the stream by conduction or radiation from sources external to the main gaseous stream, per unit mass of gas entering the control surface. Likewise, dW_x is the net external work delivered to outside bodies per unit mass of gas entering the control boundary. The external work includes shaft work, electrical work, and shear work on moving bodies adjacent to the control-surface boundaries. The symbols h_{gT} and h_g denote, respectively, the enthalpy of the injected gas dw_g at the temperature T , and the enthalpy at the temperature T_g with which dw_g enters the control volume. The symbol h_V denotes the enthalpy of the evaporated liquid dw_L at the temperature T , and h_L denotes the enthalpy of the liquid at out to evaporate as it enters the control volume.

Eq. 8.9 may be rearranged in the form

$$\begin{aligned} dQ - dW_x = & dh + d \frac{V^2}{2} + \left[h_{gT} - h_g + \frac{V^2 - V_g^2}{2} \right] \frac{dw_g}{w} \\ & + \left[h_V - h_L + \frac{V^2 - V_L^2}{2} \right] \frac{dw_L}{w} \end{aligned} \quad (8.10)$$

The enthalpy change of the main gas stream, dh , is the sum of the changes due to chemical reaction and to temperature change. Thus

$$dh = -dh_{pr} + c_p dT \quad (8.11)$$

where dh_{pr} , the enthalpy increase at the temperature T and pressure p for a change from products to reactants, is positive for exothermic reactions. It is usually called the constant-pressure heat of reaction and, in special cases, the constant-pressure heat of combustion. In evaluating dh_{pr} , one considers of course only the chemical changes which actually occur, but computes dh_{pr} per unit mass of the main gas stream.

We may also write

$$h_{gT} - \left[h_g + \frac{V_g^2}{2} \right] = h_{gT} - h_{0g} = \bar{c}_{pg}(T - T_{0g}), \quad (8.12)$$

where

$$\bar{c}_{pg} = \frac{1}{T - T_{0g}} \int_{T_{0g}}^T c_{pg} dT \quad (8.13)$$

and h_{0g} and T_{0g} are, respectively, the stagnation enthalpy and stagnation temperature of the injected gas stream.

Inserting Eqs. 8.11 and 8.12 into 8.10, and rearranging, the energy equation is finally put into the convenient form

$$dQ - dW_x + dH = c_p dT + d(V^2/2) \quad (8.14)$$

where dH is an energy term defined by

$$dH = dh_{pr} - [\bar{c}_{pg}(T - T_{0g}) + V^2/2] \frac{dw_g}{w} - \left[h_L - h_V + \frac{V^2 - V_L^2}{2} \right] \frac{dw_L}{w} \quad (8.15)$$

Dividing Eq. 8.14 by $c_p T$, we obtain

$$\frac{dQ - dW_x + dH}{c_p T} = \frac{dT}{T} + \frac{k-1}{2} M^2 \frac{dV^2}{V^2} \quad (8.16)$$

Momentum Equation. The net force acting on the material within the control surface of Fig. 8.1 is equal to the increase of momentum flux of the streams flowing through the control surface.

Consider forces in the direction of flow acting on the control surface in Fig. 8.1a. Assuming that the injected gas and liquid streams are at the control-surface pressure as they cross the boundary and that the angle of divergence of the walls is small, the momentum equation may be written *

$$pA + p dA - (p + dp)(A + dA) - \tau_w dA_w - dX = (w + dw_g + dw_L)(V + dV) - V_g' dw_g - V_L' dw_L - wV \quad (8.17)$$

In the foregoing expression τ_w represents the frictional shearing stress acting on the pipe wall area dA_w ; dX is the sum of (i) the drag of stationary bodies immersed in the stream within the control-surface boundaries; (ii) the drag of liquid droplets and filaments traveling more slowly than

* If the injected gas stream is not at the control-surface pressure as it crosses the boundary, the term $(p_g - p)dA_g'$ should be added to the left-hand side of Eq. 8.17, where p_g is the pressure of the injected stream at the boundary and dA_g' is the projected area of the part of the control surface occupied by the injected gas stream.

the main gas stream, and (iii) the component of body or gravity forces acting on the material within the control surface in the direction opposite to that of the velocity vector; V_g' is the forward component of the velocity V_g with which the injected gas dw_g crosses the control surface, and similarly for V_L' .

The wall shearing stress is related to the coefficient of friction, f , though the definition of the latter:

$$\tau_w \equiv f \rho V^2 / 2 \quad (8.18)$$

It is convenient to define the quantities

$$y_g = V_g' / V \quad \text{and} \quad y_L = V_L' / V \quad (8.19)$$

From the definition of the mean hydraulic diameter D , we obtain

$$dA_w / A = 4dx / D \quad (8.20)$$

Substituting Eqs. 8.18, 8.19, and 8.20 into Eq. 8.17, and noting that $\rho V^2 = k p M^2$, we obtain, following rearrangement,

$$\frac{dp}{p} + \frac{kM^2}{2} \frac{dV^2}{V^2} + \frac{kM^2}{2} \left(4f \frac{dx}{D} + \frac{dX}{\frac{1}{2} k p A M^2} \right) + kM^2(1-y) \frac{dw}{w} = 0 \quad (8.21)$$

where

$$(1-y) \frac{dw}{w} \equiv (1-y_g) \frac{dw_g}{w} + (1-y_L) \frac{dw_L}{w} \quad (8.22a)$$

$$\frac{dw}{w} = \frac{dw_g}{w} + \frac{dw_L}{w} \quad (8.22b)$$

$$y \frac{dw}{w} \equiv y_g \frac{dw_g}{w} + y_L \frac{dw_L}{w} \quad (8.22c)$$

These equations apply also for the methods of injection shown in Figs. 8.1b and 8.1c, provided that A is always taken as the cross-sectional area of the main gas stream.

Definition of Impulse Function. The impulse function, which is defined by

$$F = pA + \rho AV^2 = pA(1 + kM^2) \quad (8.23)$$

is useful for evaluating the thrust of propulsion systems. The increase in this function represents the total force exerted by the stream on the internal walls of the duct and acting on the duct walls in the direction opposite to the flow. In differential form,

$$\frac{dF}{F} = \frac{dA}{A} + \frac{dp}{p} + \frac{kM^2}{1+kM^2} \frac{dM^2}{M^2} + \frac{kM^2}{1+kM^2} \frac{dk}{k} \quad (8.24)$$

Second Law of Thermodynamics. Application of the Second Law of Thermodynamics is simplified through use of the entropy. For a semi-perfect gas and no changes in chemical composition, the entropy change of the main gas stream alone is

$$\frac{ds}{c_p} = \frac{dT}{T} - \frac{k-1}{k} \frac{dp}{p} \quad (8.25)$$

More important, however, is the total entropy change of the main stream plus injected gas and evaporated liquid. It may be shown that for unchanged chemical composition

$$d\bar{s} = ds + (s - s_g) \frac{dw_g}{w} + (s - s_L) \frac{dw_L}{w} \quad (8.26)$$

where $d\bar{s}$ is the total entropy change per unit mass of main gas stream.

8.3. Working Equations and Tables of Influence Coefficients

Eight independent relations between the differential parameters have been set forth, namely, Eqs. 8.2, 8.4, 8.6, 8.8, 8.16, 8.21, 8.24, and 8.25. As there are fourteen differential variables, six may be chosen as independent variables and eight as dependent variables. For the independent variables we choose those most easily controlled in practice, as indicated below.

Independent	Dependent
dA/A	dM^2/M^2
$(dQ - dW_x + dH)/c_p T$	dV/V
$4f \frac{dx}{D} + \frac{dX}{\frac{1}{2}kpAM^2} - 2y \frac{dw}{w}$	dc/c
dw/w	$d\rho/\rho$
dW/W	dF/F
dk/k	$d\bar{s}/c_p$

The usual methods for solving a system of simultaneous, linear, algebraic equations may be employed for obtaining each dependent variable in terms of the six independent parameters. For example, by elimination we obtain for dM^2/M^2 the equation

$$\begin{aligned} dM^2/M^2 = & - \frac{2 \left(1 + \frac{k-1}{2} M^2 \right)}{1 - M^2} \frac{dA}{A} + \frac{1 + kM^2}{1 - M^2} \frac{dQ - dW_x + dH}{c_p T} \\ & + \frac{kM^2 \left(1 + \frac{k-1}{2} M^2 \right)}{1 - M^2} \left[4f \frac{dx}{D} + \frac{dX}{\frac{1}{2}kpAM^2} - 2y \frac{dw}{w} \right] \\ & + \frac{2(1 + kM^2) \left(1 + \frac{k-1}{2} M^2 \right)}{1 - M^2} \frac{dw}{w} - \frac{1 + kM^2}{1 - M^2} \frac{dW}{W} - \frac{dk}{k} \end{aligned} \quad (8.27)$$

Influence Coefficients. We shall call the coefficients of the independent variables *influence coefficients*, since they indicate the influence of each independent variable on each of the dependent parameters. Table 8.1 lists the influence coefficients found by solution of the simultaneous equations. The examples presented later illustrate the usefulness of these influence coefficients in treating a variety of practical problems.

Useful Integral Relations. In addition to the differential relations summarized by Table 8.1, a number of useful integral relations are obtainable from Eqs. 8.1, 8.5, 8.7, 8.16, and 8.23. They may be summarized as follows:

$$Q - W_x + \Delta H \cong c_{p2} T_2 \left(1 + \frac{k_2 - 1}{2} M_2^2 \right) - c_{p1} T_1 \left(1 + \frac{k_1 - 1}{2} M_1^2 \right) - (c_{p2} - c_{p1}) \frac{T_1 + T_2}{2} \quad (8.28)$$

$$\frac{p_2}{p_1} = \frac{w_2}{w_1} \frac{A_1}{A_2} \frac{M_1}{M_2} \sqrt{\frac{T_2}{T_1}} \sqrt{\frac{k_1 W_1}{k_2 W_2}} \quad (8.29)$$

$$\frac{V_2}{V_1} = \frac{M_2}{M_1} \sqrt{\frac{k_2}{k_1} \frac{T_2}{T_1} \frac{W_1}{W_2}} \quad (8.30)$$

$$\frac{\rho_2}{\rho_1} = \frac{w_2}{w_1} \frac{A_1}{A_2} \frac{V_1}{V_2} = \frac{p_2}{p_1} \frac{T_1}{T_2} \frac{W_2}{W_1} \quad (8.31)$$

$$\frac{F_2}{F_1} = \frac{p_2}{p_1} \frac{A_2}{A_1} \frac{1 + k_2 M_2^2}{1 + k_1 M_1^2} \quad (8.32)$$

These formulas are derived by writing the energy equation and continuity equation for two sections (1 and 2) of the flow, and by introducing

TABLE 8.1

INFLUENCE COEFFICIENTS FOR VARIABLE SPECIFIC HEAT AND MOLECULAR WEIGHT

$\frac{dA}{A}$	$\frac{dQ - dW_x + dH}{c_p T}$	$4f \frac{dx}{D} + \frac{1}{2} \frac{k p A M^2}{1 - M^2} - 2 \frac{dw}{w}$	$\frac{dw}{w}$	$\frac{dW}{W}$	$\frac{dk}{k}$
$\frac{dM^2}{M^2}$	$2 \left(1 + \frac{k-1}{2} M^2 \right)$	$\frac{1 + k M^2}{1 - M^2}$	$\frac{k M^2 \left(1 + \frac{k-1}{2} M^2 \right)}{1 - M^2}$	$\frac{2(1 + k M^2) \left(1 + \frac{k-1}{2} M^2 \right)}{1 - M^2}$	$-\frac{1 + k M^2}{1 - M^2}$
$\frac{dV}{V}$	$-\frac{1}{1 - M^2}$	$\frac{1}{1 - M^2}$	$\frac{k M^2}{2(1 - M^2)}$	$\frac{1 + k M^2}{1 - M^2}$	$-\frac{1}{1 - M^2}$
$\frac{dc}{c}$	$\frac{k-1}{2} M^2$	$\frac{1 - k M^2}{2(1 - M^2)}$	$-\frac{k(k-1) M^4}{4(1 - M^2)}$	$-\frac{k-1}{2} M^2 (1 + k M^2)$	0
$\frac{dT}{T}$	$\frac{(k-1) M^2}{1 - M^2}$	$\frac{1 - k M^2}{1 - M^2}$	$-\frac{k(k-1) M^4}{2(1 - M^2)}$	$-\frac{(k-1) M^2 (1 + k M^2)}{1 - M^2}$	$\frac{k M^2 - 1}{2(1 - M^2)}$
$\frac{dp}{p}$	$\frac{M^2}{1 - M^2}$	$\frac{1}{1 - M^2}$	$-\frac{k M^2}{2(1 - M^2)}$	$-\frac{(k+1) M^2}{1 - M^2}$	$\frac{1}{1 - M^2}$
$\frac{dp}{p}$	$\frac{k M^2}{1 - M^2}$	$-\frac{k M^2}{1 - M^2}$	$-\frac{k M^2 (1 + (k-1) M^2)}{2(1 - M^2)}$	$-\frac{2k M^2 (1 + \frac{k-1}{2} M^2)}{1 - M^2}$	0
$\frac{dw}{w}$	$\frac{1}{1 + k M^2}$	0	$-\frac{k M^2}{2(1 + k M^2)}$	0	0
$\frac{dw}{w}$ (Note 2)	0	1	$\frac{(k-1) M^2}{2}$	$(k-1) M^2$	0

Notes: (1) Each influence coefficient represents the partial derivative of the variable in the left-hand column with respect to the variable in the top row; for example

$$\frac{dM^2}{M^2} = -2 \left(1 + \frac{k-1}{2} M^2 \right) \frac{dA}{A} + \frac{1 + k M^2}{1 - M^2} \frac{dQ - dW_x + dH}{c_p T} + \dots \dots - \frac{dk}{k}$$

(2) For unaltered chemical composition only, and referring to entropy change of main stream. See Eq. 8.26 for total entropy change.

the definitions of M and F together with the relations $p = \rho RT$ and $c = \sqrt{k \mathcal{R} T / W}$.

In deriving Eq. 8.28 it was assumed that for a moderate temperature interval it is valid to write

$$\int_{T_1}^{T_2} c_p dT \leq \frac{c_{p1} + c_{p2}}{2} (T_2 - T_1)$$

8.4. Flow with Constant Specific Heat and Molecular Weight

There are many instances where the changes in molecular weight and specific heat are of secondary importance and may, therefore, be neglected for the sake of simplicity.

The equations of Arts. 8.2 and 8.3 remain valid, of course, but are simplified by noting that

$$dW = dc_p = dk = 0$$

and

$$W_1 = W_2; \quad c_{p1} = c_{p2}; \quad k_1 = k_2$$

Stagnation Temperature and Pressure. The stagnation temperature and stagnation pressure are, as we have seen, useful parameters for problems of one-dimensional flow.

Although these stagnation properties are always significant, they have not been brought explicitly into the equations of Arts. 8.2 and 8.3 because there are no simple algebraic relations connecting the local properties with the stagnation properties in the general case of variable specific heat and molecular weight.

STAGNATION TEMPERATURE. With the assumptions of constant c_p and W , however, we may express the stagnation temperature as

$$T_0 = T + \frac{V^2}{2c_p} = T \left(1 + \frac{k-1}{2} M^2 \right) \quad (8.33)$$

or, in differential form, as

$$\frac{dT_0}{T_0} = \frac{dT}{T} + \frac{\frac{k-1}{2} M^2}{1 + \frac{k-1}{2} M^2} \frac{dM^2}{M^2} \quad (8.34)$$

Eq. 8.14, when combined with Eq. 8.33, yields

$$dQ - dW_x + dH = c_p dT + d(V^2/2) = c_p dT_0 \quad (8.35)$$

or

$$\frac{dQ - dW_x + dH}{c_p T} = \left(1 + \frac{k-1}{2} M^2 \right) \frac{dT_0}{T_0} \quad (8.36)$$

Eq. 8.35 shows that the change in T_0 is a measure of the total energy effects produced by heat transfer, shear and shaft work, chemical reaction, change of phase, injection of gases, etc. We shall, therefore, employ Eq. 8.34 rather than Eq. 8.16 as a representation of the energy equation. The parameter $(dQ - dW_x + dH)/c_p T$ is then replaced by dT_0/T_0 in our system of equations. These parameters are related through Eq. 8.36.

STAGNATION PRESSURE. The isentropic stagnation pressure is related to the local pressure and Mach Number through the familiar formula

$$p_0 = p \left(1 + \frac{k-1}{2} M^2 \right)^{\frac{k}{k-1}} \quad (8.37)$$

or, in differential form,

$$\frac{dp_0}{p_0} = \frac{dp}{p} + \frac{kM^2/2}{1 + \frac{k-1}{2} M^2} \frac{dM^2}{M^2} \quad (8.38)$$

The change of entropy, in terms of p_0 and T_0 , is then

$$\frac{ds}{c_p} = \frac{dT_0}{T_0} - \frac{k-1}{k} \frac{dp_0}{p_0} \quad (8.39)$$

Working Equations and Table of Influence Coefficients. As in Art. 8.3, the differential working equations are arranged in terms of independent parameters, influence coefficients, and dependent parameters.

For example, Eq. 8.27 becomes

$$\begin{aligned} \frac{dM^2}{M^2} = & - \frac{2 \left(1 + \frac{k-1}{2} M^2 \right)}{1 - M^2} \frac{dA}{A} + \frac{(1 + kM^2) \left(1 + \frac{k-1}{2} M^2 \right)}{1 - M^2} \frac{dT_0}{T_0} \\ & + \frac{kM^2 \left(1 + \frac{k-1}{2} M^2 \right)}{1 - M^2} \left(4f \frac{dx}{D} + \frac{dX}{\frac{1}{2} kpAM^2} - 2y \frac{dw}{w} \right) \\ & + \frac{2(1 + kM^2) \left(1 + \frac{k-1}{2} M^2 \right)}{1 - M^2} \frac{dw}{w} \end{aligned} \quad (8.40)$$

The complete array of influence coefficients is given in Table 8.2.

TABLE 8.2
INFLUENCE COEFFICIENTS FOR CONSTANT SPECIFIC HEAT AND MOLECULAR WEIGHT

	$\frac{dA}{A}$	$\frac{dT_0}{T_0}$	$\frac{dX}{\frac{1}{2} kpAM^2}$	$-2y \frac{dw}{w}$	$\frac{dw}{w}$
$\frac{dM^2}{M^2}$	$-\frac{2 \left(1 + \frac{k-1}{2} M^2 \right)}{1 - M^2}$	$\frac{(1 + kM^2) \left(1 + \frac{k-1}{2} M^2 \right)}{1 - M^2}$	$\frac{kM^2 \left(1 + \frac{k-1}{2} M^2 \right)}{1 - M^2}$	$\frac{2(1 + kM^2) \left(1 + \frac{k-1}{2} M^2 \right)}{1 - M^2}$	
$\frac{dV}{V}$	$-\frac{1}{1 - M^2}$	$\frac{1 + \frac{k-1}{2} M^2}{1 - M^2}$	$\frac{kM^2}{2(1 - M^2)}$	$\frac{1 + kM^2}{1 - M^2}$	
$\frac{dc}{c}$	$\frac{k-1}{2} \frac{M^2}{1 - M^2}$	$\frac{1 - kM^2 \left(1 + \frac{k-1}{2} M^2 \right)}{2(1 - M^2)}$	$\frac{k(k-1)M^4}{4(1 - M^2)}$	$\frac{k-1}{2} \frac{M^2(1 + kM^2)}{1 - M^2}$	
$\frac{dT}{T}$	$\frac{(k-1)M^2}{1 - M^2}$	$\frac{(1 - kM^2) \left(1 + \frac{k-1}{2} M^2 \right)}{1 - M^2}$	$\frac{k(k-1)M^4}{2(1 - M^2)}$	$\frac{(k-1)M^2(1 + kM^2)}{1 - M^2}$	
$\frac{dp}{p}$	$\frac{M^2}{1 - M^2}$	$-\frac{1 + \frac{k-1}{2} M^2}{1 - M^2}$	$-\frac{kM^2}{2(1 - M^2)}$	$-\frac{(k+1)M^2}{1 - M^2}$	
$\frac{dp}{p}$	$\frac{kM^2}{1 - M^2}$	$-\frac{kM^2 \left(1 + \frac{k-1}{2} M^2 \right)}{1 - M^2}$	$-\frac{kM^2(1 + (k-1)M^2)}{2(1 - M^2)}$	$-\frac{2kM^2 \left(1 + \frac{k-1}{2} M^2 \right)}{1 - M^2}$	
$\frac{dw}{p_0}$	0	$-\frac{kM^2}{2}$	$-\frac{kM^2}{2}$	$-kM^2$	
$\frac{dF}{F}$	$\frac{1}{1 + kM^2}$	0	$-\frac{kM^2}{2(1 + kM^2)}$	0	$(k-1)M^2$
$\frac{ds}{c_p}$	0	$1 + \frac{k-1}{2} M^2$	$\frac{(k-1)M^2}{2}$		

Note: Each influence coefficient represents the partial derivative of the variable in the left-hand column with respect to the variable in the top row; for example

$$\frac{dM^2}{M^2} = -\frac{2 \left(1 + \frac{k-1}{2} M^2 \right)}{1 - M^2} \frac{dA}{A} + \frac{(1 + kM^2) \left(1 + \frac{k-1}{2} M^2 \right)}{1 - M^2} \frac{dT_0}{T_0} + \frac{kM^2 \left(1 + \frac{k-1}{2} M^2 \right)}{1 - M^2} \left(4f \frac{dx}{D} + \frac{dX}{\frac{1}{2} kpAM^2} - 2y \frac{dw}{w} \right)$$

$$+ \frac{2(1 + kM^2) \left(1 + \frac{k-1}{2} M^2 \right)}{1 - M^2} \frac{dw}{w}$$

USEFUL INTEGRAL RELATIONS. The several useful integral relations between the properties at two cross-sections may be summarized as follows:

$$Q - W_x + \Delta H = c_p(T_{02} - T_{01}) \quad (8.41)$$

$$\frac{p_2}{p_1} = \frac{w_2 A_1 M_1}{w_1 A_2 M_2} \sqrt{\frac{1 + \frac{k-1}{2} M_1^2}{1 + \frac{k-1}{2} M_2^2}} \sqrt{\frac{T_{02}}{T_{01}}} \quad (8.42)$$

$$\frac{V_2}{V_1} = \frac{M_2}{M_1} \sqrt{\frac{T_2}{T_1}} \quad (8.43)$$

$$\frac{\rho_2}{\rho_1} = \frac{w_2 A_1 V_1}{w_1 A_2 V_2} = \frac{p_2 T_1}{p_1 T_2} \quad (8.44)$$

$$\frac{T_2}{T_1} = \frac{T_{02}}{T_{01}} \frac{1 + \frac{k-1}{2} M_1^2}{1 + \frac{k-1}{2} M_2^2} \quad (8.45)$$

$$\frac{p_{02}}{p_{01}} = \frac{p_2}{p_1} \left[\frac{1 + \frac{k-1}{2} M_2^2}{1 + \frac{k-1}{2} M_1^2} \right]^{\frac{k}{k-1}} \quad (8.46)$$

8.5. General Features of Flow Patterns

The influence coefficients are indicative of some interesting aspects of compressible flow patterns.

Effects of Independent Parameters. The influence coefficients for M , V , T , ρ , and p have, with the exception of those pertaining to the independent parameter dk/k , the term $(1 - M^2)$ in the denominator. From this it is evident that the Mach Number, velocity, temperature, pressure, and density, all change at an infinite rate in the neighborhood of Mach Number unity. Moreover, wherever the signs of the influence coefficients change at $M = 1$, the effects of the independent variables are of opposite sign for subsonic and supersonic flow. An exception concerns the effect of heating on the temperature, for which it will be noted that the influence coefficient changes sign at $M = 1/\sqrt{k}$ as well as at $M = 1$.

The individual influence of each independent variable is readily found from Table 8.1. From Eqs. 8.27 and 8.40 these influences are seen to be independent of each other, i.e., the incremental effects of small changes in the independent variables are linearly additive.

EFFECTS ON M . An increase in area tends to reduce M in subsonic flow and to increase it in supersonic flow.

Heating or combustion tends to increase M at subsonic speeds, and to decrease M at supersonic speeds.

The effect of friction, or drag of internal bodies, acts to increase M at subsonic speeds, and to decrease M at supersonic speeds. Note that the friction term, $f dx$, and internal-drag term, dX , are always positive, while the other independent variables may be either positive or negative.

An increase in mass flow (with $y < 1$ for the added flow) tends to increase M at subsonic speeds and to decrease M at supersonic speeds.

When the molecular weight is increased, the Mach Number tends to decrease for subsonic flow and to increase for supersonic flow.

An increase in the isentropic exponent k always tends to reduce M , for either subsonic or supersonic speeds.

EFFECTS ON STAGNATION PRESSURE. Changes in area have no effect on stagnation pressure, at least when c_p and W are constant.

An increase in stagnation temperature always tends toward a reduction in p_0 . Thus the stagnation-pressure loss in combustion chambers can never be entirely eliminated.

Friction and drag likewise always act to reduce p_0 .

Gas injection tends to decrease p_0 if $y < 1$, i.e., if the gas is injected with a forward velocity less than that of the main stream; while the stagnation pressure tends to be increased when gas is injected with a forward velocity greater than that of the main stream (as in a jet pump).

The Second Law of Thermodynamics. Considering the simple case where there is no combustion, no W_x , and no injection, we find from Table 8.1 that

$$ds = \frac{dQ}{T} + c_p \frac{k-1}{2} M^2 \left[4f \frac{dx}{D} + \frac{dX}{\frac{1}{2} k p A M^2} \right]$$

Application of the Second Law of Thermodynamics to the flow through the control surface yields

$$ds - \frac{dQ}{T} \geq 0$$

from which it may be shown that both $f dx$ and dX are always positive, i.e., negative friction or negative drag would constitute violations of the Second Law.

Considering next the case where there is no chemical change, no friction, no drag, and no W_x , we find from Eq. 8.26 that

$$d\bar{s} = \frac{dQ + dH}{T} + c_p(k-1)M^2(1-y) \frac{dw}{w} + (s - s_g) \frac{dw}{w}$$

As in the preceding paragraph, the Second Law of Thermodynamics requires that

$$d\bar{s} - \frac{dQ}{T} \geq 0$$

Examination of this requirement for gas injection shows that it is satisfied under all conditions.

If the foregoing equation for $d\bar{s}$ is to be valid for gas withdrawal, the withdrawn gas must cross the boundary of the control surface with exactly the same properties and direction of motion as the main stream. In other words, the withdrawal must not include an unmixing process, and, in addition, y must be unity. Obviously, gas may be withdrawn at other values of y , but in these instances the gas will cross the boundary at other than the control-surface pressure, and the equation for $d\bar{s}$ will have to be modified to take into account the added term discussed in the footnote to Eq. 8.17.

From this discussion it is to be noted that for gas withdrawal the influence coefficients in Tables 8.1 and 8.2 are applicable only for the condition $y = 1$.

Choking Effects. We have previously seen, for the simple flows of the previous chapters, that under certain conditions it is impossible to reduce the area, increase the amount of friction, or increase the amount of heating without causing a complete readjustment of the steady-state flow pattern. In subsonic flow this readjustment consists of a reduction in flow rate. In supersonic flow the readjustment usually involves, first, the appearance of shocks and, ultimately, for large alterations in the independent parameters, reductions in flow rate.

Similar effects occur for more complex types of flow patterns. To illustrate the argument, let us first reconsider a simple case, namely, one in which the area is the only independent parameter which changes. From the first column and first line of Tables 8.1 and 8.2 we see that

$$(1 - M^2) dM^2 = -2M^2 \left(1 + \frac{k-1}{2} M^2\right) \frac{dA}{A}$$

(i) If the area increases, i.e., if $dA > 0$, we see that

$$(1 - M^2) dM^2 < 0$$

Therefore,

$$\text{when } M < 1, \quad dM < 0$$

and

$$\text{when } M > 1, \quad dM > 0$$

In other words, an increase in area causes the Mach Number to decrease in subsonic flow and to increase in supersonic flow, and there seem to be no difficulties in allowing the area to increase indefinitely.

(ii) If the area decreases, i.e., if $dA < 0$, we see that

$$(1 - M^2) dM^2 > 0$$

Therefore,

$$\text{when } M < 1, \quad dM > 0$$

and

$$\text{when } M > 1, \quad dM < 0$$

In other words, a decrease in area causes the Mach Number to increase in subsonic flow and to decrease in supersonic flow, and so the Mach Number always approaches unity. If Mach Number unity is reached at some point in the duct, further reductions in area cannot be introduced without altering the entire flow pattern. This alteration usually is in the form of *choking*. It is to be noted also that after reductions in area have brought the Mach Number to unity, further changes in area without alteration in flow rate can occur only if the area is increased.

Effects similar to these have been discussed previously for flow with friction and for flow with increases in stagnation temperature.

RULES OF CHOKING. The foregoing arguments may be generalized as follows (see also Art. 8-10):

(i) If $(1 - M^2) dM^2$ is always negative, as for an area increase, no limiting effects are encountered in constructing flow patterns.

(ii) If $(1 - M^2) dM^2$ is always positive, as for an area decrease, no further changes in the stream parameters are possible after the Mach Number has reached unity.

(iii) If, with $(1 - M^2) dM^2$ at first always positive, Mach Number unity is reached, then further changes in stream properties can occur only if $(1 - M^2) dM^2$ becomes negative.

The three rules given above may be readily applied to complex flows involving variations in two or more of the independent parameters. For example, consider a process in which the area and stagnation temperature change simultaneously, and in which there are also frictional effects. Then, from the first line of Table 8.2,

$$(1 - M^2) dM^2 =$$

$$M^2 \left(1 + \frac{k-1}{2} M^2\right) \left[-2 \frac{dA}{A} + (1 + kM^2) \frac{dT_0}{T_0} + kM^2 4f \frac{dx}{D} \right]$$

The term $4f dx/D$ is always positive. Therefore, if the area continually decreases and the stagnation temperature continually increases it is clear that $(1 - M^2) dM^2$ will always be positive and that choking effects must ensue. On the other hand, if the area were continually increased and the stagnation temperature continually decreased, these effects might outweigh frictional effects and act to maintain $(1 - M^2) dM^2$ always negative, in which case there would be no difficulty in continuing the flow pattern indefinitely.

CONTINUOUS TRANSITION THROUGH SPEED OF SOUND. In order to obtain a continuous transition from subsonic to supersonic flow, or vice versa, it is evident that the rates of change of area, stagnation temperature, and frictional length must be such as to produce a change of sign in $(1 - M^2) dM^2$ at Mach Number unity. That is, $(1 - M^2) dM^2$ must be generally positive until Mach Number unity is reached, at which point $(1 - M^2) dM^2$ must pass through zero and become negative, after which the Mach Number will change in the direction away from unity. This is a delicate process near $M = 1$, since dA/A , $4f dx/D$ and dT_0/T_0 must be so controlled relative to each other as to make $(1 - M^2) dM^2$ pass from positive values through zero to negative values exactly at the moment when $M = 1$. When the flow is from subsonic to supersonic speeds, this continuous transition is easy to carry out in practice. The continuous transition from supersonic to subsonic speeds, on the other hand, is hardly ever realized in practice, and is probably unstable under most conditions.

8.6. General Method of Solution

Integration of Differential Equations. A typical problem involving simultaneous effects will usually involve known initial conditions (M_1 , p_1 , T_1 , etc.) at some point in the duct, together with certain prescribed variations in area, stagnation temperature, and in the remaining independent parameters of Tables 8.1 and 8.2. Integration of Eq. 8.27 then yields the value of the Mach Number at each section of the duct downstream of the initial section. Sometimes this integration may be carried out analytically, but more often an approximate step-wise integration is necessary.

In order to find the corresponding values of p , T , V , etc. at each section of the duct, two procedures are open. First, the differential equations of Table 8.1 for dp/p , dT/T , dV/V , etc. may be integrated analytically or numerically. Or, secondly, since the value of M is known at each section from the previous integration, Eqs. 8.28 to 8.32 and 8.41 to 8.46 may be used for finding the remaining stream properties.

Suppose that the values of M_1 , p_1 , T_1 , A_1 , etc. are known at a section 1,

and that the values of A_2 , $(Q - W_x + \Delta H)_{1-2}$, $x_2 - x_1$, w_2 , W_2 , k_2 , etc. are known for a section 2, a small distance downstream of section 1. Then, from Eq. 8.27, the value of M_2 may be found by numerical or graphical integration. Next, Eq. 8.28 is solved for T_2 , Eq. 8.29 for p_2 , and Eqs. 8.30 and 8.31 for V_2 and ρ_2 , respectively. The procedure is then repeated for a step between sections 2 and 3, and so on.

Integration Near Mach Number Unity. Special precautions in numerical integration must be taken near $M = 1$ because many of the influence coefficients there approach infinity. It is usually possible to avoid difficulty by obtaining an approximate analytical formula for a step near $M = 1$, making use of the approximation that $1 - M^2$ is negligible compared with unity. For example, consider the first two terms of Eq. 8.27:

$$\frac{dT_0}{T_0} = \frac{1 - M^2}{M^2(1 + kM^2) \left(1 + \frac{k-1}{2} M^2 \right)} dM^2$$

Define, for compactness, $N \equiv 1 - M^2$. Then, when $M \cong 1$, $N \ll 1$, and it may be shown by means of binomial expansions that

$$\frac{dT_0}{T_0} \cong \frac{2}{(k+1)^2} N(1 + N + \dots) \left(1 + \frac{2k-1}{k+1} N + \dots \right) dN$$

Retaining terms only up to the first order in N , and integrating, we finally obtain

$$(1 - M^2)^2 \cong (k+1)^2 \frac{T_0^* - T_0}{T_0}$$

where T_0^* is the stagnation temperature at Mach Number unity.

Tables of Influence Coefficients. For convenience in performing numerical calculations the influence coefficients (multiplied by M^2) are tabulated in Table B.6 for $k = 1.4$, with M as the independent argument. In order to explain the notation of these tables, we rewrite Eqs. 8.27 and 8.40 in the respective forms

$$\begin{aligned} dM^2 &= F_A \frac{dA}{A} + F_Q \frac{dQ - dW_x + dH}{c_p T} \\ &+ F_f \left(4f \frac{dx}{D} + \frac{dX}{\frac{1}{2} k p A M^2} - 2y \frac{dw}{w} \right) \\ &+ F_w \frac{dw}{w} + F_W \frac{dW}{W} - \frac{dk}{k} \end{aligned} \quad (8.47)$$

$$dM^2 = F_A \frac{dA}{A} + F_{T_0} \frac{dT_0}{T_0} + F_f \left(4f \frac{dx}{D} + \frac{dX}{\frac{1}{2} k p A M^2} - 2y \frac{dw}{w} \right) + F_w \frac{dw}{w} \quad (8.48)$$

where

$$F_A = -\frac{2M^2 \left(1 + \frac{k-1}{2} M^2\right)}{1 - M^2} \quad (8.49a)$$

$$F_Q = -F_W \equiv \frac{M^2(1 + kM^2)}{1 - M^2} \quad (8.49b)$$

$$F_f \equiv \frac{kM^4 \left(1 + \frac{k-1}{2} M^2\right)}{1 - M^2} \quad (8.49c)$$

$$F_{T_0} = \frac{F_w}{2} \equiv \frac{M^2(1 + kM^2) \left(1 + \frac{k-1}{2} M^2\right)}{1 - M^2} \quad (8.49d)$$

The influence coefficients F_A , F_Q , etc., are seen to be greater than those in Tables 8.1 and 8.2 by the factor M^2 .

Specific illustrations of both analytical and numerical procedures are given in the examples which follow.

8.7. Simple Types of Flow

A *simple type of flow* is defined here as one in which all but one of the independent differentials in Table 8.2 are zero. Thus Simple Area-Change refers to a process in which the area changes without frictional, stagnation-temperature, or gas-injection effects. Similarly, Simple T_0 -Change refers to a process in which the stagnation temperature changes (due to external heat exchange) without area change, friction, or gas injection. In each of the simple types of flow the specific heat and molecular weight are constant.

Three of the simple types of flow have, of course, been discussed in Chapters 4, 6, and 7.

The integration of Eq. 8.40 may be carried out analytically for each of the simple types of flow. For example, consider Simple Area-Change. Using the first influence coefficient in Table 8.2, we obtain

$$\int_{A^*}^A \frac{dA}{A} = - \int_1^{M^2} \frac{(1 - M^2) dM^2}{2M^2 \left(1 + \frac{k-1}{2} M^2\right)}$$

Integration yields

$$\frac{A}{A^*} = \frac{1}{M} \sqrt{\left[\frac{2 \left(1 + \frac{k-1}{2} M^2\right)}{k+1} \right]^{k+1}}$$

TABLE 8.3
FORMULAS FOR SIMPLE TYPES OF ONE-DIMENSIONAL FLOW WITH CONSTANT SPECIFIC HEAT AND MOLECULAR WEIGHT

		Friction only $\frac{dA}{dV} = 0$ $\frac{df}{dw} = 0$	Gas injection only $\frac{dy}{dV} = 0$ $\frac{dA}{dT_f} = 0$	Gas injection only $\frac{y}{M} = 0$ $\frac{dA}{dT_f} = 0$
$\frac{A}{A^*}$	$\frac{\sqrt{2 \left(1 + \frac{k-1}{2} M^2\right) \frac{k+1}{k-1}}}{M}$	1	1	1
$\frac{T_0}{T_0^*}$	$\frac{2(k+1)M^2 \left(1 + \frac{k-1}{2} M^2\right)}{(1 + kM^2)^2}$	1	1	1
$\frac{L_{max}}{D}$	0	$\frac{1 - M^2 + \frac{k+1}{2k} \log \frac{(k+1)M^2}{2 \left(1 + \frac{k-1}{2} M^2\right)}}{kM^2}$	0	0
$\frac{u}{u^*}$	1	1	$M \sqrt{2(k+1) \left(1 + \frac{k-1}{2} M^2\right)}$	$M \sqrt{2 \left(1 + \frac{k-1}{2} M^2\right) \frac{k+1}{k-1}}$
$\frac{V}{V^*}$	$M \sqrt{\frac{k+1}{2 \left(1 + \frac{k-1}{2} M^2\right)}}$	$M \sqrt{\frac{k+1}{2 \left(1 + \frac{k-1}{2} M^2\right)}}$	$M \sqrt{\frac{k+1}{2 \left(1 + \frac{k-1}{2} M^2\right)}}$	$M \sqrt{\frac{k+1}{2 \left(1 + \frac{k-1}{2} M^2\right)}}$
$\frac{T}{T^*}$	$\frac{\left(\frac{c}{c^*}\right)^2}{2 \left(1 + \frac{k-1}{2} M^2\right)}$	$\frac{(k+1)M^2}{2 \left(1 + \frac{k-1}{2} M^2\right)}$	$\frac{k+1}{2 \left(1 + \frac{k-1}{2} M^2\right)}$	$\frac{k+1}{2 \left(1 + \frac{k-1}{2} M^2\right)}$
$\frac{p}{p^*}$	$\frac{\left[\frac{2}{2 \left(1 + \frac{k-1}{2} M^2\right)}\right]^{\frac{1}{k-1}}}{\left[\frac{2}{2 \left(1 + \frac{k-1}{2} M^2\right)}\right]^{\frac{1}{k-1}}}$	$\frac{1 + kM^2}{(k+1)M^2}$	$\frac{1}{M} \sqrt{\frac{k+1}{2 \left(1 + \frac{k-1}{2} M^2\right)}}$	$\frac{1}{M} \sqrt{\frac{k+1}{2 \left(1 + \frac{k-1}{2} M^2\right)}}$
$\frac{p}{p^*}$	$\frac{\left[\frac{k+1}{2 \left(1 + \frac{k-1}{2} M^2\right)}\right]^{\frac{1}{k-1}}}{\left[\frac{k+1}{2 \left(1 + \frac{k-1}{2} M^2\right)}\right]^{\frac{1}{k-1}}}$	$\frac{k+1}{1 + kM^2}$	$\frac{1}{M} \sqrt{\frac{k+1}{2 \left(1 + \frac{k-1}{2} M^2\right)}}$	$\frac{1}{M} \sqrt{\frac{k+1}{2 \left(1 + \frac{k-1}{2} M^2\right)}}$
$\frac{T_0}{T_0^*}$	1	$\frac{k+1}{1 + kM^2} \left[\frac{2 \left(1 + \frac{k-1}{2} M^2\right)}{k+1} \right]^{\frac{1}{k-1}}$	$\frac{k+1}{1 + kM^2} \left[\frac{2 \left(1 + \frac{k-1}{2} M^2\right)}{k+1} \right]^{\frac{1}{k-1}}$	$\frac{k+1}{1 + kM^2} \left[\frac{2 \left(1 + \frac{k-1}{2} M^2\right)}{k+1} \right]^{\frac{1}{k-1}}$
$\frac{p}{p^*}$	$M \sqrt{2(k+1) \left(1 + \frac{k-1}{2} M^2\right)}$	1	$M \sqrt{2(k+1) \left(1 + \frac{k-1}{2} M^2\right)}$	$M \sqrt{2(k+1) \left(1 + \frac{k-1}{2} M^2\right)}$
$\frac{e-1}{cp}$	0	$\log M^2 \left(\frac{k+1}{1 + kM^2} \right)^{\frac{k-1}{k}}$	$\log M^2 \left[\frac{k+1}{2 \left(1 + \frac{k-1}{2} M^2\right) M} \right]^{\frac{k-1}{k}}$	$\log M^2 \left[\frac{k+1}{2 \left(1 + \frac{k-1}{2} M^2\right)} \left(\frac{k+1}{k+1} M^2 \right)^{\frac{k-1}{k}} \right]$

Note: Each quantity in the table represents the value of the variable in the left-hand column under the conditions specified in the top row.

The integration is carried out between the sections where $M = 1$, $A = A^*$, and $M = M$, $A = A$. The asterisk then indicates the critical value of A , or the value where the Mach Number is unity. Thus we obtain the well-known formula giving the ratio of local area to throat area as a function of the local Mach Number for an isentropic process.

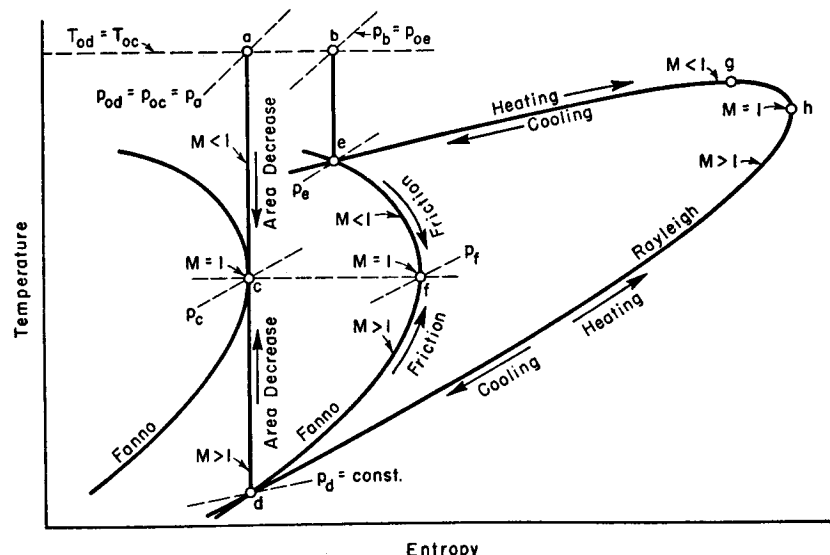


Fig. 8.2. Comparison of process curves on temperature-entropy diagram for Simple Area-Change, Simple Friction, and Simple T_0 -Change. With d as the starting point, the corresponding asterisk conditions ($M = 1$) are respectively at points c , f , and h .

Referring again to Simple Area-Change, we obtain, from the first column of Table 8.2,

$$\frac{dV/V}{dM^2/M^2} = \frac{(dV/V)/(dA/A)}{(dM^2/M^2)/(dA/A)} = \frac{1}{2\left(1 + \frac{k-1}{2}M^2\right)}$$

Upon integration between $M = 1$; $V = V^*$ and $M = M$, $V = V$, we get

$$\frac{V}{V^*} = M \sqrt{\frac{k+1}{2\left(1 + \frac{k-1}{2}M^2\right)}}$$

where V^* is the velocity where $M = 1$. This same equation might have been obtained with the help of the integral relations of Eqs. 8.41, 8.43, and 8.45.

By continuing in this manner we obtain p/p^* , T/T^* , etc., for Simple Area-Change. Similar formulas are obtainable by the same general method for the other types of simple flow. These formulas are summarized in Table 8.3. Note that the case of simple gas injection with $y = 1$ is essentially identical with the case of isentropic area change; that this must be so is evident when we remember that this type of gas injection is thermodynamically reversible, involves no change in stagnation temperature, and has as its principal effect an alteration in the mass flow per unit area.

Fig. 8.2 shows on a temperature-entropy diagram the several courses of states, beginning with state d , corresponding to Simple Area-Change, Simple T_0 -Change, and Simple Friction, respectively.

In interpreting the formulas of Table 8.3, it must be remembered that the conditions where $M = 1$ (asterisk conditions) are different for the several types of simple flow. For example, referring to Fig. 8.2, points c , f , and h represent, respectively, the asterisk conditions for Simple Area-Change, Simple Friction, and Simple T_0 -Change. The quantities marked with asterisks are best regarded as reference values which remain constant in any one type of simple flow.

Charts and tables representing the formulas for Simple Area-Change, Simple Friction, and Simple T_0 -Change have been presented in previous chapters. Fig. 8.3 shows curves for Simple Gas Injection with $y = 0$.

8.8 Example of Combined Friction and Area Change

As a simple instance where combined effects occur and an analytical solution is possible, let us examine the problem of designing a long insulated duct for constant Mach Number along its length. Changes in specific heat will be ignored.

From the first line of influence coefficients in Table 8.2, with dM , dT_0 , dX , and dw set equal to zero, we get

$$\frac{dA}{A} = \frac{kM^2}{2} 4f \frac{dx}{D} \quad (8.50)$$

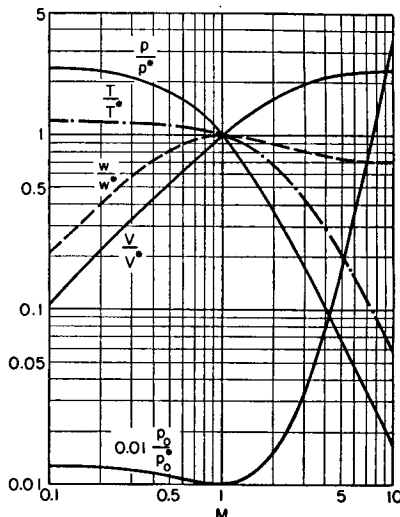


Fig. 8.3. Working chart for Simple Gas Injection with $y = 0$ and $k = 1.4$

Now, from the geometry of a duct of circular cross section

$$\frac{dA}{A} = 2 \frac{dD}{D}$$

so that

$$\tan \sigma = \frac{dD/2}{dx} = \frac{kM^2}{2} f \quad (8.51)$$

where σ is the half-angle of divergence of the duct. For a constant friction coefficient, therefore, σ must be constant, hence the duct must be conical. As a specific example, let us take $f = 0.0025$, $k = 1.4$, and $M = 2$; then $\sigma = 0.4$ degree. Note that the duct must diverge for both subsonic and supersonic flow. For typical values of f , the degree of divergence in subsonic flow is very small.

From the second line of influence coefficients in Table 8.2 and Eq. 8.50 we get

$$(1 - M^2) \frac{dV}{V} = - \frac{dA}{A} + \frac{kM^2}{2} 4f \frac{dx}{D} = 0$$

Thus the velocity is constant. Similarly, the temperature and impulse function are found to be constant.

For calculating the pressure change we find from Table 8.2 and Equation 8.50 that

$$\frac{dp}{p} = - \frac{dA}{A}, \quad \text{whence} \quad p_1 A_1 = p_2 A_2$$

In like manner, we obtain

$$\frac{dp_0}{p_0} = - \frac{kM^2}{2} 4f \frac{dx}{D} = - \frac{kM^2 f}{\tan \sigma} \frac{dD}{D} = - 2 \frac{dD}{D}$$

or

$$\frac{p_{02}}{p_{01}} = \frac{A_1}{A_2}$$

and, since the area must always increase, the stagnation pressure is always diminished.

The foregoing results for V , T , F , p , and p_0 might also have been found from Eqs. 8.41 to 8.46.

8.9. Examples of Combined Friction and Heat Transfer

An important example of flow with combined effects is that of heating of a gas flowing through a tube. The mechanisms of friction and heat transfer are so similar that one cannot be had without the other. Hence, to calculate the pressure drop and other properties of interest with

reference to heat exchangers, it is necessary to take account of friction as well as of heat transfer. We shall assume the area, specific heat, and molecular weight all to be constant.

General Analysis. Considering an infinitesimal length of duct dx , the rate of heat transfer may be expressed by means of the energy equation in terms of the increase in stagnation enthalpy; or, by means of the coefficient of heat transfer \mathcal{C} , in terms of $T_w - T_{aw}$. Thus,

$$w dQ = \frac{\pi}{4} D^2 \rho V c_p dT_0 = \mathcal{C} \pi D dx (T_w - T_{aw})$$

When the flow is subsonic, the adiabatic wall temperature T_{aw} does not differ very much from the stagnation temperature T_0 . Moreover, the error in substituting T_0 for T_{aw} will be small in any event if T_w is considerably in excess of T_{aw} . We shall assume that this substitution (which simplifies the subsequent calculations) is permissible; this is equivalent to assuming that the recovery factor \mathcal{R} is unity. Then the foregoing equation yields

$$\frac{dT_0}{T_w - T_0} = \frac{4\mathcal{C}}{\rho V c_p} \frac{dx}{D}$$

REYNOLDS ANALOGY. A further considerable simplification results when the Reynolds Analogy between friction and heat transfer is assumed to be valid. Experiments show that the analogy, which relates the heat-transfer and friction coefficients according to

$$\frac{\mathcal{C}}{\rho V c_p} = \frac{f}{2}$$

has an accuracy of a few per cent for fully developed turbulent gas flows. Substituting this formula into the preceding equation, we get

$$\frac{dT_0}{T_w - T_0} = 2f \frac{dx}{D} \quad (8.52)$$

With the help of Eq. 8.52, we may now write Eq. 8.48 as

$$dM^2 = F_{T_0} \frac{dT_0}{T_0} + F_f 4f \frac{dx}{D} = \left(F_{T_0} + \frac{2T_0}{T_w - T_0} F_f \right) \frac{dT_0}{T_0} \quad (8.53)$$

The procedure beyond this point depends on the nature of the heat-transfer process. To illustrate, we shall consider three specific problems: (i) constant wall temperature, (ii) constant heat flux, and (iii) nuclear reactors.

Case of Constant Wall Temperature. The wall temperature is approximately constant when the tube metal is a good conductor and is

surrounded by a constant-pressure bath of condensing vapor or boiling liquid (e.g., condensing steam). Since T_w is independent of x , Eq. 8.52 is easily integrated. Considering any pair of sections 1 and 2, integration yields

$$\frac{1}{2} \left[\frac{4f(x_2 - x_1)}{D} \right] = \ln \frac{T_w - T_{01}}{T_w - T_{02}} = \ln \frac{\frac{T_w}{T_{01}} - 1}{\frac{T_w}{T_{02}} - \frac{T_{02}}{T_{01}}} \quad (8.54)$$

Hence, for any initial value of T_{01} , and for known values of f , D , and T_w , Eq. 8.54 yields T_{02} as a function of x_2 .

NUMERICAL INTEGRATION FOR MACH NUMBER VARIATION. To compute the variation of M with distance, we must integrate Eq. 8.53. In the present example it is, unfortunately, not possible to separate variables and integrate in closed analytic form. Hence it is necessary to integrate either numerically or graphically. We shall first illustrate numerical integration.

Suppose that $f = 0.005$, $M_1 = 0.5$, and $T_w/T_{01} = 4$. Let us specify section 2 as that section downstream of section 1 where $T_{02}/T_{01} = 1.05$. The location of section 2 is found by direct substitution into Eq. 8.54, thus yielding

$$\frac{x_2 - x_1}{D} = \frac{1}{0.01} \ln \frac{4 - 1}{4 - 1.05} = 1.68$$

In other words, section 2 is 1.68 duct diameters downstream of section 1.

Eq. 8.53 is now integrated approximately in finite-difference form over the short interval between sections 1 and 2, the approximation being that the coefficient of dT_0 is constant (at its mean value) during the interval. Let \bar{F}_{T_0} and \bar{F}_f denote the values of the influence coefficients when evaluated at $\bar{M} = (M_1 + M_2)/2$. Furthermore, let us set $\bar{T}_0 = (T_{01} + T_{02})/2$ for the interval. Then the approximate integration yields

$$M_2^2 - M_1^2 = 2 \left(\frac{T_{02}}{T_{01}} - 1 \right) \left[\frac{\bar{F}_{T_0}}{\left(\frac{T_{02}}{T_{01}} + 1 \right)} + \frac{2\bar{F}_f}{2\left(\frac{T_w}{T_{01}} - \left(\frac{T_{02}}{T_{01}} - 1 \right) \right)} \right] \quad (8.55)$$

Equation 8.55 must be solved by iteration, inasmuch as \bar{F}_{T_0} and \bar{F}_f are functions of M_2 , which is not known. We proceed as follows:

Trial I: We guess that $M_2 = 0.60$. From Table B.6, at $\bar{M} = 0.55$, we find that $\bar{F}_{T_0} = 0.655$ and $\bar{F}_f = 0.195$. Substituting into Eq. 8.55, we get $M_2 \approx 0.54$.

Trial II: We guess that $M_2 = 0.535$. Then, at $\bar{M} = 0.518$, we find that $\bar{F}_{T_0} = 0.5317$ and $\bar{F}_f = 0.1453$. From Eq. 8.55, then, $M_2 = 0.530$.

Trial III: After plotting for Trials I and II the computed values of M_2 against the guessed values, we try $M_2 = 0.5293$ and find that this value makes the solution converge with adequate accuracy.

The corresponding values of all other properties at section 2 may be found either through numerical integration of the corresponding differential equations (as given in Table 8.2) or, more conveniently, through the integral relations of Eqs. 8.41 to 8.46. The latter method is used here.

From Eq. 8.45,

$$\frac{T_2}{T_1} = \frac{T_{02}}{T_{01}} \frac{1 + \frac{k-1}{2} M_1^2}{1 + \frac{k-1}{2} M_2^2} = 1.0440$$

From Eqs. 8.42 and 8.45, furthermore,

$$\frac{p_2}{p_1} = \frac{M_1}{M_2} \sqrt{\frac{T_2}{T_1}} = 0.9652$$

Eqs. 8.43, 8.44, and 8.46 yield

$$\frac{V_2}{V_1} = \frac{M_2}{M_1} \sqrt{\frac{T_2}{T_1}} = 1.0816$$

$$\frac{\rho_2}{\rho_1} = \frac{p_2}{p_1} \frac{T_1}{T_2} = 0.9245$$

$$\frac{p_{02}}{p_{01}} = \frac{p_2}{p_1} \left[\frac{1 + \frac{k-1}{2} M_2^2}{1 + \frac{k-1}{2} M_1^2} \right]^{\frac{k}{k-1}} = 0.9847$$

Some of the numerical computations made immediately above may be facilitated by noticing that several of the awkward functions of Mach Number which occur are tabulated in one or another of the tables of Appendix B. For example,

$$\left[1 + \frac{k-1}{2} M^2 \right]^{\frac{k}{k-1}} = \left(\frac{p_0}{p} \right)_{\text{isen}}$$

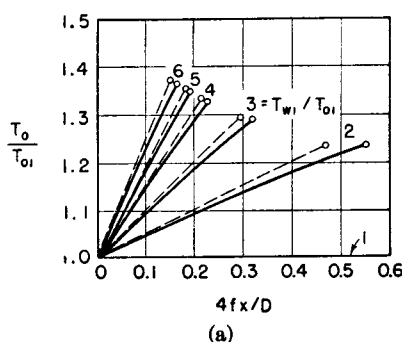
where $(p/p_0)_{\text{isen}}$, the pressure ratio for isentropic flow, is tabulated versus M in Table B.2. The last equation of the present example might therefore be written

$$\frac{p_{02}}{p_{01}} = \frac{p_2}{p_1} \left[\frac{(p/p_0)_{\text{isen}}}{M_1} \right]_{M_2}$$

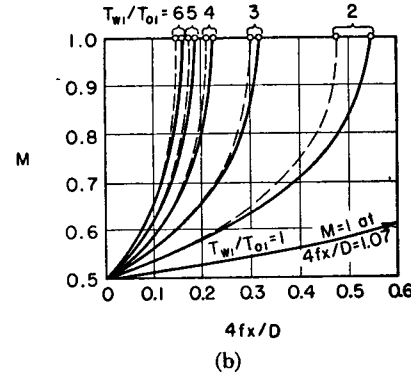
thus eliminating considerable arithmetical computations.

To illustrate still further the possibility of exploiting the tables of functions in Appendix B, it is found by combining the foregoing expressions for p_{02}/p_{01} , p_2/p_1 , and T_2/T_1 that

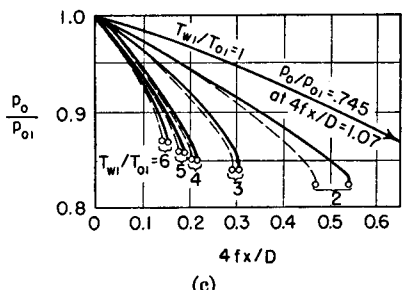
$$\frac{p_{02}}{p_{01}} = \sqrt{\frac{T_{02}}{T_{01}} \frac{M_1}{M_2}} \left[\frac{1 + \frac{k-1}{2} M_2^2}{1 + \frac{k-1}{2} M_1^2} \right]^{\frac{k+1}{2(k-1)}}$$



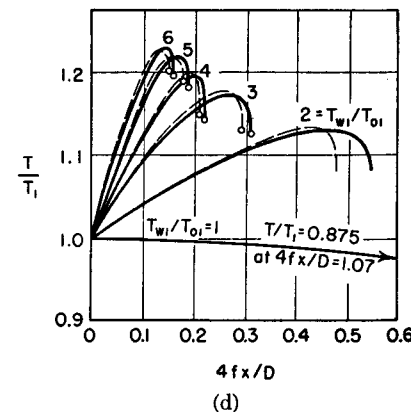
(a)



(b)



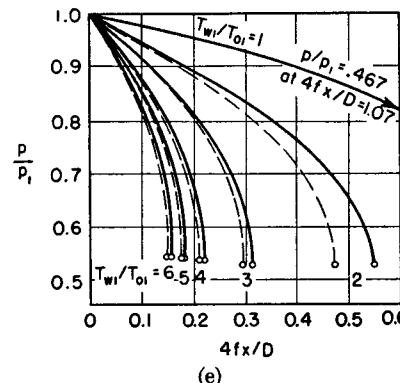
(c)



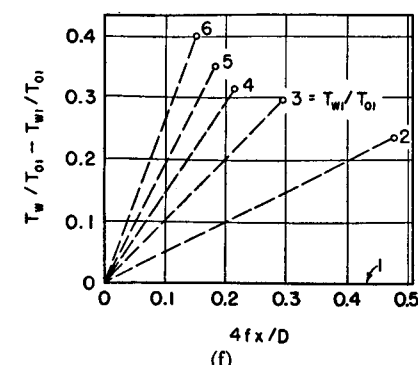
(d)

FIG. 8.4. Illustrative results of calculations for combined friction and heat transfer in a constant-area tube, with $k = 1.4$, $R = 1$, and $M_1 = 0.5$. Solid curves are for constant wall temperature and dashed curves are for constant heat flux per unit area. The circled points of each curve indicate choking ($M = 1$).

- (a) Stagnation temperature versus distance.
- (b) Mach Number versus distance.
- (c) Stagnation pressure versus distance.
- (d) Temperature versus distance. Note that just prior to choking the temperature decreases as heat is added.



(e)



(f)

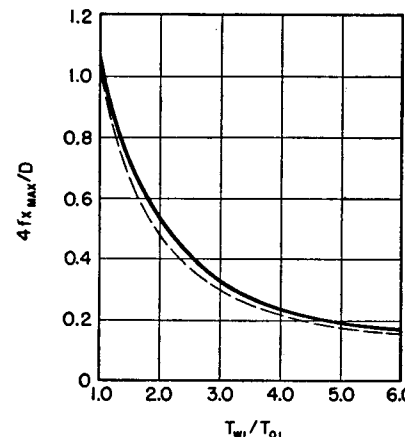


FIG. 8.4.—Continued

(e) Static pressure versus distance.

(f) Wall temperature versus distance.

(g) Duct length for choking versus initial wall temperature.

We now examine Table 8.3 to see whether any similar functions of M and k appear and discover that

$$\frac{p_{02}}{p_{01}} = \sqrt{\frac{T_{02}}{T_{01}} \frac{[(A/A^*)_{\text{isen}}]_{M_2}}{[(A/A^*)_{\text{isen}}]_{M_1}}}$$

which again allows us to use the tabulated numerical values in Table B.2.

Returning now to our illustrative problem, the changes which occur between section 2 and a section 3 further downstream are determined in the same manner as the changes between sections 1 and 2. This procedure is continued until the exit of the duct is reached, unless Mach Number unity is reached first. The latter result indicates choking, and

then either the entrance Mach Number or the length of duct must be reduced in order to obtain a steady-state solution.

The accuracy of the numerical integration naturally depends on the size of interval chosen for each step and is improved by the selection of small steps.

Fig. 8.4 shows the results of numerical calculations for the example considered here. Also shown in this figure are corresponding results for the case of constant heat flux per unit length of tube. It is seen that many of the fluid properties change very rapidly as choking is approached. Fig. 8.4g shows that high rates of heat transfer make the choking problem very serious. For example, with $T_{w1}/T_{01} \leq 5$ and $f \leq 0.005$, only about 10 diameters of duct length are allowable when $M_1 = 0.5$. Apart from the large stagnation-pressure losses associated with high Mach Numbers, therefore, considerations of choking often prohibit the use of high values of M in heat exchangers.

GRAPHICAL INTEGRATION BY THE METHOD OF ISOCLINES. To illustrate this rapid method for obtaining solutions with the accuracy typical of graphical constructions, we combine Eq. 8.53 with Eq. 8.52 and thus obtain a differential equation of the form (assuming f is constant)

$$\frac{dM^2}{d(4fx/D)} = \frac{T_w - T_0}{T_0} \frac{F_{T_0}}{2} + F_f \quad (8.56)$$

Now consider a chart with M^2 as ordinate and $4fx/D$ as abscissa (Fig. 8.5). Eq. 8.56 gives the slope on this chart of an integral curve satisfying the differential equation. Considering the same illustrative problem as before, we are given a constant value of T_w , and T_{01} is known.

The value of T_0 corresponding to any value of $4fx/D$ may, therefore, be computed immediately from Eq. 8.54. Hence T_w and T_0 are known at each value of $4fx/D$. If, for a given value of $4fx/D$, we choose various values of M^2 at convenient intervals, the corresponding slopes may be found from Eq. 8.56. These slopes are plotted in the chart as short streaks. By repeating this procedure for a great many values of $4fx/D$, the entire chart may be filled with such streaks indicative of the local slopes.

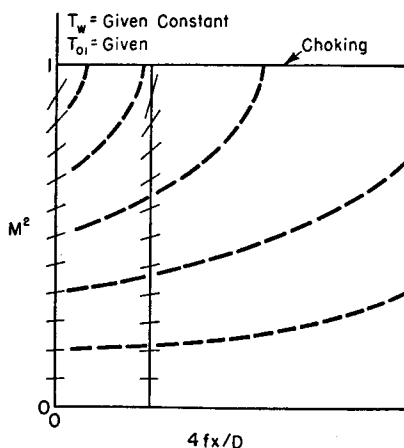


FIG. 8.5. Illustrates graphical integration by method of isoclines.

The integration is carried out by starting with one of the streaks at $4fx/D = 0$ (corresponding to a certain M_1^2) and drawing with a French curve a line which everywhere has the appropriate tangent. Such an integral curve represents a solution for the chosen value of M_1^2 , inasmuch as it satisfies the differential equation at each point and also satisfies the initial condition.

It is evident that this method is especially adaptable to finding families of solutions, for, once the slopes have been drawn in Fig. 8.5, it is easy to draw solution curves for many initial values of M^2 .

APPROXIMATE METHOD FOR LOW MACH NUMBERS. When the Mach Numbers are low, which is the situation most often met with in practice, an approximate method of calculation may be devised which has the advantage of being in closed form and which, therefore, does not require the tedious integrations described above.

Our interest lies primarily in the stagnation-pressure loss and the increase in stagnation temperature occasioned by given values of T_w , p_{01} , T_{01} , T_w , D , and L . The changes in stagnation temperature are easily calculable from Eq. 8.54 and need no further consideration.

For the variation in stagnation pressure we find from Table 8.2, for the case under consideration, that

$$\frac{dp_0}{p_0} = -\frac{kM^2}{2} \left(\frac{dT_0}{T_0} + 4f \frac{dx}{D} \right)$$

Eliminating dT_0 with the aid of Eq. 8.52, we get, in dimensionless form,

$$\frac{dp_0}{p_0} = \frac{d(p_0/p_{01})}{p_0/p_{01}} = -\frac{kM^2}{2} \left(4f \frac{L}{D} \right) \left[\frac{1}{2} \frac{T_w - T_0}{T_0} + 1 \right] d\left(\frac{x}{L}\right) \quad (8.57)$$

By eliminating p_2/p_1 from Eqs. 8.42 and 8.46, and setting $w_2/w_1 = 1$ and $A_2/A_1 = 1$, we obtain

$$M^2 = \left(\frac{p_{01}}{p_0} \right)^2 \frac{T_0}{T_{01}} \left(\frac{1 + \frac{k-1}{2} M^2}{1 + \frac{k-1}{2} M_1^2} \right)^{\frac{k+1}{k-1}} M_1^2 \quad (8.58)$$

Substitution of this relation for M^2 into Eq. 8.57 then yields the differential equation

$$-\left(\frac{p_0}{p_{01}} \right) d\left(\frac{p_0}{p_{01}} \right) = \frac{k}{2} M_1^2 \left(\frac{1 + \frac{k-1}{2} M^2}{1 + \frac{k-1}{2} M_1^2} \right)^{\frac{k+1}{k-1}} \left(4f \frac{L}{D} \right) \frac{T_0}{T_{01}} \left[\frac{1}{2} \frac{T_w - T_0}{T_0} + 1 \right] d\left(\frac{x}{L} \right)$$

The left-hand side is immediately integrable, but the right-hand side is not because of the term in M^2 . However, we find by a binomial expansion that

$$\left(1 + \frac{k-1}{2} M^2\right)^{\frac{k+1}{k-1}} \cong 1 + \frac{k+1}{2} M^2 + \dots$$

This suggests that, if M is always fairly small, this function of M is nearly constant. For example, if M never exceeds 0.3, then this function of M cannot be less than 1.0 or more than 1.113. Hence, if the function is assumed to have a constant mean value during the integration, the consequent error in Δp_0 can at most be a few per cent.

We therefore integrate as indicated above between the following limits: (i) $p_0/p_{01} = 1$ when $x/L = 0$, and (ii) $p_0/p_{01} = p_{02}/p_{01}$ when $x/L = 1$, the subscript 2 now denoting the exit of the duct. Thus we obtain

$$1 - \left(\frac{p_{02}}{p_{01}}\right)^2 = (kM_1^2) \cdot \mathfrak{G} \cdot \mathfrak{D} \cdot \left(4f \frac{L}{D}\right) \quad (8.59a)$$

where

$$\mathfrak{G} = \left[\frac{1 + \frac{k-1}{2} M^2}{1 + \frac{k-1}{2} M_1^2} \right]^{\frac{k+1}{k-1}}_{\text{mean}} \quad (8.59b)$$

$$\text{and } \mathfrak{D} = \int_0^1 \frac{T_w}{T_{01}} \left[\frac{1}{2} \frac{T_w - T_0}{T_0} + 1 \right] d\left(\frac{x}{L}\right) \quad (8.59c)$$

The quantity \mathfrak{G} depends on M_1 and M_2 , and may be set equal to unity as a first approximation. The definite integral \mathfrak{D} depends on the variation of T_w and of T_0 with x ; this integral, accordingly, depends in part on the method of heating.

As shown previously, and in accord with Eq. 8.58,

$$\frac{[(A/A^*)_{\text{isen}}]_{M_2}}{[(A/A^*)_{\text{isen}}]_{M_1}} = \frac{p_{02}}{p_{01}} \sqrt{\frac{T_{01}}{T_{02}}} \quad (8.60)$$

In order to evaluate \mathfrak{G} we take the mean of the two values of the quantity on the right-hand side of Eq. 8.59b; one of these values is found by setting $M = M_1$, and the second is found by setting $M = M_2$. When we set $M = M_1$, the right-hand side of Eq. 8.59b is unity; when we set

$M = M_2$, we find with the help of Eq. 8.58 that

$$\left(\frac{1 + \frac{k-1}{2} M_2^2}{1 + \frac{k-1}{2} M_1^2} \right)^{\frac{k+1}{k-1}} = \left(\frac{p_{02}}{p_{01}} \right)^2 \frac{T_{01}}{T_{02}} \frac{M_2^2}{M_1^2}$$

Hence it follows that

$$\mathfrak{G} = \frac{1}{2} + \frac{1}{2} \left(\frac{p_{02}}{p_{01}} \right)^2 \left(\frac{T_{01}}{T_{02}} \right) \frac{M_2^2}{M_1^2} \quad (8.61)$$

Assuming that T_w , T_{01} , L , D , and p_{01} are known to begin with, and that we wish to calculate p_{02} and M_2 corresponding to a certain inlet Mach Number M_1 , we proceed as follows: The value of \mathfrak{G} is found from Eq. 8.62, which is derived below. A first approximation for p_{02} is found from Eq. 8.59a by setting $\mathfrak{G} = 1$ (or perhaps a slightly higher value, depending on one's experience with prior calculations). The corresponding value of M_2 may then be found from Eq. 8.60, inasmuch as T_{02} is easily calculated from Eq. 8.54.

If it is desired to improve on this approximation (often it is not necessary), we employ the first approximations to p_{02} and M_2 for calculating a more accurate estimate of \mathfrak{G} from Eq. 8.61. The calculation procedure is then repeated with this new value of \mathfrak{G} . The recalculation of \mathfrak{G} and repetition of the calculation procedure are continued until convergence is obtained; in practice convergence is usually adequate on the second approximation.

In order to evaluate \mathfrak{D} , we first write Eq. 8.54 as

$$2fx/D = \ln \frac{T_w - T_{01}}{T_w - T_0}$$

which we may solve for T_0 in the form

$$T_0 = T_w - (T_w - T_{01}) e^{2f \frac{L}{D} \left(\frac{x}{L}\right)}$$

Substituting this into Eq. 8.59c, \mathfrak{D} may be worked out in terms of elementary integrals. The final result is

$$\mathfrak{D} = \frac{T_w}{T_{01}} + \frac{1}{4fL/D} \left(\frac{T_w}{T_{01}} - 1 \right) \left(e^{-\frac{1}{4f} \frac{L}{D}} - 1 \right) \quad (8.62)$$

Case of Constant Heat Flux. We now take up briefly the case where the heat flux per unit area is the same for all values of x . Such a situation results, for example, when the tube is heated electrically by passing current either through the wall of the tube itself or through resistance wires wrapped uniformly around the tube.

Assuming that \mathfrak{C} is constant, it follows from the first equation of this article that $T_w - T_0$ is independent of x . Hence we write

$$T_w - T_0 = T_{w1} - T_{01} \quad (8.63)$$

Substituting this into Eq. 8.52, we have

$$\frac{dT_0}{T_{w1} - T_{01}} = 2f \frac{dx}{D} \quad (8.64a)$$

and integration then yields

$$\frac{T_{02} - T_{01}}{T_{w1} - T_{01}} = 2f \frac{x_2 - x_1}{D} \quad (8.64b)$$

which allows us to compute T_0 at any value of x .

The variation of M with x may, as in the case of constant T_w , be found either by (i) an iterative integration using finite-difference methods, or (ii) a graphical integration using the method of isoclines. For the former, the finite-difference equation is written as

$$M_2^2 - M_1^2 = \left(\frac{T_{02}}{T_{01}} - 1 \right) \left[\frac{2\bar{F}_{T_0}}{(T_{02}/T_{01}) + 1} + \frac{\bar{F}_f}{(T_{w1}/T_{01}) - 1} \right] \quad (8.65)$$

The corresponding values of p , T , etc., are found from the integral relations, Eqs. 8.41 to 8.46.

The approximate analytical method for low Mach Numbers, as embodied in Eqs. 8.59 to 8.61, is also applicable here. It should be noted, however, that \mathfrak{D} is no longer given by Eq. 8.62 but rather has to be recalculated for the specific temperature distributions of the present example.

Case of Heat Transfer in a Nuclear Reactor. One possible arrangement of a gas-cooled nuclear reactor is to have the gas flow through tubes in parallel, with the radioactive material incorporated in the tube walls. Apart from the problems of choking and of maintaining reasonable pressure drops, it is desirable to have large rates of heat flux and yet not exceed wall temperatures injurious to the material. Hence we are interested in $T_{w_{\max}}$, the maximum wall temperature.

One interesting feature of a nuclear reactor is that, as a result of neutron leakage, the heat flux is usually a maximum at the center of the reactor and tends to become small at the outer periphery. We shall not concern ourselves with the actual heat-flux distribution, but shall, rather, use for illustrative purposes a simple distribution which embodies the heat-flux characteristics described above.

A simple heat-flux distribution which lends itself to calculation is parabolic, with a maximum value at the center of the tube and a zero

value at the ends. Assuming that the tube has a length L , and employing the dimensionless length variable $\xi \equiv x/L$, the equation representing such a parabolic distribution of heat input is

$$\frac{dQ}{d\xi} = 4 \left(\frac{dQ}{d\xi} \right)_{\max} (\xi - \xi^2) = \frac{c_p dT_0}{d\xi} \quad (8.66)$$

where the term $c_p dT_0$ is found from the energy equation.

Separating variables and integrating, we find

$$\int_{T_{01}}^{T_0} dT_0 = \frac{4}{c_p} \left(\frac{dQ}{d\xi} \right)_{\max} \int_0^\xi (\xi - \xi^2) d\xi \quad (8.67a)$$

$$T_{02} - T_{01} = \frac{4}{c_p} \left(\frac{dQ}{d\xi} \right)_{\max} \left(\frac{1}{6} \right) \quad (8.67b)$$

where T_{02} is the stagnation temperature at the tube exit, corresponding to $\xi = 1$. Hence

$$\frac{T_0 - T_{01}}{T_{02} - T_{01}} = 3\xi^2 - 2\xi^3 \quad (8.67c)$$

Furthermore, from Eqs. 8.66 and 8.67b,

$$\frac{dT_0}{T_{02} - T_{01}} = 6(\xi - \xi^2) d\xi \quad (8.67d)$$

Eq. 8.52 yields, moreover,

$$\frac{dT_0}{T_w - T_0} = \frac{1}{2} 4f \frac{L}{D} d\left(\frac{x}{L}\right) = 4f \frac{L}{D} \frac{d\xi}{2} \quad (8.68)$$

We now form a dimensionless expression for the wall temperature by means of the identity

$$\frac{T_w - T_{01}}{T_{02} - T_{01}} \equiv \frac{T_w - T_0}{dT_0} \cdot \frac{dT_0}{T_{02} - T_{01}} + \frac{T_0 - T_{01}}{T_{02} - T_{01}}$$

The three ratios on the right-hand side are now expressed in terms of ξ by means of Eqs. 8.67c, 8.67d, and 8.68, and thus yielding

$$\frac{T_w - T_{01}}{T_{02} - T_{01}} = \frac{6}{4fL/D} (\xi - \xi^2) + 6\xi \left(\frac{\xi}{2} - \frac{\xi^2}{3} \right) \quad (8.69)$$

In order to find $T_{w_{\max}}$, we set

$$\frac{\partial}{\partial \xi} \left(\frac{T_w - T_{01}}{T_{02} - T_{01}} \right) = 0$$

Carrying out the indicated differentiation and setting the derivative

equal to zero, we find the following value of ξ_o for which the wall temperature is a maximum:

$$\xi_o = \frac{1}{2} - \frac{1}{4fL/D} + \sqrt{\frac{1}{4} + \left(\frac{1}{4fL/D}\right)^2} \quad (8.70)$$

The maximum wall temperature corresponding to selected values of T_{01} , T_{02} , and $4fL/D$ is then easily found by substitution in Eq. 8.69. It is of interest to note that $T_{w_{\max}}$ depends only on the three variables mentioned and is independent of M_1 , of pressure level, of pressure drop, of the gas constant, etc. Indeed, the ratio T_w/T_{01} depends only on T_{02}/T_{01} and on $4fL/D$.

The temperature characteristics of a gas-cooled reactor tube with parabolic heat-flux distribution are indicated in dimensionless form in Fig. 8.6.

The calculation of the Mach Number distribution and of the distribution of fluid properties is carried out in substantially the same way as for the case of constant T_w , and the remarks made in the latter case are applicable here.

Eqs. 8.59 to 8.61, comprising a rapid, approximate method for determining the loss in stagnation pressure, are also valid for the present case. However, the definite integral \mathfrak{D} of Eq. 8.59c must be recalculated, as Eq. 8.62 is no longer applicable.

8.10. Special Conditions at the Sonic Point

The discussion on pp. 234-36 is here amplified and generalized to indicate clearly the special circumstances of choking and of the continuous transition through Mach Number unity.

Form of Differential Equation. To illustrate the thinking, let us consider the case of constant specific heat and molecular weight. Then Eq. 8.40 may be written as

$$\frac{dM^2}{dx} = \frac{G(x)}{1 - M^2} \quad (8.71a)$$

$$G(x) \equiv M^2 \left(1 + \frac{k-1}{2} M^2\right) \left[-2 \frac{d(\ln A)}{dx} + (1 + kM^2) \frac{d(\ln T_0)}{dx} + kM^2 \frac{4f}{D} + \dots \right] \quad (8.71b)$$

where $d(\ln A)/dx$, $d(\ln T_0)/dx$, and $4f/D$ are assumed to be functions of x , and where dx is of course always positive.

From Eq. 8.71a it is clear that whether the local Mach Number increases or decreases depends on whether the local Mach Number is

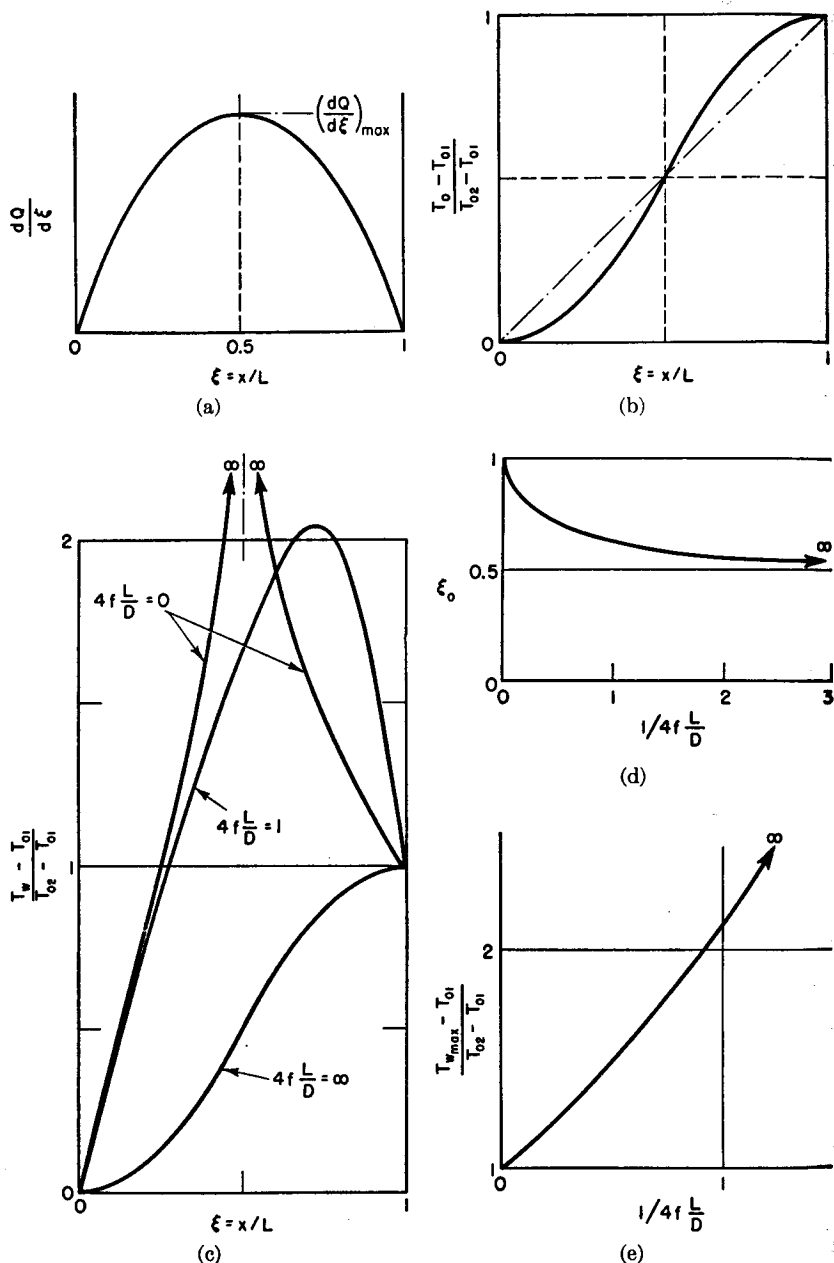


FIG. 8.6. Some general performance features of gas-cooled nuclear reactor tube with parabolic heat-flux distribution.

- Heat-flux distribution.
- Stagnation-temperature distribution.
- Wall-temperature distribution.
- Location of maximum wall temperature.
- Maximum wall temperature.

greater or less than unity and also on whether G is positive or negative, according to the following table:

VALUE OF dM^2/dx

	$M < 1$	$M = 1$	$M > 1$
$G < 0$	—	∞	+
$G = 0$	0	indeterminate	0
$G > 0$	+	∞	—

Therefore the curve of M versus x may have many different forms, depending on whether the initial Mach Number (M_1) is less than or greater than unity, and also depending on whether G is always positive, always negative, or changes sign. We shall now explore the various possibilities.

CASE I: G IS ALWAYS NEGATIVE. (Fig. 8.7a.) If the flow is initially subsonic, the Mach Number continually decreases. If it is initially supersonic, on the other hand, the Mach Number continually increases.

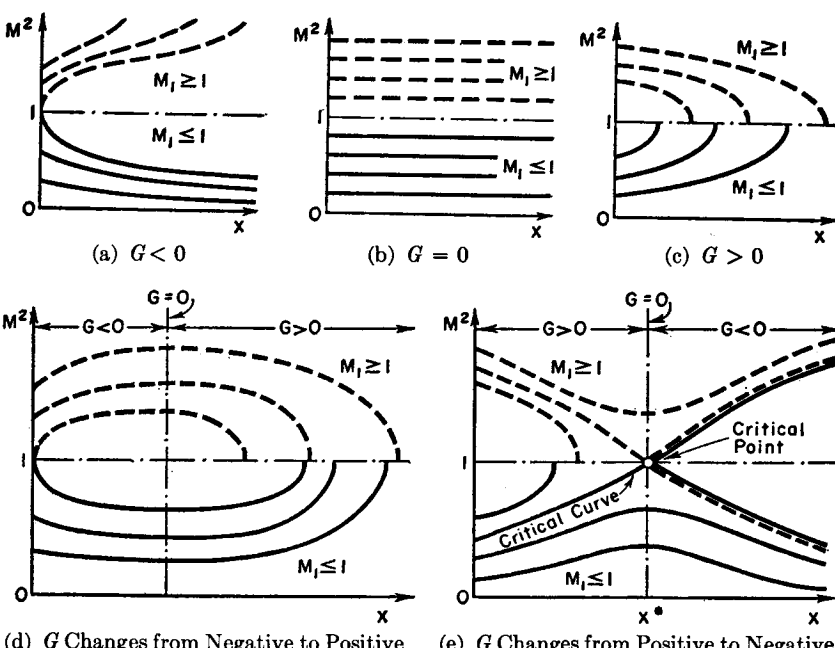


FIG. 8.7. Illustrates possible variations of Mach Number versus distance.

In brief, the Mach Number always proceeds away from unity. There are no limits on the flow.

Examples: (i) Isentropic flow in a diverging passage; (ii) Flow with cooling only; (iii) Adiabatic flow with friction in a diverging passage, with $d(\ln A)/dx > 2kM^2f/D$.

CASE II: G IS ALWAYS ZERO. (Fig. 8.7b.) The Mach Number always remains constant, irrespective of whether the flow is subsonic or supersonic. There are no limits on the flow.

Example: Adiabatic flow with friction in a diverging passage, with $d(\ln A)/dx = 2kM^2f/D$.

CASE III: G IS ALWAYS POSITIVE. (Fig. 8.7c.) If the flow is initially subsonic, the Mach Number tends continually to increase. If it is initially supersonic, on the other hand, the Mach Number tends continually to decrease. In brief, the Mach Number always proceeds toward unity. Consequently, the flow reaches a limiting condition when $M = 1$, for it may then proceed no further. This phenomenon, called *choking*, is discussed more fully below.

Examples:

- (i) Isentropic flow in a converging passage
- (ii) Flow with heating only
- (iii) Adiabatic flow with friction in a straight or in a converging passage
- (iv) Adiabatic flow with friction in a diverging passage with $d(\ln A)/dx < 2kM^2f/D$

Choking. When G is always positive, it is impossible for the flow to pass continuously through $M = 1$. To prove this, assume that the flow is initially subsonic, and that Mach Number unity is reached at some point where $x = x_0$. Suppose that the flow subsequently became supersonic. Then, at a value of $x = x_0 + \delta x$, where δx is positive, dM^2/dx would, according to Eq. 8.71a, be negative. This, however, contradicts the supposition, for if M^2 at $x_0 + \delta x$ is greater than unity, dM^2/dx must be positive in the interval between x_0 and $x_0 + \delta x$. Hence it is impossible for the flow to become supersonic if it is initially subsonic. A similar argument may be used to demonstrate that the flow cannot pass continuously from supersonic to subsonic speeds.

At the choking point, dM^2/dx is infinite, and in fact most of the fluid properties change at an infinite rate.

If choking occurs, and there is an increase in x while G remains positive, it will not be possible for a steady-state flow to exist. After a transient period of readjustment, a new steady-state condition will be established for which choking does not occur (this usually involves a reduction in the initial Mach Number, the appearance of shock waves, or both).

CASE IV: G CHANGES FROM NEGATIVE TO POSITIVE. (Fig. 8.7d.) If the flow is initially subsonic, the Mach Number first decreases, passes through a minimum where $G = 0$, and then increases until finally choking occurs. If the flow is initially supersonic, however, the Mach Num-

ber first increases, passes through a maximum where $G = 0$, and then decreases until choking occurs.

Example: Isentropic flow through a diverging-converging passage.

CASE V: G CHANGES FROM POSITIVE TO NEGATIVE. (Fig. 8.7e.) There are several interesting possibilities for either initially subsonic or initially supersonic flow. We shall consider in detail only flows which are initially subsonic, but we note that similar circumstances prevail for initially supersonic flows.

(i) If M_1 in the initially subsonic flow is quite low, the Mach Number at first increases, passes through a maximum where $G = 0$, and then continually decreases.

(ii) If M_1 is sufficiently high, the flow chokes before $G = 0$, and the solution may not be continued.

(iii) If, for a given variation of G with x , a particular value of M_1 is chosen, the flow will reach Mach Number unity at the exact point where G also passes through zero. Under these conditions, as described in detail below, the flow may pass continuously into the supersonic range or may pass continuously back into the subsonic zone.

Continuous Passage Through Sonic Point. Examining the right-hand side of Eq. 8.71a, we see (i) that in general there is a maximum or minimum in the curve of M versus x at the point where $G = 0$; (ii) that in general choking occurs when $M = 1$; (iii) that dM^2/dx is of the indeterminate form $0/0$ when G passes through zero simultaneously with M becoming unity. The latter singular condition is the one we shall now examine, for it permits a continuous passage from subsonic to supersonic speeds (or vice versa).

RELATION BETWEEN INDEPENDENT VARIABLES AT CRITICAL POINT. Using an asterisk to denote conditions at the *critical point* where $G = 0$ and $M = 1$ simultaneously, Eq. 8.71b yields the following relation among the independent variables which must be fulfilled at this point:

$$G^* = 0 = -2 \frac{d(\ln A)}{dx} + (k+1) \frac{d(\ln T_0)}{dx} + k \frac{4f}{D} + \dots \quad (8.72)$$

VALUE OF $(dM^2/dx)^*$ AT CRITICAL POINT. The limiting value of $(dM^2/dx)^*$ at the critical point is found by applying L'Hospital's rule to the right-hand side of Eq. 8.71a. Thus,

$$\left(\frac{dM^2}{dx} \right)^* = \frac{[G'(x)]^*}{-(dM^2/dx)^*} \quad (8.73)$$

where $G'(x) \equiv dG/dx$, from which we obtain

$$(dM^2/dx)^* = \pm \sqrt{-[G'(x)]^*} \quad (8.74)$$

as the value of the slope of M^2 versus x at the critical point. Thus, at the critical point, the flow may be continued through the speed of sound provided that $[G'(x)]^*$ is negative and is not zero. Under these conditions it is clear from Eq. 8.74 that the solution may be continued from the critical point in either of two directions: into the supersonic range, or back into the subsonic range.

The critical point is a singular point in the solution and is in fact a saddle point (see Fig. 8.7e). The critical curve passing through the critical point is a singular curve of the family of solutions.

Since $G(x)$ depends on M^2 as well as on the independent variables $d(\ln A)/dx$, $d(\ln T_0)/dx$, etc., it follows that $G'(x)$ in Eq. 8.74 contains terms in dM^2/dx . However, if, as is usually the case, Eq. 8.71 is being integrated numerically or graphically, the terms in dM^2/dx implicitly contained in $G'(x)$ will be automatically accounted for provided that one plots G versus x and then determines the value of the slope $G'(x)$ as $M^2 \rightarrow 1$ and $G \rightarrow 0$.

SPECIAL RELATION FOR $(dM^2/dx)^*$ AT CRITICAL POINT. When the only independent variables are $d(\ln A)/dx$, $d(\ln T_0)/dx$, and $4f/D$, and when these are functions of x only, then one may proceed as follows:

The value of $[G'(x)]^*$ is found from Eq. 8.71b by differentiating with respect to x and then setting $M^2 = 1$. Thus we obtain

$$(G')^* = \Psi^* + \Phi^* (dM^2/dx)^* \quad (8.75a)$$

$$\Phi^* \equiv -2k \frac{d(\ln A)}{dx} + \frac{3k}{2} (k+1) \frac{d(\ln T_0)}{dx} + \frac{k}{2} (3k+1) \frac{4f}{D} \quad (8.75b)$$

$$\Psi^* \equiv -(k+1) \frac{d^2(\ln A)}{dx^2} + \frac{(k+1)^2}{2} \frac{d^2(\ln T_0)}{dx^2} + \frac{k(k+1)}{2} \frac{d(4f/D)}{dx} \quad (8.75c)$$

Using Eq. 8.72, Eq. 8.75b may also be written as

$$\Phi^* \equiv \frac{k(k+1)}{2} \frac{d(\ln T_0)}{dx} + \frac{k(k+1)}{2} \frac{4f}{D} \quad (8.75d)$$

Inserting Eq. 8.75a into Eq. 8.74, and solving the resulting quadratic for $(dM^2/dx)^*$, we finally obtain

$$\left(\frac{dM^2}{dx} \right)^* = -\frac{\Phi^*}{2} \pm \sqrt{\left(\frac{\Phi^*}{2} \right)^2 - \Psi^*} \quad (8.76)$$

In most practical situations, however, such independent variables as $d(\ln T_0)/dx$ will depend on M^2 as well as on x . In such cases it is best to proceed from Eq. 8.74.

Examples: (i) The most familiar example of continuous passage through the speed of sound is at the throat of a nozzle. Assuming friction and heat transfer to be negligible, Eq. 8.72 shows that dA/dx must be zero at the sonic point, i.e., the area must have an extremum. In addition, Eqs. 8.76 and 8.75 show that $d^2(\ln A)/dx^2$ must be positive at the sonic point, i.e., the area must be decreasing upstream of x^* and must be increasing downstream of x^* , and the sonic point must therefore have a *minimum* area.

(ii) The author and his associates have succeeded experimentally in producing the critical curve of Fig. 8.7e by injecting water at low speed into a high-speed subsonic hot gas stream. At first drag is controlling, and G is positive. After the water droplets have been accelerated, evaporative cooling is controlling, and G is negative. In this way all the solid curves of Fig. 8.7e have been realized, and an acceleration from subsonic to supersonic speeds has been achieved in a constant-area pipe.

Stability of Passage Through Sonic Point. The foregoing considerations refer to steady flows, and provide no information as to whether the steady-state solutions are in fact stable to small time-dependent disturbances in the boundary conditions. This question has hardly begun to be explored, but what has been done theoretically suggests that the transition from subsonic to supersonic flow is stable whereas the transition from supersonic flow to subsonic flow is unstable. Experimental results thus far seem to confirm this tentative finding.

REFERENCES AND SELECTED BIBLIOGRAPHY

- SHAPIRO, A. H., and HAWTHORNE, W. R. The Mechanics and Thermodynamics of Steady, One-Dimensional Gas Flow, *Jour. App. Mach.*, Vol. 14, No. 4 (1947), p. A317.
- TURNER, L. R., ADDIE, A. N., and ZIMMERMAN, R. H. Charts for the Analysis of One-Dimensional Steady Compressible Flow, *NACA Tech. Note*, No. 1419 (1948).
- HICKS, B. L., MONTGOMERY, D. J., and WASSERMAN, R. H. The One-Dimensional Theory of Steady Compressible Fluid Flow in Ducts with Friction and Heat Addition, *NACA Tech. Note*, No. 1336 (1947).

PROBLEMS

8.1. Plot on a temperature-entropy diagram the curves corresponding to Simple Friction, Simple T_0 -Change, and Simple Gas Injection with $y = 0$. Choose the starting point of each curve such that in all the processes the corresponding stream properties are identical at $M = 2$.

8.2. A stream flowing in an insulated duct with friction is to be maintained at *constant Mach Number* through suitable changes in duct area.

Assume that a one-dimensional treatment is acceptable and that at section 1 of the duct the properties are M_1 , p_1 , A_1 , etc.

(a) Starting with fundamental principles, show that the product of area and pressure is the same for all cross sections.

(b) Find an expression for the area at a point downstream of section 1 in terms of the area at 1, the Mach Number, the friction coefficient, and the number of length-diameter ratios (based on D_1) between section 1 and the downstream section.

(c) If $M_1 = 0.5$, $p_1 = 1$ atm, and $f = 0.005$, compute the ratios A_2/A_1 , p_2/p_1 , and p_{02}/p_{01} if section 2 is 50 diameters downstream of section 1.

8.3. Air flows adiabatically in a tube of circular cross section with an initial Mach Number of 0.5, temperature of 1000°R , and pressure of 100 psia, all at section 1.

The tube is to be changed in cross-sectional area so that, taking friction into account, there is no change in the temperature of the stream.

Assuming the friction coefficient to be 0.005 and that the exit section (2) is downstream of the inlet by a distance 100 times as large as the initial diameter, find:

- The final Mach Number, M_2
- The ratio of diameters, D_2/D_1
- The final stagnation pressure, p_{02} , in psia

8.4. A hydrocarbon gas is to be injected step-wise and burned in a high-speed stream of air. It is desired to carry out the combustion at a constant Mach Number of 0.5, and changes in cross-sectional area will therefore be necessary.

To simplify the analysis, a one-dimensional point of view will be adopted, and the following assumptions will be made: (a) variations in specific heat and molecular weight are negligible, (b) wall friction is negligible, (c) the hydrocarbon is injected at low speed, and (d) enthalpy effects associated with the difference between the gas temperature and the stream temperature are negligible compared with the enthalpy effects due to combustion.

Assuming that the constant-pressure heat of reaction is 15,000 Btu per pound of hydrocarbon gas, $T_{01} = 1000^{\circ}\text{R}$, and $T_{02} = 2500^{\circ}\text{R}$, estimate the area ratio A_2/A_1 and the pressure ratio p_2/p_1 .

8.5. A gas flows in a conical duct of circular cross section, the included angle between the walls being θ . If f is the coefficient of friction, find a relation between θ , D/D^* , M , and f , where D is the diameter at Mach Number M and D^* is the diameter at Mach Number unity. Find a similar relation between p_0/p_0^* , M , θ , and f .

8.6. Consider the compressible flow of air in an electrically heated tube of constant cross-sectional area. It is agreed to assume a recovery factor of unity and to employ the Reynolds analogy between heat transfer and friction.

The electrical resistance of the tube wall is such that the rate of heat transfer varies linearly from a maximum at the inlet end to zero at the outlet end, i.e.,

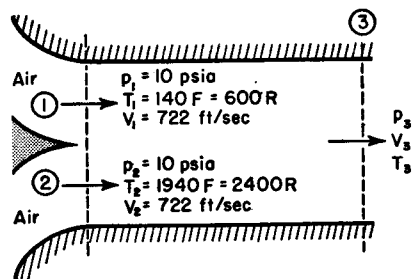
$$\frac{dQ}{d\frac{x}{L}} = \left(1 - \frac{x}{L}\right) \left(\frac{dQ}{d\frac{x}{L}}\right)_{\max}$$

(a) Plot $4fL/D$ versus $\frac{T_{w_{\max}} - T_{01}}{T_{02} - T_{01}}$.

(b) Plot M and p_0 versus x/L , if $M_1 = 0.25$, $T_{01} = 500^{\circ}\text{R}$, $T_{02} = 1500^{\circ}\text{R}$, and $T_{w_{\max}} = 2000^{\circ}\text{R}$.

8.7. Consider the compressible flow of air in a heated tube with friction. A constant Mach Number of 0.5 is to be maintained through suitable changes in area. It is agreed to assume a recovery factor of unity, a constant wall temperature T_w , and to employ the Reynolds analogy between friction and heat transfer. The stream properties at the inlet section will be denoted by A_1 , T_{01} , T_1 , etc., and at a distance x from the inlet by A , T_0 , T , etc. Since the flow is turbulent, f varies as D to the -0.2 power, i.e., $f \sim D^{-0.2}$.

Plot A/A_1 , T/T_1 , T_0/T_{01} , p/p_1 , and p_0/p_{01} , all versus $4fx/D_1$, for a value of T_w/T_{01} of 2.0. Carry the computations up to a value of 1 for $4fx/D_1$.



PROB. 8.9.

8.8. Investigate the possibility of raising the stagnation pressure of a high-speed gas stream by cooling the stream as it flows through a duct. Show with the help of Reynolds' analogy that there is always a net loss in stagnation pressure if the cooling is accomplished by conduction to the walls.

shown in the sketch. It is agreed to assume

- (i) That just before mixing the individual streams have equal cross-sectional areas
- (ii) That wall friction in the mixing section is negligible and that the walls of the mixing section are insulated against heat transfer
- (iii) That the streams are completely mixed at section 3
- (iv) That air behaves as a perfect gas

Calculate

- (a) The isentropic stagnation pressure (psia) for stream 1
- (b) The mass flow per unit area (lbm/sec ft²) for stream 1
- (c) The stagnation temperature at section 3 (degrees R)
- (d) The isentropic stagnation pressure at section 3 (psia)

8.10. The throat of a circular passage has a wall of the shape $r/r_0 = 1 + \alpha(x/r_0)^2$, where r_0 is the radius at the minimum section, r is the radius at the longitudinal distance x , x is the distance from the minimum section, and α is a dimensionless constant. Assuming adiabatic flow with a constant friction factor f , determine

- (a) The location x^*/r_0 of the critical point
- (b) The value of dM/dx at the geometric throat and also at the critical point

PART III

INTRODUCTION TO FLOW IN TWO AND THREE DIMENSIONS

Chapter 9

THE EQUATIONS OF MOTION FOR STEADY, IRROTATIONAL FLOW

9.1. Introductory Remarks

The analyses previously given for one-dimensional flow are exactly correct only for the flow through an infinitesimal stream tube. For all real problems the assumption of one-dimensionality for the entire flow is at best an approximation. In many instances, especially those relating to the flow in ducts, the one-dimensional treatment is adequate. In other cases, however, the one-dimensional methods are not only inadequate but often can provide no information whatsoever about important aspects of the flow. As examples where the flow field must be thought of as two-dimensional or three-dimensional in order to obtain results of value, we may mention the flow past the wings, fuselage, and control surfaces of aircraft; the flow through the blade passages of turbines and compressors; and the flow through ducts of rapidly varying cross-sectional area or through ducts the axes of which undergo rapid changes in direction.

To treat the most general case of three-dimensional motion—including friction, heat transfer, shocks, and a fluid with a complex equation of state— involves mathematical difficulties so great that the task is well-nigh hopeless using present-day methods of analysis. Hence, as in most engineering problems, it is necessary to conceive simple models of the flow which lend themselves to analytical treatment, but which at the same time furnish information of value concerning the real, and more complex, flow patterns.

Using Prandtl's concept of the *boundary layer*—a concept well verified by experiment—it is possible to ignore friction and heat transfer for the region of *potential flow* outside of the boundary layer. According to this concept shearing stresses and heat transfer may be ignored compared to other effects, except in a thin film near solid boundaries. In this thin film, usually called the boundary layer, the velocity and temperature gradients are so large that the shearing stresses and heat transfer cannot be neglected. Thus, the flow is assumed to be adiabatic and frictionless outside a fictitious body whose outline is displaced

from the outline of the actual body by an amount equal to the *displacement thickness* of the boundary layer at each point. The flow within the boundary layer is treated separately by methods specially adapted to the characteristics of flow in a boundary layer. An important premise in this line of attack is that to first-order effects the potential flow is independent of the flow in the boundary layer.

Shock waves cannot occur in regions where the flow is entirely subsonic. In transonic and supersonic flow, on the other hand, it is difficult if not impossible to avoid shocks. Even with shocks present, however, the flow patterns upstream and downstream of the shock can each be treated as shock-free, and the shock is then thought of as a discontinuity dividing the two continuous domains of flow. It will be shown in this chapter that a flow which is initially uniform and parallel has the special property of being *irrotational* outside the boundary layer as long as shocks are absent, and that the assumption of irrotationality leads to important simplifications in the analysis.

When shocks appear in an initially irrotational flow, however, the flow downstream of the shock is in general rotational, except in the special circumstance of a plane or conical shock. The amount of rotation introduced by a curved shock is often so small, however, that there is little error in treating the downstream flow as irrotational.

In connection with the boundary-layer concept, it should be noted that when shocks are present, the flow outside the boundary layer may be substantially influenced by the boundary layer itself. Experiments indicate a marked interaction between shock waves and boundary layers, in which the extraordinary pressure gradient of the shock wave significantly alters the flow in the boundary layer, and this alteration in turn influences the external flow to such an extent that the shock pattern becomes itself dependent on the effects it produces on the boundary layer.

For most problems in compressible flow the assumption that the fluid is a perfect gas permits great mathematical simplifications with scarcely any sacrifice in accuracy. This assumption would have to be abandoned, however, for thermodynamic states near the critical state or near the condensation state.

In this chapter the differential equations of motion will be derived for the irrotational, frictionless, adiabatic, shock-free motion of a perfect gas. The fluid will be treated as a continuum and all stream properties will be assumed to vary in a continuous manner in all directions. Gravity effects will be ignored since they are seldom of importance in the flow of gases. For convenience in later reference, several coordinate systems will be employed.

NOMENCLATURE

<i>a</i>	acceleration	<i>T</i>	absolute temperature
<i>A</i>	area	<i>u</i>	velocity component in <i>x</i> -direction
A	area vector	<i>v</i>	velocity component in <i>y</i> -direction
<i>c</i>	speed of sound	V	velocity
<i>F</i>	force	V	velocity vector
<i>g</i>	acceleration of gravity	<i>w</i>	velocity component in <i>z</i> -direction; mass rate of flow
<i>h</i>	enthalpy per unit mass	<i>x, y, z</i>	Cartesian coordinates
<i>i, j, k</i>	unit vectors in the <i>x</i> -, <i>y</i> -, and <i>z</i> -directions respectively		
<i>k</i>	ratio of specific heats		
<i>l</i>	length		
<i>m</i>	mass	α	angle
<i>n</i>	curvilinear coordinate measured normal to streamline	Γ	circulation
<i>p</i>	pressure	θ	angle
<i>q</i>	rotation vector	ρ	density
<i>r</i>	radius; cylindrical coordinate	φ	velocity potential
<i>r</i>	radius vector	ψ	stream function
<i>R</i>	radius of curvature of streamline	ω	rotation; cylindrical coordinate
<i>s</i>	entropy per unit mass	Ω	angular velocity
<i>t</i>	time	() ₀	signifies stagnation state

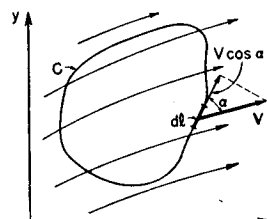
9.2. The Physical Significance of Irrotational Motion

Before proceeding to a development of the differential equations of motion, we shall first discuss the meaning of *rotation* in a fluid and the implications of *irrotational motion* as to the nature of the flow pattern.

Circulation. The *circulation* is defined as the line integral of the velocity around any closed curve. Mathematically, the *line integral of the velocity* is the sum of the products of the element dl of the curve and the corresponding component of velocity tangent to the curve. Referring to the closed curve *C* of Fig. 9.1, and using the symbol Γ to denote circulation, we may write

$$\Gamma \equiv \oint_C V \cos \alpha \, dl$$

Fig. 9.1. Illustrates the concept of circulation.



In vector notation this may be written in terms of the scalar product as

$$\Gamma \equiv \oint_C \mathbf{V} \cdot d\mathbf{r}$$

where \mathbf{V} denotes the vector velocity and \mathbf{r} the vector radius from any fixed origin. If u , v , and w denote respectively the velocity components in the x -, y -, and z -directions, the Cartesian form of Eqs. 9.1a and 9.1b becomes

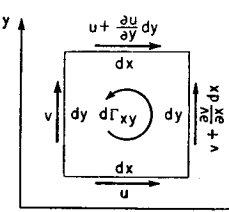


FIG. 9.2. Circulation for elementary closed curve.

COUNTER-CLOCKWISE from the origin, we obtain

$$d\Gamma_z = u \, dx + \left(v + \frac{\partial v}{\partial x} \, dx \right) dy - \left(u + \frac{\partial u}{\partial y} \, dy \right) dx - v \, dy$$

or, simplifying,

$$d\Gamma_z = \left(\frac{\partial v}{\partial x} - \frac{\partial u}{\partial y} \right) dx \, dy = \left(\frac{\partial v}{\partial x} - \frac{\partial u}{\partial y} \right) dA_z \quad (9.2)$$

The circulation per unit area in the x,y -plane is therefore given by

$$\frac{d\Gamma_z}{dA_z} = \frac{\partial v}{\partial x} - \frac{\partial u}{\partial y} \quad (9.3)$$

Similar expressions for the other directions may be found by the usual rotation of indices.

GREEN'S THEOREM. Considering now the circulation around an area of finite size, we note from Fig. 9.3 that the line integral around the bounding curve C is the algebraic sum of the line integrals around the elementary square elements comprising the area within C , since each interior line of each element is traversed an equal number of times in opposite directions, and hence only the exterior lines of the elements (which comprise curve C) contribute to the circulation. Therefore, employing Eq. 9.2, we find that the circulation around any finite closed curve C in the x,y -plane may in the limit be expressed in terms of a surface integral, namely,

$$\Gamma_z = \iint_A \left(\frac{\partial v}{\partial x} - \frac{\partial u}{\partial y} \right) dx \, dy \quad (9.4)$$

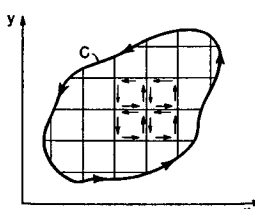


FIG. 9.3. The circulation around any closed curve is the sum of the circulations around all the closed curves bounding the elementary areas comprising the region within C .

Likewise, Eq. 9.1c gives

$$\Gamma_z = \oint_C (u \, dx + v \, dy) \quad (9.5)$$

A comparison between Eqs. 9.4 and 9.5 shows that taken together they represent *Green's Theorem* for the transformation from line to surface integrals in two-dimensional space.

STOKES' THEOREM. The general form of Eq. 9.4, expressed in vector notation, is,

$$\Gamma = \iint_A \nabla \times \mathbf{V} \cdot d\mathbf{A} \quad (9.6)$$

This equation taken together with Eq. 9.1b is an expression of *Stokes' Theorem* for converting from a line integral to a surface integral in three-dimensional space.

FLUID ROTATION AT A POINT. The *angular velocity of a rigid body* is defined as the time rate of change of the angle between any fixed line on the object and a reference line fixed in space. With deformable bodies such as fluids or elastic solids the angular velocity thus defined is ambiguous and must be modified. The difficulty here is that an initially straight line of the body becomes curved owing to deformations, and the angle referred to above can have many values. This suggests that we consider a *point* of the body and measure the angle with respect to the tangent to a curve fixed in the body and passing through the point. However, a new difficulty is thus raised, inasmuch as the angular velocities of tangents to different curves passing through the same point will not be identical. Obviously what is required is some generalization of the concept of angular velocity which defines the average angular velocity at a point in a manner which is invariant with orientation.

Such a generalization is given by the following definition: The *fluid rotation at a point* is the mean angular velocity of two infinitesimal and mutually perpendicular fluid curves instantaneously passing through the point. A *fluid curve* is defined as a curve passing through a set of fluid particles of fixed identity.

The rotation at a point, it should be noted, reduces to the familiar angular velocity for rigid-body motion. Hence the rotation as defined above is an extension of the concept of angular velocity to bodies which are deformable.

ROTATION IN TWO DIMENSIONS. In order to find an analytical expression for the fluid rotation at a point in a two-dimensional flow, let us consider the infinitesimal and mutually perpendicular fluid lines OA and OB of Fig. 9.4. The motion of each of these lines may be resolved into a translation plus a rotation. Considering the fluid line OA , a

rotation will take place only if the y -component of velocity at A is different from that at O . Since only the difference in velocity is important, we imagine that we move with point O ; the upward velocity at A relative to that at point O is, then, $(\partial v / \partial x) dx$. During an infinitesimal time interval dt , OA rotates to the position OA' , and the relative vertical displacement AA' is

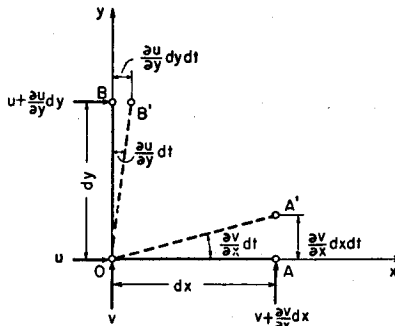


FIG. 9.4. Illustrates fluid rotation at a point. OA and OB are mutually perpendicular fluid lines.

Similarly, it may be shown that the angular velocity of the fluid line OB is $-\partial u / \partial y$.

From the definition of rotation, therefore,

$$\omega_z = \frac{1}{2} \left(\frac{\partial v}{\partial x} - \frac{\partial u}{\partial y} \right) \quad (9.7)$$

Referring to Eq. 9.3, we see that the circulation per unit area is twice the average rotation of a fluid particle:

$$\frac{d\Gamma_z}{dA_z} = 2\omega_z = \frac{\partial v}{\partial x} - \frac{\partial u}{\partial y} \quad (9.8)$$

ROTATION IN THREE DIMENSIONS. The rotation of a fluid at a point, like the angular velocity of a rigid body, is a vector quantity. Eq. 9.7 can be taken to represent the z -component of rotation, and the x - and y -components may then be found from Eq. 9.7 by rotation of indices. In terms of the unit vectors \mathbf{i} , \mathbf{j} , \mathbf{k} , the vector rotation \mathbf{q} is then given by

$$2\mathbf{q} = \mathbf{i} \left(\frac{\partial w}{\partial y} - \frac{\partial v}{\partial z} \right) + \mathbf{j} \left(\frac{\partial u}{\partial z} - \frac{\partial w}{\partial x} \right) + \mathbf{k} \left(\frac{\partial v}{\partial x} - \frac{\partial u}{\partial y} \right)$$

which is more compactly expressed as the curl of the velocity vector:

$$2\mathbf{q} = \nabla \times \mathbf{V}$$

RATE OF SHEAR DEFORMATION. Before leaving Fig. 9.4, it is of interest to note that the rate of shear deformation in a fluid is defined as the

rate of change of the angle between two mutually perpendicular fluid lines. Referring to the angle between the lines OA and OB , we get

$$\left\{ \begin{array}{l} \text{Rate of shear} \\ \text{deformation} \end{array} \right\} = \frac{(\partial v / \partial x) dt + (\partial u / \partial y) dt}{dt} = \frac{\partial v}{\partial x} + \frac{\partial u}{\partial y} \quad (9.9)$$

The shear deformation is connected with the shearing stresses in the fluid through the coefficient of viscosity.

It may be of interest here to point out also the analogue between the expressions given above and corresponding expressions encountered in the mechanics of deformable solids. In the case of a fluid particle we deal with velocities, whereas for a deformable solid particle we deal with displacements. The average rotation of a fluid particle corresponds to the average rotation of a solid particle, and the rate of shear deformation of a fluid particle corresponds to the shearing strain of an elastic solid particle.

EXAMPLE OF ROTATIONAL MOTION. A simple example of rotational motion in a fluid is the solid-body type (or wheel type) of angular motion about an axis. Referring to Fig. 9.5, the streamlines are concentric circles, and, since the individual fluid particles maintain their relative positions as in the case of a rigid solid, we may write for the velocity along a streamline

$$V = \Omega r$$

where Ω is the angular velocity in the rigid-body sense. Then, evaluating the circulation along any circular streamline of radius r , we get

$$\Gamma = \int_0^{2\pi} Vr d\theta = \Omega r^2 \int_0^{2\pi} d\theta = 2\pi\Omega r^2$$

or

$$\frac{\Gamma}{A} = \frac{\Gamma}{\pi r^2} = 2\Omega$$

and, referring to Eq. 9.8, we conclude that the angular velocity Ω of the entire mass is, as we expect, identical with the average rotation of each particle.

EXAMPLE OF IRROTATIONAL MOTION. A simple but important example of irrotational motion is the *potential vortex*, which describes approximately the motion in tornadoes and whirlpools, and which plays an important role in the theory of flight and the theory of turbines and compressors. In its simplest form a potential vortex is a two-dimensional

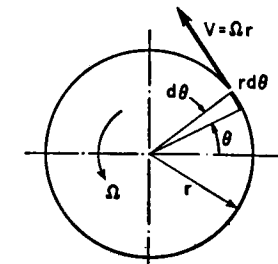


FIG. 9.5. Forced vortex

motion in which the streamlines form concentric circles, and the tangential velocity along any streamline is inversely proportional to the radius of the streamline. Thus,

$$Vr = K \quad (9.10)$$

where K is a constant. Consider the circulation around the element $ABCD$ of Fig. 9.6. Noting that the line integral is zero along the sides AB and CD , we obtain

$$\begin{aligned} d\Gamma_{ABCD} &= (V + dV)(r + dr) d\theta - Vr d\theta = (V dr + r dV) d\theta \\ &= [d(Vr)] d\theta \end{aligned}$$

Then, using Eq. 9.10, we see that

$$d\Gamma_{ABCD} = 0$$

Thus the circulation of any element not enclosing the origin is zero, and, employing the theorem illustrated by Fig. 9.3, we conclude that the circulation of any area *not enclosing the origin* of the vortex is zero.

Considering next the circulation around the streamline of radius r in Fig. 9.6, we obtain

$$\Gamma = \int_0^{2\pi} Vr d\theta = K \int_0^{2\pi} d\theta = 2\pi K$$

so that Eq. 9.10 becomes

$$Vr = \frac{\Gamma}{2\pi} \quad (9.11)$$

where Γ is the circulation for *any* closed circuit *enclosing the origin*.

Each particle of fluid in the vortex undergoes a shearing deformation but the average rotation of each particle is zero. We conclude that a potential vortex is in general irrotational, except for a singularity at the origin where the rotation is infinite.

To illustrate in another way the fact that the motion in a potential vortex is irrotational even though the fluid particles follow circular paths, consider a cork floating in a pan of water in which the water moves as in a potential vortex. The cork will travel in circles, but if a straight line is painted on the top of the cork it will be observed that this line has a purely rectilinear motion, that is, the line always remains parallel to its original direction and consequently has zero angular velocity.

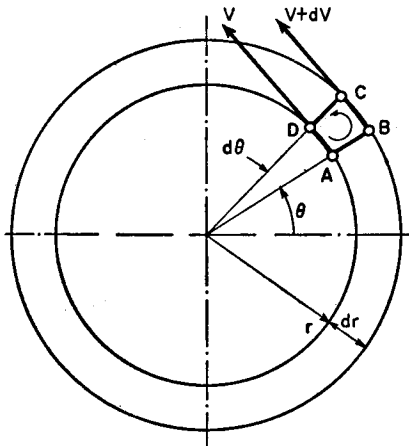


FIG. 9.6. Free, or potential, vortex.

The line on the cork will in fact have the same type of rectilinear motion as the magnetic needle of a compass when the compass travels through a circular path in a horizontal plane.

9.3. Euler's Equations of Motion

In this article we shall consider the application of Newton's second law of motion to a fluid flowing without friction and without body forces (gravity, electromagnetic, etc.) in three-dimensional space. Since we are interested in the details of the flow pattern, we shall write the equations in differential form. It will be assumed that all stream properties vary continuously in all directions; this implies that shocks are excluded.

Euler's Equations in Cartesian Coordinates. We begin by considering the forces acting on and the accelerations experienced by a particular

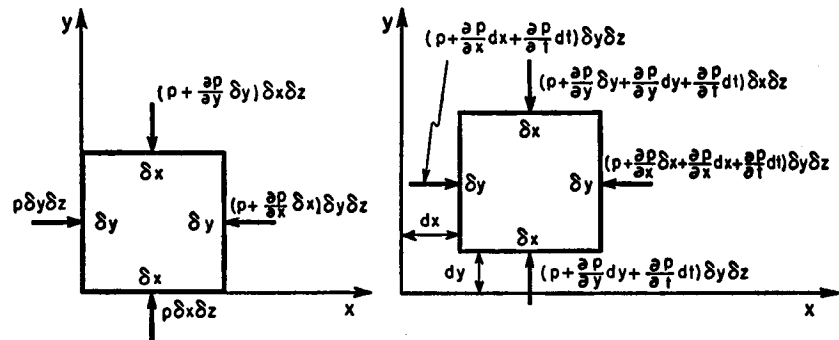


FIG. 9.7. Pressure forces acting on isolated body.

- (a) At time t .
(b) At time $t + dt$.

particle of fluid of fixed mass and identity. This system is taken to be an elementary cube of dimensions δx , δy , and δz . The respective locations of the system at the times t and $t + dt$ are indicated in Figs. 9.7a and 9.7b, respectively.

Newton's second law can be written for each of the three Cartesian directions as

$$F_x = ma_x = m \frac{Du}{Dt} \quad (9.12a)$$

$$F_y = ma_y = m \frac{Dv}{Dt} \quad (9.12b)$$

$$F_z = ma_z = m \frac{Dw}{Dt} \quad (9.12c)$$

where F_x , F_y , and F_z denote the respective forces acting on the system in the x -, y -, and z -directions, and u , v , and w are the corresponding components of velocity. The symbol D/Dt represents the *substantial derivative* with respect to time and denotes that the differentiation is to be carried out *while following a particular fluid particle*.

Since shearing forces and body forces are excluded from this analysis, the only forces acting on the system are pressure-area forces. The magnitudes of these forces acting on the various faces in the x, z - and y, z -planes are shown in Figs. 9.7a and 9.7b at the times t and $t + dt$, respectively.

Considering first the x -direction, the *average* force during the time interval dt is

$$F_x = \left(p + \frac{1}{2} \frac{\partial p}{\partial x} dx + \frac{1}{2} \frac{\partial p}{\partial t} dt \right) \delta y \delta z - \left(p + \frac{\partial p}{\partial x} \delta x + \frac{1}{2} \frac{\partial p}{\partial x} dx + \frac{1}{2} \frac{\partial p}{\partial t} dt \right) \delta y \delta z$$

or, after simplifying,

$$F_x = - \frac{\partial p}{\partial x} \delta x \delta y \delta z$$

For the y - and z -directions we obtain, similarly,

$$F_y = - \frac{\partial p}{\partial y} \delta y \delta z \delta x$$

$$F_z = - \frac{\partial p}{\partial z} \delta z \delta x \delta y$$

The mass of the system is the product of the mass density and the volume:

$$m = \rho \delta x \delta y \delta z$$

The acceleration in the x -direction, a_x , may be written

$$a_x = \frac{Du}{Dt} = \frac{(u)_{x+dx, y+dy, z+dz, t+dt} - (u)_{x, y, z, t}}{dt}$$

$$= \frac{\left(u + \frac{\partial u}{\partial x} dx + \frac{\partial u}{\partial y} dy + \frac{\partial u}{\partial z} dz + \frac{\partial u}{\partial t} dt \right) - u}{dt}$$

$$= \frac{\frac{\partial u}{\partial x} dx + \frac{\partial u}{\partial y} dy + \frac{\partial u}{\partial z} dz + \frac{\partial u}{\partial t} dt}{dt}$$

Now, since dx is the x -displacement of the fluid particle during the time dt , it follows that $u = dx/dt$. Likewise, $v = dy/dt$ and $w = dz/dt$. Hence

$$\frac{Du}{Dt} = \frac{\partial u}{\partial t} + u \frac{\partial u}{\partial x} + v \frac{\partial u}{\partial y} + w \frac{\partial u}{\partial z}$$

For the y - and z -directions we obtain similar expressions:

$$\frac{Dv}{Dt} = \frac{\partial v}{\partial t} + u \frac{\partial v}{\partial x} + v \frac{\partial v}{\partial y} + w \frac{\partial v}{\partial z}$$

$$\frac{Dw}{Dt} = \frac{\partial w}{\partial t} + u \frac{\partial w}{\partial x} + v \frac{\partial w}{\partial y} + w \frac{\partial w}{\partial z}$$

Inserting the foregoing expressions for m , for F_x , F_y , and F_z , and for a_x , a_y , and a_z into Eqs. 9.12, and simplifying, we finally obtain *Euler's equations of motion* in Cartesian coordinates:

$$-\frac{1}{\rho} \frac{\partial p}{\partial x} = \frac{\partial u}{\partial t} + u \frac{\partial u}{\partial x} + v \frac{\partial u}{\partial y} + w \frac{\partial u}{\partial z} = \frac{Du}{Dt} \quad (9.13a)$$

$$-\frac{1}{\rho} \frac{\partial p}{\partial y} = \frac{\partial v}{\partial t} + u \frac{\partial v}{\partial x} + v \frac{\partial v}{\partial y} + w \frac{\partial v}{\partial z} = \frac{Dv}{Dt} \quad (9.13b)$$

$$-\frac{1}{\rho} \frac{\partial p}{\partial z} = \frac{\partial w}{\partial t} + u \frac{\partial w}{\partial x} + v \frac{\partial w}{\partial y} + w \frac{\partial w}{\partial z} = \frac{Dw}{Dt} \quad (9.13c)$$

There are two special sets of conditions for which this system of equations may be easily integrated: first, along a streamline; and second, throughout the entire flow field, provided that the flow is irrotational.

Integration of Euler Equation Along a Streamline in Steady Flow.

Since a streamline is defined by the condition that at each instant the velocity vector is tangent to the streamline (Fig. 9.8), we may write the equation of the streamline in the form

$$\frac{dy}{dx} = \frac{v}{u}; \quad \frac{dz}{dy} = \frac{w}{v}; \quad \frac{dx}{dz} = \frac{u}{w} \quad (9.14)$$

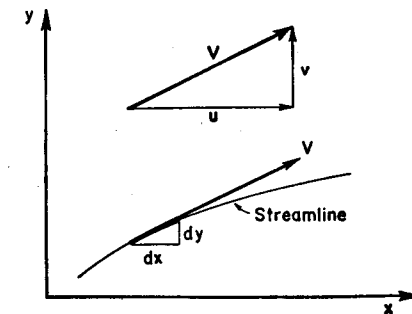


Fig. 9.8. Illustrates the equation of a streamline.

ourselves to considering only changes along a particular streamline:

$$\begin{aligned}
 -\frac{1}{\rho} \frac{\partial p}{\partial x} dx &= u \frac{\partial u}{\partial x} dx + v \frac{\partial u}{\partial y} dx + w \frac{\partial u}{\partial z} dx \\
 &= u \frac{\partial u}{\partial x} dx + u \frac{\partial u}{\partial y} dy + u \frac{\partial u}{\partial z} dz \\
 -\frac{1}{\rho} \frac{\partial p}{\partial y} dy &= u \frac{\partial v}{\partial x} dy + v \frac{\partial v}{\partial y} dy + w \frac{\partial v}{\partial z} dy \\
 &= v \frac{\partial v}{\partial x} dy + v \frac{\partial v}{\partial y} dy + v \frac{\partial v}{\partial z} dz \\
 -\frac{1}{\rho} \frac{\partial p}{\partial z} dz &= u \frac{\partial w}{\partial x} dz + v \frac{\partial w}{\partial y} dz + w \frac{\partial w}{\partial z} dz \\
 &= w \frac{\partial w}{\partial x} dz + w \frac{\partial w}{\partial y} dy + w \frac{\partial w}{\partial z} dz
 \end{aligned}$$

Adding these equations, and noting that

$$\begin{aligned}
 dp &= \frac{\partial p}{\partial x} dx + \frac{\partial p}{\partial y} dy + \frac{\partial p}{\partial z} dz \\
 du &= \frac{\partial u}{\partial x} dx + \frac{\partial u}{\partial y} dy + \frac{\partial u}{\partial z} dz; \text{ etc.}
 \end{aligned}$$

we obtain

$$-\frac{1}{\rho} dp = u du + v dv + w dw = d \left(\frac{u^2 + v^2 + w^2}{2} \right)$$

or,

$$-\frac{1}{\rho} dp = d \left(\frac{V^2}{2} \right) \quad (9.15)$$

where V is the resultant velocity. Eq. 9.15 may be put in the form

$$dp = -\rho d \left(\frac{V^2}{2} \right) = -\rho V dV \quad (9.16a)$$

or it may be integrated to give

$$\int \frac{dp}{\rho} + \frac{V^2}{2} = \text{constant along streamline} \quad (9.16b)$$

The constant of integration is usually called the *Bernoulli constant* of the streamline. It should be especially noted that Eq. 9.16 is, within

the assumptions given here, valid only from point to point of a given streamline. Or, to put it differently, the Bernoulli constant may in general vary from one streamline to another. Of course, if all the streamlines originated in a region of uniform flow, the same Bernoulli constant would prevail throughout the entire field of flow.

Integration of Euler Equation for Steady, Irrotational Flow. We now abandon the restriction that only points along the same streamline are to be considered and introduce instead the assumption that the motion is irrotational and steady. According to Eq. 9.7, then,

$$\frac{\partial v}{\partial x} - \frac{\partial u}{\partial y} = 0 \quad (9.17a)$$

$$\frac{\partial w}{\partial y} - \frac{\partial v}{\partial z} = 0 \quad (9.17b)$$

$$\frac{\partial u}{\partial z} - \frac{\partial w}{\partial x} = 0 \quad (9.17c)$$

the last two equations being obtained from the first through rotation of indices.

We now multiply Eq. 9.13a by dx , Eq. 9.13b by dy , and 9.13c by dz , and introduce the assumption of irrotationality through Eq. 9.17, thus getting

$$\begin{aligned}
 -\frac{1}{\rho} \frac{\partial p}{\partial x} dx &= u \frac{\partial u}{\partial x} dx + v \frac{\partial u}{\partial y} dx + w \frac{\partial u}{\partial z} dx \\
 &= u \frac{\partial u}{\partial x} dx + v \frac{\partial v}{\partial x} dx + w \frac{\partial w}{\partial x} dx \\
 -\frac{1}{\rho} \frac{\partial p}{\partial y} dy &= u \frac{\partial v}{\partial x} dy + v \frac{\partial v}{\partial y} dy + w \frac{\partial v}{\partial z} dy \\
 &= u \frac{\partial u}{\partial y} dy + v \frac{\partial v}{\partial y} dy + w \frac{\partial w}{\partial y} dy \\
 -\frac{1}{\rho} \frac{\partial p}{\partial z} dz &= u \frac{\partial w}{\partial x} dz + v \frac{\partial w}{\partial y} dz + w \frac{\partial w}{\partial z} dz \\
 &= u \frac{\partial u}{\partial z} dz + v \frac{\partial v}{\partial z} dz + w \frac{\partial w}{\partial z} dz
 \end{aligned}$$

Adding these equations, and noting that

$$u \frac{\partial u}{\partial x} = \frac{\partial}{\partial x} \left(\frac{u^2}{2} \right), \text{ etc.}$$

that

$$\frac{\partial}{\partial x} \left(\frac{u^2 + v^2 + w^2}{2} \right) = \frac{\partial}{\partial x} \left(\frac{V^2}{2} \right), \text{ etc.}$$

and that

$$\frac{\partial}{\partial x} \left(\frac{V^2}{2} \right) dx + \frac{\partial}{\partial y} \left(\frac{V^2}{2} \right) dy + \frac{\partial}{\partial z} \left(\frac{V^2}{2} \right) dz = d \left(\frac{V^2}{2} \right)$$

we obtain finally

$$-\frac{1}{\rho} dp = d \left(\frac{V^2}{2} \right)$$

which is identical with Eq. 9.15 as derived along a streamline in the preceding section. Integration yields

$$\int \frac{dp}{\rho} + \frac{V^2}{2} = \text{constant throughout flow field} \quad (9.18)$$

Thus, for steady, continuous, frictionless, and irrotational flow the Bernoulli constant is the same for all streamlines, and Eq. 9.18 may be used for relating the flow properties between any two points in the flow field. The assumption of irrotational flow is therefore an important simplification, as will be seen more fully in subsequent sections.

BERNOULLI'S EQUATION FOR INCOMPRESSIBLE FLOW. Finally, we note that for frictionless, steady, incompressible flow the Euler equation reduces to the familiar *Bernoulli equation*,

$$p + \frac{1}{2} \rho V^2 = \text{constant} \quad (9.19)$$

where the constant has a particular value for each streamline, except for irrotational flow in which case the constant is the same for all streamlines.

9.4. Kelvin's Theorem

Several significant conclusions follow from the theorem first demonstrated by Thomson (Lord Kelvin), which states in part that *in a frictionless, homogeneous fluid without body forces the circulation along a*

closed fluid line remains constant with respect to time. A homogeneous, or barotropic, fluid is one whose density depends only on the pressure.

To demonstrate this theorem, we first evaluate the substantial derivative of the line integral of the velocity along a fluid line (Fig. 9.9), namely

$$\frac{D}{Dt} \int_A^B (u dx + v dy + w dz)$$

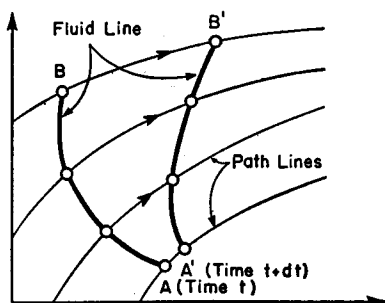


FIG. 9.9. Illustrates Kelvin's theorem.

Considering the first term, we may write

$$\frac{D}{Dt} \int u dx = \int \frac{D}{Dt} (u dx)$$

inasmuch as a consideration of the meaning of the integration and differentiation operations indicates that the two operations may be performed in any order. We may then differentiate by parts, thus getting

$$\frac{D}{Dt} \int u dx = \int \frac{Du}{Dt} dx + \int u \frac{D}{Dt} (dx)$$

Now, from Eq. 9.13a, we note that in the absence of friction,

$$\frac{Du}{Dt} = -\frac{1}{\rho} \frac{\partial p}{\partial x}$$

and, since we are following a particular fluid particle,

$$\frac{Dx}{Dt} = u; \quad \text{and} \quad \frac{D}{Dt} (dx) = du$$

Hence

$$\frac{D}{Dt} \int u dx = -\int \frac{1}{\rho} \frac{\partial p}{\partial x} dx + \int u du$$

Carrying out similar operations on the other two terms of the line integral, we obtain

$$\begin{aligned} \frac{D}{Dt} \int_A^B (u dx + v dy + w dz) &= - \int_A^B \frac{1}{\rho} \left(\frac{\partial p}{\partial x} dx + \frac{\partial p}{\partial y} dy + \frac{\partial p}{\partial z} dz \right) \\ &\quad + \int_A^B (u du + v dv + w dw) \\ &= - \int_A^B \frac{1}{\rho} dp + \int_A^B d \left(\frac{u^2 + v^2 + w^2}{2} \right) \\ &= \int_A^B \frac{dp}{\rho} + \frac{V_B^2 - V_A^2}{2} \end{aligned}$$

Now, if the density is a function only of the pressure, it is clear that the line integral depends only on the fluid properties at points *A* and *B*, and not on the path of integration. Points *A* and *B* coincide if the fluid line is closed, and then the line integral is zero. The proof of the theorem is completed by noting that the line integral of the velocity around a closed curve is by definition the circulation.

When body forces, such as gravity, are present, Kelvin's Theorem remains valid provided that the body force may be written as the gradient of a potential. Such body forces are usually said to be conservative.

IRROTATIONAL MOTION. If the fluid starts from rest, or if in some region the flow is uniform and parallel, the rotation in these regions is zero. Kelvin's theorem then leads to the important conclusion that the entire flow is irrotational, subject to the assumptions of no friction, a homogeneous fluid, the existence of potentials for the body forces, and the absence of discontinuities.

Since in many practical problems the flow may as a first approximation be thought of as frictionless and as having started as a uniform, parallel flow, Kelvin's theorem and the concept of irrotational motion play an important role in the understanding of many flow phenomena. They indicate, for example, that while in most flow patterns observed in nature the fluid particles follow curved paths, the flow is nevertheless likely to be irrotational except in those regions where viscous stresses are an important factor.

9.5. The Connection Between the Rotation and the Thermodynamic Properties of the Flow

It was shown in Art. 9.4 that a steady flow which starts from a region of uniform, parallel motion remains irrotational if the fluid is frictionless and homogeneous and if there are no discontinuities.

We shall now demonstrate the connection between the rotation, which is a purely kinematic property of the motion, and some of the thermodynamic properties of the fluid. To bring out the salient points,

we shall make the simplifying assumptions that the flow is steady, that the fluid is frictionless, and that all fluid properties vary in a continuous manner from point to point. Such would be the case, for example, downstream of a curved shock. We shall also assume the flow to be two-dimensional.

Rotation in Streamline Coordinates. It will be convenient to work in a system of curvilinear coordinates comprising the streamlines and the system of lines normal to the streamlines. Referring to Fig. 9.10, let us first calculate the rotation of the element $ABCD$. Since the line integral of the velocity is

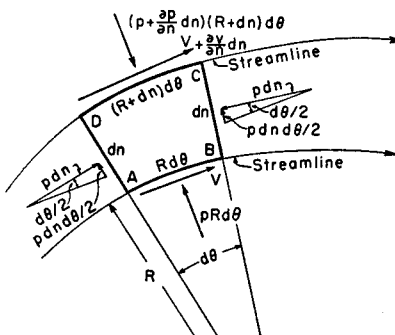


FIG. 9.10. Pressure forces and velocities for an elementary fluid particle in a streamline coordinate system.

normal to the streamlines. Referring to Fig. 9.10, let us first calculate the rotation of the element $ABCD$. Since the line integral of the velocity is

zero along sides BC and DA , we get

$$d\Gamma = VR d\theta - \left(V + \frac{\partial V}{\partial n} dn \right) (R + dn) d\theta = - \left(R \frac{\partial V}{\partial n} + V \right) d\theta dn$$

or

$$2\omega = \frac{d\Gamma}{dA} = \frac{d\Gamma}{R d\theta dn} = - \frac{\partial V}{\partial n} - \frac{V}{R} \quad (9.20)$$

Dynamic Equation Normal to Streamlines. Next we apply Newton's second law of motion in the direction n normal to the streamlines. The mass of the element is $\rho R d\theta dn$, and its acceleration toward the center of curvature of the streamline is the familiar expression for centrifugal acceleration, V^2/R . In the absence of friction and body forces, the only forces acting are those owing to pressure. From Fig. 9.10 we see that the net force acting toward the center of curvature is given by

$$\left(p + \frac{\partial p}{\partial n} dn \right) (R + dn) d\theta - pR d\theta - 2 \left(p dn \frac{d\theta}{2} \right)$$

or, after simplifying,

$$\frac{\partial p}{\partial n} R dn d\theta$$

Finally, after equating the force to the product of mass and acceleration, and simplifying, we get the steady-state form of Euler's equation in a direction normal to the streamline direction:

$$\frac{\partial p}{\partial n} = \frac{\rho V^2}{R} \quad (9.21)$$

Combining Eqs. 9.20 and 9.21, we find that

$$2\omega = - \frac{\partial V}{\partial n} - \frac{1}{\rho V} \frac{\partial p}{\partial n}$$

Crocco's Theorem. Now the stagnation enthalpy, h_0 , is related to the velocity and enthalpy through the steady-flow energy relation:

$$h_0 = h + \frac{V^2}{2}$$

or, differentiating in the n -direction,

$$\frac{\partial h_0}{\partial n} = \frac{\partial h}{\partial n} + V \frac{\partial V}{\partial n}$$

The thermodynamic relation for the entropy,

$$T ds = dh - \frac{1}{\rho} dp$$

may be differentiated to give

$$\frac{\partial h}{\partial n} = T \frac{\partial s}{\partial n} + \frac{1}{\rho} \frac{\partial p}{\partial n}$$

Combination of the two thermodynamic equations then yields

$$\frac{\partial p}{\partial n} = -\rho T \frac{\partial s}{\partial n} + \rho \frac{\partial h_0}{\partial n} - \rho V \frac{\partial V}{\partial n}$$

Substituting this into the expression for the rotation, we obtain finally a special form of *Crocco's Theorem* for two-dimensional flows:

$$2\omega = \frac{1}{V} \left(T \frac{\partial s}{\partial n} - \frac{\partial h_0}{\partial n} \right) \quad (9.22)$$

The rotation is therefore seen to depend on the rates of change of entropy and stagnation enthalpy *normal to the streamlines*.

If the fluid is originally in parallel motion with uniform properties, and if the fluid along each streamline undergoes adiabatic, reversible changes, it follows from Eq. 9.22 that the flow is everywhere irrotational. But the stipulation of reversible flow is equivalent to the statement that there is no friction, and hence the results obtained from this partially thermodynamic treatment coincide with the results of Kelvin's Theorem.

It is conceivable that all streamlines might have the same stagnation enthalpy, but that the entropy would vary from streamline to streamline. Such would be the case in the region downstream of a curved shock, because the entropy change depends on the angle of the shock. Under these circumstances the flow downstream of a shock would be rotational even though the upstream flow were irrotational.

In a boundary layer near a solid wall viscous stresses and heat conduction give rise to variations in entropy and stagnation enthalpy between neighboring streamlines. Hence, according to Eq. 9.22, the boundary layer flow is rotational. From a purely kinematic point of view, the rotational nature of the flow may be seen by examining the angular velocities of the two arms of a fluid cross or by computing the circulation around a closed line in the boundary layer.

9.6. The Equation of Continuity

To express the principle of conservation of mass, we consider a control surface of dimensions dx, dy, dz at a fixed location in space, and equate the net incoming mass rate of flow to the time rate of change of mass within the control surface.

Referring to Fig. 9.11, which shows the mass rates of flow entering and leaving the $dy dz$ and the $dx dz$ areas of the control surface, it is seen that the net flow into the control surface in the x -direction only is the flow through the left-hand face minus the flow through the right-hand face, or,

$$-\frac{\partial}{\partial x} (\rho u dy dz) dx = -\frac{\partial}{\partial x} (\rho u) dx dy dz$$

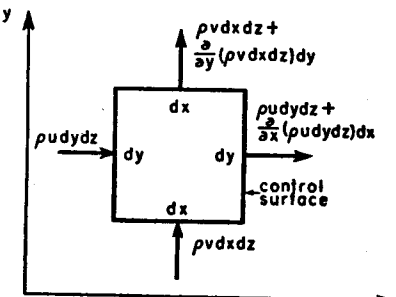


FIG. 9.11. Mass flows through elementary control surface.

Likewise, the net flows into the control surface in the y - and z -directions only are, respectively,

$$-\frac{\partial}{\partial y} (\rho v) dy dx dz$$

and

$$-\frac{\partial}{\partial z} (\rho w) dz dx dy$$

so that the total net flow into the control surface is

$$-\left[\frac{\partial}{\partial x} (\rho u) + \frac{\partial}{\partial y} (\rho v) + \frac{\partial}{\partial z} (\rho w) \right] dx dy dz$$

The time rate of change of mass within the control surface is expressed by

$$\frac{\partial}{\partial t} (\rho dx dy dz) = \frac{\partial \rho}{\partial t} dx dy dz$$

Hence the principle of conservation of mass takes the general form

$$\frac{\partial \rho}{\partial t} + \frac{\partial (\rho u)}{\partial x} + \frac{\partial (\rho v)}{\partial y} + \frac{\partial (\rho w)}{\partial z} = 0 \quad (9.23)$$

This expression is usually called the *equation of continuity* in Cartesian coordinates.

For *steady flow* the equation of continuity becomes

$$\frac{\partial(\rho u)}{\partial x} + \frac{\partial(\rho v)}{\partial y} + \frac{\partial(\rho w)}{\partial z} = 0 \quad (9.24)$$

When the *flow is both incompressible and steady*, we have

$$\frac{\partial u}{\partial x} + \frac{\partial v}{\partial y} + \frac{\partial w}{\partial z} = 0 \quad (9.25)$$

9.7. The Laws of Thermodynamics

In the treatment of irrotational, frictionless motion, we are dealing with a conservative system which can be almost completely described by Newton's laws of motion and by the principle of conservation of mass, the sole contribution of thermodynamics being information concerning the relation between pressure and density for the isentropic process under consideration. For a perfect gas, as an example, we have the familiar isentropic equation,

$$p/\rho^k = \text{constant} \quad (9.26)$$

For adiabatic or isentropic flows of a perfect gas an important relation previously derived (see Eq. 4.8) is

$$c^2 = c_0^2 - \frac{k-1}{2} V^2 = c_0^2 - \frac{k-1}{2} (u^2 + v^2 + w^2) \quad (9.27)$$

Although, in the previous derivation, use was made of the First Law of Thermodynamics in the form of the steady-flow energy equation, Eq. 9.27 may be obtained for isentropic flows with no recourse to thermodynamics except the p - ρ relation of Eq. 9.26. The reader may verify that Eq. 9.27 may be derived from the Euler equation (Eq. 9.18), the definition of the sound velocity (Eq. 3.3), and the isentropic pressure-density relation for a perfect gas (Eq. 9.26). The steady-flow energy equation in reality embodies Newton's second law in the form of the kinetic-energy term, and it is only the latter term which entered into the previous derivation of Eq. 9.27.

Thermodynamics plays a more important role, it will be seen later, when shock waves, friction, heat transfer, or work effects are important factors in the flow pattern.

9.8. Differential Equations in Terms of the Velocity Potential

The Velocity Potential. Restricting our remarks now to irrotational motion, the definition of circulation shows that for irrotational motion the line integral of the velocity around a closed curve is zero. From this

it follows that the line integral of the velocity between any two points *A* and *B* depends only on the location of the points and not on the path of integration. For, referring to Fig. 9.12 (see also Fig. 9.1), we may write for the closed curves *A1B3A* and *A2B3A*:

$$\begin{aligned} \textcircled{1} \int_A^B V \cos \alpha \, dl + \textcircled{3} \int_B^A V \cos \alpha \, dl &= 0 \\ \textcircled{2} \int_A^B V \cos \alpha \, dl + \textcircled{3} \int_B^A V \cos \alpha \, dl &= 0 \end{aligned}$$

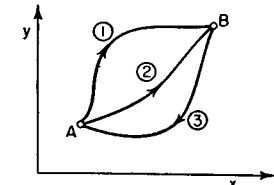


FIG. 9.12. Line integral of velocity between two points in an irrotational motion is independent of path of integration.

from which we see that

$$\textcircled{1} \int_A^B V \cos \alpha \, dl = \textcircled{2} \int_A^B V \cos \alpha \, dl$$

Since paths 1 and 2 were chosen arbitrarily, it follows that the line integral of the velocity is independent of the path.

This means that $V \cos \alpha \, dl$ is an exact differential, and may, therefore, be considered as the differential of a point function whose value depends only on x , y , and z . This function is called the *velocity potential*, φ , and is defined through the relation

$$\begin{aligned} d\varphi &= V \cos \alpha \, dl \\ \text{or} \\ \frac{d\varphi}{dl} &= V \cos \alpha \end{aligned} \quad (9.28)$$

Thus, the derivative of the velocity potential in a given direction represents the component of velocity in the same direction. In Cartesian coordinates we have

$$u = \frac{\partial \varphi}{\partial x} = \varphi_x \quad (9.29a)$$

$$v = \frac{\partial \varphi}{\partial y} = \varphi_y \quad (9.29b)$$

$$w = \frac{\partial \varphi}{\partial z} = \varphi_z \quad (9.29c)$$

where the symbol φ_x is shorthand for $\partial \varphi / \partial x$, φ_{xx} is correspondingly $\partial^2 \varphi / \partial x^2$, and φ_{xy} is $\partial^2 \varphi / \partial x \partial y$.

Using the Cartesian notation, it is easy to see that the condition of irrotationality is the necessary and sufficient condition for the existence of a scalar potential function whose gradient is the velocity. For, using Eqs. 9.29, and noting that the order of differentiation of a point function with continuous derivatives is immaterial, we see that

$$\frac{\partial u}{\partial y} - \frac{\partial v}{\partial x} = \frac{\partial}{\partial y} \frac{\partial \varphi}{\partial x} - \frac{\partial}{\partial x} \frac{\partial \varphi}{\partial y} = 0$$

$$\frac{\partial v}{\partial z} - \frac{\partial w}{\partial y} = \frac{\partial}{\partial z} \frac{\partial \varphi}{\partial y} - \frac{\partial}{\partial y} \frac{\partial \varphi}{\partial z} = 0$$

$$\frac{\partial w}{\partial x} - \frac{\partial u}{\partial z} = \frac{\partial}{\partial x} \frac{\partial \varphi}{\partial z} - \frac{\partial}{\partial z} \frac{\partial \varphi}{\partial x} = 0$$

which show that the conditions of irrotationality specified by Eq. 9.17 are automatically satisfied by the assumption that a velocity potential exists.

Eqs. 9.29 may be summarized in vector notation by

$$\mathbf{V} = \text{grad } \varphi = \nabla \varphi$$

That this definition of φ automatically satisfies the condition of irrotationality is seen by writing

$$2\mathbf{q} \equiv \nabla \times \mathbf{V} = \nabla \times \nabla \varphi = 0$$

where the last term is set equal to zero because the cross product of two parallel vectors is zero.

The concept of the velocity potential derives historically from the concept in mechanics of the potential of a force. It may be recalled that for conservative systems, the work, or the line integral of the force, is zero around a closed curve, and hence a *force potential* exists whose derivative in any direction is the force in that direction.

Because a velocity potential always exists for irrotational motion, the terms *potential motion* and *irrotational motion* are often used interchangeably.

The Differential Equation of the Velocity Potential. We shall now derive a single differential equation representing the steady, irrotational, frictionless, isentropic flow of a perfect gas.

The condition of irrotationality is automatically satisfied through the introduction of the velocity potential, φ , which is assumed to be a point function with continuous derivatives, and which is defined through Eq. 9.29.

The principle of conservation of mass is represented by the continuity equation, Eq. 9.24, which, in terms of the velocity potential, takes the form

$$\frac{\partial}{\partial x} (\rho \varphi_x) + \frac{\partial}{\partial y} (\rho \varphi_y) + \frac{\partial}{\partial z} (\rho \varphi_z) = 0$$

or, expanding,

$$\rho(\varphi_{xx} + \varphi_{yy} + \varphi_{zz}) + \varphi_x \frac{\partial \rho}{\partial x} + \varphi_y \frac{\partial \rho}{\partial y} + \varphi_z \frac{\partial \rho}{\partial z} = 0 \quad (9.30)$$

Newton's second law under the conditions assumed here may be written in the form of the Euler equation:

$$dp = -\rho d\left(\frac{V^2}{2}\right) = -\rho d\left(\frac{u^2 + v^2 + w^2}{2}\right) = -\rho d\left(\frac{\varphi_x^2 + \varphi_y^2 + \varphi_z^2}{2}\right) \quad (9.31)$$

The sound velocity is given by $c^2 = (\partial p / \partial \rho)_s$, but, since we are in fact dealing with isentropic flow, this may be written in terms of the actual pressure and density changes. Thus, $c^2 = dp/d\rho$. Introducing Eq. 9.31, we obtain

$$dp = \frac{dp}{c^2} = -\frac{\rho}{c^2} d\left(\frac{\varphi_x^2 + \varphi_y^2 + \varphi_z^2}{2}\right)$$

from which, by differentiation, we get

$$\frac{\partial \rho}{\partial x} = -\frac{\rho}{c^2} (\varphi_x \varphi_{xx} + \varphi_y \varphi_{xy} + \varphi_z \varphi_{xz})$$

$$\frac{\partial \rho}{\partial y} = -\frac{\rho}{c^2} (\varphi_x \varphi_{yx} + \varphi_y \varphi_{yy} + \varphi_z \varphi_{yz})$$

$$\frac{\partial \rho}{\partial z} = -\frac{\rho}{c^2} (\varphi_x \varphi_{zx} + \varphi_y \varphi_{zy} + \varphi_z \varphi_{zz})$$

Substituting these expressions into Eq. 9.30 and rearranging, we finally obtain

$$\left(1 - \frac{\varphi_x^2}{c^2}\right) \varphi_{xx} + \left(1 - \frac{\varphi_y^2}{c^2}\right) \varphi_{yy} + \left(1 - \frac{\varphi_z^2}{c^2}\right) \varphi_{zz} - 2 \frac{\varphi_x \varphi_y}{c^2} \varphi_{xy} - 2 \frac{\varphi_y \varphi_z}{c^2} \varphi_{yz} - 2 \frac{\varphi_z \varphi_x}{c^2} \varphi_{xz} = 0 \quad (9.32)$$

The local sound velocity is, of course, not constant, but varies with φ according to Eq. 9.27:

$$c^2 = c_0^2 - \frac{k-1}{2} (u^2 + v^2 + w^2) = c_0^2 - \frac{k-1}{2} (\varphi_x^2 + \varphi_y^2 + \varphi_z^2) \quad (9.33)$$

Substitution of Eq. 9.33 into Eq. 9.32 would yield a single differential equation for φ in terms of x , y , and z , an equation which simultaneously satisfies the law of conservation of mass, Newton's second principle of motion, and the laws of thermodynamics.

DIRECT AND INVERSE METHODS. Having obtained Eqs. 9.32 and 9.33, how do we employ them for the solution of problems? Two approaches are possible:

(i) Most often, we are interested in the flow through a duct or around a body of known shape, and with certain additional boundary conditions as to velocity and pressure. We must, therefore, seek a function $\varphi(x, y, z)$ which satisfies Eq. 9.32 and which also satisfies all the boundary conditions. This is often difficult, if not impossible, and experience and intuition rather than a prescribed procedure are likely to lead to successful results. Thus, although for practical reasons the direct approach is preferable, it is often necessary to use the second approach.

(ii) In this case we find, more or less at random, functions $\varphi(x, y, z)$ which satisfy the differential equation, Eq. 9.32, and then proceed to determine the corresponding streamline patterns. If one or more of the streamlines coincides approximately with the shape of a solid body or duct which is of interest, then the solution is useful; otherwise, it is not. Evidently, this procedure is at best haphazard.

In either case, if we have a solution of Eq. 9.32 for φ in terms of x, y , and z , the entire flow pattern may then be determined. From Eq. 9.29 it is possible to calculate the three velocity components and the Mach Number at each point and thus to construct the streamline pattern. Furthermore, from the equations for isentropic flow, Eqs. 4.14a, 4.14b, and 4.14c, all the fluid properties may be found at each point. The integration of the pressure-area forces on the solid boundaries then gives the resultant force acting on the duct or on the body immersed in the stream.

MATHEMATICAL REMARKS. Mathematically speaking, Eq. 9.32 is of the second order. A differential equation is said to be *linear* when the dependent variable and its derivatives appear only in linear form. In Eq. 9.32, however, we find quadratic terms of the form φ_x^2 , and cubic terms of the forms $\varphi_x^2\varphi_{xx}$ and $\varphi_x\varphi_y\varphi_{xy}$, which means that Eq. 9.32 is nonlinear. An important feature of linear equations is that solutions may be superposed; that is, if $\varphi_1(x, y, z)$ and $\varphi_2(x, y, z)$ are respective solutions of a linear differential equation, then $A_1\varphi_1 + A_2\varphi_2$ is also a solution, where A_1 and A_2 are arbitrary constants. Many of the mathematical difficulties encountered in compressible fluid mechanics are traceable to the fact that the equations are nonlinear, for it is not possible to build up complex solutions by superposition of a few simple, known solutions. Later, it will be seen that, at the expense of other complications, the *hodograph method* removes this difficulty, for the differential equations prove to be linear when the velocity components rather than the physical coordinates are used as the independent variables.

PLANE, TWO-DIMENSIONAL FLOW. For plane, two-dimensional flow, Eqs. 9.32 and 9.33 are simplified to give

$$\left(1 - \frac{\varphi_x^2}{c^2}\right)\varphi_{xx} + \left(1 - \frac{\varphi_y^2}{c^2}\right)\varphi_{yy} - 2\frac{\varphi_x\varphi_y}{c^2}\varphi_{xy} = 0 \quad (9.34)$$

$$c^2 = c_0^2 - \frac{k-1}{2}(\varphi_x^2 + \varphi_y^2) \quad (9.35)$$

INCOMPRESSIBLE FLOW. When the flow is incompressible, the sound velocity is infinite compared to the stream velocity, so that Eq. 9.32 becomes

$$\frac{\partial^2\varphi}{\partial x^2} + \frac{\partial^2\varphi}{\partial y^2} + \frac{\partial^2\varphi}{\partial z^2} = 0 \quad (9.36)$$

For plane, two-dimensional flow Eq. 9.34 takes the form

$$\frac{\partial^2\varphi}{\partial x^2} + \frac{\partial^2\varphi}{\partial y^2} = 0 \quad (9.37)$$

These may be recognized as two forms of *Laplace's equation*, an equation which plays an important role in such other fields as heat conduction through a solid and flow of electricity through a conductor. Many of the solutions which have been found in these well-explored fields may therefore be borrowed to give solutions in the field of incompressible fluid mechanics; furthermore, analogue techniques may be employed so that experimental results in one field may be directly applied to one of the other fields.

In two-dimensional, incompressible flow, the mathematical techniques are especially convenient, for it may be shown that Eq. 9.37 is satisfied by both the real and imaginary parts of any analytic function of a complex variable. Thus, the formal mathematical methods in the theory of functions of a complex variable may be applied to plane, incompressible flow.

Since Eqs. 9.36 and 9.37 are linear, solutions may be superposed. Consequently, even the second method described previously has been fruitful in incompressible flow, for after some experience it becomes possible to select a few simple solutions which when superposed will give a flow pattern approximating the pattern desired.

The Differential Equation in Cylindrical Coordinates. For certain types of problems, such as flow over bodies of revolution, it is convenient to use cylindrical coordinates. We shall adopt the notation shown in Fig. 9.13, where u , v , and w are the velocity components in the r -, ω -, and z -directions, respectively.

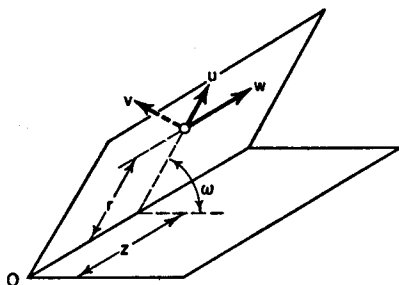


FIG. 9.13. Nomenclature for cylindrical coordinate system.

coordinates. By either method we obtain the following relations:

Irrotationality.

$$\frac{\partial u}{\partial \omega} - \frac{\partial(vr)}{\partial r} = 0; \quad \frac{\partial(vr)}{\partial z} - \frac{\partial w}{\partial \omega} = 0; \quad \frac{\partial w}{\partial r} - \frac{\partial u}{\partial z} = 0 \quad (9.39)$$

Definition of φ .

$$u = \frac{\partial \varphi}{\partial r} = \varphi_r; \quad v = \frac{1}{r} \frac{\partial \varphi}{\partial \omega} = \frac{\varphi_\omega}{r}; \quad w = \frac{\partial \varphi}{\partial z} = \varphi_z \quad (9.40)$$

Equation of continuity.

$$\frac{\partial}{\partial r} (\rho u) + \frac{\partial}{\partial \omega} (\rho v) + r \frac{\partial}{\partial z} (\rho w) = 0 \quad (9.41)$$

Euler equation.

$$dp = -\frac{\rho}{2} d \left(\varphi_r^2 + \frac{\varphi_\omega^2}{r^2} + \varphi_z^2 \right) \quad (9.42)$$

Sound velocity in isentropic process.

$$c^2 = dp/d\rho \quad (9.43)$$

The combination of Eqs. 9.40 to 9.43 in the same manner as that used previously for Cartesian coordinates yields finally

$$\left(1 - \frac{\varphi_r^2}{c^2}\right) \varphi_{rr} + \left(1 - \frac{\varphi_\omega^2}{r^2 c^2}\right) \frac{\varphi_{\omega\omega}}{r^2} + \left(1 - \frac{\varphi_z^2}{c^2}\right) \varphi_{zz} - 2 \frac{\varphi_r \varphi_\omega}{r^2 c^2} \varphi_{r\omega} - 2 \frac{\varphi_\omega \varphi_z}{r^2 c^2} \varphi_{\omega z} - 2 \frac{\varphi_z \varphi_r}{c^2} \varphi_{zr} + \frac{\varphi_r}{r} \left(1 + \frac{\varphi_\omega^2}{r^2 c^2}\right) = 0 \quad (9.44)$$

where

$$c^2 = c_0^2 - \frac{k-1}{2} \left(\varphi_r^2 + \frac{\varphi_\omega^2}{r^2} + \varphi_z^2 \right) \quad (9.45)$$

AXIALLY SYMMETRIC FLOW. When a body of revolution is placed in a uniform flow at zero angle of attack, the flow pattern will possess axial symmetry. The flow pattern is then the same in all meridian planes passing through the axis of symmetry, and the flow is two-dimensional.

Placing the z -axis along the direction of flow, and noting that for axial symmetry all the derivatives with respect to ω vanish, we find that Eqs. 9.44 and 9.45 reduce to

$$\left(1 - \frac{\varphi_r^2}{c^2}\right) \varphi_{rr} + \left(1 - \frac{\varphi_z^2}{c^2}\right) \varphi_{zz} - 2 \frac{\varphi_z \varphi_r}{c^2} \varphi_{rz} + \frac{\varphi_r}{r} = 0 \quad (9.46)$$

$$c^2 = c_0^2 - \frac{k-1}{2} (\varphi_r^2 + \varphi_z^2) \quad (9.47)$$

PLANE, TWO-DIMENSIONAL FLOW. When the flow pattern is identical in all planes normal to the z -axis, we obtain in polar coordinates the following equations corresponding to Eqs. 9.34 and 9.35:

$$\left(1 - \frac{\varphi_r^2}{c^2}\right) \varphi_{rr} + \left(1 - \frac{\varphi_\omega^2}{r^2 c^2}\right) \frac{\varphi_{\omega\omega}}{r^2} - 2 \frac{\varphi_r \varphi_\omega}{r^2 c^2} \varphi_{r\omega} + \frac{\varphi_r}{r} \left(1 + \frac{\varphi_\omega^2}{r^2 c^2}\right) = 0 \quad (9.48)$$

$$c^2 = c_0^2 - \frac{k-1}{2} \left(\varphi_r^2 + \frac{\varphi_\omega^2}{r^2} \right) \quad (9.49)$$

9.9. Differential Equations in Terms of the Stream Function

The Stream Function. Just as the condition of irrotationality is the necessary and sufficient condition for the existence of a velocity potential, so the equation of continuity for steady, two-dimensional flow is the necessary and sufficient condition that another point function, the *stream function*, exist. The flow need be two-dimensional in the sense that only two space coordinates are necessary to describe the motion, so that both plane flow and axially symmetric flow fall in this category.

Considering two-dimensional, plane, steady flow, and using Cartesian coordinates, the continuity equation may be written

$$\frac{\partial}{\partial x} (\rho u) + \frac{\partial}{\partial y} (\rho v) = 0 \quad (9.50)$$

We now define the stream function through the relations

$$u = \frac{\rho_0}{\rho} \frac{\partial \psi}{\partial y} = \frac{\rho_0}{\rho} \psi_y \quad (9.51a)$$

$$v = -\frac{\rho_0}{\rho} \frac{\partial \psi}{\partial x} = -\frac{\rho_0}{\rho} \psi_x \quad (9.51b)$$

where ρ_0 is the isentropic stagnation density (or any other convenient constant) and is brought in so that ψ will have the same dimensions as the velocity potential.

Next, we form the expression

$$\frac{\partial}{\partial x}(\rho u) + \frac{\partial}{\partial y}(\rho v) = \rho_0 \left(\frac{\partial}{\partial x} \frac{\partial \psi}{\partial y} - \frac{\partial}{\partial y} \frac{\partial \psi}{\partial x} \right)$$

If ψ is a point function, the order of differentiation is immaterial. By comparison of the foregoing equation with Eq. 9.50 we see that the statement that there exists a point function ψ defined through Eq. 9.51 is equivalent to the statement of the continuity equation. Conversely, the continuity equation is the necessary and sufficient condition that ψ be a point function.

The magnitude of the velocity vector at any point is given in terms of the stream function by the relation

$$V^2 = u^2 + v^2 = \left(\frac{\rho_0}{\rho} \right)^2 (\psi_x^2 + \psi_y^2) \quad (9.52)$$

PHYSICAL INTERPRETATION OF STREAM FUNCTION. What is the physical significance, if any, of the stream function? Since ψ is a point function we may write

$$d\psi = \frac{\partial \psi}{\partial x} dx + \frac{\partial \psi}{\partial y} dy = \frac{1}{\rho_0} (\rho u dy - \rho v dx) \quad (9.53)$$

Now, referring to Fig. 9.14, the mass rate of flow dw across any surface AB (of unit width normal to the paper) connecting two neighboring surfaces of constant ψ is given by

$$dw = \rho u dy - \rho v dx$$

and hence we see that the change in the magnitude of ψ between two lines of constant ψ is a measure of the mass rate of flow between the two ψ lines, according to the relations

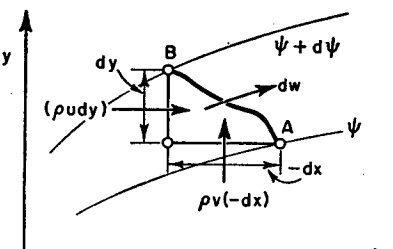
$$dw = \rho_0 d\psi \quad (9.54a)$$

$$w = \rho_0(\psi_B - \psi_A) \quad (9.54b)$$

FIG. 9.14. Illustrates physical significance of stream function.

Since, for steady flow, the mass rate of flow between streamlines is constant, it follows that lines of constant ψ are streamlines, hence the term "stream function."

The Differential Equation of the Stream Function. We shall now derive a single differential equation representing the steady, two-dimensional, irrotational, frictionless, isentropic flow of a perfect gas.



The equation of continuity is automatically satisfied through the introduction of the point function ψ as defined by Eq. 9.51.

In terms of the stream function, the condition of irrotationality (Eq. 9.17a) takes the form

$$\frac{\partial}{\partial y} \left(\frac{\rho_0}{\rho} \frac{\partial \psi}{\partial y} \right) = \frac{\partial}{\partial x} \left(- \frac{\rho_0}{\rho} \frac{\partial \psi}{\partial x} \right)$$

or, after differentiation and rearrangement, the equation of irrotationality becomes

$$\rho(\psi_{xx} + \psi_{yy}) = \psi_x \frac{\partial \rho}{\partial x} + \psi_y \frac{\partial \rho}{\partial y} \quad (9.55)$$

From the Euler equation and the expression for the sound velocity in isentropic flow, we obtain

$$d\rho = \frac{dp}{c^2} = - \frac{\rho}{2c^2} d(u^2 + v^2) = - \frac{\rho}{2c^2} d \left[\left(\frac{\rho_0}{\rho} \right)^2 (\psi_x^2 + \psi_y^2) \right]$$

or

$$d\rho = - \frac{\rho}{c^2} \left[\left(\frac{\rho_0}{\rho} \right)^2 (\psi_x d\psi_x + \psi_y d\psi_y) - (\psi_x^2 + \psi_y^2) \left(\frac{\rho_0}{\rho} \right)^2 \frac{dp}{\rho} \right] \quad (9.56)$$

The partial derivatives $\partial \rho / \partial x$ and $\partial \rho / \partial y$ may now be formed from Eq. 9.56. When these derivatives are substituted into Eq. 9.55, and the resulting expression simplified, there is obtained

$$\left[1 - \left(\frac{\rho_0}{\rho} \right)^2 \frac{\psi_y^2}{c^2} \right] \psi_{xx} + \left[1 - \left(\frac{\rho_0}{\rho} \right)^2 \frac{\psi_x^2}{c^2} \right] \psi_{yy} + 2 \left(\frac{\rho_0}{\rho} \right)^2 \frac{\psi_x \psi_y}{c^2} \psi_{xy} = 0 \quad (9.57)$$

where, from Eqs. 9.27 and 9.52,

$$c^2 = c_0^2 - \frac{k-1}{2} \left(\frac{\rho_0}{\rho} \right)^2 (\psi_x^2 + \psi_y^2) \quad (9.58)$$

and, from Eqs. 4.14c and 9.52,

$$\frac{\rho_0}{\rho} = \left[1 + \frac{k-1}{2} \left(\frac{\rho_0}{\rho} \right)^2 \frac{\psi_x^2 + \psi_y^2}{c^2} \right]^{\frac{1}{k-1}} \quad (9.59)$$

Eqs. 9.57, 9.58, and 9.59 on the one hand are completely equivalent to Eqs. 9.34 and 9.35 on the other. However, the differential equations in terms of φ are simpler in form than those in terms of ψ , and hence it is customary to work with Eq. 9.34.

INCOMPRESSIBLE FLOW. For incompressible flow, the sound velocity is infinite relative to the velocity of the gas, and Eq. 9.57 reduces to

$$\psi_{xx} + \psi_{yy} = 0 \quad (9.60)$$

This is the Laplace equation in two dimensions, and because of its similarity in form with Eq. 9.37, a solution for the potential lines in plane, incompressible flow represents also a solution for the streamlines, and vice versa.

Axially Symmetric Flow. Since in steady, axially symmetric flow there are only two space coordinates, the statement of the continuity equation is the necessary and sufficient condition for the existence of a stream function. Bearing in mind that partial derivatives with respect to ω are zero, Eq. 9.41 takes the form

$$\frac{\partial}{\partial r}(\rho ur) + r \frac{\partial}{\partial z}(\rho w) = 0 \quad (9.61a)$$

But, since r is independent of z , this may be written

$$\frac{\partial}{\partial r}(\rho ur) + \frac{\partial}{\partial z}(\rho wr) = 0 \quad (9.61b)$$

It may be verified by direct substitution that this relation is automatically satisfied by a point function ψ defined by

$$u = -\frac{\rho_0}{\rho} \frac{1}{r} \frac{\partial \psi}{\partial z} \quad (9.62a)$$

$$w = \frac{\rho_0}{\rho} \frac{1}{r} \frac{\partial \psi}{\partial r} \quad (9.62b)$$

The equation of irrotationality is now

$$\frac{\partial}{\partial r} \left(\frac{\rho_0}{\rho} \frac{1}{r} \frac{\partial \psi}{\partial r} \right) = \frac{\partial}{\partial z} \left(-\frac{\rho_0}{\rho} \frac{1}{r} \frac{\partial \psi}{\partial z} \right) \quad (9.63)$$

Using the Euler equation and the expression for the sound velocity in isentropic flow, we get

$$d\rho = \frac{dp}{c^2} = -\frac{\rho}{2c^2} d \left[\left(\frac{\rho_0}{\rho} \right)^2 \frac{1}{r^2} (\psi_r^2 + \psi_z^2) \right] \quad (9.64)$$

Combination of Eqs. 9.63 and 9.64 in a manner similar to that described previously finally yields

$$\begin{aligned} & \left[1 - \left(\frac{\rho_0}{\rho} \right)^2 \frac{1}{r^2} \frac{\psi_z^2}{c^2} \right] \psi_{rr} + \left[1 - \left(\frac{\rho_0}{\rho} \right)^2 \frac{1}{r^2} \frac{\psi_r^2}{c^2} \right] \psi_{zz} \\ & + 2 \left(\frac{\rho_0}{\rho} \right)^2 \frac{1}{r^2} \frac{\psi_r \psi_z}{c^2} \psi_{rz} - \frac{\psi_r}{r} = 0 \end{aligned} \quad (9.65)$$

where

$$c^2 = c_0^2 - \frac{k-1}{2} \left[\left(\frac{\rho_0}{\rho} \right)^2 \frac{1}{r^2} (\psi_z^2 + \psi_r^2) \right] \quad (9.66)$$

and

$$\frac{\rho_0}{\rho} = \left[1 + \frac{k-1}{2} \left(\frac{\rho_0}{\rho} \right)^2 \frac{1}{r^2} \frac{\psi_z^2 + \psi_r^2}{c^2} \right]^{\frac{1}{k-1}} \quad (9.67)$$

9.10. Relations Between the Velocity Potential and the Stream Function

For the velocity potential to exist it is only necessary that the flow be irrotational; hence we may employ the velocity potential for unsteady flow or for three-dimensional flow. For the stream function to exist it is only necessary that the flow be steady and describable by two space coordinates; hence the stream function may be used when the flow is rotational. However, it should be noted that the differential equations for φ and ψ which have been developed in this chapter refer to flow patterns which are both steady and irrotational. If the flow were unsteady, Eq. 9.32 would be different in form. Likewise, if the flow were rotational, Eq. 9.57 would be different in form.

Orthogonality of Streamlines and Equipotential Lines. When the flow is steady, irrotational, and two-dimensional, the stream function and velocity potential are related through Eqs. 9.29 and 9.51:

$$u = \varphi_x = \frac{\rho_0}{\rho} \psi_y \quad (9.68)$$

$$v = \varphi_y = -\frac{\rho_0}{\rho} \psi_x \quad (9.69)$$

That the lines of constant ψ are also streamlines may be shown by noting that, since ψ is a point function,

$$d\psi = \psi_x dx + \psi_y dy$$

Setting $d\psi$ equal to zero and using Eqs. 9.68 and 9.69, we find the slope of a line of constant ψ to be given by

$$\left(\frac{dy}{dx} \right)_\psi = -\frac{\psi_x}{\psi_y} = \frac{v}{u}$$

But, by definition, the slope of a streamline is given by

$$\left(\frac{dy}{dx} \right)_{\text{streamline}} = \frac{v}{u}$$

and hence the ψ lines and streamlines are identical.

Turning next to a consideration of the equipotential lines, we have, similarly,

$$d\varphi = \varphi_x dx + \varphi_y dy$$

Using Eqs. 9.68 and 9.69, we get for the slope of an equipotential line,

$$\left(\frac{dy}{dx}\right)_\varphi = -\frac{\varphi_x}{\varphi_y} = -\frac{u}{v}$$

so that

$$\left(\frac{dy}{dx}\right)_\varphi = -1 / \left(\frac{dy}{dx}\right)_\psi \quad (9.70)$$

from which we conclude that a line of constant φ is normal to a line of constant ψ . In other words, the equipotential lines and streamlines form an *orthogonal network*.

Spacing of Net Lines. To investigate the relative spacing of the network, we note that the gradient of the potential in any direction is the velocity component in that direction. Referring to Fig. 9.15, the gradient of φ along the streamline gives the magnitude of the velocity vector,

$$V = \Delta\varphi/l$$

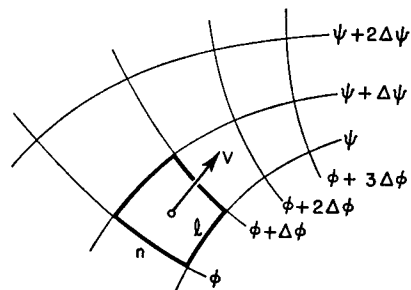


FIG. 9.15. Illustrates relation between streamlines and equipotential lines

ψ along the equipotential line, we have, for the resultant velocity

$$V = \frac{\rho_0 \Delta\psi}{\rho n}$$

We may arbitrarily select equal numerical magnitudes for the values of $\Delta\psi$ and $\Delta\varphi$ between neighboring lines in the grid. In that case we find that

$$\frac{l}{n} = \frac{\rho}{\rho_0} \quad (9.71)$$

Since ρ/ρ_0 cannot be greater than unity, it follows that the potential lines are more closely spaced than the streamlines. And, since ρ/ρ_0 is near unity at low Mach Numbers and far less than unity at high Mach Numbers, the difference between the spacings will be most marked in

regions of high Mach Number. These results may be verified by inspection of the potential and streamline nets of Fig. 9.16 for the two-dimensional flow past a circular cylinder in the x direction.

INCOMPRESSIBLE FLOW. For incompressible flow each small element of the net is, in the limit, a square. Steady, two-dimensional, incompressible, irrotational motion might even be said to be a problem in pure geometry, for any orthogonal network of lines, each small element of

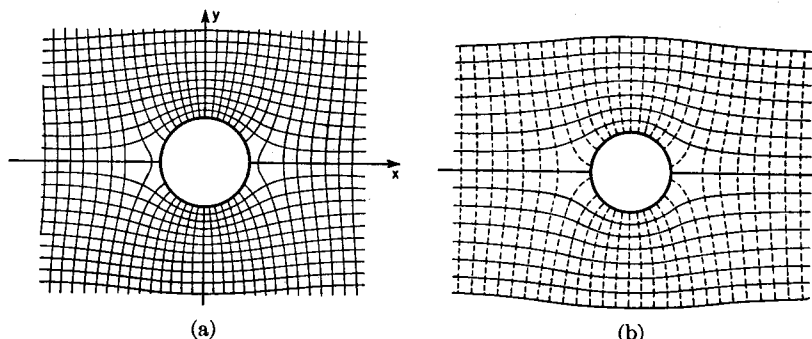


FIG. 9.16. Streamlines and equipotential lines for two-dimensional, irrotational, isentropic, frictionless flow past circular cylinder (after Busemann).

- (a) Incompressible ($M = 0$).
- (b) Free-stream Mach Number of 0.4, giving nearly sonic velocity at shoulders of cylinder.

which is a square, represents a possible solution to the equations of motion. In this respect we note that the conditions of irrotationality and steady flow are purely kinematic for an incompressible fluid, and only these conditions enter into the derivation of Laplace's equation for the velocity potential or stream function. The dynamic conditions, represented by Bernoulli's equation, are not at all involved in the determination of the streamline pattern. For these reasons, incompressible flow patterns may be at least rudely constructed by drawing square nets by trial with the help of paper, pencil, and eraser. Or a more organized procedure, such as the relaxation method, may be used. In any case, for incompressible flow the φ lines and ψ lines are interchangeable, so that any single flow pattern embodies two possible solutions.

COMPRESSIBLE FLOW. The situation is quite different for compressible flow. Although the condition of irrotationality remains kinematic, the equation of continuity contains the density, which is in turn related to the pressure and, therefore, to the dynamic requirements. In compressible flow the streamline and potential network depends on both kinematic and dynamic considerations, and the φ and ψ lines when interchanged do not represent a solution.

REFERENCES AND SELECTED BIBLIOGRAPHY

1. PRANDTL, L., and TIETJENS, O. G. *Fundamentals of Hydro- and Aeromechanics*. New York: McGraw-Hill Book Co., Inc., 1934.
2. PRANDTL, L., in *The Physics of Solids and Fluids*, by EWALD, POSCHL, and PRANDTL. 2d Ed. London: Blackie & Sons, 1936.
3. LAMB, H. *Hydrodynamics*. 6th Ed. New York: Dover Publications, 1945.
4. SAUER, R. *Theoretical Gas Dynamics*. Translated by F. K. HILL and R. A. ALPHER. Ann Arbor: J. W. Edwards, 1947.
5. MILNE-THOMPSON, L. M. *Theoretical Hydromechanics*. 2d Ed. London: Macmillan & Co., Ltd. 1949.

PROBLEMS

- 9.1. Show that Euler's equation for unsteady, irrotational motion can, with the introduction of the velocity potential φ , be integrated to give

$$\frac{\partial \varphi}{\partial t} + \int \frac{dp}{\rho} + \frac{V^2}{2} = f(t)$$

where the "constant" of integration $f(t)$ is a function of time only.

- 9.2. In Art. 9.3 Euler's equations in Cartesian coordinates (Eq. 9.13) were obtained by applying Newton's second law of motion to a fluid particle of *fixed mass and identity*, and with sides $\delta x, \delta y, \delta z$.

Show that the same results may be derived by applying the momentum theorem to the flow through a cubical *control surface* fixed in space and with sides dx, dy, dz .

- 9.3. In Art. 9.6 the equation of continuity (Eq. 9.23) in Cartesian coordinates was derived by applying the principle of conservation of mass to conditions within and at the boundaries of a *control surface* fixed in space and with sides dx, dy, dz .

Show that the same result may be obtained by applying the principle of conservation of mass to the motion of a particle of *fixed mass and identity* and with sides $\delta x, \delta y, \delta z$.

- 9.4. Starting with first principles, verify Eqs. 9.39 through 9.45, expressing the steady, irrotational, frictionless, isentropic motion of a perfect gas in terms of the velocity potential and in terms of cylindrical coordinates.

- 9.5. Verify the derivation of Eq. 9.57.

- 9.6. Derive a single differential equation for steady, plane, two-dimensional, irrotational, frictionless, isentropic motion, expressing the stream function in terms of the polar coordinates r and ω .

- 9.7. Show that the stream function for axially symmetric flow, as defined by Eq. 9.62, defines surfaces which are generated by streamlines. Derive the relation between the magnitudes of ψ between two streamline surfaces and the corresponding mass rate of flow between these surfaces.

- 9.8. Consider axially symmetric flow, with the streamlines lying in planes containing the axis of symmetry. Use the following notation for a spherical system of coordinates:

- R radius vector, measured from the origin O
 σ angle of the radius vector with respect to the axis of symmetry
 u velocity component along radius vector
 v velocity component perpendicular to radius vector

- (a) Show that the condition of irrotationality may be written

$$\frac{\partial u}{\partial \sigma} = \frac{\partial}{\partial R} (Rv)$$

- (b) Show that the equation of continuity may be written

$$\frac{\partial}{\partial R} (\rho u) + \frac{2}{R} (\rho u) + \frac{1}{R} \frac{\partial}{\partial \sigma} (\rho v) + \frac{\rho v}{R \tan \sigma} = 0$$

- 9.9. Show that the stream function

$$\psi = \frac{w}{2\pi\rho_0} \omega$$

represents in polar coordinates a plane source motion for which w is the mass flow issuing from the line source per unit length of source.

Assuming the flow is frictionless and adiabatic, calculate the corresponding expression for the velocity potential for

- (a) Incompressible flow
(b) Compressible flow with a stagnation sound velocity c_0

- 9.10. Show that the potential function

$$\varphi = \frac{\Gamma}{2\pi} \omega$$

satisfies Eq. 9.48 and that it represents a line vortex of circulation Γ .

Assuming the motion to be steady and frictionless, and that all streamlines have the same entropy and stagnation temperature, determine the corresponding expression for the stream function ψ for

- (a) Incompressible flow
(b) Compressible flow with a stagnation sound velocity c_0

PART IV
SUBSONIC FLOW

Chapter 10

TWO-DIMENSIONAL, SUBSONIC FLOW WITH SMALL PERTURBATIONS

10.1. Introductory Remarks

Although the differential equations in terms of the velocity potential for steady, irrotational, isentropic motion were derived rather easily in the preceding chapter, exact solutions of these equations for particular flow problems often involve such complex or tedious mathematical procedures as to be impractical. Two courses then seem to be open—either (i) to find exact solutions for a relatively few problems in the hope of obtaining a qualitative understanding of the nature of other flow patterns for which solutions are not obtainable; or (ii) to find simple, though approximate, solutions suitable for practical computations. Both methods of approach yield useful information and, in a sense, complement each other, as the few exact solutions serve as a check on the accuracy and reliability of the approximate methods. In this chapter we shall show how the second method may be applied to some important problems of two-dimensional, subsonic flow.

The assumption of two-dimensional flow serves as a first approximation to the flow past the wings of airplanes and to the flow through the blade systems of propellers and of axial-flow compressors and turbines. In many such applications the velocity perturbations produced by the body or bodies immersed in the flowing stream are small, because the bodies are very thin. Here we have the essence of the linearized method—that the flow pattern may be thought of as the combination of a uniform, parallel velocity on which is superposed small perturbation velocities.

The advantage of making such an assumption, we shall see, lies in the fact that the equation of motion is greatly simplified and also becomes linear. From this method, which is called the *linearized theory* or the *method of small perturbations*, we shall draw useful approximate information as to the effects of Mach Number for subsonic flow. The linearized theory also makes evident an approximate *similarity law* for subsonic flow; that is, a rule connecting the pressure field of a given compressible flow with that of a related incompressible flow. Analogous similarity laws for transonic, supersonic, and hypersonic flow are derived in later chapters.

NOMENCLATURE

<i>a</i>	angle of attack	<i>V</i>	velocity
<i>A</i>	area	<i>x, y</i>	Cartesian coordinates
<i>c</i>	sonic speed		
<i>c_p</i>	specific heat at constant pressure	β	$\sqrt{1 - M_\infty^2}$
<i>C_L</i>	coefficient of lift	γ	camber ratio
<i>C_M</i>	moment coefficient	δ	thickness ratio
<i>C_P</i>	pressure coefficient	Δc_p	interference pressure coefficient
<i>h</i>	amplitude of wave-shaped wall	λ	affine transformation factor
<i>k</i>	ratio of specific heats	ρ	mass density
<i>l</i>	chord length of air foil; also wave length of wave-shaped wall	φ	perturbation velocity potential
<i>L</i>	a characteristic dimension; also lift force	Φ	velocity potential
<i>M</i>	Mach Number		
<i>p</i>	pressure	() ₀	signifies stagnation state
<i>R</i>	gas constant	() _∞	signifies free-stream condition
<i>T</i>	absolute temperature	() _s	signifies state at solid boundaries
<i>u</i>	perturbation velocity compo- nent in <i>x</i> -direction	()'	signifies incompressible flow ($M_\infty = 0$)
<i>v</i>	perturbation velocity compo- nent in <i>y</i> -direction	[O]	signifies "of the order of mag- nitude of"

10.2. Linearization of the Potential Equation

Equation of Motion. For steady, two-dimensional, irrotational, isentropic motion, the differential equation for the velocity potential is given by Eqs. 9.34 and 9.35:

$$\left(1 - \frac{\Phi_x^2}{c^2}\right)\Phi_{xx} + \left(1 - \frac{\Phi_y^2}{c^2}\right)\Phi_{yy} - 2\frac{\Phi_x\Phi_y}{c^2}\Phi_{xy} = 0 \quad (10.1)$$

$$c^2 = c_0^2 - \frac{k-1}{2}(\Phi_x^2 + \Phi_y^2) \quad (10.2)$$

where the symbol Φ represents the complete velocity potential as defined in Chapter 9, and is to be distinguished from the perturbation velocity potential denoted by φ in this chapter.

The Perturbation Components. We now assume the velocity at any point to be given by the vector sum of a constant velocity V_∞ along the *x*-axis, together with perturbation velocities u and v in the *x*- and *y*-directions, respectively. As an example, for a thin profile moving through an infinite medium (Fig. 10.1) at the speed $-V_\infty$, the velocity

ART. 10.2 LINEARIZATION OF THE POTENTIAL EQUATION

of the gas relative to the profile would be V_∞ at points very far from the profile; and near the profile the *x*- and *y*-components would be $(V_\infty + u)$ and v , respectively. The *perturbation velocities*, u and v , are considered to be small compared with the *free-stream velocity*, V_∞ .

Following this line of thought, we express the velocity potential Φ as the sum of the potential due to the main velocity V_∞ and of a *perturbation potential* φ associated with the perturbation velocities u and v :

$$\Phi = V_\infty x + \varphi \quad (10.3)$$

FIG. 10.1. Nomenclature.

Taking derivatives, and noting that V_∞ is a constant, we obtain

$$\Phi_x = V_\infty + \varphi_x = V_\infty + u \quad (10.4)$$

$$\Phi_{xx} = \varphi_{xx} = \frac{\partial u}{\partial x} \quad (10.5)$$

$$\Phi_y = \varphi_y = v \quad (10.6)$$

$$\Phi_{yy} = \varphi_{yy} = \frac{\partial v}{\partial y} \quad (10.7)$$

$$\Phi_{xy} = \varphi_{xy} = \frac{\partial u}{\partial y} = \frac{\partial v}{\partial x} \quad (10.8)$$

Comparisons of Orders of Magnitude. We wish to simplify Eq. 10.1 by dropping those terms which, according to the assumption of small perturbations, may be regarded as negligible compared with the remaining terms. The second derivatives in Eq. 10.1, according to Eqs. 10.5, 10.7, and 10.8, are given by

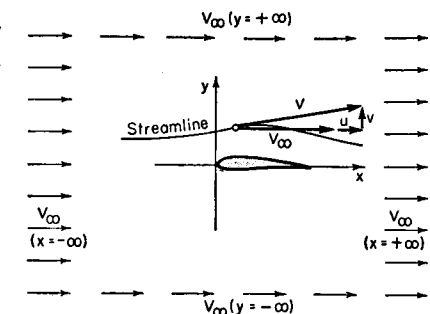
$$\Phi_{xx} = \frac{\partial u}{\partial x}; \quad \Phi_{yy} = \frac{\partial v}{\partial y}; \quad \Phi_{xy} = \frac{\partial u}{\partial y} = \frac{\partial v}{\partial x}$$

Now the perturbation velocities u and v are of the same order of magnitude. Also, since Eq. 10.1 is to be applied throughout the entire flow field, the lengths in the denominators of $\partial u/\partial x$, $\partial v/\partial y$, and $\partial v/\partial x$ must all be regarded as being of the same order of magnitude. Hence, the derivatives Φ_{xx} , Φ_{xy} , and Φ_{yy} are all of the same order of magnitude.

We next examine the relative magnitudes of the coefficients of Φ_{xx} , Φ_{yy} , and Φ_{xy} . Using Eqs. 10.2, 10.4, and 10.6, we obtain, upon noting that c_0 is constant,

$$c^2 + \frac{k-1}{2}[(V_\infty + u)^2 + v^2] = c_\infty^2 + \frac{k-1}{2}V_\infty^2$$

where c_∞ is the sound velocity at points where the stream velocity is V_∞ .



Simplifying and rearranging this expression, we obtain

$$\frac{c_\infty^2}{c^2} = \frac{1}{1 - \frac{k-1}{2} M_\infty^2 \left(2 \frac{u}{V_\infty} + \frac{u^2 + v^2}{V_\infty^2} \right)} \quad (10.9)$$

where M_∞ is the free-stream Mach Number, defined by

$$M_\infty = V_\infty/c_\infty \quad (10.10)$$

Expanding Eq. 10.9 with the help of the binomial theorem, we obtain

$$\frac{c_\infty^2}{c^2} = 1 + \frac{k-1}{2} M_\infty^2 \left(2 \frac{u}{V_\infty} + \frac{u^2 + v^2}{V_\infty^2} \right) + [O] \left(M_\infty^4 \frac{u^2}{V_\infty^2} \right) + \dots \quad (10.11)$$

where the symbol $[O]$ means "of the order of magnitude of."

For the coefficient of Φ_{xx} we get, using Eq. 10.4,

$$1 - \frac{\Phi_x^2}{c^2} = 1 - \frac{(V_\infty + u)^2}{c^2} = 1 - \frac{(V_\infty + u)^2}{V_\infty^2} \frac{V_\infty^2}{c_\infty^2} \frac{c_\infty^2}{c^2}$$

Introducing Eqs. 10.10 and 10.11, this expression becomes

$$\begin{aligned} 1 - \frac{\Phi_x^2}{c^2} &= 1 - M_\infty^2 - 2M_\infty^2 \frac{u}{V_\infty} - (k-1)M_\infty^4 \frac{u}{V_\infty} \\ &\quad + [O] \left(M_\infty^2 \frac{u^2}{V_\infty^2} \right) + \dots \end{aligned}$$

together with terms of higher order. We now assume that the perturbation velocities are so small compared with V_∞ that we may write

$$M_\infty^2 \left(\frac{u}{V_\infty} \right)^2 \ll 1 \quad (10.12)$$

$$M_\infty^2 \left(\frac{v}{V_\infty} \right)^2 \ll 1 \quad (10.13)$$

$$M_\infty^2 \left(\frac{uv}{V_\infty^2} \right) \ll 1 \quad (10.14)$$

Consequently the equation preceding Eq. 10.12 may be approximated by

$$1 - \frac{\Phi_x^2}{c^2} \cong 1 - M_\infty^2 - [2M_\infty^2 + (k-1)M_\infty^4] \frac{u}{V_\infty} \quad (10.15)$$

Turning now to the second term of Eq. 10.1, we have

$$1 - \frac{\Phi_y^2}{c^2} = 1 - \frac{v^2}{c^2} = 1 - \frac{v^2}{V_\infty^2} \frac{V_\infty^2}{c_\infty^2} \frac{c_\infty^2}{c^2}$$

Introducing Eqs. 10.10 and 10.11 as before, we obtain

$$1 - \frac{\Phi_y^2}{c^2} = 1 - M_\infty^2 \frac{v^2}{V_\infty^2} + [O] \left(M_\infty^4 \frac{uv^2}{V_\infty^3} \right) + \dots$$

However, with the assumption of Eq. 10.13, this becomes

$$1 - \frac{\Phi_y^2}{c^2} \cong 1 \quad (10.16)$$

For the coefficient of the third term of Eq. 10.1, we have

$$2 \frac{\Phi_x \Phi_y}{c^2} = 2 \frac{(V_\infty + u)v}{c^2} = 2 \frac{V_\infty v + uv}{V_\infty^2} \frac{V_\infty^2}{c_\infty^2} \frac{c_\infty^2}{c^2}$$

Again introducing Eqs. 10.10 and 10.11, we obtain

$$2 \frac{\Phi_x \Phi_y}{c^2} = 2M_\infty^2 \frac{v}{V_\infty} + [O] \left(M_\infty^2 \frac{uv}{V_\infty^2} \right) + \dots$$

Using the assumption of Eq. 10.14, however, this becomes

$$2 \frac{\Phi_x \Phi_y}{c^2} \cong 2M_\infty^2 \frac{v}{V_\infty} \quad (10.17)$$

Substituting Eqs. 10.5, 10.7, 10.8, 10.15, 10.16, and 10.17 into Eq. 10.1, we get the approximate differential equation

$$\begin{aligned} (1 - M_\infty^2) \left[1 - \left(\frac{2M_\infty^2}{1 - M_\infty^2} \right) \left(\frac{u}{V_\infty} \right) \left(1 + \frac{k-1}{2} M_\infty^2 \right) \right] \frac{\partial u}{\partial x} \\ + \frac{\partial v}{\partial y} - 2M_\infty^2 \frac{v}{V_\infty} \frac{\partial v}{\partial x} = 0 \end{aligned} \quad (10.18)$$

The Linearized Equation of the Velocity Potential. Unfortunately, despite the assumptions already made, this equation is not linear, since there remain the quadratic terms $u \partial u / \partial x$ and $v \partial v / \partial x$. We therefore introduce the further assumptions that

$$\frac{M_\infty^2}{1 - M_\infty^2} \frac{u}{V_\infty} \ll 1 \quad (10.19)$$

$$M_\infty^2 \frac{v}{V_\infty} \ll 1 \quad (10.20)$$

and thus we get the following linear differential equation:

$$(1 - M_\infty^2) \frac{\partial u}{\partial x} + \frac{\partial v}{\partial y} = 0; \quad \text{or} \quad \beta^2 \frac{\partial^2 \varphi}{\partial x^2} + \frac{\partial^2 \varphi}{\partial y^2} = 0 \quad (10.21a)$$

where

$$\beta = \sqrt{1 - M_\infty^2} \quad (10.21b)$$

Examination of Assumptions Underlying Linearized Equations. The assumptions underlying the linearized differential equation are embodied in Eqs. 10.12, 10.13, 10.14, 10.19, and 10.20. Examination of these equations indicates that the latter two include the former three, and are, therefore, the most stringent.

As M_∞ approaches unity, Eq. 10.19 becomes invalid. Hence, except for extraordinarily small perturbations, the conclusions set out in the remainder of the chapter are not valid for transonic flow, i.e., for values of M_∞ greater than about 0.8.

The perturbation ratios u/V_∞ and v/V_∞ depend chiefly on the thickness ratio of the body. The accuracy of Eqs. 10.19 and 10.20 will, for thin profiles, be good up to high subsonic (but not transonic) Mach Numbers. For thick profiles, on the other hand, the assumptions are reasonably valid only for very low Mach Numbers.

10.3. Linearization of the Pressure Coefficient

The pressure distribution in a given flow pattern is of primary practical importance. A knowledge of the pressure distribution is necessary for the calculation of the forces and moments produced by the fluid on solid boundaries. Moreover, the pressure gradient at a solid boundary influences the development of the boundary layer, and the nature of the pressure gradient must be known before the behavior of the boundary layer may be predicted.

Dimensional Analysis. Since we are dealing with an inviscid fluid, the motion of a fluid particle is determined by a balance between pressure forces and inertia forces. Let us assume that we are dealing with the flow of a particular gas past a series of geometrically similar bodies, so that in any particular experiment the specification of one characteristic dimension L (perhaps the length of the body) suffices to determine the body geometry.

The pressure forces on a given fluid particle are due to the differences in pressure acting on the various faces of the particle. They may, therefore, be represented by some characteristic pressure difference, $p - p_\infty$, and by the characteristic length L . Here p is the pressure at the desired point in the flow pattern and p_∞ is the free-stream static pressure.

The inertia force of the particle depends upon the local density and the local acceleration as well as upon the particle size. The local density is characterized by the free-stream density ρ_∞ together with some index of compressibility which is conveniently taken as the free-stream speed of sound c_∞ . The local acceleration may be characterized by the characteristic velocity V_∞ and the characteristic length L . The particle size is, of course, characterized by L .

From the foregoing considerations, we may write a physical equation in the implicit form

$$p - p_\infty = f(V_\infty, \rho_\infty, c_\infty, L)$$

which may be rearranged to give, implicitly,

$$\frac{p - p_\infty}{\frac{1}{2} \rho_\infty V_\infty^2} = f_1 \left(\frac{V_\infty}{c_\infty}, \rho_\infty, c_\infty, L \right)$$

Since the left-hand side has zero dimensions, the right-hand side must also be dimensionless. But ρ_∞ , c_∞ , and L can in no way be formed into a dimensionless group. From this we conclude that, when the physical equation is rearranged as indicated, these three terms disappear from the equation except insofar as ρ_∞ and c_∞ appear in the dimensionless groups.

PRESSURE COEFFICIENT. The group containing the local pressure is called the *pressure coefficient*, and may be variously written as

$$C_p = \frac{p - p_\infty}{\frac{1}{2} \rho_\infty V_\infty^2} = \frac{p_\infty (p/p_\infty - 1)}{\frac{1}{2} k p_\infty M_\infty^2} = \frac{\frac{p}{p_\infty} - 1}{\frac{1}{2} k M_\infty^2} \quad (10.22)$$

From the dimensional analysis we conclude that the local pressure coefficient at a given point depends only on the free-stream Mach Number M_∞ . The size of the body is seen to enter not at all. For the same free-stream Mach Number the pressures at corresponding points in two flows are, therefore, related through the condition that the value of C_p is the same at both points.

The Pressure Coefficient for Small Perturbations. We shall now develop a special form of Eq. 10.22 which is consistent with the assumptions of the linear theory. From the energy equation and the velocity vector diagram of Fig. 10.1, we may write

$$T_\infty - T = \frac{V^2 - V_\infty^2}{2c_p} = \frac{[(V_\infty + u)^2 + v^2] - V_\infty^2}{2c_p} = \frac{2uV_\infty + u^2 + v^2}{2c_p}$$

We now solve this expression for T/T_∞ , and, after employing the relations

$$c_\infty^2 = kRT_\infty$$

$$M_\infty = V_\infty/c_\infty$$

we obtain

$$\frac{T}{T_\infty} = 1 - \frac{k-1}{2} M_\infty^2 \left(2 \frac{u}{V_\infty} + \frac{u^2 + v^2}{V_\infty^2} \right) \quad (10.23)$$

Since the flow is isentropic, the pressure ratio may be written as

$$\frac{p}{p_\infty} = \left(\frac{T}{T_\infty} \right)^{\frac{k}{k-1}} = \left[1 - \frac{k-1}{2} M_\infty^2 \left(2 \frac{u}{V_\infty} + \frac{u^2 + v^2}{V_\infty^2} \right) \right]^{\frac{k}{k-1}}$$

We now note that the second term in the bracket is less than unity, and so we develop a series expansion for p/p_∞ with the help of the binomial theorem:

$$\frac{p}{p_\infty} = 1 - \frac{k}{2} M_\infty^2 \left(2 \frac{u}{V_\infty} + \frac{u^2 + v^2}{V_\infty^2} \right) + \frac{k}{8} M_\infty^4 \left[4 \frac{u^2}{V_\infty^2} + \dots \right] + \dots$$

Substituting this expression into Eq. 10.22, and simplifying, we get

$$C_p = -2 \frac{u}{V_\infty} \left[1 + \frac{1 + v^2/u^2 - M_\infty^2}{2} \frac{u}{V_\infty} + [O] \left(M_\infty^4 \frac{u^2 + v^2}{V_\infty^2} \right) + \dots \right] \quad (10.24)$$

We now introduce the assumptions of Eqs. 10.12, 10.14, and 10.19, and, since mathematical simplicity is the main purpose of the linearized theory, we make the additional assumption that

$$\frac{u}{V_\infty} \ll 1 \quad (10.25)$$

The final expression for the pressure coefficient of the linearized theory is then

$$C_p \cong -2 \frac{u}{V_\infty} \quad (10.26)$$

Eq. 10.25 is a more severe restriction than Eq. 10.19. However, in many applications, Eq. 10.26 for C_p is used only when comparing corresponding values of C_p for two flows wherein the two values of C_p do not differ by much. Such is the case, for example, in the formulation of the Gothert and Prandtl-Glauert similarity rules to be discussed later in this chapter. In cases of this sort, it may be shown by detailed consideration that the use of Eq. 10.26 in computing the ratio of two values of C_p involves only the assumption that $(u/V_\infty)^2 \ll 1$, rather than the assumption of Eq. 10.25.

10.4. Flow Past a Wave-Shaped Wall

We shall now investigate a particular solution ⁽¹⁾ of the linearized equations, the practical significance of which rests on the fact that in a relatively simple way we may demonstrate the quantitative and qualitative effects of compressibility on the streamline pattern and on the pressure distribution.

Velocity Potential. Let us consider the following expression for the perturbation velocity potential:

$$\varphi = \frac{V_\infty}{\beta} h \left(\sin \frac{2\pi x}{l} \right) e^{-2\pi\beta y/l} \quad (10.27)$$

where h and l are length constants whose physical meanings will be evident later and β is defined by Eq. 10.21b. Whether or not this assumed function satisfies the conditions of continuity, momentum, energy, and irrotationality depends on whether it satisfies Eq. 10.21a. To determine this, we first take derivatives as follows:

$$u = \frac{\partial \varphi}{\partial x} = \frac{V_\infty h}{\beta} \frac{2\pi}{l} \left(\cos \frac{2\pi x}{l} \right) e^{-2\pi\beta y/l} \quad (10.28)$$

$$\frac{\partial u}{\partial x} = \frac{\partial^2 \varphi}{\partial x^2} = - \frac{V_\infty h}{\beta} \left(\frac{2\pi}{l} \right)^2 \left(\sin \frac{2\pi x}{l} \right) e^{-2\pi\beta y/l} \quad (10.29)$$

$$v = \frac{\partial \varphi}{\partial y} = - V_\infty h \frac{2\pi}{l} \left(\sin \frac{2\pi x}{l} \right) e^{-2\pi\beta y/l} \quad (10.30)$$

$$\frac{\partial v}{\partial y} = \frac{\partial^2 \varphi}{\partial y^2} = \beta V_\infty h \left(\frac{2\pi}{l} \right)^2 \left(\sin \frac{2\pi x}{l} \right) e^{-2\pi\beta y/l} \quad (10.31)$$

Substitution of Eqs. 10.29 and 10.31 into Eq. 10.21a shows that the function $\varphi(x, y)$ of Eq. 10.27 satisfies the differential Eq. 10.21a identically. Hence we conclude that Eq. 10.27 represents a flow pattern satisfying the conditions of continuity, momentum, energy, and irrotationality.

Streamlines. To determine the form of the streamlines, we make use of the definition that the slope of the streamline is identical with the slope of the velocity vector, so that, referring to Fig. 10.1, we write

$$\left(\frac{dy}{dx} \right)_{\text{streamline}} = \frac{v}{u} = \frac{v/V_\infty}{1 + u/V_\infty} \quad (10.32)$$

The values of v/V_∞ and u/V_∞ are known in terms of x and y through Eqs. 10.28 and 10.30, but on substituting these values into Eq. 10.32 there seems to be no simple way of separating variables and thus integrating to find the equations of the streamlines. However, this difficulty may be avoided by introducing approximations in keeping with the assumptions of small perturbations. We write the identity

$$1 + \frac{u}{V_\infty} = 1 + \beta^2 \frac{u}{V_\infty} + (1 - \beta^2) \frac{u}{V_\infty} = 1 + \beta^2 \frac{u}{V_\infty} + M_\infty^2 \frac{u}{V_\infty}$$

Now, according to the assumption of Eq. 10.19, the value of $M_\infty^2 u/V_\infty$ is negligible compared with unity, hence

$$\left(\frac{dy}{dx}\right)_{\text{streamline}} \cong \frac{v/V_\infty}{1 + \beta^2 \frac{u}{V_\infty}} \quad (10.33)$$

Now, substituting u/V_∞ and v/V_∞ from Eqs. 10.28 and 10.30 into Eq. 10.33, and rearranging, we obtain

$$\begin{aligned} dy &= -2\pi \frac{h}{l} \left(\sin \frac{2\pi x}{l} \right) e^{-2\pi\beta y/l} dx - 2\pi\beta \frac{h}{l} \left(\cos \frac{2\pi x}{l} \right) e^{-2\pi\beta y/l} dy \\ &= h d \left[\left(\cos \frac{2\pi x}{l} \right) e^{-2\pi\beta y/l} \right] \end{aligned}$$

This may now be integrated directly to give the equation of the streamline,

$$y = \text{constant} + h \left(\cos \frac{2\pi x}{l} \right) e^{-2\pi\beta y/l} \quad (10.34)$$

where each streamline has associated with it a particular value of the constant of integration.

Suppose that the streamline for which the constant of integration is zero is taken to be a solid wall, defined by the coordinates y_s and x_s . If we also stipulate that the solid wall lies very close to the x -axis (i.e., y_s is very small), the value of the exponential term of Eq. 10.34 is nearly unity, and hence the shape of the solid wall may be expressed by the relation

$$y_s \cong h \cos \frac{2\pi x_s}{l} \quad (10.35)$$

At very large distances from the wall (i.e., very large values of y), it is evident from Eq. 10.34 that the streamlines have constant values of y and are therefore parallel to the x -axis.

The physical nature of the flow pattern defined by Eq. 10.27 is now clear. We are dealing with the flow past a wave-shaped wall which has the shape of a cosine curve. Referring to Eq. 10.35 and to Fig. 10.2, we see that l and h are the wave length and lateral amplitude, respectively, of the wave-shaped wall.

From Eqs. 10.28 and 10.30 we see that the perturbation velocities u and v are zero at very large values of y . This means that at an infinite distance from the wall the flow is parallel to the x -axis and has the uniform velocity V_∞ .

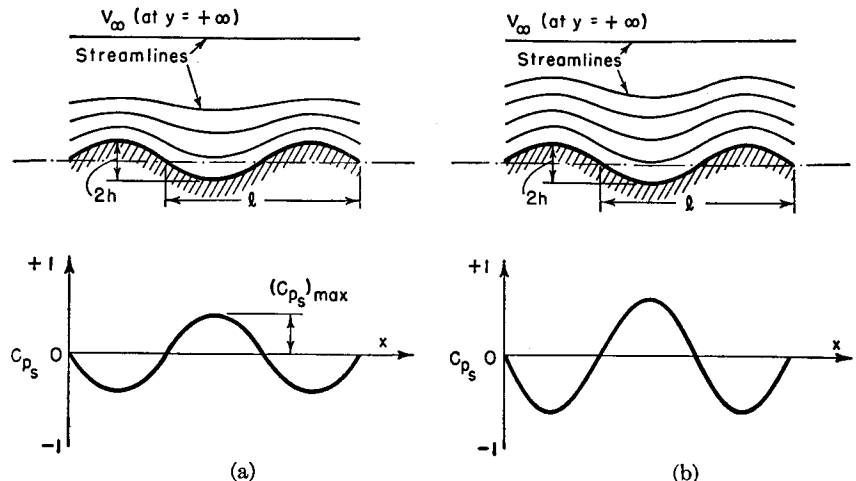


FIG. 10.2. Flow past wave-shaped wall, showing streamlines and pressure distribution at surface. Amplitude of wave in wall is exaggerated.

- (a) Incompressible flow ($M_\infty = 0$).
 (b) Subsonic flow ($M_\infty < 1$).

Pressure Distribution. The perturbation velocities at the wall, according to Eqs. 10.28 and 10.30, are

$$\begin{aligned} u_s &\cong \frac{2\pi V_\infty h}{\beta l} \cos \frac{2\pi x}{l} \\ v_s &\cong -2\pi V_\infty \frac{h}{l} \sin \frac{2\pi x}{l} \end{aligned} \quad (10.36)$$

Using the approximate expression for the pressure coefficient given by Eq. 10.26, we obtain

$$C_p = -\frac{4\pi h}{\beta l} \cos \frac{2\pi x}{l} e^{-2\pi\beta y/l} \quad (10.37)$$

$$C_{ps} \cong -\frac{4\pi h}{\beta l} \cos \frac{2\pi x}{l} \quad (10.38)$$

$$C_{p\infty} = 0 \quad (10.39)$$

From Eq. 10.38 it is evident that on the solid wall the pressure is a maximum in the lowest points of the troughs and is a minimum at the highest points of the crests. The variation in pressure along the contour is one-half wave length out of phase with the shape of the wall (Fig. 10.2). By tracing the cross-sectional area of a stream tube formed by two neighboring streamlines, it will be observed that the pressure is a maximum at the largest cross-sectional area and a minimum at the smallest

cross-sectional area, a result which fits in with one-dimensional considerations.

The streamlines at any distance from the wall are also approximately cosine in shape and are *in phase* with the wave-shaped wall, but the amplitude of the wave in the streamline shape dies off with increasing distance from the wall, according to the negative exponential term of Eq. 10.34. Likewise, the disturbance produced by the wall, as measured by the perturbation velocity u and by the pressure coefficient, decays with increasing distance from the wall according to the factor

$$e^{-2\pi\beta y/l}$$

Effect of Mach Number. How does compressibility influence the flow pattern? Suppose that we have a wall whose contour is given by Eq. 10.35, with fixed values of h and l . Now, for high Mach Numbers, β is small, while for low Mach Numbers, β approaches unity. Hence we see first of all from Eq. 10.38 that the difference between the free-stream pressure and wall pressure increases with Mach Number according to the factor $1/\sqrt{1 - M_\infty^2}$. Examination of Eqs. 10.34 and 10.37 shows also that with increasing Mach Number the disturbance produced by the wall on the flowing stream decays at a slower rate. Thus, increasing the Mach Number acts not only to augment the pressure difference acting on the solid body, but the effects of the solid body are felt at greater lateral distances from the body.

The conclusions reached in the preceding paragraphs are illustrated in Figs. 10.2 and 10.3.

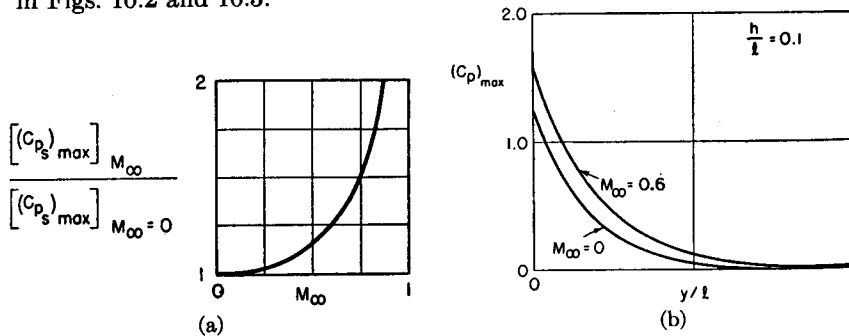


FIG. 10.3. Effect of Mach Number on pressure disturbance for flow past wave-shaped wall.

(a) Peak pressure coefficient at wall.

(b) Lateral decay of peak pressure coefficient.

Although the flow past a wave-shaped surface is by no means the same as the flow past a thin profile, it nevertheless seems plausible that the effects of Mach Number would be much the same and that we may use the example of the wave-shaped wall as a guide in estimating com-

pressibility effects. Thus, since the lift and moment acting on a profile are found by suitable integration of the pressures acting over the surface of the profile, we might expect from Eq. 10.38 that as a first approximation the lift and moment coefficients would be inversely proportional to β , i.e.,

$$\frac{(C_L)_{M_\infty}}{(C_L)_{M_\infty=0}} = \frac{(C_M)_{M_\infty}}{(C_M)_{M_\infty=0}} \cong \frac{1}{\sqrt{1 - M_\infty^2}}$$

Still another important conclusion to be drawn from this simple example is that in wind tunnel experiments the interference effects due to the walls of the tunnel are likely to become increasingly important at high Mach Numbers, because the lateral influence of a solid profile immersed in a stream increases with increasing Mach Number. For similar reasons, the mutual interference effects between blades in an axial flow turbine or compressor may be expected to grow larger as the Mach Number is increased.

A further interesting conclusion is that for small perturbations the effect of Mach Number on the pressure coefficient is independent of the specific-heat ratio. Of course this is valid only to the order of approximation of the linearized method.

10.5. Gothert's Rule

General Remarks Concerning Similarity Laws. In this article we shall derive an expression which relates the subsonic compressible flow past a certain profile to the incompressible flow past a second profile derived from the first through an affine transformation. Such an expression is called a *similarity law*. Since we shall subsequently derive other similarity laws for transonic, supersonic, and hypersonic flow, it is appropriate to discuss the philosophy underlying such similarity laws.

If the equations of motion could be solved easily, the solutions themselves would indicate quite clearly the nature of any similarities which might exist among members of a family of flow patterns. A separate derivation of similarity laws would, therefore, be superfluous.

We are in fact unable, in the majority of instances, to solve the equations of motion. However, even though solutions are lacking, we may exploit our knowledge of the *forms* of the differential equations (and the associated boundary conditions), and thus derive the similarity laws which of necessity would appear in the solutions if the latter could be found.

The derivation of similarity laws is a form of dimensional analysis involving *distorted models* rather than geometrically similar models.

Similarity laws may be useful in a number of practical ways. For example, Gothert's rule for subsonic flow, which is derived in this article,

allows us to predict the details of the subsonic flow past a body at subsonic speeds if we know the details of an incompressible flow past an affinely related body. Similarly, the transonic and hypersonic similarity rules show how experimental data for a certain body at a certain M_∞ can be made applicable to a related body at a different M_∞ .

Transformation of Variables Leading to Laplace's Equation. Suppose that a thin, two-dimensional airfoil is moving at the constant speed $-V_\infty$ through an infinite gas medium which is at rest at great distances from the airfoil. To an observer traveling with the uniform velocity of the airfoil, the airfoil is stationary, and the gas at great distances from the airfoil flows past the airfoil with the uniform, parallel velocity V_∞ (Fig. 10.1).

The flow pattern is in first approximation governed by the linearized differential equation of the perturbation velocity potential,

$$\beta^2 \frac{\partial^2 \varphi}{\partial x^2} + \frac{\partial^2 \varphi}{\partial y^2} = 0 \quad (10.21a)$$

This equation, however, is not a complete description of the problem, since it is necessary also to specify the boundary conditions. At an infinite distance in any direction from the airfoil the velocity is V_∞ , and the perturbation velocity is zero. Hence we may write

$$\text{at } x = \pm\infty: \begin{cases} u = \partial\varphi/\partial x = 0 \\ v = \partial\varphi/\partial y = 0 \end{cases} \quad (10.40a)$$

$$\text{at } y = \pm\infty: \begin{cases} u = \partial\varphi/\partial x = 0 \\ v = \partial\varphi/\partial y = 0 \end{cases} \quad (10.40b)$$

In addition, the velocity vector at the surface of the profile must be tangent to the profile itself. Denoting the coordinates of the surface of the profile by x_s, y_s , we express this boundary condition (Fig. 10.1) by the relation

$$\text{at } x_s, y_s: \frac{dy_s}{dx_s} = \frac{v_s}{V_\infty + u_s} = \frac{v_s/V_\infty}{1 + u_s/V_\infty}$$

where the subscript s denotes conditions at the surface of the profile. According to Eq. 10.25, however, we have agreed in the linearized theory to ignore u/V_∞ as compared with unity. Hence the boundary condition at the profile becomes

$$\text{at } x_s, y_s: \frac{dy_s}{dx_s} = \frac{v_s}{V_\infty} = \frac{1}{V_\infty} \left[\frac{\partial\varphi(x, y)}{\partial y} \right]_{x_s, y_s} \quad (10.41)$$

For a profile of given shape, that is, with a contour given by a certain function $f(x_s, y_s) = 0$, the solution of Eq. 10.21a, subject to the boundary

conditions given by Eqs. 10.40 and 10.41, is at best not easy. However, it will be noticed that Eq. 10.21a is not very different in form from the exact equation for incompressible flow, the latter being found merely by setting β equal to unity. Also, it may be recalled that one of the devices used for solving unfamiliar differential equations is to seek a transformation of variables which reduces the differential equation to a familiar form for which a solution is available. These remarks suggest that by a suitable transformation it might be possible to reduce Eq. 10.21a to the Laplace equation and thus open the possibility of employing the well-developed store of theory and experiment for incompressible flow.

A generalized transformation which leads to the desired result is found by defining new variables x', y' and $\varphi'(x', y')$ as follows:

$$x' = \lambda_x x \quad (10.42)$$

$$y' = \lambda_y y \quad (10.43)$$

$$\varphi'(x', y') = \lambda_\varphi \varphi(x, y) \quad (10.44)$$

where λ_x , λ_y , and λ_φ are constants whose values are to be determined. We now transform Eq. 10.21a into the x' , y' , φ' system of variables through the following relations:

$$u = \frac{\partial[\varphi(x, y)]}{\partial x} = \frac{\partial[\varphi'(x', y')/\lambda_\varphi]}{\partial(x'/\lambda_x)} = \frac{\lambda_x \partial\varphi'}{\lambda_\varphi \partial x'} = \frac{\lambda_x}{\lambda_\varphi} u' \quad (10.45a)$$

$$\frac{\partial u}{\partial x} = \frac{\partial}{\partial x} \frac{\partial[\varphi(x, y)]}{\partial x} = \frac{\partial}{\partial(x'/\lambda_x)} \frac{\lambda_x \partial\varphi'}{\lambda_\varphi \partial x'} = \frac{\lambda_x^2 \partial^2\varphi'}{\lambda_\varphi \partial x'^2} = \frac{\lambda_x^2}{\lambda_\varphi} \frac{\partial u'}{\partial x'} \quad (10.45b)$$

$$v = \frac{\partial[\varphi(x, y)]}{\partial y} = \frac{\partial[\varphi'(x', y')/\lambda_\varphi]}{\partial(y'/\lambda_y)} = \frac{\lambda_y \partial\varphi'}{\lambda_\varphi \partial y'} = \frac{\lambda_y}{\lambda_\varphi} v' \quad (10.45c)$$

$$\frac{\partial v}{\partial y} = \frac{\partial}{\partial y} \frac{\partial[\varphi(x, y)]}{\partial y} = \frac{\partial}{\partial(y'/\lambda_y)} \frac{\lambda_y \partial\varphi'}{\lambda_\varphi \partial y'} = \frac{\lambda_y^2 \partial^2\varphi'}{\lambda_\varphi \partial y'^2} = \frac{\lambda_y^2}{\lambda_\varphi} \frac{\partial v'}{\partial y'} \quad (10.45d)$$

Substituting these into Eq. 10.21a, we obtain

$$\frac{\beta^2 \lambda_x^2}{\lambda_\varphi} \frac{\partial^2 \varphi'}{\partial x'^2} + \frac{\lambda_y^2}{\lambda_\varphi} \frac{\partial^2 \varphi'}{\partial y'^2} = 0 \quad (10.46)$$

Now, if we set

$$\beta^2 \lambda_x^2 = \lambda_y^2; \quad \text{or} \quad \lambda_y/\lambda_x = \beta \quad (10.47)$$

we obtain

$$\frac{\partial^2 \varphi'}{\partial x'^2} + \frac{\partial^2 \varphi'}{\partial y'^2} = 0 \quad (10.48)$$

which means that the x' , y' , φ' system of variables describes the motion of an incompressible fluid if λ_x and λ_y are so chosen that $\lambda_y/\lambda_x = \beta$.

Transformed Boundary Conditions. To discover the complete relation between the compressible flow $\varphi(x, y)$ and the incompressible flow $\varphi'(x', y')$, we must see what form the transformed boundary conditions take.

At infinite distance from the airfoil, by employing Eq. 10.40 with Eq. 10.45, we see that

$$\left\{ \begin{array}{l} \text{at } x' = \pm\infty \\ \text{or} \\ y' = \pm\infty \end{array} \right\} : \left\{ \begin{array}{l} u' = \partial\varphi'/\partial x' = 0 \\ v' = \partial\varphi'/\partial y' = 0 \end{array} \right\} \quad (10.49a)$$

$$y' = \pm\infty \quad (10.49b)$$

From these relations we conclude that in the incompressible flow there are no velocity perturbations at great distances from the airfoil and hence the velocity is uniform and parallel at infinity.

Turning now to the boundary condition at the airfoil, we first note that the profile slopes are related by

$$\frac{dy_s}{dx_s} = \frac{d(y_s'/\lambda_y)}{d(x_s'/\lambda_x)} = \frac{\lambda_x}{\lambda_y} \frac{dy_s'}{dx_s'} \quad (10.50)$$

where x_s' and y_s' represent the coordinates of the transformed profile as given by

$$x_s' = \lambda_x x_s \quad (10.51a)$$

$$y_s' = \lambda_y y_s \quad (10.51b)$$

In addition, we note that the transformation formulas give

$$\left[\frac{\partial\varphi(x, y)}{\partial y} \right]_{x_s, y_s} = \frac{\lambda_y}{\lambda_\varphi} \left[\frac{\partial\varphi'(x', y')}{\partial y'} \right]_{x_s', y_s'} \quad (10.52)$$

Substituting Eqs. 10.52 and 10.50 into the boundary condition of Eq. 10.41, we get after rearrangement

$$\frac{dy_s'}{dx_s'} = \frac{\lambda_y^2}{\lambda_x \lambda_\varphi} \frac{1}{V_\infty} \left[\frac{\partial\varphi'(x', y')}{\partial y'} \right]_{x_s', y_s'} \quad (10.53)$$

If we now set

$$\lambda_y^2 = \lambda_x \lambda_\varphi \quad (10.54)$$

and if we also define V_∞' to be equal to V_∞ (which may be done without loss of generality), we obtain

$$\frac{dy_s'}{dx_s'} = \frac{1}{V_\infty'} \left[\frac{\partial\varphi'(x', y')}{\partial y'} \right]_{x_s', y_s'} \quad (10.55)$$

Comparison of Eq. 10.55 with Eq. 10.41 shows that the boundary conditions for the incompressible flow past a new profile defined by x_s' , y_s' are satisfied when $V_\infty' = V_\infty$ and $\lambda_y^2 = \lambda_x \lambda_\varphi$.

To recapitulate what has been accomplished thus far, we have found that the function $\varphi'(x', y')$ describes the uniform, parallel incompressible flow past a new profile x_s' , y_s' , provided that λ_x , λ_y , and λ_φ are chosen so as to satisfy Eqs. 10.47 and 10.54 and that the velocity at infinity is the same for both flows.

Relation Between Geometries of Corresponding Profiles. How does the newly found incompressible flow compare with the compressible flow to which it is related? We see from Eqs. 10.50 and 10.47 that

$$\frac{dy_s/dx_s}{dy_s'/dx_s'} = \frac{\lambda_x}{\lambda_y} = \frac{1}{\beta} = \frac{1}{\sqrt{1 - M_\infty^2}} \quad (10.56)$$

which means that the slope of the profile in the compressible flow pattern is larger by the factor $1/\beta$ than the slope of the corresponding profile in the related incompressible flow pattern. But if the slope of the profile at each point is greater by the factor $1/\beta$, it is also true that the *camber ratio*, *angle of attack*, and *thickness ratio* must all be greater for the compressible airfoil by the factor $1/\beta$. Thus, denoting the camber ratio by γ , the angle of attack by α and the thickness ratio by δ , we have

$$\frac{\gamma}{\gamma'} = \frac{\alpha}{\alpha'} = \frac{\delta}{\delta'} = \frac{1}{\beta} = \frac{1}{\sqrt{1 - M_\infty^2}} \quad (10.57)$$

To demonstrate this relation for the thickness ratio, for note that

$$\delta \equiv \frac{t_{\max}}{l}$$

where t_{\max} is the difference in profile ordinates at the point of maximum thickness of the profile, and l is the chord length (which direction). But, from Eq. 10.51,

$$t_{\max} = t'_{\max}/\lambda_y; \quad l = l'/\lambda_x$$

and hence

$$\delta = \frac{\lambda_x}{\lambda_y} \frac{t'_{\max}}{l'} = \frac{\lambda_x}{\lambda_y} \delta' = \frac{1}{\beta} \delta'$$

which was to be proved.

The geometrical results discussed above are illustrated in form in Fig. 10.4. It will be noted that the individual constants λ_x and λ_y are unimportant, since it is the ratio of the two which determines changes in the shape of the profile. Thus, we can set $\lambda_y = \beta$, thereby keeping the same chord but changing the camber ratio. We can get equivalent results by setting $\lambda_y = 1$ and $\lambda_x = \beta$, thereby keeping the same ordinates but changing the chord. The geometrical transformation involved here is termed *affine*, m

coordinates in a given direction are changed by a uniform ratio. If a profile were printed on a thin, uniform sheet of rubber, and the rubber were then stretched with uniform strain in both the x - and y -directions, the profile would change shape in an affine manner.

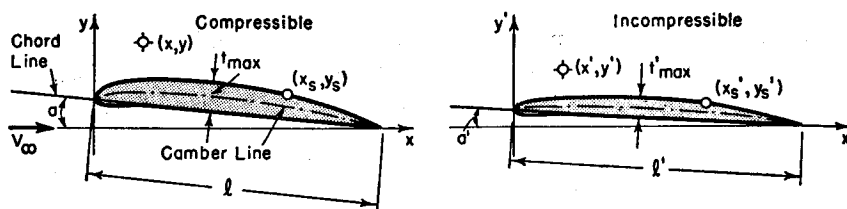


FIG. 10.4. Coordinate transformation for Goert's rule.

$$\begin{aligned} x' &= \lambda_x x; & x'_s &= \lambda_x x_s \\ y' &= \lambda_y y; & y'_s &= \lambda_y y_s \\ t'_{\max} &\equiv \lambda_y t_{\max}; & l' &\equiv \lambda_x l \\ a' &\equiv (\lambda_y / \lambda_x) a \end{aligned}$$

Relation Between Forces on Corresponding Profiles. The lift on the profile is determined by the pressure distribution on the surface of the airfoil, which in turn may be expressed in terms of the pressure coefficient at the surface. From Eq. 10.26 we have

$$C_{ps} = -2 \frac{u_s}{V_\infty} = -\frac{2}{V_\infty} \left[\frac{\partial \varphi(x, y)}{\partial x} \right]_{x_s, y_s}$$

Similarly, noting that we have already set $V'_\infty = V_\infty$,

$$C'_{ps} = -2 \frac{u'_s}{V_\infty} = -\frac{2}{V_\infty} \left[\frac{\partial \varphi'(x', y')}{\partial x'} \right]_{x'_s, y'_s}$$

But

$$\left[\frac{\partial \varphi(x, y)}{\partial x} \right]_{x_s, y_s} = \frac{\lambda_x}{\lambda_\varphi} \left[\frac{\partial \varphi'(x', y')}{\partial x'} \right]_{x'_s, y'_s}$$

and hence, with the aid of Eqs. 10.47 and 10.54, we find that

$$\frac{C_{ps}}{C'_{ps}} = \frac{\lambda_x}{\lambda_\varphi} = \frac{\lambda_x^2}{\lambda_y^2} = \frac{1}{\beta^2} = \frac{1}{1 - M_\infty^2} \quad (10.58)$$

The lift is found by integrating the vertical component of pressure force over the surface of the profile. Hence the lift coefficient is found by integrating the pressure coefficient over the surface, as indicated by the following operations:

$$C_L \equiv \frac{L}{\frac{1}{2} \rho_\infty V_\infty^2 l} = \frac{\oint p_s dx_s}{\frac{1}{2} \rho_\infty V_\infty^2 l} = \frac{\oint (p_s - p_\infty) dx_s}{\frac{1}{2} \rho_\infty V_\infty^2 l} = \oint C_{ps} d \left(\frac{x}{l} \right)$$

At equal values of x_s/l , C_{ps} and C'_{ps} are related by Eq. 10.58. Therefore the ratio C_L/C'_L must be the same as the ratio C_{ps}/C'_{ps} . A similar argument leads to the same conclusion for the moment coefficient, C_M . Thus we may write

$$\frac{C_L}{C'_L} = \frac{C_M}{C'_M} = \frac{1}{\beta^2} = \frac{1}{1 - M_\infty^2} \quad (10.59)$$

which means that if the two profiles are related affinely as described previously, the lift and moment coefficients for the compressible flow pattern will be greater than for the related incompressible flow pattern by the factor $1/\beta^2$.

We might inquire whether these results have any practical significance. There has been accumulated fairly extensive theoretical and experimental information on the properties of classes of affinely related profiles in incompressible flow, with systematic variations in camber, thickness ratio, and angle of attack. If it is desired to find the lift coefficient of one of these profiles at a finite Mach Number M_∞ , one first finds (either theoretically or experimentally) the lift coefficient in incompressible flow of an affinely related profile whose camber, thickness ratio, and angle of attack are all *smaller* than the corresponding values for the original profile by the ratio β . Then, by multiplying this lift coefficient by $1/\beta^2$, one finds the desired lift coefficient for the compressible flow.

This method of projecting experimental data for incompressible flow is sometimes awkward, since it requires incompressible data for a large range of thickness ratios. It would be more convenient in many cases to know how Mach Number affects the performance of a profile of fixed shape. The *Prandtl-Glauert rule*, which is discussed in the next article, yields information of this type.

10.6. The Prandtl-Glauert Rule

Similarity Law for Incompressible Flow. For the present let us consider the *incompressible*, two-dimensional flow past a family of affinely related thin profiles. It is known that for such affinely related profiles the pressure coefficients at corresponding points are approximately proportional to the thickness ratios (and, of course, simultaneously to the camber ratios and angles of attack). For example, if in the case of the wave-shaped wall we consider h/l to be the appropriate "thickness ratio," it is evident from Eqs. 10.37 and 10.38 that the pressure coefficient is proportional to the thickness ratio. As a second example, consider incompressible flow past an inclined flat plate: classical aerodynamic theory shows that the lift is proportional to the angle of attack.

Following this line of thought, consider two affine profiles in *incompressible* flow which are related as follows:

$$\frac{\gamma'}{\gamma''} = \frac{a'}{a''} = \frac{\delta'}{\delta''} = \beta$$

Then it follows that, at least approximately,

$$\frac{C_{ps}'}{C_{ps}''} = \frac{C_L'}{C_L''} = \frac{C_{\mathfrak{M}}'}{C_{\mathfrak{M}}''} = \beta$$

Combination of Goert's Rule with Incompressible Similarity Law. The foregoing rule for incompressible flow gives us an opportunity to derive further similarity criteria between incompressible and compressible flow. For if we combine the relations immediately above with Eqs. 10.57, 10.58, and 10.59, we find that if the compressible profile (unprimed) is affinely related to the incompressible profile (double primed) in such a way that

$$\frac{\gamma}{\gamma''} = \frac{a}{a''} = \frac{\delta}{\delta''} = 1 \quad (10.60)$$

then the forces acting in the two flows are related through

$$\frac{C_{ps}}{C_{ps}''} = \frac{C_L}{C_L''} = \frac{C_{\mathfrak{M}}}{C_{\mathfrak{M}}''} = \frac{1}{\beta} = \frac{1}{\sqrt{1 - M_\infty^2}} \quad (10.61)$$

These equations mean that for the same profile at the same angle of attack the pressure coefficient, lift coefficient and moment coefficient are all affected by Mach Number in proportion to the factor $1/\sqrt{1 - M_\infty^2}$.

From Eqs. 10.60 and 10.61 it also follows that for a given profile the lift-curve slope is proportional to $1/\beta$:

$$\frac{dC_L/da}{dC_L''/da''} = \frac{1}{\beta} = \frac{1}{\sqrt{1 - M_\infty^2}} \quad (10.62)$$

It is profitable to carry this line of attack one step further. Let us now consider two affinely related profiles in incompressible flow for which

$$\frac{\gamma'}{\gamma'''} = \frac{a'}{a'''} = \frac{\delta'}{\delta'''} = \beta^2$$

so that, at least approximately,

$$\frac{C_{ps}'}{C_{ps}'''} = \frac{C_L'}{C_L'''} = \frac{C_{\mathfrak{M}}'}{C_{\mathfrak{M}}'''} = \beta^2$$

Now let us combine these relations with Eqs. 10.57, 10.58, and 10.59. We find that if the compressible profile (unprimed) is affinely related to the incompressible profile (triple primed) in such a way that

$$\frac{\gamma}{\gamma'''} = \frac{a}{a'''} = \frac{\delta}{\delta'''} = \beta = \sqrt{1 - M_\infty^2} \quad (10.63)$$

then

$$\frac{C_{ps}}{C_{ps}'''} = \frac{C_L}{C_L'''} = \frac{C_{\mathfrak{M}}}{C_{\mathfrak{M}}'''} = 1 \quad (10.64)$$

These equations mean that the dimensionless pressure distribution, lift coefficient, and moment coefficient will be the same for compressible and incompressible flow if the profiles are affinely related in such a way that the compressible profile is smaller in camber ratio, thickness ratio, and angle of attack by the factor $\sqrt{1 - M_\infty^2}$.

This form of the similarity rule is sometimes useful for making predictions concerning boundary-layer separation, for the latter is largely dependent upon the dimensionless pressure gradient at the surface of the profile. If the effect of Mach Number on boundary-layer separation is assumed to be small, for example, then Eqs. 10.63 and 10.64 show that, in order to avoid stalling the profile in a compressible flow, the profile must be thinner, have a smaller value of γ , and be at a lesser angle of attack than would be allowable with an incompressible flow.

Summary of Similarity Laws. The three laws of similarity may be conveniently summarized by the following symbolic statements:

Rule I:

$$[C_p]_{M_\infty, a, \delta, \gamma} = \frac{1}{1 - M_\infty^2} [C_p]_{0, \beta a, \beta \delta, \beta \gamma} \quad (10.65)$$

Rule II:

$$[C_p]_{M_\infty, a, \delta, \gamma} = \frac{1}{\sqrt{1 - M_\infty^2}} [C_p]_{0, a, \delta, \gamma} \quad (10.66)$$

Rule III:

$$[C_p]_{M_\infty, a, \delta, \gamma} = [C_p]_{0, a/\beta, \delta/\beta, \gamma/\beta} \quad (10.67)$$

Identical statements apply to C_L and $C_{\mathfrak{M}}$.

Eq. 10.65 corresponds to Eqs. 10.57 and 10.58, and is to be read: "The pressure coefficient at a certain point for compressible flow with Mach Number M_∞ past a profile having geometric parameters of magnitude a , δ , and γ is greater by the factor $1/\beta^2$ than the pressure coefficient at the corresponding point for incompressible flow ($M_\infty = 0$) past an affinely related profile having geometric parameters of magnitude βa , $\beta \delta$, and $\beta \gamma$."

The three rules are illustrated in Fig. 10.5. Rule I is Gothert's rule, and is the most exact of the three. Rules II and III are known as the *Prandtl-Glauert rule*, and were originally derived incorrectly, inasmuch as the transformed boundary conditions were not taken into account. For two-dimensional flows this oversight was not serious, or at least introduced errors no worse than are already inherent in the linearized equations. The oversight was not appreciated for some twenty years, until anomalous results were obtained in comparing Rule II with experimental and exact theoretical results for flow past thin bodies of

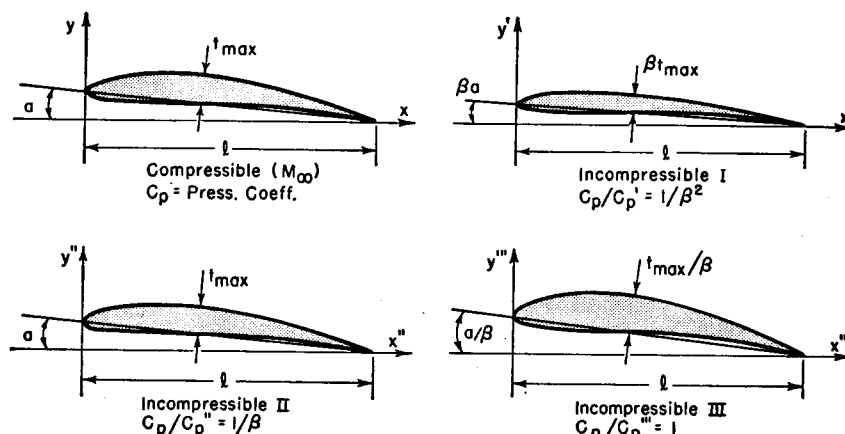


FIG. 10.5. Similarity Rules I, II, and III for subsonic flow.

revolution. For such axi-symmetric flows the incompressible pressure coefficient is not proportional to the thickness ratio, and hence Rules II and III are not applicable. Gothert⁽²⁾ formulated the more general Rule I and showed the correct way of extending it to three-dimensional flows (Chapter 13).

Effect of Mach Number on Flow Far from Profile. Thus far we have considered the influence of M_∞ on the pressure distribution at the surface of the profile. At great distances from a given profile it may be shown that, at a given point (see Problem 10.6)

$$\frac{[C_p]_{M_\infty}}{[C_p]_0} = \frac{1}{(1 - M_\infty^2)^{\frac{1}{2}}} \quad \text{when } \frac{y}{x} \rightarrow \infty$$

$$\frac{[C_p]_{M_\infty}}{[C_p]_0} = \frac{1}{\sqrt{1 - M_\infty^2}} \quad \text{when } \frac{x}{y} \rightarrow \infty$$

Laitone's Modification of Prandtl-Glauert Rule. An improvement on Rule II has been suggested by Laitone.⁽⁹⁾

The linearized theory is evidently not applicable for large perturbations. Or, stated differently, it is only applicable for regions where C_p is very small and for low values of M_∞ . A better approximation is obtained by writing Rule II in terms of the local Mach Number M_L rather than in terms of the free-stream Mach Number M_∞ . This procedure implies that the linearized equations are applied not to the entire field of flow but instead to the local flow field which is considered to be approximately uniform in a small region.

Let C_p be the pressure coefficient at a certain point for compressible flow past a profile, and let C_{p0} be the pressure coefficient at the same point for incompressible flow past the same profile. Then, by Laitone's hypothesis,

$$C_p = \frac{C_{p0}}{\sqrt{1 - M_L^2}} \quad (10.68)$$

Eq. 10.22 for C_p is in this case written with p_L/p_∞ on the right-hand side. The latter ratio is given by the isentropic relations of Chapter 4 as

$$\frac{p_L}{p_\infty} = \left(\frac{1 + \frac{k-1}{2} M_\infty^2}{1 + \frac{k-1}{2} M_L^2} \right)^{\frac{k}{k-1}}$$

Substituting this into Eq. 10.22, and solving for M_L^2 , we obtain

$$M_L^2 = \left(M_\infty^2 + \frac{2}{k-1} \right) \left(1 + \frac{k M_\infty^2}{2} C_p \right)^{-\frac{k-1}{k}} - \frac{2}{k-1}$$

However, since the linearized theory ignores terms of greater than first order in C_p , the foregoing expression may be expanded by the binomial theorem to give

$$M_L^2 \cong M_\infty^2 - \left(1 + \frac{k-1}{2} M_\infty^2 \right) M_\infty^2 C_p + \dots$$

Substituting this into Eq. 10.68, and solving for C_p , we finally obtain

$$C_p = \frac{C_{p0}}{\sqrt{1 - M_\infty^2} + \frac{\sqrt{1 - M_\infty^2}}{2\sqrt{1 - M_\infty^2}} C_{p0}} \quad (10.69)$$

For very small values of C_{p0} , this is seen to be substantially identical with the Prandtl-Glauert rule. Usually we are interested in regions where the pressure coefficient is negative. For such regions Eq. 10.69

indicates a greater influence of Mach Number on C_p than does the Prandtl-Glauert rule. Moreover, Eq. 10.69 is in agreement with experimental results in predicting that the effects of compressibility are proportionately greater for regions of high negative pressure coefficient than for regions of low negative pressure coefficient.

The pressure correction rule of Eq. 10.69 cannot be extended to the prediction of forces, because the effect of Mach Number on C_p is different at each point of the profile. If the pressure distribution for incompressible flow is known, however, the pressure distribution for compressible flow may be found from Eq. 10.69. Then, by integration, the lift and moment coefficients for compressible flow may be computed.

10.7. Experimental Results for Thin Profiles

In comparing the similarity rules with experimental data, it must be remembered that they represent primitive attempts to obtain useful information in the simplest possible manner. It is evident that the

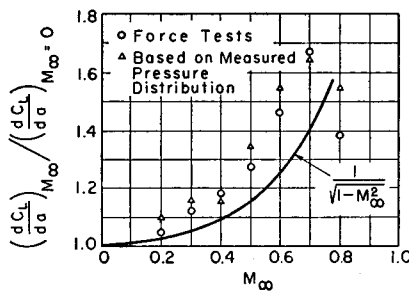


FIG. 10.6. Comparison of measured lift-curve slope for NACA 4412 profile (12% thickness) with Prandtl-Glauert rule (after Stack, Lindsey, and Littell).

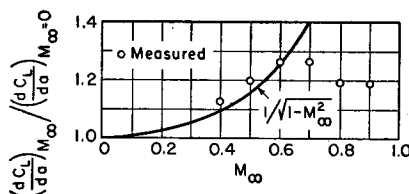


FIG. 10.7. Comparison of measured lift-curve slope for propeller section of 6% thickness with Prandtl-Glauert rule (after Ferri).

assumptions on which the rule is based are in most practical cases satisfied only in a very approximate way. For example, although the perturbation velocity is taken to be negligible compared to the free-stream velocity, at the stagnation point the perturbation velocity is exactly equal to the free-stream velocity.

Fig. 10.6 shows in a typical way the experimental effect of M_∞ on the lift-curve slope for a 12%-thick profile. Similar data for a propeller section of 6% thickness ratio is shown in Fig. 10.7. Up to the Mach Number where the lift begins to drop sharply because of "compressibility burble," the Prandtl-Glauert rule predicts the general effect of M_∞ but underestimates the magnitude of the effect. As might be expected from the nature of the linear theory, the Prandtl-Glauert rule is more accurate for the thinner profile. The "compressibility burble"

is associated with the appearance of shock waves near the profile which, by virtue of adverse pressure gradients, produce flow separation. This effect is very similar to stalling at high angles of attack.

Fig. 10.8 shows the effect of M_∞ on the pressure coefficient at 30% chord on the upper surface of NACA 4412 operating with an angle of attack of -2° . Here again it is evident that the Prandtl-Glauert rule is correct as regards order of magnitude, but underestimates the effects of compressibility.

From these typical results we may conclude that the Prandtl-Glauert rule predicts the effects of M_∞ with good accuracy for very thin profiles at low Mach Numbers. For thick profiles and high Mach Numbers, the rule provides a guide to orders of magnitude but is not accurate enough for design purposes.

For additional experimental data illustrating the validity of the Prandtl-Glauert rule, the reader is referred to Chapters 11 and 12.

Laitone's modification of the Prandtl-Glauert rule is seen from Fig. 10.8 to predict the variation of C_p with M_∞ somewhat better than does the Prandtl-Glauert rule. It should be noted here that no single similarity rule can be correct for all profiles, and hence the different similarity laws compare more or less favorably with experiment, depending upon the profile shape, angle of attack, position of measurement, etc.

It is not amiss here to point out that the Karman-Tsien pressure correction formula (Chapter 11) is generally in better agreement with experiment than is the Prandtl-Glauert rule.

10.8 Wind Tunnel Corrections

Definition of Problem. When a wing profile is tested in a wind tunnel, corrections must be made to the measured lift and moment coefficients in order to obtain the corresponding coefficients for the same profile in an infinite air stream. These corrections are necessary because the boundary conditions of the flow in a tunnel are different from those in a large air stream. For two-dimensional tests, with the wing spanning a rectangular test section, the tunnel correction depends chiefly on the ratio l/h , where l is the chord of the profile and h is the half-height of the tunnel (Fig. 10.9a). In incompressible flow the methods of making

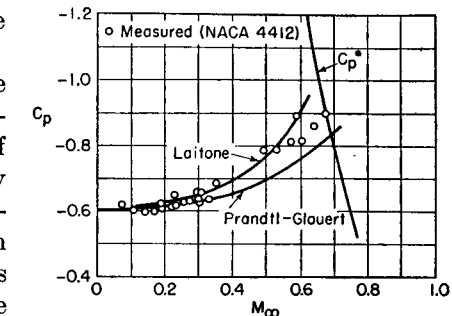


FIG. 10.8. Pressure coefficient versus M_∞ at 30% chord on upper surface of NACA 4412, with $\alpha = -2^\circ$. Comparison of measured data with Eqs. 10.66 and 10.69. The curve marked C_p^* denotes the local sonic condition (after Stack, Lindsey, and Littell).

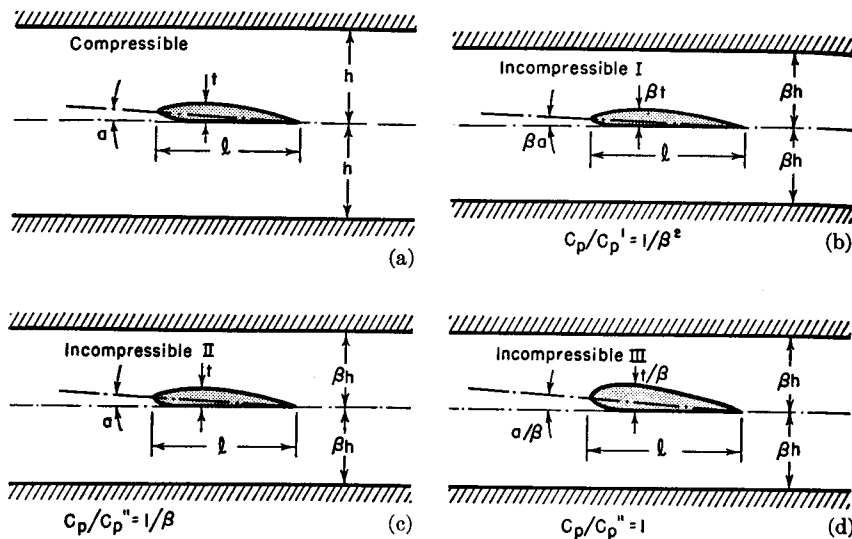


FIG. 10.9. Similarity Rules I, II, and III for thin profile in wind tunnel.

such corrections are well developed. We shall now derive similarity rules which show the effect of compressibility on the tunnel correction factors.

Similarity Transformations. The differential equation describing the flow is, as before, Eq. 10.21a. Introducing the transformation formulas, Eqs. 10.42, 10.43, and 10.44, we get Eq. 10.46 and find as before that $\varphi'(x', y')$ represents an incompressible flow pattern if $\lambda_y/\lambda_x = \beta$.

Far upstream and far downstream of the profile, the boundary condition is

$$\text{at } x = \pm\infty: \begin{cases} u = \partial\varphi/\partial x = 0 \\ v = \partial\varphi/\partial y = 0 \end{cases}$$

Using Eqs. 10.42 and 10.45, we see that the corresponding boundary condition in the incompressible flow is

$$\text{at } x' = \pm\infty: \begin{cases} u' = \partial\varphi'/\partial x' = 0 \\ v' = \partial\varphi'/\partial y' = 0 \end{cases}$$

which means that in the incompressible flow the stream is undisturbed far upstream and far downstream of the profile.

The boundary condition at the tunnel wall is

$$\text{at } y = \pm h: v = \left[\frac{\partial\varphi(x, y)}{\partial y} \right]_{y=\pm h} = 0$$

For the incompressible case, the corresponding boundary condition, according to the transformation formulas, is

$$\text{at } y' = \pm\lambda h: \frac{\lambda_y}{\lambda_\varphi} \left[\frac{\partial\varphi'(x', y')}{\partial y'} \right]_{y'=\pm\lambda h} = 0$$

from which it follows that v' is zero at $y' = \pm h'$, where

$$h' = \lambda_y h$$

In the incompressible flow the tunnel-wall boundary condition is therefore satisfied when the half-height is h' .

Hence it follows that

$$\frac{h/l}{h'/l'} = \frac{h}{h'} \cdot \frac{l'}{l} = \frac{\lambda_x}{\lambda_y} = \frac{1}{\beta}$$

Regarding the boundary conditions at the profile, Eqs. 10.50 to 10.55 are applicable here, and yield the requirement that $\lambda_y^2 = \lambda_x \lambda_\varphi$. Similarly, Eq. 10.58, showing the connection between the corresponding pressure coefficients, is also valid for the present case.

Similarity Rules. Combining the foregoing considerations, we obtain the following similarity rule:

Rule I:

$$[C_{ps}]_{M_\infty, a, \delta, \gamma, \frac{h}{l}} = \frac{1}{\beta^2} [C_{ps}]_{0, \beta a, \beta \delta, \beta \gamma, \beta \frac{h}{l}} \quad (10.70)$$

If h/l is considerably larger than unity, then, as in the case of a single profile in an infinite stream, there is a similarity law for incompressible flow which states that

$$[C_{ps}]_{0, a, \delta, \gamma, \frac{h}{l}} = \frac{1}{n} [C_{ps}]_{0, na, n\delta, n\gamma, \frac{h}{l}}$$

where n is a constant.

By employing this approximate rule for incompressible flow, there may be derived from Eq. 10.70 the following rules:

Rule II:

$$[C_{ps}]_{M_\infty, a, \delta, \gamma, \frac{h}{l}} = \frac{1}{\beta} [C_{ps}]_{0, a, \delta, \gamma, \beta \frac{h}{l}} \quad (10.71)$$

Rule III:

$$[C_{ps}]_{M_\infty, a, \delta, \gamma, \frac{h}{l}} = [C_{ps}]_{0, \frac{a}{\beta}, \frac{\delta}{\beta}, \frac{\gamma}{\beta}, \beta \frac{h}{l}} \quad (10.72)$$

None of these, it may be noted, shows the effect of M_∞ on a test arrangement of fixed geometry.

The three rules are illustrated in Fig. 10.9.

Identical rules apply to the lift and moment coefficients.

The *interference pressure coefficient* ΔC_p is defined as the value of C_p with the tunnel walls present minus the value of C_p with the tunnel walls

absent. It may be shown (see Problem 10.10) that the effect of compressibility on the interference pressure coefficient at a fixed point on a profile of fixed shape in a tunnel of fixed size is given approximately by

$$\frac{[\Delta C_p]_{M_\infty}}{[\Delta C_p]_0} = \frac{1}{(1 - M_\infty^2)^{1/2}}$$

10.9 Flow Inside Two-Dimensional Passages

Consider the two-dimensional flow inside a passage such as is shown in Fig. 10.10. We shall suppose that the wall contours are such that

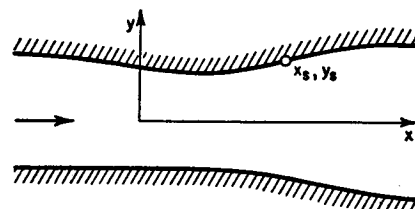


FIG. 10.10. Flow in two-dimensional duct.

the velocity perturbations are small enough to permit application of the linear theory.

Application of Goert's Rule. In applying the similarity analysis, only Rule I (Goert's rule) is permissible, since the approximations involved in the boundary conditions near thin profiles for Rules II and III are not applicable when applied to the boundary conditions at the duct walls of Fig. 10.10.

Using the previous results, Goert's rule for the present case may be easily applied. We consider an affine transformation of the duct such that

$$x_s' = \lambda_x x_s; \quad y_s' = \lambda_y y_s \quad (10.73)$$

and, in order that the primed quantities shall correspond to incompressible flow, we stipulate that

$$\frac{y_s/x_s}{y_s'/x_s'} = \frac{dy_s/dx_s}{dy_s'/dx_s'} = \frac{\lambda_x}{\lambda_y} = \frac{1}{\beta} \quad (10.74)$$

At corresponding points in the incompressible and compressible flow, the following relations then prevail:

$$\frac{C_p}{C_p'} = \frac{u}{u'} = \frac{1}{\beta^2} \quad (10.75)$$

$$\frac{v}{v'} = \frac{1}{\beta} \quad (10.76)$$

Thus, using one of the many methods for obtaining incompressible flow patterns, it is possible with this rule to construct approximately a series of corresponding patterns for compressible flow.

One-Dimensional Flow. The method given here refers to flows which are essentially two-dimensional and serve no useful purpose for one-dimensional flow because in the latter case there are simple and more accurate methods at hand. However, we may employ one-dimensional considerations to verify for a limiting case the validity of the rule as given above. Suppose that we have a long duct of uniform width followed by a slight change in area, after which the duct is again constant in width (Fig. 10.11). Far upstream and far downstream of the change,

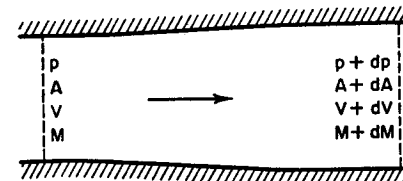


FIG. 10.11. Illustrates verification of Goert's rule for one-dimensional flow.

the flow is nearly one-dimensional, and therefore we may use one-dimensional formulas for calculating changes between the two sections.

What does Goert's rule tell us about this problem? First of all, since the transformation is affine, Eq. 10.73 shows that the fractional change in area, dA/A , taken in a one-dimensional sense, is the same for the compressible and incompressible patterns which are to be compared. Eq. 10.75 then indicates that, *for the same fractional change in area*,

$$C_p \sim \frac{1}{1 - M^2}$$

Using the Euler equation, the pressure coefficient for small changes may be written

$$C_p = \frac{dp}{\frac{1}{2}\rho V^2} = -\frac{\rho V dV}{\frac{1}{2}\rho V^2} = -2 \frac{dV}{V}$$

Now, employing the one-dimensional considerations previously referred to, we find from Table 8.1 that for isentropic flow,

$$\frac{dV}{V} = -\frac{1}{1 - M^2} \frac{dA}{A}$$

and, accordingly,

$$C_p = \frac{2}{1 - M^2} \frac{dA}{A}$$

which shows that the pressure coefficient is indeed proportional to

$1/(1 - M^2)$ for a given area ratio. Consequently we have verified Gothert's rule for the limiting case considered here.

REFERENCES AND SELECTED BIBLIOGRAPHY

- ACKERET, J. Über Luftkräfte bei sehr grossen Geschwindigkeiten insbesondere bei ebenen Strömungen, *Helvetica Physica Acta*, Vol. 1 (1928), pp. 301-22.
- GOTHERT, B. Plane and Three-Dimensional Flow at High Subsonic Speeds, *NACA Tech. Memo.*, No. 1105 (1946). (Translation from original German paper in Lilienthal Gesellschaft 127.)
- STACK, J., LINDSEY, W. F., and LITTELL, R. E. The Compressibility Bubble and the Effect of Compressibility on the Pressure and Forces Acting on an Airfoil, *NACA Tech. Rep.*, No. 640 (1938).
- FERRI, A. Investigations and Experiments in the Guidonia Supersonic Wind Tunnel, *NACA Tech. Memo.*, No. 946 (1940).
- TSIEN, H. S., and LEES, L. The Glauert-Prandtl Approximation for Subsonic Flows of a Compressible Fluid, *Jour. Aero. Sci.*, Vol. 12, No. 2 (1945), p. 173.
- HUNSAKER, J. C., and RIGHTMIRE, B. G. *Engineering Applications of Fluid Mechanics*, New York: McGraw-Hill Book Co., Inc., 1947.
- GLAUERT, H. The Effect of Compressibility on the Lift of Airfoils, *Proc. Roy. Soc. (A)*, Vol. 118 (1927), p. 113.
- GOLDSTEIN, S., and YOUNG, A. D. The Application of the Linear Perturbation Theory of Compressible Fluid to Wind Tunnel Interference, *British A.R.C., R & M No. 1909* (1943).
- LAITONE, E. V. New Compressibility Correction for Two-Dimensional Subsonic Flow, *Jour. Aero. Sci.*, Vol. 18, No. 5 (1951), p. 350.

PROBLEMS

10.1. Consider subsonic, two-dimensional flow with small perturbations, and assume that the Prandtl-Glauert rule is valid.

If the free-stream Mach Number at which the local speed on a profile first becomes sonic is 0.80, what is the maximum negative pressure coefficient on the profile at very low Mach Numbers?

10.2. The local pressure coefficient is defined as

$$C_p = \frac{p - p_\infty}{\frac{1}{2} \rho_\infty V_\infty^2}$$

Show that the value of the pressure coefficient corresponding to the critical velocity on the surface of an airfoil is given by

$$C_p^* = \frac{\left(\frac{2}{k+1}\right)^{\frac{k}{k-1}} \left[1 + \frac{k-1}{2} (M_\infty)_{\text{crit}}^2\right]^{\frac{k}{k-1}} - 1}{\frac{k}{2} (M_\infty)_{\text{crit}}^2}$$

Plot C_p^* versus $(M_\infty)_{\text{crit}}$ between values of 0 and 1 for $k = 1.4$.

10.3. The wing of a high-speed airplane has, owing to inaccuracies of manufacture, a bump in a region where the local Mach Number is 0.70. The bump

extends 0.1 inch above the surrounding surface and is about two inches long in the direction of flow.

(a) Estimate the peak Mach Number on the bump, neglecting the boundary layer.

(b) Suppose that a static pressure tap were at the highest point of the bump. What would be the per cent error in static pressure owing to the presence of the bump?

(c) What effect would the presence of a boundary layer have on the foregoing results?

10.4. Show that the potential function

$$\varphi = \frac{V_\infty}{\beta} \frac{h}{1 - e^{-4\pi\beta H/l}} \left(\sin \frac{2\pi x}{l} \right) e^{-2\pi\beta y/l} [1 + e^{4\pi\beta \frac{y-H}{l}}]$$

is a solution of the linearized equation of motion and that it represents the flow in a two-dimensional passage formed by one wavy wall (amplitude h and wave length l) and one straight wall, the two walls being at a lateral distance H from each other.

Explore the flow pattern corresponding to this solution.

Compare the streamlines and wall-pressure distributions with the corresponding quantities when H is infinite.

Compare the influence of the straight wall at a fixed value of H in incompressible flow with that in subsonic flow.

Determine how the "interference velocity perturbation" varies with M_∞ .

10.5. In deriving the similarity rules of this chapter it was assumed arbitrarily that $V_\infty' = V_\infty$. Demonstrate that this is not a restriction on the results by starting anew with the more general form, $V_\infty' = \lambda_v V_\infty$, and showing that the similarity rules thus obtained are the same as those previously obtained.

10.6. In estimating the effect of distance from a profile on the disturbance produced by the profile in incompressible flow, the shape of the profile is not important at very large distances from the profile. For large distances, then, we might consider the disturbance of a doublet to be representative of that of any profile.

The perturbation potential for a doublet at the origin which is superposed on a parallel flow V_∞ is

$$\varphi = \frac{V_\infty x}{x^2 + y^2}$$

and from this it may be shown that, for incompressible flow,

$$u \sim \frac{y^2 - x^2}{(x^2 + y^2)^2}$$

(a) Using this result show that at a fixed point at a large lateral distance ($y/x \rightarrow \pm\infty$) from a fixed profile at a fixed angle of attack, the effect of compressibility on pressure coefficient is given by

$$C_p \sim \frac{1}{(1 - M_\infty^2)^{\frac{3}{2}}}$$

(b) Show that at a fixed large longitudinal distance ($x/y \rightarrow \pm\infty$) from a fixed profile at a fixed angle of attack,

$$C_p \sim \frac{1}{\sqrt{1 - M_\infty^2}}$$

10.7. The NACA profiles in the 4-digit series are defined in the following way. The first digit represents the maximum camber, in per cent of the chord; the second digit the location of the point of maximum camber, in tenths of the chord; and the last two digits the maximum thickness, in per cent of chord. Arbitrary camber equations and thickness functions, together with the number of the airfoil, serve to specify the shape of the profile.

It is proposed to predict the performance of the NACA 4412 profile at a Mach Number of 0.6 and at an angle of attack of 4° , starting with data taken in a low-speed wind tunnel.

For each of the three similarity rules, stipulate the number of the profile which should be tested at zero Mach Number, specify in each case the angle of attack for the low-speed test, and explain how you would extrapolate the data to Mach Number 0.6.

10.8. NACA Report No. 646 gives the following data on lift-curve slopes for the NACA 4412 airfoil, where M is the Mach Number and a is the angle of attack in degrees:

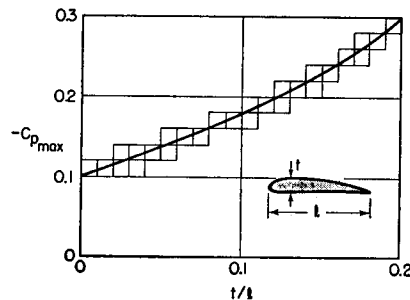
$M:$	0.2	0.3	0.4	0.5	0.6	0.65	0.7	0.75
$dC_L/da:$.108	.113	.115	.124	.130	.132	.127	.100

(a) Plot dC_L/da versus M , using these data.

(b) Starting with the value of dC_L/da at $M = 0.2$, calculate the value of dC_L/da at high Mach Numbers with the aid of the Prandtl-Glauert rule. Plot these results on the chart of part (a).

(c) Plot on the same chart the theoretical lift-curve slope for a flat plate. The lift coefficient of the latter, for zero Mach Number, is $C_L = 2\pi a_r$, where a_r is in radians.

10.9. Wind tunnel tests of a series of affinely related profiles at low speeds and at zero angle of attack yielded the attached curve of maximum negative pressure coefficient versus thickness ratio.



PROB. 10.9.

Using the method of small perturbations, estimate the free-stream Mach Number at which sonic velocity would first be reached at zero angle of attack at the surface of a profile in this series having a 10% thickness ratio.

10.10. In wind tunnel testing the "interference" velocity is defined as the perturbation velocity at a certain point (usually on the profile) minus the perturbation velocity which would exist at the same point if there were no tunnel walls.

For *incompressible*, two-dimensional flow it may be shown that, at least approximately,

$$\left(\frac{\Delta u}{V_\infty}\right)_{\text{incomp}} \sim \left(\frac{l}{2h}\right)^2$$

where l is the profile chord, $2h$ is the height of the tunnel, and Δu is the "interference" velocity.

From this and the similarity rules demonstrate that the effect of compressibility on the interference velocity for a profile of fixed shape in a tunnel of fixed size is given by

$$\frac{(\Delta u/V_\infty)_{\text{comp}}}{(\Delta u/V_\infty)_{\text{incomp}}} = \frac{1}{(1 - M_\infty^2)^{1/2}}$$

10.11. Test Goert's rule for flow inside two-dimensional ducts against results obtained from a one-dimensional analysis according to the type of argument presented in Art. 10.9. Assume that two long sections of straight duct having different cross-sectional areas are joined together. Defining

$$C_p = \frac{p_2 - p_1}{\frac{1}{2}\rho_1 V_1^2}$$

plot C_p/C_p' versus M_1 for a fixed ratio $A_1/A_2 = 1.05$. Compare the results thus obtained with the corresponding results predicted by Goert's rule.

10.12. Consider the two-dimensional flow past an elliptical cylinder at zero angle of attack.

For incompressible flow the maximum velocity at the surface of the ellipse is related to the free-stream velocity by $V_{\max}/V_\infty = 1 + \delta$, where δ is the thickness ratio.

From this information, compute the lower critical Mach Number (the value of M_∞ for which sonic velocity is first reached at the profile surface) for an ellipse with $\delta = 0.15$, using Goert's rule, the Prandtl-Glauert rule, and Laitone's modification of the latter.

Compare your result with the nearly exact result of $M_{\infty\text{crit}} = 0.771$ found by the Rayleigh-Janzen method (cf. Chapter 12).

Chapter 11

HODOGRAPH METHOD FOR TWO-DIMENSIONAL,
SUBSONIC FLOW

11.1. Introductory Remarks

It has already been observed that the nonlinearity and complexity of the partial differential relation (Eq. 9.34) for the velocity potential φ as a function of x and y make it very difficult to obtain solutions for subsonic flow. One of the few simple approaches is the approximate linearized method of the preceding chapter, leading to the Gotthert and Prandtl-Glauert rules. Other techniques are discussed in Chapter 12, including the Rayleigh-Janzen method, numerical relaxation methods, etc., but these are all so cumbersome that they have been used thus far only to solve in a nearly exact manner a few simple problems which are useful for indicating typical results and as a basis of comparison for approximate methods.

The hodograph method is a powerful mathematical approach to problems of two-dimensional flows which are either subsonic or mixed subsonic-supersonic. The term *hodograph* stems from a choice of the velocity coordinates (i.e., u and v in Cartesian coordinates, or V and θ in polar coordinates) as the independent variables, in place of the physical coordinates x and y which have hitherto been employed. One great advantage of this change in variables is that the differential relation for φ or ψ as a function of V and θ is linear, thus allowing complex solutions to be formed by linear superposition of elementary solutions. If, in addition, an approximate form of the isentropic pressure-density relation for the gas (the *tangent-gas relation*) is adopted, the hodograph equations are reducible to the Laplace equation, thus making them accessible to the powerful tool of analytic functions of a complex variable.

Relation Between Physical and Hodograph Streamlines. The nature of the transformation between the physical and hodograph planes and some of the difficulties of the hodograph method may be illustrated by considering the flow past the symmetrical profile of Fig. 11.1a. Two streamlines are identified—the boundary streamline 1-2-3-4-5, and an external streamline 6-7-8. The images of these streamlines in the hodograph plane, Fig. 11.1b, are sketched in by noting that V is the resultant magnitude of the velocity at a point and that θ is the slope of a stream-

line. Along 1-2, for example, θ , for reasons of symmetry, is zero, but the velocity decreases from its free-stream value to zero at the stagnation point. Along 2-3 the speed increases, while the angle θ first increases

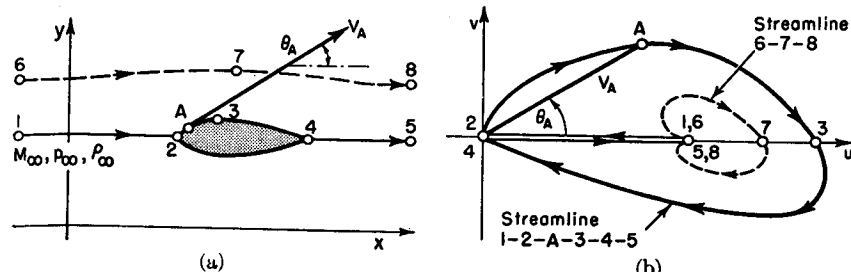


FIG. 11.1. Corresponding streamlines in:

(a) Physical plane.
(b) Hodograph plane.

and then decreases until it is zero at 3. A continuation of this reasoning leads to the streamline shapes of Fig. 11.1b.

Several difficulties are now evident, namely:

(i) The entire physical flow at infinity (points 1, 5, 6, 8, etc.) is mapped into the singular point 1 of the hodograph plane. Furthermore, all stagnation points (2, 4, etc.) are mapped as a single point in the hodograph plane.

(ii) The entire upper half of the physical plane maps into a finite region of the hodograph plane, and this latter region represents also the lower half of the physical plane.

(iii) By far the most serious problem is that the streamline patterns in the two planes are totally dissimilar. Therefore, given a complete solution in the hodograph plane, the physical streamlines can be found only by a laborious transformation. For practical problems, given a body shape in the physical plane, it is very difficult to obtain a solution for the given boundaries by the hodograph method.

Scope of This Chapter. Although the hodograph method is almost unique in providing analytical flow patterns involving both subsonic and supersonic flow, we shall reserve the discussion of mixed flow to Volume II, Chapter 20, and consider now only subsonic flow.

Furthermore, we shall in this chapter discuss in detail only the Karman-Tsien pressure-correction formula for subsonic flow. Other procedures for subsonic flow using the hodograph variables are too lengthy to be treated here, and will be mentioned only briefly.

We shall assume throughout the chapter that the flow is two-dimensional, steady, frictionless, and irrotational.

Additional material relevant to the subject matter of this chapter may be found in Chapter 12 and in Volume II, Chapter 20.

NOMENCLATURE

b	see Fig. 11.10	x, y	Cartesian coordinates
c	speed of sound	z	complex coordinate variable, $x + iy$
C_p	pressure coefficient	\bar{z}	conjugate complex coordinate, $x - iy$
$C_{p, \text{cr}}$	critical pressure coefficient, corresponding to $M = 1$	δ	thickness ratio
$(-C_p)_{\text{max}}$	peak negative pressure coefficient	ζ	complex variable (see Fig. 11.10)
C_D	drag coefficient	θ	direction of velocity vector
i	$\sqrt{-1}$, imaginary operator for complex variable	λ	see Eq. 11.27
k	ratio of specific heats	ρ	mass density
M	Mach Number	σ	see Fig. 11.10
$M_{\infty, \text{cr}}$	free-stream Mach Number for which local sonic velocity is first attained	φ	velocity potential
p	pressure	ψ	stream function
u, v	Cartesian components of velocity vector	$(\cdot)_0$	denotes stagnation state
V	velocity	$(\cdot)_{\infty}$	denotes free-stream conditions
w	complex velocity, $u + iv$	$(\cdot)_i$	denotes incompressible flow
\bar{w}	conjugate complex velocity, $u - iv$		

11.2. Derivation of the Hodograph Equations

Our first task is to derive the differential equations representing the governing physical laws in terms of V and θ as independent variables.

Introduction of Potential and Stream Functions. The condition of irrotationality is satisfied through the introduction of a velocity potential function (see Chapter 9):

$$u = \partial\varphi/\partial x = \varphi_x; \quad v = \partial\varphi/\partial y = \varphi_y \quad (11.1)$$

Similarly, the equation of continuity is satisfied through the introduction of a stream function (see Chapter 9)

$$u = (\rho_0/\rho)(\partial\psi/\partial y) = (\rho_0/\rho)\psi_y; \\ v = -(\rho_0/\rho)(\partial\psi/\partial x) = -(\rho_0/\rho)\psi_x \quad (11.2)$$

Polar Coordinates in Velocity Plane. It is convenient to use polar coordinates for the velocity, as illustrated by Fig. 11.2. Thus

$$u = V \cos \theta; \quad v = V \sin \theta \quad (11.3)$$

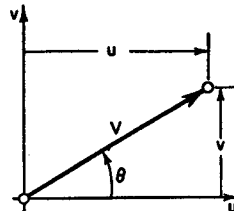


FIG. 11.2. Velocity coordinates.

Art. 11.2 DERIVATION OF THE HODOGRAPH EQUATIONS

Now, noting that φ and ψ are functions of x and y , and making use of Eqs. 11.1 and 11.3, we may write

$$d\varphi = \varphi_x dx + \varphi_y dy = V(\cos \theta dx + \sin \theta dy) \quad (11.4a)$$

$$d\psi = \psi_x dx + \psi_y dy = (\rho_0/\rho)V(-\sin \theta dx + \cos \theta dy) \quad (11.4b)$$

Elimination of Physical Coordinates. Considering these relations as two simultaneous equations for dx and dy in terms of $d\varphi$ and $d\psi$, we may by elimination solve for dx and dy , thus obtaining

$$dx = \frac{\cos \theta}{V} d\varphi - \frac{\rho_0 \sin \theta}{\rho} \frac{d\psi}{V} \quad (11.5a)$$

$$dy = \frac{\sin \theta}{V} d\varphi + \frac{\rho_0 \cos \theta}{\rho} \frac{d\psi}{V} \quad (11.5b)$$

Now, V and θ are functions of x and y . Since φ and ψ are also functions of x and y , it follows that φ and ψ may be considered to be functions of V and θ . Thus, we may write

$$d\varphi = \frac{\partial \varphi}{\partial V} dV + \frac{\partial \varphi}{\partial \theta} d\theta = \varphi_V dV + \varphi_{\theta} d\theta \quad (11.6a)$$

$$d\psi = \frac{\partial \psi}{\partial V} dV + \frac{\partial \psi}{\partial \theta} d\theta = \psi_V dV + \psi_{\theta} d\theta \quad (11.6b)$$

Next, we substitute $d\varphi$ and $d\psi$ from Eqs. 11.6 into Eqs. 11.5:

$$dx = \left(\frac{\cos \theta}{V} \varphi_V - \frac{\rho_0 \sin \theta}{\rho} \psi_V \right) dV + \left(\frac{\cos \theta}{V} \varphi_{\theta} - \frac{\rho_0 \sin \theta}{\rho} \psi_{\theta} \right) d\theta \quad (11.7a)$$

$$dy = \left(\frac{\sin \theta}{V} \varphi_V + \frac{\rho_0 \cos \theta}{\rho} \psi_V \right) dV + \left(\frac{\sin \theta}{V} \varphi_{\theta} + \frac{\rho_0 \cos \theta}{\rho} \psi_{\theta} \right) d\theta \quad (11.7b)$$

Since V and θ are independent of each other,

$$\partial V/\partial V = 1; \quad \partial \theta/\partial \theta = 1; \quad \partial V/\partial \theta = 0; \quad \partial \theta/\partial V = 0$$

Therefore from Eqs. 11.7 we may form

$$\frac{\partial x}{\partial V} = x_V = \frac{\cos \theta}{V} \varphi_V - \frac{\rho_0 \sin \theta}{\rho} \psi_V \quad (11.8a)$$

$$\frac{\partial x}{\partial \theta} = x_{\theta} = \frac{\cos \theta}{V} \varphi_{\theta} - \frac{\rho_0 \sin \theta}{\rho} \psi_{\theta} \quad (11.8b)$$

$$\frac{\partial y}{\partial V} = y_V = \frac{\sin \theta}{V} \varphi_V + \frac{\rho_0 \cos \theta}{\rho} \psi_V \quad (11.8c)$$

$$\frac{\partial y}{\partial \theta} = y_{\theta} = \frac{\sin \theta}{V} \varphi_{\theta} + \frac{\rho_0 \cos \theta}{\rho} \psi_{\theta} \quad (11.8d)$$

We may now eliminate x and y from these equations by noting that

$$\frac{\partial^2 x}{\partial V \partial \theta} = \frac{\partial^2 x}{\partial \theta \partial V}; \quad \frac{\partial^2 y}{\partial \theta \partial V} = \frac{\partial^2 y}{\partial V \partial \theta}$$

The derivative of Eq. 11.8a with respect to θ is therefore set equal to the derivative of Eq. 11.8b with respect to V , and similar operations are performed on the y -derivatives. Thus we obtain after simplification (noting that ρ depends only on V),

$$\begin{aligned} -\frac{\sin \theta}{V} \varphi_V - \frac{\rho_0 \cos \theta}{\rho} \psi_V &= -\frac{\cos \theta}{V^2} \varphi_\theta + \frac{\rho_0 \sin \theta}{\rho} \psi_\theta \\ &\quad - \frac{\sin \theta}{V} \left[\frac{d}{dV} \left(\frac{\rho_0}{\rho} \right) \right] \psi_\theta \end{aligned} \quad (11.9a)$$

$$\begin{aligned} \frac{\cos \theta}{V} \varphi_V - \frac{\rho_0 \sin \theta}{\rho} \psi_V &= -\frac{\sin \theta}{V^2} \varphi_\theta - \frac{\rho_0 \cos \theta}{\rho} \psi_\theta \\ &\quad + \frac{\cos \theta}{V} \left[\frac{d}{dV} \left(\frac{\rho_0}{\rho} \right) \right] \psi_\theta \end{aligned} \quad (11.9b)$$

Now we multiply Eq. 11.9a by $\cos \theta$ and Eq. 11.9b by $\sin \theta$, and add, thus getting

$$\varphi_\theta = (\rho_0/\rho) V \psi_V \quad (11.10)$$

Similarly, we multiply Eq. 11.9a by $\sin \theta$ and Eq. 11.9b by $\cos \theta$, and subtract, thus getting

$$\varphi_V = \left[-\frac{\rho_0}{\rho} \frac{1}{V} + \frac{d}{dV} \left(\frac{\rho_0}{\rho} \right) \right] \psi_\theta = V \left[\frac{d}{dV} \left(\frac{1}{V} \frac{\rho_0}{\rho} \right) \right] \psi_\theta \quad (11.11)$$

Introduction of Dynamic Equation. Since the flow is isentropic, the pressure is uniquely related to the density through the speed of sound, i.e., $dp/d\rho = c^2$. Also, Euler's equation for frictionless, irrotational motion is $dp = -\rho V dV$. With these relations we now form the expression

$$\frac{d}{dV} \left(\frac{\rho_0}{\rho} \right) = -\frac{\rho_0}{\rho^2} \frac{dp}{dV} = -\frac{\rho_0}{\rho} \frac{dp}{dp} \frac{dp}{dV} = -\frac{\rho_0}{\rho} \left(\frac{1}{c^2} \right) (-\rho V) = \frac{\rho_0}{\rho} \frac{V}{c^2} \quad (11.12)$$

Substituting this into Eq. 11.11, we have, after rearrangement,

$$\varphi_V = -\frac{\rho_0}{\rho} \frac{1}{V} \left(1 - \frac{V^2}{c^2} \right) \psi_\theta = -\frac{\rho_0}{\rho} \frac{1}{V} (1 - M^2) \psi_\theta \quad (11.13)$$

To eliminate φ from Eqs. 11.10 and 11.13, we set $\varphi_{\theta V} = \varphi_{V \theta}$. Thus, noting that ρ and M depend only on V , and using Eq. 11.12,

$$\frac{\partial}{\partial V} \left(\frac{\partial \varphi}{\partial \theta} \right) = \frac{\partial}{\partial V} \left[\frac{\rho_0}{\rho} V \psi_V \right] = \frac{\rho_0}{\rho} (V \psi_{VV} + \psi_V) + V \psi_V \left(\frac{\rho_0}{\rho} \frac{V}{c^2} \right)$$

$$\frac{\partial}{\partial \theta} \left(\frac{\partial \varphi}{\partial V} \right) = \frac{\partial}{\partial \theta} \left[-\frac{\rho_0}{\rho} \frac{1}{V} \left(1 - \frac{V^2}{c^2} \right) \psi_\theta \right] = -\frac{\rho_0}{\rho} \frac{1}{V} (1 - M^2) \psi_{\theta \theta}$$

Differential Equation of the Stream Function in the Hodograph Plane. Equating the two preceding equations, and simplifying, we finally get

$$\frac{\partial}{\partial V} \left(\frac{\rho_0}{\rho} V \psi_V \right) + \frac{\rho_0}{\rho} \frac{1}{V} (1 - M^2) \psi_{\theta \theta} = 0 \quad (11.14a)$$

or

$$V^2 \frac{\partial^2 \psi}{\partial V^2} + V \left(1 + \frac{V^2}{c^2} \right) \frac{\partial \psi}{\partial V} + \left(1 - \frac{V^2}{c^2} \right) \psi_{\theta \theta} = 0 \quad (11.14b)$$

which is the desired relation giving ψ as a function of V and θ , since c is a function of V only. This differential equation is linear in the dependent variable ψ .

Procedure for Obtaining Physical Flow Pattern from Hodograph Solution. Assuming that a function $\psi = \psi(V, \theta)$ has been found which satisfies Eq. 11.14, the procedure for determining the flow pattern is as follows:

- (i) The derivatives ψ_V and ψ_θ as functions of V and θ are found by direct differentiation of $\psi = \psi(V, \theta)$.
- (ii) Using Eqs. 11.10 and 11.13, φ_θ and φ_V are found as functions of V and θ .
- (iii) Eqs. 11.7 are integrated to give x and y as functions of V and θ .

Since we started with a solution for ψ in terms of V and θ , we thus have ψ in terms of x and y . That is, we have the physical streamlines. If these physical streamlines represent a practical problem of interest, the solution is useful—otherwise not. The great disadvantage of the hodograph method may now clearly be seen, namely, that the problem of flow past given boundaries is not susceptible to direct treatment by the hodograph method.

11.3. The Tangent-Gas Approximation

The principal application of Eq. 11.14 which we shall discuss in this chapter is the Karman-Tsien pressure correction formula. This is arrived at through the use of an approximate pressure-density relation, the use of which allows us to construct compressible flows from known incompressible flows.

Definition of Tangent Gas. Referring to Fig. 11.3, the $p-\rho$ relation which we shall call the *tangent gas* approximation is defined by drawing a tangent to the true isentropic curve of p versus $1/\rho$ at the point representing free-stream conditions, p_∞ and ρ_∞ .

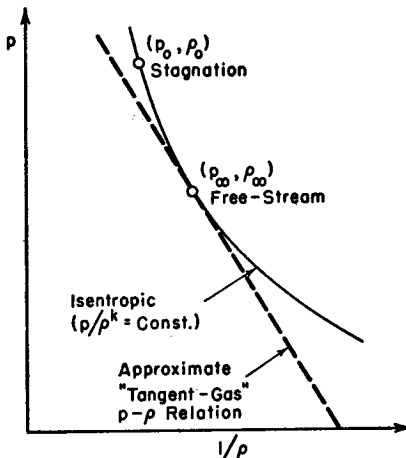


FIG. 11.3. Illustrates definition of tangent gas.

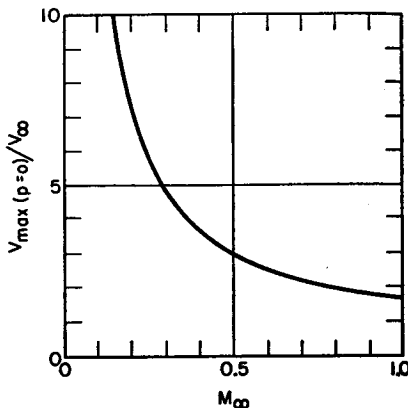


FIG. 11.4. Limiting velocity for tangent gas.

The straight-line relation between pressure and specific volume has a constant slope which may be written (remembering that $dp/d\rho = c^2$) as

$$-\frac{dp}{d(1/\rho)} = \rho^2 \frac{dp}{d\rho} = \rho^2 c^2 = \rho_\infty^2 c_\infty^2 = p_0^2 c_0^2 = \text{constant} \quad (11.15)$$

Separation of variables and integration of Eq. 11.15 now yields the tangent-gas pressure-density relation in terms of free-stream properties:

$$p - p_\infty = c_\infty^2 \rho_\infty \left(1 - \frac{\rho_\infty}{\rho} \right) \quad (11.16)$$

Dynamic Equation for Tangent Gas. Combining Euler's equation of motion with Eq. 11.15, we get

$$\int_{V_\infty}^V V dV = - \int_{p_\infty}^p \frac{dp}{\rho} = - \int_{p_\infty}^p \frac{dp}{d\rho} \frac{d\rho}{\rho} = - \rho_\infty^2 c_\infty^2 \int_{p_\infty}^p \frac{d\rho}{\rho^3}$$

Integrating, we get

$$V^2 - V_\infty^2 = \rho_\infty^2 c_\infty^2 \left(\frac{1}{\rho^2} - \frac{1}{\rho_\infty^2} \right) = c_\infty^2 \left(\frac{\rho_\infty}{\rho} \right)^2 - c_\infty^2 = c^2 - c_\infty^2$$

from which it follows that

$$V^2 - c^2 = V_\infty^2 - c_\infty^2 = \text{constant} \quad (11.17a)$$

Furthermore, since V is zero at the stagnation state,

$$V^2 = c^2 - c_0^2 \quad (11.17b)$$

Now, combining Eq. 11.17 with Eq. 11.15 in various ways, we find

$$\left(\frac{V}{c} \right)^2 = 1 - \left(\frac{c_0}{c} \right)^2 = 1 - \left(\frac{\rho}{\rho_0} \right)^2; \quad \left(\frac{\rho}{\rho_0} \right)^2 = 1 - \left(\frac{V}{c} \right)^2 = 1 - M^2 \quad (11.18a)$$

$$\left(\frac{V}{c_0} \right)^2 = \left(\frac{c}{c_0} \right)^2 - 1 = \left(\frac{\rho_0}{\rho} \right)^2 - 1; \quad \left(\frac{\rho_0}{\rho} \right)^2 = 1 + \left(\frac{V}{c_0} \right)^2 \quad (11.18b)$$

$$\left(\frac{V}{c_\infty} \right)^2 = \left(\frac{c}{c_\infty} \right)^2 - \left(\frac{c_0}{c_\infty} \right)^2 = \left(\frac{\rho_\infty}{\rho} \right)^2 - \left(\frac{\rho_\infty}{\rho_0} \right)^2 \quad (11.18c)$$

Equations 11.15, 11.16, 11.17, and 11.18 give the relations between the various fluid properties for the tangent gas, and replace the customary isentropic relations. The accuracy of these formulas of course depends on how close the fluid properties in the flow field are to the free-stream properties.

Let us see what happens during an acceleration of this fictitious gas. As V increases, Eq. 11.18b shows that ρ decreases. But Eq. 11.17 shows that c increases! From Eq. 11.18a, on the other hand, M increases, but can never exceed unity. Hence the approximate methods outlined here are applicable only to subsonic flow.

Limitations of Tangent-Gas Approximation. Another way of examining the limitations of the tangent gas is to note that for sufficiently large accelerations the pressure may become negative. We proceed to determine when the latter condition is reached. Setting $p = 0$, Eq. 11.16 becomes

$$\frac{p_\infty}{c_\infty^2 \rho_\infty} = \frac{\rho_\infty}{\rho} - 1$$

But, at the point of tangency, the true isentropic relations may be employed. Thus, $c_\infty^2 = kp_\infty/\rho_\infty$, and the preceding relation becomes simply

$$\frac{\rho_\infty}{\rho} - 1 = \frac{1}{k}; \quad \frac{\rho_\infty}{\rho} = \frac{k+1}{k}$$

Combining this expression with Eqs. 11.18c and 11.18a, we have

$$\left(\frac{V_{\max}}{c_\infty} \right)^2 = \left(\frac{k+1}{k} \right)^2 - (1 - M_\infty^2)$$

Then, forming V_{\max}/V_∞ , we obtain

$$\frac{V_{\max}}{V_\infty} = \frac{V_{\max}}{c_\infty} \cdot \frac{c_\infty}{V_\infty} = \frac{1}{M_\infty} \sqrt{\left(\frac{k+1}{k} \right)^2 - 1 + M_\infty^2} \quad (11.19)$$

which shows, for any given values of M_∞ and V_∞ , the maximum local velocity which can be reached without the attainment of negative pressures. The relation is shown graphically in Fig. 11.4. For thin profiles, it is known that the maximum local velocity seldom exceeds twice the free-stream velocity. Fig. 11.4 shows, therefore, that the possibility of the pressure becoming negative is not often an important limitation.

11.4. The Karman-Tsien Pressure Correction Formula

Differential Equation for Case of Tangent Gas. Multiplication of Eq. 11.14a by $V\rho/\rho_0(1 - M^2)$ gives the differential relation for ψ in terms of V and θ in the form

$$\frac{\rho}{\rho_0} \frac{V}{1 - M^2} \frac{\partial}{\partial V} \left(\frac{\rho_0}{\rho} V \psi_V \right) + \psi_{\theta\theta} = 0 \quad (11.20)$$

For the tangent gas, however, Eq. 11.18a shows that

$$\rho/\rho_0 = \sqrt{1 - M^2}$$

We introduce this relation into Eq. 11.20, and thus obtain, subject to the tangent-gas approximation,

$$\frac{V}{\sqrt{1 - M^2}} \frac{\partial}{\partial V} \left(\frac{V}{\sqrt{1 - M^2}} \psi_V \right) + \psi_{\theta\theta} = 0 \quad (11.21)$$

Introduction of Transformed Incompressible Velocity. By means of a transformation, this equation may be reduced to that of an incompressible flow. We define a new variable, V_i , which is a function only of the velocity V , through the relation

$$\frac{dV_i}{V_i} = \sqrt{1 - M^2} \frac{dV}{V} \quad (11.22)$$

Since V_i and V are uniquely related through Eq. 11.22, Eq. 11.21 may now be expressed in terms of V_i rather than V . Noting that, according to Eq. 11.22,

$$\frac{d}{dV} = \left(\frac{dV_i}{dV} \right) \left(\frac{d}{dV_i} \right) = \frac{V_i}{V} \sqrt{1 - M^2} \frac{d}{dV_i}$$

and replacing V -derivatives in Eq. 11.21 by V_i -derivatives, we get

$$\frac{V}{\sqrt{1 - M^2}} \left[\frac{V_i}{V} \sqrt{1 - M^2} \right] \frac{\partial}{\partial V_i} \left[\frac{V}{\sqrt{1 - M^2}} \cdot \frac{V_i}{V} \sqrt{1 - M^2} \frac{\partial \psi}{\partial V_i} \right] + \psi_{\theta\theta} = 0$$

or, after simplifying,

$$V_i \frac{\partial}{\partial V_i} (V_i \psi_{V_i}) + \psi_{\theta\theta} = 0 \quad (11.23a)$$

Incompressible Flows as a Basis for Constructing Compressible Flows. Eq. 11.23a is evidently identical in form with Eq. 11.21 if we set $M = 0$ in the latter relation. Hence Eq. 11.23a is the differential equation, in hodograph coordinates, for an incompressible flow with the velocity (V_i, θ) , and its solution, $\psi_i = \psi_i(V_i, \theta)$, therefore represents the flow pattern of an incompressible fluid.

The significance of this result is that it now allows us to obtain results, at least approximately, for *given* boundary conditions (e.g., a specific profile) in the physical plane. Suppose we have the solution for incompressible flow past the given profile, $\psi_i = \psi_i(x_i, y_i)$. From this we may find the incompressible velocity components in terms of x_i and y_i , and so we have the incompressible solution in hodograph coordinates, $\psi_i = \psi_i(V_i, \theta)$. But, if the latter is a solution of Eq. 11.23a, a function $\psi(V, \theta)$ of the same form must also be a solution of Eq. 11.21 because Eqs. 11.23a and 11.21 are transformations of each other through the medium of Eq. 11.22. Note that the compressible solution is found from the incompressible solution merely by replacing V_i by V , i.e., we set

$$\psi(V, \theta) = \psi_i(V_i, \theta) \quad (11.23b)$$

From the compressible solution, $\psi = \psi(V, \theta)$, the profile shape in the physical plane may be found by integration of Eq. 11.7. The compressible-flow profile thus found will, in general, be different from the original incompressible-flow profile. However, we can at least make them similar by insuring that the compressible solution merges continuously into the incompressible one as M_∞ approaches zero. This is done by integrating Eq. 11.22 with such limits that $V \rightarrow V_i$ as $M_\infty \rightarrow 0$.

Two distinct steps are involved in this method: first, finding the relation between the corresponding velocities in the compressible and incompressible flows; second, finding the relation between the corresponding profile shapes. Let us proceed now to the determination of the relation between the corresponding velocities.

Relation Between Corresponding Velocities. Combining Eq. 11.22 with Eqs. 11.18a and 11.18b, we have,

$$\frac{dV_i}{V_i} = \frac{\rho}{\rho_0} \frac{dV}{V} = \frac{dV}{V \sqrt{1 + \frac{c_0^2}{V^2}}} = \frac{c_0 dV}{V \sqrt{c_0^2 + V^2}}$$

Integrating, and letting K be the constant of integration, we have

$$\log V_i = - \log \frac{c_0 + \sqrt{c_0^2 + V^2}}{V} + \log K$$

or,

$$V_i = \frac{KV}{c_0 + \sqrt{c_0^2 + V^2}} = \frac{KV}{c_0[1 + \sqrt{1 + (V/c_0)^2}]}$$

Now, for reasons given previously, we let $V = V_i$ when $V/c_0 = 0$. Thus we get $K = 2c_0$, and, therefore,

$$V_i = \frac{2V}{1 + \sqrt{1 + (V/c_0)^2}} \quad (11.24a)$$

Solving explicitly for V in terms of V_i we obtain

$$V = \frac{4c_0^2 V_i}{4c_0^2 - V_i^2} \quad (11.24b)$$

We would like to obtain the relation between V and V_i in terms of M_∞ rather than c_0 . To do this, we proceed as follows. In terms of free-stream conditions, Eq. 11.24b may be written

$$V_\infty = \frac{4c_0^2 V_\infty}{4c_0^2 - V_\infty^2} \quad (11.25)$$

Dividing Eq. 11.24b by Eq. 11.25, we obtain

$$\frac{V}{V_\infty} = \frac{V_i}{V_\infty} \cdot \frac{4c_0^2 - V_\infty^2}{4c_0^2 - V_i^2} = \frac{V_i}{V_\infty} \cdot \frac{1 - \left(\frac{V_\infty}{2c_0}\right)^2}{1 - \left(\frac{V_\infty}{2c_0}\right)^2 \left(\frac{V_i}{V_\infty}\right)^2} = \frac{\frac{V_i}{V_\infty} (1 - \lambda)}{1 - \lambda \left(\frac{V_i}{V_\infty}\right)^2} \quad (11.26)$$

where, for brevity, we have defined

$$\lambda \equiv (V_\infty/2c_0)^2$$

Now, combining the latter relation with Eq. 11.24a written for free-stream conditions, we have

$$\sqrt{\lambda} = \frac{V_\infty/c_0}{1 + \sqrt{1 + (V_\infty/c_0)^2}} = \frac{(V_\infty/c_\infty)(c_\infty/c_0)}{1 + \sqrt{1 + (V_\infty/c_\infty)^2(c_\infty/c_0)^2}}$$

But, from Eq. 11.18a,

$$(c_0/c_\infty)^2 = 1 - M_\infty^2$$

and thus we obtain after simplification,

$$\lambda = \frac{M_\infty^2}{(1 + \sqrt{1 - M_\infty^2})^2} \quad (11.27)$$

Eqs. 11.26 and 11.27 taken together comprise the relation between the corresponding compressible and incompressible velocities. We now come to the final and most important step, namely, finding a relation between the corresponding pressure coefficients.

Pressure-Coefficient Correction Formula. Using Eq. 11.16, the pressure coefficient becomes

$$C_p = \frac{p - p_\infty}{\frac{1}{2} \rho_\infty V_\infty^2} = \frac{2c_\infty^2 \left(1 - \frac{\rho_\infty}{\rho}\right)}{V_\infty^2} = \frac{2}{M_\infty^2} \left(1 - \frac{\rho_\infty}{\rho}\right)$$

Dividing Eq. 11.17a by c_∞^2 , and introducing Eq. 11.15, we form

$$\left(\frac{V}{V_\infty}\right)^2 \left(\frac{V_\infty}{c_\infty}\right)^2 - \left(\frac{V_\infty}{c_\infty}\right)^2 = \left(\frac{c}{c_\infty}\right)^2 - 1 = \left(\frac{\rho_\infty}{\rho}\right)^2 - 1$$

Solving for ρ_∞/ρ , and substituting in the formula for C_p , we get

$$C_p = \frac{2}{M_\infty^2} \left[1 - \sqrt{1 - M_\infty^2 + M_\infty \left(\frac{V}{V_\infty}\right)^2} \right]$$

Now, for incompressible flow, Bernoulli's equation yields

$$C_{p_i} = 1 - (V_i/V_\infty)^2$$

Therefore, Eq. 11.26 may be written as

$$\frac{V}{V_\infty} = \frac{\sqrt{1 - C_{p_i}} (1 - \lambda)}{1 - \lambda (1 - C_{p_i})}$$

Substituting this expression for V/V_∞ into the previous relation for C_p , and simplifying, we finally obtain the Karman-Tsien pressure-correction formula:

$$C_p = \frac{C_{p_i}}{\sqrt{1 - M_\infty^2} + \frac{M_\infty^2}{1 + \sqrt{1 - M_\infty^2}} \frac{C_{p_i}}{2}} \quad (11.28)$$

Application of Karman-Tsien Rule. As mentioned previously, the two pressure coefficients in this formula correspond to slightly different profiles, and so do not strictly indicate the influence of Mach Number for a profile of given shape. However, the distortion of the profile during the transformation is usually very small, and Eq. 11.28 is commonly employed to estimate the effect of M_∞ on the pressure coefficient for a profile of fixed shape. It is the most widely accepted pressure-correction formula for two-dimensional, subsonic flow.

Fig. 11.5a is a graphical version of Eq. 11.28, showing how C_p varies with M_∞ for various values of C_{p_i} . Also indicated are lines of constant

local Mach Number, based on the isentropic relation between Mach Number and pressure ratio, from which may be found

$$C_p = \frac{2}{kM_\infty^2} \left[\left(\frac{1 + \frac{k-1}{2} M_\infty^2}{1 + \frac{k-1}{2} M^2} \right)^{\frac{k}{k-1}} - 1 \right]$$

Lower Critical Mach Number. Where the line for a particular value of C_{p_i} intersects the line marked $M = 1$ (sonic line) in Fig. 11.5a, there may be read on the horizontal scale the value of M_∞ for which the sonic velocity is reached locally at the point having the particular low-speed coefficient C_{p_i} . It is known from experience that soon after supersonic speeds are reached locally, there are usually rapid increases in the drag coefficient, and the corresponding value of M_∞ is called the *lower critical Mach Number*, $M_{\infty \text{ cr}}$. Fig. 11.5b, which is based on the Karman-Tsien pressure-correction curves of Fig. 11.5a, shows $M_{\infty \text{ cr}}$ as a function of C_{p_i} . Given the peak negative pressure coefficient for a profile at low speeds, Fig. 11.5b shows approximately the free-stream Mach Number at which compressibility effects begin to have a serious adverse effect on drag.

Comparison with Prandtl-Glauert Rule. For very small values of the pressure coefficient, that is, for very small perturbations from free-stream conditions, Eq. 11.28 reduces to the Prandtl-Glauert rule, $C_p = C_{p_i} / \sqrt{1 - M_\infty^2}$.

When C_p is negative, corresponding to regions of velocity higher than free-stream velocity, the Karman-Tsien (K-T) formula indicates a greater influence of compressibility than does the Prandtl-Glauert (P-G) formula. As a result, the K-T rule leads to a value of the lower critical Mach Number smaller than that computed by the P-G rule.

For positive values of C_p , on the other hand, the K-T rule predicts a compressibility effect which is smaller than that predicted by the P-G rule. This is not of great practical importance, however.

Since the effects of compressibility depend on the local pressure coefficient, the K-T rule does not allow the derivation of a simple relation showing the effects of compressibility on the force coefficients of a given profile. If low-speed pressure distributions for the profile are available, however, these may be corrected to higher Mach Numbers by the K-T formula, and then, by integration, the high-speed force coefficients may be found.

Accuracy of Karman-Tsien Pressure-Correction Formula. The reliability of the Karman-Tsien pressure-correction formula may be tested by (i) comparing it with experimental data, or (ii) comparing it

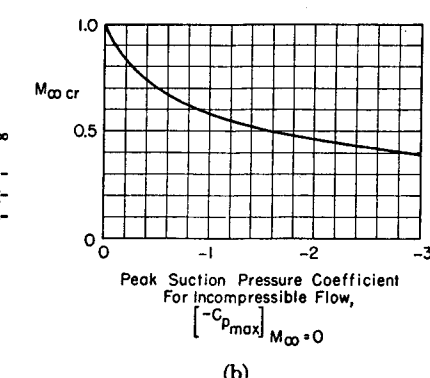
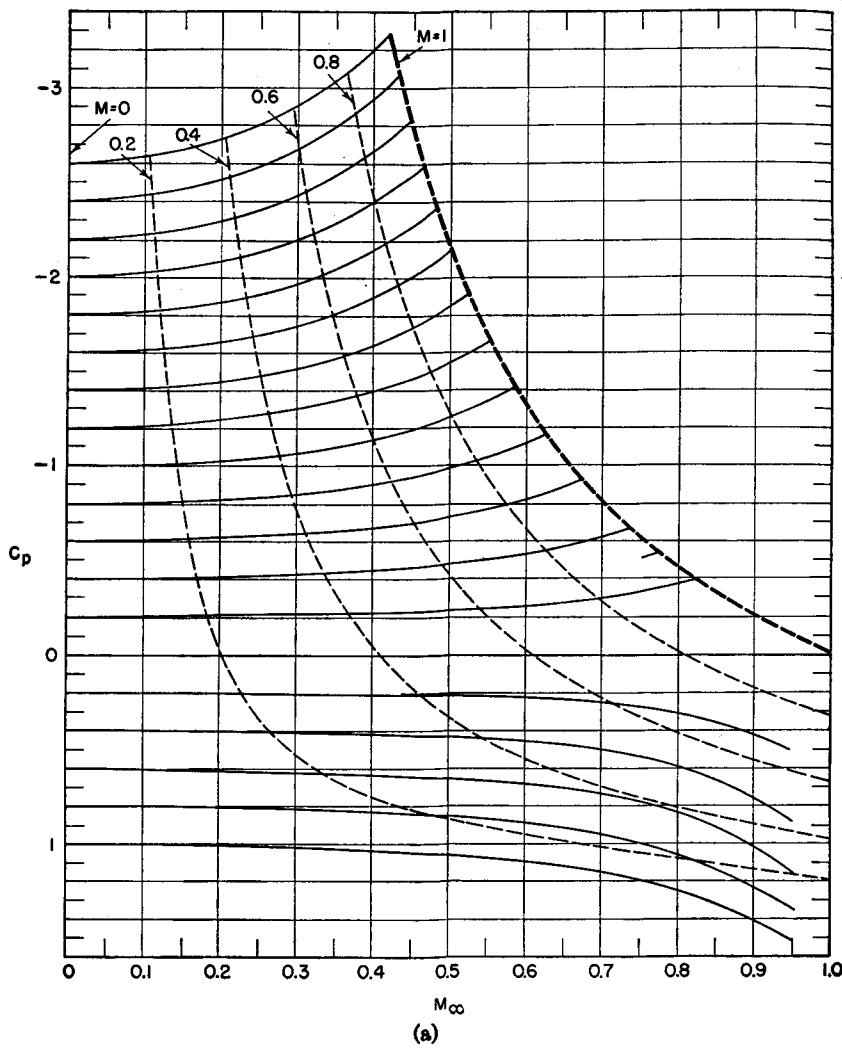


FIG. 11.5. (a) Variation of C_p with M_∞ according to Karman-Tsien rule.

(b) Corresponding curve of lower critical Mach Number versus maximum negative pressure coefficient for incompressible flow.

with more accurate analytical results for simple cases where this is possible.

Fig. 11.6, which is a typical comparison ⁽²⁾ between experimental data, the K-T rule, and the P-G rule, indicates good agreement between the measurements and the K-T rule, but shows the P-T rule to underestimate the effect of compressibility.

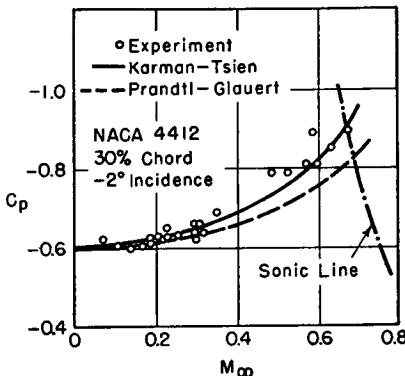


FIG. 11.6. Comparison of Karman-Tsien rule with experiment.

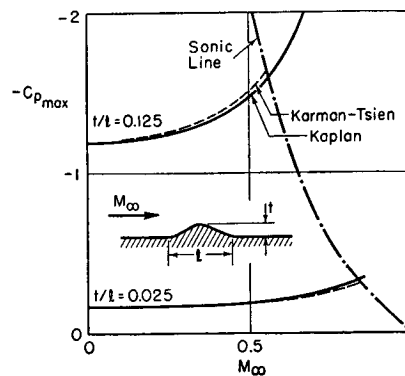


FIG. 11.7. Comparison of Karman-Tsien rule with exact theoretical result (Kaplan) for flow over a bump.

Fig. 11.7 shows excellent agreement between (i) exact analytical results for the maximum negative pressure coefficient as a function of M_∞ for flow over a bump ⁽⁴⁾ and (ii) the predictions of the Karman-Tsien formula as to the shape of the curve of $(-C_p)_{\max}$ versus M_∞ .

An examination of the assumptions underlying both the Prandtl-Glauert and Karman-Tsien rules shows that both rules are limited by the restriction of small perturbations, and hence can reasonably be expected to be reliable only for thin profiles at small angles of attack. However, the P-G rule is also limited to small Mach Numbers, whereas the K-T rule is not so limited. Hence, as verified by experimental and analytical results, the K-T rule may be expected to be more accurate than the P-G rule at high subsonic speeds.

Fig. 11.3 shows that in the range of negative pressure coefficients, i.e., the range of greatest practical significance, the tangent gas produces a lesser density change for a given pressure change than does the true isentropic. It would seem, therefore, that the Karman-Tsien rule should underestimate the effects of compressibility. However, as discussed below, the coordinate correction in the corresponding flows is such as to make the compressible profile thicker than the corresponding incompressible profile. Thus the compressibility effect would be overestimated if we took no account of the coordinate correction in comparing the compressible flow with its corresponding incompressible flow. By apply-

Art. 11.5 CALCULATION OF PROFILE SHAPE CORRECTION

351

ing the K-T formula to profiles of fixed shape we thus produce two errors in opposite directions, and the experimental evidence seems to indicate that they nearly cancel each other.

11.5. Calculation of Profile Shape Correction

Incompressible flow patterns may, for the tangent-gas approximation, be transformed to corresponding compressible flow patterns as indicated by Eq. 11.23b. The corresponding velocities in the two flows are related by Eq. 11.22, from which we derived Eqs. 11.26 and 11.28. It now remains to find the corresponding streamline patterns in the physical plane, or, in other words, to find the relation between the incompressible and compressible profiles. The relation between the various planes in the corresponding flows is shown by Fig. 11.8.

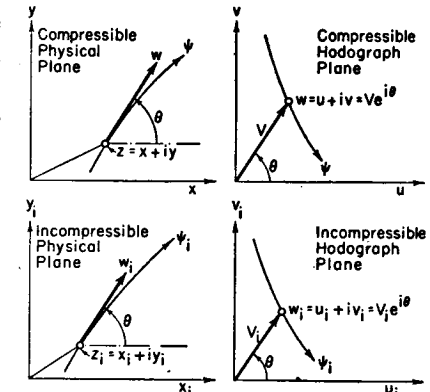


FIG. 11.8. Complex physical and velocity planes for incompressible and compressible flow.

Introduction of Complex Variables. The calculations are greatly abbreviated through the use of complex variables. Let the locations of corresponding points in the compressible and incompressible physical planes be represented respectively by the complex quantities

$$z = x + iy; \quad z_i = x_i + iy_i$$

where $i = \sqrt{-1}$. Also, after noting that the flow direction θ is the same for the corresponding flows, let the corresponding velocities be represented by the complex quantities

$$w = u + iv = Ve^{i\theta}$$

$$w_i = u_i + iv_i = V_i e^{i\theta}$$

Now, for incompressible, steady, irrotational, two-dimensional flow, the velocity components may be written in terms of the velocity potential and stream function as

$$u_i = \partial\varphi_i/\partial x_i = \partial\psi_i/\partial y_i$$

$$v_i = \partial\varphi_i/\partial y_i = -\partial\psi_i/\partial x_i$$

These may be recognized as the Cauchy-Riemann equations. We know

from the theory of functions that the incompressible complex potential, $\varphi_i + i\psi_i$, may accordingly be expressed as an analytic function of z_i , i.e.,

$$\varphi_i + i\psi_i = F(z_i) \quad (11.29a)$$

It is also well known⁽⁵⁾ that the conjugate complex velocity is then given by

$$w_i = u_i - iv_i = V_i e^{-i\theta} = \frac{dF}{dz_i} \quad (11.29b)$$

Since this relation gives w_i as an analytic function $w_i(z_i)$ of z_i , it follows that z_i is an analytic function of w_i . Then, from Eq. 11.29a, $\varphi_i + i\psi_i$ must be expressible as an analytic function of w_i :

$$\varphi_i + i\psi_i = F[z_i(w_i)] = G(w_i) \quad (11.30)$$

By changing the signs of the imaginary parts of Eqs. 11.29 and 11.30, we get

$$\varphi_i - i\psi_i = \tilde{F}(\bar{z}_i) = \tilde{G}(w_i) \quad (11.31)$$

and

$$w_i = u_i + iv_i = V_i e^{i\theta} = d\tilde{F}/d\bar{z}_i \quad (11.32)$$

Now Eq. 11.23b tells us that an incompressible solution $\psi_i(V_i, \theta) = 0$ yields a corresponding compressible solution $\psi(V, \theta) = 0$ if we merely replaced V_i by V in the former equation, provided that V_i and V are connected by Eq. 11.24. Noting that θ is constant in the transformation, it follows that

$$\varphi + i\psi = G(w); \quad \varphi - i\psi = \tilde{G}(w)$$

It seems reasonable to suppose that the functions $G(w)$ and $\tilde{G}(w)$ may be respectively approximated with good accuracy by the functions $G(w_i)$ and $\tilde{G}(w_i)$, inasmuch as w and w_i are nearly alike. Hence we write

$$\varphi + i\psi = G(w_i) = F(z_i); \quad d\varphi + i d\psi = dF \quad (11.33)$$

$$\varphi - i\psi = \tilde{G}(w_i) = \tilde{F}(\bar{z}_i); \quad d\varphi - i d\psi = d\tilde{F} \quad (11.34)$$

In Eqs. 11.5 there appears the term ρ_0/ρ , for which we now write with the help of Eqs. 11.18b and 11.24b,

$$\frac{\rho_0}{\rho} = \sqrt{1 + \left(\frac{4c_0 V_i}{4c_0^2 - V_i^2} \right)^2} = \frac{4c_0^2 + V_i^2}{4c_0^2 - V_i^2} \quad (11.35)$$

Coordinate Correction Formula. Having set down these preliminaries, we now rewrite Eqs. 11.5 in the following form, using Eq. 11.24b to substitute for V , and Eq. 11.35 to substitute for ρ_0/ρ :

$$dx = \frac{4c_0^2 - V_i^2}{4c_0^2 V_i} \cos \theta d\varphi - \frac{4c_0^2 + V_i^2}{4c_0^2 V_i} \sin \theta d\psi$$

$$dy = \frac{4c_0^2 - V_i^2}{4c_0^2 V_i} \sin \theta d\varphi + \frac{4c_0^2 + V_i^2}{4c_0^2 V_i} \cos \theta d\psi$$

With these relations we now form, noting that $(\cos \theta + i \sin \theta) = e^{i\theta}$,

$$\begin{aligned} dz &= dx + i dy = \frac{1}{V_i} \left(1 - \frac{V_i^2}{4c_0^2} \right) e^{i\theta} d\varphi + \frac{i}{V_i} \left(1 + \frac{V_i^2}{4c_0^2} \right) e^{i\theta} d\psi \\ &= \frac{e^{i\theta}}{V_i} (d\varphi + i d\psi) - \frac{e^{i\theta} V_i^2}{V_i 4c_0^2} (d\varphi - i d\psi) \end{aligned}$$

Now, making use of Eqs. 11.29 to 11.34, this may be brought into the form

$$dz = dz_i - \frac{1}{4c_0^2} \left(\frac{d\tilde{F}}{d\bar{z}_i} \right)^2 d\bar{z}_i$$

Finally, noting that $\lambda = (V_{\infty}/2c_0)^2$, we get

$$dz = dz_i - \lambda \left(\frac{1}{V_{\infty}} \frac{d\tilde{F}}{d\bar{z}_i} \right)^2 d\bar{z}_i \quad (11.36)$$

where λ is given in terms of M_{∞} by Eq. 11.27.

Eq. 11.36 is the desired relation connecting corresponding points in the two physical planes. Upon integration, and noting that the constant of integration is immaterial to the shape of the flow pattern, we have

$$z = z_i - \lambda \int \left(\frac{1}{V_{\infty}} \frac{d\tilde{F}}{d\bar{z}_i} \right)^2 d\bar{z}_i \quad (11.37)$$

Thus, the compressible physical coordinates are equal to the corresponding incompressible physical coordinates plus a correction term proportional to λ . As shown by Fig. 11.9, λ is small, especially at moderate Mach Numbers, and goes to zero as M_{∞} approaches zero, thus proving that the compressible flow pattern merges gradually into the incompressible flow pattern. In specific examples the correction term usually proves to be very small, and, consequently, there is little difference in profile shape between the corresponding flows.

The complete Karman-Tsien method may now be summarized thus: If the pressure distribution in incompressible flow for a given profile is

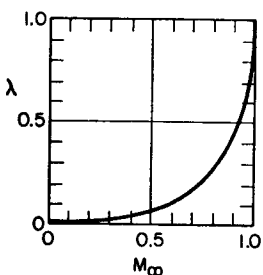


FIG. 11.9. The factor λ in the Karman-Tsien coordinate correction formula.

known, then a corresponding compressible flow at any other Mach Number, M_∞ , may be constructed, using Eq. 11.37 as a coordinate correction formula and Eq. 11.28 as a pressure correction formula to relate the location and pressure coefficient at corresponding points in the two flows.

Application of Shape-Correction Formula to Flow Past Elliptical Cylinder. To illustrate the procedure for profile correction, let us consider the incompressible flow past the ellipse of Fig. 11.10a. The incompressible flow past an ellipse in the z_i -plane may be found from the in-

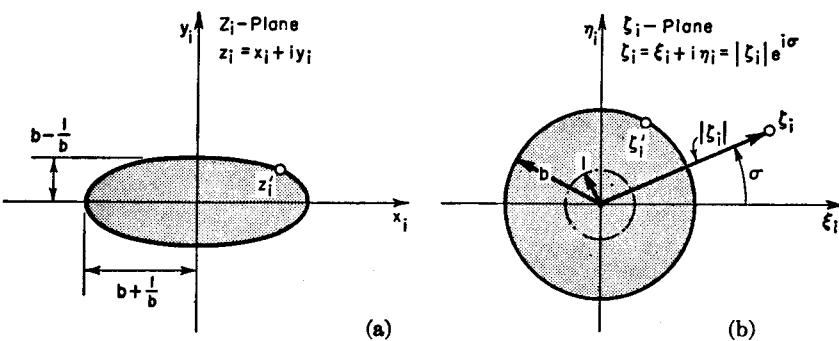


FIG. 11.10. Transformation of a circle to an ellipse (incompressible flow).

compressible flow past the circle of radius b in the ζ_i -plane of Fig. 11.10b through the conformal transformation

$$z_i = \zeta_i + \frac{1}{\zeta_i}; \quad \tilde{z}_i = \zeta_i + \frac{1}{\zeta_i} \quad (11.38)$$

To prove this, note that, at the surface of the circle of radius b , the ζ_i -coordinate is $\zeta_i' = be^{i\sigma}$, and hence

$$z_i' = \zeta_i' + \frac{1}{\zeta_i'} = be^{i\sigma} + \frac{1}{b}e^{-i\sigma} = \left(b + \frac{1}{b}\right)\cos\sigma + i\left(b - \frac{1}{b}\right)\sin\sigma$$

Separating real and imaginary parts, we have

$$x_i' = \left(b + \frac{1}{b}\right)\cos\sigma; \quad y_i' = \left(b - \frac{1}{b}\right)\sin\sigma$$

and, eliminating σ through the relation, $\sin^2\sigma + \cos^2\sigma = 1$, we get

$$\left(\frac{x_i'}{b + \frac{1}{b}}\right)^2 + \left(\frac{y_i'}{b - \frac{1}{b}}\right)^2 = 1$$

This is the equation of an ellipse in the z_i -plane, with thickness ratio

$$\delta_i = \frac{b - \frac{1}{b}}{b + \frac{1}{b}} = \frac{b^2 - 1}{b^2 + 1} \quad (11.39)$$

The complex potential for the flow past the circle in the ζ_i -plane is well known⁽⁶⁾ and is given by the superposition of a uniform flow and a doublet:

$$F(\zeta_i) = V_{i\infty} \left(\zeta_i + \frac{b^2}{\zeta_i} \right) \quad (11.40a)$$

Changing the sign of the imaginary part gives the conjugate complex potential,

$$\tilde{F}(\zeta_i) = V_{i\infty} \left(\zeta_i + \frac{b^2}{\zeta_i} \right) \quad (11.40b)$$

Now, since z_i and ζ_i are uniquely related, we may write, after taking the derivatives of Eqs. 11.38 and 11.40b,

$$\frac{d\tilde{F}}{d\tilde{z}_i} = \frac{d\tilde{F}/d\zeta_i}{d\tilde{z}_i/d\zeta_i} = \frac{V_{i\infty} \left(1 - \frac{b^2}{\zeta_i^2} \right)}{1 - \frac{1}{\zeta_i^2}}$$

Taking the differential of Eq. 11.38, we have also

$$d\tilde{z}_i = \left(1 - \frac{1}{\zeta_i^2} \right) d\zeta_i$$

Inserting the foregoing relations into Eq. 11.37, we find

$$z = z_i - \lambda \int \frac{\left(1 - \frac{b^2}{\zeta_i^2} \right)^2}{1 - \frac{1}{\zeta_i^2}} d\zeta_i$$

Carrying out the integration, we get

$$z = \left(\zeta_i + \frac{1}{\zeta_i} \right) - \lambda \left[\zeta_i + \frac{(b^2 - 1)^2}{2} \ln \frac{\zeta_i - 1}{\zeta_i + 1} + \frac{b^4}{\zeta_i} \right] \quad (11.41)$$

Since ζ_i is related to z_i , it is evident that any point of the incompressible (z_i) flow yields a corresponding point (z) of the compressible flow. We are of course particularly interested in the distortion of the elliptical

profile. Accordingly, inserting into Eq. 11.41 the coordinates of the profile in the ξ -plane, as listed below,

$$\xi'_i = be^{i\sigma} = b(\cos \sigma + i \sin \sigma)$$

$$1/\xi'_i = \frac{1}{b} e^{-i\sigma} = \frac{1}{b} (\cos \sigma - i \sin \sigma)$$

$$\xi'_i = be^{-i\sigma} = b(\cos \sigma - i \sin \sigma)$$

$$1/\xi'_i = \frac{1}{b} e^{i\sigma} = \frac{1}{b} (\cos \sigma + i \sin \sigma)$$

and taking the real and imaginary parts of the resulting expression, we obtain the x - and y -coordinates of the profile in the compressible flow:

$$x' = \left(b + \frac{1}{b} \right) \cos \sigma - \lambda \left[b(1 + b^2) \cos \sigma + \frac{(b^2 - 1)^2}{4} \ln \frac{(b^2 - 1)^2 + 4b^2 \sin^2 \sigma}{b^2 + 2b \cos \sigma + 1} \right]$$

$$y' = \left(b - \frac{1}{b} \right) \sin \sigma + \lambda \left[b(1 - b^2) \sin \sigma + \frac{(b^2 - 1)^2}{2} \tan^{-1} \frac{2b \sin \sigma}{b^2 - 1} \right]$$

The compressible profile is therefore approximately elliptical if λ is small. To find the half-chord, x'_{\max} , we set $\sigma = 0$; and to find the half-thickness, y'_{\max} , we set $\sigma = \pi/2$. By taking the ratio of the two, we find, after rearrangement, the thickness ratio of the compressible profile:

$$\delta = \delta_i \frac{1 + \lambda \left[-b^2 + \frac{b(b^2 - 1)}{2} \tan^{-1} \frac{2b}{b^2 - 1} \right]}{1 - \lambda \left[b^2 + \frac{b(b^2 - 1)^2}{2(b^2 + 1)} \ln \frac{b - 1}{b + 1} \right]} \quad (11.42)$$

Analysis of Eq. 11.42 shows that $\delta > \delta_i$, which means that the transformed compressible profile is slightly thicker than the original incompressible profile. For example, at M_∞ with $\delta_i = 0.095$, Eq. 11.42 yields $\delta/\delta_i = 1.02$. This seems to be generally the case for other examples treated in the literature. It appears, therefore, that if profile distortion is neglected in applying the K-T method, the effects of compressibility are exaggerated, which is exactly opposite to the sense of the error owing to the linear pressure-density relation.

11.6. Extension of Karman-Tsien Method

Flows with Circulation. One of the weaknesses of the Karman-Tsien method as given here is that it is restricted to flows past closed bodies without circulation. In the case of a profile with circulation, the coordinate transformation changes a closed profile into one which is not closed.

This difficulty was resolved by Lin,⁽⁶⁾ among others, who devised a logical extension of the Karman-Tsien method which not only may be used for flows with circulation but has the further advantage of leading to the calculation of the compressible flow past a *given* profile with about the same degree of difficulty as for incompressible flow past a given profile.

For details of the method, the reader is referred to References 6 and 3. It is worth mentioning here, however, that Lin's extension shows that the Karman-Tsien pressure-correction formula (Eq. 11.28) is equally applicable to flows with circulation as to flows without circulation.

A detailed application of the method for determining the airfoil shape having a prescribed velocity distribution is given in Reference 7.

Polygonal Approximation Method. A natural extension of the Karman-Tsien method involves using for the tangent-gas approximation not one but several straight-line segments in the pressure-volume plane. The method was suggested and developed by Poritsky.⁽⁸⁾

11.7. Miscellaneous Examples

The mathematical details involved in the application of the hodograph method with the tangent-gas approximation to various examples are too lengthy to be given here. For these details the reader is referred to the original papers and to Reference 3. However, it seems desirable to summarize briefly those results of examples worked out in the literature which are of greatest practical interest.

Flow Past Circular Cylinder in Two-Dimensional Wind Tunnel. Suzuki⁽⁹⁾ has worked out the calculations for the physical arrangement of Fig. 11.11a. Perhaps the most significant effect to be looked for here is the influence of wind tunnel interference on the lower critical Mach Number, $M_{\infty, cr}$, that is, the value of M_∞ at which sonic velocity is first reached at the surface of the profile. This effect, based on the Karman-Tsien pressure-correction formula, is shown in Fig. 11.11b, wherein it may be seen that a 10 per cent blockage of the channel reduces the lower

critical Mach Number from 0.40 to 0.393. Also shown is the difference in the calculated results produced by ignoring the coordinate correction in comparing the compressible and incompressible flows. For reasons given previously, it may be desirable to ignore this correction.

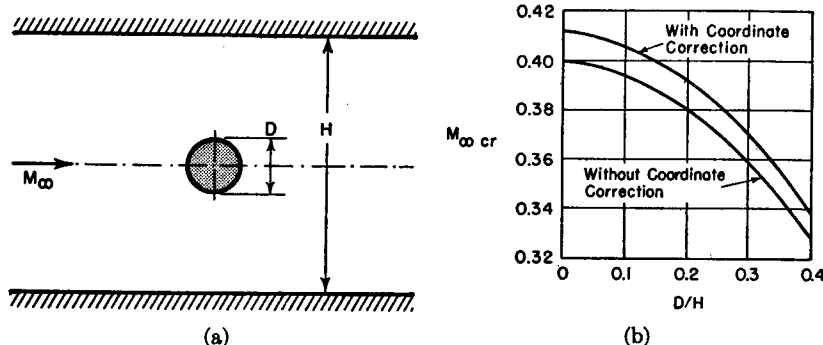


FIG. 11.11. Theoretical effect of wind tunnel walls on lower critical Mach Number for circle (after Suzuki).

Elliptic Cylinder at Angle of Attack with Circulation. This case has been worked out by the Karman-Tsien method in Reference 10, wherein

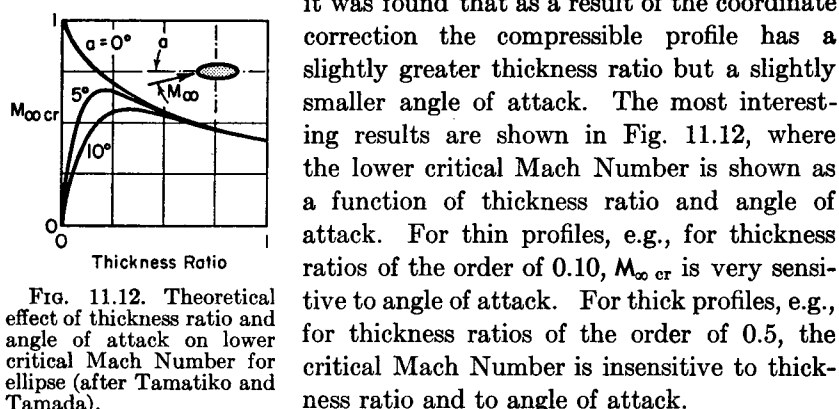


FIG. 11.12. Theoretical effect of thickness ratio and angle of attack on lower critical Mach Number for ellipse (after Tamatiko and Tamada).

Contraction Ratio for Jet from Sharp-Edged Two-Dimensional Orifice. A jet escaping from a two-dimensional slit, Fig. 11.13a, was studied by Busemann,⁽¹¹⁾ using the tangent-gas approximation. At infinite distance from the slit, the streamlines become uniform and parallel, the Mach Number is M_2 , and the jet width is b_2 . The entire free surface of the jet is at uniform pressure and at the speed M_2 . For practical purposes, the asymptotic conditions are substantially arrived at within a few jet widths of the slit.

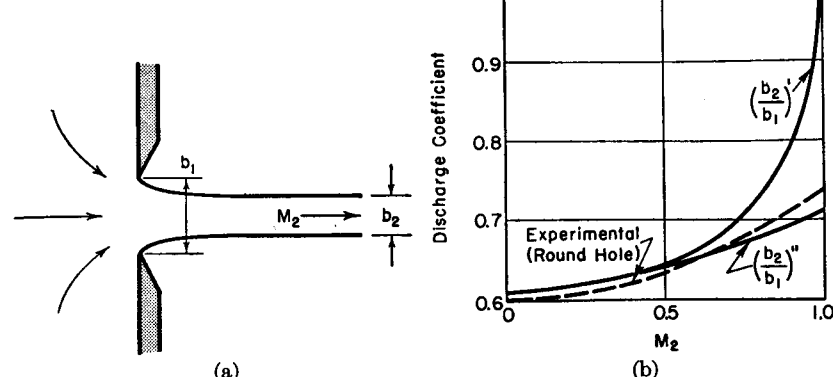


FIG. 11.13. Theoretical coefficient of contraction for jet escaping from sharp-edged slit (after Busemann).

The contraction ratio of the jet was found to be

$$\frac{b_2}{b_1} = \frac{\pi}{\pi + 2 \frac{\rho_2}{\rho_0}}$$

If we evaluate ρ_2/ρ_0 for the tangent gas, we have

$$\left(\frac{b_2}{b_1}\right)' = \frac{\pi}{\pi + 2\sqrt{1 - M_2^2}}$$

whereas if we use the exact isentropic relation for ρ_2/ρ_0 , we get

$$\left(\frac{b_2}{b_1}\right)'' = \frac{\pi}{\pi + \frac{2}{\left(1 + \frac{k-1}{2} M_2^2\right)^{1/(k-1)}}}$$

Both these relations are plotted in Fig. 11.13b, where there is plotted also the results of typical experiments⁽¹⁴⁾ on *round* sharp-edged orifices. The theoretical results follow the experimental results in a qualitative way. Both indicate a substantial rise in discharge coefficient owing to compressibility effects.

Elbows for Accelerated Flows. A method for designing passages which simultaneously turn and accelerate the flow, Fig. 11.14, has

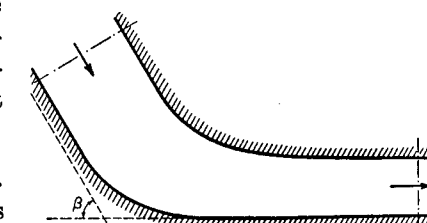


FIG. 11.14. Efficient turning channel (after Carrier).

been developed by Carrier,⁽¹²⁾ based on the tangent-gas approximation. The passages have the following desirable properties:

- The velocity increases monotonically along each streamline, thus reducing the possibility of boundary-layer separation and transition to turbulence.
- Each streamline turns monotonically.
- The ratio of total length of bend to exit width is a minimum, thus reducing frictional effects and space requirements.

Drag of Flat Plate Placed Normal to Gas Stream. In a pioneer paper on the hodograph method, Chaplygin⁽¹³⁾ solved the problem of a two-dimensional flat plate immersed normal to the flow in an infinite gas stream, assuming as in Fig. 11.15a a surface of discontinuity extending downstream from the edges.

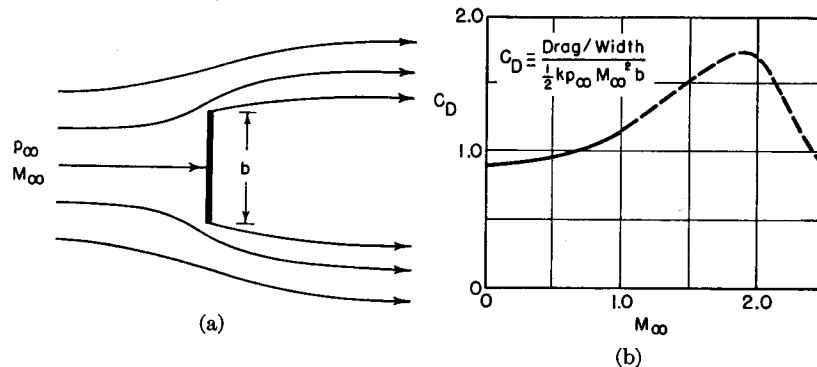


FIG. 11.15. Theoretical drag of flat plate placed normal to stream (after Chaplygin).

The calculated drag coefficient of the plate, Fig. 11.15b, begins at 0.88 for incompressible flow, and increases to 1.16 at Mach Number unity. Although the calculated coefficient is less than half the measured coefficient for flat plates, the rise in drag coefficient with Mach Number is similar to the observed increase in drag for blunt bodies. The dashed portion of the curve is an approximate extrapolation to supersonic speeds, and also agrees well with the general shape of the experimentally determined curves of C_D versus M_∞ for blunt projectiles.

REFERENCES AND SELECTED BIBLIOGRAPHY

1. TSIEN, H. S. Two-Dimensional Subsonic Flow of Compressible Fluids, *Jour. Aero. Sci.*, Vol. 6, No. 10 (Aug., 1939), p. 399.
2. VON KARMAN, TH. Compressibility Effects in Aerodynamics, *Jour. Aero. Sci.*, Vol. 8, No. 9 (July, 1941), p. 337.
3. EHRLERS, F. E., and CARRIER, G. F. Monograph IV—Methods of Linearization in Compressible Flow. Part II: Hodograph Method, *Air Material Command Report*, No. F-TR-1180B-ND (Feb., 1948).

4. KAPLAN, C. The Flow of a Compressible Fluid Past a Curved Surface, *NACA Rep.*, No. 768 (1943).
5. PRANDTL, L., and TIETJENS, O. G. *Fundamentals of Hydro- and Aeromechanics*, New York: McGraw-Hill Book Co., Inc., 1934.
6. LIN, C. C. On an Extension of the von Karman-Tsien Method to Two-Dimensional Subsonic Flows with Circulation Around Closed Profiles, *Quarterly App. Math.*, Vol. 4, No. 3 (Oct., 1946), p. 291.
7. COSTELLO, G. R. Method of Designing Airfoils with Prescribed Velocity Distributions in Compressible Potential Flows, *NACA Tech. Note*, No. 1913 (Aug., 1949).
8. PORITSKY, H. Polygonal Approximation Method in the Hodograph Plane, *Jour. App. Mech.*, Vol. 16, No. 1 (June, 1949), p. 123.
9. SUZUKI, H. On the Subsonic Flow of a Compressible Fluid Past a Circular Cylinder Between Parallel Walls, *Proc. Phys. Math. Soc. Japan*, Vol. 23 (1941), p. 337.
10. TAMAKI, S., and TAMADA, K. Application of the Hodograph Method to the Flow of a Compressible Fluid Past an Elliptic Cylinder, *Proc. Phys. Math. Soc. Japan*, Vol. 23 (1941), p. 958.
11. BUSEMANN, A. Hodographenmethode der Gasdynamik, *Z.a.M.M.*, Vol. 17 (1937), p. 73.
12. CARRIER, G. F. Elbows for Accelerated Flows, *Jour. App. Mech.*, Vol. 14 (1947), p. 108.
13. CHAPLYGIN, S. A. On Gas Jets, *NACA Tech. Memo.*, No. 1063 (1944).
14. PERRY, J. A., Jr. Critical Flow Through Sharp-Edged Orifices, *Trans. A.S.M.E.*, Vol. 71, No. 7, p. 757.

PROBLEMS

11.1. Derive the partial differential equation for two-dimensional, steady, irrotational, isentropic motion with V and θ as independent variables and the velocity potential φ as the dependent variable.

11.2. (a) Demonstrate by series expansions that the exact isentropic relation between density ratio and Mach Number may be written

$$\rho/\rho_0 = 1 - \frac{1}{2}M^2 - \frac{k}{8}M^4 + \dots$$

whereas the corresponding expression for the tangent-gas approximation is

$$\rho/\rho_0 = 1 - \frac{1}{2}M^2 + \frac{1}{8}M^4 + \dots$$

Determine the per cent error for $M = 0.1, 0.5$, and 0.8 . Note from these results that the Karman-Tsien pressure correction formula (ignoring coordinate correction) is correct up to terms of the order of M^2 .

(b) Determine corresponding expressions for ρ/ρ_∞ in terms of M and M_∞ .

11.3. It is often said that the tangent gas is equivalent to a perfect gas with $k = -1$.

(a) Compare the various tangent-gas relations with the corresponding isentropic relations for a perfect gas with $k = -1$.

(b) Compare the pressure-specific volume curve of the tangent gas with that corresponding to isentropic expansion of a perfect gas having $k = -1$.

(c) Compare the various tangent-gas relations with approximate formulas found by developing the exact isentropic relations for small changes from free-stream conditions.

(d) What conclusions do you reach?

11.4. (a) Demonstrate, for the tangent-gas approximation, that the stagnation pressure is related to the free-stream properties by the formula

$$p_0/p_\infty = 1 + k(1 - \sqrt{1 - M_\infty^2})$$

For a gas like air, should this formula be used with a value for k of 1.4 or of (-1) ? Explain.

(b) Show that if a perfect gas changes state along the line of states defined by the tangent gas, the entropy change is given by

$$\frac{ds}{c_v} = \frac{(k+1)(p_\infty - p)}{(k+1)p_\infty - p} \frac{dp}{p}$$

Verify the argument that if the processes are without friction, the tangent-gas formulas may be thought of as referring to the nonadiabatic flow of a perfect gas. Show that if the velocity changes are such that the pressure is changing in a direction away from the free-stream pressure, heat must be rejected from the gas; whereas if the pressure is changing toward the free-stream pressure, heat must be added to the gas.

11.5. Determine the isentropic relations between density, pressure, sound velocity, speed, and Mach Number, for a tangent gas having the point of tangency at the stagnation point.

11.6. Demonstrate that in the Karman-Tsien method,

$$z = \int \frac{d[G(\tilde{w}_i)]}{\tilde{w}_i} - \frac{1}{4c_0^2} \int w_i d[\tilde{G}(w_i)]$$

11.7. The complex potential

$$\varphi_i + i\psi_i = V_\infty \left(z_i + b \ln \frac{z_i}{b} \right)$$

represents the superposition of a uniform, parallel flow and a source flow, and hence yields the incompressible flow past an infinite half-body.

Using the Karman-Tsien method, determine the corresponding profile shapes for incompressible flow and for flow at $M_\infty = 0.5$.

11.8. The incompressible flow past a circular cylinder of radius R has the complex potential

$$\varphi_i + i\psi_i = V_\infty \left(z_i + \frac{R^2}{z_i} \right)$$

Using the Karman-Tsien method, determine the shape of the transformed cylinder as a function of M_∞ .

11.9. Consider incompressible flow past an ellipse of thickness ratio 0.5. Plot on the same sheet this elliptical profile together with the corresponding profile for $M_\infty = 0.5$ according to the Karman-Tsien method.

11.10. The incompressible flow without circulation past a circle of radius b at an angle of attack α is given by the complex potential

$$F(\zeta_i) = V_\infty \left(\zeta_i e^{-i\alpha} + \frac{b^2}{\zeta_i e^{-i\alpha}} \right)$$

Using the mapping function between a circle and an ellipse, namely,

$$z_i = \zeta_i + \frac{1}{\zeta_i}$$

find an expression for the coordinates in compressible flow corresponding to the incompressible flow past an elliptical profile, according to the Karman-Tsien method.

If the incompressible flow is past an elliptical profile of 25% thickness ratio at an angle of attack of 10° , and if the compressible flow is at $M_\infty = 0.5$, plot on the same sheet the corresponding incompressible and compressible profiles.

Note the important result that the compressible profile is slightly thicker but is at a smaller angle of attack.

11.11. Compare the blockage effects shown in Fig. 11.11 with a simple one-dimensional approach in which the profile is assumed to be in an infinite channel at a free-stream Mach Number corresponding to the flow in the minimum section of the actual channel.

What conclusions do you draw?

Chapter 12

MISCELLANEOUS METHODS AND RESULTS FOR TWO-DIMENSIONAL, SUBSONIC FLOW

12.1. Introductory Remarks

The purpose of this chapter is to summarize briefly a variety of important methods and results for subsonic flow, both analytical and experimental, falling into categories not classified elsewhere in this book.

On the analytical side, we shall discuss certain methods which are too lengthy for general use, but which provide nearly exact answers to a limited number of simple problems. These exact solutions are useful for testing the validity and range of application of such quick but approximate methods as the Prandtl-Glauert rule and the Karman-Tsien rule. Equally important, the exact solutions are exemplary: that is, they indicate correctly the general nature of the flow pattern for certain simple cases, and these results are a useful guide to the thinking of the designer for more complex problems.

The principal lines of attack underlying the theoretical methods will be outlined briefly, without going into details. Significant results found with each method will be summarized, again omitting laborious details.

On the experimental side, we shall present some important results connected with drag and lift for subsonic flow. These are important for practical purposes but are not easily connected with analytical studies.

Additional material relevant to the subject matter of the present chapter may be found in Volume II, Chapters 21, 22, and 28.

NOMENCLATURE

c	speed of sound	$(-C_p)_{\max}$	tional, steady flow is not possible
C_D	drag coefficient		peak negative pressure coefficient
C_L	lift coefficient	k	ratio of specific heats
C_p	pressure coefficient	M	Mach Number
$C_{p, cr}$	pressure coefficient corresponding to $M = 1$	M_{∞} or	free-stream Mach Number for which sonic velocity is first reached on profile
$(-C_p)_{\lim}$	limiting peak negative pressure coefficient, above which irrotational flow is not possible		

NOMENCLATURE—Continued

n	empirical exponent defined by Eq. 12.14; also distance along equipotential line, measured away from center of streamline curvature	δ	thickness ratio
ρ	mass density	ρ	mass density
φ	velocity potential	$()_{\infty}$	signifies free-stream conditions
p	pressure	$()_s$	signifies conditions at profile surface
R	radius of curvature of streamline	$()_0$	signifies stagnation conditions
t	characteristic thickness parameter	$()_i$	signifies incompressible flow
U_{∞}, V_{∞}	free-stream velocity		
V	velocity		
x, y	Cartesian coordinates		

12.2. The Rayleigh-Janzen Method of Expansion in Series of the Mach Number

The Rayleigh-Janzen method is a method of successive approximations, applicable to either two-dimensional or three-dimensional subsonic potential flows.

Outline of Method. To illustrate the procedure, let us consider two-dimensional potential flow, for which the differential equation of the velocity potential may be written (Chapter 9) as

$$\varphi_{xx} + \varphi_{yy} = \frac{1}{c^2} (\varphi_x^2 \varphi_{xx} + \varphi_y^2 \varphi_{yy} + 2\varphi_x \varphi_y \varphi_{xy}) \quad (12.1)$$

where

$$c^2 = c_0^2 - \frac{k-1}{2} (\varphi_x^2 + \varphi_y^2) = c_{\infty}^2 + \frac{k-1}{2} [V_{\infty}^2 - (\varphi_x^2 + \varphi_y^2)] \quad (12.2)$$

It is well known that subsonic compressible flows about a given body are not different qualitatively from incompressible flow about the same body. This suggests that the exact expression for the velocity potential, $\varphi(x, y)$, of a compressible flow may be expressed as the velocity potential, $\varphi_0(x, y)$, for incompressible flow past the same body, plus a series of correction terms whose magnitudes would depend on the Mach Number.

Accordingly, the zeroth approximation, $\varphi_0(x, y)$, is found by setting the right-hand side of Eq. 12.1 equal to zero ($c = \infty$ for incompressible flow), and using classical potential theory or function theory for solving the resultant Laplace equation for the given boundary conditions.

Having thus determined $\varphi_0(x, y)$, the right-hand side of Eq. 12.1 is evaluated approximately on the basis of this zeroth approximation, but retaining terms only up to the order of M_∞^2 . Let us call the right-hand side, as so evaluated, $F_0(x, y)$. The next step is to obtain the first approximation to compressible flow, $\varphi_1(x, y)$, by solving the linear Poisson equation,

$$\varphi_{xx} + \varphi_{yy} = F_0(x, y) \quad (12.3)$$

This process is continued to get higher approximations, but becomes prohibitively laborious, even for simple cases, after the second or third approximation.

When the mathematical details are carried out, it is found that the exact solution for the velocity potential may be expressed as

$$\varphi = \varphi_0 + M_\infty^2 \varphi_1 + M_\infty^4 \varphi_2 + \dots \quad (12.4)$$

where the function φ_0 is found by solving the Laplace equation,

$$\frac{\partial^2 \varphi_0}{\partial x^2} + \frac{\partial^2 \varphi_0}{\partial y^2} = 0 \quad (12.5)$$

after which the function φ_1 is found by solving the Poisson equation,

$$\frac{\partial^2 \varphi_1}{\partial x^2} + \frac{\partial^2 \varphi_1}{\partial y^2} = \left(\frac{\partial \varphi_0}{\partial x} \right)^2 \frac{\partial^2 \varphi_0}{\partial x^2} + 2 \frac{\partial \varphi_0}{\partial x} \frac{\partial \varphi_0}{\partial y} \frac{\partial^2 \varphi_0}{\partial x \partial y} + \left(\frac{\partial \varphi_0}{\partial y} \right)^2 \left(\frac{\partial^2 \varphi_0}{\partial y^2} \right) \quad (12.6)$$

and so on, inserting the appropriate boundary conditions:

$$\frac{\partial \varphi_0}{\partial x} = U_\infty \quad \text{and} \quad \frac{\partial \varphi_0}{\partial y} = 0 \quad \text{at} \quad x = y = \infty$$

$$\frac{\partial \varphi_0}{\partial n} = 0 \quad \text{at solid boundary} \quad (n \text{ is normal to boundary})$$

$$\frac{\partial \varphi_1}{\partial x} = \frac{\partial \varphi_1}{\partial y} = 0 \quad \text{at} \quad x = y = \infty$$

$$\frac{\partial \varphi_1}{\partial n} = 0 \quad \text{at solid boundary}$$

Note that the method gives the compressible and incompressible flows about the same body. The iteration method converges, however, only if the flow is everywhere subsonic. It is not, however, restricted to thin bodies nor to flows without stagnation points.

Important improvements in the details of carrying out the method were developed by Kaplan⁽⁴⁾ and Imai.⁽⁵⁾ For complete details as to

the techniques employed by various investigators for numerous examples, the reader is referred to Reference 1 and the complete bibliography contained therein.

We now turn to some of the significant results which have been found with the Rayleigh-Janzen method.

Flow Past Circular Cylinder. Fig. 12.1⁽⁶⁾ shows the velocity distribution for flow past a circular cylinder at $M_\infty = 0.4$. Besides indicating a comparison with incompressible flow, the various curves show the differences between the first, second, and third approximations and indicate the degree of convergence of the method. For $\theta < 45^\circ$, the increase in local surface velocity is greater for incompressible flow than for compressible flow; whereas, for $90^\circ > \theta > 45^\circ$, the opposite effect holds.

The lower critical Mach Number $M_{\infty \text{ cr}}$, i.e., the free-stream Mach Number at which sonic velocity is first reached locally in the flow, is found by the third approximation to be 0.404. The Prandtl-Glauert rule together with the incompressible solution yields $M_{\infty \text{ cr}} = 0.418$, and the Karman-Tsien rule correspondingly yields $M_{\infty \text{ cr}} = 0.40$.

The maximum local velocity, which occurs at the point of maximum thickness, is related to the free-stream velocity and Mach Number as follows:

$$\frac{V_{\max}}{U_\infty} = 2 + \frac{7}{6} M_\infty^2 + \left[\frac{281}{120} + \frac{71}{120} (k - 1) \right] M_\infty^4 + \dots$$

This illustrates that up to terms in M_∞^2 the specific-heat ratio has no effect on the flow pattern, a typical result not confined to circular cylinders, and demonstrated also by the various linearized theories. When the above expression is evaluated for $k = 1.40$, one gets

$$V_{\max}/U_\infty = 2.00 + 1.167 M_\infty^2 + 2.58 M_\infty^4 + 7.53 M_\infty^6 + \dots$$

which illustrates that the convergence of the method becomes poorer as M_∞ increases. This is the main reason why the method is so clumsy for high subsonic Mach Numbers.

Circular Cylinder in Wind Tunnel. Fig. 12.2⁽⁷⁾ shows how the presence of wind tunnel walls decreases the lower critical Mach Number for

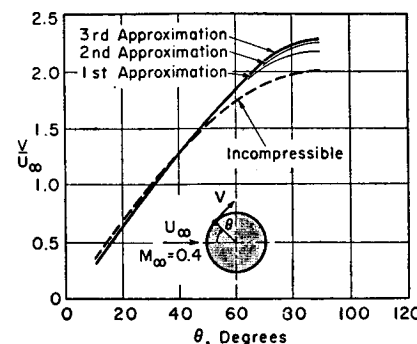


FIG. 12.1. Velocity distribution on circular cylinder (after Imai).

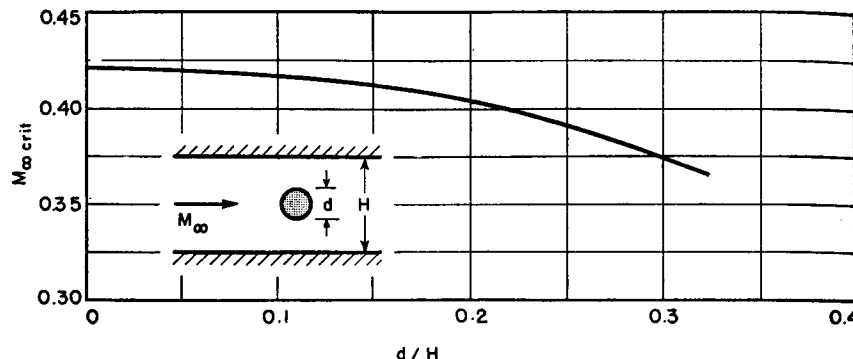


FIG. 12.2. Lower critical Mach Number for circular cylinder in wind tunnel (after Hasimoto).

flow past a circular cylinder, and indicates that caution must be used in interpreting wind tunnel results.

Circular Cylinder in Two-Dimensional Free Jet. For a circular cylinder in a free jet of limited lateral extent, as in an open wind tunnel, Lamla⁽⁸⁾ gives the following results (see Fig. 12.3):

$$\frac{V_{\max}}{U_{\infty}} = 2 + \frac{7}{6} M_{\infty}^2 - \frac{\pi^2}{12} \left(\frac{d}{H} \right)^2 \left(1 + \frac{43}{12} M_{\infty}^2 \right) + \dots$$

$$\frac{W_{\max} - H}{H} = \frac{\pi}{2} \left(\frac{d}{H} \right)^2 \left(1 + \frac{5}{6} M_{\infty}^2 \right) + \dots$$

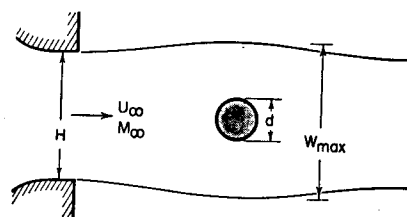


FIG. 12.3. Circular cylinder in free wind tunnel jet.

The maximum increase in local velocity is seen to be less when the free stream is limited than when the latter is infinite, and hence the lower critical Mach Number is increased as the jet becomes more limited in width. Notice that this effect is exactly opposite to that in a closed wind tunnel.

The maximum widening of the jet owing to the presence of the profile is increased as the result of compressibility effects.

Flow Past Elliptic Cylinder. An elliptic cylinder may be thought of as approximating a wing of large span or a compressor or turbine blade,

and, because of its relatively simple geometry, has received much theoretical attention.^(4 and 9)

Fig. 12.4 is a comparison of the pressure distributions over an ellipse for incompressible and compressible flow. The effect of compressibility

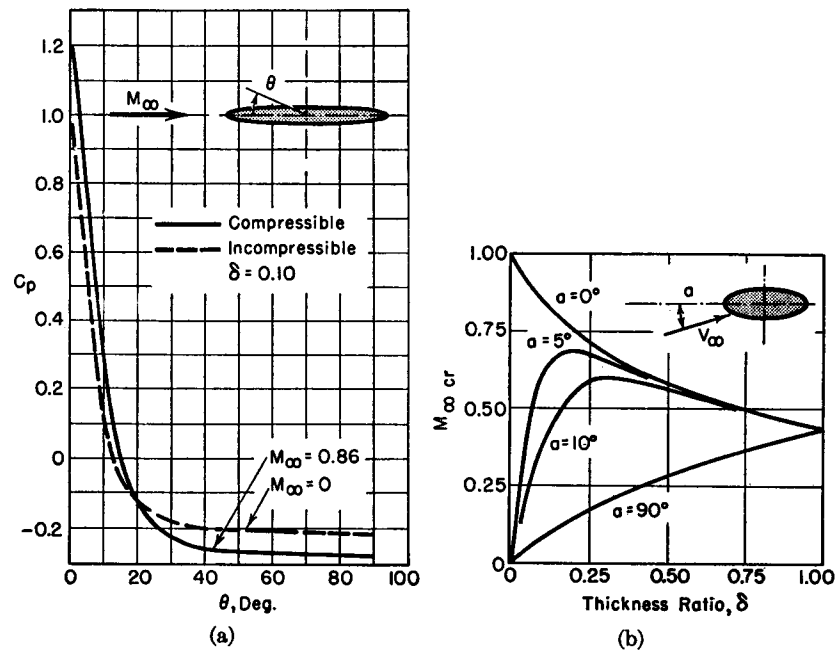


FIG. 12.4. Flow past elliptic cylinder (after Kaplani).

(a) Effect of Mach Number on pressure distribution.

(b) Lower critical Mach Number as function of thickness ratio and angle of incidence.

is to steepen pressure gradients and to increase considerably the peak negative pressure coefficient.

On Fig. 12.4b is shown the lower critical Mach Number as a function of thickness ratio and angle of attack. For moderate angles of attack, there is a particular thickness ratio having the highest critical Mach Number. Below this particular thickness ratio, the nose of the profile is too sharp, whereas above this ratio the profile is too thick.

Symmetrical Joukowski Profile. The Joukowski class of profiles, although not used in practice, do resemble some real profiles both geometrically and in respect to flow pattern. Also, since their aerodynamic properties may be found relatively easily, they are suitable for analytic studies, the results of which are sometimes a useful guide to the characteristics of real profiles.

The most significant results which have been worked out for this type of profile⁽¹⁰⁾ are summarized in Fig. 12.5. The lower critical Mach Number for symmetrical Joukowski profiles is shown in dependence on thickness ratio and angle of attack in Fig. 12.5b. The curves are like those of Fig. 12.4b, for much the same physical reasons.

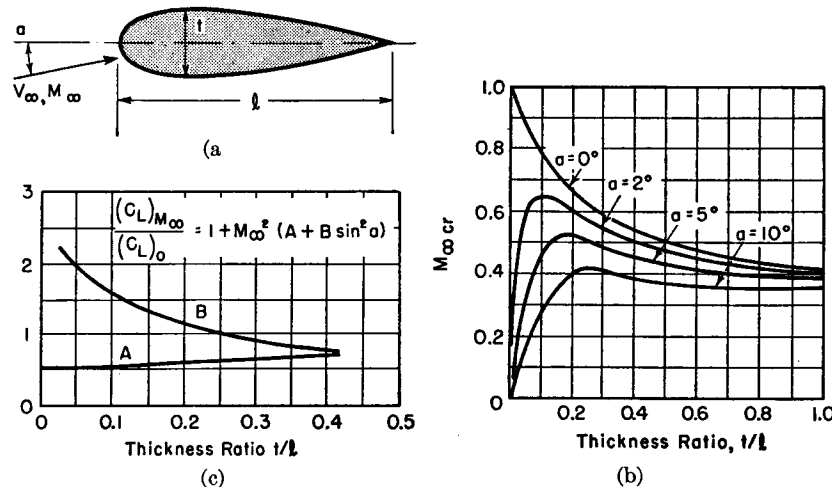


FIG. 12.5. Flow past symmetrical Joukowski profile (after Tamatiko and Umemoto).

- Shape of profile.
- Lower critical Mach Number as function of thickness ratio and angle of incidence.
- Effect of M_∞ on lift coefficient.

In practice, the Mach Number at which large drag increases appear for modern profiles is significantly greater than that indicated by Fig. 12.5b. This is explained by the fact that modern high-speed profiles are designed to give much flatter pressure distributions than do Joukowski profiles, and hence have lower peak negative pressures.

Fig. 12.5c shows the theoretical effect of Mach Number on the lift of symmetrical Joukowski profiles. The correction to the incompressible lift is seen to depend on thickness ratio and angle of attack as well as on M_∞ . In this connection, it may be remembered that the Prandtl-Glauert rule takes no account of these, whereas the Karman-Tsien rule does, at least approximately. For small thickness ratios, small angles of attack, and low Mach Numbers, Fig. 12.5c yields the same compressibility correction as the Prandtl-Glauert rule.

12.3. The Prandtl-Glauert Method of Expansion in Series of a Shape Parameter

Whereas in the Rayleigh-Janzen method we expand the velocity potential in a series of the Mach Number, in the Prandtl-Glauert method

we expand the velocity potential (or stream function) in a series of some shape parameter, such as the thickness ratio of a class of related profiles. Although the difficulty of working out the Rayleigh-Janzen method is scarcely influenced by the thickness of the body under study, the method converges very slowly at high Mach Numbers and becomes very clumsy. The Prandtl-Glauert method, on the other hand, works well at high Mach Numbers, but converges slowly for bodies of large thickness ratio or camber ratio. Thus, the Rayleigh-Janzen method is especially suitable for finding the flow past thick bodies at low Mach Numbers, whereas the Prandtl-Glauert method is especially suitable for the flow past thin bodies at high Mach Numbers. The latter method, incidentally, is not limited to flows where the velocity is everywhere subsonic. It is, however, limited to two-dimensional flows.

Outline of Method. The basic differential relation describing the flow is given by Eqs. 12.1 and 12.2. We now assume that we are dealing with an initially uniform, parallel flow past a thin body. Then it is physically plausible to assume that the velocity potential is the sum of the velocity potential for the undisturbed flow plus a series of terms whose magnitudes depend on a shape parameter. This is expressed mathematically by

$$\varphi = U_\infty x + t\varphi_1(x, y) + t^2\varphi_2(x, y) + \dots \quad (12.7)$$

where t is a characteristic parameter of the shape, such as the thickness ratio or camber ratio. The problem now is to find the functions φ_1, φ_2 , etc.

The derivatives $\varphi_x, \varphi_y, \varphi_{xx}, \varphi_{yy}$, and φ_{xy} are taken in Eq. 12.7 and these, together with Eq. 12.2, are introduced into Eq. 12.1. As the equation is to be valid for all values of t , the coefficient of each power of t in the resulting equation is equated to zero. In this manner the following differential equations for φ_1, φ_2 , etc., are found:

$$(1 - M_\infty^2) \frac{\partial^2 \varphi_1}{\partial x^2} + \frac{\partial^2 \varphi_1}{\partial y^2} = 0 \quad (12.8)$$

$$(1 - M_\infty^2) \frac{\partial^2 \varphi_2}{\partial x^2} + \frac{\partial^2 \varphi_2}{\partial y^2}$$

$$= \frac{M_\infty^2}{V_\infty} \left[(k+1) \frac{\partial \varphi_1}{\partial x} \frac{\partial^2 \varphi_1}{\partial x^2} + (k-1) \frac{\partial \varphi_1}{\partial x} \frac{\partial^2 \varphi_1}{\partial y^2} + 2 \frac{\partial \varphi_1}{\partial y} \frac{\partial^2 \varphi_1}{\partial x \partial y} \right] \quad (12.9)$$

The corresponding expression for φ_3 is given in Reference 11.

Eq. 12.8 is recognized as the linearized equation for two-dimensional flow, and its solution for subsonic flow leads to the familiar Prandtl-Glauert rule, which states that for a given profile the pressure coefficient at any point varies in proportion to $1/\sqrt{1 - M_\infty^2}$. The solutions of

Eq. 12.9 and of the equations for φ_3 , φ_4 , etc., provide higher approximations to the flow of a compressible fluid and may be expected to hold good for larger departures from a uniform, parallel flow.

To apply the method to the flow past boundaries of specified shape, Eq. 12.8 is first solved for the function φ_1 . In finding φ_1 it is only necessary to determine the incompressible solution for the chosen boundaries and then to apply the Prandtl-Glauert rule. Now, having determined $\varphi_1(x, y)$, the right-hand side of Eq. 12.9 may be expressed as a function of x and y . In order to determine the function φ_2 it is then necessary to solve the resulting linear Poisson equation. The process is repeated for higher approximations. Naturally the boundary conditions for each approximation need be satisfied for each approximation only to the same order of t which is involved in the velocity potential.

The detailed calculations for specific problems are too lengthy to be given here, but we shall summarize some of the results of practical significance which have been found with this method.

Flow Past a Bump and Past a Symmetrical Profile Without Stagnation Points. Kaplan⁽¹¹⁾ has developed the method for uniform flow past a symmetrical shape with cusps at both the leading and trailing edges (thus insuring against stagnation points). The results are applicable to the flow past the cusped profile of Fig. 12.6a, and also to the flow

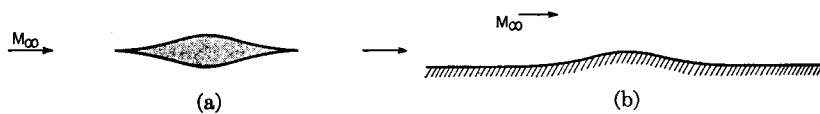


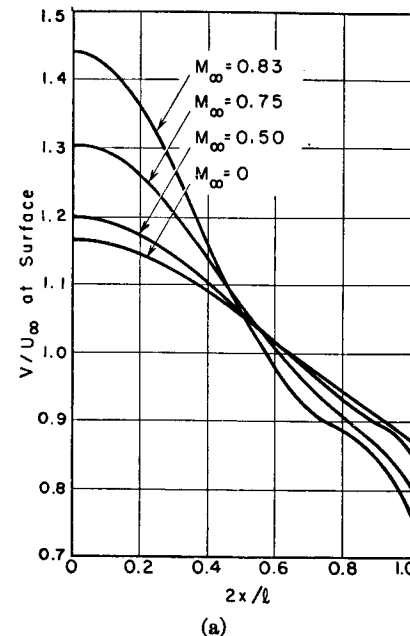
FIG. 12.6. Flow past Kaplan bump (after Kaplan).

- (a) Application to profile without stagnation points.
- (b) Application to bump on wall.

near the bump on the plane wall of Fig. 12.6b. The latter interpretation, for example, would be useful in estimating the effects of roughness or waviness on a surface in subsonic flow.

Fig. 12.7a shows the velocity distribution at the surface of a profile of 10% thickness ratio, for values of M_∞ from zero to 0.83. As found previously, compressibility tends generally to augment the local departures from free-stream velocity. For the 10% profile, the value of $M_{\infty, cr}$ is 0.742, i.e., at this free-stream Mach Number the velocity is exactly sonic at the point of maximum thickness. It is found that the solution is regular up to M_∞ of 0.83, beyond which the series diverges. Beyond this limiting Mach Number, denoted by $M_{\infty, lim}$, and sometimes called the *upper critical Mach Number*, no irrotational potential flow for the given boundary is possible. Presumably, for $M_\infty > M_{\infty, lim}$ shock

waves would appear in the flow field. With the limiting value $M_{\infty, lim}$ for the 10% profile, the zone of supersonic flow is shown in Fig. 12.7b,



(a)

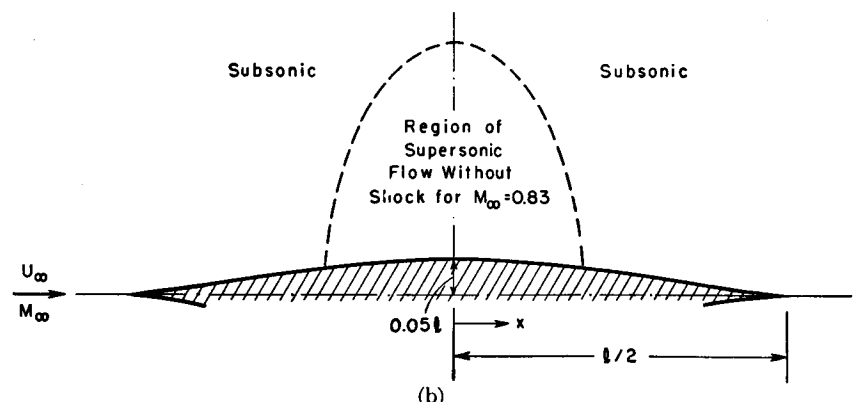


FIG. 12.7. Flow past cusped profile with 10% thickness ratio (after Kaplan).

- (a) Velocity distribution at surface.
- (b) Region of supersonic flow for $M_\infty = 0.83$.

and is seen to extend to a distance on each side of about seven times the half-width. This example is significant in that it demonstrates that there is no theoretical reason to expect shock waves in a potential flow merely because the flow becomes supersonic locally.

Fig. 12.8a shows, for various thickness ratios, the variation of peak negative pressure coefficient with M_∞ . Also shown is the curve denoting the local attainment of the sonic speed, marked $(-C_p)_{cr}$, and the curve beyond which irrotational flow is impossible, marked $(-C_p)_{lim}$. The

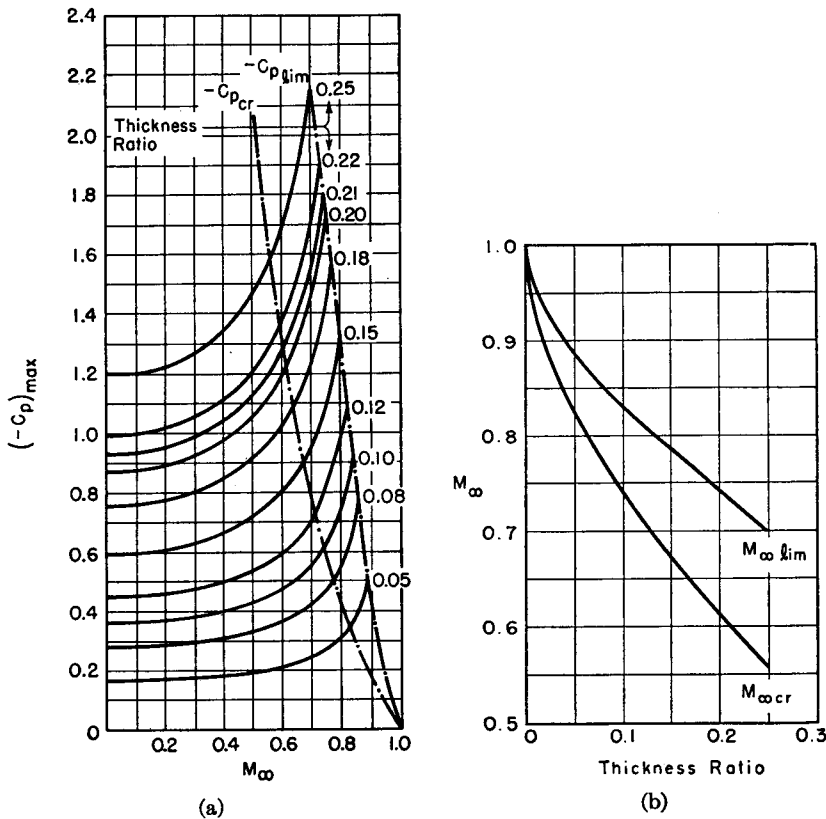


FIG. 12.8. Flow past cusped profile (after Kaplan).

- (a) Maximum negative pressure coefficient. Also shown are the sonic line and the limiting line beyond which steady potential flow is impossible.
 (b) Upper and lower critical Mach Numbers.

Karman-Tsien rule proves to be in good accord with the curves of $(-C_p)_{max}$ up to $M_{\infty cr}$, but of course deviates considerably beyond this value, because the tangent-gas approximation of the K-T rule limits the latter to purely subsonic flow.

From the intersections on Fig. 12.8a it is possible to construct Fig. 12.8b, showing the upper and lower critical Mach Numbers as a function of thickness ratio. The difference between the two curves is of the order of 0.10 for conventional thickness ratios.

Flow Past a Circular Arc Profile. The results given above refer to an uncambered profile. To investigate the effects of camber, Kaplan⁽¹²⁾ studied the flow past a circular arc profile of zero thickness (Fig. 12.9a) at zero angle of attack, with the circulation adjusted to satisfy the Kutta condition of a stagnation point at the trailing edge.

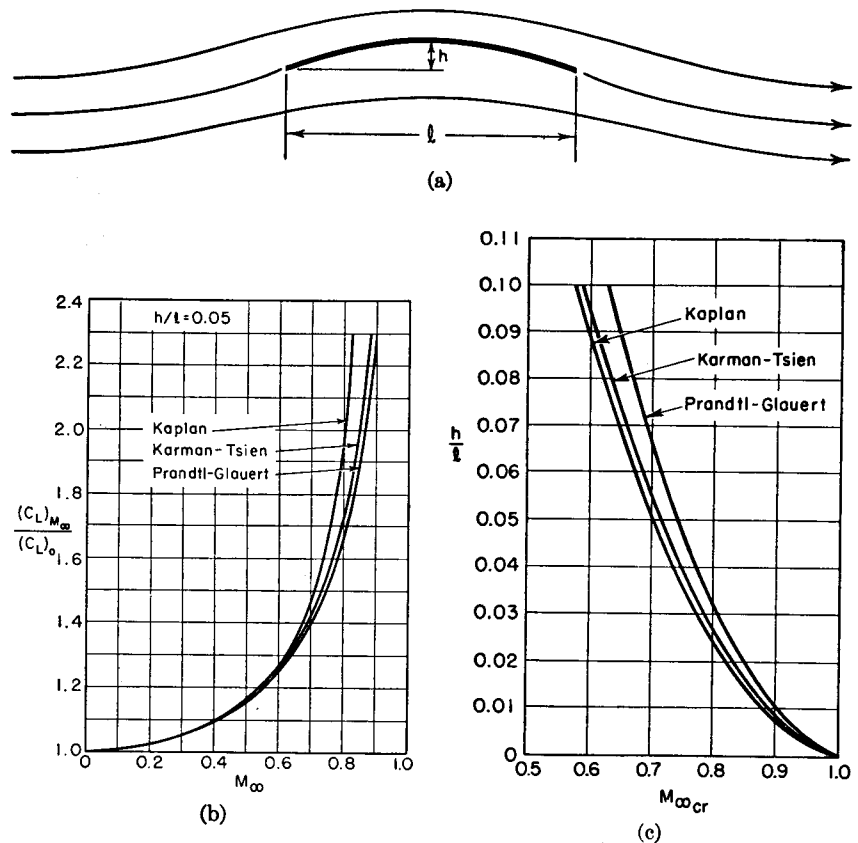


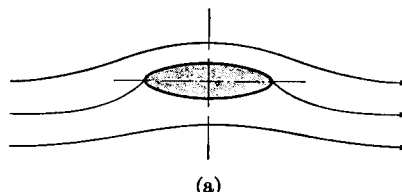
FIG. 12.9. Flow past circular arc profile (after Kaplan).

- (a) Streamlines.
 (b) Effect of M_∞ on lift coefficient.
 (c) Lower critical M_∞ as function of camber.

The increase of lift coefficient with M_∞ for a typical camber ratio is seen from Fig. 12.9b to be slightly more rapid than the increase predicted by the Karman-Tsien and Prandtl-Glauert rules, although the former is a good approximation.

Fig. 12.9c shows the relation between lower critical Mach Number and camber ratio, and indicates that the K-T and P-G rules both overestimate $M_{\infty cr}$.

Lift of Elliptic Cylinders at Small Angles of Attack. To investigate further the effects of compressibility on the lift of profiles of finite thickness, Kaplan⁽¹³⁾ studied the compressible flow past an elliptic cylinder at an angle of attack (Fig. 12.10a), with the circulation adjusted to



(a)

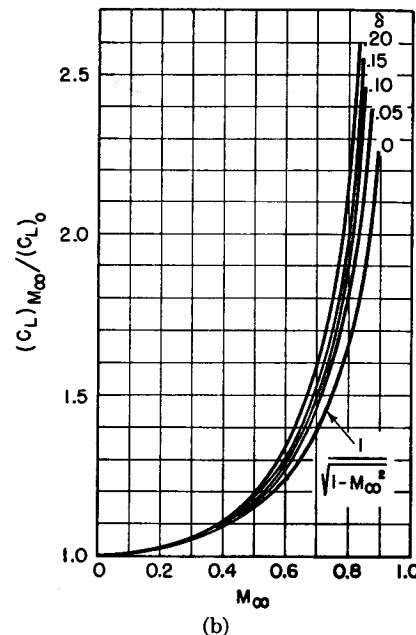


FIG. 12.10. Flow past elliptic cylinder at small angle of attack (after Kaplan).

- (a) Streamlines.
(b) Effect of M_{∞} on lift coefficient.

give the Kutta condition at the trailing edge of the major axis. The results of this study are summarized by the following formula relating the lift coefficients about the same elliptical profile in compressible and incompressible flow:

$$\frac{(C_L)_{M_{\infty}}}{(C_L)_0} = \frac{1}{\sqrt{1 - M_{\infty}^2}} + \frac{\delta}{1 - \delta} \left[\frac{1}{1 - M_{\infty}^2} - \frac{1}{\sqrt{1 - M_{\infty}^2}} + \frac{k + 1}{4} \left(\frac{M_{\infty}^2}{1 - M_{\infty}^2} \right)^2 \right] \quad (12.10)$$

where δ is the thickness ratio. It is shown in Reference 13 that this formula is approximately true also for any slender symmetrical profile.

For zero thickness ratio this relation reduces to the Prandtl-Glauert rule. The second term on the right-hand side represents the first-order thickness correction to the P-G rule. The order of magnitude of the thickness effect is illustrated by Fig. 12.10b, which is a plot of Eq. 12.10. For profiles of finite thickness, this analysis shows that the P-G rule underestimates the compressibility effect, a result which is in accord

with experiment. The curves of Fig. 12.10b are in fairly good agreement with experimental results on profiles having the same thickness coefficients as the elliptical profiles.

12.4. Relaxation Method

The so-called *relaxation method* of obtaining solutions to differential equations is a numerical technique which occupies a unique place in that it can usually be made to give answers where other methods fail. In the field of high-speed flow, for example, it is the only available method of calculation for flow patterns containing regions of subsonic and supersonic flow together with shock waves.

Some General Remarks. The procedure for solving Eq. 12.1 with specified boundary conditions begins with guesses of the values of φ at the net points of a grid in the x, y plane. Then, by writing Eq. 12.1 in finite difference form, it is possible to calculate at each point by how much the differential equation is violated. The values of φ are then adjusted systematically from point to point until ultimately the finite-difference equations are satisfied everywhere. This indicates that the correct value of φ at each point has been found. When this is done, the velocity and pressure distributions are easily computed.

For further details of the method and hints as to how the method may be made to converge most rapidly, the reader is referred to Volume II, Chapter 21 and to References 14 and 15.

When the flow is incompressible, i.e., when Laplace's equation is valid, the relaxation technique gives final answers to practical problems in a time measured in hours. For compressible flow, on the other hand, the time is measured in days, weeks, or months, so that for this class of flows the method is useful chiefly in an exemplary way, i.e., to provide theoretical solutions to a few typical problems which are not accessible to other methods of analysis.

Illustrative Results. As an illustration of the type of results obtained with this method, consider the flow past an NACA 0012 profile at zero angle of attack in a wind tunnel (Fig. 12.11a). The theoretical flow patterns were calculated in Reference 16 and corresponding experimental results were obtained in Reference 17.

A typical theoretical result is shown in Fig. 12.11b for a free-stream Mach Number of 0.75. This example is of special interest because it shows a shock attached to the airfoil at about 32% chord, followed immediately by a small expansion.

Up to a free-stream Mach Number of 0.60, the theoretical and experimental pressure distributions, Fig. 12.11c, are in good accord. At higher Mach Numbers there is serious disagreement. For example, at $M_{\infty} = 0.75$, Fig. 12.11d shows that the measured peak negative pressure coefficient is considerably less than

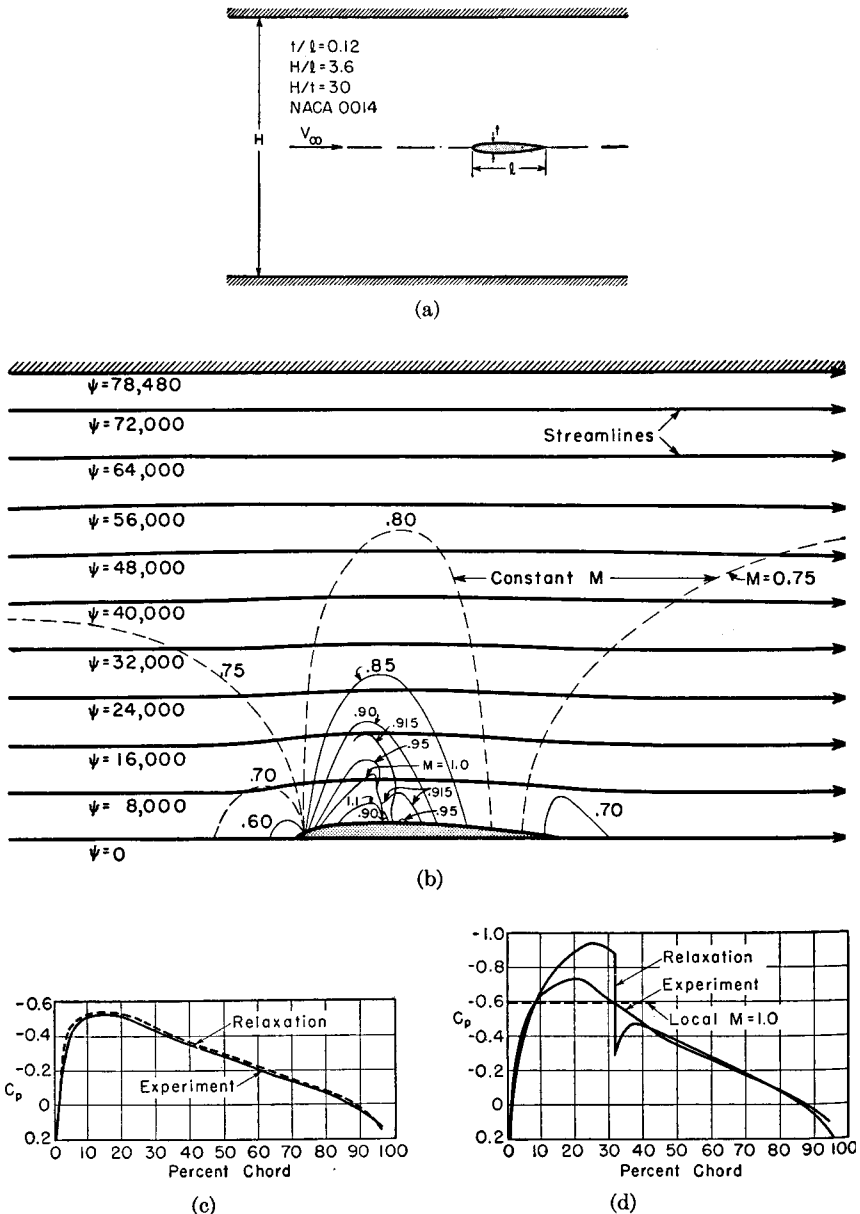


FIG. 12.11. (a) Flow past NACA 0012 profile in wind tunnel.

(b) Streamlines and lines of constant Mach Number, as worked out by relaxation method for $M_\infty = 0.75$ (after Emmons).

(c) Theoretical and experimental pressure distributions on profile for $M_\infty = 0.60$ (after Emmons; Amick).

(d) Theoretical and experimental pressure distributions on profile for $M_\infty = 0.75$ (after Emmons; Amick).

the theory indicates. Furthermore, in practice there seem to occur a series of weak shocks near the surface rather than a single large shock. The probable explanation of the discrepancy lies in the change in the effective boundaries of the profile owing to a shock-boundary layer interaction.

12.5. Some Measured Effects of Compressibility in Subsonic Flow

General Considerations. From theoretical and experimental work on compressible boundary layers (Volume II, Chapters 26 and 27), it appears that for subsonic flow the local skin-friction coefficient is almost independent of Mach Number, all other things remaining constant. Nevertheless, one might expect the drag coefficient of airfoil profiles to increase with free-stream Mach Number, for three reasons:

(i) As M_∞ increases, the local velocity outside the boundary layer at a given point on the profile generally increases more rapidly than V_∞ . But the local shear stress is a function primarily of the local V , whereas the drag coefficient C_D is defined in terms of V_∞ , whence it follows that C_D increases even though the local skin-friction remains approximately constant.

(ii) An increase in M_∞ generally increases the local pressure coefficients for the profile, and hence increases pressure gradients. This is particularly significant on the rearward portions of the profile where pronounced thickening of the boundary layer usually occurs. When the adverse pressure gradient near the trailing edge is steepened by compressibility, this thickening becomes greater and there is consequently a rise in drag coefficient.

(iii) As M_∞ increases, the maximum local Mach Number increases even more rapidly, until, after a zone of supersonic flow has appeared, shock waves are found to occur. These shock waves are serious not only because of the losses they occasion directly, but even more so because of the way in which they produce a very rapid thickening and sometimes separation of the boundary-layer flow.

PRESSURE DISTRIBUTION. Fig. 12.12, showing the measured pressure distributions⁽¹⁸⁾ at various Mach Numbers for the NACA 4412 profile, illustrates the steepening adverse gradient of point (ii) above. At $M_\infty = 0.66$, there is also evident at about 55% of chord a sudden rise in pressure on the upper (convex) surface, which, by the simultaneous evidence of schlieren photographs, is associated with a shock wave near the surface at that point. As M_∞ increases further, the shock moves rearwards, and the pressure distribution aft of the shock is considerably altered as the result of boundary-layer separation. In Fig. 12.12, the short horizontal dashes marked " $M = 1$ " indicate the point where the

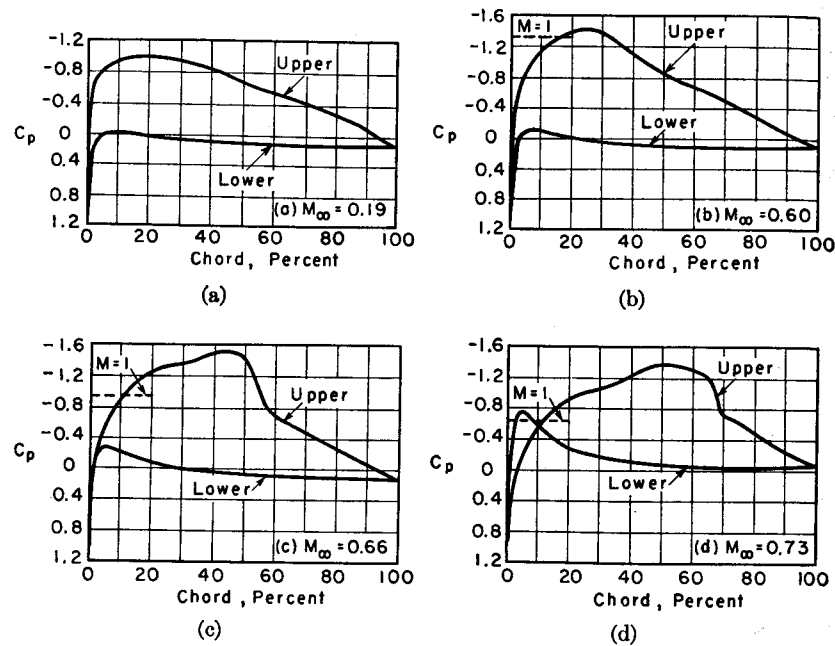


FIG. 12.12. Pressure distribution on NACA 4412 profile at angle of attack of $1^{\circ}52'$ (after Stack, Lindsey, and Littell).

- (a) $M_{\infty} = 0.19$.
- (b) $M_{\infty} = 0.60$.
- (c) $M_{\infty} = 0.66$ (note shock at 55% chord).
- (d) $M_{\infty} = 0.73$ (note shock at 67% chord).

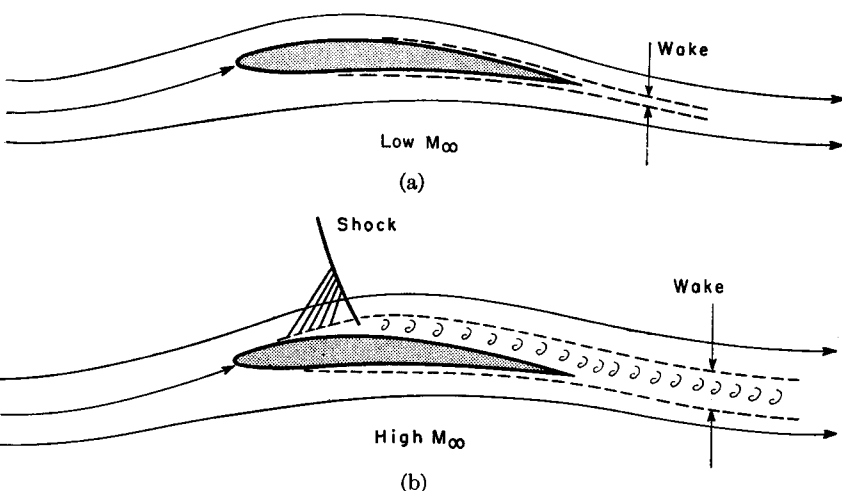


FIG. 12.13. (a) Flow past profile at low Mach Number.
(b) Flow at high Mach Number, with boundary-layer separation owing to shock wave.

local sonic velocity is first reached on the profile. It is of particular interest that shock waves do not necessarily appear immediately upon the appearance of supersonic speeds somewhere in the flow.

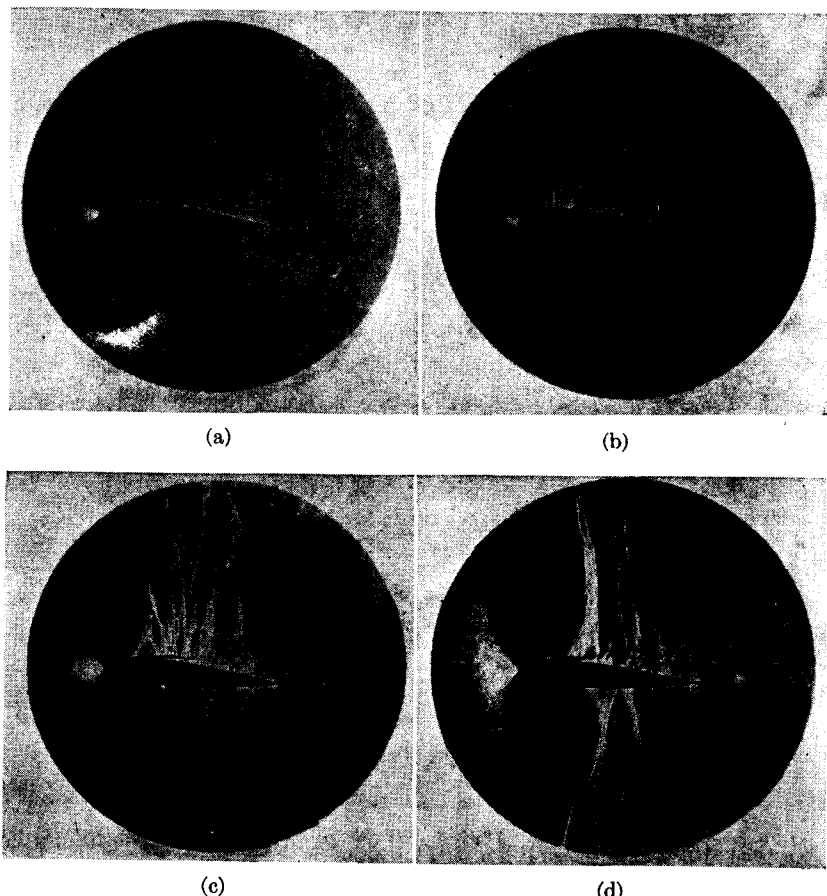


FIG. 12.14. Schlieren photographs of flow past NACA 23015 profile at angle of attack of 3° (after Stack). Flow from left to right.

- (a) $M_{\infty} = 0.40$. Flow entirely subsonic.
- (b) $M_{\infty} = 0.60$. Small zone of supersonic flow at 25% chord, with weak repeated shocks.
- (c) $M_{\infty} = 0.70$. Large zone of supersonic flow, with lambda shock and boundary-layer separation.
- (d) $M_{\infty} = 0.80$. Extensive shock pattern with so much boundary-layer separation that profile is stalled.

SHOCK-BOUNDARY LAYER INTERACTION. The effect of the interaction between the shock wave and the boundary layer is shown in Figs. 12.13, 12.14, and 12.15. As a result of the very large adverse pressure gradient imposed by the shock wave, the boundary layer thickens

rapidly, generally becomes turbulent, and often separates from the profile, thus producing a large increase in the thickness of the wake. The change in effective body shape usually acts to decrease the lift and increase the drag.

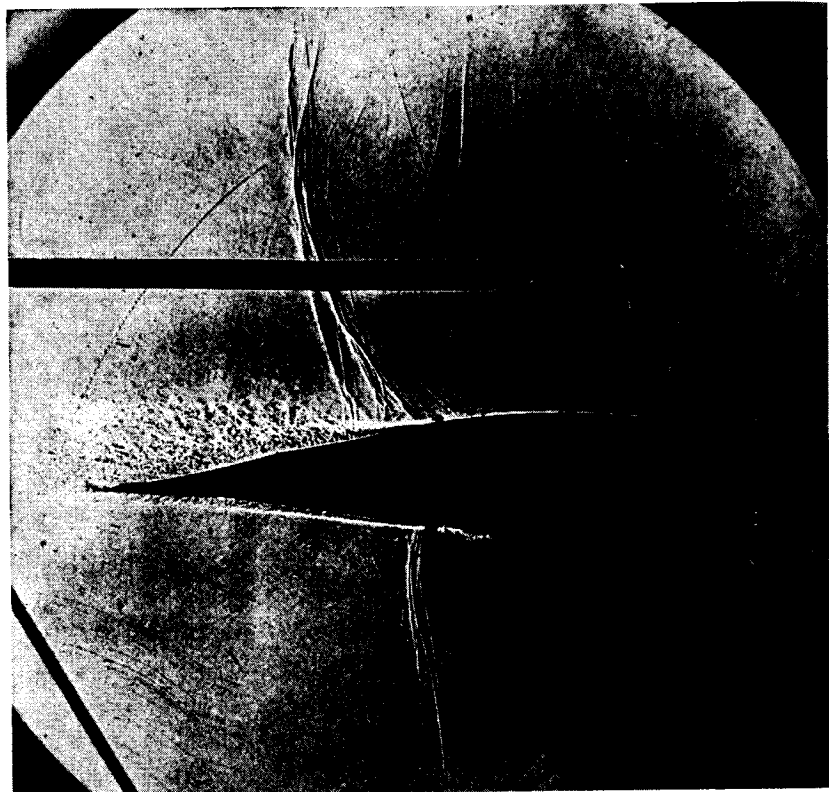


FIG. 12.15. Schlieren photograph of flow past Mustang wing at $M_\infty = 0.78$, with angle of attack of 2° (after Hilton). Flow from right to left.

Fig. 12.16 shows the results of wake-survey measurements⁽¹⁹⁾ behind a symmetrical profile. At $M_\infty = 0.708$, the wake is narrow, the maximum loss in total pressure is small, and the drag coefficient is small. At $M_\infty = 0.910$, however, for which schlieren photographs show strong shock waves, the wake is wide, with a large maximum loss in total pressure. The middle portion of this diagram represents viscous and separation losses in the boundary layer, whereas the "wings" of the diagram represent direct losses in stagnation pressure across the shocks.

FORCE COEFFICIENTS. Fig. 12.17 shows typical effects of compressibility on the force coefficients of airfoils.⁽²⁰⁾ For Mach Numbers up to and somewhat beyond the lower critical Mach Number (correspond-

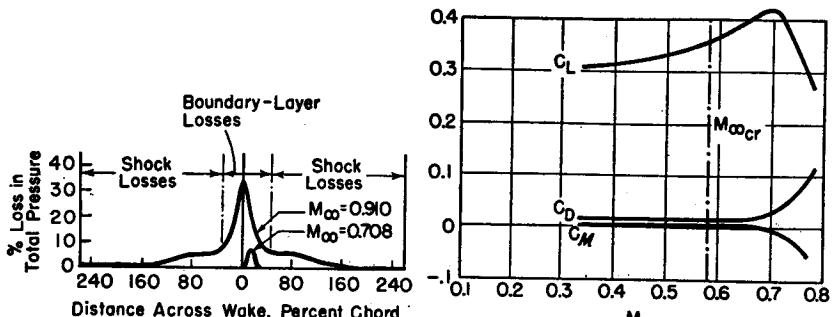


FIG. 12.16. Loss of total pressure in wake of symmetrical NACA 0012 profile (12% thick) at zero incidence (after Stack).

ing to the initial appearance locally of supersonic flow), the drag and moment coefficients remain nearly constant, while the lift coefficient increases approximately according to the Prandtl-Glauert rule. At a Mach Number of about 0.7, as compared with M_∞ cr of about 0.58, there is a "force break," i.e., the drag coefficient suddenly increases, the lift coefficient suddenly falls off, and the moment coefficient decreases. An extensive summary of such results is given in Reference 20.

Application of the Prandtl-Glauert Rule to Drag. Karman⁽²¹⁾ has suggested a method, based on the Prandtl-Glauert rule, for predicting the effect of M_∞ on drag coefficient in the range of Mach Numbers where shock waves are not present. It is assumed that if the surface distributions of pressure coefficient are the same in an incompressible and in a compressible flow, then the local skin-friction coefficient will be alike at corresponding points, and hence the drag coefficient will be the same

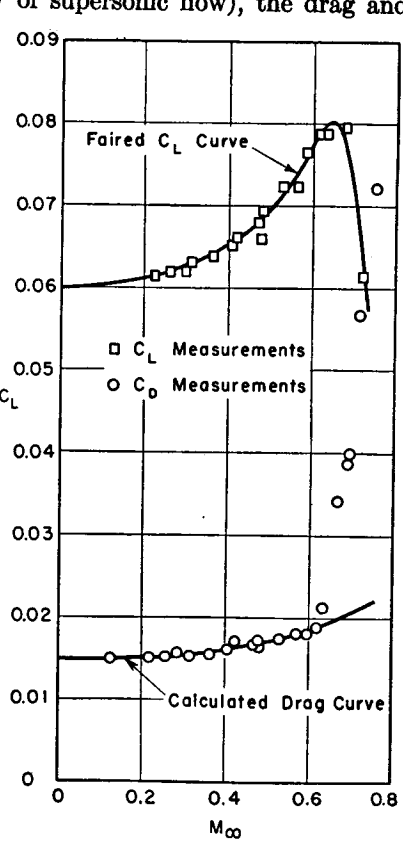


FIG. 12.17. Effect of Mach Number on force coefficients of NACA 23015 profile at zero incidence (after Stack).

FIG. 12.18. C_L and C_D versus M_∞ for NACA 4412 profile at $\alpha = 1^\circ 52'$, showing comparison of calculated drag with measured drag (after von Karman).

for both profiles. The drag coefficient of a given profile at M_∞ and with a certain value of $C_{L_{M_\infty}}$ is, therefore, taken to be equal to the drag coefficient in incompressible flow of an affinely related profile operating at an angle of attack to give the same lift coefficient $C_{L_{M_\infty}}$; the incompressible profile must have its thickness and camber larger by the factor $1/\sqrt{1 - M_\infty^2}$ than the corresponding quantities for the original profile. A comparison of this method with experimental results for the NACA 4412 profile at $\alpha = 1.88^\circ$ (Fig. 12.18) shows, for this example at least, that the method works well up to the value of M_∞ at which the "force break" or "compressibility burble" takes place.

Effects of Thickness, Camber, and Angle of Attack on Relation Between Mach Number and Force Coefficients. Fig. 12.19 shows the effects of thickness, camber, and angle of attack on the way in which the lift coefficient is altered by increasing M_∞ .⁽²²⁾

Considering first the uncambered sections, the effect of thickness is seen to be quite marked. Whereas the 6% profile experiences at constant incidence a significant increase in C_L followed by a moderate drop, the C_L of the 12% profile at first remains nearly constant, then suddenly drops severely, and finally recovers slightly. Whereas the M_∞ for peak C_L at constant incidence is about 0.85 for the 6% section, the corresponding figure for the 12% profile is only about 0.75. A comparison of the two cambered profiles, Figs. 12.19c and 12.19d, shows similar effects of thickness.

By comparing Fig. 12.19c with Fig. 12.19a, and Fig. 12.19d with Fig. 12.19b, it is evident that an increase in camber reduces the Mach Number for lift-force break at a prescribed C_L .

A similar set of results showing variations in drag coefficient⁽²²⁾ is shown in Fig. 12.20. Here it is seen that the typical sudden increase in C_D at high speeds occurs at lower and lower Mach Numbers as the incidence is increased. By comparing the thin with the thick sections, it is evident that the Mach Number for sudden drag rise is more favorable for the thin sections.

Force-Divergence Mach Numbers. The NACA 4-digit series profiles of Figs. 12.19 and 12.20 do not have as favorable high-speed characteristics as the NACA 6-series profiles. Fig. 12.21 summarizes the high-speed characteristics of the NACA 66-210 profile in terms of the Mach Numbers for *drag divergence* and *lift divergence* at selected values of C_L . These special Mach Numbers are defined as the values of M_∞ where $(d^2C_L/dM_\infty^2)_a = 0$ (for lift), and $(dC_D/dM_\infty)_a = 0.1$ (for drag). In this example the force-divergent M_∞ for lift is about 0.01 higher than that for drag; and the latter, over a range of lift coefficients near the design lift coefficient of 0.2, is about 0.02 higher than the theo-

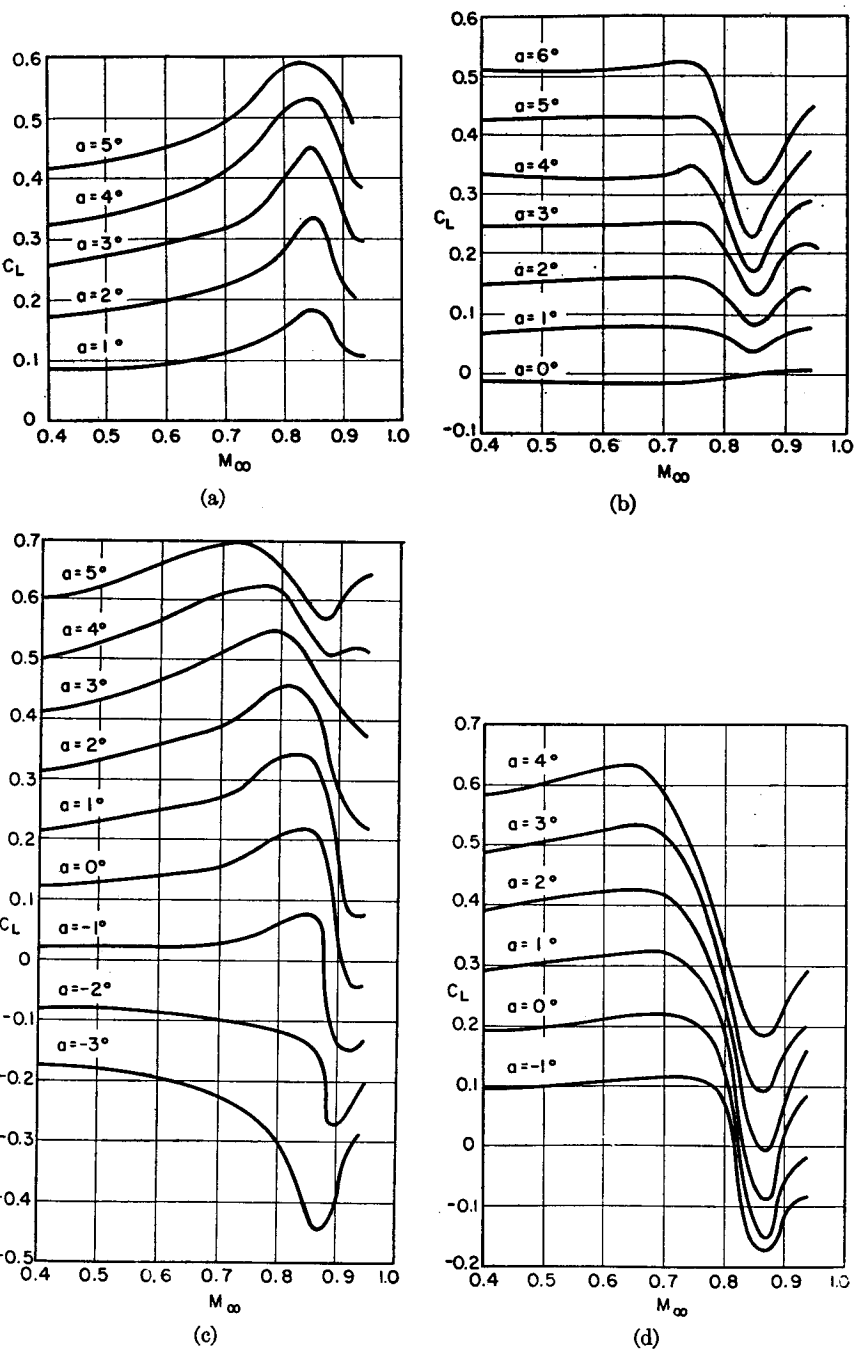


FIG. 12.19. Effect of Mach Number on lift coefficient (after Ferri).

- (a) NACA 0006-34, having 6% thickness and 0% camber.
- (b) NACA 0012-34, having 12% thickness and 0% camber.
- (c) NACA 2306, having 6% thickness and 2% camber.
- (d) NACA 2312, having 12% thickness and 2% camber.

retical lower critical Mach Number at each C_L . It is especially significant that the range of C_L over which the force-divergent Mach Numbers remain high is about three times as wide as the range of C_L for which $M_{\infty \text{ cr}}$ is high.

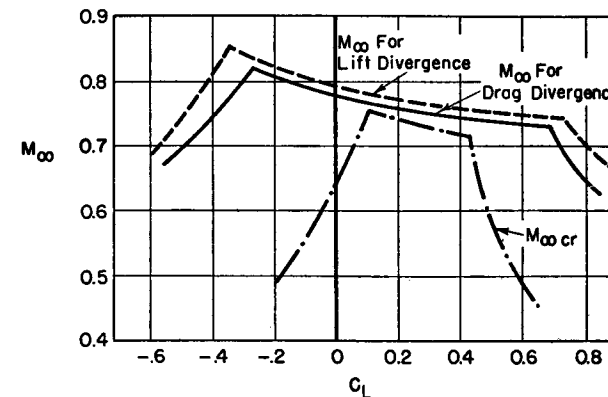
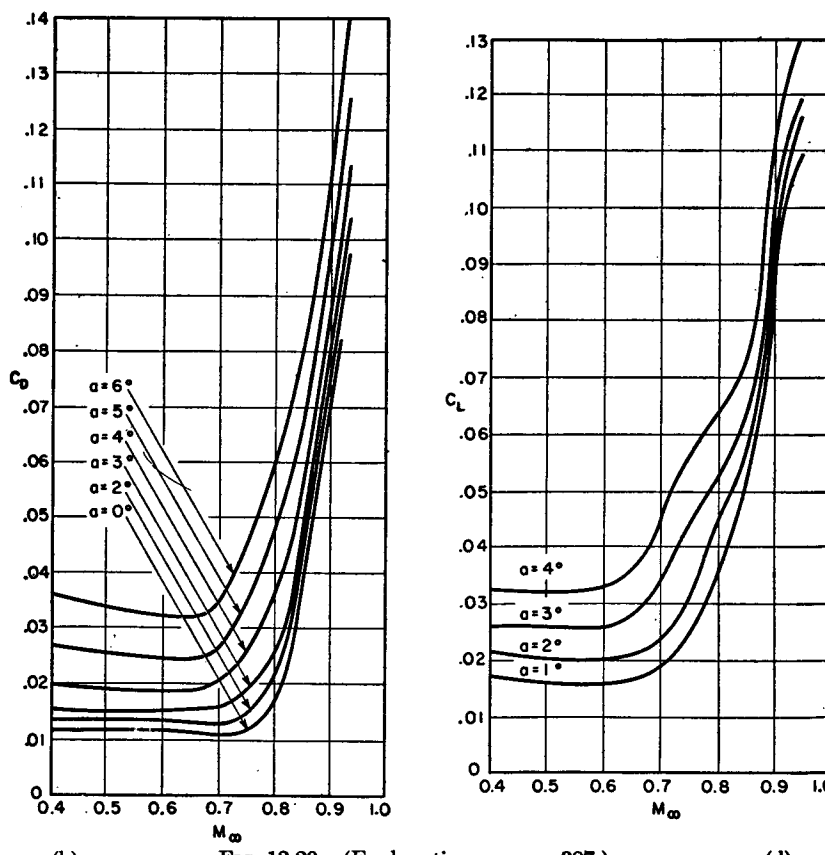


FIG. 12.21. Force-divergence Mach Numbers for NACA 66-210 profile designed for C_L of 0.2 (NACA).



(b)

FIG. 12.20. (Explanation on page 387.)

12.6. The Streamline Curvature Method

A simple, approximate method of analyzing two-dimensional frictionless flows has been developed by Perl.⁽²³⁾

The method is a so-called *integral method*, inasmuch as it satisfies the equations of motion in the large, but does not satisfy them in the small.

Governing Physical Equations. Consider the potential flow past the thin profile of Fig. 12.22. Point P is any point in the flow field and has the local velocity V . Point s is the point on the airfoil surface lying on the same equipotential line as P , and has the local velocity V_s . The streamlines and equipotential lines may be regarded as curvilinear coordinates, with n representing distance along the equipotential line (in the direction away from the center of curvature of the streamlines).

IRROTATIONALITY. In Chapter 9 it was shown that the condition of irrotationality at point P is

$$\frac{\partial V}{\partial n} + \frac{V}{R} = 0 \quad (12.11)$$

where R is the radius of curvature of the streamline at P .

Fig. 12.20. Effect of Mach Number on drag coefficient (after Ferri).

- (a) NACA 0006-34, having 6% thickness and 0% camber.
- (b) NACA 0012-34, having 12% thickness and 0% camber.
- (c) NACA 2306, having 6% thickness and 2% camber.
- (d) NACA 2312, having 12% thickness and 2% camber.

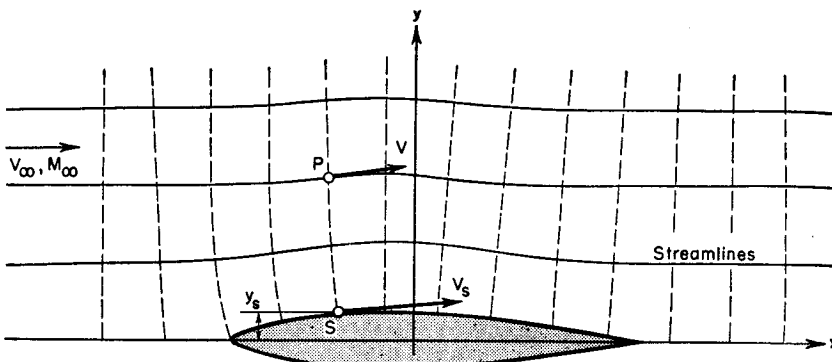


FIG. 12.22. Nomenclature for streamline curvature method.

If the profile is thin the equipotential lines are nearly parallel to the y -axis. Hence, we may, with little error, write $dn \equiv dy$, and the condition of irrotationality accordingly becomes

$$dy = -R \frac{dV}{V} \quad (12.12)$$

where it is to be understood that the differentials are to be taken at constant x .

CONTINUITY. The mass flow between the stagnation streamline and a streamline far from the profile must be the same for all values of x . Hence, we write, in accordance with the previous assumption that $dn \equiv dy$,

$$\rho_\infty V_\infty y_\infty \equiv \rho_\infty V_\infty y_s + \rho_\infty V_\infty (y_\infty - y_s) = \int_{y_s}^{y_\infty} \rho V dy$$

where y_∞ is so large that the corresponding streamline is parallel to the x -axis and the corresponding velocity is V_∞ . The integral is evaluated at constant x on a vertical line passing through point s . Rearrangement of the foregoing equation yields

$$y_s = \int_{y_s}^{y_\infty} \frac{\rho V}{\rho_\infty V_\infty} dy - (y_\infty - y_s) = \int_{y_s}^{y_\infty} \left(\frac{\rho V}{\rho_\infty V_\infty} - 1 \right) dy$$

and introduction of Eq. 12.12 gives

$$y_s = \int_1^{V_s/V_\infty} \frac{R}{V/V_\infty} \left(\frac{\rho}{\rho_\infty} \frac{V}{V_\infty} - 1 \right) d\left(\frac{V}{V_\infty}\right) \quad (12.13)$$

where the variable of integration has been changed to V/V_∞ .

Approximation of Streamline Curvature. If R were known as a function either of y or of V/V_∞ , then Eq. 12.13 could be integrated to yield the value of V_s/V_∞ for each value of y_s . This is tantamount to determining the pressure distribution on the profile, and constitutes the desired solution. In order to determine R exactly, however, it would be necessary to solve the complete equations of motion, and this is just what we are trying to avoid.

It is known that R is infinite at $y = \infty$, and has the radius of curvature of the profile, R_s , at $y = y_s$. Hence we postulate that R may be approximately represented in terms of V/V_∞ by means of the empirical relation

$$\frac{R}{R_s} = \left(\frac{V_s/V_\infty - 1}{V/V_\infty - 1} \right)^n \quad (12.14)$$

where n is a constant the value of which is to be determined later. Eq. 12.14 shows a monotonic variation of R with V , which is as it should be for stations near the station of maximum thickness.

From the isentropic relations of Chapter 4, it may be shown that

$$\frac{\rho}{\rho_\infty} = \left[1 - \frac{k-1}{2} M_\infty^2 \left(\frac{V^2}{V_\infty^2} - 1 \right) \right]^{\frac{1}{k-1}}$$

Substituting this equation for ρ/ρ_∞ , together with Eq. 12.14 for R , into Eq. 12.13, we obtain

$$\frac{y_s}{R_s} = \left(\frac{V_s}{V_\infty} - 1 \right)^n \int_1^{V_s/V_\infty} \frac{\frac{V}{V_\infty} \left[1 - \frac{k-1}{2} M_\infty^2 \left(\frac{V^2}{V_\infty^2} - 1 \right) \right]^{\frac{1}{k-1}}}{\frac{V}{V_\infty} \left(\frac{V}{V_\infty} - 1 \right)^n} d\left(\frac{V}{V_\infty}\right) \quad (12.15)$$

Determination of Parameter n . The pressure distribution for incompressible flow past the given profile can be found relatively easily. Assuming that this is known, the value of V_s/V_∞ is computed at each value of x for incompressible flow. Then, integrating Eq. 12.15 with $M_\infty = 0$, and inserting the incompressible value of V_s/V_∞ , we are able to compute n for each value of x .

By assuming the values of n as found above to be independent of M_∞ , Eq. 12.15 may be solved for the velocity distribution on the airfoil for any value of M_∞ less than unity.

Details of the method, together with useful tables and charts for numerical computations, are given in Reference 24. The method may

also be extended to supersonic flows⁽²³⁾ and to flow through turning channels, where the equipotential lines may not be assumed parallel.⁽²⁴⁾

Application to Flow with Small Perturbations. As an example of the method, consider flow with small perturbations. Then it is appropriate to expand the integrand of Eq. 12.15 in powers of $(V/V_\infty - 1)$. Proceeding in this way and assuming this variable to be small compared with unity, we obtain by detailed expansions

$$\begin{aligned} \frac{y_s}{R_s} &\cong \\ &\left(\frac{V_s}{V_\infty} - 1\right)^n \int_1^{V_s/V_\infty} \frac{\frac{V}{V_\infty} \left[1 - \frac{M_\infty^2}{2} \left(\frac{V}{V_\infty} + 1 \right) \left(\frac{V}{V_\infty} - 1 \right) + \dots \right] - 1}{\frac{V}{V_\infty} \left(\frac{V}{V_\infty} - 1 \right)^n} d\left(\frac{V}{V_\infty}\right) \\ &\cong \left(\frac{V_s}{V_\infty} - 1\right)^n (1 - M_\infty^2) \int_1^{V_s/V_\infty} \left(\frac{V}{V_\infty} - 1\right)^{1-n} d\left(\frac{V}{V_\infty}\right) \end{aligned}$$

This may be readily integrated and solved for $(V_s/V_\infty - 1)$ in the form

$$\frac{V_s}{V_\infty} - 1 = \sqrt{\frac{2-n}{1-M_\infty^2}} \sqrt{\frac{y_s}{R_s}} \quad (12.16)$$

The value of n is now found by setting $M_\infty = 0$. Thus

$$\frac{V_{si}}{V_\infty} - 1 = \sqrt{2-n} \sqrt{\frac{y_s}{R_s}} \quad (12.17)$$

where V_{si} is the velocity at point s for incompressible flow. Combining Eqs. 12.16 and 12.17, we obtain finally

$$\frac{V_s}{V_\infty} - 1 = \frac{1}{\sqrt{1-M_\infty^2}} \left(\frac{V_{si}}{V_\infty} - 1 \right) \quad (12.18)$$

which may be recognized as the Prandtl-Glauert rule. This result gives some assurance that the curvature function, Eq. 12.14, is reasonably accurate for flows involving large perturbations.

Accuracy of Streamline Curvature Method. To appraise the accuracy of the streamline curvature method, it has been compared⁽²³⁾ with the substantially exact results in the example of Fig. 12.7. As may be seen

from Fig. 12.23, the streamline curvature method gives an excellent approximation to the exact results at $M_\infty = 0.75$; a similar comparison (not shown here) at $M_\infty = 0.50$ shows almost perfect agreement.

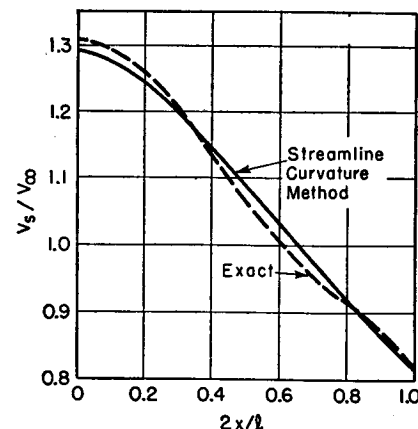


FIG. 12.23. Velocity distribution (at $M_\infty = 0.75$) for flow past 10%-thick profile of Fig. 12.7b. Curve marked "exact" is taken from Fig. 12.7a (after Perl).

REFERENCES AND SELECTED BIBLIOGRAPHY

1. EHLERS, F. E., and CARRIER, G. F. Monograph IV, Methods of Linearization in Compressible Flow. Part I: Janzen-Rayleigh Method, *Air Materiel Command Report*, No. F-TR-1180A-ND (Feb., 1948).
2. SAUER, R. *Theoretical Gas Dynamics*. Ann Arbor: J. W. Edwards, 1947, p. 135.
3. RAYLEIGH, LORD. On the Flow of a Compressible Fluid Past an Obstacle, *Phil. Mag.*, Vol. 32 (1916), p. 1.
4. KAPLAN, C. On the Use of Residue Theory for Treating the Subsonic Flow of a Compressible Fluid, *NACA Tech. Rep.*, No. 728 (1942).
5. IMAI, I. A New Method of Successive Approximation for Dealing with the Two-Dimensional Flow of a Compressible Fluid, *Proc. Phys. Math. Soc. Japan*, Vol. 24 (1942).
6. IMAI, I. On the Flow of a Compressible Fluid Past a Circular Cylinder, II, *Proc. Phys. Math. Soc. Japan*, Vol. 23 (1941), p. 181.
7. HASIMOTO, Z. On the Subsonic Flow of a Compressible Fluid Past a Circular Cylinder Between Two Parallel Walls, *Proc. Phys. Math. Soc. Japan*, Vol. 25 (1943), pp. 563-74.
8. LAMLA, E. Die symmetrische Potentialstromung eines kompressiblen Gases um einen Kreiszylinder in Freistrahl im unterkritischen Gebiet, *Luftfahrtforschung*, Vol. 19 (1943), pp. 358-62.
9. KAPLAN, C. A Theoretical Study of the Moment on a Body in a Compressible Fluid, *NACA Tech. Rep.*, No. 671 (1939).
10. TAMATIKO, S., and UMEMOTO, H. On the Subsonic Flow of a Compressible Fluid Past a Symmetrical Joukowski Aerofoil, Report 201 of Aero. Res. Inst., Tokyo Imp. Univ. (1941).
11. KAPLAN, C. The Flow of a Compressible Fluid Past a Curved Surface, *NACA Rep.*, No. 768 (1943).
12. KAPLAN, C. The Flow of a Compressible Fluid Past a Circular Arc Profile, *NACA Rep.*, No. 994 (1944).

13. KAPLAN, C. Effect of Compressibility at High Subsonic Velocities on the Lifting Force Acting on an Elliptic Cylinder, *NACA Rep.*, No. 834 (1946).
14. EMMONS, H. W. The Numerical Solution of Compressible Fluid Flow Problems, *NACA Tech. Note*, No. 932 (1944).
15. EMMONS, H. W. The Theoretical Flow of a Frictionless, Adiabatic, Perfect Gas Inside of a Two-Dimensional Hyperbolic Nozzle, *NACA Tech. Note*, No. 1003 (1946).
16. EMMONS, H. W. Flow of a Compressible Fluid Past a Symmetrical Airfoil in a Wind Tunnel and in Free Air, *NACA Tech. Note*, No. 1746 (1948).
17. AMICK, J. L. Comparison of the Experimental Pressure Distribution on an NACA 0012 Profile at High Speeds with that Calculated by the Relaxation Method, *NACA Tech. Note*, No. 2174 (1950).
18. STACK, J. L., LINDSEY, W. F., and LITTELL, R. E. The Compressibility Bubble and the Effects of Compressibility on Pressures and Forces Acting on an Airfoil, *NACA Rep.*, No. 646 (1938).
19. STACK, J. Compressible Flows in Aeronautics, *Jour. Aero. Sci.*, Vol. 12, No. 2 (1945).
20. ABBOTT, I. H., and von DOENHOFF, A. E. *Theory of Wing Sections*. New York: McGraw-Hill Book Co., Inc., 1949.
21. von KARMAN, TH. Compressibility Effects in Aerodynamics, *Jour. Aero. Sci.*, Vol. 8, No. 9 (1941), p. 337.
22. FERRI, A. Completed Tabulation in the United States of Tests of 24 Airfoils at High Mach Numbers, *NACA ACR*, No. L5E21 (1945). (*Wartime Report*, No. L-143.)
23. PERL, W. Calculation of Compressible Flows Past Aerodynamic Shapes by Use of the Streamline Curvature, *NACA Tech. Note*, No. 1328 (1947).
24. ALPERT, S. Design Method for Two-Dimensional Channels for Compressible Flow with Application to High-Solidity Cascades, *NACA Tech. Note*, 1931 (1949).

Chapter 13

THREE-DIMENSIONAL, SUBSONIC FLOW

13.1. Introductory Remarks

Most practical problems are three-dimensional in nature but their mathematical complexity usually makes the exact analysis of such problems prohibitively difficult. An idealized approach is usually adopted, therefore, the results of which are taken as a general guide to what might take place in more complex situations. This simplified approach might consist of the exact analysis of certain mathematically simple forms, such as ellipsoids; or it might involve the determination of approximate rules of comparison between three-dimensional flows and plane two-dimensional flows, since analysis of the latter is less difficult; or it might depend on a linearized theory, based on the assumption of small perturbations, and leading to approximate rules showing the effect of Mach Number.

All these techniques, alone and in combination, will be discussed in this chapter, the purpose mainly being to arrive at a general understanding of subsonic flow about three-dimensional bodies.

Our analytical considerations will be limited to potential flows, and will, therefore, give information concerning the pressure distribution and streamline pattern in the flow outside of the boundary layer. However, the pressure distribution of the potential flow controls to a large extent the behavior of the boundary layer. We shall therefore inject boundary-layer considerations into the discussion of experimental drag results.

NOMENCLATURE

\mathcal{A}	aspect ratio	try normal to leading edge
α	angle of attack (radians)	
b	span of wing	C_{m} moment coefficient
c	speed of sound	l chord
C_p	pressure coefficient	M Mach Number
$(-C_p)_{\text{max}}$	peak negative pressure coefficient	$M_{\infty \text{ cr}}$ lower critical free-stream Mach Number
C_D	drag coefficient	p pressure
C_L	lift coefficient	r radius in cylindrical coordinates
C_{LN}	section lift coefficient, based on flow and geom-	t thickness of profile

NOMENCLATURE—Continued

u	x -component of perturbation velocity	σ	sweepback angle
v	y -component of perturbation velocity	φ	perturbation velocity potential
V	resultant velocity	$(\cdot)'$	signifies transformed coordinates
w	z -component of perturbation velocity	$(\cdot)_s$	signifies conditions at profile surface
x, y, z	Cartesian coordinates	$(\cdot)_c$	signifies compressible flow
β	$\sqrt{1 - M_\infty^2}$	$(\cdot)_i$	signifies incompressible flow
δ	thickness ratio	$(\cdot)_\infty$	signifies free-stream conditions
δ_N	thickness ratio in plane normal to leading edge		

13.2. Gothert's Rule for Uniform Flow with Small Perturbations

We shall consider in this article the irrotational, isentropic, steady, subsonic flow of a perfect gas under the assumption that there are only small deviations from a uniform, parallel flow. Let the uniform flow be along the x -axis with a speed V_∞ . The body producing the disturbances in the flow must then be very thin in at least one direction normal to x , say the y -direction; that is, the thickness ratio of the body in the x, y -plane must be small compared to unity, but may be anything whatsoever in the x, z -plane (Fig. 13.1).

Linearization of the Differential Equation. The exact differential equation of the velocity potential, without the assumption of small perturbations, is Eq. 9.32. In Chapter 10, the linearization of this equation for two-dimensional flow was undertaken very carefully, with special consideration of the significance of the various assumptions, and Eq. 10.21a for the perturbation velocity potential was arrived at.

Employing similar assumptions, Eq. 9.32 for three-dimensional flow may be linearized to give

$$\beta^2 \frac{\partial^2 \varphi}{\partial x^2} + \frac{\partial^2 \varphi}{\partial y^2} + \frac{\partial^2 \varphi}{\partial z^2} = 0 \quad (13.1)$$

where $\beta \equiv \sqrt{1 - M_\infty^2}$, $M_\infty \equiv V_\infty/c_\infty$, and φ is the *perturbation velocity potential*, the derivatives of which are the *perturbation velocity components* u , v , and w in the x -, y -, and z -directions, respectively:

$$u = \partial \varphi / \partial x; \quad v = \partial \varphi / \partial y; \quad w = \partial \varphi / \partial z \quad (13.2)$$

At any point in the flow the complete velocity components in the x -, y -, z -directions are, respectively, $(V_\infty + u)$, v , and w .

A review of Art. 10.2 will show that the most stringent assumptions underlying Eq. 13.1 are that

$$(M_\infty)^2 (u/V_\infty) \ll 1; \quad M_\infty^2 (v/V_\infty) \ll 1; \quad M_\infty^2 (w/V_\infty) \ll 1 \quad (13.3)$$

$$M_\infty^2 (u/V_\infty) / (1 - M_\infty^2) \ll 1 \quad (13.4)$$

Equation 13.4 bars from the present analysis the transonic region, that is to say, free-stream Mach Numbers near unity. In the subsonic region Eq. 13.3 shows that the value of M_∞ up to which the analysis is accurate depends on the relative magnitudes of the perturbation velocities produced by the body.

Boundary Conditions. Let us suppose that the fluid streams past a thin body B (Fig. 13.1) whose surface is defined implicitly by the relation $S(x_s, y_s, z_s) = 0$. At infinity the boundary conditions are

$$\text{at } \begin{cases} x = \pm \infty \\ y = \pm \infty \end{cases}: \quad u = v = w = 0 \quad (13.5)$$

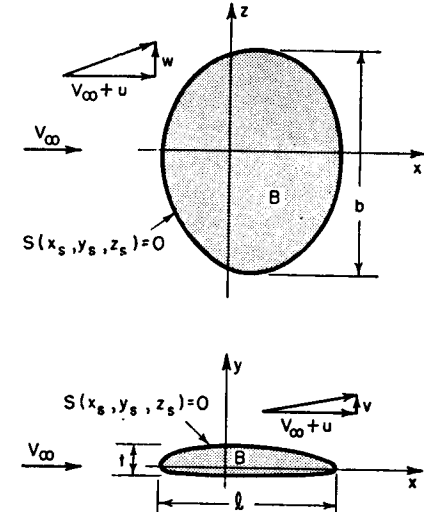


FIG. 13.1. Nomenclature for flow with small perturbations past body B .

At the surface of the body the boundary condition is that the streamline be tangent to the surface, or, mathematically,

$$(V_\infty + u_s) : v_s : w_s = dx_s : dy_s : dz_s$$

This may also be written

$$(V_\infty + u_s) / dx_s = v_s / dy_s = w_s / dz_s = \sqrt{(V_\infty + u_s)^2 + v_s^2 + w_s^2} / \sqrt{dx_s^2 + dy_s^2 + dz_s^2}$$

where u_s , v_s , and w_s are the perturbation velocities at a point on the surface S . On the surface S we may also write, however,

$$ds = \frac{\partial S}{\partial x_s} dx_s + \frac{\partial S}{\partial y_s} dy_s + \frac{\partial S}{\partial z_s} dz_s = 0$$

Elimination of dx_s , dy_s , and dz_s with the help of the preceding relations then gives us the boundary condition in the form

$$(V_\infty + u_s) (\partial S / \partial x_s) + v_s (\partial S / \partial y_s) + w_s (\partial S / \partial z_s) = 0$$

or, within the approximations of the linear theory,

$$V_\infty \partial S / \partial x_s + v_s \partial S / \partial y_s + w_s \partial S / \partial z_s = 0 \quad (13.6)$$

Affine Transformation to Corresponding Incompressible Flow. Now, using the detailed analysis of Art. 10.5 as a guide, we may effect a transformation which permits a comparison of the original compressible flow with an incompressible flow over a modified body B' having a surface defined by $S'(x_s', y_s', z_s') = 0$. The results of Art. 10.5 suggest that we define new coordinates x', y', z' and a new perturbation potential function φ' as follows:

$$x' \equiv x; \quad y' \equiv \beta y; \quad z' \equiv \beta z; \quad \varphi'(x', y', z') \equiv \beta^2 \varphi(x, y, z) \quad (13.7)$$

These same relations define the new body B' with surface coordinates $x_s' \equiv x_s; y_s' \equiv \beta y_s; z_s' \equiv \beta z_s$. Hence, we may write $S(x_s, y_s, z_s) = S'(x_s', y_s', z_s') = 0$.

Substituting these expressions for x, y, z , and φ into Eq. 13.1, and simplifying, we get

$$\frac{\partial^2 \varphi'}{\partial x'^2} + \frac{\partial^2 \varphi'}{\partial y'^2} + \frac{\partial^2 \varphi'}{\partial z'^2} = 0 \quad (13.8)$$

which is evidently the differential equation for the perturbation potential of an incompressible flow.

From Eqs. 13.2 and 13.7, we may find

$$u = \frac{\partial \varphi}{\partial x} = \frac{\partial(\varphi'/\beta^2)}{\partial x'} = \frac{1}{\beta^2} \frac{\partial \varphi'}{\partial x'} = \frac{u'}{\beta^2} \quad (13.9a)$$

$$v = \frac{\partial \varphi}{\partial y} = \frac{\partial(\varphi'/\beta^2)}{\partial y'} = \frac{1}{\beta} \frac{\partial \varphi'}{\partial y'} = \frac{v'}{\beta} \quad (13.9b)$$

$$w = \frac{\partial \varphi}{\partial z} = \frac{\partial(\varphi'/\beta^2)}{\partial z'} = \frac{1}{\beta} \frac{\partial \varphi'}{\partial z'} = \frac{w'}{\beta} \quad (13.9c)$$

where u', v', w' are the velocity components in the incompressible flow.

By applying the transformation formulas of Eqs. 13.7 and 13.9 to the boundary condition of Eq. 13.5, we get

$$\text{at } \begin{cases} x' = \pm\infty \\ y' = \pm\infty \end{cases}: \quad u' = v' = w' = 0 \quad (13.10)$$

which means that in the incompressible flow, the flow is uniform and parallel at infinity.

Next, applying Eqs. 13.7 and 13.9 to the boundary condition at the body as expressed by Eq. 13.6, we obtain, after simplification,

$$V_\infty \frac{\partial S'}{\partial x_s'} + v_s' \frac{\partial S'}{\partial y_s'} + w_s' \frac{\partial S'}{\partial z_s'} = 0 \quad (13.11)$$

Without loss of generality, we may set $V_\infty' = V_\infty$. Then Eq. 13.11 (by

comparison with the form of Eq. 13.6) is exactly the condition that the incompressible flow follow the boundaries of B' . The latter, according to Eq. 13.7, is thinner than B in all lateral dimensions by the factor β .

Linearized Pressure Coefficient. In Art. 10.3, it was shown that the linearized pressure coefficient is $C_p = -2u/V_\infty$. This expression is based on the assumption that $u/V_\infty \ll 1$. However, it is important to note that the ratio of two linearized pressure coefficients when based on this expression has an accuracy dependent on the assumption $(u/V_\infty)^2 \ll 1$, and hence the *comparison* of pressure coefficients by the linear theory is considerably more accurate than the calculation of a single pressure coefficient by linearized methods.

Now, using Eqs. 13.9, we get

$$C_p = -2 \frac{u}{V_\infty} = -2 \frac{u'}{V_\infty'} \cdot \frac{V_\infty'}{V_\infty} \cdot \frac{u}{u'} = \frac{1}{\beta^2} C_p' \quad (13.12)$$

Gothert's Rule. The bodies B' and B are affinely related, so that in going from B to B' , the thickness ratio in the x, y -plane, the aspect ratio seen in the x, z -plane, the angle of attack seen in the x, y -plane, etc., are all altered in the same proportion, namely, they are reduced by the factor β . Letting δ denote the thickness ratio, and using the convention that in affine transformations a change in δ produces proportionate changes in angle of attack, a , aspect ratio, A , etc., we may summarize the entire analysis by the symbolic relation

$$(C_p)_{M_\infty, \delta, a, A, x/l, y/t, z/b} = \frac{1}{\beta^2} (C_p)_{0, \beta\delta, \beta a, \beta A, x/l, y/t, z/b} \quad (13.13)$$

or, in words, *the pressure coefficient at a given point for the compressible flow at Mach Number M_∞ past a body of thickness δ is $1/\beta^2$ times as large as the pressure coefficient at the corresponding point for incompressible flow past a thinner affine body of thickness $\beta\delta$.*

This will be recognized as Rule I of Chapter 10. But, whereas for two-dimensional incompressible flow the pressure coefficient for affine thin profiles is approximately proportional to the thickness ratio, no such simple rule applies to three-dimensional incompressible flow. For three-dimensional flows, therefore, it is not possible to arrive at the simple Prandtl-Glauert rule showing the effect of Mach Number on the pressure coefficient for a body of fixed shape.

In applying Eq. 13.13 to a compressible flow at Mach Number M_∞ , it is necessary to consider the incompressible flow past a different body all of whose lateral dimensions are reduced by the ratio $\sqrt{1 - M_\infty^2}$. The pressure coefficient for the incompressible flow is found either from systematic experiments or by means of analytical methods.

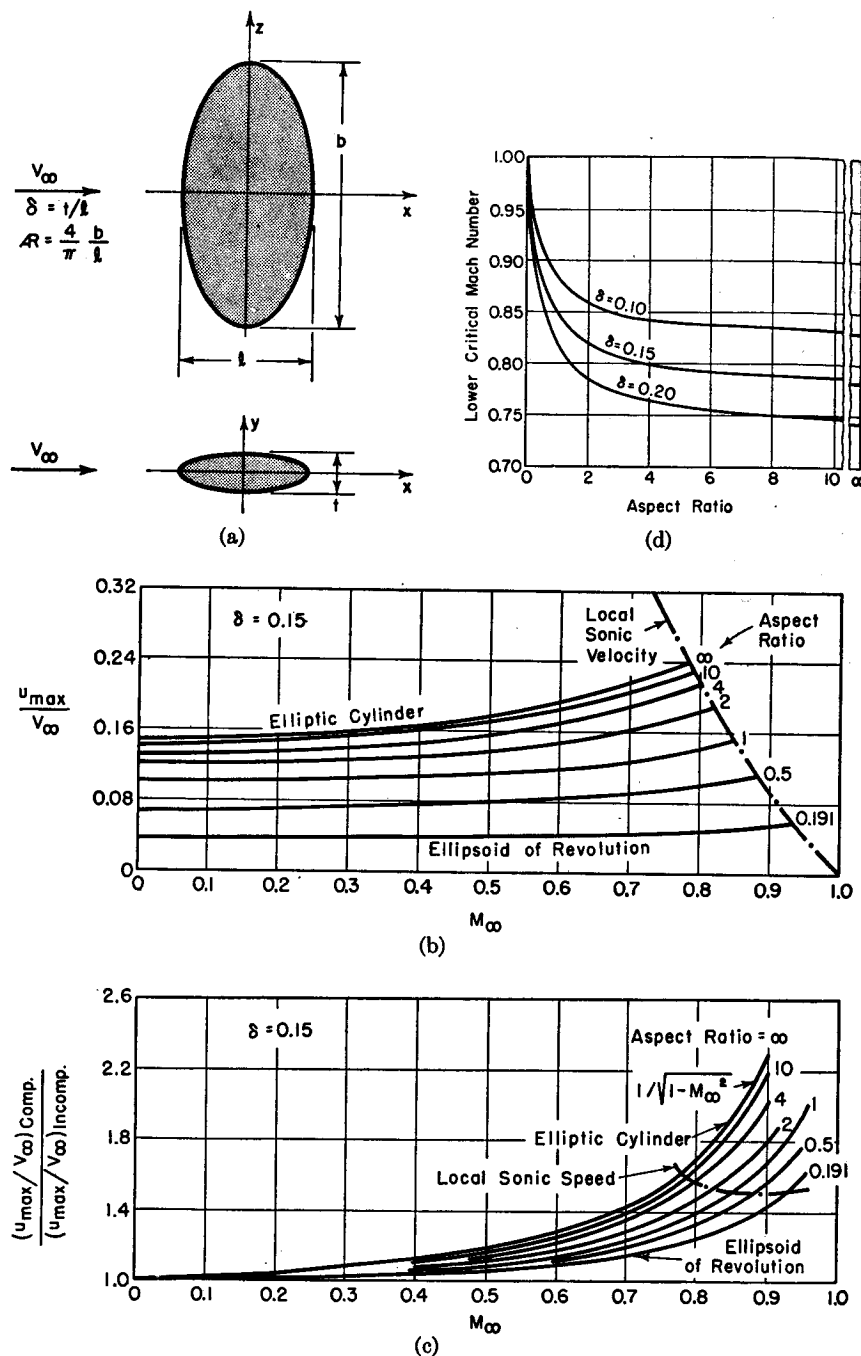


FIG. 13.2. Flow past ellipsoids (after Hess and Gardner). (See explanation on page 399.)

The lift and moment coefficients are found by integrating the pressure forces acting on the surface of the body. Within the linear theory Eq. 13.13 holds at all corresponding points of the two flows. It follows, therefore, that the rule expressed by Eq. 13.13 applies also to the lift and moment coefficients.

13.3. Flow Past Ellipsoids

Method of Calculation. Since in three-dimensional flow there is no simple rule showing the effect of Mach Number on the pressure distribution around a given body, a knowledge of this effect may be gained only by working out typical examples.

A particularly convenient example is the family of ellipsoids (Fig. 13.2a) with axes l , t , and b . As $b/l \rightarrow \infty$, we get the case of an elliptic cylinder, whereas as $b/l \rightarrow t/l$ we get the case of an ellipsoid of revolution. For intermediate values of b/l the ellipsoid is similar to a wing of elliptic planform with thickness ratio t/l .

In applying Goethert's rule to an ellipsoid in compressible flow, with thickness ratio $\delta = t/l$, and aspect ratio

$$\mathcal{R} = \frac{\text{span}}{\text{planform area/span}} = \frac{b^2}{\pi(b/2)(l/2)} = \frac{4b}{\pi l}$$

we consider the incompressible flow about an ellipsoid with $\delta' = \beta(t/l)$ and $\mathcal{R}' = \beta(4b/\pi l)$. Using the classical solution for incompressible flow past an ellipsoid (e.g., Reference 8), the incremental velocity for the compressible flow at any point is found from the incremental velocity of the incompressible flow through Eq. 13.9a:

$$\left(\frac{u}{V_{\infty}} \right)_{M_{\infty}, \delta, \mathcal{R}, x/l, y/l, z/b} = \frac{1}{\beta^2} \left(\frac{u}{V_{\infty}} \right)_{0, \beta\delta, \beta\mathcal{R}, x/l, y/l, z/b}$$

Typical results of calculations of this type ⁽²⁾ are shown in Fig. 13.2.

Three-Dimensional Relief Effect. The maximum local velocity on the surface of the profile occurs at the half-chord line, i.e., at $x = 0$, and is the same at all points on the half-chord line. Fig. 13.2b shows the effect of Mach Number on u_{\max}/V_{∞} for various aspect ratios, the thick-

(Explanation for Fig. 13.2):

- Nomenclature.
- Maximum perturbation velocity on ellipsoid of 15% thickness ratio, showing effects of M_{∞} and aspect ratio.
- Ratio of maximum perturbation velocity for compressible flow to that for incompressible flow.
- Effect of aspect ratio and thickness ratio on lower critical Mach Number.

ness ratio remaining fixed. It is clear that the pressure coefficient for a given thickness ratio is very much less in three-dimensional flow than in two-dimensional flow. This is the result of a *three-dimensional relief effect* which arises because, in a three-dimensional flow, the stream may deviate from the original direction in both the y - and z -directions, whereas only the y -direction is allowable for a two-dimensional flow. Thus a three-dimensional body produces a lesser disturbance in the uniform, parallel flow, and, consequently, it has a smaller peak negative pressure coefficient.

One of the very important conclusions to be drawn from this example is that for practical problems the linearized theory is more reliable for three-dimensional flow than for two-dimensional flow because the relief effect makes the assumptions of Eq. 13.3 more likely to be met.

Influence of Aspect Ratio on Compressibility Effect. To bring out more clearly the effect of M_∞ at various aspect ratios, the results of Fig. 13.2b are replotted in Fig. 13.2c to show the *ratio* of the peak negative pressure coefficients for compressible and incompressible flow past ellipsoids of 15% thickness ratio. For infinite aspect ratio, corresponding to two-dimensional flow past an elliptic cylinder, the curve of Fig. 13.2c corresponds to the Prandtl-Glauert rule, namely, $C_p \sim 1/\sqrt{1 - M_\infty^2}$. For finite aspect ratios the effect of Mach Number is considerably less, until for ellipsoids of revolution with small thickness ratios the pressure coefficient is almost independent of Mach Number. For a thickness ratio of 0.15 and an aspect ratio of 2 the effect of Mach Number is approximately midway between that of the ellipsoid of revolution and that of the elliptical cylinder.

Lower Critical Mach Number. On Fig. 13.2b is plotted the curve of u_{\max}/V_∞ versus M_∞ for which the value of u_{\max} is exactly sonic. The intersection of this curve with each of the aspect ratio curves gives the value of $M_{\infty\ cr}$, the *lower critical Mach Number*, at which sonic velocity is first reached at the surface of the ellipsoid. By plotting $M_{\infty\ cr}$ versus aspect ratio for constant thickness ratio, the curves of Fig. 13.2d are obtained. This chart shows that the lower critical Mach Number is markedly increased as the aspect ratio decreases to values less than about 2.0. The increase in lower critical Mach Number is the result of the three-dimensional relief effect, which reduces both the magnitude of the incremental velocity and also the effect of Mach Number on this magnitude.

Effect of Aspect Ratio on "Compressibility Bubble." The lower critical Mach Number, $M_{\infty\ cr}$, is of practical significance because experience has shown that, as the result of a shock wave-boundary layer interaction, the drag of a body rises when velocities on the surface substan-

tially exceed the sonic velocity. From the results on ellipsoids, therefore, it would be expected that the Mach Number at which the *compressibility burble* appears would be increased as the aspect ratio is decreased. No direct data for ellipsoids are available, but Fig. 13.3,⁽⁹⁾ showing the results of measurements on a wing having a rectangular planform and a symmetrical profile of 12% thickness ratio, gives evidence of the beneficial influence of three-dimensional effects in delaying the sharp drag rise associated with compressibility. Corresponding schlieren photographs are given in Fig. 13.16.

It is also well known that shock waves first appear on the wings of high-speed subsonic aircraft rather than on the fuselage or on the tail surfaces. This is further confirmation of the three-dimensional relief effect.

13.4. Bodies of Revolution

A special but important case of three-dimensional flow is that of flow with axial symmetry past bodies of revolution. Strictly, only two length dimensions are involved here, which are in cylindrical coordinates x and $r = \sqrt{y^2 + z^2}$, but the flow possesses the "relief" effects of three-dimensional space flow, and is therefore included in the latter category.

Method of Sources and Sinks. Incompressible flows with axial symmetry may be analyzed in the classical manner by distributing sources and sinks along the x -axis, the distribution being determined by the requirement that one of the streamlines have the form of the desired body of revolution.⁽¹¹⁾ By applying Goertler's rule to the formulas of this method, a set of similar formulas for compressible flow with small perturbations may be derived.

Using this procedure, Laitone⁽⁶⁾ derived the following approximate formula for the pressure coefficient at the surface of a body of revolution:

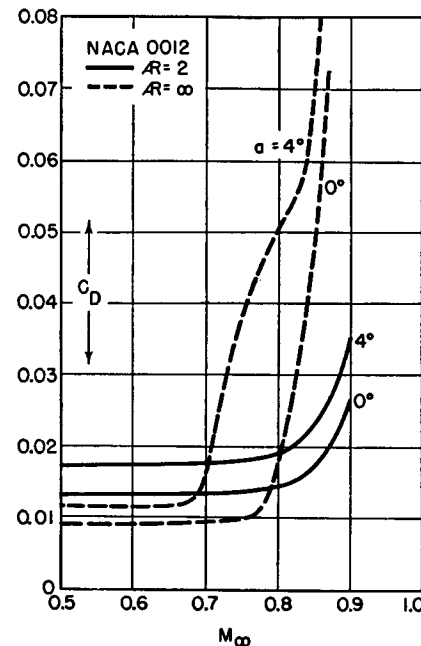


FIG. 13.3. Experimental curves showing influence of wing aspect ratio on curve of drag coefficient versus Mach Number (after Stack and Lindsey).

$$C_{p_s} = \frac{1}{\pi} \left[\frac{1 - \frac{2x}{L} A'}{1 - \frac{x}{L} 2x} - \left(1 + \ln \frac{\beta r_s}{2L \sqrt{\frac{x}{L} \left(1 - \frac{x}{L} \right)}} A'' \right) + \frac{L}{4} \left(1 - \frac{2x}{L} \right) A''' + \frac{L^2}{24} \left(1 - \frac{2x}{L} + \frac{2x^2}{L^2} \right) A'''' + \dots \right] \quad (13.14)$$

where L is the length of the body; x is the distance aft of the nose; r_s is the radius from the axis to the body surface; $A = \pi r_s^2$; $A' = dA/dx$; $A'' = d^2A/dx^2$; and so forth.

The results given by this approximate formula agree well with the exact results for an ellipsoid of revolution, discussed later.

Disturbance Produced by Body of Revolution. To determine the effects of wind tunnel wall interference, or to estimate the effects of a body of revolution on the pressure coefficient at large distances from the body, we may assume that in incompressible flow the influence of the body at remote points may be approximately represented by a three-dimensional doublet. The incompressible velocity potential of the latter is

$$\varphi \sim \frac{x}{(x^2 + r^2)^{3/2}}$$

so that, for a given body of revolution in incompressible flow,

$$u = \partial \varphi / \partial x \sim \frac{r^2 - 2x^2}{(x^2 + r^2)^{5/2}}$$

Furthermore, exact solutions for incompressible flow past very slender ellipsoids of revolution show the effect of thickness ratio on the perturbation velocity far from the body to be given approximately by $u \sim \delta^2$.

Now, referring to Fig. 13.4, let points 1 and 2 be corresponding points in compressible and incompressible flow about corresponding bodies, S and S' , in the sense demanded by Goert's rule; let point 3 refer to incompressible flow past S' , but at the same physical coordinates as point 1; and let point 4 refer to incompressible flow, at the coordinates of point 1, past the original body S . Then to find the effect of Mach Number on the pressure coefficient for a *fixed* body at a *fixed* point, we first write the identity

$$\left(\frac{u}{V_\infty} \right)_1 / \left(\frac{u}{V_\infty} \right)_4 = \frac{u_1}{u_4} = \frac{u_1}{u_2} \cdot \frac{u_2}{u_3} \cdot \frac{u_3}{u_4}$$

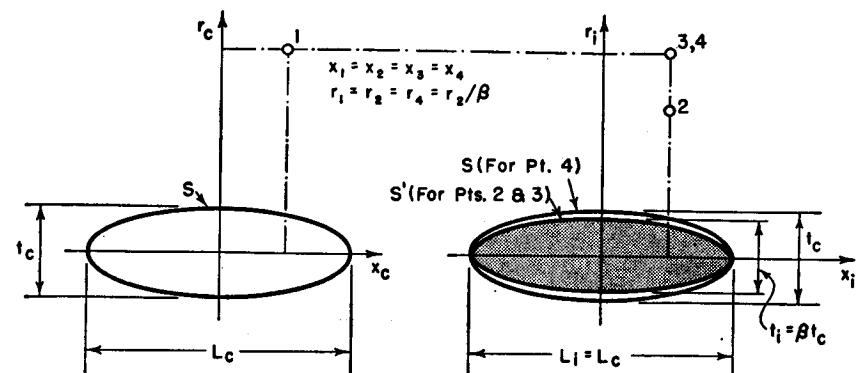


FIG. 13.4. Illustrates application of Goert's rule.

By using Goert's rule and the approximate rules for incompressible flow mentioned above, we may evaluate the three ratios on the right-hand side, and thus we get

$$\frac{u_1}{u_4} \cong \frac{1}{\beta^2} \left[\frac{r_2^2 - 2x_2^2}{r_3^2 - 2x_3^2} \cdot \frac{(x_3^2 + r_3^2)^{5/2}}{(x_2^2 + r_2^2)^{5/2}} \right] \left(\frac{\delta_3}{\delta_4} \right)^2$$

By the definitions of terms, however,

$$x_2 = x_3 = x_4 = x_1$$

$$r_1 = r_3 = r_4 = r_2/\beta$$

$$\delta_4 = \delta_1 = \delta_3/\beta$$

Making these substitutions, and simplifying, we get

$$\frac{u_1}{u_4} \cong \frac{\beta^2 r_1^2 - 2x_1^2}{r_1^2 - 2x_1^2} \cdot \frac{(x_1^2 + r_1^2)^{5/2}}{(x_1^2 + \beta^2 r_1^2)^{5/2}}$$

At great lateral distances from the body, i.e., as $x_1/r_1 \rightarrow 0$, this formula becomes $u_1/u_4 \cong 1/\beta^3$, which means that the effect of compressibility is given by

$$C_p \cong 1/(1 - M_\infty^2)^{3/2}$$

This is the same result as was obtained for two-dimensional flow. It shows that if Δu represents the *interference velocity* produced at the body in a test because of wind tunnel walls, the effect of compressibility on the interference velocity is given by $\Delta u \cong 1/\beta^3$.

It is especially curious that at the surfaces of two-dimensional and axially symmetric bodies the effects of compressibility are markedly different; whereas at great lateral distances the effects are the same.

At great longitudinal distances from a body of revolution, i.e., $r_1/x_1 \rightarrow 0$ the results of this analysis show the pressure coefficient to be independent

of Mach Number. In Chapter 10 it was shown that for two-dimensional bodies the pressure coefficient at great longitudinal distances varies as $1/\beta$.

Comparison of Goert's Rule with Experiment. Fig. 13.5 shows the measured surface pressure coefficients⁽⁷⁾ at various sections of a semi-infinite half-body of revolution with an ellipsoidal nose. Also shown

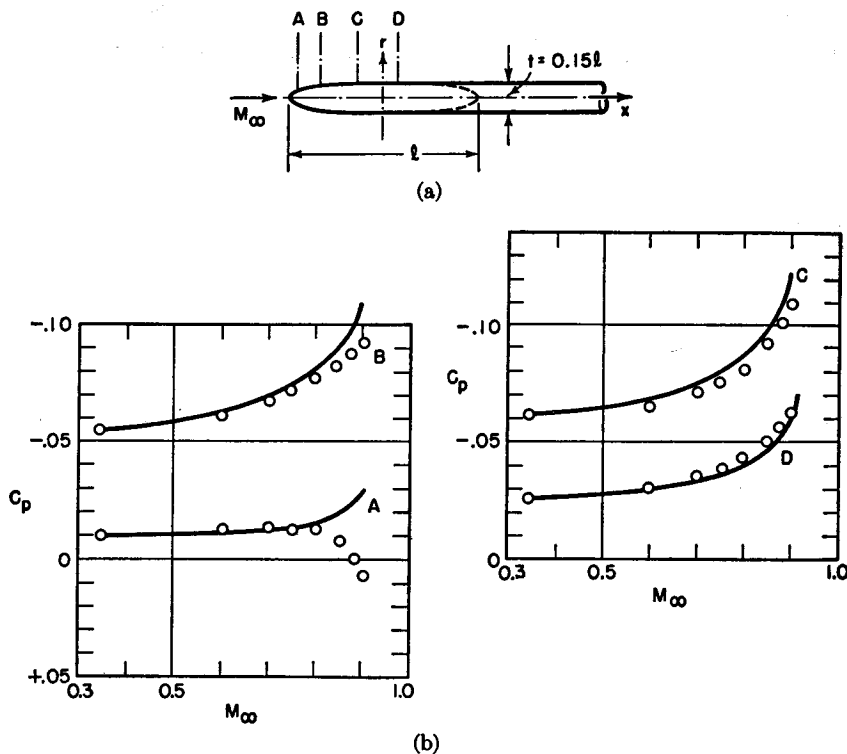


FIG. 13.5. Flow past semi-infinite half-body of revolution (after van Driest).

(a) Nomenclature.

(b) Comparison of Goert's rule with experimental data.

are solid lines indicating the effect of Mach Number on pressure coefficient as found by Goert's rule. To apply the latter, the theoretical solution for incompressible flow was first worked out as a function of thickness ratio by the method of sources and sinks, and then Goert's rule applied in the usual manner.

The agreement between theory and experiment is on the whole fairly satisfactory, even up to Mach Numbers of 0.9. Thanks to the several effects mentioned earlier in reference to the flow past ellipsoids, the method of small perturbations is seen to be considerably more reliable

at high Mach Numbers for axi-symmetric flow than for two-dimensional flow.

Thin Ellipsoid of Revolution. The ellipsoid of revolution remains such during an affine transformation. Since the exact incompressible solution is known, we may derive an analytical formula in closed form relating the peak negative pressure coefficient to the Mach Number and thickness ratio δ .

PRESSURE CORRECTION FORMULA. According to Lamb,⁽¹⁰⁾ the maximum disturbance velocity for incompressible flow occurs at the point of maximum thickness, and for potential flow is given exactly by

$$\left(\frac{u_{\text{incomp}}}{V_{\infty}}\right)_{\text{max}} = \frac{\left[\delta^2 \ln \frac{1 + \sqrt{1 - \delta^2}}{1 - \sqrt{1 - \delta^2}} - 2\delta^2 \sqrt{1 - \delta^2}\right]}{\left[2\sqrt{1 - \delta^2} - \delta^2 \ln \frac{1 + \sqrt{1 - \delta^2}}{1 - \sqrt{1 - \delta^2}}\right]} \quad (13.15)$$

By restricting our considerations to small thickness ratios (less than about 20%), it may be shown by expanding this expression and ignoring terms of higher order that

$$\left(\frac{u_{\text{incomp}}}{V_{\infty}}\right)_{\text{max}} \cong \delta^2 \left(\ln \frac{2}{\delta} - 1\right) \quad (13.16)$$

Applying Goert's rule to this expression, we obtain for the maximum incremental velocity in compressible flow past a thin ellipsoid of revolution of thickness δ ,

$$\left(\frac{u_{\text{comp}}}{V_{\infty}}\right)_{\text{max}} = \frac{1}{\beta^2} (\beta \delta)^2 \left(\ln \frac{2}{\beta \delta} - 1\right) \cong \delta^2 \left(\ln \frac{2}{\delta \sqrt{1 - M_{\infty}^2}} - 1\right) \quad (13.17)$$

To find the effect of compressibility for a fixed value of δ , we combine Eqs. 13.17 and 13.16 to give

$$\begin{aligned} \frac{(-C_p)_{\text{max}}}{(-C_{p_i})_{\text{max}}} &= \frac{(u_{\text{comp}})_{\text{max}}}{(u_{\text{incomp}})_{\text{max}}} \\ &= \frac{\frac{2}{\sqrt{1 - M_{\infty}^2} \delta} - 1}{\frac{2}{\delta} - 1} = 1 + \frac{\ln \sqrt{1 - M_{\infty}^2}}{1 - \ln 2 + \ln \delta} \end{aligned} \quad (13.18a)$$

In the absence of better information, Eqs. 13.17 and 13.18 may also be used as a guide for estimating the peak negative pressure coefficient on slender bodies of revolution of shapes other than ellipsoidal. For this

purpose an equivalent δ should be used, so chosen as to produce equal peak negative pressure coefficients in incompressible flow for the ellipsoid and for the body under investigation.

A theoretical investigation of the flow past a prolate spheroid⁽²⁰⁾ gives exactly the same result as Eq. 13.18a, thus lending strength to the

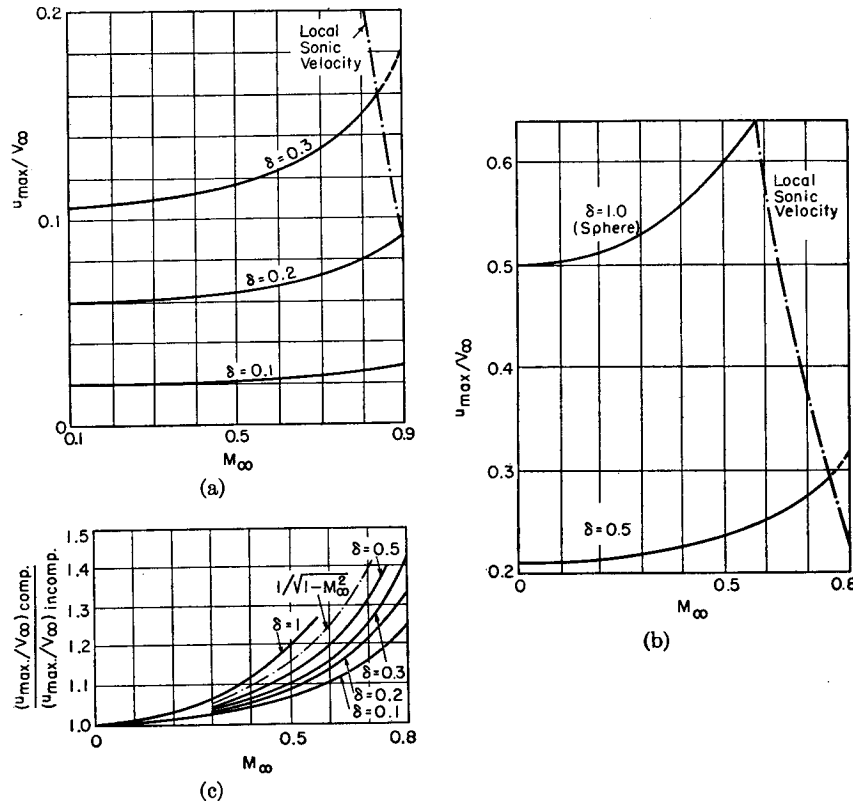


FIG. 13.6. Substantially exact theoretical results for flow past ellipsoid of revolution (after Schmieden and Kawalki).

(a) and (b) Maximum perturbation velocity.
(c) Ratio of maximum perturbation velocity for compressible flow to that for incompressible flow.

hypothesis that Eq. 13.18a may be used as a general rule for thin bodies of revolution. In Reference 20 it is also shown that, within the approximations of the perturbation theory,

$$(-C_p)_{\max} - (-C_{p_i})_{\max} = 2\delta^2 \ln \sqrt{1 - M_\infty^2} \quad (13.18b)$$

RESULTS OF EXACT THEORETICAL ANALYSIS. Substantially exact results for potential, compressible flow past ellipsoids of revolution⁽³⁾ are shown in Fig. 13.6. For thickness ratios below 0.20, the approximate

formulas of Eqs. 13.17 and 13.18 are found to fit these results to within a few per cent.

Figs. 13.6a, b show, as was mentioned previously, that the maximum disturbance velocity produced by a thin body of revolution is small compared with that of a two-dimensional body. Fig. 13.6c shows further the relatively small effect of Mach Number on the pressure coefficient of slender bodies of revolution, as compared with the factor $1/\sqrt{1 - M_\infty^2}$ for two-dimensional flow. Indeed, for the limiting case of zero thickness ratio, Eq. 13.18 shows the pressure coefficient to be independent of Mach Number.

By plotting on Figs. 13.6a, b the relation between $(V^* - V_\infty)/V_\infty$ and M_∞ for isentropic flow, corresponding to the local appearance of sonic velocity, the value of the lower critical Mach Number for each thickness ratio may be found at the appropriate intersection point. Fig. 13.7 accordingly shows the lower critical Mach Number as a function of thickness ratio. For comparison, the corresponding relation for the elliptic cylinder is also shown. For $\delta = 0.20$, as an example, the lower critical Mach Number of the cylinder is 0.74, as compared with 0.90 for the body of revolution, thus showing again that compressibility effects become serious at an earlier stage for wing-type bodies than for fuselage-type bodies.

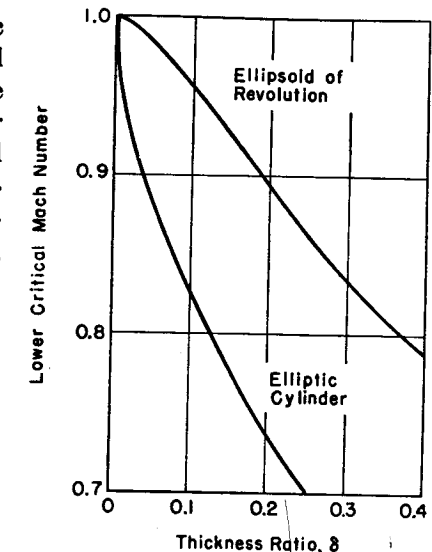


FIG. 13.7. Lower critical Mach Number for ellipsoid of revolution and for elliptic cylinder.

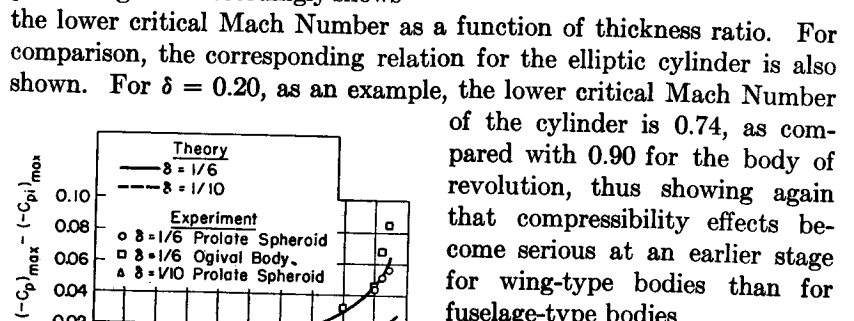


FIG. 13.8. Experimental results for flow past prolate spheroid and ogival body of revolution (after Matthews). Theoretical curves represent Eq. 13.18b.

shown is the pressure correction formula of Eq. 13.18b for the relevant thickness ratios of 1/6 and 1/10.

COMPARISON WITH EXPERIMENT. Fig. 13.8 shows the experimental effect of M_∞ on the peak negative pressure coefficient of two prolate spheroids and of an ogival body of revolution. Also

Up to $M_\infty = 0.9$ the agreement of theory with experiment is quite good. It is also of practical interest that the two shapes with $\delta = 1/6$ show substantially the same effect of Mach Number.

Drag. Fig. 13.9 shows the results of drag measurements⁽¹²⁾ made on a bomb.

This body of revolution has a comparatively large thickness ratio, namely, $\delta \cong 0.25$. Hence it is to be expected that the drag will be predominantly form drag, i.e., pressure drag. In the range of M_∞ where

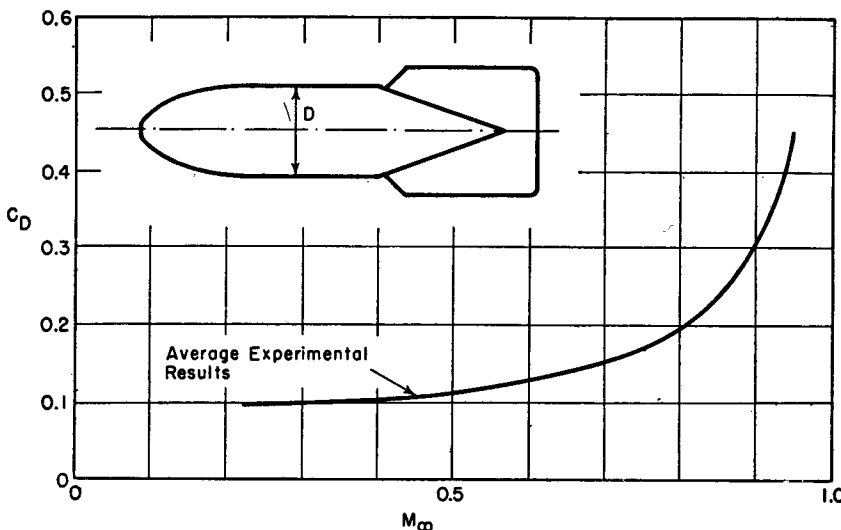


FIG. 13.9. Drag of bomb at subsonic speed (after Gothert).

$$C_D = \text{drag} / \frac{1}{2} \rho_\infty V_\infty^2 \left(\frac{\pi}{4} D^2 \right)$$

the flow is entirely subsonic, the pressure drag should, therefore, exhibit a variation with M_∞ somewhat similar to the variation of pressure coefficient for inviscid flow. A comparison of the bomb drag in the range of low Mach Numbers with the pressure-coefficient curve for $\delta \cong 0.25$ in Fig. 13.6 shows that the rise of drag coefficient is about twice as large as this argument would indicate, most likely because the shape of the bomb produces higher incremental velocities than does an ellipsoid of like thickness ratio.

According to Fig. 13.6, for $\delta \cong 0.25$, the lower critical Mach Number is about 0.86. At about this point Fig. 13.9 indicates a very rapid increase in drag coefficient, owing probably to the appearance of shock waves.

13.5. Spheres

Gothert's Rule. The sphere is of some interest because of its simple geometry and also because it represents the limiting case of a body of revolution. Since a sphere is far from slender, Eq. 13.15 must be used for the exact incompressible solution. Then, noting that $\delta = 1$ for a sphere, Gothert's rule applied to Eq. 13.15 yields the prediction that for compressible flow

$$\left(\frac{u_{\text{comp}}}{V_\infty} \right)_{\text{max}} = \left[\ln \frac{1 + M_\infty}{1 - M_\infty} - 2M_\infty \right] / \left[2M_\infty - (1 - M_\infty^2) \ln \frac{1 + M_\infty}{1 - M_\infty} \right] \quad (13.18c)$$

Rayleigh-Janzen Method. The accuracy of Gothert's rule may be tested by comparing Eq. 13.18c with the substantially exact solution for

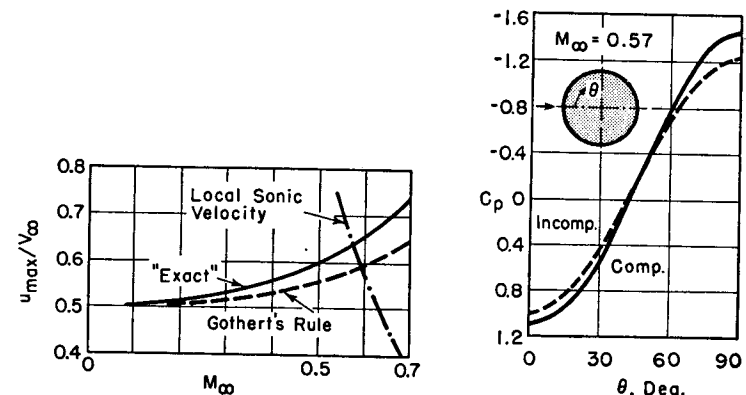


FIG. 13.10. Maximum perturbation velocity for flow past sphere as function of Mach Number. Comparison of exact solution (after Kaplan) with Gothert's rule.

flow past a sphere obtained by the Janzen-Rayleigh method.⁽¹³⁾ This comparison appears in Fig. 13.10. Considering the severity of this test of the method of small perturbations when applied to a body as thick as a sphere, this comparison lends confidence in Gothert's rule for the range of moderate thickness ratios.

Fig. 13.10 shows the lower critical M_∞ for the sphere to be 0.57. For this speed, as well as for incompressible flow, the pressure distribution over the surface of the sphere is shown in Fig. 13.11. These results, which are typical for symmetrical bodies of revolution, show that over practically all of the surface the effect of Mach Number is to augment the absolute magnitude of the pressure coefficient.

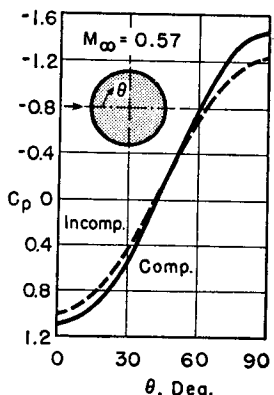


FIG. 13.11. Pressure distribution on sphere for compressible and incompressible flow (after Kaplan).

Drag. Experimental measurements⁽¹⁴⁾ of the drag of spheres at high speeds are summarized in Fig. 13.12. The range of Reynolds Numbers for these tests is in the region where the flow is separated over the downstream part of the sphere, and hence the drag is substantially all pressure drag.

Up to $M_\infty \leq 0.5$, there is little effect of Mach Number on drag coefficient, in conformity with the effect of Mach Number on peak disturbance velocity shown in Fig. 13.10. Above the lower critical Mach

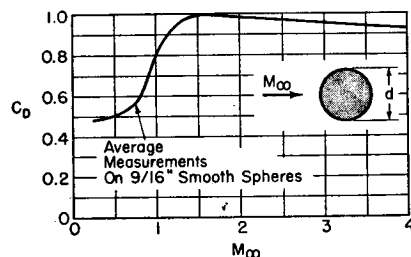


FIG. 13.12. Experimental drag of smooth spheres of $\frac{9}{16}$ -inch diameter. Drag coefficient is based on frontal area (after Charters).

Number of 0.57, however, there is a sharp rise in drag. Spark shadowgraphs of the flow past the sphere show this rise in drag to be associated with the appearance of shock waves.

13.6. Wings of Finite Span

Goertert's Rule. Consider a wing of span b , chord l , thickness t , and aspect ratio \mathcal{R} , operating at an angle of attack α in a stream of Mach Number M_∞ . The pressure coefficient at any point in the flow may, by Goertert's rule, be related to the pressure coefficient at a corresponding point for incompressible flow past an affinely related wing. The relation may be written implicitly as

$$(C_p)_{M_\infty, \delta, \mathcal{R}, \alpha, x/l, y/t, z/b} = \frac{1}{\beta^2} (C_{p_i})_{0, \beta\delta, \beta\mathcal{R}, \beta\alpha, x/l, y/t, z/b} \quad (13.19)$$

Since the lift and moment coefficients are found by integrating the pressure coefficient over the entire surface of the wing, it follows from Eq. 13.19 that the similarity rules for the lift and moment coefficients are

$$\frac{(C_L)_{M_\infty, \delta, \mathcal{R}, \alpha}}{(C_{L_i})_{0, \beta\delta, \beta\mathcal{R}, \beta\alpha}} = \frac{(C_M)_{M_\infty, \delta, \mathcal{R}, \alpha}}{(C_{M_i})_{0, \beta\delta, \beta\mathcal{R}, \beta\alpha}} = \frac{1}{1 - M_\infty^2} \quad (13.20)$$

Lift-Curve Slope. This similarity relation, which holds for any planform, compares wings of different aspect ratio and thickness ratio and at different angles of attack. To obtain a relation showing clearly the

effect of Mach Number on a wing of *fixed* aspect ratio, *fixed* thickness ratio, and *fixed* angle of attack, we introduce some approximate relations obtained by lifting-line theory for incompressible flow past wings of finite aspect ratio. The lift-curve slope in incompressible flow for a wing of finite aspect ratio is approximately related to that for infinite aspect ratio by the formula

$$\left(\frac{dC_{L_i}}{da} \right)_{\mathcal{R}} = \frac{(dC_{L_i}/da)_\infty}{1 + \frac{1}{\pi\mathcal{R}} \left(\frac{dC_{L_i}}{da} \right)_\infty} \quad (13.21a)$$

But, for incompressible two-dimensional flow

$$(dC_{L_i}/da)_\infty \approx 0.9(2\pi) \quad (13.21b)$$

where the factor 0.9 takes account of an average departure for existing wings from the theoretical value of 2π . Combining the last two relations, we get

$$\left(\frac{dC_{L_i}}{da} \right)_{\mathcal{R}} = \frac{5.65}{1 + \frac{1.8}{\mathcal{R}}} \quad (13.21c)$$

We may now write the identity

$$\frac{(dC_L/d\alpha)_{M_\infty, \delta, \mathcal{R}}}{(dC_{L_i}/da)_{0, \delta, \mathcal{R}}} = \frac{(dC_L/d\alpha)_{M_\infty, \delta, \mathcal{R}}}{(dC_{L_i}/da)_{0, \beta\delta, \beta\mathcal{R}}} \cdot \frac{(dC_{L_i}/da)_{0, \beta\delta, \beta\mathcal{R}}}{(dC_{L_i}/da)_{0, \delta, \beta\mathcal{R}}} \cdot \frac{(dC_{L_i}/da)_{0, \delta, \beta\mathcal{R}}}{(dC_{L_i}/da)_{0, \delta, \mathcal{R}}}$$

The first ratio on the right-hand side is found from Goertert's rule; the second is found from the approximate rule that the lift of affinely related profiles is proportional to the angle of attack; and the third is found from Eq. 13.21c. Thus we get

$$\frac{(dC_L/d\alpha)_{M_\infty, \delta, \mathcal{R}}}{(dC_{L_i}/da)_{0, \delta, \mathcal{R}}} = \frac{1}{\beta^2} \cdot \beta \left(\frac{1 + \frac{1.8}{\mathcal{R}}}{1 + \frac{1.8}{\beta\mathcal{R}}} \right) = \frac{1.8 + \mathcal{R}}{1.8 + \sqrt{1 - M_\infty^2} \mathcal{R}} \quad (13.22)$$

Fig. 13.13, which is based on Eq. 13.22, shows how the aspect ratio modifies the effect of compressibility on the lift coefficient. For infinite aspect ratio, Eq. 13.22 reduces to the Prandtl-Glauert rule for two-dimensional flow, namely: for a fixed profile, $dC_L/d\alpha \sim 1/\sqrt{1 - M_\infty^2}$. At the other extreme of zero aspect ratio, the lift-curve slope is independent of Mach Number. For aspect ratios in the neighborhood of 3, the augmentation of lift coefficient by compressibility is only about half what it would be for infinite aspect ratio.

In a high-speed airplane, the tail surfaces have a much smaller aspect ratio than the wing, and hence become relatively less effective at high

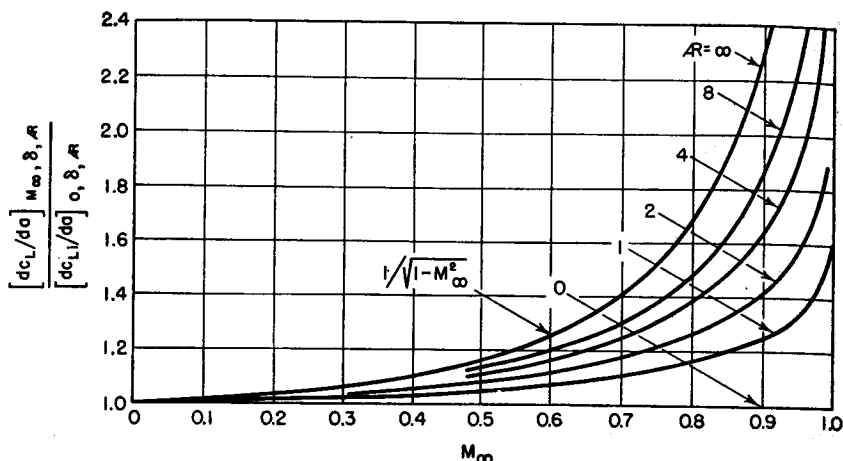


FIG. 13.13. Influence of aspect ratio on the way in which the lift-curve slope varies with Mach Number.

Mach Numbers. This may have an important bearing on aircraft stability at very high subsonic speeds.

Induced Drag. The minimum induced drag for linearized compressible flow may be shown to be given by the same relation as for incompressible flow, namely,

$$C_{D_{ind}} = \frac{C_L^2}{\pi AR} \quad (13.23)$$

Combining this with Eq. 13.22, we have

$$\frac{(C_{D_{ind}})_{M_\infty}}{(C_{D_{ind}})_0} = \frac{(C_L^2)_{M_\infty}}{(C_L^2)_0} = \left(\frac{1.8 + AR}{1.8 + \sqrt{1 - M_\infty^2} AR} \right)^2 \quad (13.24)$$

which shows that the induced drag increases less rapidly with Mach Number for wings of small aspect ratio than it does for wings of large aspect ratio.

Experimental Results. The effect of Mach Number on the lift-curve slope of a 12%-thickness profile with $AR = 1.15$ is shown in Fig. 13.14a.⁽¹⁵⁾ It is seen that the Prandtl-Glauert correction factor for two-dimensional flow is much too large and that the approximate theory developed in this chapter agrees rather well with the measurements up to the point where the lift-curve slope drops off as the result of local shock waves.

The moment-curve slope for the same wing is shown in Fig. 13.14b. The change in the sign of the moment-curve slope at $M_\infty \approx 0.75$ has a crucial bearing on aircraft stability at high speeds.

Fig. 13.15 represents the results of measurements on wings having a 12%-thickness profile and various aspect ratios.⁽¹⁶⁾ At low Mach Num-

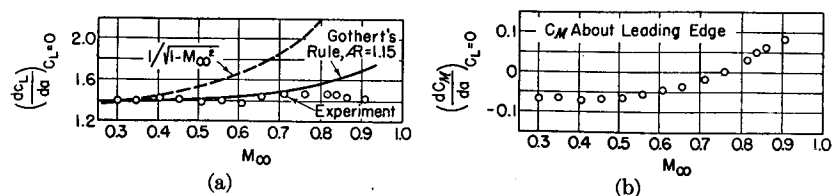


FIG. 13.14. Experimental results for wing having aspect ratio of 1.15 and NACA 0012 profile (after Goert).

- (a) Lift-curve slope at zero incidence versus Mach Number, showing comparison with Goert's rule.
 (b) Moment-curve slope at zero incidence versus Mach Number.

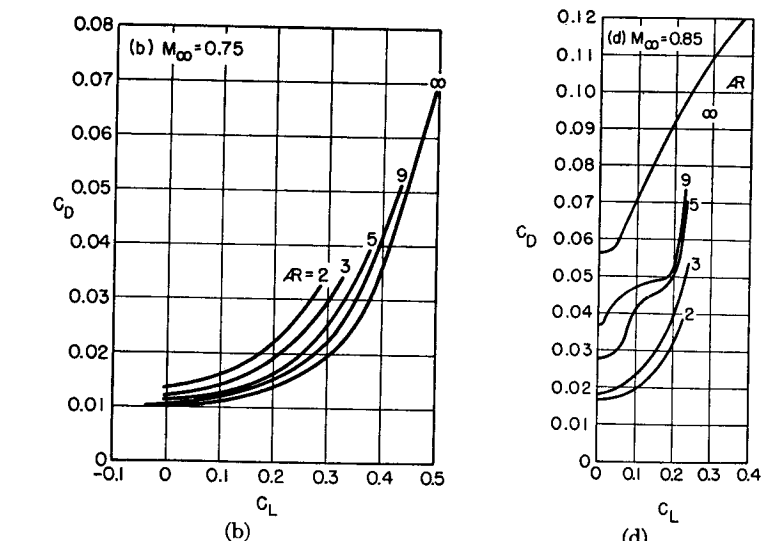
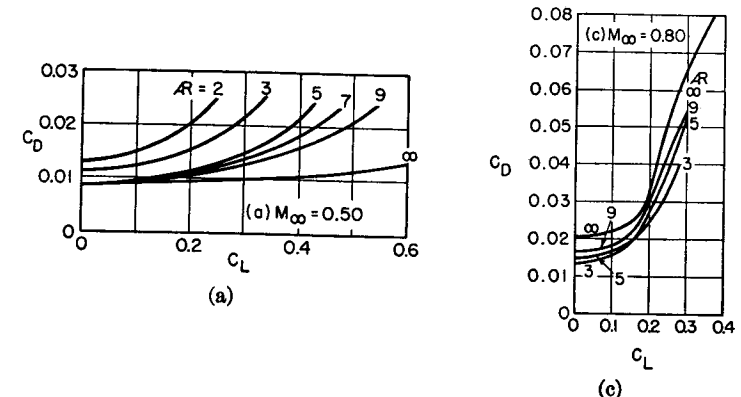


FIG. 13.15. Experimental lift-drag polars for NACA 0012 profile in wings of various aspect ratio (after Stack and Lindsey).

bers, Fig. 13.15a, it is aerodynamically desirable to have large aspect ratios in order to avoid the induced drag that goes with wings of finite span. As the Mach Number increases there is at first little change in

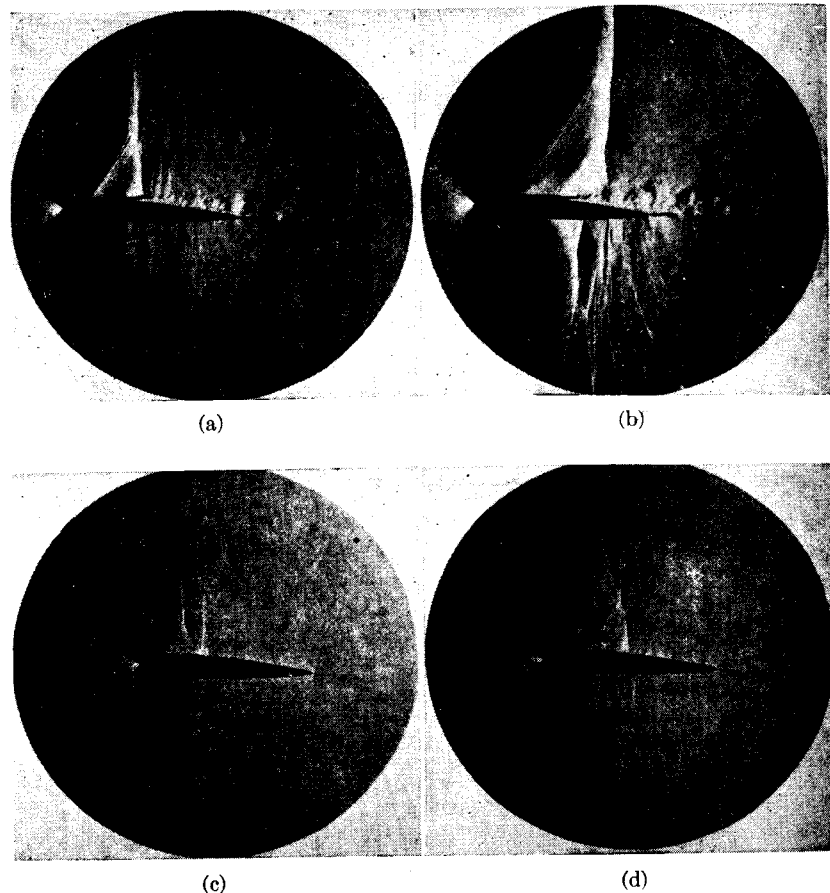


FIG. 13.16. Schlieren photographs of flow past wings with NACA 0012 profile at 4° angle of attack (after Lindsey and Humphreys). See also Fig. 13.3.

- (a) $AR = \infty; M_\infty = 0.78$.
- (b) $AR = \infty; M_\infty = 0.87$.
- (c) $AR = 2; M_\infty = 0.78$.
- (d) $AR = 2; M_\infty = 0.86$.

the relative positions of the lift-drag polars because the relation between lift and induced drag, Eq. 13.23, is substantially independent of Mach Number. At higher Mach Numbers, and especially at high lift coefficients, local compressibility effects give rise to shock waves, but this effect is smaller for wings of low aspect ratio because of the three-dimensional "relief effect." Thus, at $M_\infty = 0.85$, Fig. 13.15d, the order of

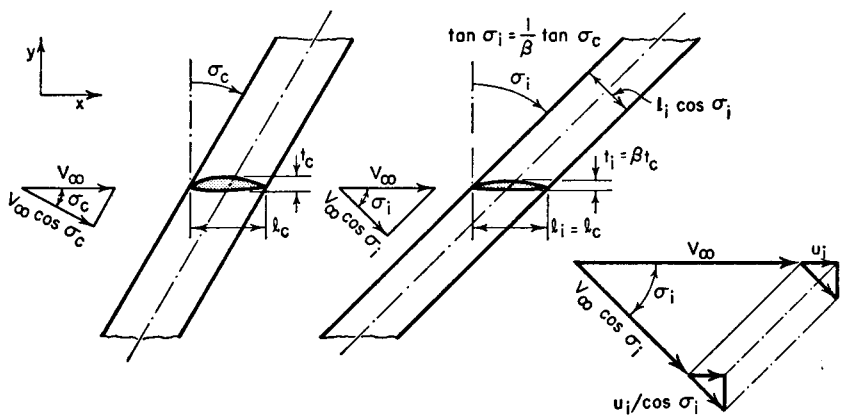
aerodynamic efficiency for the wings of various aspect ratios is completely reversed as compared with the low-speed tests of Fig. 13.15a. At high speeds, therefore, wings of low aspect ratio have some distinct aerodynamic advantages over wings of high aspect ratio.

The changes in flow pattern corresponding to the data of Fig. 13.15 are illustrated by the schlieren photographs of Fig. 13.16. It is seen that separation owing to shock waves is strongly dependent upon aspect ratio.

13.7. Sweptback Wings

A most effective method for delaying compressibility effects on lifting surfaces, and one which is commonly employed for high-speed aircraft, is the use of sweepback. A sweptback wing is one the mean chord line of which is not perpendicular to the undisturbed flow.

Physical Considerations. The physical concepts underlying this scheme may best be understood by considering a uniform wing of infinite span with its leading edge swept back at an angle σ_c from the normal to the free-stream velocity vector V_∞ (Fig. 13.17a). Now imagine the



(a) Compressible

(b) Incompressible

FIG. 13.17. Nomenclature for analysis of sweptback wing.

- (a) Compressible flow.
- (b) Incompressible flow past affinely related wing according to lateral contraction required by Gothert's rule.

observer to move along the span of the wing at the uniform speed $V_\infty \sin \sigma_c$. The approach flow then appears to be normal to the leading edge, and has the speed $V_\infty \cos \sigma_c$. The tangential velocity of the original flow, $V_\infty \sin \sigma_c$, does not influence the pressure distribution on the wing, but is important only in the determination of the frictional stresses on the surface. Since only the normal component of velocity is significant

in the potential flow, it follows that the effective Mach Number of the flow is $M_\infty \cos \sigma_c$. Thus, although the free-stream Mach Number M_∞ may be of the order of unity or even greater, the effective Mach Number, $M_\infty \cos \sigma_c$, may, through sufficient sweepback, be made small enough to avoid the adverse effects of shocks.

In the coordinate transformation mentioned above, the effective thickness normal to the leading edge is also increased, which is unfavorable as regards the maximum local velocity. This effect, however, is considerably smaller than that of reducing the effective Mach Number normal to the leading edge.

On the other side of the picture, sweepback has two disadvantages: First, the lift coefficient is lessened by reducing the normal component of velocity, thus leading to larger wing areas. Second, severe structural problems are associated with sweptback wings.

Sweepback may also be used advantageously to improve the efficiency of propeller tips at high speeds and to ameliorate compressibility problems with compressors pumping gases of very high molecular weight (i.e., low sound velocity).

Another way of picturing the physical effects of sweepback is to imagine a wing in a rectangular wind tunnel. If there is no sweepback, the wing produces a blocking effect in complete planes normal to the flow. If the wing is swept back, however, there is a comparatively small blocking effect in any plane normal to the flow. Hence, a three-dimensional "relief" effect is present, inasmuch as the air may avoid the wing by flowing laterally in two dimensions. The corresponding reduction in the perturbation velocity has a cumulative effect in compressible flow because the effects of Mach Number are decreased as the incompressible disturbance velocity itself is decreased.

Goert's Rule. In applying Goert's rule of similarity, we compare the original compressible flow, Fig. 13.17a, with an incompressible flow, Fig. 13.17b, past a body whose longitudinal dimensions are unchanged, but whose lateral dimensions are all decreased by the ratio β .

Assuming infinite aspect ratio, the geometric relations between the two wings are

$$\frac{t_i}{l_i} = \frac{t_c}{l_c} \cdot \frac{l_c}{l_i} \cdot \frac{t_i}{t_c} = \beta \frac{t_c}{l_c} \quad (13.25)$$

$$\tan \sigma_i = \left(\frac{dx_i}{dy_i} \right)_{\text{lead edge}} = \left(\frac{dx_c}{dy_c} \right)_{\text{lead edge}} \cdot \frac{y_c}{y_i} \cdot \frac{x_i}{x_c} = \frac{1}{\beta} \left(\frac{dx_c}{dy_c} \right)_{\text{lead edge}} = \frac{1}{\beta} \tan \sigma_c \quad (13.26)$$

Then, at corresponding points in the two flows, the disturbance velocities are related by

$$(u/V_\infty)_c = (u/V_\infty)_i / \beta^2 \quad (13.27)$$

Influence of Sweepback on Compressibility Effects. From a practical point of view, we are interested in knowing how sweepback alters the influence of Mach Number on the maximum local velocity. To arrive at an approximate but general rule, let us suppose that the profile is elliptical. For an elliptical profile with no sweepback, it is known that in incompressible flow the maximum perturbation velocity divided by the free-stream velocity is equal to the thickness ratio. Now let us apply this result to the flow seen by an observer moving along the span of the wing of Fig. 13.17b at such a speed that the approach flow appears to be normal to the leading edge. For this observer the thickness is t_i ; the chord is $l_i \cos \sigma_i$; the free-stream velocity is $V_\infty \cos \sigma_i$; and the disturbance velocity is $u_i / \cos \sigma_i$, where u_i is the perturbation velocity for the incompressible flow seen by a stationary observer. Thus we may write

$$\left(\frac{u_i / \cos \sigma_i}{V_\infty \cos \sigma_i} \right)_{\text{max}} = \frac{t_i}{l_i \cos \sigma_i}$$

or

$$\left(\frac{u_i}{V_\infty} \right)_{\text{max}} = \left(\frac{t}{l} \right)_i \cos \sigma_i = \frac{t_i}{l_i} \frac{1}{\sqrt{1 + \tan^2 \sigma_i}} \quad (13.28)$$

Then, by substituting Eqs. 13.25, 13.26, and 13.27 into Eq. 13.28, simplifying, and dropping the subscript c for the compressible flow, we get

$$\left(\frac{u}{V_\infty} \right)_{\text{max}} = \frac{t/l}{\sqrt{\beta^2 + \tan^2 \sigma}} = \frac{t/l}{\sqrt{1 - M_\infty^2 + \tan^2 \sigma}} \quad (13.29)$$

For the same profile in incompressible flow ($\beta = 1$), we get

$$\left(\frac{u_i}{V_\infty} \right)_{\text{max}} = \frac{t/l}{\sqrt{1 + \tan^2 \sigma}} \quad (13.30)$$

Finally, division of Eq. 13.29 by Eq. 13.30 yields

$$\frac{(u/V_\infty)_{\text{max}}}{(u_i/V_\infty)_{\text{max}}} = \frac{(-C_p)_{\text{max}}}{(-C_{p_i})_{\text{max}}} = \frac{\sqrt{1 + \tan^2 \sigma}}{\sqrt{1 - M_\infty^2 + \tan^2 \sigma}} \quad (13.31)$$

This formula, which may be expected to apply at least approximately to conventional subsonic profiles, shows how sweepback modifies the effect of Mach Number on the peak negative pressure coefficient, and is plotted in Fig. 13.18. For zero sweepback, Eq. 13.31 reduces to the Prandtl-Glauert rule in two-dimensional flow. For 90°-sweepback, the peak negative pressure coefficient is independent of Mach Number. To illustrate how sweepback reduces the effects of compressibility on pressure coefficient, Eq. 13.31 shows that for an increase from $M_\infty = 0$ to $M_\infty = 0.8$, the pressure coefficient is increased by 67% without sweep-

back; by 39% for 30°-sweepback; by 21% for 45°-sweepback; and by only 9% for 60°-sweepback.

An important fact shown by Eq. 13.29 is that whereas for unswept wings the incremental velocity tends to become infinite as M_∞ approaches unity, for swept wings this tendency occurs at supersonic speeds, according to the relation $M_\infty = \sqrt{1 + \tan^2 \sigma}$. This result must be looked on as only indicative, inasmuch as the linear theory fails for large perturbation velocities and also near $M_\infty = 1$.

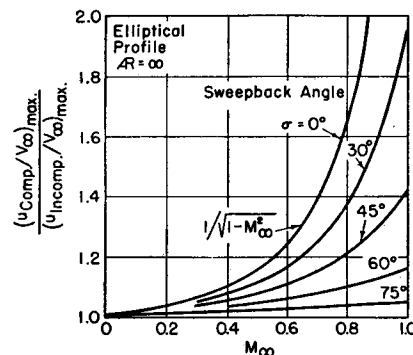


FIG. 13.18. Effect of sweepback on the way in which the maximum perturbation velocity for thin elliptical profiles varies with Mach Number.

Effect of Sweepback on Lower Critical Mach Number. Suppose that a wing is a “bent-back” type of swept wing, i.e., the wing as a whole is rotated so that the profile in a plane normal to the leading edge remains unchanged. This means that the profile in a plane parallel to V_∞ becomes thinner as σ increases. Therefore, if δ is the thickness ratio in the flight direction, and δ_N is the thickness ratio in the direction normal to the leading edge, $\delta = \delta_N \cos \sigma$, so that Eq. 13.29 may be written

$$\left(\frac{u}{V_\infty}\right)_{\max} = \frac{\delta_N \cos \sigma}{\sqrt{1 - M_\infty^2 + \tan^2 \sigma}} \quad (13.32)$$

With bent-back wings, δ_N remains constant as σ increases. Furthermore, the value of u/V_∞ is uniquely related to the local Mach Number and M_∞ through the isentropic relations. From Eq. 13.32, therefore, we may plot, for a given thickness ratio, curves of maximum local Mach Number versus M_∞ , one curve being required for each sweepback angle. The value of M_∞ where each of these curves reaches a maximum local Mach Number of unity defines the corresponding lower critical speed, $M_{\infty \text{ cr}}$, for the given δ_N and σ .

The results of such calculations⁽¹⁶⁾ for sweptback wings of infinite span with elliptical profiles are summarized in Fig. 13.19. As an example, for a profile of 10% thickness ratio normal to the leading edge, a change

from an unswept wing to 45°-sweepback raises the $M_{\infty \text{ cr}}$ from 0.82 to 0.93.

If the wing is “sheared back” in such a way that the profile parallel to V_∞ remains constant, then Eq. 13.29 rather than Eq. 13.32 is to be used. Since shear-back increases the thickness normal to the leading edge, this type of sweepback is not as effective as bend-back. As an example, for an elliptical profile of 10% thickness ratio parallel to V_∞ ,

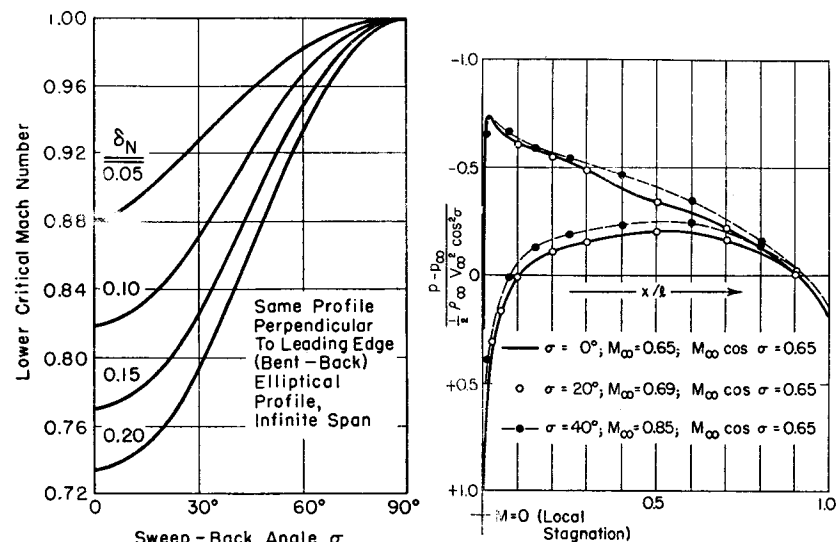


FIG. 13.19. Lower critical Mach Number as a function of sweepback angle and thickness ratio normal to leading edge, for thin elliptical profiles (after Goertler).

a change from 0°-sweepback to 45°-sweepback increases $M_{\infty \text{ cr}}$ from 0.82 to 0.90, as compared with the change from 0.82 to 0.93 for the corresponding bent-back wing.

These estimates of lower critical Mach Number are based on the criterion of the local total velocity becoming sonic. If, as an opposite extreme, only the normal component of velocity were assumed to be significant, the resulting lower critical Mach Numbers would be substantially greater than those shown in Fig. 13.19, and could easily exceed unity for large angles of sweepback. The true state of affairs probably lies between the two simplified extremes.

Experimental Results. To illustrate the principle that the pressure distribution is determined primarily by the normal component of velocity, Fig. 13.20 shows the results of experiments⁽¹⁷⁾ on a 9%-thick symmetrical profile, with maximum thickness at 40% chord, at an angle of

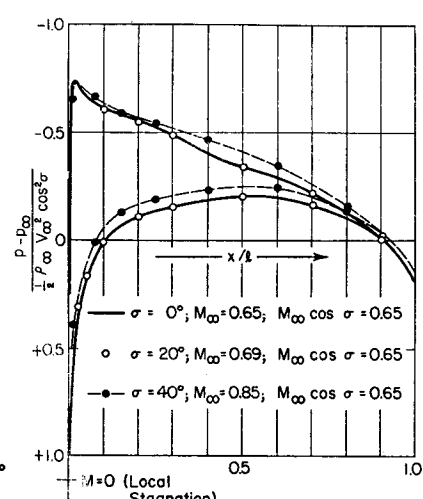


FIG. 13.20. Experimental results for flow past sweptback wings of infinite span with 9%-thick profile (normal to leading edge) at incidence of -2° (after Lippisch and Beuschausen).

attack of -2° . Data are shown for three conditions, with different values of σ and M_∞ but with the same value of $M_\infty \cos \sigma$. The ordinate represents the pressure coefficient based, in each case, on the corresponding normal component of velocity. The principle under discussion is, at least approximately, verified by the fact that the three sets of data are nearly superposed when plotted in this manner.

Fig. 13.21a, from the same set of experiments, demonstrates the same principle by showing that curves of $C_L/\cos^2 \sigma$ versus $M_\infty \cos \sigma$ are almost

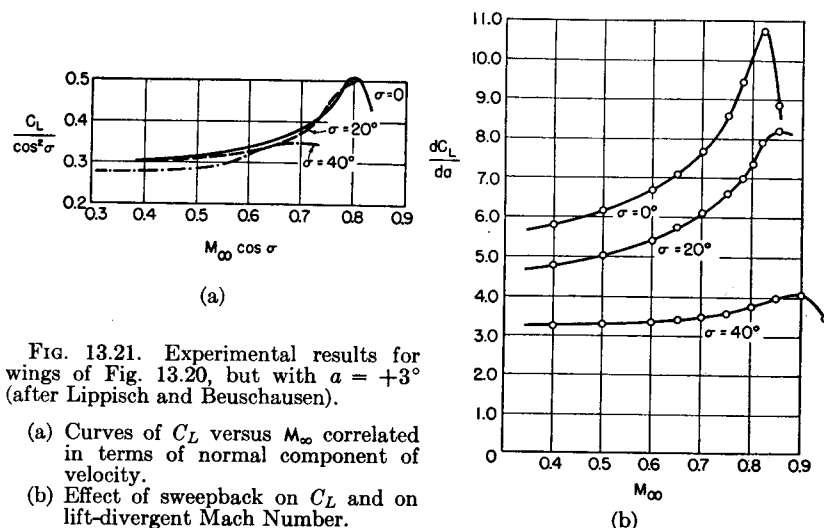


FIG. 13.21. Experimental results for wings of Fig. 13.20, but with $\alpha = +3^\circ$ (after Lippisch and Beuschausen).

- (a) Curves of C_L versus M_∞ correlated in terms of normal component of velocity.
- (b) Effect of sweepback on C_L and on lift-divergent Mach Number.

independent of sweepback angle σ . In Fig. 13.21b, where the effect of σ is omitted from the coordinates, we see that sweepback reduces the lift coefficient significantly but also increases the Mach Number at which compressibility produces a sudden droop in lift-curve slope. For example, 40° -sweepback reduces the lift coefficient by some 40%, but increases the lower critical Mach Number from about 0.82 to about 0.90.

13.8. Sweptback Wings of Finite Span

In practice, of course, wings are of finite span, and the beneficial effects of sweepback on compressibility are reinforced by the effects of aspect ratio. Fig. 13.22 shows the results of experiments⁽¹⁸⁾ on bent-back wings of constant span along the 50%-chord line, formed by rotating the original unswept wing halves about the intersection of the line of symmetry and the 50%-chord line. The lift-drag polars of Fig. 13.22b show the considerable improvement at high subsonic speeds produced by 45° -sweepback. Fig. 13.22c shows that, for a fixed C_L , sweepback has scarcely any effect up to $M_\infty \approx 0.7$. At Mach Numbers between

0.8 and 1.2, however, sweepback produces remarkable reductions in drag coefficient.

An extensive comparison between the theoretical similarity methods outlined here and a large number of experiments on wings of various aspect ratios and sweepback is given in Reference 19.

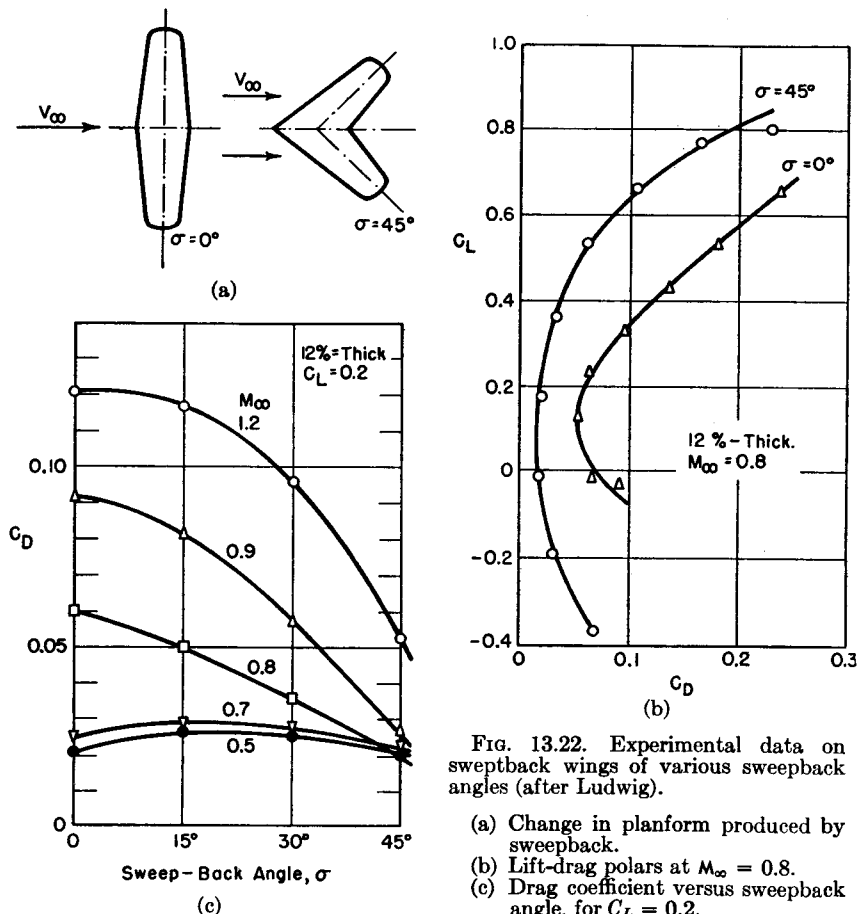


FIG. 13.22. Experimental data on sweptback wings of various sweepback angles (after Ludwig).

- (a) Change in planform produced by sweepback.
- (b) Lift-drag polars at $M_\infty = 0.8$.
- (c) Drag coefficient versus sweepback angle, for $C_L = 0.2$.

A generalized correlation incorporating the effects of both aspect ratio and sweepback, and based on the methods outlined in this chapter, has been proposed by Diederich.⁽²¹⁾ The correlation is based on the parameter

$$F = \frac{AR}{\frac{1}{2\pi} \left(\frac{dC_{LN}}{da} \right) \cos \sigma}$$

where C_{LN} is the section lift coefficient of the profile, measured with respect to the speed and chord in a plane normal to the mean chord line;

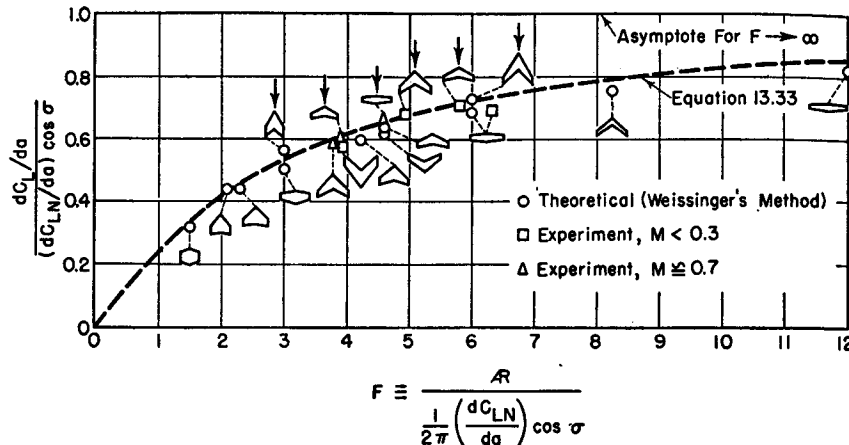


FIG. 13.23. Correlation of lift-curve slopes for various planforms (after Diederich).

and α is the angle of attack (in radians) of the entire wing measured in a plane parallel to the axis of symmetry of the wing.

Using C_L to denote the lift coefficient of the entire wing, based on V_∞ , the total planform area, and the incidence α , the semi-empirical law proposed⁽²¹⁾ is

$$\frac{dC_L/d\alpha}{(dC_{LN}/d\alpha) \cos \sigma} = \frac{F}{2 + F \sqrt{1 + \frac{4}{F^2}}} \quad (13.33)$$

A comparison of this formula with accurate theoretical and experimental results is shown in Fig. 13.23 for a wide variety of planforms. The validity of Eq. 13.33 as a general correlation rule is seen to be quite satisfactory.

REFERENCES AND SELECTED BIBLIOGRAPHY

1. GOTHERT, B. Plane and Three-Dimensional Flow at High Subsonic Speeds, *NACA Tech. Memo.*, No. 1105 (Oct., 1946).
2. HESS, R. V., and GARDNER, C. S. Study by the Prandtl-Glauert Method of Compressibility Effects and Critical Mach Number for Ellipsoids of Various Aspect Ratios and Thickness Ratios, *NACA RM*, No. L7B03a (March, 1947).
3. SCHMIEDEN, C., and KAWALKI, K. H. Contribution to the Problem of Flow at High Speed. Part II: Effect of Compressibility in Axially Symmetrical Flow around an Ellipsoid, *NACA Tech. Memo.*, No. 1233 (June, 1949).
4. LEES, L. A Discussion of the Prandtl-Glauert Method to Subsonic Compressible Flow Over a Slender Body of Revolution, *NACA Tech. Note*, No. 1127 (Sept., 1946).
5. HERRIOT, J. G. The Linear Perturbation Theory of Axially Symmetric Compressible Flow with Application to the Effect of Compressibility on the Pressure Coefficient at the Surface of a Body of Revolution, *NACA RM*, No. A6H19 (July, 1947).

6. LAITONE, E. V. The Subsonic Axial Flow About a Body of Revolution, *Quarterly App. Math.*, Vol. 5, No. 2 (1947), p. 227.
7. VAN DRIEST, E. R. Die linearisierte Theorie der dreidimensionale kompressiblen Unterschallstromung und die experimentelle Untersuchung von Rotationskorpern in einem geschlossenen Windkanal, *Mitt. Nr. 16*, Institut für Aerodynamik, E.T.H., Zurich, 1949.
8. MUNK, M. M. Fluid Mechanics, Part II, Division C, of *Aerodynamic Theory*, edit. by W. F. Durand, Vol. I, p. 293. (Reprinted by Durand Reprinting Committee, Calif. Inst. of Tech., Pasadena, 1943.)
9. STACK, J., and LINDSEY, W. F. Characteristics of Low-Aspect-Ratio Wings at Supercritical Mach Numbers, *NACA Tech. Note*, No. 1665 (Aug., 1948).
10. LAMB, H. *Hydrodynamics*. 6th ed. New York: Dover Publications, 1945, p. 141.
11. VON KARMAN, TH. Calculation of Pressure Distribution on Air Ship Hulls, *NACA Tech. Memo.*, No. 574 (1930).
12. GOTHERT, B. Comparison of Drop and Wind-Tunnel Experiments on Bomb Drag at High Subsonic Speeds, *NACA Tech. Memo.*, No. 1186 (May, 1948).
13. KAPLAN, C. The Flow of a Compressible Fluid Past a Sphere, *NACA Tech. Note*, No. 762 (May, 1940).
14. CHARTERS, A. C., and THOMAS, R. N. The Aerodynamic Performance of Small Spheres from Subsonic to High Supersonic Velocities, *Jour. Aero. Sci.*, Vol. 12, No. 4 (Oct., 1945), p. 468.
15. GOTHERT, B. H. High-Velocity Measurements for a Wing of Small Aspect Ratio, *Air Materiel Command Report*, No. F-TS-646-RE (Sept., 1946).
16. GOTHERT, B. Calculation of the Velocity Field of Swept-Back Wings at High Subsonic Speeds, *Air Materiel Command Report*, No. F-TS-3183-RE (Feb., 1948).
17. LIPPISCH, A., and BEUSCHAUSEN, W. Pressure Distribution Measurements at High Speed and Oblique Incidence of Flow, *NACA Tech. Memo.*, No. 1115 (Mar., 1947).
18. LUDWIG, H. Test Results on Arrow-Head Wings at High Velocities, *Air Materiel Command Report*, No. F-TS-417-RE (Oct., 1946).
19. MURRAY, H. E. Comparison with Experiment of Several Methods of Predicting the Lift of Wings in Subsonic Compressible Flow, *NACA Tech. Note*, No. 1739 (Oct., 1948).
20. MATTHEWS, C. W. A Comparison of the Experimental Subsonic Pressure Distributions About Several Bodies of Revolution with Pressure Distributions Computed by Means of the Linearized Theory, *NACA RM*, No. L9F28 (1949).
21. DIEDERICH, F. W. A Plan-Form Parameter for Correlating Certain Aerodynamic Characteristics of Swept Wings, *NACA Tech. Note*, No. 2335 (1951).

PROBLEMS

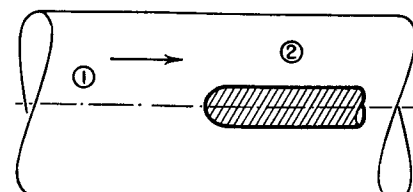
- 13.1. A tunnel of circular cross-sectional area A_1 is blocked by a model of circular cross-sectional area A_m .

Demonstrate by Goert's rule that the incremental velocity produced by the blocking is given approximately by

$$\frac{V_2 - V_1}{V_1} \approx \frac{1}{1 - M_1^2} \frac{A_m}{A_1}$$

Compare this with the exact result of one-dimensional isentropic flow, namely,

$$\frac{dV}{V} = -\frac{1}{1 - M^2} \frac{dA}{A}$$

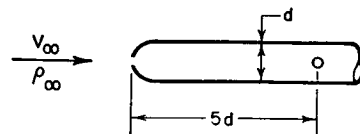


PROB. 13.1.

13.2. A certain wind tunnel of circular cross section has a contraction section designed for incompressible flow to avoid at all points on the wall regions of minimum pressure followed by adverse pressure gradients. Show that this same contraction section will have no adverse pressure gradients for compressible subsonic flow.



PROB. 13.2.



PROB. 13.3.

13.3. At low speeds the static-pressure hole of a pitot-static tube registers an error given by

$$\frac{p - p_{\infty}}{\frac{1}{2} \rho_{\infty} V_{\infty}^2} = -0.01$$

Estimate how large the corresponding error would be at $M_{\infty} = 0.85$.

13.4. Assuming that for slender bodies of revolution in incompressible flow the curve of peak negative pressure coefficient versus thickness ratio is the same as for an ellipsoid of revolution, plot the lower critical Mach Number versus the low-speed peak negative pressure coefficient.

13.5. Using Eq. 13.21a, show that the compressible lift-curve slope for wings of finite aspect ratio is related to the corresponding low-speed slope by

$$\left(\frac{dC_L}{da} \right)_{\infty} / \left(\frac{dC_{L_i}}{da} \right)_{\infty} = \frac{1}{\sqrt{1 - M_{\infty}^2} + \frac{1 - \sqrt{1 - M_{\infty}^2}}{\pi A} \left(\frac{dC_{L_i}}{da} \right)_{\infty}}$$

13.6. It has been shown by Bollay [Z.a.M.M., Bd. 19 (1939), p. 21], that for incompressible flow past a flat plate of vanishingly small aspect ratio, the lift coefficient is related to the angle of attack by the formula

$$C_L = 2\pi \sin^2 a$$

Using Gothert's rule, find a similar relation for compressible flow. Compare your results with the discussion in Art. 13.6.

13.7. Consider a wing of infinite span with 45°-sweepback and a 10% elliptical profile. Assuming that the tangential component of velocity is of no consequence, find the value of M_{∞} for which the local sonic velocity is first reached at the surface of the wing. Compare your result with Fig. 13.19.

PART V

SUPERSONIC FLOW

Chapter 14

TWO-DIMENSIONAL, SUPERSONIC FLOW WITH SMALL PERTURBATIONS

NOMENCLATURE FOR CHAPTER 14

a	angle of attack	x, y	Cartesian coordinates
c	speed of sound	α	Mach angle
C_D	drag coefficient	δ	thickness ratio; angle
C_L	lift coefficient	η	coordinate normal to chord
C_M	moment coefficient	θ	turning angle of streamline (radians)
C_p	pressure coefficient	Θ	$180 \theta/\pi$
D	drag	ξ	coordinate along chord
h	amplitude of wave-shaped wall	ρ	mass density
k	ratio of specific heats	σ	surface slope of profile with respect to chord line
l	wave length of wave-shaped wall; also chord of airfoil	φ	perturbation velocity potential
L	lift	$(\cdot)_\infty$	signifies free-stream condition
M	Mach Number	$(\cdot)_U$	signifies upper surface of airfoil
M	counter-clockwise moment about leading edge	$(\cdot)_L$	signifies lower surface of airfoil
p	pressure	$(\cdot)_I$	signifies step <i>along</i> Mach wave of family <i>I</i> , or <i>across</i> Mach wave of family <i>II</i> .
P	pressure index (Eq. 14.20)	$(\cdot)_{II}$	signifies step <i>along</i> Mach wave of family <i>II</i> , or <i>across</i> Mach wave of family <i>I</i> .
s	surface area of profile		
S	area between chord line and profile surface		
u, v	perturbation velocity compo- nents		
V	velocity		

14.1. Introductory Remarks

By virtue of a radical change in the properties of the differential equations, the exact solution of problems in two-dimensional, frictionless, supersonic flow is far easier than for subsonic flow. When the flow is shock-free and irrotational the exact solution of supersonic problems may even be said to be simple. Even with shocks and rotation present, methods of solution are available which, although requiring extensive numerical computations, are still manageable.

On the other hand, these exact solutions (Chapters 15 and 16) almost always require either numerical or graphical, rather than analytical, procedures. Therefore, in spite of the existence of such exact numerical methods, there is a useful place for analytical, but approximate, methods. Such approximate analytical methods provide the rapid means of calculation which are so important for making preliminary estimates. And, by showing clearly the relationships among the variables, they provide a better insight into problems and permit general conclusions to be drawn.

In this chapter we shall discuss an approximate analytical method which applies to two-dimensional, supersonic flows which are everywhere shock-free and irrotational and in which there are only small perturbations from a uniform, parallel flow. It is true that most supersonic flows involve shocks, but, as will be seen in Chapter 16, the entropy changes across weak oblique shocks are so small that they may often be disregarded. Accordingly, in many problems, the magnitude of the rotation is negligible.

The method of small perturbations yields useful results for such practical problems as the flow past thin airfoils with sharp leading and trailing edges, the flow through turbine and compressor cascades with thin blades and small turning angles, the flow inside of two-dimensional ducts, and the flow at the exit of supersonic nozzles discharging into a region of variable back pressure.

The solutions for linearized supersonic flow show, in especially simple form, many of the important features of more complex supersonic flow patterns. Hence it is often helpful to work out the approximate linearized solution to a problem prior to carrying out the comparatively laborious exact solution.

A further advantage of the linearized procedure is that it brings home clearly the vast differences between subsonic and supersonic flow without at this stage becoming lost in the mathematical complexities of a more general approach.

Additional material relevant to the subject matter of the present chapter may be found in Chapters 15 and 16 and in Volume II, Chapter 17.

14.2. Linearization of the Equations

Perturbation Velocity Potential. Assuming that the flow is two-dimensional, irrotational, and isentropic, and that there are only small perturbations from a uniform, parallel flow along the x -axis, we may follow exactly the procedure of Art. 10.2 for subsonic flow. In this way we arrive at the linearized equation of motion, Eq. 10.21. We write the latter in the form

$$\frac{\partial^2 \varphi}{\partial y^2} = (M_\infty^2 - 1) \frac{\partial^2 \varphi}{\partial x^2} \quad (14.1)$$

where φ is the perturbation velocity potential. The perturbation velocity components are given by

$$u = \partial \varphi / \partial x; \quad v = \partial \varphi / \partial y \quad (14.2)$$

Restrictions on Linear Theory. In arriving at the linearized equation, it was necessary to assume that

$$\frac{M_\infty^2 \frac{u}{V_\infty}}{1 - M_\infty^2} \ll 1 \quad \text{and} \quad M_\infty^2 \frac{v}{V_\infty} \ll 1$$

Thus, as in subsonic flow, Eq. 14.1 loses validity in the transonic region, i.e., near Mach Number unity.

In supersonic flow still another restriction appears, namely, that the Mach Number may not be too high. Although no definite upper limits can be given, it seems clear from the above assumptions that for practical purposes the maximum allowable order of magnitude of M_∞^2 is about ten. Or, more precisely, since u/V_∞ and v/V_∞ are of the same order of magnitude as the thickness ratio δ of thin bodies, we may say that the linearized theory may be used when $M_\infty^2 \delta$ is small compared with unity.

Pressure Coefficient. Making assumptions similar to those of Art. 10.3, we find that the linearized pressure coefficient for supersonic flow is the same as in subsonic flow, namely,

$$C_p = -2 \frac{u}{V_\infty} \quad (14.3)$$

provided that u/V_∞ is small compared with unity.

14.3. The General Solution for Linearized Supersonic Flow

Subsonic Versus Supersonic Flow. It might at first appear from the similarity between Eqs. 14.1 and 10.21 that the linearized solutions for subsonic and supersonic flow should be much the same. However, the nature of the flow pattern proves to be entirely different depending on whether M_∞ is greater or less than unity. It may be recalled that in the various one-dimensional analyses the sign of the term $(M_\infty^2 - 1)$ was a determining factor in the qualitative nature of the flow. If we write Eqs. 14.1 and 10.21 in the form

$$\frac{\partial v}{\partial y} = (M_\infty^2 - 1) \frac{\partial u}{\partial x}$$

and note that $\partial u / \partial x$ denotes longitudinal accelerations while $\partial v / \partial y$ is connected with the convergence or divergence of the elementary stream tube formed between two neighboring streamlines, we see that this equation represents the already familiar fact that an acceleration requires an increase in cross-sectional area for supersonic flow and a decrease for subsonic flow. Because $\partial v / \partial y$ and $\partial u / \partial x$ are of the same sign for supersonic flow and of different sign for subsonic flow, the resulting flow patterns are of different type. As in the one-dimensional simplification, the long-familiar concepts of incompressible flow prove to be misleading if applied to supersonic flows.

For subsonic flow Eq. 14.1 is said to be *elliptic* in type, and in fact may be reduced to the Laplace equation by the transformation given in Chapter 10. Hence subsonic flows are, at least qualitatively, similar to incompressible flow. For supersonic flow Eq. 14.1 is said to be *hyperbolic* in type, and may be reduced to the classical *wave equation* by a simple transformation. Hence, linearized supersonic flows have many properties akin to the properties of vibrating metal bars, air columns, and strings. A fuller explanation of the mathematical properties of elliptic and hyperbolic differential equations is presented in Appendix A.

Solution to the Differential Equation. We shall now show that for supersonic flow the general solution to Eq. 14.1 is given by

$$\varphi = \varphi_1(x + \sqrt{M_\infty^2 - 1} y) + \varphi_2(x - \sqrt{M_\infty^2 - 1} y) \quad (14.4)$$

where φ_1 is an arbitrary function of the argument $(x + \sqrt{M_\infty^2 - 1} y)$, and φ_2 is an arbitrary function of the argument $(x - \sqrt{M_\infty^2 - 1} y)$.

To demonstrate that this is indeed the solution, we first examine the particular solution φ_1 . Taking derivatives,* we have

* The derivative $\partial \varphi(Q) / \partial x$, where $Q = Q(x, y)$, is found by noting that

$$d\varphi = \frac{\partial \varphi}{\partial Q} dQ = \frac{\partial \varphi}{\partial Q} \left(\frac{\partial Q}{\partial x} dx + \frac{\partial Q}{\partial y} dy \right) \quad \text{so that} \quad \frac{\partial \varphi}{\partial x} = \frac{\partial \varphi}{\partial Q} \frac{\partial Q}{\partial x} = \varphi' \frac{\partial Q}{\partial x}$$

where φ' is the first derivative of φ with respect to the argument Q .

$$\frac{\partial \varphi_1}{\partial x} = \varphi_1'; \quad \frac{\partial \varphi_1}{\partial y} = \sqrt{M_\infty^2 - 1} \varphi_1'$$

$$\frac{\partial^2 \varphi_1}{\partial x^2} = \varphi_1''; \quad \frac{\partial^2 \varphi_1}{\partial y^2} = (\sqrt{M_\infty^2 - 1})^2 \varphi_1''$$

By direct substitution, we see that the arbitrary function φ_1 satisfies Eq. 14.1 exactly, and is therefore a particular solution. Similarly, it may be shown that the arbitrary function φ_2 is also a solution. Our problem now is to find the particular forms of these functions corresponding to any desired flow pattern.

Streamlines and Pressure Distribution. The arbitrary nature of the functions φ_1 and φ_2 is a great simplification, for any number of solutions may now be found at will merely by specifying the forms of these functions. Even better, we may easily determine the flow pattern corresponding to specified boundaries. Let us write Eq. 14.4 in the following equivalent form:

$$\varphi = V_\infty f_1(x + \sqrt{M_\infty^2 - 1} y) + V_\infty f_2(x - \sqrt{M_\infty^2 - 1} y) \quad (14.5)$$

Then

$$u = \frac{\partial \varphi}{\partial x} = V_\infty (f_1' + f_2')$$

$$v = \frac{\partial \varphi}{\partial y} = V_\infty \sqrt{M_\infty^2 - 1} (f_1' - f_2')$$

For the differential equation of the streamline we write

$$\begin{aligned} \left(\frac{dy}{dx} \right)_{\text{str}} &= \frac{v}{V_\infty + u} = \frac{v/V_\infty}{1 + \frac{u}{V_\infty}} \cong \frac{v/V_\infty}{1 - (M_\infty^2 - 1) \frac{u}{V_\infty}} \\ &= \frac{\sqrt{M_\infty^2 - 1} (f_1' - f_2')}{1 - (M_\infty^2 - 1)(f_1' + f_2')} \end{aligned}$$

where (to facilitate the subsequent integration) we have inserted in the denominator the term $M_\infty^2 u/V_\infty$, which has been assumed small compared with unity. Rearranging, we have

$$\begin{aligned} dy &= \sqrt{M_\infty^2 - 1} \left[(f_1' dx + \sqrt{M_\infty^2 - 1} f_1' dy) \right. \\ &\quad \left. - (f_2' dx - \sqrt{M_\infty^2 - 1} f_2' dy) \right] \\ &= \sqrt{M_\infty^2 - 1} (df_1 - df_2) \end{aligned}$$

where the last relation is obtained by noting that

$$df_1 = \frac{\partial f_1}{\partial x} dx + \frac{\partial f_1}{\partial y} dy = f_1' dx + \sqrt{M_\infty^2 - 1} f_1' dy, \quad \text{etc.},$$

the symbol f_1' denoting differentiation of the function f_1 with respect to the argument $(x + \sqrt{M_\infty^2 - 1} y)$.

Integrating, we get for the equation of the streamline,

$$y_{\text{str}} = \text{constant} + \sqrt{M_\infty^2 - 1} (f_1 - f_2) \quad (14.6)$$

in which the magnitude of the constant identifies a particular streamline.

The pressure coefficient is now found to be

$$C_p \cong -2 \frac{u}{V_\infty} = -2(f_1' + f_2') \quad (14.7)$$

Within the assumptions of the linear theory, this may also be written as

$$C_p \cong \frac{2}{\sqrt{M_\infty^2 - 1}} \frac{f_1' + f_2'}{f_2' - f_1'} \left(\frac{dy}{dx} \right)_{\text{str}} \quad (14.8)$$

If the functions f_1 and f_2 are specified, the shapes of the streamlines and the pressure distribution may be found from Eqs. 14.6 and 14.7. Or, conversely, if the shape of a solid body immersed in the stream is known, and if the functions f_1 and f_2 are chosen to satisfy the body streamlines according to Eq. 14.6 and also to satisfy the remaining initial conditions necessary to determine (but not to overdetermine) the problem, then Eqs. 14.5 through 14.8 give the linearized solution for the flow past the solid body.

Flow with Waves of One Family. The general nature of supersonic flow with small perturbations may best be brought out by considering the two simple cases where either the function f_1 or the function f_2 is degenerate, i.e., the function is constant throughout the entire flow field. The particular solutions then obtained are referred to as *simple wave* solutions, or solutions with *waves of one family* only. For the two classes of simple-wave solutions, the foregoing results take the simple form shown in the following table:

$f_1 = \text{constant}$	$f_2 = \text{constant}$
$y_{\text{str}} = \text{const} - \sqrt{M_\infty^2 - 1} f_2$	$y_{\text{str}} = \text{const} + \sqrt{M_\infty^2 - 1} f_1$
$\left(\frac{dy}{dx} \right)_{\text{str}} = \frac{-\sqrt{M_\infty^2 - 1} f_2'}{1 + f_2'}$	$\left(\frac{dy}{dx} \right)_{\text{str}} = \frac{\sqrt{M_\infty^2 - 1} f_1'}{1 + f_1'}$
$\cong -\sqrt{M_\infty^2 - 1} f_2'$	$\cong \sqrt{M_\infty^2 - 1} f_1'$
$C_p = -2f_2'$	$C_p = -2f_1'$
$\cong \frac{2}{\sqrt{M_\infty^2 - 1}} \left(\frac{dy}{dx} \right)_{\text{str}}$	$\cong -\frac{2}{\sqrt{M_\infty^2 - 1}} \left(\frac{dy}{dx} \right)_{\text{str}}$

Flow with Left-Running Mach Waves. Consider the simple-wave flow for which the function f_1 is everywhere constant. We see from Eq. 14.10 that the slopes of the streamlines are then constant along lines on which f_2' is constant. However, f_2' is a function only of the argument $(x - \sqrt{M_\infty^2 - 1} y)$. Consequently the slopes of the streamlines are constant on lines for which

$$x - \sqrt{M_\infty^2 - 1} y = \text{constant}$$

These form a family of parallel straight lines with slope $dy/dx = 1/\sqrt{M_\infty^2 - 1}$. Referring to the velocity triangle of Fig. 14.1, we see

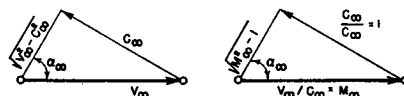


FIG. 14.1. Illustrates definition of Mach angle.

from the definition of the Mach angle (Chapter 3) that

$$\sin \alpha_\infty = \frac{c_\infty}{V_\infty} = \frac{1}{M_\infty}; \quad \tan \alpha_\infty = \frac{1}{\sqrt{M_\infty^2 - 1}}$$

Hence the lines of constant f_2' (and of constant f_2) are inclined at the angle α_∞ to the direction of flow. Thus the lines of constant f_2 are identified with the *left-running Mach lines* of the flow. The left-running Mach lines are those which, for an observer looking downstream, appear to be going downstream in a generally leftward direction; consequently the left-running Mach lines lie at the angle α_∞ above the x -axis, while *right-running Mach lines* lie at the angle α_∞ below the x -axis.

The general relation between the streamlines must be as shown in Fig. 14.2. All the streamlines are similar to each other and, moreover,

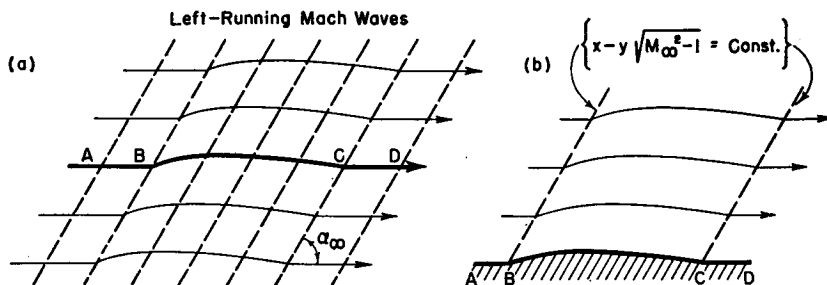


FIG. 14.2. Flow with only left-running Mach waves present.

have equal slopes along each left-running Mach line. According to Eq. 14.11 the pressure, velocity components, and all other fluid properties are also constant along the left-running Mach lines. Moreover, the

local pressure coefficient, according to Eq. 14.11, depends only on the local inclination of the streamline, that is, only on the local direction of the velocity vector.

In the case considered here, the changes in fluid properties may be said to be propagated along the left-running Mach lines. A propagation of this type is usually called a wave. It is customary, therefore, to refer to the Mach lines as *Mach waves*. The latter may also be thought of as *pressure waves* propagating along the Mach lines, according to the simple descriptions of Chapter 3.

Similar results are obtained if we consider the other class of simple flows, that is, with the function f_2 everywhere constant. In this case, however, the Mach lines are inclined at the angle $-\alpha_\infty$ to the direction of flow (Fig. 14.3).

Choice of Wave Family. Consider the streamline $ABCD$, which is the same in Figures 14.2a and 14.3a. Suppose the region below $ABCD$

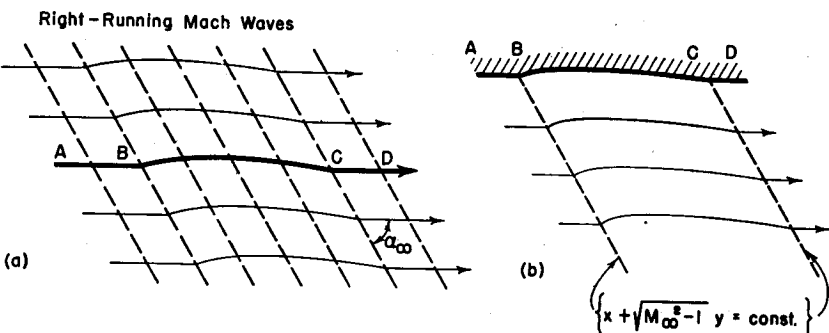


FIG. 14.3. Flow with only right-running Mach waves present.

(Fig. 14.2b) were made solid. Then $ABCD$ might be considered the surface of a body with unbounded flow above the surface. We now inquire which of the two solutions (f_1 or f_2) is valid, or whether some combination of the two might be valid. The answer depends partly on the boundary conditions. If we specify no upper boundary to the flow and that the flow far upstream is uniform and parallel, then the function f_1 must be everywhere constant, for otherwise the flow far upstream could not be uniform and parallel. From another point of view, if we consider the Mach lines as representing the lines of propagation of pressure waves produced by changes in direction at the solid boundary, these waves can physically be propagated only downstream in supersonic flow, and hence only the pressure waves corresponding to the function f_2 can appear in the solution. Accordingly, the flow pattern must be as indicated in Fig. 14.2b.

By similar arguments, if the region above $ABCD$ were made solid, the flow pattern would be as shown in Fig. 14.3b.

If the curve BC represented a thin airfoil moving at supersonic speed through still air (or, equivalently, located in a supersonic wind tunnel having a uniform, parallel air stream), the flow pattern would be as shown in Fig. 14.4. The pressure distribution on the upper and lower

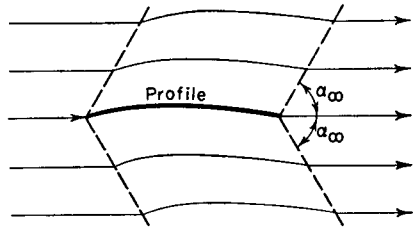


FIG. 14.4. Flow past thin cambered profile. Above the profile the flow is affected only by left-running Mach waves; below, only by right-running Mach waves.

surfaces of the airfoil (at each point of which the slope of the streamline is known) may easily be calculated from Eq. 14.11. That the flow downstream of the airfoil must have the direction and pressure of the upstream flow follows from the fact the two streamlines which join at the trailing edge must have the same pressure and direction; from the two forms of Eq. 14.11, this will be so only when the flow is as shown in Fig. 14.4.

14.4. Geometrical Interpretation of the General Solution

Physical Description of Flow. From the results of the preceding article, we see that the general mathematical solution to linearized supersonic flow may be interpreted physically by portraying the flow as being influenced by two families of pressure waves which are inclined at the Mach angle to the velocity vector. Having arrived at this concept, it is unnecessary to work with the potential functions directly. Instead, it is easier to proceed by constructing the wave pattern which produces a flow corresponding to specified boundary conditions. In order to do this, however, we must have a method for calculating the changes produced in a streamline as the streamline crosses waves of either family. The relations between changes in pressure and changes in direction are given by Eq. 14.11. Here we shall derive the same relations by a geometrical construction, due to Ackeret, which emphasizes the physical rather than the mathematical aspects of the problem.

From the form of the general solution, Eq. 14.4, it is evident that the perturbation potential φ may be considered as the sum of the perturbation potentials of two families of waves, denoted by the symbols I and II , and corresponding to the functions φ_1 and φ_2 , respectively. The waves of family I are the right-running Mach lines, and those of family II are

the left-running Mach lines. Now, since φ_1 depends only on the argument $(x + \sqrt{M_\infty^2 - 1} y)$, the lines of constant φ_1 are all inclined at the angle $-\alpha_\infty$ to the flow; similarly, the lines of constant φ_2 are all inclined at the angle α_∞ to the flow. We may then consider the flow field to be covered with these lines, as shown in Fig. 14.5; the specific nature of the flow pattern then depends on the numerical magnitudes of φ_1 and φ_2 attached to each of these lines.

Suppose that in a small region only the function φ_2 undergoes any change in numerical value, that is, the function φ_1 is a constant, and we have waves of only one family. Then, since the gradient of the perturbation potential is equal to the vector change in velocity, and since the gradient of the perturbation potential is normal to the lines of constant perturbation potential, it follows that as the streamline crosses the specified region the change in the velocity vector must lie in the direction normal to the lines of family II . The velocities before and after the change are, therefore, related geometrically as shown in Fig. 14.6.

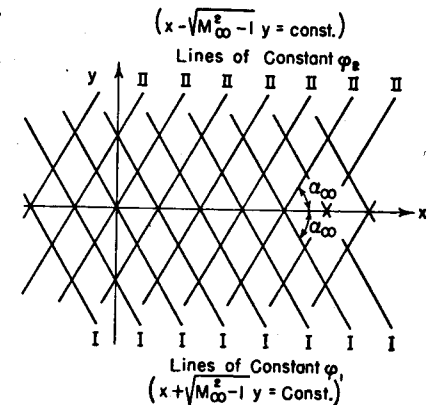


FIG. 14.5. Two families of Mach lines.

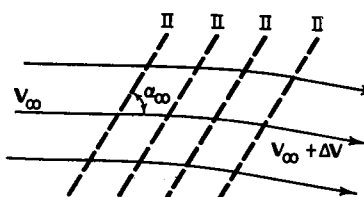
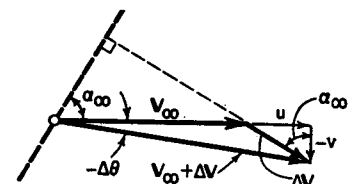


FIG. 14.6. Velocity vector diagram for a streamline influenced by left-running pressure waves.



Pressure-Turning Angle Relation for Mach Wave. To calculate the relation between the change in pressure and the change in direction as the streamline crosses a region where there are pressure waves only of family II , we start with the linearized form of the Euler equation,

$$p - p_\infty = -\rho_\infty V_\infty u$$

But, from the geometry of Fig. 14.6,

$$u = -v \tan \alpha_\infty$$

Furthermore, if $\Delta\theta$ is the change in direction of the streamline, and if it

is assumed positive when measured counter-clockwise, then Fig. 14.6 shows that, to first-order terms,

$$v = V_\infty \Delta\theta$$

Hence, we find that

$$(p - p_\infty)_I = \rho_\infty V_\infty^2 \Delta\theta \tan \alpha_\infty = \frac{\rho_\infty V_\infty^2}{\sqrt{M_\infty^2 - 1}} \Delta\theta = \frac{k p_\infty M_\infty^2}{\sqrt{M_\infty^2 - 1}} \Delta\theta \quad (14.12a)$$

The pressure coefficient is accordingly given by the simple formula

$$C_{pI} = \frac{p - p_\infty}{\frac{1}{2} \rho_\infty V_\infty^2} = \frac{2 \Delta\theta}{\sqrt{M_\infty^2 - 1}} \quad (14.12b)$$

The subscript *I* is used here to indicate that in *crossing* a Mach wave of family *II* we are following a course of states for which the function φ_1 is constant or on which the argument of φ_1 is constant. Or, more in line with the generalization of these ideas by the method of characteristics (Chapter 15), the subscript *I* signifies that the crossing of a Mach line of family *II* may be accomplished by *following* a Mach line of family *I*.

Similarly, if we were to consider the influence of a system of waves of family *I*, we would find that

$$(p - p_\infty)_{II} = - \frac{\rho_\infty V_\infty^2}{\sqrt{M_\infty^2 - 1}} \Delta\theta = - \frac{k p_\infty M_\infty^2}{\sqrt{M_\infty^2 - 1}} \Delta\theta \quad (14.13a)$$

$$C_{pII} = - \frac{2 \Delta\theta}{\sqrt{M_\infty^2 - 1}} \quad (14.13b)$$

It may be seen by comparison that these relations agree with Eq. 14.11.

Four Basic Waves. In constructing solutions by means of waves, we may synthesize a flow pattern corresponding to specified boundary conditions out of four fundamental types of changes, depending (i) on whether the wave is of family *I* or of family *II*, and (ii) on whether the stream is accelerated or decelerated. These four types of changes are illustrated in Fig. 14.7. From these sketches and Eqs. 14.12 and 14.13, we see that the pressure increases for a deceleration and decreases for an acceleration, as required by momentum considerations. Furthermore, during a compression the streamline bends *toward* the Mach line, whereas during an expansion the streamline bends *away* from the Mach line; by considering the cross-sectional area of a stream tube formed by two neighboring streamlines, it will be seen that in a compression the area decreases while in an expansion the area increases, as might be expected from simple one-dimensional considerations for supersonic flow.

When a streamline is influenced by a wave, it may be seen from Fig. 14.6 that the velocity component parallel to the wave is unaltered. Only the velocity component normal to the wave is changed in magni-

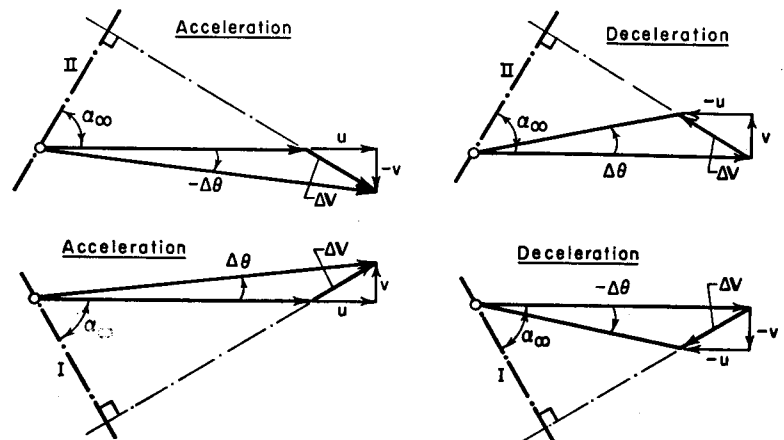


FIG. 14.7. Four basic types of Mach waves.

tude. Or, stated differently, the vector change in velocity is in the direction for which the component of velocity is equal to the local sound velocity.

Fig. 14.8 shows the compression Mach waves of family *I* and family *II* generated at the nose of a thin wedge-shaped body.

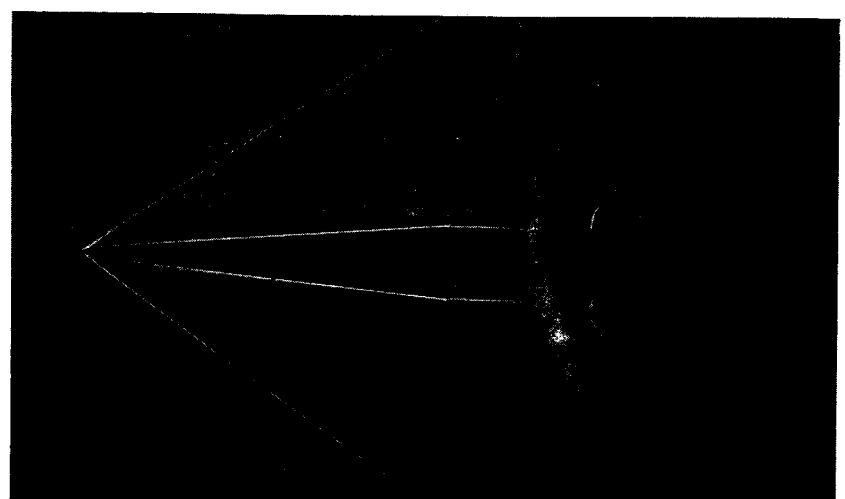


FIG. 14.8. Shadow photograph of flow (from left to right) past thin wedge-shaped body (M.I.T. Gas Turbine Laboratory).

14.5. Flow Past a Wave-Shaped Wall

As an application of the foregoing ideas, let us consider the wave shaped wall of Art. 10.4, having the equation

$$y_s = h \cos \frac{2\pi x_s}{l}$$

Perturbation Potential. Assuming that the wall has only a small waviness ($y_s \ll x_s$) and that the flow is from left to right and above the wall, we may eliminate pressure waves of family I on the grounds that they cannot physically be propagated upstream. To satisfy the equation of the streamline at the wall, the function f must, in accordance with Eq. 14.9, be given by

$$\frac{\varphi}{V_\infty} = f_2 = - \frac{h}{\sqrt{M_\infty^2 - 1}} \cos \left[\frac{2\pi}{l} (x - \sqrt{M_\infty^2 - 1} y) \right] + \text{constant}$$

Pressure Distribution. Using Eq. 14.11, we find that

$$C_p = - \frac{4\pi}{\sqrt{M_\infty^2 - 1}} \frac{h}{l} \sin \left[\frac{2\pi}{l} (x - \sqrt{M_\infty^2 - 1} y) \right]$$

$$C_{p_s} \cong - \frac{4\pi}{\sqrt{M_\infty^2 - 1}} \frac{h}{l} \sin \frac{2\pi x_s}{l}$$

Comparison of Subsonic and Supersonic Flow. The streamlines and pressure distribution are shown in Fig. 14.9a. How the maximum pressure coefficient varies with Mach Number is shown in Fig. 14.9b for both supersonic and subsonic flow. Many of the qualitative differences between subsonic and supersonic flow are illustrated by comparing this solution with the subsonic solution of Art. 10.4. In supersonic flow the effect of the wall is propagated out to infinity along the Mach lines with undiminished intensity; in subsonic flow the effect is propagated in all directions, but decays rapidly with increasing distance from the wall. In supersonic flow the flow pattern is unsymmetrical about a vertical axis through a crest or trough; in subsonic flow it is symmetrical. In supersonic flow the pressure coefficient goes through maxima and minima where the streamline has its greatest inclination; in subsonic flow the pressure coefficient goes through maxima and minima where the streamline has its largest curvature. In supersonic flow the pressure coefficient decreases as the free-stream Mach Number increases; in subsonic flow the opposite is true. In subsonic flow it was possible to

specify that the perturbation velocity shall vanish at large distances from the wall; in supersonic flow this is not possible, thus indicating that the necessary and allowable amount of initial data (that is, boundary-value information) are different in the two types of flow, corresponding to the difference in the types of differential equation describing the

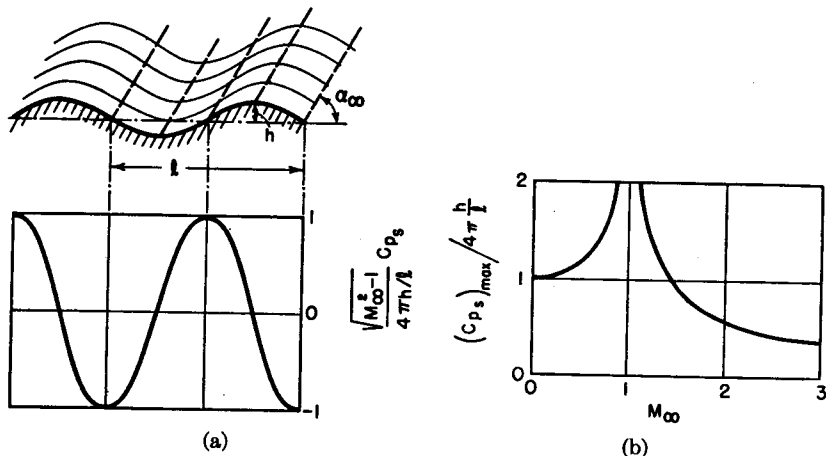


FIG. 14.9. Flow past wave-shaped wall (after Ackeret).

- (a) Streamlines and surface pressure distribution.
(b) Effect of Mach Number on peak pressure coefficient.

motion. This simple example thus demonstrates that the experience gained from dealing with subsonic flow problems does not help in the understanding of supersonic flow.

Solution by Construction of Wave Pattern. The solution given above was obtained by seeking the proper form of the potential function. We could also have proceeded by constructing the wave pattern. Suppose that we were to start with the known shape of wall extending upstream and downstream to infinity, with the flow unbounded on top of the wall. Then, since there is no way of originating pressure waves of family I, there can be present only waves of family II. From each point of the wall of Fig. 14.8 an infinitesimal wave is propagated at the Mach angle into the flow, the turning angle of the stream across the wave being determined by the differential change of angle at the wall. Since the waves are propagated with unchanged intensity (i.e., pressure rise), it follows that the velocity vector and all stream properties are constant along each of the Mach lines. The streamlines may therefore be constructed simply by transferring slopes along the Mach lines. Eq. 14.12a shows that for simple waves the pressure coefficient is linearly proportional to the turning angle of the stream; hence, the local pres-

sure coefficient on a given streamline depends only on the local slope of the streamline. For the solid wall, as an example,

$$\Delta\theta_s = \left(\frac{dy}{dx}\right)_s = -2\pi \frac{h}{l} \sin \frac{2\pi x_s}{l}$$

and, using Eq. 14.12b, we get

$$C_{p_s} = -\frac{4\pi}{\sqrt{M_\infty^2 - 1}} \frac{h}{l} \sin \frac{2\pi x_s}{l}$$

which is identical with the result obtained previously.

14.6. Supersonic Airfoils

One of the most important applications of the method of small perturbations is to bring out in an approximate but general way the

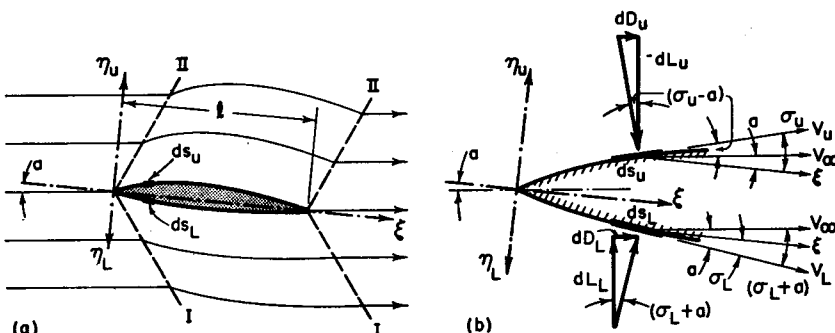


FIG. 14.10. Nomenclature for analysis of thin supersonic profile.

properties of supersonic airfoils of infinite span. Experience has shown that the leading and trailing edges of supersonic airfoils should be sharp, or at most there should be only a slight rounding of the leading edge; otherwise, there are large penalties in drag owing to the presence of detached shocks which stand ahead of the airfoil. We shall consider, therefore, profiles of the general form shown in Fig. 14.10, while keeping in mind that the results will be valid only for small angles of attack and for values of $M_\infty^2 \delta$ small compared with unity.

Flow Pattern. Using the concept of pressure waves generated at the surface of the airfoil, we construct the wave pattern and streamline pattern of Fig. 14.10a. Since the pressure disturbances can be propagated only downstream, the pressure waves on the upper surface must be of family II (left-running) and those on the lower surface of family I (right-running). Thus the flow field is divided into several regions in

each of which there are simple-wave patterns. From Eqs. 14.12 and 14.13, therefore, the local pressure at any point on the surface depends only on the local inclination of the tangent to the surface.

Pressure Distribution. Let ξ, η be a system of coordinates which lie in the airfoil and which are therefore independent of angle of attack, and for convenience let ξ lie along the chord line. Also, let σ denote the local inclination of the surface measured from the chord line, and let subscripts U and L refer to the upper and lower surfaces respectively. Note that η_U is measured upward and η_L downward; similarly, σ_U is measured counterclockwise and σ_L clockwise.

Referring to the geometry of Fig. 14.10b, the local directions of the streamlines at the surface, relative to the undisturbed flow, are

$$\Delta\theta_U = (\sigma_U - a); \quad \Delta\theta_L = -(\sigma_L + a)$$

From Eqs. 14.12 and 14.13 we find the local surface pressures to be

$$p_L - p_\infty = \frac{kp_\infty M_\infty^2}{\sqrt{M_\infty^2 - 1}} (\sigma_L + a)$$

$$p_U - p_\infty = \frac{kp_\infty M_\infty^2}{\sqrt{M_\infty^2 - 1}} (\sigma_U - a)$$

Subtracting the second from the first of this pair of equations, we get, for the pressure difference at any chordwise location,

$$p_L - p_U = \frac{kp_\infty M_\infty^2}{\sqrt{M_\infty^2 - 1}} (\sigma_L - \sigma_U + 2a)$$

Lift Coefficient. The forces on the profile may now be found by integrating the pressure over the entire surface. Resolving the pressure-area forces on the typical surface elements shown, and making use of the approximations permitted by the linear theory, we have

$$dL_L = p_L ds_L \cos(\sigma_L + a) \cong p_L d\xi$$

$$dL_U = -p_U ds_U \cos(\sigma_U - a) \cong -p_U d\xi$$

so that

$$dL = dL_U + dL_L = (p_L - p_U) d\xi = \frac{kp_\infty M_\infty^2}{\sqrt{M_\infty^2 - 1}} (\sigma_L - \sigma_U + 2a) d\xi$$

Integrating this expression between $\xi = 0$ and $\xi = l$, we find the total lift per unit span to be simply

$$L = \frac{kp_\infty M_\infty^2}{\sqrt{M_\infty^2 - 1}} 2al$$

inasmuch as

$$\int_0^l \sigma_L d\xi \cong \int_0^l \left(\frac{d\eta}{d\xi} \right)_L d\xi = \int_0^l d\eta_L = 0$$

and, likewise,

$$\int_0^l \sigma_U d\xi = 0$$

The lift coefficient and lift-curve slope are now computed as

$$C_L \equiv \frac{L}{\frac{1}{2} k p_\infty M_\infty^2 l} = \frac{4a}{\sqrt{M_\infty^2 - 1}} \quad (14.14a)$$

$$dC_L/da = 4/\sqrt{M_\infty^2 - 1} \quad (14.14b)$$

Drag Coefficient. Proceeding similarly, we calculate the elementary drags as

$$dD_L = p_L d\sigma_L \sin(\sigma_L + a) \cong p_L(\sigma_L + a) d\xi$$

$$dD_U = p_U d\sigma_U \sin(\sigma_U - a) \cong p_U(\sigma_U - a) d\xi$$

Using the previous expressions for p_L and p_U , we find

$$\begin{aligned} dD &= dD_L + dD_U \\ &= \frac{kp_\infty M_\infty^2}{\sqrt{M_\infty^2 - 1}} [(\sigma_L + a)^2 + (\sigma_U - a)^2] d\xi \\ &\quad + p_\infty [(\sigma_L + a) + (\sigma_U - a)] d\xi \end{aligned}$$

Expanding this expression, integrating, and noting that, as before,

$$\int_0^l \sigma_L d\xi \cong 0; \quad \int_0^l \sigma_U d\xi \cong 0$$

we get

$$D = \frac{kp_\infty M_\infty^2 l}{\sqrt{M_\infty^2 - 1}} [2a^2 + \overline{\sigma_L^2} + \overline{\sigma_U^2}] \quad (14.15a)$$

where $\overline{\sigma_L^2}$ and $\overline{\sigma_U^2}$ are the mean squares of the slopes, as defined by

$$\overline{\sigma_L^2} \equiv \frac{1}{l} \int_0^l \sigma_L^2 d\xi; \quad \overline{\sigma_U^2} \equiv \frac{1}{l} \int_0^l \sigma_U^2 d\xi \quad (14.15b)$$

The drag coefficient is then

$$C_D = \frac{D}{\frac{1}{2} k p_\infty M_\infty^2 l} = \frac{4}{\sqrt{M_\infty^2 - 1}} \left[a^2 + \frac{1}{2} (\overline{\sigma_L^2} + \overline{\sigma_U^2}) \right] \quad (14.15c)$$

INDUCED DRAG. We see that the pressure drag may be thought of as the sum of two parts. The first part is independent of the profile shape

and depends only on the angle of attack. Since the angle of attack is, by Eq. 14.14a, directly associated with the generation of lift, this part of the drag is known as the *wave drag due to lift*, or, following the nomenclature of subsonic fluid dynamics, the *induced drag*:

$$C_{D_{\text{ind}}} = \frac{4}{\sqrt{M_\infty^2 - 1}} a^2$$

However, the analogy to subsonic flow is somewhat overextended. In subsonic flow the induced drag is associated with the kinetic energy in the tip vortices which (according to Thomson's vortex theorem) are shed from lifting wings of finite span. The term "induced drag" for supersonic flow, on the other hand, is associated with the energy in the ever-spreading wave system of wings of infinite span.

THICKNESS DRAG. The second part of the drag depends only on the profile shape, and is known as the *wave drag due to thickness*:

$$C_{D_{\text{th}}} = \frac{4}{\sqrt{M_\infty^2 - 1}} \frac{1}{2} (\overline{\sigma_L^2} + \overline{\sigma_U^2})$$

SKIN-FRICTION DRAG. So far we have calculated only the drag forces resulting from pressure stresses acting on the surface of the profile. If the concept of a thin boundary layer flow which does not interact with the potential flow is applicable, it is clear that we may add the shear drag directly to the pressure drag. Letting C_{D_f} denote the skin-friction coefficient, the total drag coefficient is then given by

$$C_{D_{\text{total}}} = C_{D_{\text{ind}}} + C_{D_{\text{th}}} + C_{D_f}$$

It appears from experiment that C_{D_f} is approximately the same as in subsonic flow, i.e., it is of the order of magnitude of 0.005.

Lift-Drag Ratio. The lift-drag ratio may now be found with the help of Eqs. 14.14a and 14.15c. Including the skin-friction drag, we have

$$\frac{L}{D} = \frac{C_L}{C_D} = \frac{a}{a^2 + \frac{1}{2} (\overline{\sigma_L^2} + \overline{\sigma_U^2}) + \frac{1}{4} C_{D_f} \sqrt{M_\infty^2 - 1}} \quad (14.16)$$

To find the maximum lift-drag ratio, we differentiate Eq. 14.16 with respect to a and set the derivative equal to zero. The angle of attack a' corresponding to $(L/D)_{\max}$ is thus found as

$$a' = \sqrt{\frac{1}{2} (\overline{\sigma_L^2} + \overline{\sigma_U^2}) + \frac{1}{4} C_{D_f} \sqrt{M_\infty^2 - 1}}$$

Inserting this into Eq. 14.16, we find that

$$\left(\frac{L}{D} \right)_{\max} = \frac{1}{2 \sqrt{\frac{1}{2} (\overline{\sigma_L^2} + \overline{\sigma_U^2}) + \frac{1}{4} C_{D_f} \sqrt{M_\infty^2 - 1}}} = \frac{1}{2a'} \quad (14.17)$$

Moment Coefficient. To obtain the counter-clockwise moment, \mathfrak{M} , about the leading edge, we again employ the approximations of the linear theory, and write

$$d\mathfrak{M} \cong (p_L - p_U)\xi d\xi = \frac{kp_\infty M_\infty^2}{\sqrt{M_\infty^2 - 1}} (\sigma_L - \sigma_U + 2a)\xi d\xi$$

Integrating between $\xi = 0$ and $\xi = l$, we first evaluate the integrals

$$\int_0^l \xi d\xi = l^2/2$$

and

$$\begin{aligned} \int_0^l (\sigma_L - \sigma_U)\xi d\xi &\cong \int_0^l \left(\frac{d\eta_L}{d\xi} - \frac{d\eta_U}{d\xi} \right) \xi d\xi \\ &= \int_0^l \xi (d\eta_L - d\eta_U) = -S_L + S_U \end{aligned}$$

where S_L is the area between the lower surface and the chord (positive when the lower surface lies below the chord), and S_U is the area above the chord. With these integrals we obtain

$$\mathfrak{M} = \frac{kp_\infty M_\infty^2}{\sqrt{M_\infty^2 - 1}} [al^2 + (S_U - S_L)] \quad (14.18a)$$

and

$$C_{\mathfrak{M}} = \frac{\mathfrak{M}}{\frac{1}{2}kp_\infty M_\infty^2 l^2} = \frac{2}{\sqrt{M_\infty^2 - 1}} \left(a + \frac{S_U - S_L}{l^2} \right) \quad (14.18b)$$

Center of Pressure. Suppose that $l_{c.p.}$ denotes the distance aft of the leading edge through which the resultant force is applied. To first-order effects,

$$\mathfrak{M} = Ll_{c.p.}; \quad \text{or} \quad \frac{l_{c.p.}}{l} = \frac{\mathfrak{M}}{Ll}$$

Then, using Eqs. 14.14 and 14.18, we get

$$\frac{l_{c.p.}}{l} = 0.5 + \frac{S_U - S_L}{2al^2} \quad (14.19)$$

Characteristic Parameters for Flat Plate and Double Wedge. Considering the special cases of a flat plate and a symmetrical double-wedge profile of thickness ratio δ , for which the streamlines and surface pres-

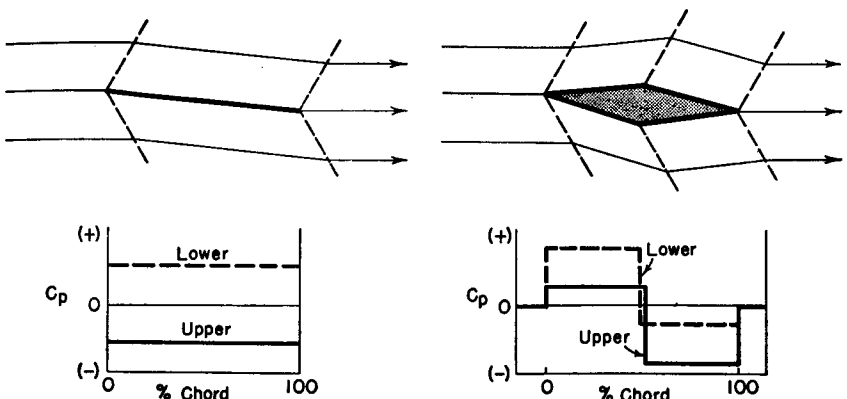


FIG. 14.11. Pressure distributions at surface of flat-plate and symmetrical, double-wedge profiles.

sure distributions are shown in Fig. 14.11, we obtain the following characteristic parameters:

Parameter	Flat Plate	Double-Wedge
$dC_L/d\alpha$	$4/\sqrt{M_\infty^2 - 1}$	$4/\sqrt{M_\infty^2 - 1}$
C_{D_f}	$4a^2/\sqrt{M_\infty^2 - 1}$	$4a^2/\sqrt{M_\infty^2 - 1}$
$C_{D_{th}}$	0	$4\delta^2/\sqrt{M_\infty^2 - 1}$
a' (for $C_{D_f} = 0$)	0	δ
$(L/D)_{\max}$ (for $C_{D_f} = 0$)	∞	$1/2\delta$
$dC_{\mathfrak{M}}/da$	$2/\sqrt{M_\infty^2 - 1}$	$2/\sqrt{M_\infty^2 - 1}$
$l_{c.p.}/l$	0.5	0.5

Performance Characteristics of Supersonic Profiles. Let us review the results obtained thus far and draw some general conclusions.

Lift. From Eq. 14.14b we see that the lift-curve slope, $dC_L/d\alpha$, is the same for all thin profiles at small angles of attack, irrespective of the specific shape of the profile. Fig. 14.12 shows the variation of $dC_L/d\alpha$ with M_∞ ; for convenience in comparison, there is also shown the curve of $dC_L/d\alpha \cong 2\pi/\sqrt{1 - M_\infty^2}$ for subsonic flow, based on the

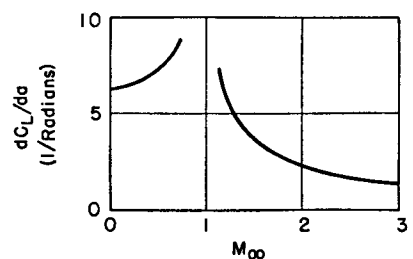


FIG. 14.12. Lift-curve slope for thin profiles.

Prandtl-Glauert rule and on the well known value of 2π for the theoretical lift-curve slope of a flat plate in incompressible flow.

DRAG. It may be seen from Eq. 14.15c that at small angles of attack the thickness and skin-friction drag predominate, whereas at large angles of attack the induced drag predominates.

For a given profile at a fixed Mach Number, Eqs. 14.14a and 14.15c define a *polar* relation between C_L and C_D with the angle of attack as a parameter. As in subsonic flow, the lift-drag polar has the form of a

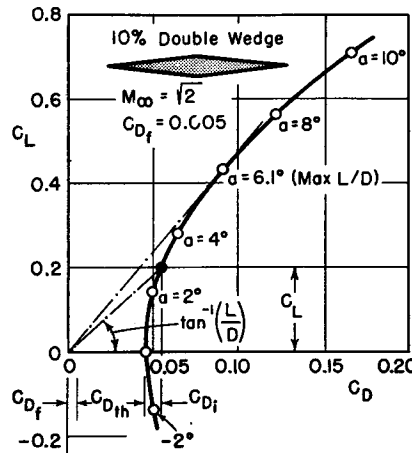


FIG. 14.13. Lift-drag polar for typical supersonic profile.

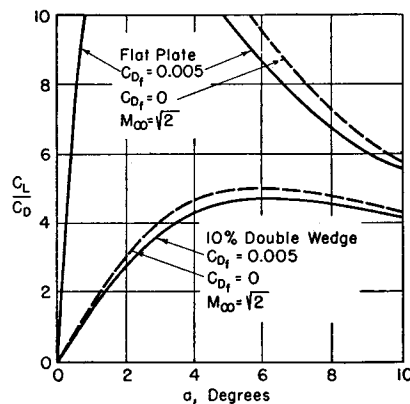


FIG. 14.14. Lift-drag ratios for flat-plate and double-wedge profiles, showing effect of skin friction.

parabola. Fig. 14.13 shows the lift-drag polar for a symmetrical double-wedge profile of 10% thickness ratio operating at $M_\infty = \sqrt{2}$. Fig. 14.14 shows how the lift-drag ratio of the 10% double-wedge and of the flat plate vary with angle of attack at $M_\infty = \sqrt{2}$. The angle of attack for maximum lift-drag ratio, together with the value of $(L/D)_{\max}$, are independent of Mach Number and depend only on the shape of the profile, provided of course that $C_{Df} = 0$. It is clear from Eq. 14.15c that, from the aerodynamic point of view, it is desirable to use profiles with small thickness ratios in order to minimize the thickness drag.

CENTER OF PRESSURE. The center of pressure is in the neighborhood of the mid-chord point for profiles symmetrical about the chord, whereas for subsonic flow the center of pressure is at about 25% of the chord aft of the leading edge. If an aircraft must fly at both subsonic and supersonic speeds, therefore, the control problem will be seriously complicated by the large changes in aerodynamic moments and in hinge moments of the control surfaces as the aircraft passes from subsonic to supersonic

speeds. We also conclude from Eq. 14.19 that the control problem is simplified if the profile is symmetrical about the chord line, for then the center of pressure does not change with angle of attack. To first-order effects the center of pressure is independent of Mach Number.

The foregoing generalizations, it should be emphasized, rest on the linearized theory. Consequently they are not entirely correct. More accurate methods of calculation are presented in Chapters 15 and 16. For the present it will suffice to state that the linear theory is reasonably correct as regards the lift and drag, but is unreliable as regards the center of pressure.

Comparison with Experiment. Fig. 14.15 shows the theoretical and experimental⁽¹⁾ surface-pressure distributions on a biconvex circular-arc

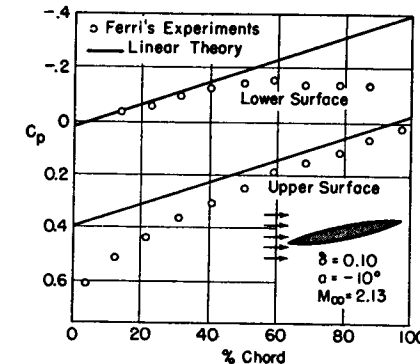


FIG. 14.15. Comparison of linear theory with measured pressure coefficient at surface of 10% biconvex profile (after Ferri).

profile of 10% thickness ratio. The agreement is quite good for small deviations from the free-stream direction and is very poor for large deviations in direction, as might be expected from the assumptions of the linear theory. Schlieren photographs indicate that the curious variation of C_p near the trailing edge of the lower surface is the result of boundary-layer interaction with the oblique shock wave which, according to a more exact theory, must be present near the trailing edge (Chapter 16).

Although the pressure distributions are in poor agreement with the linear theory, the errors are largely self-canceling as far as the resultant forces are concerned, since the respective areas between the experimental and theoretical curves for the upper and lower surfaces are nearly the same. For this reason, the agreement as to lift and drag coefficients is much better than the pressure distribution would indicate. For example, Figs. 14.16a and 14.16b show that the linear theory furnishes a good approximation to the lift and drag coefficients. However, the

errors in pressure distribution are quite serious in respect to the moment coefficient, as may be seen from Fig. 14.16c.

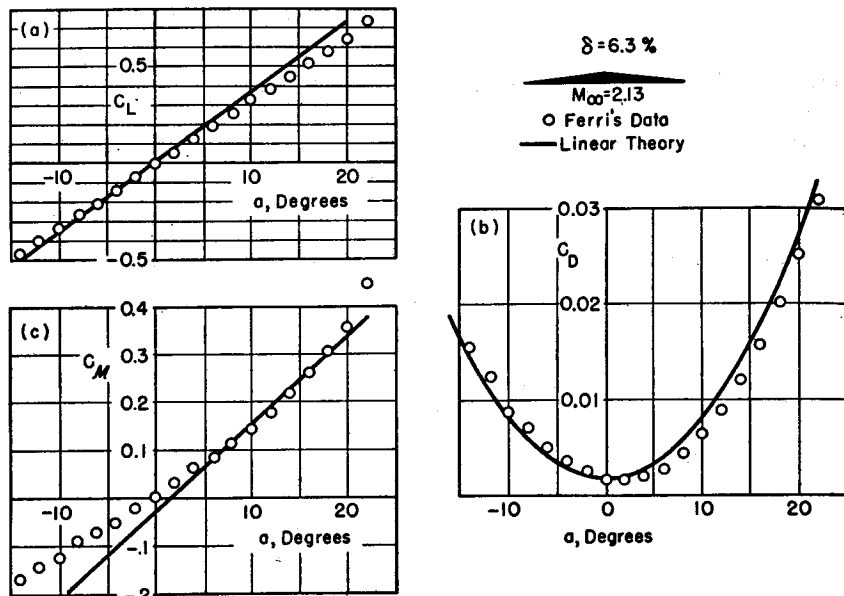


FIG. 14.16. Comparison of linear theory with force coefficients of 6.3% single-wedge profile (after Ferri).

To sum up, the linearized theory is useful for showing in a general way the properties of supersonic airfoils. In addition, it furnishes a simple method for approximating the lift and drag coefficients with fair accuracy.

Flat-Plate Airfoil in Subsonic and Supersonic Flow. It is instructive to compare a flat-plate airfoil in a frictionless fluid for incompressible flow with the corresponding situation for supersonic flow. The streamline patterns are shown in Fig. 14.17. In supersonic flow the static

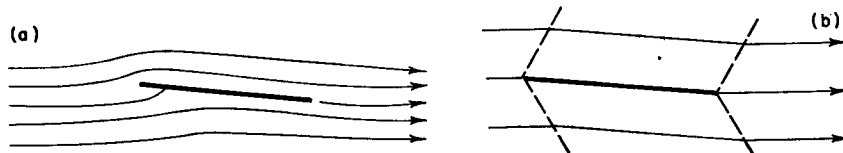


FIG. 14.17. Streamlines for flat-plate airfoil.

- (a) Subsonic flow.
- (b) Supersonic flow.

pressure is uniform over the top and bottom surfaces; in incompressible flow it undergoes wide variations. There are stagnation points in sub-

sonic flow, but none in supersonic flow. Near the nose of the flat plate in incompressible flow the velocities approach infinity and there are infinite "suction pressures," but no singularities of this sort appear in the supersonic pattern. In incompressible flow the resultant force on the plate is normal to the direction of the distant flow, that is, there is no drag (the d'Alembert Paradox); in supersonic flow the resultant force is normal to the plate, that is, there is a wave drag even though the fluid is frictionless. The center of pressure is at about 25% of chord for incompressible flow, but at about 50% of chord for supersonic flow. These comparisons again illustrate the complete difference in character between subsonic and supersonic flow.

14.7. Reflection and Intersection of Waves

All the examples of the linear theory thus far cited have referred to simple-wave flows. We now consider flow patterns in which waves of both families are present.

For flow with simple waves it is usually possible to obtain analytical solutions, and hence the flow pattern may with no difficulty be thought of as containing an infinite number of infinitesimal pressure waves. For flow with mixed waves, on the other hand, it is usually necessary to make stepwise calculations, and hence it has been found convenient to condense the wave system into a finite number of waves which divide the flow field into regions of uniform, parallel flow.

Representation of Continuous Flow by Lumped Pressure Waves. To illustrate this idea, suppose that an initially uniform parallel flow passes over the curved surface *AB* of Fig. 14.18a. Then, by the theory of

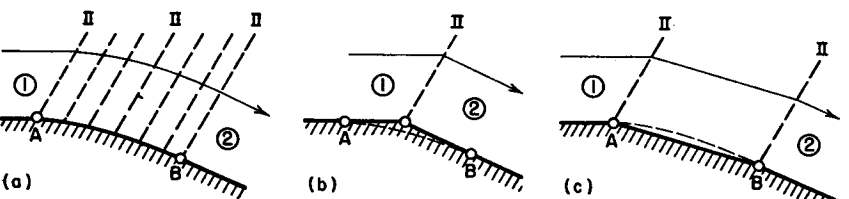


FIG. 14.18. Replacement of a continuous wave system by lumped discontinuities.

simple-wave flow, the change in direction of the wall generates at each point an infinitesimal pressure wave which bends each streamline by an equal amount. In Fig. 14.18b, as an approximation, the curved wall has been replaced by a single sharp change in direction with the same angle of turn, and the infinite system of pressure waves has been condensed into a single wave across which the entire change of stream properties is concentrated. A better approximation is furnished by

Fig. 14.18c, and still better approximations could be had by dividing the curved wall into a larger number of straight chords. According to Eq. 14.12, the change in pressure (and of Mach Number) for a turn of given $\Delta\theta$ will be the same for the three patterns of Fig. 14.18; the approximation lies only in the construction of the wave pattern and streamline pattern.

In calculating the pressure change and wave angle for the flow pattern of Fig. 14.18b, using Eqs. 14.12 and the definition of Mach angle, we might in the first instance choose the Mach Number and direction in zone 1 as the mean-stream conditions. However, after finding the pressure in zone 2 the Mach Number in zone 2 may be calculated from the isentropic relation. We could then make a better approximation by taking the mean-stream conditions as those corresponding to the average Mach Number and direction between zones 1 and 2. However, since one of the functions of the linear theory is to provide answers with a minimum of computation, such averaging refinements are generally not worth employing, especially since methods more accurate than the linear theory are available (Chapters 15 and 16).

Unit Processes. Wave patterns may be synthesized from a few unit processes, namely, (i) reflection of a wave from a straight wall, (ii) cancellation of a wave at a boundary, (iii) reflection of a wave from a boundary of constant pressure, and (iv) intersection of two waves.

Direction and Pressure Indexes. Before taking these up in turn, let us for convenience define

$$\Theta = \frac{180}{\pi} \theta$$

where Θ is the inclination of the streamline to the x -axis, in degrees, and θ is the corresponding inclination in radians. Also, let us define a dimensionless pressure index

$$P = \frac{180 \sqrt{M_\infty^2 - 1}}{\pi k p_\infty M_\infty^2} p + \text{constant}$$

where the constant is so chosen that P has convenient numerical values. Then it follows from Eq. 14.12 that as a streamline crosses waves of family II (left-running),

$$\Delta P_I = \Delta\Theta \quad (14.20a)$$

and as it crosses waves of family I (right-running),

$$\Delta P_{II} = -\Delta\Theta \quad (14.20b)$$

The local pressure index P of course determines the local Mach Number through the isentropic relationships.

Reflection of Wave from Straight Wall. In Fig. 14.19a the flow is assumed to be uniform and parallel in region 1, with $\Theta_1 = 0$ and say $P_1 = 100$. At the 1° bend in the lower wall, rarefaction wave a of family II is generated. In region 2, then, $\Theta_2 = -1$, and, from Eq. 14.20a, $P_2 = 99$.

Now, what happens when wave a strikes the upper wall? It cannot merely end on the upper wall, for then the flow would separate from the upper wall. The continuity of flow at the upper wall is maintained if we assume that wave b , of family I, originates where wave a strikes the

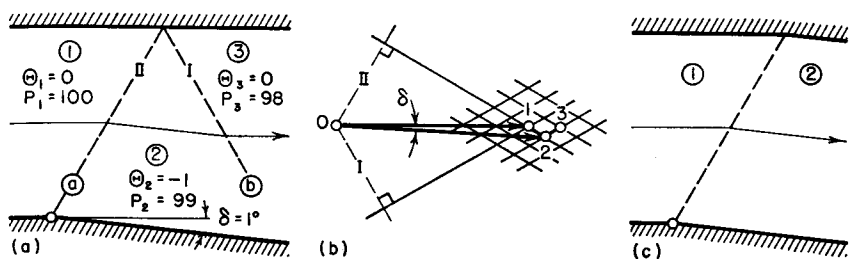


FIG. 14.19. Reflection of expansion wave.

- (a) Reflection from straight wall in like sense.
 (b) Hodograph diagram for (a).
 (c) Cancellation of wave by bend in wall.

upper wall. Wave b is called the reflection of wave a . In region 3, if the flow follows the wall, it is necessary that $\Theta_3 = 0$. Applying Eq. 14.20b to the flow across wave b , we get $P_3 = 98$.

In this example, the incident wave a is an expansion wave in the sense that the fluid crossing the wave undergoes a drop in pressure and an increase in velocity. The reflected wave b is also an expansion wave. If a had been a compression wave, similar reasoning would show that b would also be a compression wave. We therefore reach the important conclusion that *pressure waves are reflected from a straight wall in like sense*. Furthermore, for waves of small strength, to which the linear theory is limited, the angle of reflection equals the angle of incidence, and the strengths of the reflected and incident waves (as measured by the respective pressure changes) are equal.

Fig. 14.19b shows the *hodograph diagram* for this example. In the hodograph diagram all velocity vectors are drawn from the common origin O . A region in the physical plane of Fig. 14.19a is mapped as a point in the hodograph diagram. After locating point 1 on the hodograph, point 2 is found from the known direction of the velocity vector in region 2 and from the fact that the vector change in velocity between regions 1 and 2 is normal to the direction of the pressure wave of family II. Point 3 may similarly be located in the hodograph diagram.

Fig. 14.20a illustrates the generation of a compression wave by a wedge, together with two subsequent reflections.

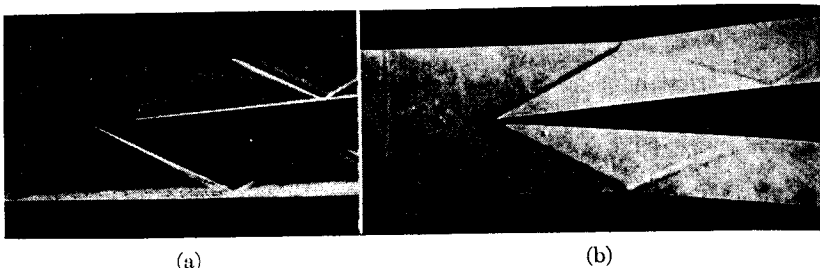


FIG. 14.20. Schlieren photographs of wave reflection (M.I.T. Gas Turbine Laboratory).

- (a) Compression waves generated by wedge are reflected in like sense at duct walls. Reflected waves are subsequently reflected in like sense at wedge surface.
- (b) Compression wave generated by wedge is incident on a corner, the turning angle of which is slightly greater than that of the wedge. The compression wave is more than canceled by the expansion generated at the corner, and the net result is a very weak expansion emanating from the corner.

Cancellation of Wave. Referring again to Fig. 14.19, and following the same reasoning as in the previous example, we see that wave a would have no reflection if the upper wall were, at the point of incidence of wave a , bent in the direction of the lower wall. Fig. 14.19c shows the resulting flow pattern.

Fig. 14.20b illustrates the near cancellation of a wave by a bend in the wall.

Reflection of Wave from Boundary of Constant Pressure. Suppose that in Fig. 14.21a a uniform, parallel jet leaves a nozzle and is exposed on the upper side to an atmosphere of constant pressure. Assume that

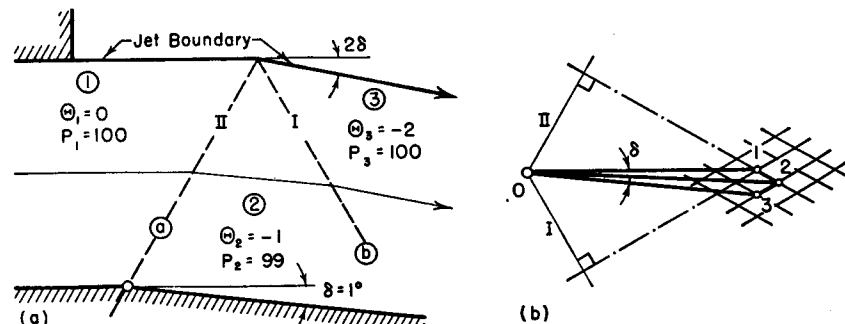


FIG. 14.21. Reflection of a wave from a free (constant-pressure) boundary.

- (a) Wave system, streamlines, and fluid properties.
- (b) Hodograph diagram.

in region 1 the flow properties are $\Theta_1 = 0$, $P_1 = 100$ and that there is a 1° bend in the lower wall. Then, as in the example of Fig. 14.19, we may construct expansion wave a and compute $\Theta_2 = -1$, $P_2 = 99$.

The upper boundary of the jet by assumption remains at constant pressure. Hence, wave a must be reflected as the compression wave b . In region 3 we have $P_3 = P_1 = 100$, and, applying Eq. 14.20b across wave b , we find that $\Theta_3 = -2$.

The upper boundary of the jet therefore undergoes a turning angle twice as large as that of the bend in the lower wall. We conclude furthermore that *a pressure wave is reflected from a boundary of constant pressure in unlike sense*.

The hodograph diagram for this example is shown in Fig. 14.21b. Note that since regions 1 and 3 have the same pressure, they must also have the same speed. Points 1 and 3 therefore lie on a circle with the origin O as center.

Intersection of Waves. Fig. 14.22a shows the intersection of two waves of opposite family. Our problem is to find the state in region 4 from the known state in region 1 and the known turning angles δ_a and δ_b .

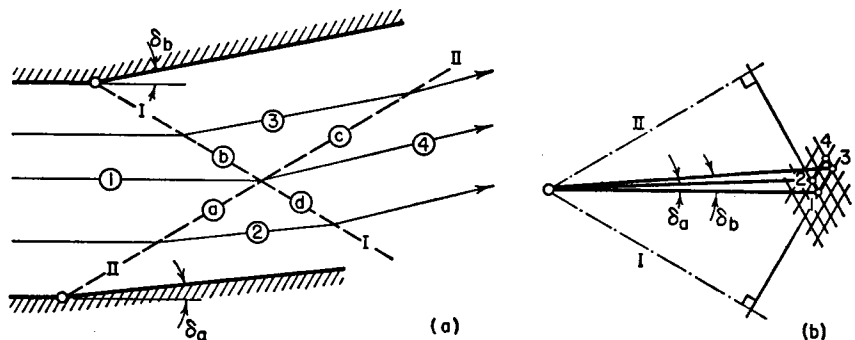


FIG. 14.22. Crossing of waves.

- (a) Wave system, streamlines, and fluid properties.
- (b) Hodograph diagram.

Region 4 may be reached along a streamline from region 1 either through region 3 or through region 2. We therefore apply Eqs. 14.20a and 14.20b in the following manner:

$$\begin{aligned}
 P_4 - P_1 &= (P_4 - P_2) + (P_2 - P_1) \\
 &= -(\Theta_4 - \Theta_2) + (\Theta_2 - \Theta_1) = -\Theta_4 + 2\Theta_2 - \Theta_1 \\
 P_4 - P_1 &= (P_4 - P_3) + (P_3 - P_1) \\
 &= (\Theta_4 - \Theta_3) - (\Theta_3 - \Theta_1) = \Theta_4 - 2\Theta_3 + \Theta_1
 \end{aligned}$$

If we first add and then subtract these two equations we obtain the desired answers in the form

$$P_4 - P_1 = \Theta_2 - \Theta_3 = \delta_a - \delta_b \quad (14.21a)$$

$$\Theta_4 - \Theta_1 = (\Theta_2 - \Theta_1) + (\Theta_3 - \Theta_1) = \delta_a + \delta_b \quad (14.21b)$$

A general conclusion to be drawn from this example is that, for wave strengths within the linear theory, intersecting waves do not interfere with each other. This inference is reached by noting that waves *a* and *c* have identical pressure changes and turning angles, and likewise for waves *b* and *d*. We may therefore ignore the crossing of the waves and simply assume that a certain wave has associated with it a constant turning angle and pressure change, irrespective of the fact that it may be crossed by waves of the other family.

Example of Overexpanded and Underexpanded Jets. In Chapter 5 it was remarked that when a supersonic nozzle discharges into a region

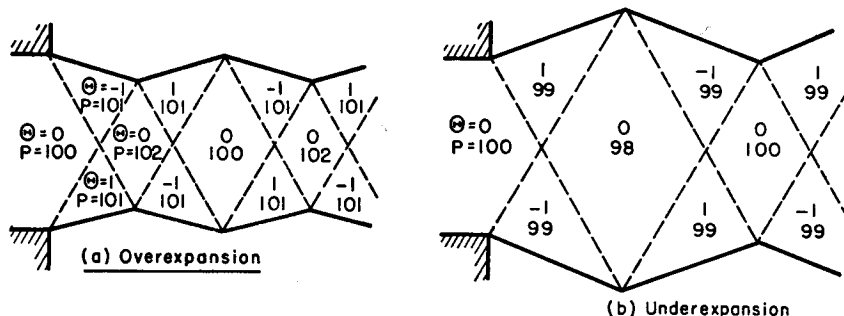


FIG. 14.23. Flow patterns at exit of two-dimensional nozzle.

- (a) Overexpanded nozzle.
(b) Underexpanded nozzle.

of variable back pressure, there is a range of back pressures for which the one-dimensional approach yields no answers. Problems of this type may now be solved, at least approximately, by linear methods.

In Fig. 14.23a the pressure of the exhaust region is higher than the pressure in the exit plane of the two-dimensional nozzle. On leaving the nozzle the jet boundaries must be immediately adjusted to the back pressure. Hence we assume that compression waves originate at the corners of the nozzle exit. The strengths of the waves are such as to make the pressure at the jet boundaries equal to the back pressure. For the specific case shown it was assumed that the pressure rise across the first wave corresponds to a change in *P* of one unit. The subsequent intersections and reflections of the original waves are handled according to the unit process methods previously described. It may be seen

that the wave and flow patterns undergo cyclic changes which extend to infinity in the absence of friction. In adjusting itself to the back pressure, the jet in a sense "overshoots," for there are zones in the jet where the pressure is higher than the back pressure.

Fig. 14.23b shows the wave pattern and flow properties for an under-expanded jet, i.e., for the case where the exhaust-region pressure is less than the exit-plane pressure.

Example of Supersonic Flat-Plate Biplane. Fig. 14.24 shows how the linearized theory may be used to determine approximately the aerodynamic properties of a supersonic biplane. The particular example of

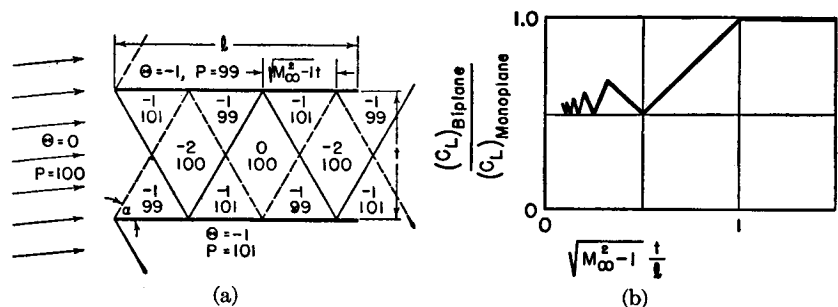


FIG. 14.24. Flat-plate biplane at 1° incidence.

- (a) Wave pattern, streamlines, and pressure distribution. Dashed lines show expansion waves; full lines compression waves.
(b) Ratio of lift coefficient of biplane (based on area of both plates) to that of monoplane.

the sketch is for an angle of attack of one degree. From the pressure distribution of Fig. 14.24a, it may be seen that over certain areas of the plate there is no net force acting, whereas over the remaining areas the force per unit area is the same as for a single flat-plate airfoil. From the geometry of the wave pattern, it is found that the fraction of the area over which there are pressure differences depends on the parameter $t\sqrt{M_\infty^2 - 1}/l$. Fig. 14.24b indicates how the ratio of lift coefficient for the biplane to lift coefficient for the monoplane at the same angle of attack varies with the parameter $t\sqrt{M_\infty^2 - 1}/l$. Further consideration shows that the location of the center of pressure also depends in marked degree on the parameter $t\sqrt{M_\infty^2 - 1}/l$. From the viewpoints considered here, the flat-plate biplane is inferior to the monoplane, but for thick profiles the biplane has certain advantages over the monoplane.

The method of applying the linearized theory as given in this article should be considered as a simple and rapid means for obtaining qualitative results and rough quantitative results. Accurate numerical results may be obtained by this method only when there are very small perturbations from a mean parallel flow. For large changes in velocity and

direction the linear theory remains useful for portraying the flow pattern in a general way, but the calculations must be based on more exact techniques, such as the method of characteristics (Chapter 15) and the theory of oblique shocks (Chapter 16).

REFERENCES AND SELECTED BIBLIOGRAPHY

1. FERRI, ANTONIO. Experimental Results with Airfoils Tested in the High-Speed Tunnel at Guidonia, *NACA Tech. Memo.*, No. 946 (1940).
2. TAYLOR, G. I. Application to Aeronautics of Ackeret's Theory of Airfoils Moving at Speeds Greater than That of Sound, *British A.R.C., R & M No. 1467* (1932).
3. ACKERET, J. Air Forces on Airfoils Moving Faster than Sound Velocity, *NACA Tech. Memo.*, No. 317 (1925).
4. ACKERET, J. Über Luftkräfte bei sehr grossen Geschwindigkeiten insbesondere bei ebenen Stromungen, *Helvetica Physica Acta*, Vol. 1 (1928), pp. 301-22.
5. LIEPMANN, H. W., and PUCKETT, A. E. *Introduction to Aerodynamics of a Compressible Fluid*. New York: John Wiley & Sons, Inc., 1947.
6. SAUER, R. *Introduction to Theoretical Gas Dynamics*. Ann Arbor: J. W. Edwards, 1947.
7. BONNEY, E. A. *Engineering Supersonic Aerodynamics*. New York: McGraw-Hill Book Co., Inc., 1950.

PROBLEMS

14.1. Consider a nearly uniform, parallel flow with the following perturbation velocity potential:

$$\varphi = 0 \quad \text{for } (x - \sqrt{M_\infty^2 - 1} y) < 0$$

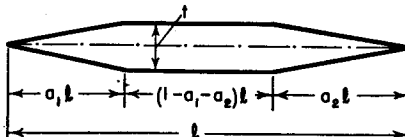
$$\varphi = \frac{V_\infty \epsilon}{A \sqrt{M_\infty^2 - 1}} e^{-A(x - \sqrt{M_\infty^2 - 1} y)} \quad \text{for } (x - \sqrt{M_\infty^2 - 1} y) > 0$$

where A is a constant.

(a) Investigate the streamlines and pressure distribution.

(b) Show that when A approaches zero, the flow pattern is that corresponding to flow from left to right above a wall which has a sharp corner with a turning angle ϵ .

14.2. If the value of $p_2 - p_1$ across a weak pressure wave is calculated from the linear theory, and if the values of M_2 and of p_2/p_1 are calculated from the isentropic relations, it is found that the equation of continuity is violated across the wave. Explain why this is so.



PROB. 14.3.

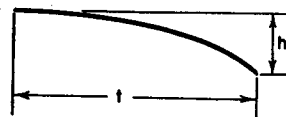
14.3. Consider the thin supersonic airfoil shown in the sketch. The airfoil is symmetrical about the chord line.

Find expressions for the lift, drag, and moment coefficients in terms of the Mach Number, the constants a_1 and a_2 , and the thickness ratio $\delta = t/l$.

Show that for a fixed thickness ratio, the wave drag due to thickness is a minimum when $a_1 = a_2 = 0.5$.

14.4. Consider a thin, curved profile of parabolic shape (see sketch), expressed by the curve, $y = -h(x/t)^2$. The leading edge of the profile is tangent to the direction of the oncoming air stream. Using the linearized theory,

(a) Find expressions for the lift and drag coefficients, for the lift-drag ratio, and for the moment coefficient, all in terms of M_∞ and the thickness ratio, M_∞



PROB. 14.4.

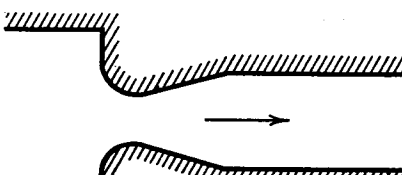
(b) Plot the pressure coefficient for the upper and lower surfaces against per cent chord, for $M_\infty = 2$ and $h/t = 0.10$.

(c) For $M_\infty = 2$ and $h/t = 0.10$, compare the pressure drag of this airfoil with the pressure drag of the flat-plate airfoil and of the 10% double-wedge profile, assuming that both the latter have the same lift coefficient as the parabolic profile.

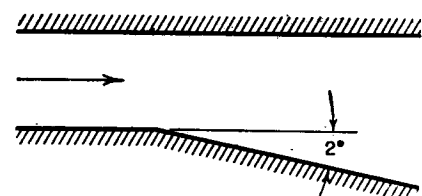
14.5. A converging-diverging nozzle with straight divergent sides discharges into a straight duct (see sketch). The total included angle between the straight sides is 12° . At the nozzle exit the Mach Number is 2.0. Two static pressure taps are placed in the wall near the sharp corner which joins the nozzle to the duct, one just upstream and one just downstream of the corner.

Estimate the pressure rise across the corner in (a) per cent of the pressure at the nozzle exit, and (b) per cent of the pressure at the nozzle entrance.

Are your answers dependent on whether the nozzle is two-dimensional or axially symmetric?



PROB. 14.5.



PROB. 14.6.

14.6. A certain two-dimensional passage has one straight wall and one curved wall (see sketch). The shape of the latter may, as a first approximation, be replaced by two straight-line segments joined at an angle of 2° , as shown in the sketch.

The Mach Number and pressure are initially 2.0 and 1000 respectively.

Using linearized theory, make a sketch to scale, showing streamlines, disturbance lines, and pressures in the various regions of constant velocity. Carry out the flow pattern until two complete reflections of the original wave have occurred.

14.7. A frictionless, two-dimensional, converging-diverging nozzle is supplied with air at 100 psia. The diverging section is shaped so that the stream passes through the exit plane of the nozzle in parallel flow with a Mach Number of 2.0. The pressure in the exhaust region is variable. Using linearized theory, make a

sketch to scale of the streamlines and disturbance lines in the region outside the nozzle exit and indicate the pressures in the various regions of constant velocity,

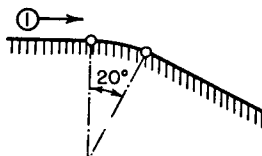
- For an exhaust-region pressure of 14.7 psia
- For an exhaust-region pressure of 10.5 psia

14.8. A two-dimensional, supersonic stream of air is bounded by a solid wall on one side only (see sketch). The wall is shaped so that the stream undergoes a 20° change in direction along an arc of a circle. It is agreed to replace the actual wall by a series of straight-line segments of equal length, and it is proposed to investigate the effect of the number of segments on the calculated values of the final Mach Number and pressure.

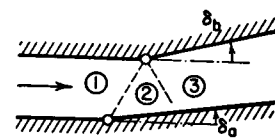
A modified linear theory is to be used, that is, linear theory will be used for each disturbance line, but the Mach Number downstream of each disturbance line will be modified so that it corresponds to the newly found pressure.

For an initial Mach Number of 2.0 and an initial pressure of 100 psia, calculate the final Mach Number and pressure when the arc of the circle is replaced in turn by 2, 4, and 6 equal line segments.

Estimate the asymptotic solution by graphically plotting the results against the reciprocal of the number of line segments, and compare with the exact solution (from Prandtl-Meyer theory) of $M = 2.83$, $p = 27.4$ psia.



PROB. 14.8.

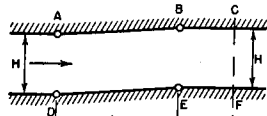


PROB. 14.9.

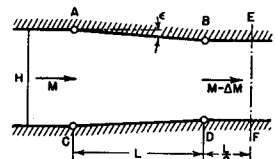
14.9. Considering the wave pattern shown in the sketch, find $(\Theta_3 - \Theta_1)$ and $P_3 - P_1$ as functions of δ_a and δ_b . Investigate the special cases where $\delta_a = \delta_b$ and $\delta_a = -\delta_b$.

14.10. The sketch shows a two-dimensional duct having an offset formed by 10° -turns at the corners A, B, D, and E.

Assuming that at section AD the stream is uniform and parallel and that $M = \sqrt{2}$ and $p = 100$ psia, determine for section CF the way in which the pressure, Mach Number, and stream direction vary over the cross section, for values of L/H of 1, 2, and 3.



PROB. 14.10.



PROB. 14.11.

14.11. The sketch shows a simple form of diffuser for decelerating a supersonic stream by very small amounts. Upstream of section AC the flow is uniform and parallel.

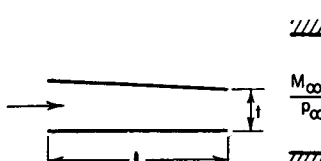
form and parallel, and it is desired to design the passage so that the flow downstream of section BD will be uniform and parallel.

(a) Show that for small changes in Mach Number, the correct ratio L/H is related only to M , and find the relationship.

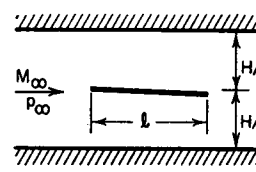
(b) Find the relation between ϵ and ΔM .

(c) Suppose that $M = \sqrt{2}$, $L/H = 0.75$, and $\epsilon = 0.01$ radian. Compute (i) the ratio of the maximum variation in pressure over the section EF to the average pressure difference between AC and EF, and (ii) the ratio of the maximum difference in stream direction over section EF to the wall angle ϵ .

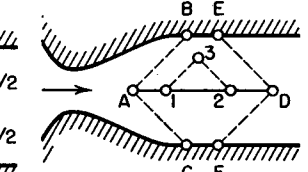
14.12. Consider a supersonic biplane with the lower flat plate always at zero angle of attack (see sketch). Explore the characteristics of such a biplane and compare the lift coefficient and center of pressure with the corresponding parameters for a flat plate. Demonstrate the significance of the parameter $t\sqrt{M_\infty^2 - 1}/l$ as suggested by Fig. 14.24b.



PROB. 14.12.



PROB. 14.13.



PROB. 14.14.

14.13. A two-dimensional supersonic airfoil of chord l is to be tested in a two-dimensional supersonic wind tunnel of height H (see sketch).

(a) Derive a general criterion among the variables l , H , and M_∞ which will insure that there is no effect of the tunnel walls on the performance of the airfoil, for the case of very small angles of attack.

(b) Indicate qualitatively how this criterion would be modified for larger angles of attack.

(c) Consider a flat-plate airfoil at an angle of attack 2° , with $M_\infty = \sqrt{2}$, $H/l = 2/3$, and a test-section pressure of 10 psia. Calculate approximately the lift coefficient, the drag coefficient, and the location of the center of pressure (in fractions of the chord aft of the leading edge), using the method of small perturbations.

14.14. One of the most important problems in supersonic wind tunnel design is the design of the contours for producing in the test section a stream which is exactly uniform and parallel.

The sketch shows a two-dimensional nozzle which is symmetrical about the center line and in which the flow is intended to be uniform and parallel in the region downstream of the line BAC, where B and C are the ends of the curved contours, and AB and BC are the Mach lines corresponding to the test-section Mach Number.

Because of errors in machining the contours, inaccuracies in the design, and uncertainty as to boundary-layer behavior, it is necessary to calibrate every tunnel.

(a) Assuming that the flow is two-dimensional, show that if the calibration yields data on the velocity vector along the line AD , it is then not necessary to do any calibration in the remainder of the region $ABEDFC$, where ED and FD are Mach lines. That is, show that information as to the velocity vector determines completely the state of the flow in the region $ABEDFC$.

(b) In the region $ABEDFC$ the flow is very nearly uniform and parallel. If the lines 1-3 and 1-2 are Mach lines, show that the pressure and stream direction at a typical point 3 may be found from similar data at points 1 and 2 from the formulas

$$p_3 = \frac{p_1 + p_2}{2} + \frac{kpM^2}{\sqrt{M^2 - 1}} \frac{\theta_1 - \theta_2}{2}$$

$$\theta_3 = \frac{\theta_1 + \theta_2}{2} + \frac{\sqrt{M^2 - 1}}{kpM^2} \frac{p_1 - p_2}{2}$$

where p and M are respectively the mean pressure and mean Mach Number in the test section.

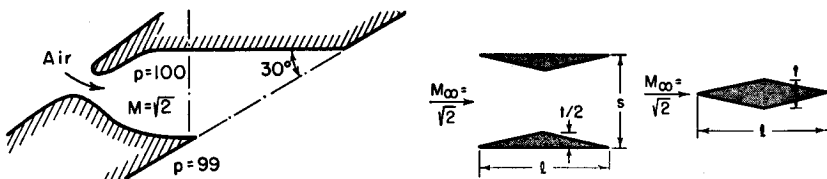
14.15. Show that the lift per unit span for a flat-plate airfoil at small incidence in a supersonic stream is given by

$$L = -\rho_\infty V_\infty \Gamma$$

where Γ is the circulation around the profile.

14.16. The sketch shows a turbine nozzle cut off at an angle of 30° to the nozzle axis. The nozzle is designed for a Mach Number of $\sqrt{2}$. It operates with a pressure of 100 psia in the plane shown and discharges into a region where the pressure is 99 psia.

Ignoring friction, draw a sketch showing the wave pattern and the jet boundaries. Indicate compression waves by solid lines and rarefaction waves by dashed lines. In each zone of flow show the pressure (psia) and flow direction (degrees). Continue the sketch at least to the point where the jet pattern begins to repeat itself, and indicate which portion of the pattern repeats itself infinitely.



PROB. 14.16.

PROB. 14.17.

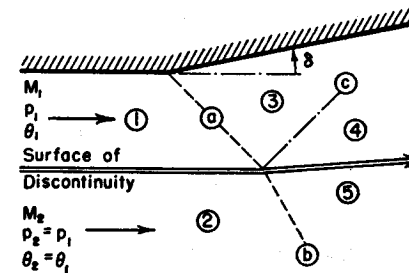
14.17. A supersonic biplane is constructed as shown from the two halves of a symmetrical double-wedge profile.

It is desired to compute $C_{D_0''}/C_{D_0'}$, where $C_{D_0''}$ is the pressure drag of the biplane at zero angle of attack, and $C_{D_0'}$ is the pressure drag of the symmetrical double wedge at zero angle of attack.

Assume that $M_\infty = \sqrt{2}$ in both cases, that t/l is very small compared with unity, and that the linearized theory is valid.

Make a chart approximately to scale of $C_{D_0''}/C_{D_0'}$ as a function of s/l , for values of the latter between 0.25 and 2.

14.18. The sketch shows a two-dimensional, supersonic flow with wave a incident on a surface of discontinuity which separates two regions of flow having the same directions and pressures but different velocities. The situation illustrated in the sketch might serve as a crude model of a shock entering a boundary layer.



PROB. 14.18.

The problem is to determine the strengths of the transmitted wave b and of the reflected wave c compared with the strength of the original wave a .

Carry out the analysis for the limiting case where the turning angle δ for wave a is extremely small, so that the linearized theory for the flow across a wave is valid. The Mach Numbers M_1 and M_2 may, however, have any value greater than unity.

Demonstrate that

$$\frac{\theta_b - \theta_a}{\delta} = \frac{2}{1 + \frac{M_2^2}{M_1^2} \sqrt{\frac{M_1^2 - 1}{M_2^2 - 1}}}$$

and

$$\frac{p_4 - p_1}{p_3 - p_1} = \frac{2}{1 + \frac{M_1^2}{M_2^2} \sqrt{\frac{M_2^2 - 1}{M_1^2 - 1}}}$$

Chapter 15

METHOD OF CHARACTERISTICS FOR TWO-DIMENSIONAL, SUPERSONIC FLOW

15.1. Introductory Remarks

The linearized approximation of Chapter 14 has its place in obtaining simple analytical relations for thin supersonic profiles and for quickly obtaining simplified stepwise solutions to other problems of supersonic flow. Of course, there are many instances in which more accurate calculations are necessary, and for that purpose we shall discuss in this chapter the *method of characteristics*.

Our analysis will at first be limited to two-dimensional, irrotational, isentropic, supersonic flow, and we shall make the further assumptions that the fluid is a perfect gas, that the flow is steady, and that gravity forces are negligible. There are many problems involving supersonic wings, supersonic compressor cascades, supersonic wind tunnel nozzles, etc., where the method of characteristics, based on these assumptions, can be and has been highly successful. In Art. 15.12 the method of characteristics is extended to rotational flows of a nonviscous fluid.

The method of characteristics will be developed in two ways: first, by an extension of the linearized theory, in which physical concepts are emphasized; and second, by formal mathematical methods. The latter development is more rigorous and leads to a better appreciation of the concept of characteristic curves, an appreciation which will be useful in attacking other types of problems involving the method of characteristics.

NOMENCLATURE

A	cross-sectional area for isentropic flow	k	ratio of specific heats
b	slope of physical characteristic	M	Mach Number
c	speed of sound	M^*	V/c^*
c^*	critical speed of sound for isentropic flow	p	pressure
c_v	specific heat at constant volume	p_0	isentropic stagnation pressure
h	distance along Mach line (Fig. 15.11a)	r	radius measured outward from sharp corner
		s	entropy per unit mass
		T	absolute temperature

NOMENCLATURE—Continued

u	x -component of velocity	φ	velocity potential
v	y -component of velocity	ω	defined by Eq. 15.6
V	resultant velocity	I, II	characteristic coordinates
x, y	Cartesian coordinates	$(\cdot)_I$	signifies characteristic curve of family I
α	Mach angle	$(\cdot)_{II}$	signifies characteristic curve of family II
θ	inclination of velocity vector to x -axis	$(\cdot)_E$	signifies exit of nozzle
ρ	density		

15.2. Flow with Waves of One Family by Extension of Linear Theory

Modified Linear Theory. From the linearized theory of Chapter 14, we learned that small disturbances in a two-dimensional, supersonic flow are propagated in the form of pressure waves along the Mach lines,

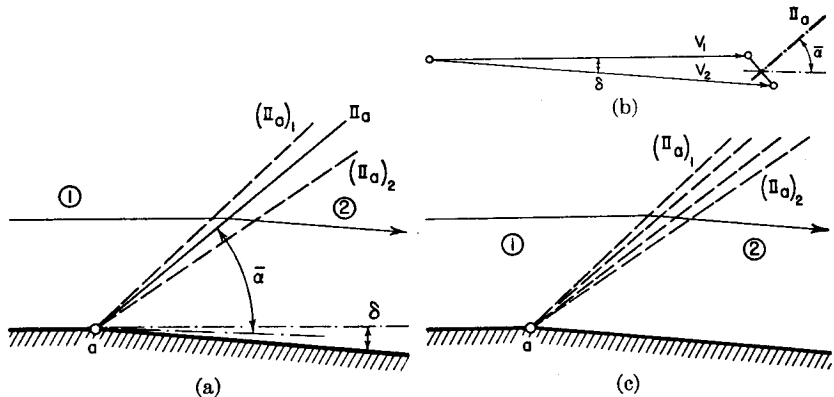


FIG. 15.1. Propagation of disturbance produced by bend in wall at point a .

- Streamlines and Mach lines according to linear theory. Mean Mach line II_a lies midway between Mach lines of upstream flow $(II_a)_1$, and of downstream flow $(II_a)_2$.
- Hodograph diagram according to linear theory.
- Exact Prandtl-Meyer solution for corner flow.

that these lines are also lines of constant perturbation potential, and that the *vector* change in velocity produced by a pressure wave must accordingly have a direction normal to the Mach direction. From these considerations, all the calculations can be reduced to a single unit process, illustrated by Fig. 15.1.

In Fig. 15.1a, an initially uniform parallel flow in region 1 is influenced by a small turn in the wall at point a . The effect of this turn is propagated along the left-running Mach line II_a , which makes the Mach angle α_1 to the initial flow. Fig. 15.1b shows how the velocity V_2 is

determined from the known turning angle δ and from the rule that the vector change in velocity is normal to the line II_a . The inclination of the latter depends on the Mach Number. As a first approximation the Mach line II_a may be drawn at the Mach direction corresponding to the upstream flow, i.e., as line $(II_a)_1$. However, after V_2 and other stream properties are tentatively found in region 2 by means of this first approximation, the accuracy of the approximation may be improved by taking the line II_a at the *mean* Mach angle $\bar{\alpha}$ to the *mean* flow direction. In this way, by several iterations, a better value of the stream properties in region 2 may be computed with the help of Fig. 15.1b, and the direction of the mean Mach line II_a may be more accurately drawn in the physical plane, Fig. 15.1a.

These ideas may be extended to the flow around the curved wall of Fig. 15.2a. As an approximation, the continuous wall is replaced by a

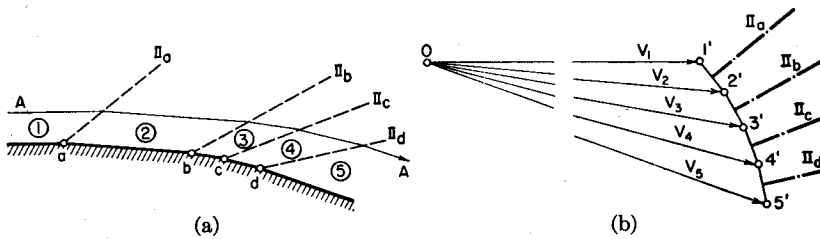


FIG. 15.2. Flow past curved wall by modified linear theory.

- (a) Streamlines and Mach waves.
- (b) Hodograph diagram.

series of straight-line chords with corners at a , b , c , and d . From each corner a pressure wave is propagated of such strength as to preserve continuity at the wall. Using the iteration process described above, the conditions in region 2 and the direction of the Mach line II_a are found from the *mean* flow conditions between zones 1 and 2. Next, the conditions in region 3 and the direction of the Mach line II_b are found by iteration from the *mean* flow conditions between zones 2 and 3. Thus, by stepwise increments, the entire flow field is determined. This type of flow, in which pressure waves of only one family appear, is known variously as *flow with waves of one family*, *simple-wave flow*, *Prandtl-Meyer flow*, and *corner-type flow*. It is distinguished by the features that (i) all flow properties are uniform along each Mach line and the Mach lines are straight, and that (ii) for given initial conditions, the magnitude of the velocity at any point depends only on the flow direction at that point. Later we shall see that these two features necessarily go hand-in-hand mathematically.

The construction of the velocity vectors for the flow of Fig. 15.2a is shown in Fig. 15.2b. If we denote the end points of the velocity vectors

representing the flows in fields 1, 2, etc., by the respective image points $1'$, $2'$, etc., Fig. 15.2b becomes the *hodograph plane*, or the *velocity plane*. A line drawn from the origin to any point such as $1'$ gives the magnitude and direction of the velocity vector pertaining to that point; hence the velocity V and stream direction θ are polar coordinates in the hodograph plane. The Cartesian coordinates in the hodograph plane are u and v , the x - and y -components of velocity, respectively. Since the velocity at each point of the physical plane may be represented by a corresponding point in the hodograph plane, any line in the physical plane is in general mapped into a corresponding line in the hodograph plane. For example, the physical streamline AA of Fig. 15.2a is mapped into the hodograph streamline $1'2'3'4'5'$ of Fig. 15.2b. We observe that in a flow with waves of one family, *all* physical streamlines are imaged by a *single* hodograph streamline.

Exact Solution for Simple Waves. The method of solution indicated above for the curved wall of Fig. 15.2a becomes more and more exact as we increase the number of chords by which the wall is replaced. We obtain an exact solution in the limit by carrying out the process with infinitesimal steps.

LEFT-RUNNING WAVE. Let us imagine that a Mach wave of family II (Fig. 15.3a) turns the flow through the positive angle $d\theta$, with correspond-

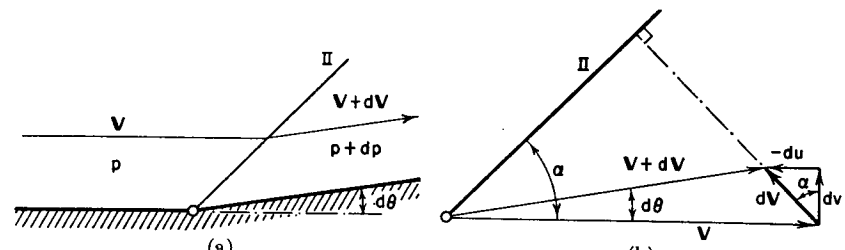


FIG. 15.3. Infinitesimal Mach wave.

- (a) Physical plane.
- (b) Hodograph plane.

ing infinitesimal changes in all stream properties. The hodograph diagram of Fig. 15.3b is constructed with the rule that the *vector* change in velocity produced by the wave is normal to the wave direction. From the geometry of the figure, noting that du is in the limit the *algebraic* increment in velocity, dV , we get

$$dv = V d\theta$$

$$du = dV$$

$$-du/dv = \tan \alpha = 1/\sqrt{M^2 - 1}$$

Elimination of du and dv from this set of equations yields

$$\frac{1}{V} \frac{dV}{d\theta} = - \frac{1}{\sqrt{M^2 - 1}} \quad (15.1)$$

Now, from the adiabatic relations of Chapter 4, the relation between dV and dM is

$$\frac{dV}{V} = \frac{dM^2}{2M^2 \left(1 + \frac{k-1}{2} M^2 \right)} \quad (15.2)$$

hence Eq. 15.1 may be written

$$d\theta = - \frac{\sqrt{M^2 - 1} dM^2}{2M^2 \left(1 + \frac{k-1}{2} M^2 \right)} \quad (15.3)$$

Integration of this equation by standard methods yields

$$\theta = - \sqrt{\frac{k+1}{k-1}} \arctan \sqrt{\frac{k-1}{k+1} (M^2 - 1)} + \arctan \sqrt{M^2 - 1} + \text{constant} \quad (15.4)$$

It is often more convenient to work with the dimensionless velocity $M^* = V/c^*$ rather than the Mach Number M . Using the adiabatic relation that

$$M^2 = \frac{2}{k+1} M^{*2} / \left(1 - \frac{k-1}{k+1} M^{*2} \right)$$

Eq. 15.4 may be put into the form

$$\theta_I = -\omega(M^*) + 2I - 1000 \quad (15.5)$$

where the function $\omega(M^*)$ is given by

$$\omega(M^*) = \sqrt{\frac{k+1}{k-1}} \arctan \sqrt{\frac{M^{*2} - 1}{\frac{k+1}{k-1} - M^{*2}}} - \arctan \sqrt{\frac{M^{*2} - 1}{1 - \frac{k-1}{k+1} M^{*2}}} \quad (15.6)$$

The constant of integration, denoted by $(2I - 1000)$ in Eq. 15.5, is determined from the initial values of θ and M^* for any particular problem. Why the constant of integration is put in this particular form will be made clear when we discuss waves of two families.

RIGHT-RUNNING WAVE. If we had been dealing with a problem in which there were Mach waves only of family I, the sign on the right-hand side of Eq. 15.1 would have been reversed, and we would have ended with

$$\theta_{II} = +\omega(M^*) + 2II - 1000 \quad (15.7)$$

NOMENCLATURE. The subscript I in the symbol θ_I of Eq. 15.5 signifies that pressure waves of family I are *absent*, that the process occurs at a *constant value* of I, and that changes in flow properties take place as the streamline crosses Mach waves of family II, i.e., as it crosses left-running Mach waves. Similarly for the nomenclature of Eq. 15.7. The rationality of this nomenclature will be made more evident in connection with the later derivation of these same results by the mathematical theory of characteristics.

WORKING CHART. The curves of ω versus M^* and ω versus M , corresponding to Eqs. 15.6 and 15.4, are shown in Fig. 15.4. Since the Mach

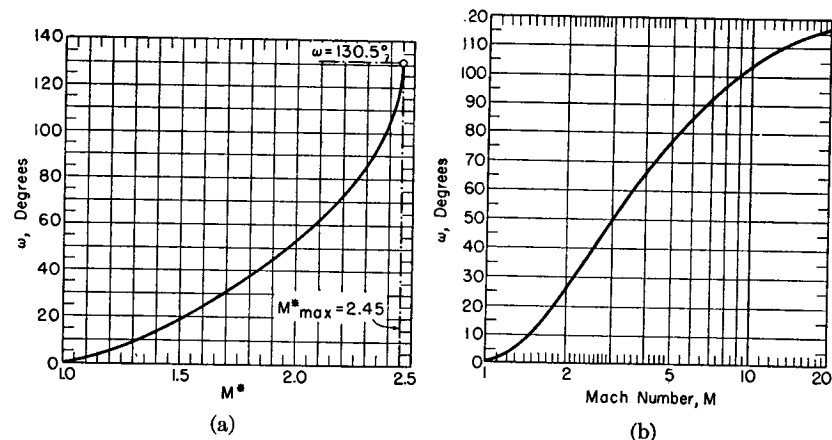


FIG. 15.4. Hodograph characteristic function ($k = 1.4$).

(a) ω versus M^* .
(b) ω versus M .

Number uniquely determines the pressure ratio, temperature ratio, etc., for isentropic flow, it follows that ω is also directly related to the pressure ratio, temperature ratio, etc.

SUMMARY OF CALCULATION RULES. From Eqs. 15.5 and 15.7 we derive the convenient rules of computation,

$$\theta_2 - \theta_1 = -(\omega_2 - \omega_1) \text{ for left-running Mach waves} \quad (15.8a)$$

$$\theta_2 - \theta_1 = \omega_2 - \omega_1 \text{ for right-running Mach waves} \quad (15.8b)$$

TABULATED FUNCTIONS. To facilitate numerical calculations, the relationships between M , M^* and ω are tabulated in Table B.7 for $k = 1.4$. Table B.7 also has certain other isentropic functions of Mach Number which will be found useful.

The argument of this table is the variable ω . It will be seen from subsequent examples that it is convenient to select regular and equal intervals of ω for a problem, corresponding to equal turning angles across each Mach wave.

Example of Simple-Wave Flow. Suppose that in the flow of Fig. 15.1, $M_1 = 2.059$, $\theta_1 = 0$, and $\theta_2 = -5^\circ$. From Fig. 15.4, at $M_1 = 2.059$, we get $\omega_1 = 28.0^\circ$. Then, since only left-running Mach waves are involved, Eq. 15.8a gives $\omega_2 = \theta_1 - \theta_2 + \omega_1 = 0 - (-5) + 28 = 33^\circ$. Then, using Fig. 15.4 again, for $\omega_2 = 33.0^\circ$ we get $M_2 = 2.249$. To find the relation between the pressures in regions 1 and 2, we get, with the help of the isentropic tables,

$$p_2/p_1 = (p/p_0)_2/(p/p_0)_1 = 0.0866/0.1165 = 0.743$$

These exact answers for the problem of Fig. 15.1 will of course be slightly different from the linearized solution described earlier. In the exact solution (Fig. 15.1c), the single pressure wave II_a of the approximate solution (Fig. 15.1a) is replaced by an infinite number of infinitesimal Mach waves lying in the zone between $(II_a)_1$ and $(II_a)_2$, and the streamline undergoes continuous changes as it passes through this zone.

Hodograph Characteristics. If all velocities are divided by c^* , the hodograph diagram becomes dimensionless, with polar coordinates M^* and θ . Then, if Eqs. 15.5 and 15.7, which represent respectively the hodograph streamlines for simple left-running waves and simple right-running waves, are plotted in the hodograph plane, we get the two families of curves of Fig. 15.5. The curves marked I are defined by Eq. 15.5, each curve being identified by a particular value of the constant, I , in Eq. 15.5; similarly for the curves of family II defined by Eq. 15.7. Obviously the two families of curves are mirror images of each other, and any curve of a given family may be found from a single curve of the same family merely by rotating the latter around the origin.

The hodograph curves of family I in Fig. 15.5 are evidently a more exact version of the curve 1'2'3'4'5' of Fig. 15.2b. They are known as the hodograph characteristics. We then have the rule that with simple left-running waves the Mach line at a given point in the physical plane is normal to the hodograph characteristic of family I at the image point

in the hodograph plane; and, with simple right-running waves, the Mach line at a given point is normal to the hodograph characteristic of family II at the image point.

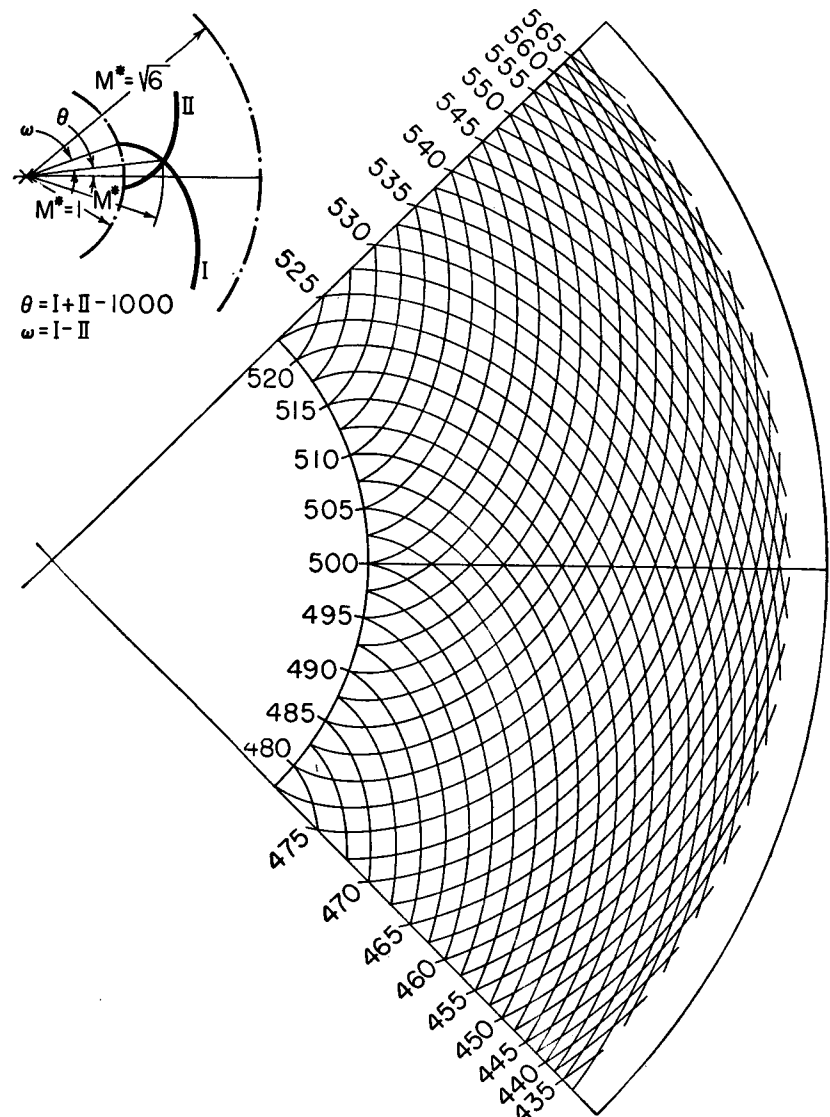


FIG. 15.5. Hodographic characteristic curves on M^* , θ -plane.

For a perfect gas it may be shown that the hodograph characteristic curve on the $M^* - \theta$ plane is an epicycloid formed by rolling on the circle of radius unity another circle of radius $[\sqrt{(k+1)/(k-1)} - 1]$.

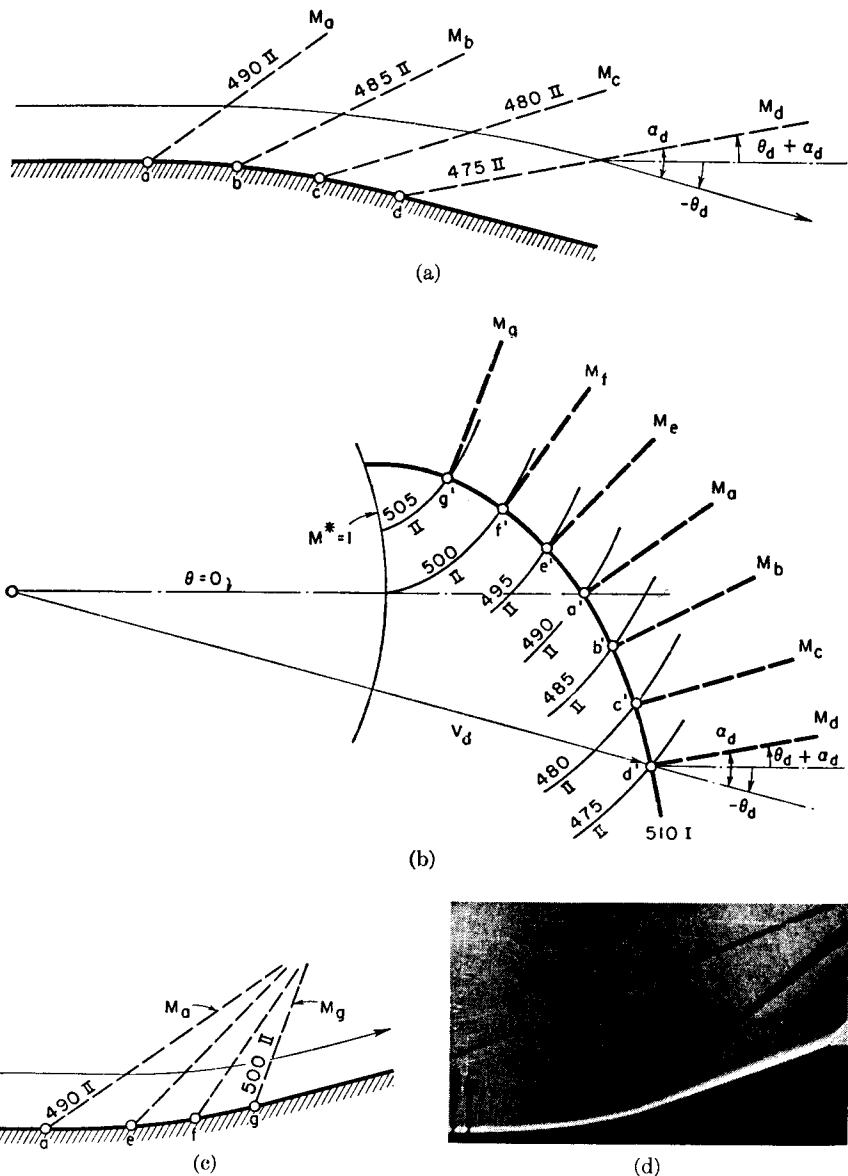


FIG. 15.6. Simple-wave flow past curved wall.

- (a) Left-running expansion waves.
- (b) Hodograph diagram for (a) and (c).
- (c) Left-running compression waves.
- (d) Schlieren photograph showing convergence of simple compression waves (after Drougge). Flow from left to right in concave corner, with wall shaped for centered Prandtl-Meyer compression. Note convergence of Mach lines to form shock, and contact discontinuity (vortex sheet) extending from junction of continuous waves with shock (see Chapter 16).

Features of Simple-Wave Flow. To make the method clear let us consider the flow past the curved wall of Fig. 15.6a. Suppose that the curve begins at point a , and that the flow upstream of a is uniform and parallel, with properties $\theta_a = 0$ and $M_a^* = 1.66$. From these data, point a' may be located in the hodograph diagram of Fig. 15.6b. Then, since the upstream flow was given as uniform and parallel, right-running waves cannot be present, and we are dealing with a case of simple left-running waves. All fluid states must therefore lie on the hodograph characteristic of family I passing through point a' . Points b' , c' , and d' may then be located on this characteristic because the flow directions at points b , c , and d are known. From the values of M^* all other fluid properties may be found at these points. Furthermore, all fluid properties are constant on the Mach lines originating from points a , b , c , and d . The Mach lines themselves are drawn normal to the hodograph characteristic at the appropriate points (Fig. 15.6b), and lie at an angle $(\theta + \alpha)$ to the horizontal. Thus the entire flow field is determined. Each streamline is a transformation of the boundary streamline $abcd$, as the slopes of the streamlines are constant on the Mach lines.

It may be noted from Fig. 15.6a that the Mach lines diverge. This must always be so in an expansive flow: the streamline, from momentum considerations, bends *away* from the Mach line, and, moreover, the Mach angle becomes smaller; hence the Mach lines necessarily diverge. Mathematically, since the left-running Mach wave is at the counter-clockwise angle α to the velocity direction, and the latter is at the angle θ to the horizontal, the Mach wave is inclined at the angle $(\theta + \alpha)$ to the horizontal. In the flow of Fig. 15.6a, both θ and α decrease, and the Mach lines therefore diverge. The pressure gradients for streamlines far from the wall are consequently smaller than for those near the wall.

Conversely, as in Fig. 15.6c, the Mach lines always converge for a simple-wave compressive flow. This gives rise to compression shocks (Fig. 15.6d), as explained in Chapter 16.

Fig. 15.7 shows examples of right-running simple waves of both expansion and compression type. Note that whereas the left-running Mach lines are inclined at the angle $(\theta + \alpha)$, measured counter-clockwise, the right-running Mach lines lie at the angle $(\theta - \alpha)$, measured counter-clockwise.

Many different simple-wave flow patterns may have the same image in the hodograph diagram. For example, Fig. 15.8 shows the flows along three curved walls, all with the same initial Mach Number, and all of which are represented by the same hodograph characteristic. At each point of each wall the flow properties are determined uniquely by the streamline direction, and these flow properties are propagated out from the wall along the corresponding Mach lines.

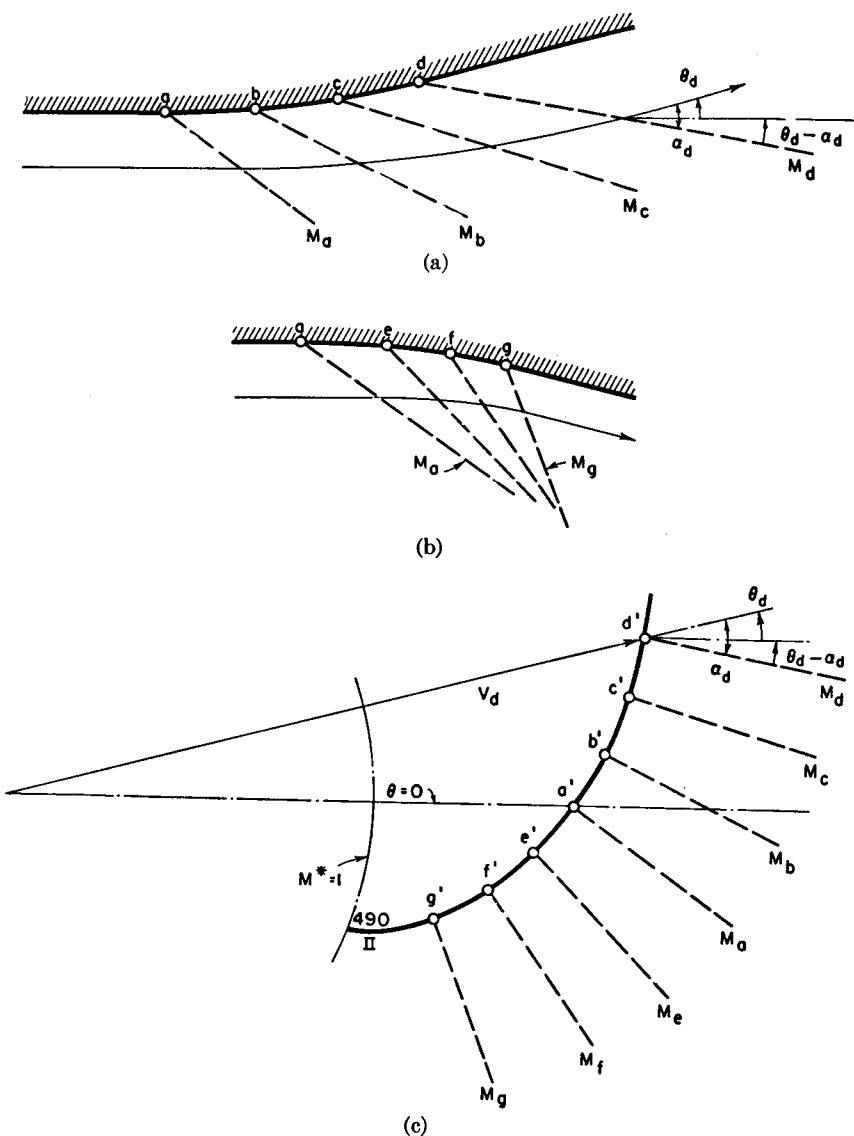


FIG. 15.7. Right-running simple-wave flow.

- (a) Expansion waves.
- (b) Compression waves.
- (c) Hodograph diagram.

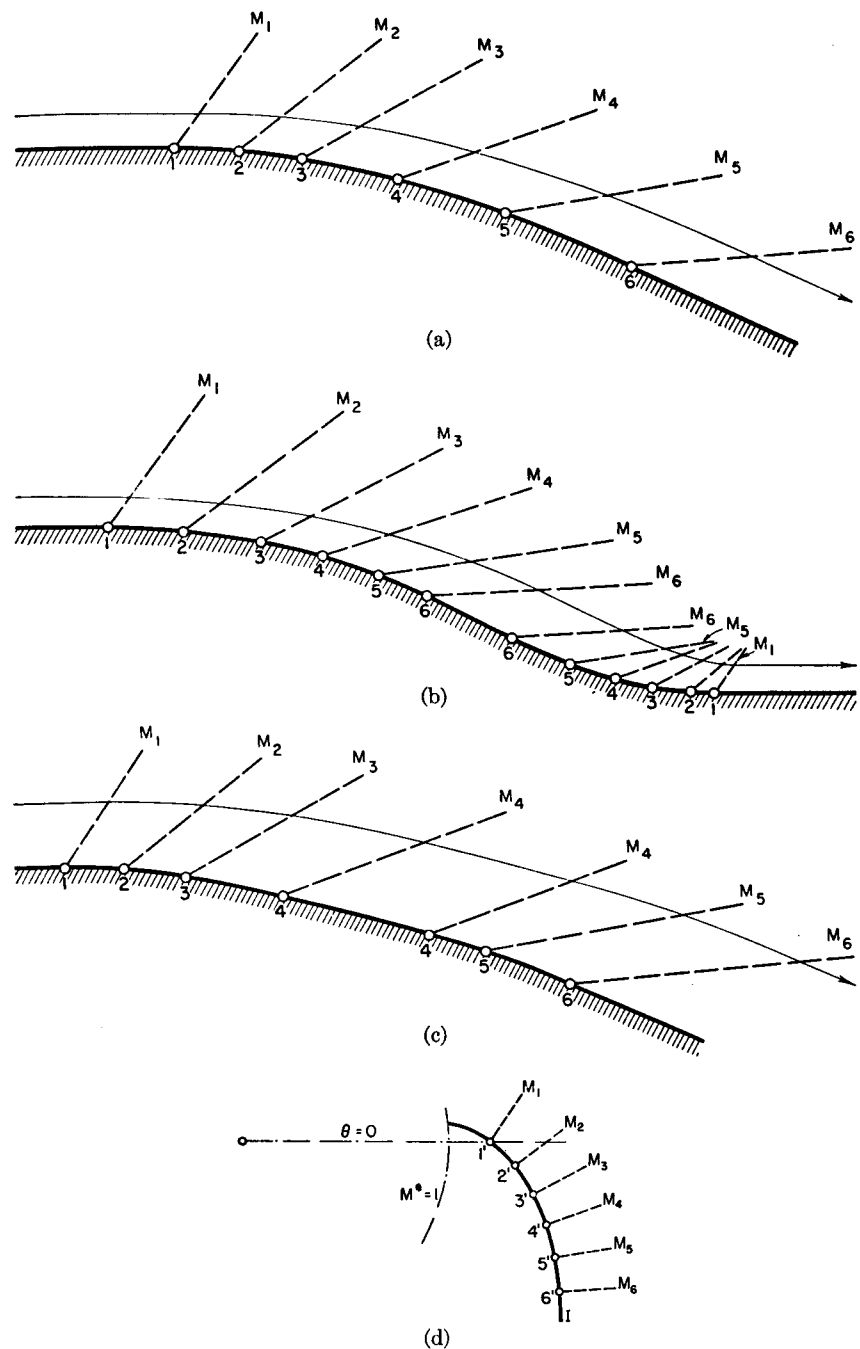


FIG. 15.8. Three simple-wave flows represented by the same hodograph characteristic.

- (a, b, c) Physical plane.
- (d) Hodograph plane.

Centered Waves. A special but important case of simple-wave flow is that in which the streamlines are so shaped that all the Mach lines pass through a common point O (Fig. 15.9a). In Fig. 15.9b is shown a special case of this special case, of even greater practical importance, in which the boundary streamline itself passes through the center O . Either of these is a flow with *centered simple waves*, and is often called

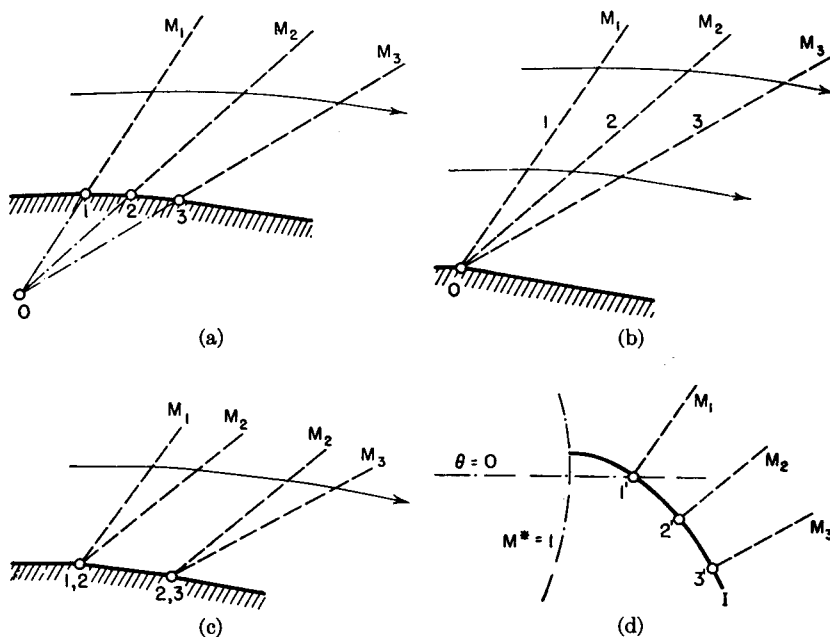


FIG. 15.9. Centered simple waves.

corner-type flow, or *Prandtl-Meyer flow*. The corner-type flow is characterized by the rules that (i) all flow properties are uniform on straight rays emanating from the corner, and (ii) these rays make the local Mach angle to the local flow direction.

A peculiarity of corner-type flow is that it incorporates a rarefaction shock at the corner. However, this rarefaction discontinuity is confined to a singular point, and hence there is no violation of the Second Law of Thermodynamics. As the rarefaction wave propagates outward from the corner, along the Mach lines, it becomes less steep, in accordance with the considerations of Chapter 5.

A *complete simple-wave flow* is one in which the Mach Number goes from unity to infinity. Fig. 15.10c shows the hodograph representation of a complete simple wave, and Fig. 15.10a shows the wave and streamline patterns if this complete simple-wave flow is of Prandtl-Meyer type.

From Eq. 15.6, for $k = 1.4$, $\omega = 130.5^\circ$ at M^*_{\max} . It follows from Eq.

15.8 that the maximum possible turning angle of the flow is also 130.5° . With this turning angle the stream would expand to zero pressure and temperature. Since $\alpha_1 = 90^\circ$ and $\alpha_2 = 0$, the tangent to the hodograph characteristic is along the radius at the $M^* = 1$ circle, and is normal to the radius at the M^*_{\max} circle (Fig. 15.10c). This may also be deduced from Eq. 15.3.

Query: what is the flow pattern when a flow with Mach Number unity approaches a corner which turns through an angle of more than 130.5° ,

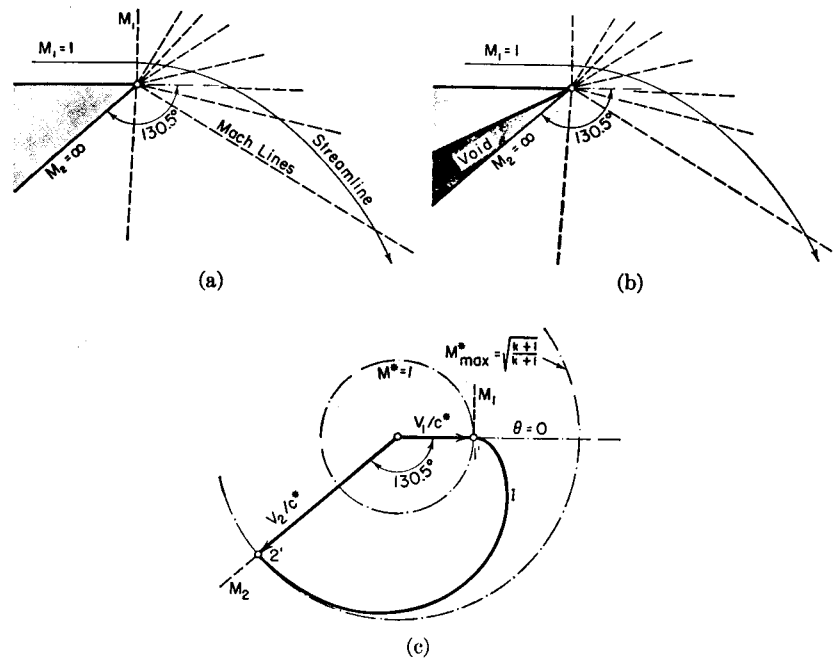


FIG. 15.10. Complete simple wave.

as in Fig. 15.10b? The flow is at zero pressure when it has expanded through 130.5° , hence there will be a void, or *cavitation region*, adjacent to the wall. This solution, however, is at best only indicative. At very low temperatures the thermodynamic properties may be very different from that of a perfect gas, especially if liquefaction occurs. At very low pressures, moreover, the assumption of a continuum is not realistic, and, in order to get meaningful theoretical results, it is necessary to employ the kinetic theory of gases.

Streamline Shapes. Suppose that in Fig. 15.11a we have simple-wave flow along a curved wall, and that we let h denote the distance, measured along the Mach line, between a point on the wall and a point on a certain streamline. Then the distance h^* is proportional to the minimum cross-

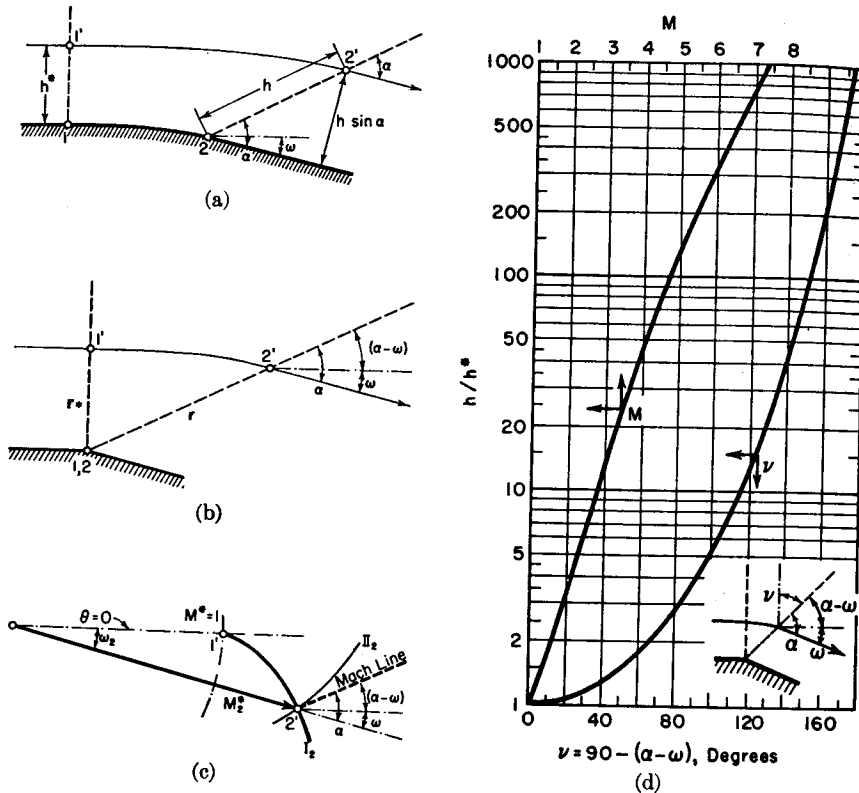


FIG. 15.11. Construction of streamlines for simple wave.

- (a) Noncentered simple wave.
- (b) Centered simple wave.
- (c) Hodograph diagram.
- (d) Chart for facilitating construction of streamlines.

sectional area for isentropic flow, and the distance $h \sin \alpha$ is proportional to the cross-sectional area for flow at any other section. We may therefore write

$$(h \sin \alpha)/h^* = A/A^*$$

where A/A^* is the area ratio for isentropic one-dimensional flow, related to the Mach Number by the formula (Chapter 4)

$$\frac{A}{A^*} = \frac{1}{M} \sqrt{\left[\frac{2}{k+1} \left(1 + \frac{k-1}{2} M^2 \right) \right]^{\frac{k+1}{k-1}}}$$

Then, since $\sin \alpha = 1/M$, we get

$$\frac{h}{h^*} = \sqrt{\left[\left(\frac{2}{k+1} \right) \left(1 + \frac{k-1}{2} M^2 \right) \right]^{\frac{k+1}{k-1}}} \quad (15.9)$$

The Mach Number at any point on the wall is uniquely determined by Eq. 15.8a, and the Mach lines for this case, wherein $\theta = -\omega$, are at the angle $(\alpha - \omega)$ to the horizontal. Since $(\alpha - \omega)$ depends only on M , for each point on the wall streamline there may be plotted with the help of Eq. 15.9 a corresponding point on any other streamline. Thus the entire streamline pattern is easily determined.

If the initial flow is not at Mach Number unity, the Mach line lies at the angle $[\alpha_2 - (\omega_2 - \omega_1)]$ to the initial direction, and the distances between streamlines, measured along the Mach lines, are related by

$$\frac{h_2}{h_1} = \frac{M_2}{M_1} \frac{(A/A^*)_2}{(A/A^*)_1} \quad (15.10)$$

The latter relation is most conveniently evaluated with the isentropic tables, and is plotted in Fig. 15.11d.

When the simple-wave flow is of Prandtl-Meyer type, as in Fig. 15.11b, we have

$$\frac{r}{r^*} = \frac{h}{h^*} = \sqrt{\left(\frac{2}{k+1} \right) \left(1 + \frac{k-1}{2} M^2 \right)^{\frac{k+1}{k-1}}} \quad (15.11)$$

and the streamlines are easily plotted with r and $(\alpha - \omega)$ as polar coordinates.

15.3. Flow with Waves of Both Families by Extension of Linear Theory

Modified Linear Theory. When waves of both families are present in a problem, it is in general not possible to obtain an analytical solution. However, a simple stepwise method may be devised which is founded on the physical fact that changes in fluid properties in a supersonic flow may be conceived as being brought about by pressure waves propagated along the Mach lines of the flow.

The underlying idea is to imagine, for purposes of calculation, that the physical flow plane is divided into many small regions, in each of which all flow properties, including velocity, direction, pressure, etc., are considered constant. Considering two of these adjacent regions, or *fields*, which differ only slightly in properties, the linearized theory of Chapter 14 may be applied to the changes in fluid properties as a streamline crosses from one field to the next. Now the linear theory shows that the changes in properties occur as the streamline crosses a Mach line, hence it follows that in general each field is a quadrilateral bounded either by Mach lines or by physical boundaries. Occasionally the *Mach quadrilateral* takes on the limiting form of a triangle, as will be seen in subsequent examples.

Practical problems are then solved by constructing the wave pattern which fits the given boundary conditions. The calculations are worked out from field to field in stepwise fashion, using the linear theory for each step in which a streamline passes from one field into another across a Mach wave. In applying the linear theory to each Mach wave, we employ the mean Mach Number between the two fields and draw the Mach line at the mean Mach angle to the mean flow direction.

Use of Hodograph Characteristics. The type of calculation outlined above is facilitated by the use of the hodograph characteristic curves of Fig. 15.5. From the analysis of the preceding article, we may set down the following rules for using the hodograph chart:

- (i) When a streamline *crosses* a left-running wave (Mach wave of family II), the hodograph of the streamline (that is, the point in the hodograph plane representing the end point of the velocity vector) moves along a hodograph characteristic of family I . The Mach line is normal to the hodograph characteristic of family I , and lies at the angle $(\theta + \alpha)$ to the horizontal.
- (ii) When a streamline *crosses* a right-running wave (Mach wave of family I), the hodograph of the streamline moves along a hodograph characteristic of family II . The Mach line is normal to the hodographic characteristic of family II , and lies at the angle $(\theta - \alpha)$ to the horizontal.

Each of the hodograph characteristic curves is identified by a particular value of I and II . These values may be thought of as curvilinear coordinates in the hodograph plane (mathematically they are the *characteristic coordinates*), and may be used in place of M^* and θ to specify the velocity vector. At a given point in the hodograph plane, Eqs. 15.5 and 15.7 may be written:

$$1000 + \omega + \theta = 2I \quad (15.12a)$$

$$1000 - \omega + \theta = 2II \quad (15.12b)$$

First subtracting and then adding this pair of simultaneous equations, we get

$$\theta = I + II - 1000 \quad (15.13a)$$

$$\omega = I - II \quad (15.13b)$$

Thus, given θ and ω , I and II may be found from Eqs. 15.12. Or, conversely, given I and II , θ and ω may be found from Eqs. 15.13. The latter relations show also that in the hodograph plane, radial lines (lines of constant flow direction) through the origin are lines of constant $(I + II)$, whereas concentric circles (circles of constant velocity and pressure) are lines of constant $(I - II)$.

Illustration of Method. The calculation procedure can best be described with the help of a specific example. Let us consider underexpanded air flow at the exit of a two-dimensional nozzle, the linearized solution for which was given in Fig. 14.23b. From symmetry considerations, the middle streamline must be straight, and may be replaced by a wall (Fig. 15.12a), thus halving the calculations.

Suppose that at the nozzle exit, in field 1, $M_1 = 1.4349$, $\theta_1 = 0$, and $p_1 = 100$. Also, suppose that the surrounding pressure is 60.45.

From Table B.7 we get $\omega_1 = 10.0^\circ$ and $(p/p_0)_1 = 0.2991$. Furthermore, from Eqs. 15.12, we get $I_1 = 505$ and $II_1 = 495$.

Now the boundary of the free jet must be everywhere at a pressure of 60.45. The sudden drop in pressure at corner A from 100 to 60.45 can only take place in an expansive corner-type flow. If 3 is the state after the corner flow, we have

$$p_3/p_0 = (p_1/p_0)(p_3/p_1) = (0.2991)(0.6045) = 0.1808$$

Hence, from Table B.7, $\omega_3 = 20^\circ$. Then, since states 1 and 3 lie on a common I -characteristic, we have $I_3 = I_1 = 505$. Eqs. 15.12 and 15.13 then give $\theta_3 = -10^\circ$ and $II_3 = 485$. Thus, there is a 10° deflection of the jet boundary as it leaves the nozzle.

All the details of the corner flow between fields 1 and 3 are known analytically from the simple-wave formulas of the preceding article. Subsequently, when waves of both families are present, however, only stepwise methods can be used. Therefore, we replace the actual Prandtl-Meyer continuous expansion by a number of individual Mach waves into which the actual changes of state are lumped. For the sake of illustration, we have here substituted two individual waves, a and b , for the actual corner flow. Assuming equal angles of turn across each of these waves, we have $\theta_2 = \theta_3/2 = -5^\circ$ and $I_2 = I_1 = 505$. Then $\omega_2 = 15.0$ and $II_2 = 490$.

Points 1', 2', and 3' may be spotted in the hodograph diagram of Fig. 15.12b. Wave a is then drawn in the direction a' , i.e., normal to the hodograph characteristic of family I at the mean conditions between fields 1 and 2. Similarly, wave b is drawn in the direction b' , normal to the hodograph characteristic of family I at the mean conditions between fields 2 and 3.

When wave a strikes the upper wall, it must be reflected as wave c in order to have the flow follow the upper wall. If the region downstream of wave c is called field 4, we have $\theta_4 = 0$ and $II_4 = II_2 = 490$. Hence $I_4 = 510$ and $\omega_4 = 20.0$. Wave c is now drawn in the direction c' , normal to the hodograph characteristic of family II at the mean conditions between fields 2 and 4. The intersection of wave c with wave b defines one corner of the Mach quadrilateral for field 2.

Now assume that wave b is continued as wave d , and that wave c is continued as wave e , and that they partially bound field 5. But field 5 is reached from field 4 along a characteristic of family I , and is reached from field 3 along a characteristic of family II . Therefore $I_5 = I_4 = 510$, and $II_5 = II_3 = 485$, whence $\omega_5 = 25.0$ and $\theta_5 = -5.0$. Waves e and d are now drawn with the respective directions e' and d' .

What happens when wave e strikes the free boundary of the jet? Since field 5 has a lower pressure than the surroundings, wave e must be reflected in the form of wave g to preserve the boundary condition of constant pressure. If the field

downstream of wave g is 7, we have $\omega_7 = \omega_3 = 20.0$ and $I_7 = I_5 = 510$, whence $II_7 = 490$ and $\theta_7 = 0$. Wave g may now be drawn with the direction g' , which, incidentally, coincides with the direction d' . The lower side of field 7 is the jet boundary, which is drawn with the appropriate streamline direction $\theta_7 = 0$.

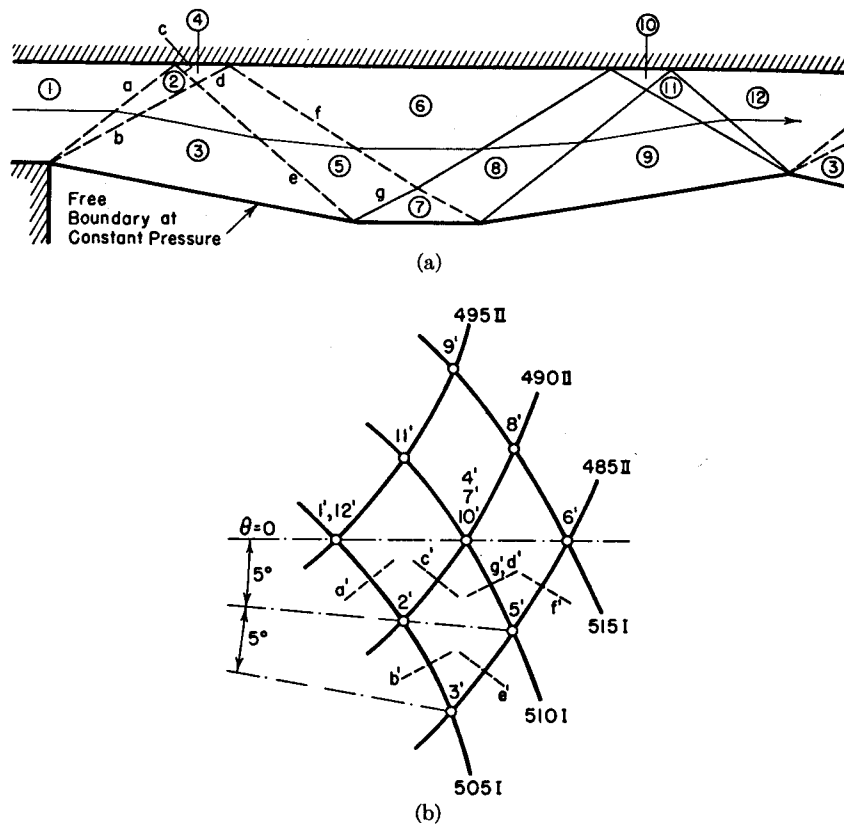


FIG. 15.12. Flow at exit of underexpanded nozzle.

- (a) Physical plane. Full lines signify compression waves; dashed lines signify expansion waves.
 - (b) Hodograph diagram.

The remainder of the flow pattern may now be constructed by applying successively the various methods outlined above. If an expansion wave is denoted as one across which the pressure on a streamline decreases in the direction of flow, and conversely for a compression wave, in Fig. 15.12a expansion waves are shown by dashed lines and compression waves by full lines. Various streamlines may also be drawn from the known flow direction in each field, and the pressure distribution plotted from the known Mach Numbers in each field.

The various properties in each field are summarized in the "Table for Fig. 15.12b." For each field, two of the four properties I , II , ω , and θ are underlined, thereby indicating the two properties in that field which are found first. The

remaining two properties in each field are of course found from the two underlined ones either algebraically from Eqs. 15.12 and 15.13, or graphically from Fig. 15.12b.

TABLE FOR FIG. 15.12a

Wave	Up-stream ($\theta + \alpha$)	Down-stream ($\theta + \alpha$)	Mean ($\theta + \alpha$)	Up-stream ($\theta - \alpha$)	Down-stream ($\theta - \alpha$)	Mean ($\theta - \alpha$)
<i>a</i>	44.2	33.6	38.9			
<i>b</i>	33.6	24.3	29.0			
<i>c</i>						
<i>d</i>	34.3	25.8	30.0	-43.6	-34.3	-39.0
<i>e</i>				-44.3	-35.8	-40.0
<i>f</i>				-35.8	-28.0	-31.9
<i>g</i>	25.8	34.3	30.0			
6-8	28.0	35.8	31.9			
7-8				-34.3	-25.8	-30.0
8-9	35.8	44.3	40.0			
8-10				-25.8	-34.3	-30.0
10-11	34.3	43.6	39.0			
9-11				-24.3	-33.6	-29.0
11-12				-33.6	-44.2	-38.9

TABLE FOR FIG. 15.12b

Field	<i>I</i>	<i>II</i>	ω	θ	α	$\theta + \alpha$	$\theta - \alpha$	p/p_0
1	505	495	10.0°	0°	44.18°	44.2°	-44.2°	0.2991
2	505	490	15.0	-5	38.55	33.6	-43.6	.2334
3	505	485	20.0	-10	34.29	24.3	-44.3	.1808
4	510	490	20.0	0	34.29	34.3	-34.3	.1808
5	510	485	25.0	-5	30.85	25.8	-35.8	.1381
6	515	485	30.0	0	27.95	28.0	-28.0	.1037
7	510	490	20.0	0	34.29	34.3	-34.3	.1808
8	515	490	25.0	5	30.85	35.8	-25.8	.1381
9	515	495	20.0	10	34.29	44.3	-24.3	.1808
10	510	490	20.0	0	34.29	34.3	-34.3	.1808
11	510	495	15.0	5	38.55	43.6	-33.6	.2334
12	505	495	10.0	0	44.18	44.2	-44.2	.2991

The table also shows in each field the direction $(\theta + \alpha)$ for left-running waves, and $(\theta - \alpha)$ for right-running waves. These may be combined as in the "Table for Fig. 15.12a" to get the inclinations of each wave. With the help of this table, Mach wave directions may be determined without graphical operations in the hodograph plane.

15.4. Application of Theory of Characteristics

The calculation method of the preceding article is based largely on the physical concept of pressure waves being propagated at the Mach angle to the flow. We shall now show that the procedure has a rigorous analytical foundation which clarifies the significance and range of validity of the calculation procedure usually termed the *method of characteristics*.

Differential Equation of the Velocity Potential. The physical conditions of a two-dimensional, steady, isentropic, irrotational flow are expressed mathematically by the differential equation of the velocity potential (see Chapter 10)

$$(c^2 - \varphi_x^2)\varphi_{xx} - 2\varphi_x\varphi_y\varphi_{xy} + (c^2 - \varphi_y^2)\varphi_{yy} = 0 \quad (15.14)$$

where u and v , which are respectively the x - and y -components of the velocity vector, are given by

$$u = \varphi_x; \quad v = \varphi_y \quad (15.15)$$

and the local sound velocity, c , is related to the derivatives of the potential by the energy equation,

$$c^2 = c_0^2 - \frac{k-1}{2}(\varphi_x^2 + \varphi_y^2) \quad (15.16)$$

Definition of the Characteristic Curves. Our problem now is to find solutions to Eq. 15.14 satisfying given boundary conditions. This differential equation is of the general type

$$A\varphi_{xx} + 2B\varphi_{xy} + C\varphi_{yy} = D \quad (15.17)$$

where the coefficients A , B , C , and D are functions generally of x , y , φ_x , and φ_y . Differential equations of this type are investigated in some detail in Appendix A, where it is shown that on the $\varphi(x, y)$ surface representing in φ , x , y -space the solution of Eq. 15.17, there lie certain *characteristic curves*, so called, having special properties, namely:

- Real characteristic curves exist for supersonic, but not subsonic flow.
- The characteristic curves satisfy the differential equation, Eq. 15.14, and hence may represent solutions of this differential equation.
- On the characteristic curves there may be discontinuities in the *derivatives* of the fluid properties. Regions of flow which are analytically different may therefore be joined or *patched* on the characteristics, the sole requirement being that there be no discontinuities in the fluid properties themselves on the patching lines.

The characteristic curves of Eq. 15.14, as developed in Appendix A, are defined by two pairs of simultaneous, ordinary differential equations of first order:

$$\left(\frac{dy}{dx}\right)_I = \frac{B + \sqrt{B^2 - AC}}{A} \quad (15.18)$$

$$\left(\frac{dy}{dx}\right)_{II} = \frac{B - \sqrt{B^2 - AC}}{A} \quad (15.18)$$

$$\left(\frac{d\varphi_y}{d\varphi_x}\right)_I = -\frac{B + \sqrt{B^2 - AC}}{C} + \frac{D}{C}\left(\frac{dy}{d\varphi_x}\right)_I \quad (15.19)$$

$$\left(\frac{d\varphi_y}{d\varphi_x}\right)_{II} = -\frac{B - \sqrt{B^2 - AC}}{C} + \frac{D}{C}\left(\frac{dy}{d\varphi_x}\right)_{II} \quad (15.19)$$

The Characteristic Curves for Two-Dimensional, Supersonic Flow. Comparing Eq. 15.17 with Eq. 15.14, we see that

$$A = c^2 - u^2; \quad B = -uv; \quad C = c^2 - v^2; \quad D = 0$$

Substituting these coefficients into Eqs. 15.18 and 15.19 we obtain, after some rearrangement,

$$\left(\frac{dy}{dx}\right)_{I, II} = \frac{-\frac{uv}{c^2} \pm \sqrt{\frac{u^2 + v^2}{c^2} - 1}}{1 - \frac{u^2}{c^2}} \quad (15.20)$$

$$\left(\frac{dv}{du}\right)_{I, II} = \frac{\frac{uv}{c^2} \mp \sqrt{\frac{u^2 + v^2}{c^2} - 1}}{1 - \frac{v^2}{c^2}} \quad (15.21)$$

Eq. 15.20 defines two characteristic directions at each point in the physical plane. These directions give the slopes of the physical characteristics at each point. Likewise, Eq. 15.21 defines the slopes of the corresponding pair of hodograph characteristics at the hodograph image point of each physical point. Shortly we shall see how these two sets of differential equations taken together permit, in effect, numerical solutions of the original Eq. 15.14 to be carried out.

It is evident from Eqs. 15.20 and 15.21 that for two-dimensional, steady, irrotational, isentropic flow the characteristic curves are real only for supersonic flow, that is, only when

$$u^2 + v^2 > c^2, \text{ or } V^2 > c^2$$

The Physical Characteristics as Mach Lines. We shall now show that the physical characteristics are inclined at the local Mach angle to the local velocity vector. Using polar coordinates V and θ for the hodograph plane, we have

$$u = V \cos \theta; \quad v = V \sin \theta \quad (15.22)$$

Introducing these into Eq. 15.20, remembering that $V/c = M$, and that $M = 1/\sin \alpha$ and $\sqrt{M^2 - 1} = 1/\tan \alpha$, we get

$$\left(\frac{dy}{dx}\right)_{I, II} = \frac{-\frac{\cos \theta \sin \theta}{\sin^2 \alpha} \pm \frac{1}{\tan \alpha}}{1 - \frac{\cos^2 \theta}{\sin^2 \alpha}}$$

After considerable rearrangement and simplification with the help of the customary trigonometric identities, this becomes

$$(dy/dx)_I = \tan(\theta - \alpha); \quad (dy/dx)_{II} = \tan(\theta + \alpha) \quad (15.23)$$

Referring to Fig. 15.13, Eq. 15.23 shows that each of the two physical characteristics is inclined at the Mach angle to the velocity vector, and that the streamline direction at a point in the physical plane bisects the characteristic directions at that point. Thus we see that the physical

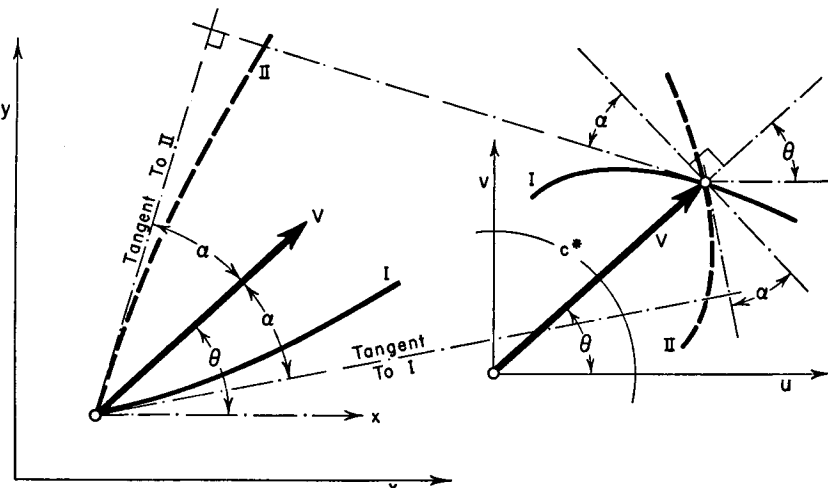


FIG. 15.13. Geometry of physical and hodograph characteristics.

characteristics are identical with the Mach lines of the flow. The left-running Mach lines are physical characteristics of family *II* and the right-running Mach lines are physical characteristics of family *I*.

These results may be seen even more easily by arbitrarily placing the x -axis parallel to the velocity vector at a given point in the flow field. At that point we would have $u = V$, $v = 0$, $M = V/c$, and $\theta = 0$; Eq. 15.20 then becomes

$$\left(\frac{dy}{dx}\right)_{I, II} = \frac{\pm \sqrt{\frac{V^2}{c^2} - 1}}{1 - \frac{V^2}{c^2}} = \mp \frac{1}{\sqrt{M^2 - 1}} = \mp \tan \alpha$$

Since, at the point in question, the velocity vector coincides with the x -axis, we conclude that the physical *I*-characteristic lies at the Mach angle below the velocity vector and the physical *II*-characteristic lies at the Mach angle above the velocity vector.

Orthogonality Relations Between Physical and Hodograph Characteristics. It may be verified by algebraic simplification, using Eqs. 15.20 and 15.21, that

$$\left(\frac{dy}{dx}\right)_I \left(\frac{dv}{du}\right)_{II} = -1; \quad \left(\frac{dy}{dx}\right)_{II} \left(\frac{dv}{du}\right)_I = -1 \quad (15.24)$$

which means that *the physical characteristic of one family is normal to the hodograph characteristic of opposite family*. This rule of reciprocal orthogonality between the hodograph and physical characteristics is illustrated schematically in Fig. 15.13, and may be used to advantage for graphical solutions.

Equations of the Hodograph Characteristics. The characteristic curves for any particular problem are found by simultaneous integration of Eqs. 15.20 and 15.21. Once these curves are established, the entire problem is solved, for the characteristic curves relate points in the physical plane to points in the hodograph plane, and hence the Mach Number and flow direction may be found for each point of the physical flow field.

Now Eq. 15.20 shows that the differential equation of the physical characteristics contains velocity terms, and must therefore be solved simultaneously with the differential equation of the hodograph characteristics. Quite differently, however, the differential equation (Eq. 15.21) of the hodograph characteristics contains only velocity terms, and may therefore be integrated in advance of any specific physical problem to give a set of universal hodograph characteristics which are independent of the flow pattern in the physical plane.

In obtaining the universal set of hodograph characteristics, it is convenient to employ polar coordinates, V, θ , rather than Cartesian coordinates u, v . Applying the transformation of Eq. 15.22 to Eq. 15.21, we get after algebraic manipulation,

$$\frac{1}{V} \left(\frac{dV}{d\theta} \right)_{I, II} = \mp \frac{1}{\sqrt{M^2 - 1}} = \mp \tan \alpha \quad (15.25)$$

An even simpler method of getting Eq. 15.25 is to use the rule which states that the normal to the hodograph I -characteristic lies at the angle $+\alpha$ to the velocity vector, while that for the II -characteristic lies at the angle $-\alpha$. Applying this rule to the graphical construction of Fig. 15.14,

Eq. 15.25 becomes immediately evident.

Eq. 15.25 is seen to be identical with Eq. 15.1. Therefore, making the substitution of Eq. 15.2, and carrying out the integration of Eq. 15.3, we arrive at

$$\theta_I = -\omega(M^*) + 2I - 1000 \quad (15.26a)$$

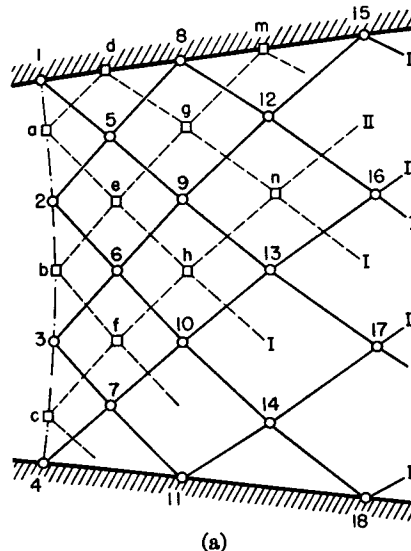
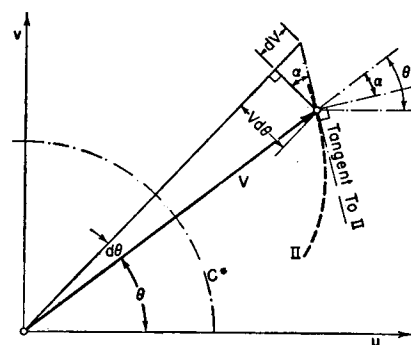
$$\theta_{II} = +\omega(M^*) + 2II - 1000 \quad (15.26b)$$

Fig. 15.14. Geometrical interpretation of the differential equation of the hodograph characteristics.

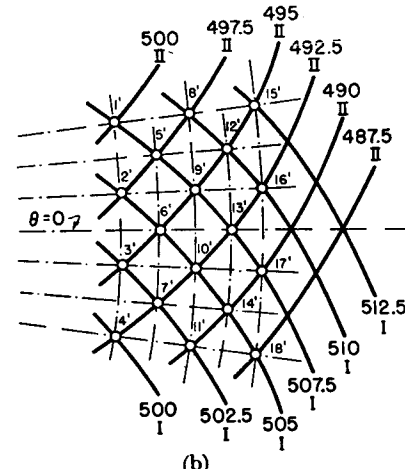
where $\omega(M^*)$ is given by Eq. 15.6 and Fig. 15.4. Obviously Eqs. 15.26, representing the hodograph characteristic curves, are identical with Eqs. 15.5 and 15.7. The two families of curves of Fig. 15.5 are in fact the unique set of hodograph characteristics which apply to any problem of two-dimensional, supersonic, irrotational, isentropic flow. The symbols I and II are the characteristic coordinates, related to the state coordinates, ω and θ , through Eqs. 15.12 and 15.13.

Example of Construction of Characteristics Nets. It has already been pointed out that, as a consequence of the special properties of the characteristic curves, the original problem of finding a solution $\varphi(x, y)$ of Eq. 15.14 for given initial conditions is replaced by the equivalent problem of constructing in the physical and hodograph planes the characteristic curves of Eqs. 15.20 and 15.21. In a sense this procedure gives the desired kinds of answers more directly, because it is the velocity vector rather than the velocity potential which is of interest.

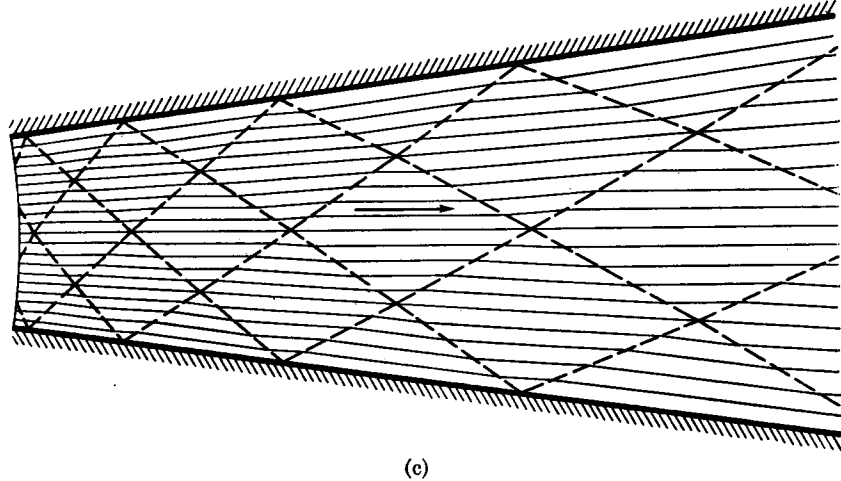
The hodograph characteristics for all problems are given by Eq. 15.26. To solve problems having specific physical boundary conditions, we construct stepwise in the physical plane a characteristics net of whatever degree of fineness is necessary to obtain the desired accuracy.



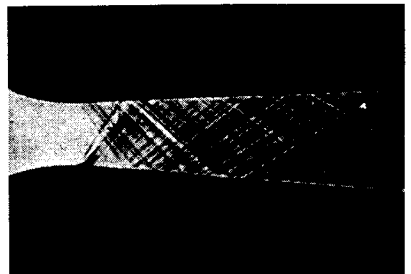
(a)



(b)



(c)



(d)

FIG. 15.15. Source flow.

- (a) Physical plane. Solid lines and circles refer to lattice-point method. Dashed lines and squares refer to field method.
- (b) Hodograph diagram for (a).
- (c) Streamlines and Mach waves.
- (d) Schlieren photograph of flow in two-dimensional nozzle with straight diverging walls. The Mach lines are made visible by small roughnesses on the nozzle walls (after Busemann).

To illustrate the method, let us discuss the problem of a two-dimensional source flow (Fig. 15.15). The exact solution to this simple problem is known from one-dimensional considerations, and hence the only practical purpose of solving the problem by the method of characteristics, other than for illustrative purposes, is to investigate the effect of the fineness of the characteristics net on the accuracy of the stepwise numerical solution.

We shall assume that we are given the straight, solid boundaries 1-8-15 and 4-11-18, inclined at an angle of 15° to each other, and that along the circular arc 1-2-3-4 the flow is radial and has a constant Mach Number of 1.348, corresponding to a constant value of $\omega = 7.5^\circ$.

We begin by choosing the evenly spaced net points 1, 2, 3, and 4 along the initial-value curve, thus arbitrarily determining the fineness of the net. Since ω and θ are known at each of these points, the corresponding values of I and II may be computed from Eqs. 15.12 and 15.13 and entered into the attached table; or, graphically, the image points $1'$, $2'$, $3'$, and $4'$ may be located in the hodograph diagram, Fig. 15.15b. Of the four interconnected quantities I , II , ω , and θ , of which two are independent and two dependent, those two which are found first at each net point are underlined in the table.

TABLE FOR FIG. 15.15b

Lattice Point	I	II	ω	θ	α	$\theta + \alpha$	$\theta - \alpha$	p/p_0
1	507.5	500.0	7.5°	7.5°	47.9°	55.4°	-40.4°	0.338
2	505.0	497.5	7.5	2.5	47.9	50.4	-45.4	.338
3	502.5	495.0	7.5	-2.5	47.9	45.4	-50.4	.338
4	500.0	492.5	7.5	-7.5	47.9	40.4	-55.4	.338
5	507.5	497.5	10.0	5.0	44.2	49.2	-39.2	.422
6	505.0	495.0	10.0	0	44.2	44.2	-44.2	.422
7	502.5	492.5	10.0	-5.0	44.2	39.2	-49.2	.422
8	510.0	497.5	12.5	7.5	41.1	48.6	-33.6	.387

TABLE FOR FIG. 15.15a

Wave *	Up-stream ($\theta + \alpha$)	Down-stream ($\theta + \alpha$)	Mean ($\theta + \alpha$)	Up-stream ($\theta - \alpha$)	Down-stream ($\theta - \alpha$)	Mean ($\theta - \alpha$)
1-5				-40.4	-39.2	-39.8
2-5	50.4	49.2	49.8			
2-6				-45.4	-44.2	-44.8
3-6	45.4	44.2	44.8			
3-7				-50.4	-49.2	-49.8
4-7	40.4	39.2	39.8			
(1-8)	(7.5)	(7.5)	(7.5)			
5-8	49.2	48.6	48.9			

* Items in parentheses refer to segments of flow boundary, and θ rather than $\theta \pm \alpha$ is tabulated.

Since the hodograph characteristics are known to begin with, points $5'$, $6'$, and $7'$ may be located immediately in the hodograph plane by means of the hodograph characteristics passing through $1'$, $2'$, $3'$, and $4'$. Or, since the values of I and II for $5'$, $6'$, and $7'$ are determined by the values of I and II for $1'$, $2'$, $3'$, and $4'$ (e.g., $I_5 = I_1$ and $II_5 = II_1$), Eqs. 15.12 and 15.13 may be used for filling in the values of ω and θ in the attached table.

To find point 5 in the physical plane, the physical I -characteristic 1-5 is drawn normal to the hodograph II -characteristic at the mean conditions between $1'$ and $5'$. Similarly the physical II -characteristic 2-5 is drawn normal to the hodograph I -characteristic at the mean conditions between $2'$ and $5'$. The intersection of the two physical characteristics establishes the location of point 5. If it is not desired to use the hodograph curves, wave 1-5 may be laid off at the appropriate mean inclination ($\theta - \alpha$), and wave 2-5 at the appropriate mean inclination ($\theta + \alpha$); these inclinations are shown in the attached table.

In locating points 8 and $8'$, we note that point 8 is on the physical boundary and that the velocity direction at $8'$ is known. This, together with the fact that 8 lies on the II -characteristic passing through 5, establishes points 8 and $8'$. Points 11 and $11'$ are found in the same way.

By continuing this process, the characteristics nets are established in both planes. In the physical plane of Fig. 15.15a they are shown as solid lines connected by small circles at the net points.

Figs. 15.15c and 15.15d show that the Mach wave pattern as determined by this method is in good agreement with the pattern observed in schlieren photographs.

15.5. Simple Waves by Theory of Characteristics

Let us now investigate simple waves more rigorously by means of the theory of characteristics.

There are several interrelated ways in which flow with simple waves may be defined. Let us use the definition that, in a region of flow with simple waves, the velocity components u and v are not independent of each other, but rather are unique functions of each other. What does this restriction imply as to other features of the flow?

We may write Eq. 15.14 in the form

$$\left(1 - \frac{u^2}{c^2}\right) \frac{\partial u}{\partial x} - 2 \frac{uv}{c^2} \frac{\partial v}{\partial x} + \left(1 - \frac{v^2}{c^2}\right) \frac{\partial v}{\partial y} = 0$$

Now, since by assumption $u = u(v)$, we may set

$$\frac{\partial u}{\partial x} = \frac{\partial v}{\partial x} \frac{du}{dv}$$

and

$$\frac{\partial v}{\partial y} = \frac{\partial u}{\partial y} \frac{dv}{du} = \frac{\partial v}{\partial x} \frac{dv}{du}$$

where the last equation is found by using the condition of irrotationality, namely, that $\partial u / \partial y = \partial v / \partial x$. Inserting these expressions into Eq. 15.14a, it is found that $\partial v / \partial x$ vanishes, and we obtain

$$\left(1 - \frac{u^2}{c^2}\right) \frac{du}{dv} - 2 \frac{uv}{c^2} + \left(1 - \frac{v^2}{c^2}\right) \frac{dv}{du} = 0$$

Solving for dv/du , we get

$$\frac{dv}{du} = \frac{\frac{uv}{c^2} \pm \sqrt{\frac{u^2 + v^2}{c^2} - 1}}{1 - \frac{v^2}{c^2}}$$

where either the positive or negative sign, but not both, is applicable, because u and v are uniquely related. By comparison with Eq. 15.21, it is seen immediately that the hodograph curve representing the unique relation between u and v must in fact be one of the hodograph characteristic curves.

Next, using the equation of irrotationality and the fact that $u = u(v)$ we carry out the following operations:

$$\frac{dv}{du} = \frac{\left(\frac{\partial v}{\partial x}\right) \frac{dv}{du}}{\frac{\partial v}{\partial x}} = \frac{\left(\frac{\partial u}{\partial y}\right) \frac{dv}{du}}{\frac{\partial v}{\partial x}} = \frac{\left(\frac{\partial v}{\partial y} \frac{du}{dv}\right) \frac{dv}{du}}{\frac{\partial v}{\partial x}} = \frac{\partial v / \partial y}{\partial v / \partial x}$$

But, since

$$dv = (\partial v / \partial x) dx + (\partial v / \partial y) dy$$

we have

$$(dy/dx)_v = -(\partial v / \partial x) / (\partial v / \partial y)$$

so that

$$\frac{dv}{du} = -1 / (dy/dx)_v$$

Now dv/du is, as we have just seen, the slope of the hodograph characteristic. Also, $(dy/dx)_v$ is the slope in the physical plane of lines of constant v , and therefore of constant fluid properties, since u depends only on v . Recalling now the reciprocal orthogonality relationships of Eq. 15.24, the equation immediately above proves that in a simple-wave flow the lines of constant fluid properties are Mach lines of opposite family to the hodograph characteristic on which the simple-wave flow is mapped. Furthermore, since u and v are constant on each such Mach line, the stream direction and Mach angle are likewise constant on each Mach line. Hence the Mach lines under consideration must be straight lines.

A flow with "simple waves" may now be summarized as follows. It is a flow for which the Mach lines of only one family are physically significant in the sense that the streamlines are influenced only as they cross Mach lines of this particular family. The physically significant Mach waves are straight, and all stream properties are constant along each of these Mach lines. All the fluid states in a region of simple waves are mapped on a single hodograph characteristic of family opposite to that of the physically significant Mach waves.

In general, for flow with waves of both families, an area in the flow field is mapped as an area in the hodograph plane. Flows with waves of one family are singly degenerate because an area in the flow plane is mapped as a line in the hodograph plane. A special case of simple-wave flow is that of uniform, parallel flow, which is doubly degenerate because an area in the flow field is mapped as a single point in the hodograph plane.

15.6. Field Method Versus Lattice-Point Method

The reader has probably noticed that the procedure used for the problem of Fig. 15.12 appears to differ from that for Fig. 15.15. The former is termed the *field method*, wherein the stream properties are found in small regions or fields bounded by Mach lines. The latter is known as the *lattice-point method*, wherein the stream properties are found at the lattice points of the Mach net.

These two methods are in substance identical. To illustrate this point, the dashed lines of Fig. 15.15a illustrate the solution which would be obtained by the field method, as compared with the solid lines obtained by the lattice-point method. Midway between the solid Mach net, we imagine a dashed Mach net, at the intersection of which are small squares. As an example, we now consider the region surrounding "lattice-point 9" to be one of uniform, parallel flow, and term this region "field 9." The boundaries of field 9 are formed by the characteristic quadrilateral e-g-n-h. In the field method the entire physical field of flow is thus divided into Mach quadrilaterals, and the direction and magnitude of the velocity vector are assumed to change only as a streamline crosses a Mach line joining two adjacent fields. An area in the physical plane then corresponds to a point in the hodograph plane, e.g., field 9 corresponds to point 9'.

In using the field method, the solid Mach net of Fig. 15.15a would of course not at first be known, and it would be necessary to construct independently the dashed Mach net dividing the fields of flow. To begin, the initial-value line 1-2-3-4 is broken up into, say, four segments, 1-a, a-b, b-c, and c-4, along each of which the velocity is considered uniform and parallel. In this case, the segment 1-a is one of the bounding sides of field 1, the latter covering only one-fourth of a Mach quadrilateral.

Similarly, the initial-value segment $a-b$ is a bounding side of field 2, the latter comprising in this case one-half of a Mach quadrilateral. The points $1'$, $2'$, $3'$, and $4'$ are located in the hodograph diagram of Fig. 15.15b in accordance with the known velocity vectors in fields 1, 2, 3, and 4, respectively.

To find the stream properties in field 6, say, we note that field 6 is reachable from field 2 along a characteristic of family I , and is reachable from field 3 along a characteristic of family II . Carrying out this construction in the hodograph diagram locates $6'$, so that the properties in this field are then known.

In addition to finding the stream properties in each Mach quadrilateral, we must determine the physical whereabouts of the Mach quadrilaterals. To find a point such as e , we note that $b-e$ is a Mach wave of family II , and is therefore normal to the hodograph I -characteristic; the direction $b-e$ is therefore drawn normal to $2'-6'$. By the same argument, the direction $a-e$ is drawn normal to $2'-5'$. The intersection of the two direction lines establishes point e . The remainder of the Mach net is found by similar constructions.

The field method conveys the physical picture of streamlines being influenced by pressure waves inclined at the Mach angle to the flow, and is advantageous in this respect. However, when it is considered that as a streamline crosses a Mach wave of one family, this is entirely equivalent to the state point moving along the physical characteristic of the opposite family, it will be seen that the field method and lattice-point method are virtually identical except for small differences in procedure owing to the finite-difference feature of the method of characteristics.

In general, the lattice-point method is slightly more convenient for problems in which the boundaries of the flow are known, whereas the field method is slightly more convenient when some of the physical boundaries are to be determined.

With either method, it is convenient to use equally spaced characteristic coordinates if possible, for this leads to a simplifying regularity in the calculations. In all the examples given thus far, for example, the characteristics net was so chosen as to give equal spacings of the I and II coordinates between fields or between lattice points, and a glance at the tables for these examples will show the type of regularity obtained. With the field method, the choice of equally spaced coordinates is equivalent to the choice of equal turning angles across each Mach wave.

15.7. Unit Processes

All the various possible flow patterns can be synthesized in terms of the corresponding wave patterns. The wave patterns themselves are con-

structed by repeated application of a relatively few operations, here termed *unit processes*. They may be summarized as follows:

Generation of Wave. This occurs when a solid boundary of the flow is curved, as in Fig. 15.6, or when the boundary of the jet is exposed to a varying pressure, as near the nozzle corner of Fig. 15.12a. From momentum considerations, we have the general rule that *across an expansion wave, the streamline bends away from the wave; whereas across a compression wave the flow bends toward the wave*.

Reflection of Wave at Plane Boundary. This is illustrated in Fig. 15.12a by wave a being reflected as wave c in order to preserve the given flow direction at the wall. We observe that the incident wave a is an expansion wave (because $V_2 > V_1$), as is the reflected wave c (because $V_4 > V_2$), and hence we arrive at the general rule that *reflection of a wave from a plane boundary is in like sense*.

Reflection of Wave from Free Boundary. This is illustrated in Fig. 15.12a by wave e being reflected as wave g in order to preserve the given pressure at the edge of the jet. Since wave e is an expansion wave, and wave g is a compression wave, we infer the rule that *reflection of a wave from a constant-pressure boundary is in unlike sense*.

Cancellation of Wave. Especially in the design of supersonic wind-tunnel nozzles, it is necessary to avoid reflection of waves incident on a

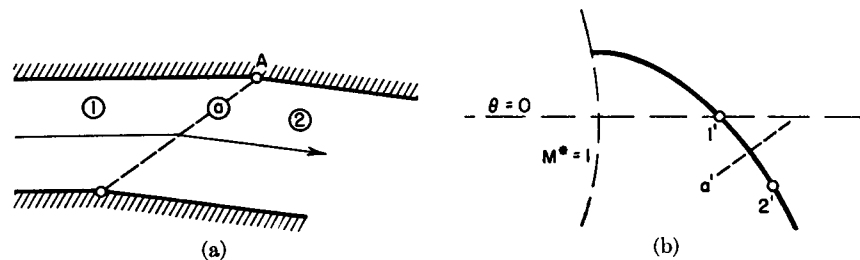


FIG. 15.16. Cancellation of a wave by appropriate curvature of wall.

wall boundary. This is done by shaping the boundary so that no reflection is necessary to preserve continuity at the wall. For example, in Fig. 15.16 wave a of given strength is incident on the upper wall, and it is desired that there be no reflection. This is easily accomplished if, at point A where wave a is incident, the wall is bent so as to have the same direction as the flow in field 2, for to satisfy this boundary condition it is necessary that no wave be reflected.

Looked at differently, if the upper wall were straight, wave a , which is shown as an expansion wave, would be reflected as an expansion wave. By bending the wall at A , however, by an amount equal to the turning

angle across wave a , a compression wave would be generated at point A . This compression wave exactly cancels the expansion wave which is the reflection of wave a , with the net result that wave a merely ends at point A . This line of argument underlines the concept of "canceling" an incident wave by bending the wall through an appropriate angle.

Crossing of Waves. This is illustrated in Fig. 15.12a by waves b and c crossing each other and emerging as waves d and e , respectively. Although the waves are refracted as they cross each other, they are unchanged in sense, and they retain their identity insofar as each has the same values of $\Delta\omega$ and $\Delta\theta$ before and after the intersection.

15.8. Graphical Versus Numerical Method

In constructing the characteristics nets for any particular problem, graphical and numerical methods may be used in several combinations, depending on considerations of accuracy and time.

Purely Graphical Construction. The entire procedure may be carried out graphically in both the hodograph and physical planes, using a large, accurately drawn set of hodograph characteristics, as was illustrated in connection with the problems of Figs. 15.12 and 15.15. This procedure requires the drawing of normals to the hodograph characteristics, which is difficult to do accurately. By use of the $M^*-\alpha$ ellipse in conjunction with the hodograph characteristics, the need for drawing normals is eliminated, and the accuracy consequently improved.⁽⁶⁾ Another technique for avoiding the troublesome task of drawing normals to a curve is by use of the *supersonic protractor*.^(6,7)

Semigraphical Construction. The graphical constructions involving the hodograph plane may be replaced by such simple and rapid arithmetical operations, based on Table B.7, that the hodograph plane may well be reserved for illustrative purposes only. The types of calculations which replace the graphical use of the hodograph diagram are shown in the "Tables for Figs. 15.12 and 15.15." In the tables for Figs. 15.12b and 15.15b are listed the flow properties in each field or at each lattice point. In the "Tables for Figs. 15.12a and 15.15a" are listed the slopes of each Mach wave in the physical plane. The Mach nets are then constructed graphically from the latter tables, using a protractor (preferably adjustable) or a drafting machine. The ease of the method can only be appreciated by working out a specific case.

Purely Numerical Construction. When the utmost in accuracy is required, it is best to eliminate graphical constructions entirely, and employ numerical calculations for the physical plane as well as the

hodograph plane. The numerical procedure may be formulated in terms of an elementary step, which is described schematically by Fig. 15.17. Except at the boundaries of the flow region, the Mach net is built up stepwise by repetitive use of an elementary step in which the fluid properties and location of two initial points completely establish the fluid properties and location at a third point lying at the intersection of the Mach waves passing through the two initial points.

In Fig. 15.17, let us suppose that we know $\omega_1, \theta_1, x_1, y_1$ and $\omega_2, \theta_2, x_2, y_2$, which is to say that we know all the fluid properties at points 1 and 2 and we also know the locations of points 1 and 2. Let point 3 lie at the intersection of the I -characteristic passing through point 1 and the II -characteristic passing through point 2. In the stepwise procedure, the curved Mach lines are replaced by a set of straight-line chords extending between the points of the nets. Let b_I be the average slope of the chord 1-3 which approximates the Mach line 1-3; and, similarly, let b_{II} be the slope of the chord 2-3.

Now, from Eqs. 15.12, we may find the values of I and II at points 1 and 2. Then, by virtue of the definition of point 3, we may find the values of I_3 and II_3 through the relations

$$I_3 = I_1; \quad II_3 = II_2$$

Having found I_3 and II_3 , Eqs. 15.13 may be used for computing ω_3 and θ_3 , thus determining fully the fluid properties at point 3.

We are now in a position to compute the average slopes b_I and b_{II} . From Eqs. 15.23, we may write approximately

$$b_I = \tan \frac{1}{2}[(\theta_3 - \alpha_3) + (\theta_1 - \alpha_1)] = \tan (\theta - \alpha)_{1-3} \quad (15.27a)$$

$$b_{II} = \tan \frac{1}{2}[(\theta_3 + \alpha_3) + (\theta_2 + \alpha_2)] = \tan (\theta + \alpha)_{2-3} \quad (15.27b)$$

and thus b_I and b_{II} are known.

Now, from the formulas of analytic geometry,

$$y_3 - y_1 = b_I(x_3 - x_1)$$

$$y_3 - y_2 = b_{II}(x_3 - x_2)$$

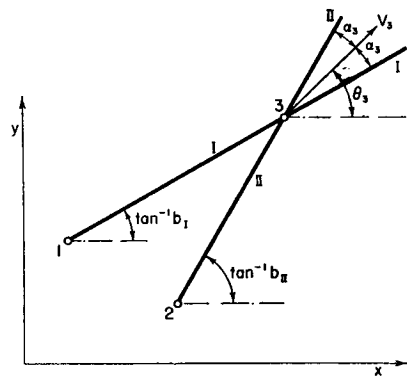


FIG. 15.17. Unit process of characteristics method.

Solving for x_3 and y_3 from this pair of simulation equations, we have

$$x_3 = \frac{(y_2 - b_{II}x_2) - (y_1 - b_Ix_1)}{b_I - b_{II}} \quad (15.28a)$$

$$y_3 = \frac{b_I(y_2 - b_{II}x_2) - b_{II}(y_1 - b_Ix_1)}{b_I - b_{II}} \quad (15.28b)$$

and thus x_3 and y_3 may be solved for in terms of the initial data and the values of b_I and b_{II} .

ORGANIZATION OF NUMERICAL CALCULATIONS. There are several ways of organizing the calculations so as to put them on a routine basis suitable for computers. One type of organization, to be used with the lattice-point method, is illustrated in Fig. 15.18. The Mach net is twice

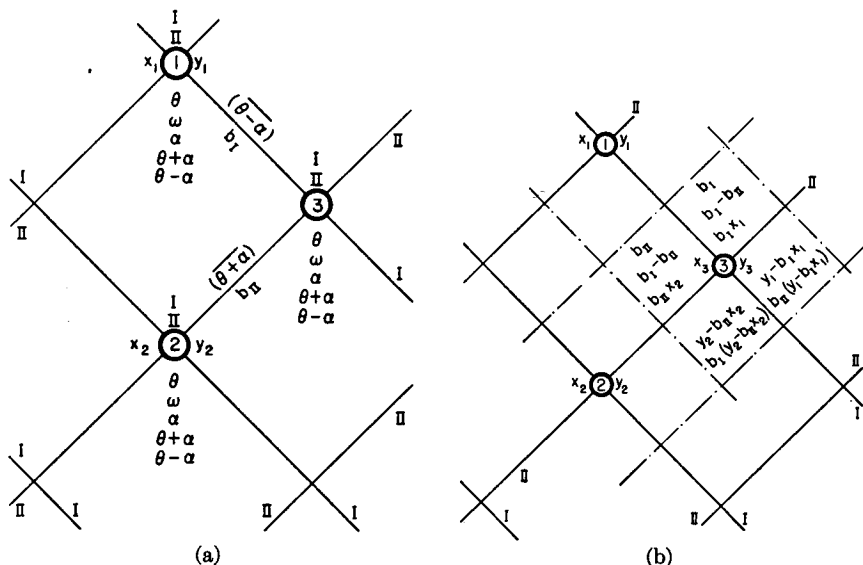


FIG. 15.18. Scheme of organization for purely numerical solution.

- (a) Schematic characteristics net; computation of fluid properties.
- (b) Schematic characteristics net; computation of coordinates of net points.

drawn *schematically* to a very large scale; for example, a $\pm 45^\circ$ net is convenient. On one net, Fig. 15.18a, are listed the variables relating to the fluid properties at each point, and also the values of b_I and b_{II} on each chord of the net. The latter are then transferred to the second net, Fig. 15.18b, where the remaining calculations required to establish the physical location of each net point are made.

A similar organizational setup may easily be devised for use with the field method.

At the boundary of the physical flow, one of the lines in Fig. 15.17 will be a segment of the boundary, and a modification of the computational technique is required. Either the flow direction or the fluid pressure is then known along one of the lines in Fig. 15.17, and equations similar to Eqs. 15.27 and 15.28 may be worked out for these special cases.

Effect of Grid Size on Accuracy. There is only one certain way of determining the required Mach net for a specified final accuracy, and that is to start with a very coarse net and obtain solutions with nets successively finer, until two successive solutions agree to the desired accuracy. Occasionally it is possible to extrapolate to zero grid size. A convenient rule is that the error owing to the finite-difference type of computation is proportional to $(\Delta\omega)^3$, where $\Delta\omega$ is a measure of the change in M^* between fields or between lattice points.⁽³⁾

For example, Fig. 15.19 shows, for the sharp-cornered supersonic wind tunnel nozzle of Fig. 15.34, the computed values of the exit coordinates

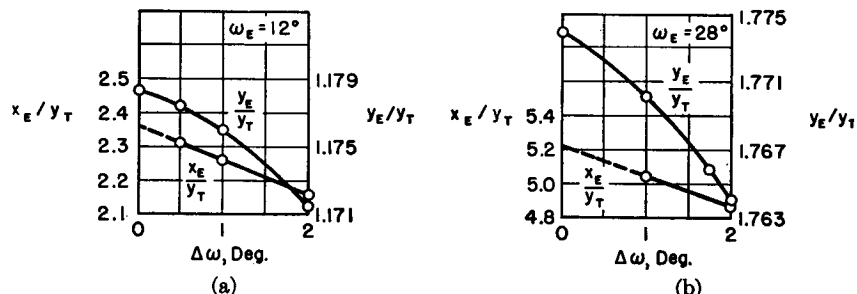


FIG. 15.19. Effect of net spacing on accuracy of solution for example of Fig. 15.34 (after Edelman).

(referred to the half-throat height) as a function of the magnitude of $\Delta\omega$ between fields. From one-dimensional considerations, the exit height can be computed exactly; this value corresponds to $\Delta\omega$ equal to zero. For $\Delta\omega = 2^\circ$, these curves show a 0.5% error in the final y -coordinate, and a 7% error in the final x -coordinate.

For most engineering work not requiring extreme accuracy, a $\Delta\omega$ of 1 or 2 degrees is satisfactory. The accuracy of an entire solution may be improved considerably by using especially small intervals near Mach Number unity, where certain derivatives vary rapidly and approach infinity.

15.9. Some Special Features of Supersonic Flow

Initial-Value Problem. Having seen several sample problems, we now ask, what initial data are necessary to obtain solutions by characteristics methods; and, for various types of initial data, within what regions of flow may the solution be established?

This question is discussed in Appendix A, where it is shown that solutions may be obtained in those flow regions within which the characteristics nets may be constructed from the given initial data. For two-dimensional, supersonic flow, the various important situations may be summarized as follows:

FIG. 15.20a. The velocity vector is given at all points of the non-characteristic line AB . The solution is then completely determined in

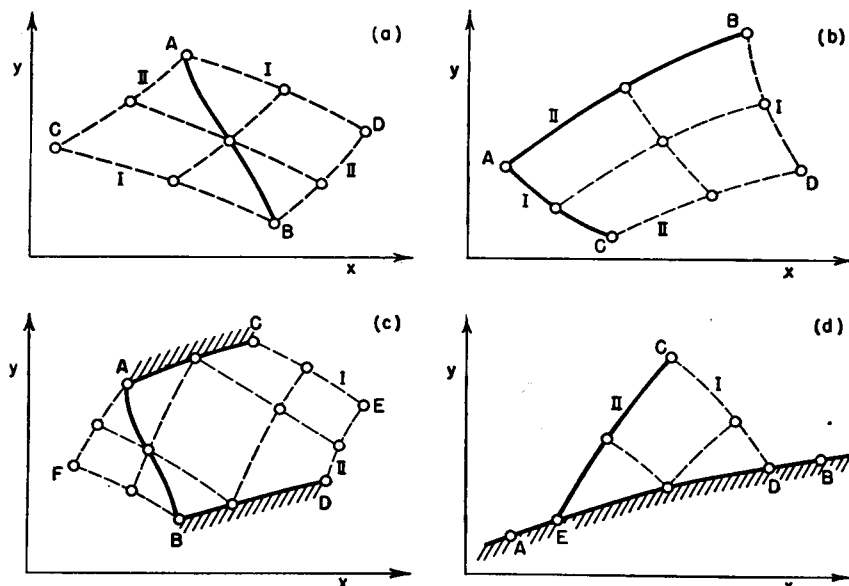


FIG. 15.20. Several initial-value problems.

the Mach quadrilateral $ADBC$. Note that the flow upstream of AB as well as the flow downstream is established by the initial data.

This type of initial data is illustrated in the example of Fig. 15.15.

FIG. 15.20b. The velocity vector is given at all points on the characteristics AB and AC . The solution is then completely determined in the Mach quadrilateral $ABDC$. As an illustration, see the example of Fig. 15.23.

FIG. 15.20c. The velocity vector is given at all points of the non-characteristic line AB , and at all points on the noncharacteristic lines AC and BD there is given *either* the velocity magnitude *or* the velocity direction. The solution is then completely determined within the figure $FACEDB$. As an illustration, see the example of Fig. 15.12a.

FIG. 15.20d. The velocity vector is given at all points of the characteristic line EC , and along the noncharacteristic line AB there is given

either the velocity magnitude *or* the velocity direction. The solution is then completely determined in the region ECD .

Other combinations of initial data may be devised, but all the important elements are included in the foregoing list.

Physical Significance of Characteristics. According to the initial-value theorem for hyperbolic equations, if the velocity components are known along the noncharacteristic curve 1-2 of Fig. 15.21, then the entire flow pattern in the Mach quadrilateral 1-4-2-3 may be solved for. Now, suppose that the velocity components are altered along 1-1'. This might be thought of as a disturbance of the flow in the neighborhood of point 1. Since the values of the velocity components remain unaltered along 1'-2, it is evident that the flow pattern in the characteristic quadrilateral 1'-4'-2-3' is not affected by disturbances along 1-1'. Hence the effects of these disturbances are confined entirely to the regions 1-4-4'-1' and 1-1'-3'-3. We see, therefore, that disturbances are propagated along the Mach lines, for if point 1' approaches 1, the effects of a small disturbance in the interval 1-1' are felt only along the characteristics 1-4 and 1-3.

These mathematical considerations have a very real physical counterpart. If small disturbances are introduced into a supersonic flow, as by roughening the walls of a passage or the surface of an airfoil, or by inserting a fine needle into the stream, schlieren and shadow photographs show that these disturbances are propagated into the stream at the Mach angle to the flow.

Domains of Influence and Dependence. The initial-value theorem indicates also that the specification of the velocity components along the line 5-6 in Fig. 15.21 completely determines the flow within the characteristic semi-quadrilateral 5-7-6. In other words, the flow pattern in the region 5-7-6 is independent of the data along 1-5 and 6-2. This means that conditions at 7 depend only on the data along 5-6. We may generalize this argument by stating that the "domain of dependence" for a given point of the flow, or the region within which events can have any effect on the conditions at the given point, is the region bounded by the upstream-running Mach lines passing through the given point.

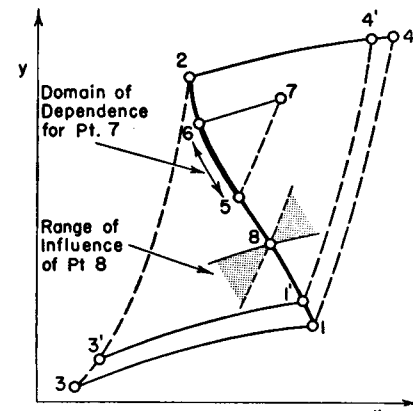


FIG. 15.21. Illustrates propagation of disturbances along Mach lines, domain of dependence, and range of influence.

From similar considerations, it may be demonstrated that the initial data at point 8 of Fig. 15.21 can affect the flow pattern only in the shaded regions bounded by the characteristics passing through point 8. Although both shaded regions appear in the mathematical argument, only the shaded region pertaining to the Mach lines downstream of point 8 is physically significant, because pressure disturbances cannot be propagated upstream in a supersonic flow. The downstream shaded region is called, therefore, the *range of influence* at point 8. Or, as von Karman has put it, the region bounded by the downstream Mach lines through a given point is the *zone of action* in which events at the given point make themselves manifest; while the entire surrounding region is the *zone of silence*, within which events at the given point are not felt. For example, if a thin, cusp-edged profile is placed in a two-dimensional, supersonic flow at zero angle of attack, the effects of the profile are confined to the regions downstream of the Mach lines attached to the leading edge.

Comparison Between Subsonic and Supersonic Flow. We have already compared subsonic with supersonic flow on several different bases. We may generalize these ideas by comparing flows defined by hyperbolic differential equations, represented for example by steady, supersonic flow, and flows defined by elliptic differential equations, represented for example by steady, subsonic flow.

In supersonic flow, the phenomena are essentially those of wave propagation, in which disturbances at individual points of the flow are propagated along the downstream Mach lines passing through these points. Thus there exist in supersonic flow domains of dependence and ranges of influence. These statements are connected, of course, with the fact that in supersonic flow analytically different regions may be connected along the characteristics, so that the solutions of the differential equations are, in general, nonanalytic.

In subsonic flow, no real characteristics exist. The solutions to the differential equations must be analytic functions which apply over the entire flow field. A disturbance at any point in the flow field makes itself felt at all other points. Or, to put it differently, the domain of dependence and range of influence for each point covers the entire field of flow. Physically, this comes about because a pressure wave generated at any point in a subsonic flow can reach any other point of the flow. Since no real characteristics exist for subsonic flow, no discontinuities in any of the velocity derivatives may in general occur. For example, if it is known that in any small finite region the flow is exactly uniform and parallel, then it follows that the flow must be uniform and parallel throughout the entire region of flow. Conversely, if the flow is non-uniform in any region, then it must be nonuniform in all regions.

15.10. Applications of Method of Characteristics

To illustrate how the method of characteristics may be used for practical calculations, a number of specific examples are discussed below.

Thin Profile. Fig. 15.22 shows a thin, curved profile whose leading edge is parallel to the oncoming air stream. Above the profile there will be only left-running Mach waves and below there will be only right-running Mach waves. At any point on the profile the local pressure

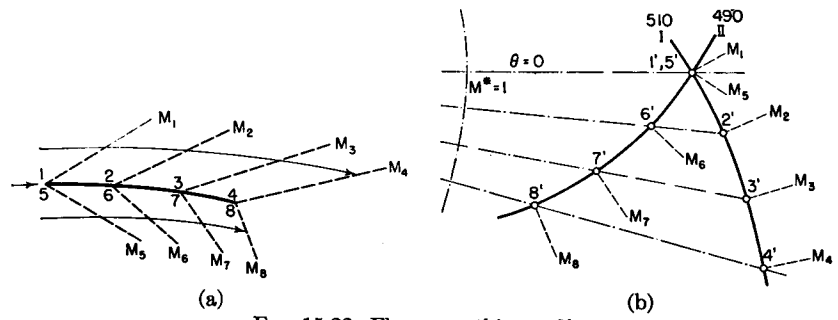


FIG. 15.22. Flow past thin profile.

(a) Flow plane.
(b) Hodograph plane.

depends only on the local inclination of the surface, on the approach Mach Number, and on whether the point is on the upper or lower surface.

Note that the compression waves generated by the lower surface converge. As described in the next chapter, they ultimately form an oblique compression shock (see Fig. 15.6d).

When a profile has thickness, oblique compression shocks are usually generated at the profile itself, and the analysis of such profiles requires the combined application of the method of characteristics and of oblique-shock theory. Such profiles are discussed in the next chapter.

Underexpanded Nozzle. Fig. 15.23 shows the complete wave pattern for a nozzle discharging into a region where the back pressure is lower than the exit-plane pressure.

This example illustrates the role of the characteristics as patching lines along which may be joined regions with analytically different types of flows. Regions 1, 2, 3, 4, and 5 are doubly degenerate, since they have uniform, parallel flows. Between 1 and 2, between 2 and 3, etc., are singly degenerate regions of simple waves. The remaining parts of the jet comprise regions in which waves of both families are present. Each of the three types of regions is analytically different. They are

joined to each other, however, only along Mach lines, which are the patching lines for supersonic flow. On the Mach lines the velocity is continuous, but there are discontinuities in the first and higher derivatives of the velocity.

The pattern shown in Fig. 15.23 is repetitive, since field 5 is identical in state with field 1.

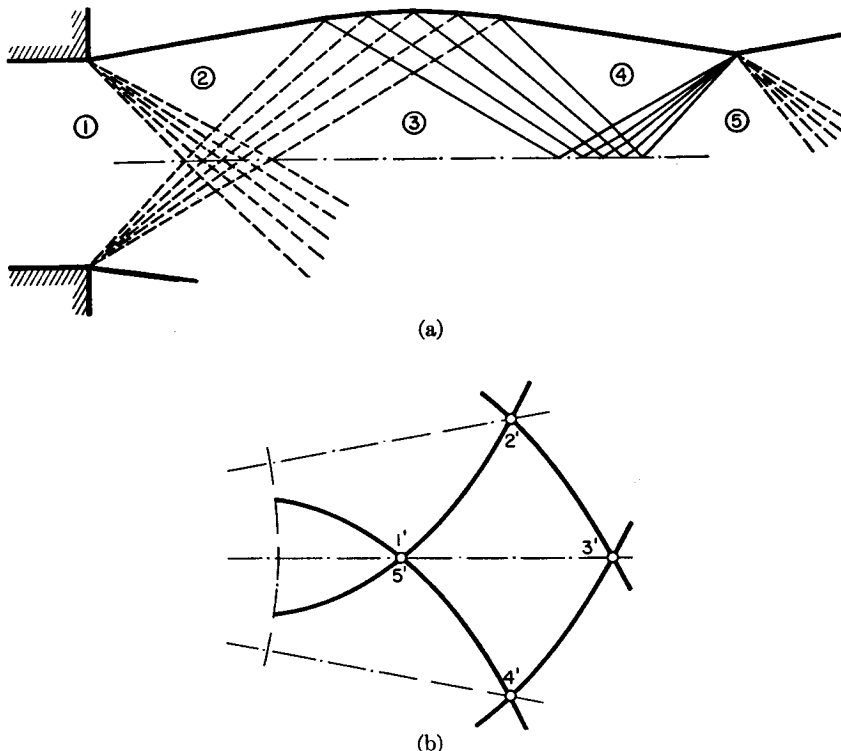


FIG. 15.23. Flow at exit of underexpanded nozzle (compare with schlieren photograph of Fig. 5.24).

- (a) Flow plane.
- (b) Hodograph plane.

Schlieren photographs of jets (Fig. 5.24) confirm beautifully the theoretical patterns of the type of Fig. 15.23, except of course that, as a result of friction between the jet and the surrounding gas, the analytical solution breaks down after one or two cycles.

A Simple Supersonic Wind Tunnel. Fig. 15.24 shows a two-dimensional passage, formed of two Prandtl-Meyer turns, which accelerates a stream from Mach Number unity at section 1 to some higher Mach Number at section 3.

If it is desired to have the stream at 3 parallel to the stream at 1, it is evident from the hodograph diagram that the turning angles must be related to the final Mach Number by the relation

$$\theta_1 - \theta_2 = \theta_3 - \theta_2 = \omega_3/2$$

Of course, parallelism of the streams at 1 and 3 is not a necessary requirement, nor is it necessary that a centered simple wave be employed,

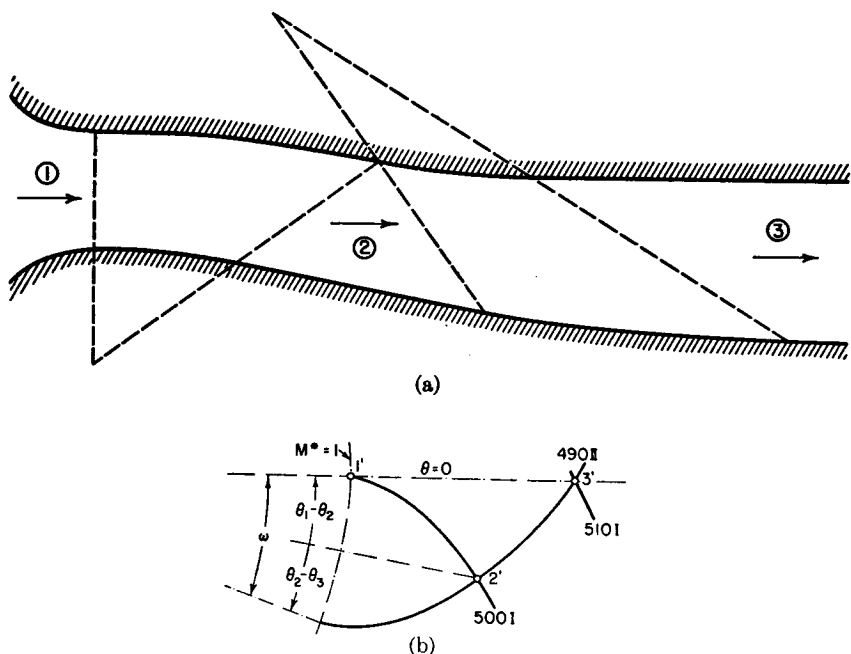


FIG. 15.24. Design of a simple supersonic wind tunnel.

- (a) Flow plane.
- (b) Hodograph plane.

for similar results may be obtained with a noncentered simple wave. However, if centered waves are used, the streamlines are Prandtl-Meyer streamlines and may be laid out very easily.

Although this design of wind tunnel nozzle would be satisfactory for an inviscid fluid, it is seldom employed in practice when a highly uniform, parallel stream is desired. The boundary layers on the passage walls produce slight deviations from the theoretical flow pattern. For the nozzle of Fig. 15.24 these deviations are not symmetrical for the two walls, and hence lead to irregularities in the final flow. The conventional type of supersonic wind tunnel nozzle is symmetrical, and is discussed in Art. 15.11.

Supersonic Elbow. Fig. 15.25 shows a two-dimensional elbow which turns a supersonic stream through the angle $(\theta_1 - \theta_3)$ without any net change in Mach Number. Two simple-wave turns are employed, in one of which left-running Mach waves expand the flow from 1 to 2, and in the other of which right-running Mach waves compress the flow from

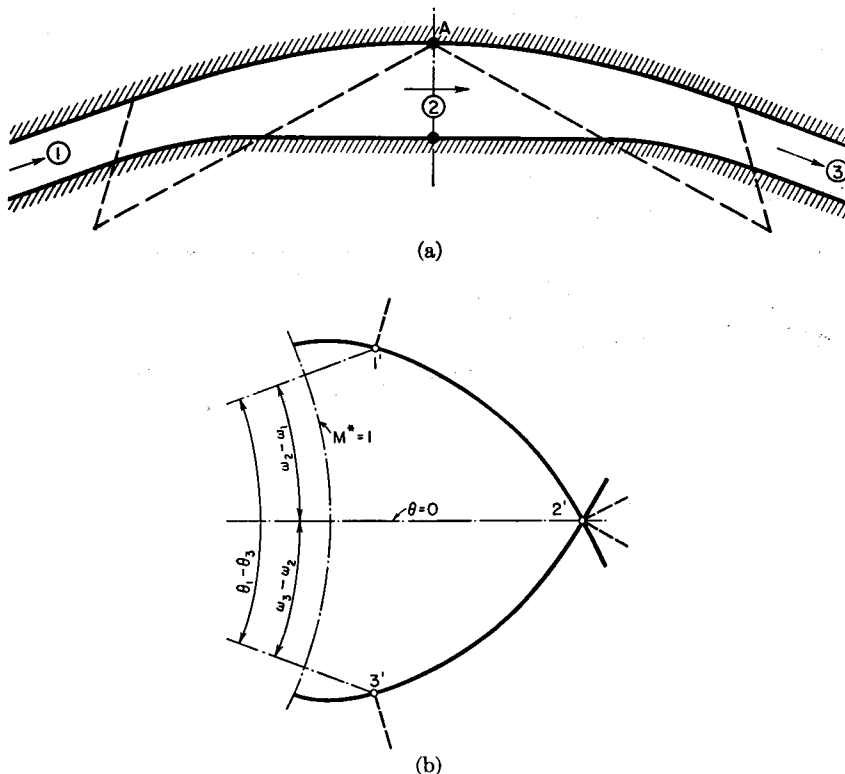


FIG. 15.25. Design of a supersonic elbow.

- (a) Flow plane.
(b) Hodograph plane.

2 to 3. In this illustrative example, the waves are assumed to be centered, and hence the streamlines are Prandtl-Meyer streamlines.

From symmetry conditions and the specification that $\omega_1 = \omega_3$, it follows that the elbow is symmetrical about $A-A$, and that

$$\theta_1 - \theta_2 = (\theta_1 - \theta_3)/2 = \omega_2 - \omega_1 = \omega_2 - \omega_3$$

Impulse Turbine Blade. In an impulse steam turbine or gas turbine, a stream approaching a set of passages is turned through a certain angle without any net change in pressure. If the flow relative to the blades

is supersonic, then the type of passage illustrated by Fig. 15.26 is theoretically suitable. The blades themselves are formed by having one of the passage walls act as the concave surface, and the other passage wall the convex surface.

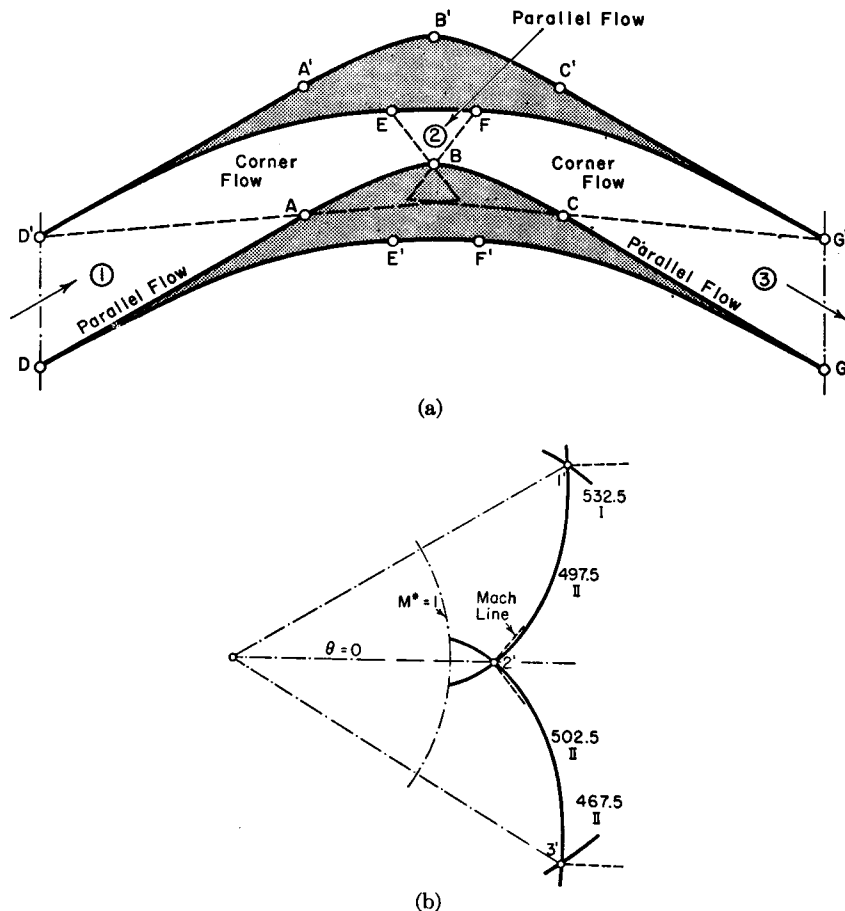


FIG. 15.26. Design of supersonic impulse blade.

- (a) Flow plane.
(b) Hodograph plane.

Supersonic Compressor Cascade. Fig. 15.27 shows a pair of blades which might be used for the stator cascade of a supersonic compressor. Gas enters supersonically at 1, is compressed by means of right-running Mach waves in a centered simple wave to a Mach Number of about 1.2 to 1.5, and is then decelerated to subsonic speeds by a normal shock, after which it is decelerated subsonically and also turned into the axial direction.

Compressors employing this principle seem to hold great promise for obtaining large pressure rises per stage with good efficiency, since the losses in a shock at $M = 1.5$ are very small if separation can be avoided.

Two-Dimensional Supersonic Inlet. Fig. 15.28 shows an inlet diffuser which might be placed in the leading edge of the wing of a super-

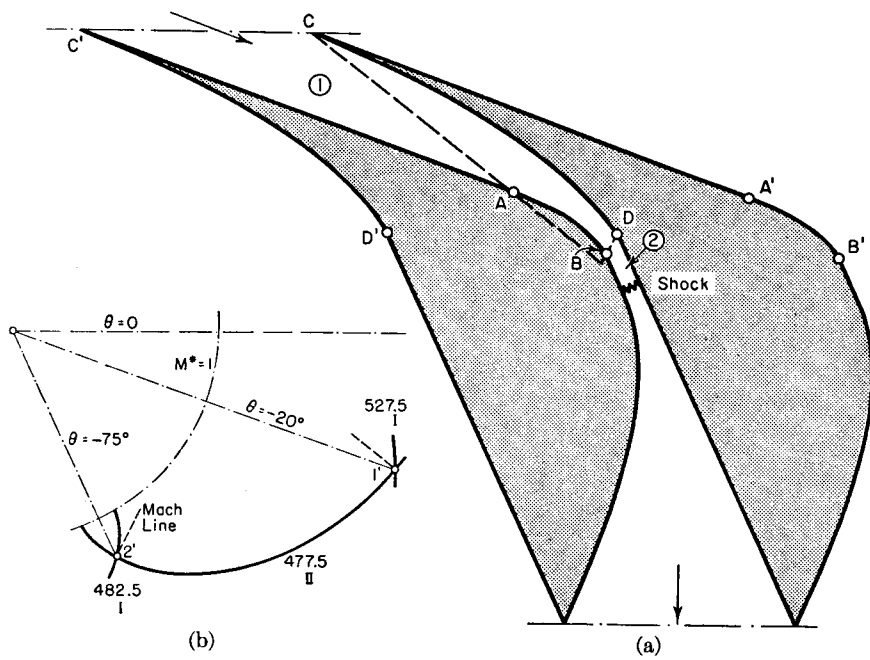


FIG. 15.27. Design of supersonic compressor cascade.

- (a) Flow plane.
(b) Hodograph plane.

sonic airplane. Two Prandtl-Meyer turns and a weak normal shock are used for reducing the incoming air speed to subsonic values.

Such a design might also be used for supersonic wind tunnel circuits if the boundary layer on the tunnel walls could be removed so as to avoid separation of the flow in a region of positive pressure gradient.

Special problems arise in the starting of supersonic diffusers because of the need for swallowing the starting shock. This problem may be met in the design of Fig. 15.28 by making the central plug retractable, so that the throat area may be temporarily enlarged.

Effects of Viscosity. The effects of viscosity are confined to a thin boundary layer unless the Reynolds Number is extremely low or unless there is back flow in the boundary layer.

In an accelerating flow, the boundary layer tends to remain very thin, and there is no tendency toward separation of the flow. Hence, flows like those in Figs. 15.15, 15.23, and 15.24 in general exhibit very good agreement between experimental results and results based upon the method of characteristics for a frictionless fluid.

In a decelerating flow, the boundary layer tends to thicken, and, owing to the adverse pressure gradient, there is a tendency to separation because of back flow in the boundary layer. The former effect produces an even larger pressure gradient in a supersonic flow, and thus tends to aggravate the latter effect. If a slight amount of separation appears,

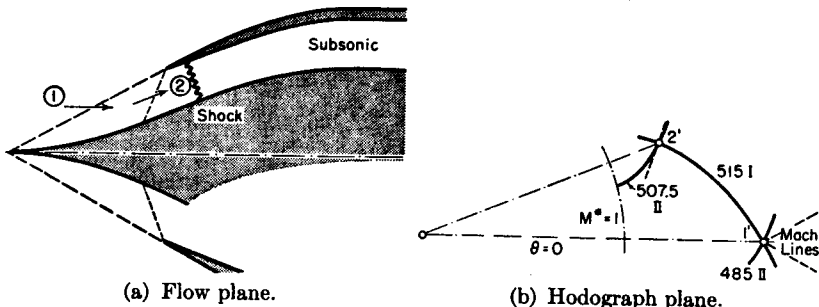


FIG. 15.28. Design of supersonic inlet.

the interaction between the resulting shock wave and the boundary layer makes the situation grow rapidly worse. There are likely to be great disappointments, therefore, in the results obtained with passages like those of Figs. 15.25, 15.26, and 15.27 unless due account is taken of these problems. Shocks will usually appear and the general flow pattern will be totally unlike what is expected. There is evidence, however, that good results may be obtained with decelerating flows if three precautions are taken: (i) very large adverse pressure gradients should be avoided, (ii) the passage walls should be displaced by the amount of a carefully computed boundary-layer displacement thickness, and (iii) any large initial boundary layer should be removed by suction. For further details, the reader should refer to Article 16.12 and to Volume II, Chapter 28.

15.11. Design of Supersonic Wind Tunnel Nozzles

The design of nozzles for two-dimensional, supersonic wind tunnels constitutes one of the important practical applications of the method of characteristics.

General Considerations as to Form of Nozzle. The function of such a nozzle is to accelerate a stream from Mach Number unity to some de-

sired final Mach Number. It is of the utmost importance, in order that free flight be simulated, that the stream entering the test section be uniform and parallel.

Referring to Fig. 15.29, if the nozzle is symmetrical, there must be a general divergence from the throat to the test section. Also, because of symmetry, the center line is a streamline, and may be considered a

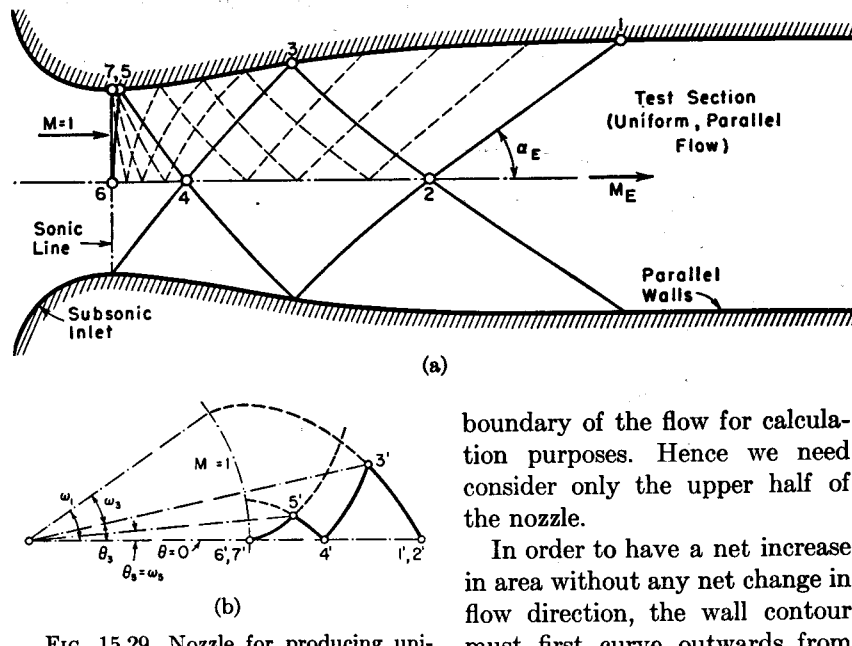


FIG. 15.29. Nozzle for producing uniform, parallel flow.

- (a) Flow plane.
- (b) Hodograph plane.

flow. Point 3 is an inflection point and is the point where the wall has its maximum slope, θ_{\max} . For the present we shall assume that the subsonic inlet is designed to give a parallel, uniform, sonic flow at the throat, section 6-7.

ZONES IN NOZZLE. Three separate zones of flow may be identified in Fig. 15.29a:

(i) The *expansion zone*, 6-7-3-2-6, bounded by the throat 6-7, by the characteristic 2-3 which on the center line of symmetry attains the required test-section Mach Number, and by the expansion portion of the nozzle wall 7-5-3. This is a zone where waves of both families are present.

(ii) The *test section*, which is the region downstream of 1-2, where the flow is uniform and parallel at the test-section Mach Number M_E . Be-

cause of the uniform, parallel flow, the Mach line 1-2 is straight, and is inclined at the angle α_F to the center line.

(iii) The *straightening section*, 3-2-1, which is bounded by the Mach lines 3-2 and 2-1, and by the straightening portion of the wall, 3-1. Since it is a general theorem that only a zone of simple waves can be patched to a uniform, parallel flow, it follows that zone 3-2-1 must have a simple-wave flow such that all flow properties are uniform on straight left-running Mach waves in this zone. The wall contour is then the streamline which begins at point 3 and crosses the left-running Mach waves until it emerges horizontal at point 1. Since it is undesirable for reasons of boundary-layer behavior to have compression waves in the nozzle, the simple wave in the straightening section must be an expansion wave, and hence the straightening contour 3-1 must be concave downward. Note that the determination of the flow in this zone from initial data on the Mach lines 3-2 and 2-1 is an initial-value problem of the type of Fig. 15.20b.

We may also discuss the main principles of the design using the physical concept of pressure waves propagating along the Mach lines. Assuming sonic flow at the throat, the wall is curved outward between 7 to 3. This generates right-running expansion waves which are reflected from the center line of symmetry as left-running expansion waves, which may be reflected again and again at the wall and the center line.

This process of generating expansion waves by curving the wall is continued to the point where one of the waves (3-2) accelerates the flow at the center line (point 2) to the desired test-section Mach Number. The left-running waves which cross line 3-2 would in general be reflected from the wall. However, the purpose of the design is to *avoid* pressure waves in the test section, and hence the straightening contour 3-1 is curved so as to cancel the waves which are incident on it. Thus the region 3-2-1 is one of simple waves.

It is clear that if the expansion contour 7-5-3 is selected arbitrarily, thus allowing the Mach line 3-2 to be constructed, it is possible then to construct the streamline 3-1 and thus complete the nozzle design. We now ask, what are the considerations that go into the selection of the expansion contour, 7-5-3?

Design of Expansion Contour, 7-5-3. The design of the expansion contour depends somewhat on the shape of the sonic line at the throat. For illustrative purposes, and to make the discussion concrete, let us suppose that the sonic line is straight and normal to the axis, as in Fig. 15.29a.

Furthermore, also for the sake of concreteness, let us assume for the present that the first test-section Mach line (2-1), when extended backward, is reflected at the wall contour twice (at points 3 and 5) before

reaching the sonic line. Now, if the radius of curvature of the contour 7-5 were finite, the waves originating at 7 would be reflected infinitely many times at the axis and the contour before the Mach Number increased above unity, because the Mach line running rightward from 7 is normal to the axis, and likewise the Mach wave reflected from 6 is also normal to the axis. Therefore, to meet the stipulation that the backwardly extended Mach line 1-2 be reflected only at 3 and 5, it is necessary that the contour 7-5 have zero radius of curvature. This means that points 5 and 7 coincide in physical location, that there is a corner at 7, and that the lines 6-7 and 5-7 are identical.

Although in the triangular region 7-4-6 there are waves of both families, the corner 7 is a singular point at which there is locally a centered simple expansion wave, so that the series of states between 7 and 5 map on a single hodograph characteristic, as in Fig. 15.29b. The latter figure also shows the hodograph characteristics corresponding to the backwardly extended Mach line 1-2.

Now, from Eqs. 15.26, since $\theta_6 = \theta_4 = \theta_1 = 0$,

$$|\theta_5| = \omega_5 - \omega_6 = \omega_4 - \omega_5$$

$$|\theta_3| = \omega_1 - \omega_3 = \omega_3 - \omega_4$$

Furthermore, since $\omega_6 = 0$,

$$\omega_1 - \omega_6 = \omega_1 = (\omega_1 - \omega_3) + (\omega_3 - \omega_4) + (\omega_4 - \omega_5) + (\omega_5 - \omega_6)$$

$$\omega_1 = |\theta_3| + |\theta_3| + |\theta_5| + |\theta_5| = 2|\theta_3| + 2|\theta_5|$$

Therefore,

$$\frac{|\theta_3|}{\omega_1/2} = 1 - \frac{|\theta_5|}{\omega_1/2} = 1 - 2 \frac{\omega_5}{\omega_1} \quad (15.29)$$

Since the expansion contour 5-3 is concave outward,

$$|\theta_3| - |\theta_5| \geq 0$$

But, from Eq. 15.29,

$$|\theta_3| - |\theta_5| = \frac{\omega_1}{2} - 2|\theta_5|$$

Hence, since $|\theta_5|$ is also greater than zero,

$$0 \leq |\theta_5| \leq \frac{\omega_1}{4}; \quad 0 \leq \omega_5 \leq \frac{\omega_1}{4} \quad (15.30)$$

and, putting this into Eq. 15.29, we find that

$$1 \geq \frac{|\theta_3|}{\omega_1/2} \geq \frac{1}{2} \quad (15.31)$$

Thus, equations 15.30 and 15.31 put certain limitations on the design. It is instructive to examine the two extremes:

(i) $\omega_5/\omega_1 = 1/4$ and $|\theta_3| = \omega_1/4$. In this case, $|\theta_5| = |\theta_3|$, so that the contour 5-3 is a straight line whose slope is related to the test-section Mach Number by

$$|\theta_3| = |\theta_5| = \omega_1/4$$

The corresponding nozzle contour and characteristics diagram are shown in Figs. 15.30a and b.

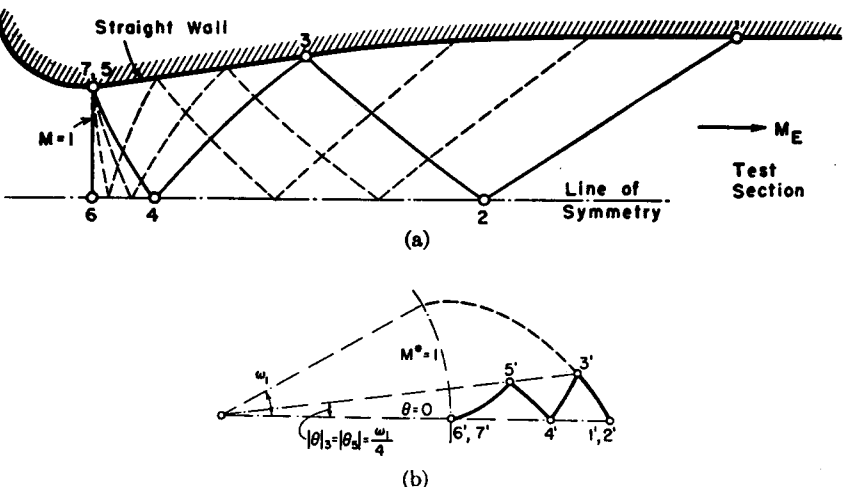


FIG. 15.30. Nozzle with $\omega_5/\omega_1 = 1/4$ and $|\theta_3| = \omega_1/4$.

(a) Flow plane.

(b) Hodograph plane.

(ii) $\omega_5/\omega_1 = 0$ and $|\theta_3| = \omega_1/2$. In this case, points 5 and 7 are identical as to both physical location and fluid properties, but, since a corner at 7 is still necessary, point 3 is coincident with 7, although it has different properties. The maximum slope of the contour is immediately

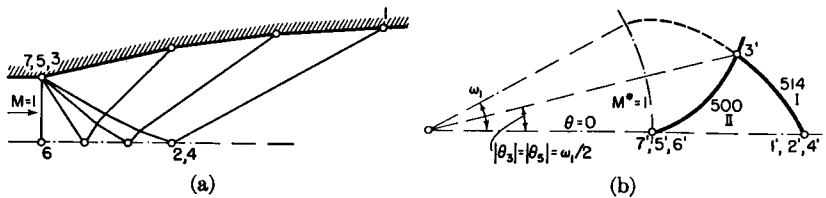


FIG. 15.31. Nozzle with $\omega_5/\omega_1 = 0$ and $|\theta_3| = \omega_1/2$.

(a) Flow plane.

(b) Hodograph plane.

downstream of the corner, and is related to the final Mach Number by $|\theta_3| = \omega_1/2$. Figs. 15.31a and b show the nozzle contour and characteristics diagram for such a nozzle.

GENERALIZATION FOR n REFLECTIONS. The relations given above may now be generalized for the case where there are n backward reflections of the first test-section Mach line on the wall contour ($n = 2$ for Fig. 15.29a). Referring to Fig. 15.32, let A be the downstream side of the

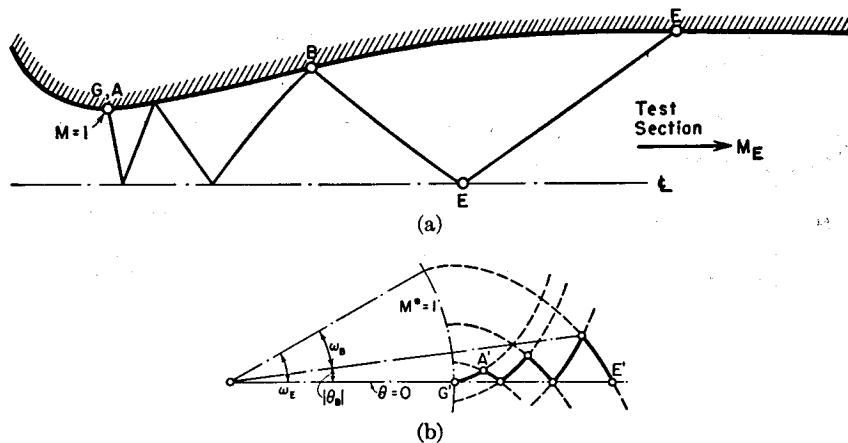


FIG. 15.32. Nomenclature for generalized nozzle-design relations.

corner, let B denote the inflection point of the contour, and let EE represent the first Mach line in the test section. Then

$$|\theta_B| + \omega_B = \omega_E \quad (15.32)$$

$$0 \leq \omega_A / \omega_E \leq 1/2n \quad (15.33)$$

$$1 \geq 2|\theta_B| / \omega_E \geq 1/n \quad (15.34)$$

At the right-hand limits of the latter two equations,

$$\omega_A = |\theta_A| = |\theta_B| = \omega_E/2n$$

$$\omega_B = \omega_E(1 - 1/2n)$$

Therefore, a straight line of inclination $\omega_E/2n$ connects points A and B , the contour BE is curved, and the nozzle contour looks like that of Fig. 15.30a.

At the left-hand limits, $\omega_A = 0$, which means that point B must be at the downstream side of the corner. Furthermore, $\theta_B = \omega_E/2$. The nozzle is therefore identical with that of Fig. 15.31a, and its maximum wall inclination, of magnitude $\omega_E/2$, is at the corner. All n reflections then occur at the corner.

Sharp-Corner Nozzle. As we have just seen, a limiting design is that for which the entire expansion contour is contracted to a sharp corner at the throat, of angle $\omega_E/2$, and for which the straightening contour extends from the corner to the exit (Fig. 15.31).

The construction of the wave pattern and wall contour for such a nozzle, using the field method, is illustrated graphically in Figs. 15.33a and b.

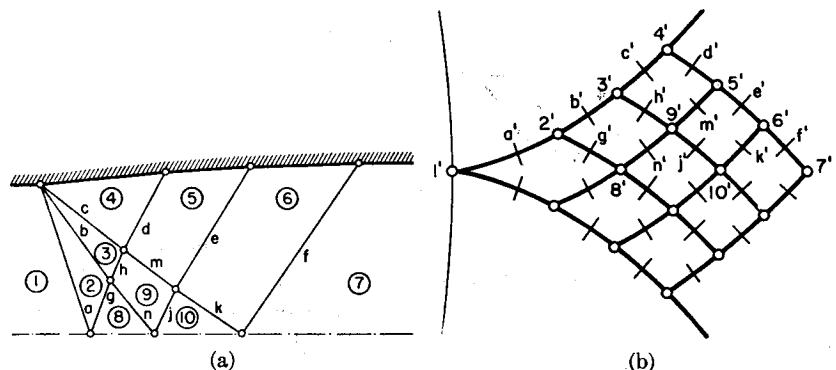


FIG. 15.33. Construction of contour of sharp-corner nozzle.

(a) Wave diagram.
(b) Hodograph plane.

A scale drawing of the Mach net for $\omega_E = 28^\circ$ ($M_E = 2.059$, $\theta_B = 14^\circ$), using 1° -intervals, is shown in Fig. 15.34. It is to this design that Fig. 15.19b, illustrating the effect of Mach-net fineness on accuracy, pertains.

No nozzle not containing compression waves can have a smaller ratio of length to throat width nor a larger value of θ_{\max} than the sharp-corner

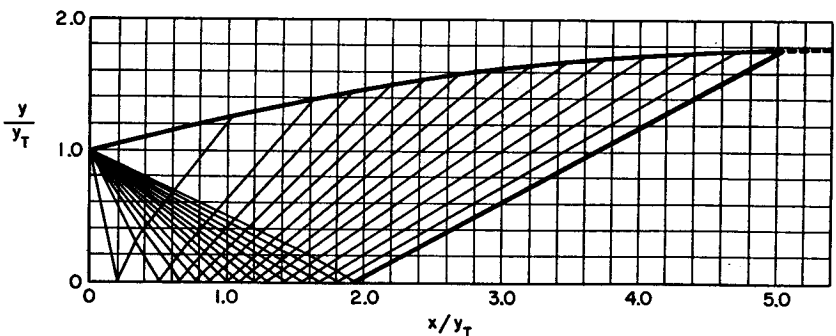


FIG. 15.34. Mach lines for sharp-corner nozzle with exit Mach Number of 2.059 ($\omega_E = 28^\circ$), based on 1° -intervals of ω . The origin of the x , y -coordinate system is in the plane of the throat, on the line of symmetry, and y_T denotes the half-height at the throat (M.I.T. Gas Turbine Laboratory).

nozzle with $\theta_{\max} = \omega_E/2$. This type of nozzle is also becoming increasingly popular because it has the most simply defined expansion contour. If the sharp corner is thought undesirable because of boundary-layer considerations, one of the interior streamlines may be employed for the wall contour.

The region with waves of both families (zone 7-4-6 in Fig. 15.31), if drawn for a very high exit Mach Number, contains within it the mixed-wave zone for all lower Mach Numbers. This is illustrated in Fig. 15.35,

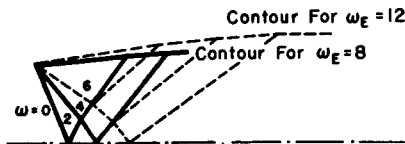


Fig. 15.35. Illustrating construction of contour for sharp-corner nozzle from "kernel."

where it is shown how a portion of the mixed-wave zone for $w_E = 12^\circ$ may be used to determine the wall contour for $w_E = 8^\circ$. Thus, if the mixed-wave zone, or "kernel," is very carefully worked out once for some particular Mach Number, the calculations for the kernel need never be repeated for lower Mach Numbers.

Coordinates of carefully calculated nozzle contours up to $w_E = 28^\circ$ are tabulated in Reference 9, and the kernel coordinates for values of M_E up to 10 are given in Reference 10.

The nozzle contours⁽⁹⁾ are shown in Fig. 15.36. In Fig. 15.37,⁽¹⁰⁾ the ratio of nozzle length to test-section height is shown as a function of final Mach Number.

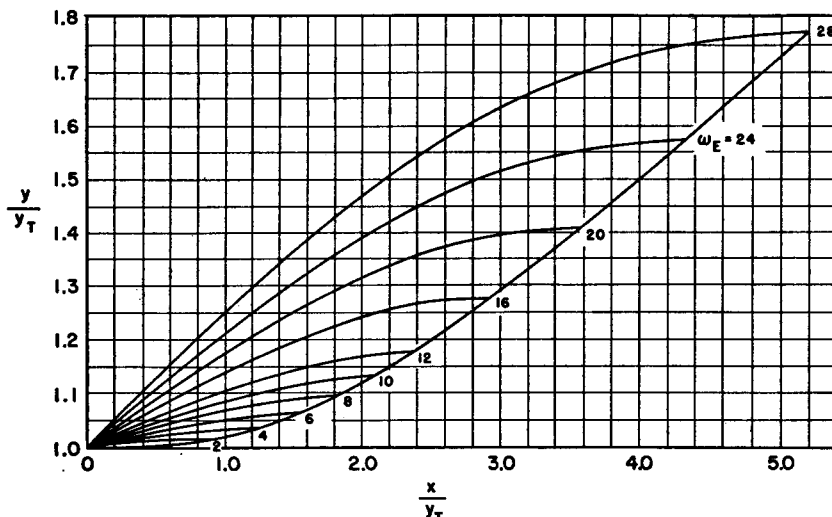


Fig. 15.36. Contours for sharp-corner nozzle (M.I.T. Gas Turbine Laboratory).

COMPARISON WITH EXPERIMENT. The very close agreement between theory and experiment for an accelerating flow is illustrated by Figs. 15.38 and 15.39.⁽⁹⁾ Fig. 15.38 shows the theoretical and experimental pressure distributions on the axis of the nozzle. Fig. 15.39a shows the

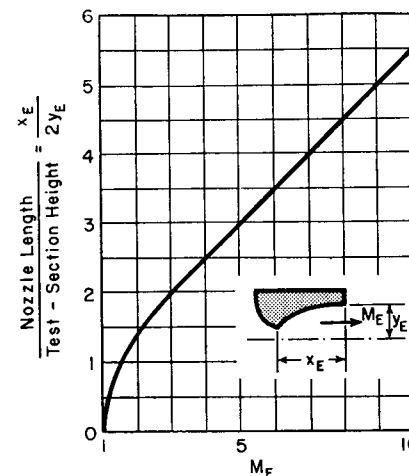


Fig. 15.37. Length of sharp-corner nozzle (after Shames and Seashore).

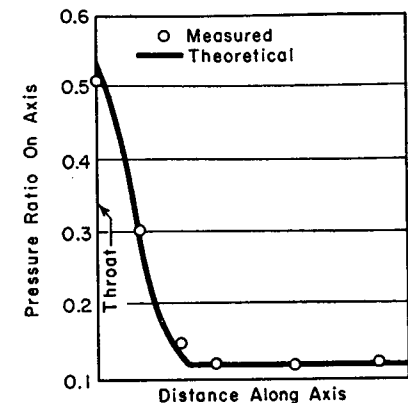


Fig. 15.38. Comparison between measured and theoretical pressure distribution on axis of sharp-corner nozzle of Fig. 15.34 (after Edelman).

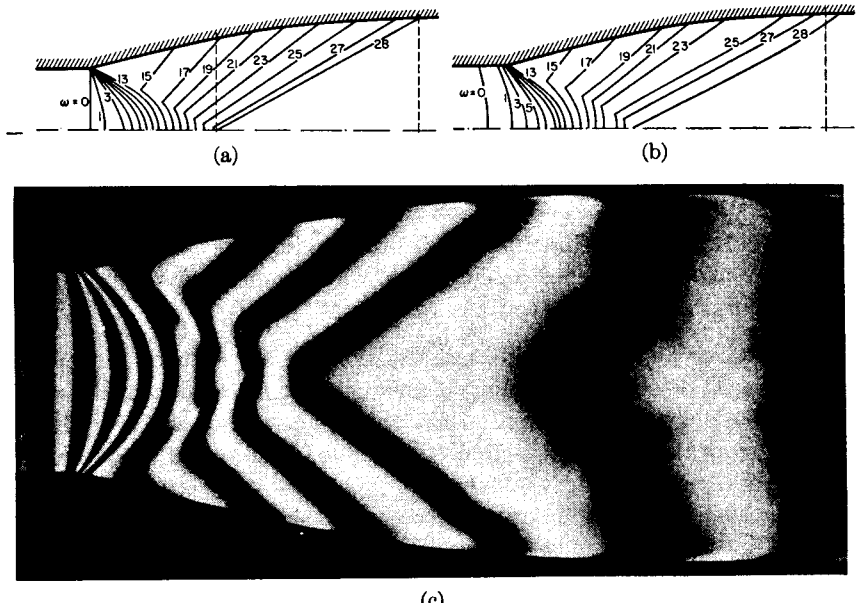


Fig. 15.39. Contours of constant pressure for sharp-corner nozzle of Fig. 15.34 (after Edelman).

- (a) From method of characteristics.
- (b) From interferogram analysis.
- (c) Typical interferogram of zero band width, showing contours of constant density.

theoretical curves of constant density and is to be compared with the measured curves of constant density of Fig. 15.39b. The latter chart was constructed with the help of interferograms similar to Fig. 15.39c. The agreement between theory and experiment is particularly good when it is considered that the test section of the nozzle was less than 1 inch by 1 inch, thus making boundary layer effects comparatively prominent.

The Subsonic Inlet. The shape of the sonic line, from which the entire nozzle design begins, depends on the shape of the subsonic inlet. There is no theoretical reason why any particular shape of sonic line is best, but the important thing is to know the shape. There are several possibilities:

- Subject to limitations of boundary-layer thickness, the subsonic inlet might be made so long and have such gentle curvature as to insure that the sonic line will be almost exactly a straight line normal to the axis.
- For a given shape of inlet the shape of the $M = 1$ line might be determined by analytical methods (see Chapter 21, Volume II).

(iii) For a given shape of inlet, preliminary tests, perhaps on a model, might be used to determine the sonic line. With this procedure it would probably be preferable to determine the conditions at some line downstream of the throat, so as to avoid the difficulty of constructing the Mach net near Mach Number unity.

In any case, to eliminate separation or thick boundary layers, the subsonic contours should be designed so that there are no local regions of rising pressure.

Construction Near Mach Number Unity. Because dM/dw approaches infinity as M approaches unity, the Mach net must be very fine in this region in order to have good accuracy.

Boundary Layer. The effects of friction are, for an accelerating flow with high Reynolds Number, confined to a thin boundary layer. In most nozzles, therefore, friction has only a perturbation effect. It acts to decrease the cross-sectional area available for flow, and thus to reduce slightly the exit Mach Number.

For best results it is desirable to correct the nozzle contour at each point by the amount of the local boundary-layer displacement thickness.

15.12. Adiabatic, Nonviscous Flow with Rotation

As shown in Chapter 16, an adiabatic nonviscous flow which is originally irrotational may become rotational as the result of passing through a curved shock. If there are no viscous or heat conduction effects, except

within the thin zone which we think of as the shock discontinuity, the stagnation enthalpy remains constant on each streamline. Moreover, the entropy on each streamline remains constant both upstream and downstream of the shock but undergoes an increase across the shock. Since the entropy increase for each streamline depends on the corresponding shock strength, the flow downstream of a curved shock is rotational (the rotation in a fluid is related to the rate of change of entropy and of stagnation enthalpy in a direction normal to the streamlines).

We shall outline in this article, therefore, the method of characteristics for a steady, two-dimensional, adiabatic, supersonic, nonviscous, rotational flow in which the stagnation enthalpy is the same for all points and in which the entropy is constant on each streamline but varies from one streamline to the next.

Governing Equations. The equation of continuity may be written

$$\rho \frac{\partial u}{\partial x} + \rho \frac{\partial v}{\partial y} + u \frac{\partial \rho}{\partial x} + v \frac{\partial \rho}{\partial y} = 0 \quad (15.35)$$

Since there are no viscous forces, Euler's equations may be written

$$u \frac{\partial u}{\partial x} + v \frac{\partial u}{\partial y} + (1/\rho) \frac{\partial p}{\partial x} = 0 \quad (15.36)$$

$$u \frac{\partial v}{\partial x} + v \frac{\partial v}{\partial y} + (1/\rho) \frac{\partial p}{\partial y} = 0 \quad (15.37)$$

Since we are considering regions of flow from which shocks are excluded, the entropy is a continuous function of x and y . Hence

$$ds = (\partial s / \partial x) dx + (\partial s / \partial y) dy$$

Now, the definition of a streamline is $dy/dx = v/u$. Furthermore, along a streamline, $ds = 0$, by assumption. Making these substitutions simultaneously, we get

$$u(\partial s / \partial x) + v(\partial s / \partial y) = 0 \quad (15.38)$$

Since the pressure is a continuous function of entropy and density,

$$dp = (\partial p / \partial s)_\rho ds + (\partial p / \partial \rho)_s d\rho \quad (15.39)$$

For a perfect gas,

$$ds/c_v = dp/p - k d\rho / \rho \quad (15.40)$$

so that $(\partial p / \partial s)_\rho = p/c_v$. Furthermore, the definition of sound velocity applied to a perfect gas gives

$$(\partial p / \partial \rho)_s = c^2 = kp / \rho$$

Thus Eq. 15.39 may be expressed as

$$dp = (\rho c^2 / k) d(s/c_v) + c^2 d\rho$$

and the partial derivatives $\partial p/\partial x$ and $\partial p/\partial y$ which appear in Eqs. 15.36 and 15.37 may therefore be written

$$\frac{\partial p}{\partial x} = (\rho c^2/k) \frac{\partial(s/c_v)}{\partial x} + c^2 \frac{\partial \rho}{\partial x} \quad (15.41)$$

$$\frac{\partial p}{\partial y} = (\rho c^2/k) \frac{\partial(s/c_v)}{\partial y} + c^2 \frac{\partial \rho}{\partial y} \quad (15.42)$$

Since u , v , ρ , and s are all continuous functions of x and y , we may write

$$du = (\partial u/\partial x) dx + (\partial u/\partial y) dy \quad (15.43)$$

$$dv = (\partial v/\partial x) dx + (\partial v/\partial y) dy \quad (15.44)$$

$$d\rho = (\partial \rho/\partial x) dx + (\partial \rho/\partial y) dy \quad (15.45)$$

$$ds = (\partial s/\partial x) dx + (\partial s/\partial y) dy \quad (15.46)$$

Solution of Equations. The expressions for $\partial p/\partial x$ and $\partial p/\partial y$ given by Eqs. 15.41 and 15.42 are now substituted into Eqs. 15.36 and 15.37, respectively. We then have eight quantities, namely, $\partial u/\partial x$, $\partial u/\partial y$, $\partial v/\partial x$, $\partial v/\partial y$, $\partial \rho/\partial x$, $\partial \rho/\partial y$, $\partial s/\partial x$, and $\partial s/\partial y$, which are connected by eight independent, linear, nonhomogeneous equations, namely, Eqs. 15.35, 15.36, 15.37, 15.38, 15.43, 15.44, 15.45, and 15.46. The solution for each of the eight quantities may be written symbolically in terms of the augmented determinant of the eight equations:

$\frac{\partial u}{\partial x}$	$\frac{\partial u}{\partial y}$	$\frac{\partial v}{\partial x}$	$\frac{\partial v}{\partial y}$	$\frac{\partial \rho}{\partial x}$	$\frac{\partial \rho}{\partial y}$	$\frac{\partial(s/c_v)}{\partial x}$	$\frac{\partial(s/c_v)}{\partial y}$	
ρ	0	0	ρ	u	v	0	0	0
u	v	0	0	c^2/ρ	0	c^2/k	0	0
0	0	u	v	0	c^2/ρ	0	c^2/k	0
0	0	0	0	0	0	u	v	0
dx	dy	0	0	0	0	0	0	du
0	0	dx	dy	0	0	0	0	dv
0	0	0	0	dx	dy	0	0	$d\rho$
0	0	0	0	0	0	dy	$d(s/c_v)$	

(15.47)

Equations of the Characteristics. In general, the characteristic curves are defined as those curves on the integral surfaces comprising the solution to the eight equations on which the eight derivatives $\partial u/\partial x$,

$\partial u/\partial y$, $\partial v/\partial x$, etc., etc., may be either indeterminate or discontinuous. The condition for this to be so is that each of the derivatives be of the form 0/0. Indeed, by selecting any one quantity, such as $\partial u/\partial x$, and setting equal to zero the determinants in both numerator and denominator of the solution for this quantity, we get after simplification the complete systems of characteristics:

$$u dy - v dx = 0 \quad (15.48a)$$

$$ds = 0 \quad (15.48b)$$

$$u du + v dv + c^2 \frac{d\rho}{\rho} = 0 \quad (15.48c)$$

$$(v^2 - c^2) dx^2 - 2uv dx dy + (u^2 - c^2) dy^2 = 0 \quad (15.49)$$

$$(u dy - v dx)(u dv - v du) + c^2 \left[\frac{d\rho}{\rho} + \frac{d(s/c_v)}{k} \right] (u dx + v dy) = 0 \quad (15.50)$$

Eq. 15.48a is the equation of the streamline. Likewise, Eq. 15.48b refers to a line of constant entropy, and hence also identifies a particular streamline. Furthermore, using the relations that

$$u du + v dv = V dV$$

$$c^2 \frac{d\rho}{\rho} = \left(k \frac{p}{\rho} \right) \left(\frac{1}{k} \frac{dp}{p} \right) = \frac{1}{\rho} dp$$

it is clear that Eq. 15.48c represents Euler's equation for changes in state along a streamline. Hence, Eqs. 15.48 state in sum that the streamlines are characteristic curves in a rotational adiabatic flow. Physically, this means that the streamlines are possible *slip lines*, or *vortex sheets* in an infinitesimal sense, on which there may be discontinuities in the derivatives of the velocity, density, entropy, and pressure.

If Eq. 15.49 is solved for dy/dx , the results will be recognized as being identical with those of Eq. 15.20. Hence Eq. 15.49 gives the differential equations of the physical characteristics, and can be reduced to the form of Eq. 15.23, namely,

$$(dy/dx)_{I, II} = \tan(\theta \mp \alpha) \quad (15.51)$$

This shows that these physical characteristics make the Mach angle to the velocity vector and are, therefore, identical with the Mach lines of the flow.

Turning to Eq. 15.50, it is convenient to express the velocity vector in terms of polar coordinates V and θ , by means of the relations $u = V \cos \theta$ and $v = V \sin \theta$. Making this transformation, and eliminating dy/dx

from Eq. 15.50 with the help of Eq. 15.51, we get the differential equation of the hodograph characteristics in the form

$$\mp \frac{d\theta}{\sin \alpha \cos \alpha} + \frac{d\rho}{\rho} + \frac{1}{k} d(s/c_v) = 0 \quad (15.52)$$

Now, since all states have the same stagnation enthalpy, it follows that

$$d(V^2/2) + c_p dT = 0; \quad \text{or} \quad V dV + (2/k - 1)c dc = 0$$

Furthermore, from the relation for the entropy of a perfect gas,

$$T ds = c_v dT + p d(1/\rho)$$

we have

$$ds/c_v = 2dc/c - (k - 1) d\rho/\rho$$

Combining these relations, we obtain

$$\frac{d\rho}{\rho} = - \frac{1}{k-1} \frac{ds}{c_v} - \frac{V dV}{c^2} \quad (15.53)$$

Substitution of Eq. 15.53 into Eq. 15.52 yields, after rearrangement,

$$\mp d\theta - \frac{1}{\tan \alpha} \frac{dV}{V} - \frac{\sin \alpha \cos \alpha}{k(k-1)} d\left(\frac{s}{c_v}\right) = 0 \quad (15.54)$$

This may be solved for $dV/d\theta$ to give

$$\frac{1}{V} \left(\frac{dV}{d\theta} \right)_{I, II} = \mp \tan \alpha - \frac{\sin^2 \alpha}{k(k-1)} \left[\frac{d(s/c_v)}{d\theta} \right]_{I, II} \quad (15.55)$$

By comparing Eq. 15.55 with Eq. 15.25 we see that the effects of vorticity are contained in the third term of Eq. 15.55. This term depends in part on the physical variables x and y , because the entropy is determined by the streamline rather than by the Mach Number. Consequently it is not possible to integrate immediately the hodograph characteristics, as was possible for irrotational flow. Instead, for each specific problem, both the physical and hodograph characteristics must be simultaneously constructed in a stepwise manner. Another consequence of the presence of the third term in Eq. 15.55 is that it eliminates the possibility of there being regions of simple waves in a rotational flow.

Numerical Method of Solution. The solution of practical problems is carried out by constructing the physical and hodograph characteristics nets piecewise by simultaneously solving Eqs. 15.51 and 15.55 in finite-

difference form, replacing an element of arc on one of the characteristic curves by a straight-line chord. Several related methods for carrying out such calculations are described in detail in Reference 3. A brief outline of one line of attack is given below in terms of the unit process required to construct the characteristics net.

Suppose that at points 1 and 2 in Fig. 15.40 we know $x_1, y_1, x_2, y_2, V_1, V_2, \theta_1, \theta_2, s_1, s_2$, thus completely defining the location and fluid properties of these two points. Let point 3 lie at the intersection of the physical II -characteristic passing through point 2 and of the physical I -characteristic passing through 1. The problem is to determine the location and the fluid properties of point 3.

Equations 15.51 may be written in finite-difference form

$$y_3 - y_1 = [\tan(\bar{\theta}_{1-3} - \bar{\alpha}_{1-3})](x_3 - x_1) \quad (15.56)$$

$$y_3 - y_2 = [\tan(\bar{\theta}_{2-3} + \bar{\alpha}_{2-3})](x_3 - x_2) \quad (15.57)$$

where $\bar{\theta}_{1-3}$ represents the arithmetic mean value of θ between points 1 and 3, i.e., $\bar{\theta}_{1-3} = (\theta_1 + \theta_3)/2$; and similarly for the other quantities with a bar.

The finite difference forms of Eq. 15.55 are

$$V_3 - V_1 = - \bar{V}_{1-3} \tan \bar{\alpha}_{1-3} (\theta_3 - \theta_1) - \frac{\bar{V}_{1-3} \sin^2 \bar{\alpha}_{1-3} s_3 - s_1}{k(k-1)} \frac{c_v}{c} \quad (15.58)$$

$$V_3 - V_2 = \bar{V}_{2-3} \tan \bar{\alpha}_{2-3} (\theta_3 - \theta_2) - \frac{\bar{V}_{2-3} \sin^2 \bar{\alpha}_{2-3} s_3 - s_2}{k(k-1)} \frac{c_v}{c} \quad (15.59)$$

From the adiabatic relation between M and V ,

$$dM/M = \left(1 + \frac{k-1}{2} M^2\right) (dV/V)$$

α and V are uniquely connected with each other. Moreover, the entropy depends only on the particular streamline on which a given point lies.

Eqs. 15.56 to 15.59 may be solved simultaneously by an iteration method. The values of V_3 and θ_3 are first chosen tentatively. Using these values, simultaneous solution of Eqs. 15.56 and 15.57 yields ap-

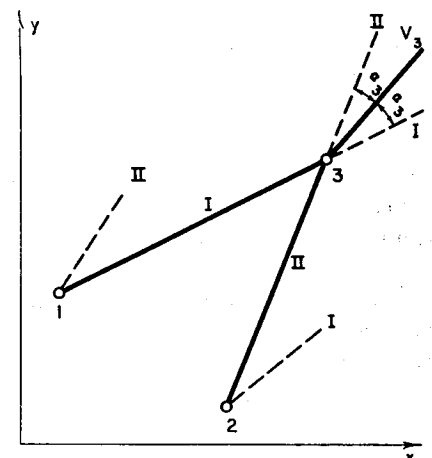


FIG. 15.40. Determination of properties at point 3 from data at points 1 and 2.

proximate values for x_3 and y_3 . By extrapolating the streamlines toward point 3, the entropy of point 3 may be tentatively determined. Then Eqs. 15.58 and 15.59 may be solved simultaneously for V_3 and θ_3 . If these values depart too greatly from the values originally assumed, the process of calculation is repeated again and again until satisfactory convergence is obtained.

Successive application of this type of calculation allows the entire characteristics net to be determined in a manner exactly like that for irrotational flow, with similar considerations applying as to the way in which various types of initial data determine the regions in which solutions may be obtained.

Semigraphical Method of Solution. The tediousness of the iteration method of calculation can be partly relieved by employing a semigraphical procedure which employs the irrotational hodograph characteristics. Noting that

$$dV/V = dM^*/M^*; \quad \sin \alpha = 1/M; \quad \tan \alpha = 1/\sqrt{M^2 - 1}$$

and using the adiabatic relation between M and M^* , we may put Eq. 15.55 in the form

$$\left(\frac{dM^*}{d\theta} \right)_{I, II} = \mp M^* \sqrt{\frac{1 - \frac{k-1}{k+1} M^{*2}}{M^{*2} - 1}} - \frac{1 - \frac{k-1}{k+1} M^{*2}}{\frac{2k(k-1)}{k+1} M^*} \left(\frac{d \frac{s}{c_v}}{d\theta} \right)_{I, II} \quad (15.60)$$

Expressed in finite-difference form, this becomes (15.60)

$$(\Delta M^*)_{I, II} = \mp \overline{M^*} \sqrt{\frac{1 - \frac{k-1}{k+1} \overline{M^{*2}}}{\overline{M^{*2}} - 1}} \Delta \theta - \frac{1 - \frac{k-1}{k+1} \overline{M^{*2}}}{2k(k-1) \overline{M^*}} \left(\Delta \frac{s}{c_v} \right)_{I, II} \quad (15.61a)$$

where \bar{M}^* refers to the mean value of M^* over the interval to which Eq. 15.61a is applied. This equation is also expressible as

$$(\Delta M^*)_{I, II} = \left[\left(\frac{\partial M^*}{\partial \theta} \right)_{I, II} \right]_s \Delta \theta + \left[\left(\frac{\partial M^*}{\partial (s/c_s)} \right)_{I, II} \right]_s \Delta \left(\frac{s}{c_s} \right) \quad (15.61b)$$

where the differential coefficients in the latter equation are functions of M^* and k as indicated by Eq. 15.61a.

Returning now to the unit process of Fig. 15.40, we may from the given initial data locate the image points 1 and 2 in the hodograph diagram of Fig. 15.41. The mean Mach lines *I* and *II* are now tentatively drawn in Fig. 15.40, thus establishing an approximate position for point 3 and allowing the entropy at 3 to be determined tentatively. The second term on the right-hand side of Eq. 15.61b may then be approximately calculated for each characteristic, and the corresponding partial values of ΔM^* laid off *radially* in Fig. 15.41 as the lines 1-1a

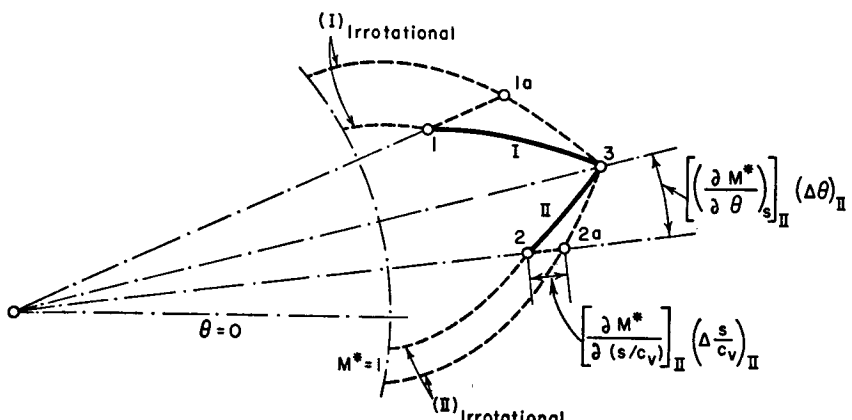


FIG. 15.41. Graphical construction in hodograph plane for flow with vorticity

and 2-2a, inasmuch as this part of ΔM^* represents the change in M^* at constant θ . Thus the intermediate points 1a and 2a are tentatively established.

The first term on the right-hand side of Eq. 15.61a gives the change of M^* for a given change of θ at constant entropy, and corresponds to irrotational flow. This term is represented graphically by the hodograph characteristics for irrotational flow, i.e., by the epicycloid curves of Fig. 15.5. The intersection of the irrotational II -characteristic passing through $2a$ with the irrotational I -characteristic passing through $1a$ therefore establishes the hodograph point 3 , at least approximately. The mean Mach lines I and II may now be redrawn to establish the physical point 3 more accurately, and the entire process of calculation repeated until the desired accuracy is obtained.

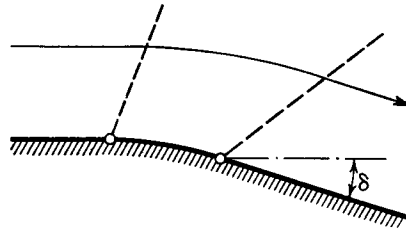
It may be shown⁽³⁾ that if iteration is not used, i.e., if the initial values rather than the mean values for each step are employed to evaluate the coefficients in Eq. 15.61a or in Eqs. 15.56 to 15.59, the error in the stepwise integration is of the order of $(\Delta\theta)^2$, where the latter is a measure of the net spacing; whereas, if iteration is employed, the error is only of the order of $(\Delta\theta)^3$.

REFERENCES AND SELECTED BIBLIOGRAPHY

1. FERRI, A. *Elements of Aerodynamics of Supersonic Flows*. New York: The Macmillan Co., 1949.
2. LIEPMANN, H. W., and PUCKETT, A. E. *Introduction to Aerodynamics of a Compressible Fluid*. New York: John Wiley & Sons, Inc., 1947.
3. ISENBERG, J. S., and LIN, C. C. The Method of Characteristics in Compressible Flow. Part I: Steady Supersonic Flow, *Air Materiel Command Report*, No. F-TR-1173A-ND (1947). Part IA: Tables and Charts, *Air Materiel Command Report*, No. F-TR-1173B-ND (1947).
4. CRONVICH, L. L. Numerical-Graphical Methods of Characteristics for Plane Potential Shock-Free Flow Problems, *Jour. Inst. Aero. Sci.*, Vol. 14, No. 4 (1947), p. 237.
5. SHAPIRO, A. H., and EDELMAN, G. M. Method of Characteristics for Two-Dimensional Supersonic Flow—Graphical and Numerical Procedures, *Jour. App. Mech.*, Vol. 14, No. 2 (1947), p. A-154.
6. TEMPLE, G. The Method of Characteristics in Supersonic Flow, *British Rep., No. S.M.E. 3282, R.A.E.* (Jan., 1944).
7. CROWN, J. C. Supersonic Nozzle Design, *NACA Tech. Note*, No. 1651 (1948).
8. PINKEL, I. I. Equations for the Design of Two-Dimensional Supersonic Nozzles, *NACA RM*, No. E8B02 (1948).
9. EDELMAN, G. M. The Design, Development, and Testing of Two-Dimensional Sharp-Cornered Nozzles, S.M. Thesis, Dept. of Mech. Eng., M.I.T. (1948).
10. SHAMES, H., and SEASHORE, F. L. Design Data for Graphical Construction of Two-Dimensional Sharp-Edge-Throat Supersonic Nozzles, *NACA RM*, No. E8J12 (1948).

PROBLEMS

- 15.1. Consider the expansive flow around a curved wall (see sketch).



PROB. 15.1.

Compare the exact theory with the linear theory by plotting curves of p_2/p_1 versus M_1 for two values of δ , namely, 2° and 10° . Use a range of M_1 from 1 to 3.

- 15.2. Compare supersonic flow past a convex corner with (a) incompressible flow, (b) subsonic flow. If the fluid is compressible, is it possible to have a purely subsonic flow in the neighborhood of the corner? How would a boundary layer near the wall influence the supersonic flow past a convex corner?

- 15.3. Plot a Prandtl-Meyer streamline from $M_1 = 1$ to $M_2 = 5$.
- 15.4. In simple-wave flows what are the maximum stream turning angles for
- Decelerating flows with initial Mach Numbers of (i) 1.0, (ii) 2.0, (iii) 5.0, and (iv) 10.0?
 - Accelerating flows with initial Mach Numbers of (i) 1.0, (ii) 2.0, (iii) 5.0, and (iv) 10.0?

- 15.5. A two-dimensional jet leaves a converging-diverging nozzle in parallel flow (see sketch) and discharges into the atmosphere, where the pressure is 14.7 psia. The area ratio of the nozzle is 2.0.

Calculate the angle δ in degrees, if

- (a) $p_0 = 200$ psia
- (b) p_0 is infinite

- 15.6. Suppose that in Fig. 15.11a the shape of the wall is given by

$$y = f(x_1, y_1, x)$$

Find the equation of the streamline passing through point $1'$, in terms of x_1' , y_1' , and the functional relation above.

Generalize your results to any arbitrary initial Mach Number, introducing M_1 as a parameter.

- 15.7. Consider a corner-type flow beginning at Mach Number unity. Derive the following equation in polar coordinates for a streamline:

$$\frac{r}{r^*} = \left[\cos \sqrt{\frac{k-1}{k+1}} \nu \right]^{-\frac{k+1}{k-1}}$$

where r is the radius vector to the streamline; r^* is the radius vector to the same streamline at $M = 1$; and ν is the angle measured clockwise from r^* to r .

- 15.8. Using the theory of characteristics as outlined in Appendix A, determine the shapes of the characteristic curves in the physical and hodograph planes for the differential equation corresponding to supersonic, uniform, parallel flow with small perturbations.

- 15.9. Consider a perfect gas with $k = 1.0$

(a) Investigate the shape of the hodograph characteristics.

- (b) For a complete corner-type flow determine in polar coordinates the equation of a streamline in terms of r , the radius vector to the streamline; r^* , the radius vector to the same streamline at $M = 1$; and ν , the angle measured clockwise from r^* to r .

- 15.10. Show that a flow region adjacent to a region of uniform, parallel flow must be a region of simple waves.

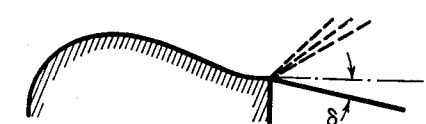
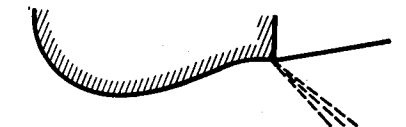
- 15.11. (a) Demonstrate that when a pressure wave is reflected from a plane wall,

$$(\Delta\theta)_{\text{reflected}} = -(\Delta\theta)_{\text{incident}}$$

$$(\Delta\omega)_{\text{reflected}} = (\Delta\omega)_{\text{incident}}$$

- (b) Show that when two pressure waves of opposite family penetrate each other, the values of $\Delta\theta$ and of $\Delta\omega$ for each wave are the same after penetration as they are before penetration.

- (c) Derive a corresponding rule for reflection of a wave from a constant-pressure boundary.



PROB. 15.5.

15.12. (a) Suppose that, in Fig. 15.17, the line 2-3 is a solid boundary, and that θ is known on this boundary. Work out the computation formulas for determining conditions at 3 from those at 1 and 2, given $\omega_1, \theta_1, x_1, y_1, \omega_2, \theta_2, x_2, y_2$, and given also θ_3 and y_3 as functions of x_3 . Note that iteration is required.

(b) Suppose that in Fig. 15.17, the line 2-3 is a constant-pressure boundary of the flow, as for a free jet. Work out the computation formulas for determining conditions at 3 from those at 1 and 2, given $\omega_1, \theta_1, x_1, y_1, \omega_2, \theta_2, x_2, y_2$, and ω_3 .

15.13. Demonstrate that if in a given region of the flow all states are mapped on a single hodograph characteristic of family I, then in that region all the left-running Mach lines are straight lines, and on each left-running Mach line all fluid properties are constant.

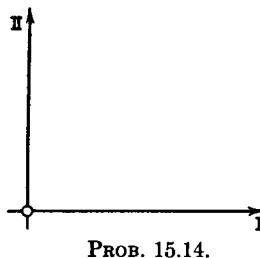
Are the right-running Mach lines straight lines for this case?

15.14. Consider a plane in which the Cartesian coordinates are the characteristic coordinates, I and II (see sketch).

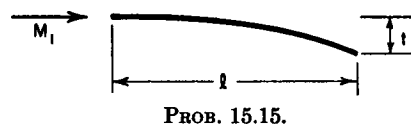
(a) Sketch in this plane lines of constant Mach Number and of constant flow direction.

(b) Plot the fields of Fig. 15.12a in this plane.

(c) Plot the net points of Fig. 15.15a in this plane.



PROB. 15.14.

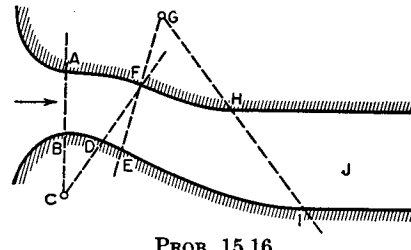


PROB. 15.15.

15.15. A thin profile has the shape of a parabola, with its leading edge parallel to the oncoming air stream (see sketch).

Assuming that $t/l = 0.10$ and $M_1 = 2.059$, find the lift and pressure drag coefficients.

15.16. A nozzle is to be designed to deliver a parallel, uniform stream of air at a Mach Number of 2.059. The general arrangement of the nozzle is as shown in the sketch.



PROB. 15.16.

The inlet section will be assumed to have a shape which produces a horizontal parallel flow at the throat section AB.

In the region AFDB the flow is an expansive "corner flow" around the corner C. The length AC is twice the length AB.

In the region FED the flow is uniform and parallel.

In the region FHIE the flow is an expansive "corner flow" around the corner G. The length GE is twice the length FE.

Region J is a uniform, parallel flow with a Mach Number of 2.059. The direction of the stream at J is the same as the direction at the throat AB.

Assuming that the throat height AB is one inch, find the lengths and inclinations to the horizontal (in degrees) of the following lines: FD, FE, DE, and HI. Using these principal dimensions and directions, make a sketch to scale of the nozzle.

15.17. Work out the problem of Fig. 15.12 by the lattice-point method.

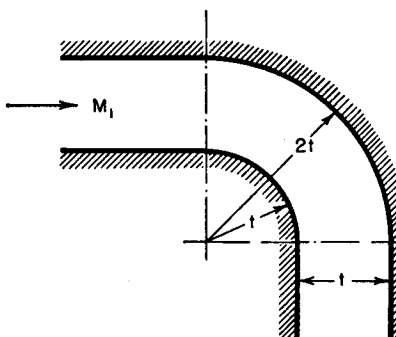
15.18. Consider a two-dimensional, source-type flow with an initial Mach Number of 1.0 and a final Mach Number of 2.0. Using the method of characteristics, plot pressure versus radius for stepwise solutions with turning angles across each wave of 8° , 4° , and 2° , and compare with the exact solution, corresponding to a turning angle across each wave of 0° .

15.19. Design a symmetrical blade for an impulse turbine with a turning angle of 120° and an entering and leaving Mach Number of 2.059.

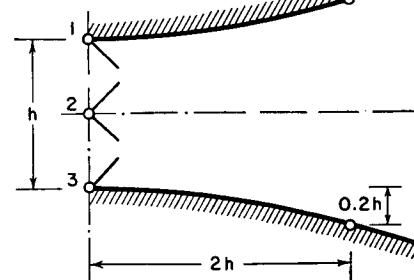
15.20. Design a stationary supersonic compressor cascade of the type shown in Fig. 15.27, assuming that $M_1 = 2.059$, $p_1 = 10$, that the air entering is inclined 60° to the axial direction, that a normal shock occurs at $M = 1.4$, and that the flow leaves in the axial direction.

Lay out a pair of blades, and determine the leaving Mach Number, pressure, and the over-all ratio of stagnation pressures.

15.21. A uniform, parallel flow with $M_1 = 2.059$ and $p_1 = 100$ approaches the two-dimensional 90° -bend shown in the sketch. Determine the flow pattern leaving the bend.



PROB. 15.21.

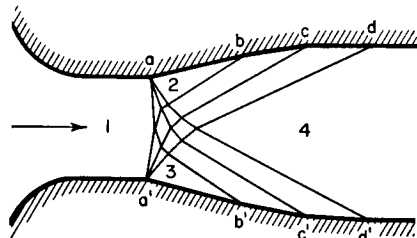


PROB. 15.22.

15.22. The two-dimensional passage shown in the sketch has parabolically shaped walls. At section 1-2-3 the flow is uniform and parallel, and $M = 1.33$. Using the coarse characteristic system suggested by the sketch, plot the pressure

distribution on the walls and along the center line for a distance of $4h$ downstream of the initial section.

15.23. A converging-diverging nozzle for a wind tunnel (see sketch) is to be designed to deliver a supersonic stream at a Mach Number of 1.915. The nozzle will draw air from the atmosphere, where the pressure and temperature are 14.7 psia and 70°F, respectively. A flow rate of 1 lb/sec is to be accommodated.



PROB. 15.23.

The design is to be based on sharp corners at the throat section aa' , at which section it may be assumed that the flow is uniform and parallel. The contours $a'b'c'd'$ are to be designed so as to produce a uniform, parallel stream in region 4. In carrying out the design, use the wave pattern suggested in the sketch, selecting the Mach lines between regions 1 and 2 to correspond to equal deflection angles across each of the Mach lines.

Assuming that the height of the nozzle at the throat (distance aa') is 2 inches, present the following design data:

- A sketch to scale of the nozzle contours.
- The height of the test section, dd' , and the width of the tunnel at the throat and at the test section.
- A plot of pressure versus distance along the axis of the tunnel, and along the wall contour.
- The maximum half-angle of divergence of the expanding portion of the nozzle.
- Draw the streamline which at the throat is midway between the axis and wall. Compare the length-height ratio of a nozzle using this streamline as a wall contour with the length-height ratio of the sharp-corner nozzle.

15.24. Determine the form of the hodograph characteristics for the tangent gas of Chapter 11.

15.25. Show, for adiabatic flow, that a plot with polar coordinates M^* and α traces out an ellipse.

Demonstrate how an $M^*-\alpha$ ellipse, drawn on a sheet of tracing paper to the same scale as the $M^*-\theta$ characteristic curves, may be used in conjunction with the latter for graphically determining wave directions without drawing normals to the hodograph characteristics.

Chapter 16

OBLIQUE SHOCKS

16.1. Introductory Remarks

Normal shocks (Chapter 5) are only special forms of pressure discontinuities within the fluid. More generally, the discontinuities observed in practice are inclined to the direction of the oncoming flow. They are called *oblique shocks*.

Oblique shocks tend to occur in supersonic flow because, as shown in Chapters 5 and 15, continuous compression waves tend to merge until they form a discontinuity. Sometimes the oblique shock is attached to the surface of a body, but this occurs only when the stream is forced to change direction suddenly, as in a sharp concave corner. Otherwise, the oblique shock is usually detached.

Oblique shock waves occur in almost all supersonic flow patterns of practical significance, although it should be pointed out that the mere existence of supersonic flow does not imply that shock waves must necessarily appear somewhere in the flow field. The subject matter of this chapter is, therefore, essential to the study of supersonic flow, and is relevant to such varied applications as nozzles, diffusers, projectiles and missiles, lifting surfaces, supersonic compressors, etc.

Additional material relevant to the subject matter of the present chapter may be found in Chapters 5, 14, 15, and in Volume II, Chapters 19 and 28.

NOMENCLATURE

a	angle of attack	J_1, J_2 , etc.	shape integrals defined by
c^*	critical speed of sound		Eqs. 16.24
c_p	specific heat at constant pressure	k	ratio of specific heats
C_1, C_2, C_3	coefficients defined by Eqs. 16.21	l	chord length of profile
C_L	lift coefficient	$l_{c.p.}$	distance from leading edge to center of pressure
C_D	drag coefficient	M	Mach Number
$C_{M\pi}$	moment coefficient, reckoned about leading edge	p	pressure
D	coefficient defined by Eq. 16.23	R	gas constant
		s	entropy per unit mass
		t	maximum thickness of profile

NOMENCLATURE—Continued

T	absolute temperature	ρ	mass density
u	x -component of velocity	σ	angle of shock to incoming flow
v	y -component of velocity	τ	slope of profile surface with respect to chord line
V	resultant velocity		
V_n	component of velocity normal to shock		
V_t	component of velocity parallel to shock	$(\cdot)_1$	signifies conditions upstream of oblique shock
α	Mach angle	$(\cdot)_2$	signifies conditions downstream of oblique shock
δ	turning angle across shock; thickness ratio of profile	$(\cdot)_0$	signifies stagnation state
δ^*	turning angle for which flow downstream of shock is sonic	$(\cdot)_x$	signifies conditions upstream of normal shock
δ_{\max}	maximum turning angle for oblique shock	$(\cdot)_y$	signifies conditions downstream of normal shock
η	coordinate normal to chord of profile	$(\cdot)_{\infty}$	signifies free-stream conditions
θ	flow direction	$(\cdot)_L$	signifies lower surface of profile
ξ	coordinate along chord of profile	$(\cdot)_U$	signifies upper surface of profile

Transformation of Normal Shock into Oblique Shock. A logical means for introducing the oblique shock is by way of the normal shock. Referring to Fig. 16.1a, suppose that a stationary observer sees the gas in state 1 suddenly decelerated and compressed to state 2 by a normal shock. Now imagine that the observer moves *along* the shock front in a downward direction with the speed V_t . The moving observer then perceives the flow pattern of Fig. 16.1b, in which the shock front is inclined to the initial direction of flow, and in which the streamline undergoes a sudden change of direction as it crosses the shock. The oblique shock flow pattern thus constructed is characterized by equal tangential components of velocity on the two sides of the shock. By allowing one of the streamlines of Fig. 16.1b to represent a solid wall, we obtain the solution for supersonic flow in the neighborhood of a concave corner (Fig. 16.1c). Obviously, by the same device of imparting a uniform velocity to the entire flow field *along* the shock, any straight segment of an oblique shock may be transformed back into a normal shock.

The relations between the fluid properties on the two sides of the oblique shock may be obtained from the familiar normal shock relations by employing the transformation equations between the flow picture of Fig. 16.1a and that of Fig. 16.1b. In this connection, note that such

thermodynamic properties as temperature, pressure, density, sound speed, and entropy are unchanged by the motion of the observer. On the other hand, the fluid velocity, Mach Number, and stagnation temperature and pressure are altered when the tangential velocity V_t is added to the normal-shock flow pattern. The magnitude of V_t is arbitrary, and hence there is an additional degree of freedom in the oblique shock relations. This means that although only one independent parameter (the approach Mach Number, say) is required for the normal shock, two independent parameters will be required for oblique shocks.

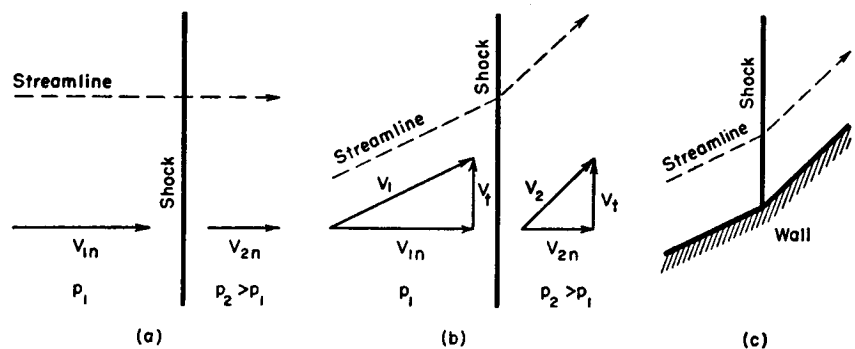


FIG. 16.1. Transformation of normal shock to oblique shock.

- (a) Stationary observer sees normal shock.
- (b) Observer moving along shock line sees oblique shock.
- (c) Flow of (b) interpreted as pattern produced near concave corner in wall.

Rather than use the transformation approach outlined above, we shall derive the oblique shock relations by returning to the principles of continuity, momentum, and energy. It will be assumed throughout this chapter that we are dealing with a perfect gas.

Distinction Between Shocks and Mach Waves. It will be recalled from Chapter 15 that when the velocity is everywhere continuous, regions having different types of flow may be “patched” together only on the characteristic curves. That is, along the characteristics there is no discontinuity in the velocity or any other fluid property, but there may be discontinuities in the derivatives of the velocity or of other fluid properties. When we deal with shocks, however, we are no longer bound by this rule, because we admit the possibility of discontinuities in all fluid properties across the shock line. Hence the shock is also a patching line which joins regions having different types of flow. But it is essential to keep in mind the distinction that the physical characteristics, or Mach lines, are patching lines for continuous flows, whereas shocks are patching lines for discontinuous flows.

16.2. Oblique Shock Equations

Governing Physical Relations. The oblique shock will be analysed by writing the continuity, momentum, and energy relations for the flow through the control surface of Fig. 16.2. Noting that the two stream-

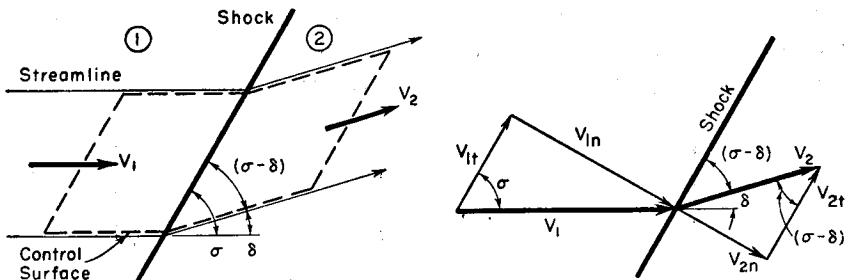


FIG. 16.2. Nomenclature for oblique-shock analysis.

lines forming part of the control surface are exact duplicates of each other, we may write

Continuity.

$$\rho_1 V_{n1} = \rho_2 V_{n2} \quad (16.1)$$

Momentum in t-direction.

$$(\rho_1 V_{n1}) V_{t1} = (\rho_2 V_{n2}) V_{t2}; \quad \therefore V_{t2} = V_{t1} = V_t \quad (16.2)$$

Momentum in n-direction.

$$p_1 - p_2 = \rho_2 V_{n2}^2 - \rho_1 V_{n1}^2 \quad (16.3)$$

Energy.

$$c_p(T_1 - T_2) = (V_t^2 - V_1^2)/2 \quad (16.4)$$

The absence of change in the tangential component of velocity (Eq. 16.2) bears out the change-in-coordinate point of view of Art. 16.1.

From Eq. 16.2 and the geometry of the velocity triangles,

$$V_2^2 - V_1^2 = (V_{n2}^2 + V_{t2}^2) - (V_{n1}^2 + V_{t1}^2) = V_{n2}^2 - V_{n1}^2$$

Furthermore, the perfect gas relations yield

$$c_p T = c_p (p/\rho R) = (k/k - 1)(p/\rho)$$

hence the energy equation may be expressed as

$$\frac{k}{k-1} \left(\frac{p_2}{\rho_2} - \frac{p_1}{\rho_1} \right) = \frac{V_{n1}^2 - V_{n2}^2}{2} \quad (16.5)$$

Eqs. 16.1, 16.2, 16.3, and 16.5, together with the perfect gas relations, define completely the relations between the states on the two sides of

the shock. For example, suppose that state 1 is completely specified by the values of p_1 , ρ_1 , V_{n1} , and V_{t1} . Then the four equations mentioned are sufficient to determine p_2 , ρ_2 , V_{n2} , and V_{t2} . Since V_{n1} and V_{t1} together specify the shock angle σ , and since V_{n2} and V_{t2} together specify the angle $(\sigma - \delta)$, the solutions also yield the shock angle σ and the turning angle δ . Furthermore, the values of p and ρ define the sound speed c , so that the Mach Numbers fore and aft of the shock, M_1 and M_2 respectively, may also be found.

The basic shock relations of Eqs. 16.1, 16.2, 16.3, and 16.5 may be combined in many ways to yield a great many algebraic relations relating various shock parameters.^(1, 2, 3) Practically, we wish to obtain those relations which lead to simple numerical calculations, or which by their forms lead to general conclusions concerning the nature of oblique shocks. We shall in the remainder of this article derive or set down some of the more useful relations of these two types.

The Rankine-Hugoniot Equations. Let us eliminate all velocity terms from the basic equations and arrive at a relation in terms of pressure and densities.

Rearranging Eq. 16.3 and employing Eq. 16.1, we have

$$\begin{aligned} p_2 - p_1 &= \rho_1 V_{n1}^2 - \rho_2 V_{n2}^2 \\ &= \rho_1 V_{n1}^2 \left(1 - \frac{\rho_2}{\rho_1} \frac{V_{n2}^2}{V_{n1}^2} \right) = \rho_1 V_{n1}^2 \left(1 - \frac{\rho_1}{\rho_2} \right) \end{aligned}$$

from which

$$V_{n1}^2 = \frac{p_2 - p_1}{\rho_2 - \rho_1} \frac{\rho_2}{\rho_1} \quad (16.6a)$$

Similarly, we may solve for V_{n2} from Eqs. 16.3 and 16.1,

$$V_{n2}^2 = \frac{p_2 - p_1}{\rho_2 - \rho_1} \frac{\rho_1}{\rho_2} \quad (16.6b)$$

Multiplying these two relations, we get

$$V_{n1} V_{n2} = \frac{p_2 - p_1}{\rho_2 - \rho_1} \quad (16.7)$$

Substituting Eqs. 16.6a and 16.6b into Eq. 16.5, and rearranging, we obtain the pressure ratio as a unique function of the density ratio, or the density ratio as a unique function of pressure ratio:

$$\frac{p_2}{p_1} = \frac{\frac{k+1}{k-1} \frac{\rho_2}{\rho_1} - 1}{\frac{k+1}{k-1} - \frac{\rho_2}{\rho_1}}; \quad \frac{\rho_2}{\rho_1} = \frac{\frac{k+1}{k-1} \frac{p_2}{p_1} + 1}{\frac{k+1}{k-1} + \frac{p_2}{p_1}} \quad (16.8)$$

These are the *Rankine-Hugoniot relations* and are represented graphically in Fig. 16.3. They show that the density ratio across the shock depends on the initial Mach Number and on the shock angle only insofar as these quantities influence the pressure ratio. A shock with a given pressure ratio has associated with it a density ratio which does not depend on the obliquity of the shock, and hence the Rankine-Hugoniot relations are valid for normal shocks as well as for oblique shocks of any shock angle. Indeed, this might have been set down from the beginning by arguing that, in a coordinate transformation which changes a normal shock to an oblique shock, the relations connecting the pressure and density changes are unaltered.

It follows further from the perfect gas laws that across shocks of any obliquity there is a unique relation between temperature ratio and pressure ratio, and a unique relation between temperature ratio and density ratio.

The Prandtl Relation. An interesting and revealing relation between the velocity components may be found by eliminating the pressures and densities from the basic equations.

Since the flow is adiabatic, we may rewrite Eq. 16.4 in terms of the stagnation temperature, T_0 :

$$c_p T_1 + (V_{n1}^2 + V_{t1}^2)/2 = c_p T_2 + (V_{n2}^2 + V_{t2}^2)/2 \equiv c_p T_0$$

But, since $c_p T = (k/k - 1)(p/\rho)$, this becomes

$$\frac{k}{k-1} \frac{p_1}{\rho_1} + \frac{V_{n1}^2 + V_{t1}^2}{2} = \frac{k}{k-1} \frac{p_2}{\rho_2} + \frac{V_{n2}^2 + V_{t2}^2}{2} = \frac{k}{k-1} \frac{p_0}{\rho_0}$$

However, from the adiabatic relations of Chapter 4,

$$\frac{k}{k-1} \frac{p_0}{\rho_0} = \frac{c_0^2}{k-1} = \frac{k+1}{2(k-1)} c^{*2}$$

We may now solve for p_1 and p_2 from the previous equation in the form

$$p_1 = \rho_1 \left[\frac{k+1}{2k} c^{*2} - \frac{k-1}{2k} (V_{n1}^2 + V_{t1}^2) \right]$$

$$p_2 = \rho_2 \left[\frac{k+1}{2k} c^{*2} - \frac{k-1}{2k} (V_{n2}^2 + V_{t2}^2) \right]$$

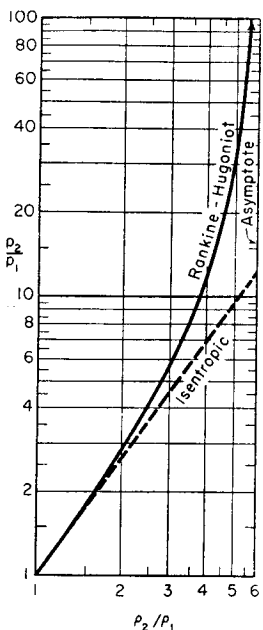


FIG. 16.3. Rankine-Hugoniot relation compared with isentropic law, for $k = 1.4$.

Substituting these expressions for p_1 and p_2 into Eq. 16.3, we get

$$\begin{aligned} \rho_1 \left[\frac{k+1}{2k} (V_{n1}^2 + c^{*2}) - \frac{k-1}{2k} V_{t1}^2 \right] \\ = \rho_2 \left[\frac{k+1}{2k} (V_{n2}^2 + c^{*2}) - \frac{k-1}{2k} V_{t2}^2 \right] \end{aligned}$$

Introducing Eqs. 16.1 and 16.2, and reducing algebraically, we finally get

$$V_{n2} V_{n1} = c^{*2} - \frac{k-1}{k+1} V_t^2 \quad (16.9)$$

which is known as the *Prandtl relation*.

For a normal shock, with $V_t = 0$, this takes the special form $V_1 V_2 = c^{*2}$.

Another useful form is found through combination of Eqs. 16.9 and 16.7,

$$\frac{p_2 - p_1}{\rho_2 - \rho_1} = c^{*2} - \frac{k-1}{k+1} V_t^2 \quad (16.10)$$

Working Formulas for Oblique Shocks. We shall now derive a convenient set of formulas for numerical calculations.

From the geometry of Fig. 16.2,

$$V_{t1} = V_1 \cos \sigma; \quad V_{t2} = V_2 \cos (\sigma - \delta) \quad (16.11)$$

$$V_{n1} = V_1 \sin \sigma; \quad V_{n2} = V_2 \sin (\sigma - \delta) \quad (16.12)$$

Since $V_{t1} = V_{t2}$, it follows from Eq. 16.11 that

$$V_1/V_2 = \cos (\sigma - \delta)/\cos \sigma$$

With Eq. 16.12, the continuity equation becomes

$$\rho_1 V_1 \sin \sigma = \rho_2 V_2 \sin (\sigma - \delta)$$

Therefore,

$$\frac{\rho_2}{\rho_1} = \frac{V_1}{V_2} \frac{\sin \sigma}{\sin (\sigma - \delta)} = \frac{\cos (\sigma - \delta)}{\cos \sigma} \frac{\sin \sigma}{\sin (\sigma - \delta)} = \frac{\tan \sigma}{\tan (\sigma - \delta)} \quad (16.13)$$

We now rearrange Eq. 16.3 with the help of Eqs. 16.1 and 16.12, and get

$$p_2 - p_1 = \rho_1 V_{n1}^2 \left(1 - \frac{\rho_2}{\rho_1} \frac{V_{n2}^2}{V_{n1}^2} \right) = \rho_1 V_1^2 (\sin^2 \sigma) \left(1 - \frac{\rho_1}{\rho_2} \right)$$

However, since $\rho_1 V_1^2 = k p_1 M_1^2$, we may solve for the pressure ratio in the form

$$\frac{p_2}{p_1} = 1 + k M_1^2 (\sin^2 \sigma) \left(1 - \frac{\rho_1}{\rho_2} \right) \quad (16.14)$$

If we had factored out $\rho_2 V_{n2}^2$ in Eq. 16.3, we would have arrived instead at

$$\frac{p_1}{p_2} - 1 = kM_2^2 \left(1 - \frac{\rho_2}{\rho_1} \right) \sin^2(\sigma - \delta) \quad (16.15)$$

Eqs. 16.8, 16.13, 16.14, and 16.15 constitute four relations among the variables σ , δ , M_1 , M_2 , p_2/p_1 , and ρ_2/ρ_1 . Any two of these variables, therefore, may be taken as independent parameters, the values of which completely determine the values of the four remaining variables. The temperature ratio, entropy change, and ratio of isentropic stagnation pressures may of course be calculated readily after the variables named above are specified.

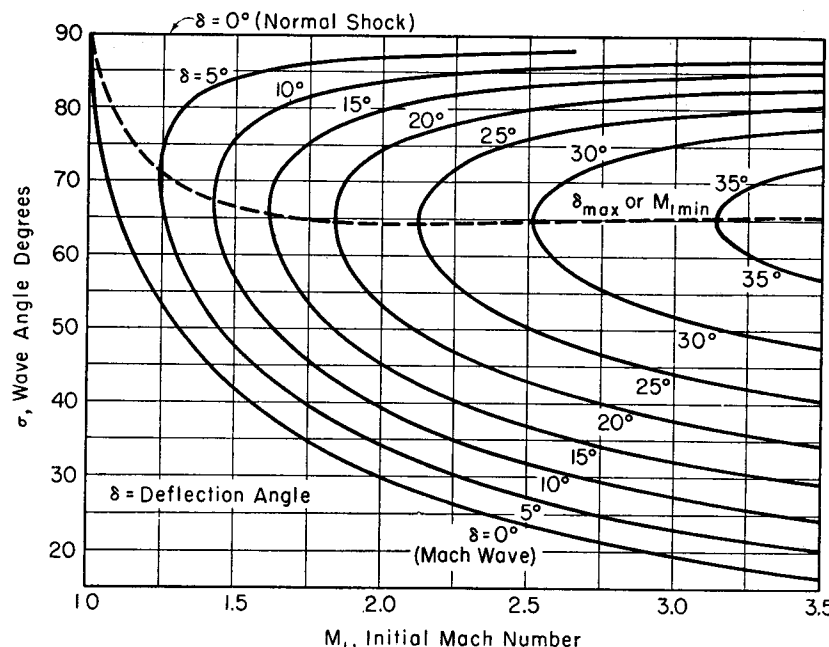


FIG. 16.4. Shock angle versus inlet Mach Number and turning angle ($k = 1.4$).

Tables and Charts. In Reference 8, tables representing the shock relations are given with σ and δ as independent arguments. In Reference 5, one set of tables has M_1 and σ as independent arguments, and another set has M_1 and δ as independent arguments. Reference 4 has convenient large-scale working charts with M_1 and δ as independent variables. Additional convenient tables and charts may be found in References 6, 7, 15, 16, and 17.

Figs. 16.4, 16.5, and 16.6 show the general orders of magnitude represented by the various shock formulas. In these charts, M_1 and δ are

taken as independent, and σ , M_2 , p_2/p_1 , and ρ_2/ρ_1 are the dependent quantities. The corresponding values of ρ_2/ρ_1 may be read approximately from Fig. 16.3, or may be found from Table B.3 at the appropriate value of p_2/p_1 .

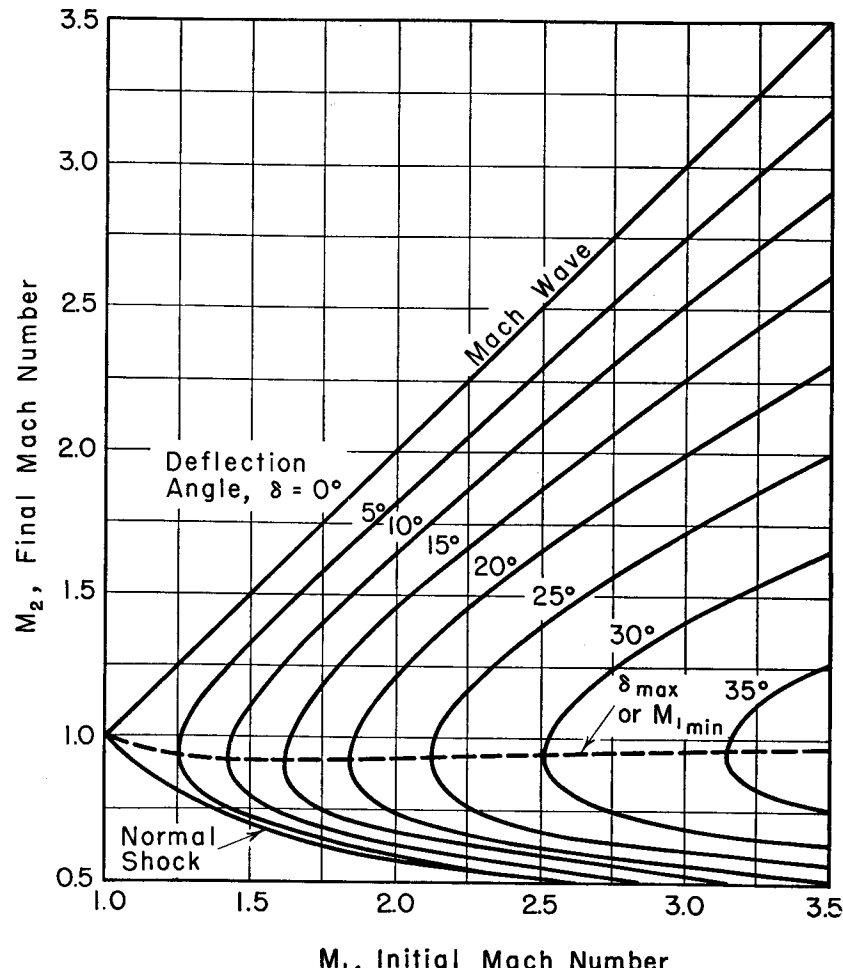


FIG. 16.5. Exit Mach Number versus inlet Mach Number, with turning angle as parameter ($k = 1.4$).

ADAPTATION OF NORMAL SHOCK TABLES TO OBLIQUE SHOCKS. Table B.3, representing the normal-shock relations, may be adapted to oblique-shock calculations. An oblique shock with an approach Mach Number M_1 may, by a transformation of the coordinate system, be reduced to a normal shock with an approach Mach Number $M_1 \sin \sigma$. Consequently, if M_x of Table B.3 is taken to represent $M_1 \sin \sigma$, then $p_y/p_x, \rho_y/\rho_x, T_y/T_x$,

and p_{0y}/p_{0x} of the table are respectively the values of p_2/p_1 , ρ_2/ρ_1 , T_2/T_1 , and p_{02}/p_{01} for an oblique shock with inlet Mach Number M_1 and shock angle σ . From the geometry of Fig. 16.2 it follows further that $M_2 = M_y/\sin(\sigma - \delta)$.

16.3. Shock Geometry

Application of Second Law of Thermodynamics. The shock formulas as previously developed do not distinguish between a compression discontinuity (pressure increase) and a rarefaction discontinuity (pressure decrease). However, since the second law of thermodynamics allows only entropy increases for adiabatic processes, it follows that $s_2 \geq s_1$. Remembering that an oblique shock may be reduced to a normal shock by means of a coordinate transformation not involving entropy changes, and that in a normal discontinuity the entropy decreases for a rarefaction shock, we conclude that the only type of oblique discontinuity which is allowable is one in which there is a pressure rise.

BENDING OF STREAMLINE. Since $p_2 > p_1$, it necessarily follows from the continuity relation (Eq. 16.1) and the momentum theorem (Eq. 16.3) that $V_{n1} > V_{n2}$. Then, since Eq. 16.2 requires that $V_{t1} = V_{t2}$, the velocity triangles of Fig. 16.2 show that δ must always be positive in magnitude. In other words, we may state the general rule that *in crossing an oblique shock the streamline always bends toward the shock line*.

DECAY OF RAREFACTION SHOCK AT CONVEX CORNER. The impossibility of a rarefaction shock is of course also connected with the fact

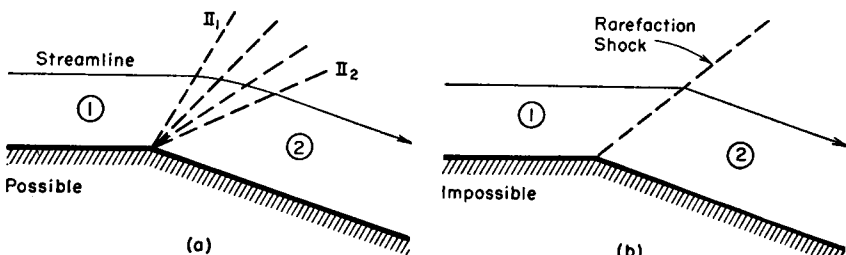
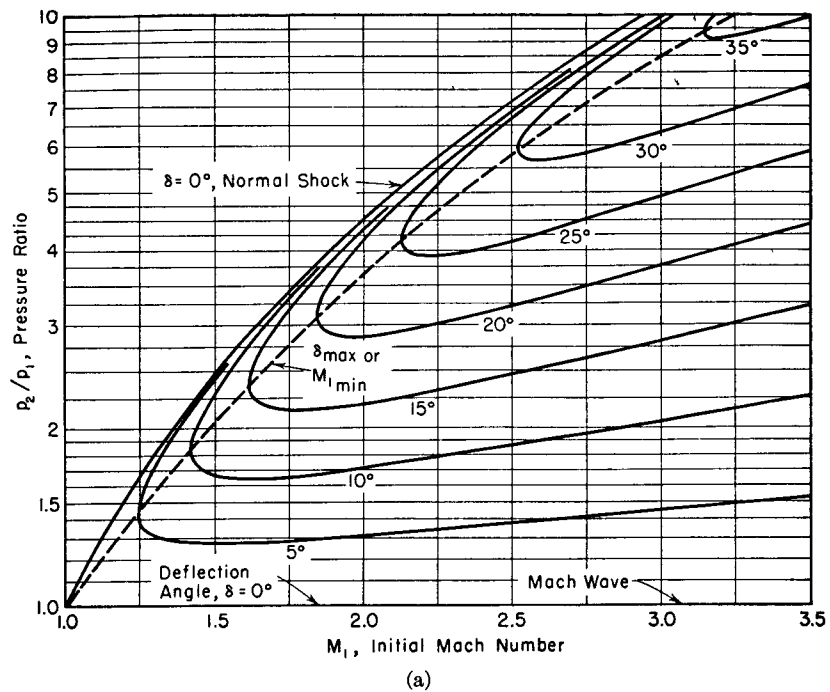


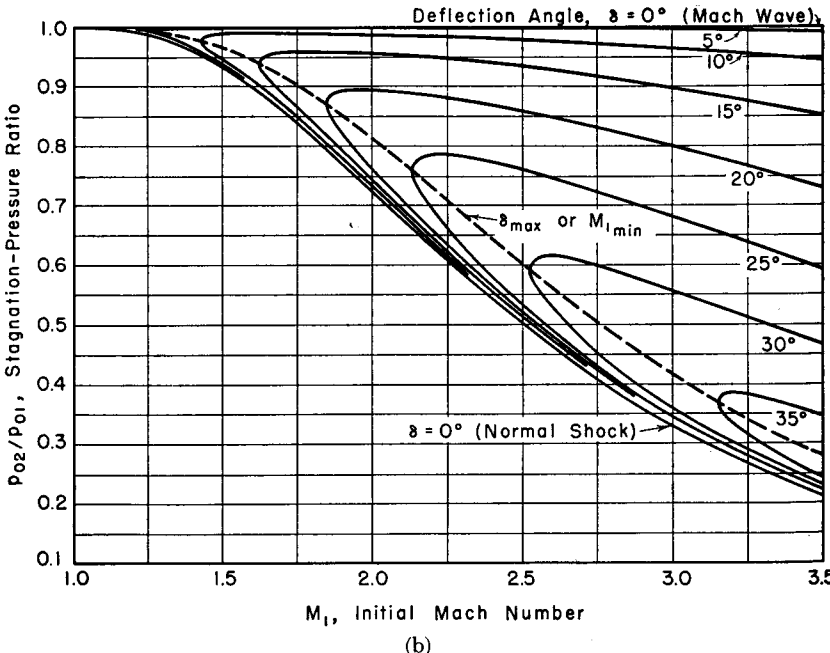
FIG. 16.7. Impossibility of oblique rarefaction shock.

- (a) Rarefaction discontinuity at corner rapidly attenuates to a continuous Prandtl-Meyer rarefaction wave.
- (b) Oblique rarefaction discontinuity would violate Second Law of Thermodynamics.

that rarefaction waves always tend to become less steep. Thus, in the expansive flow around a corner, Fig. 16.7, there is a rarefaction discontinuity confined to the singular point of the sharp corner, but this discontinuity rapidly decays to a continuous Prandtl-Meyer expansion which fills the entire expansion region.



(a)



(b)

FIG. 16.6. (a) Pressure ratio versus inlet Mach Number, with turning angle as parameter ($k = 1.4$).
(b) Stagnation-pressure ratio versus inlet Mach Number, with turning angle as parameter ($k = 1.4$).

Impossibility of Prandtl-Meyer Compression in Concave Corner. If we were to examine the possibility of a Prandtl-Meyer compression in a sharp corner (Fig. 16.8), following the analysis of Chapter 15, we would

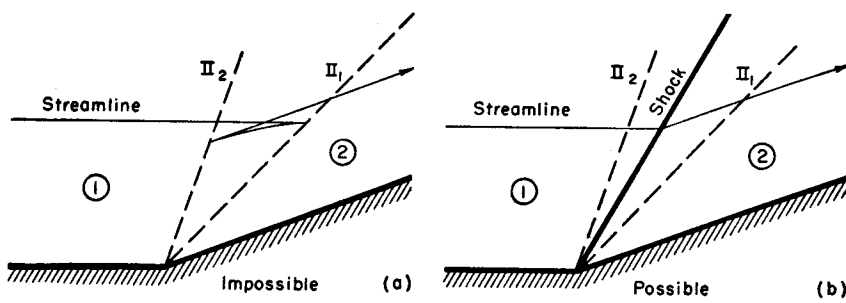


FIG. 16.8. Flow near concave corner.

- (a) Prandtl-Meyer flow is not physically possible.
(b) Oblique shock is physically possible.

find that each streamline reverses itself twice at cusps. This means that at each point in the compression region there would exist simultaneously three different pressures and velocities! Mathematically this is conceivable with the aid of multi-sheeted surfaces branched at the Mach lines, but it is physically impossible. The oblique compression shock provides a means for carrying out a sudden change in direction without involving this difficulty. The reversal of the hypothetical Prandtl-Meyer compressive flow occurs at cusps whose loci are known as *limit lines*. This example, and the example of flow reversal in a source-type

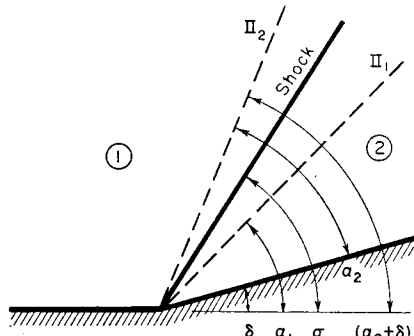
flow at a limit line where $M = 1$, are perhaps the simplest illustrations of the limit line phenomena which are discussed more fully in Volume II, Chapter 20.

Relation of Shock Line to Mach Lines. In Fig. 16.8 the shock line is shown as lying between the Mach lines of the upstream and downstream flows. We shall now demonstrate that this is always so.

Referring to Fig. 16.9, let II_1 and II_2 represent the respective directions of the left-running Mach lines

FIG. 16.9. Illustrates that left-running shock "overtakes" upstream left-running Mach wave, and is overtaken by downstream left-running Mach wave.

lines in regions 1 and 2, making the angles α_1 and α_2 to the upstream and downstream flows, respectively.



SHOCK OVERTAKES UPSTREAM MACH LINES. From Eq. 16.12 and the definition of Mach angle,

$$\sin \sigma = V_{n1}/V_1; \quad \sin \alpha_1 = c_1/V_1$$

But, since the flow in region 1 must be supersonic to an observer who sees the discontinuity as a normal shock, and since the sound velocity in region 1 does not depend on the motion of this observer, it follows that $V_{n1} \geq c_1$, whence

$$\sigma \geq \alpha_1 \quad (16.16)$$

which demonstrates that the *shock line is more steeply inclined to the flow than a Mach wave in region 1*.

SHOCK IS OVERTAKEN BY DOWNSTREAM MACH LINES. We note from Eq. 16.12 and the definition of α_2 that

$$\sin(\sigma - \delta) = V_{n2}/V_2; \quad \sin \alpha_2 = c_2/V_2$$

But the flow in region 2 must be subsonic to an observer viewing the discontinuity as a normal shock. Hence $V_{n2} \leq c_2$, from which it follows that $(\sigma - \delta) \leq \alpha_2$, or

$$\sigma \leq \alpha_2 + \delta \quad (16.17)$$

This, together with Fig. 16.9, shows clearly that *a Mach wave in region 2 is more steeply inclined to the flow than the shock line*.

RULES OF INTERACTION. From the two rules expressed by Eqs. 16.16 and 16.17 we may reach the following conclusions as to the possibility for interaction of waves of the same family:

- A shock wave always tends to interact with a continuous wave which is further downstream (Fig. 16.10a).
- A shock wave always tends to interact with a continuous wave which is further upstream (Fig. 16.10b).
- Two shock waves of the same family always tend to meet (Fig. 16.10c).

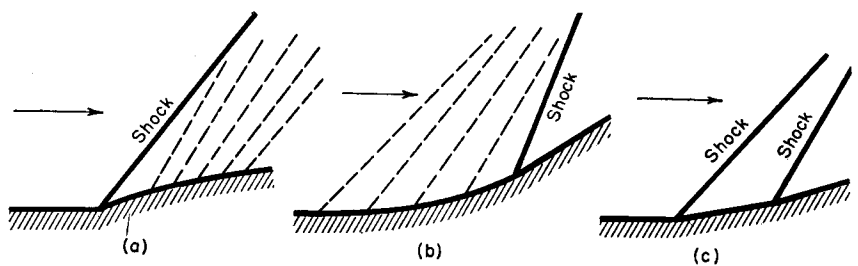


FIG. 16.10. Interaction of waves of same family.

- Shock always interacts with downstream Mach waves.
- Shock always interacts with upstream Mach waves.
- Two shocks always tend to intersect.

16.4. Shock Polars

Two types of graphical representation of the oblique shock relations which have been devised are especially useful because they include some of the geometric features of the shock.

Hodograph Shock Polar. Let the x - and y -components of velocity be denoted by u and v , respectively, and let the flow approaching the shock be in the x -direction, so that $u_1 = V_1$, and $v_1 = 0$. Then the states before and after the shock may be located in the hodograph diagram of Fig. 16.11a. For a shock of given turning angle δ , all the information

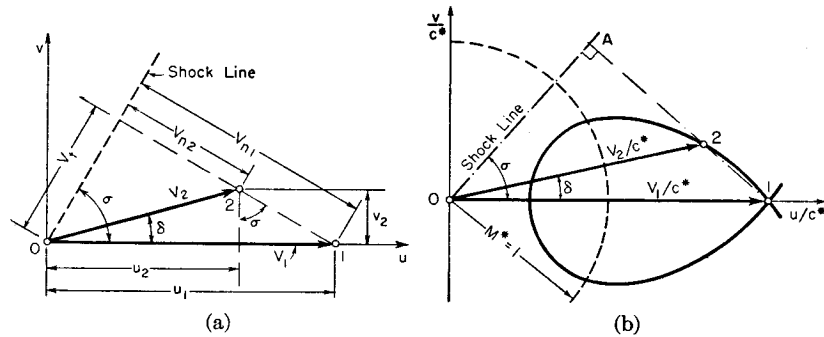


FIG. 16.11. Hodograph shock polar.

(a) Configuration of velocity vectors.

(b) Construction for determining shock angle and final velocity.

required to lay off the vector V_2 as well as the shock angle σ may be found from the preceding formulas, and thus point 2 may be located in the hodograph plane. The upstream and downstream velocity components along and parallel to the shock line must be related to each other as shown in Fig. 16.11a, with $V_{t1} = V_{t2} = V_t$. It is to be noted that Fig. 16.11a may be found by merely superposing the velocity triangles of Fig. 16.2.

Now, for each value of V_1/c^* there are an infinite number of end states (corresponding to different values of δ) in the hodograph plane which can be reached from state 1. The locus of these points is known as the hodograph shock polar for M_1 . A typical shock polar is shown in Fig. 16.11b. It is symmetrical about the horizontal axis, since there are two possible shock waves for given values of M_1 and δ , one running leftward relative to the flow, and the other rightward. Having once constructed the shock polar for a certain value of V_1/c^* , the solution for a given turning angle δ is found by laying off from the origin a line at the angle δ . Where this line intersects the shock polar is the end point of the velocity vector V_2/c^* . The normal OA to the extension of the straight line 1-2 then gives the direction of the shock line.

The complete family of *hodograph shock polars*, with V_1/c^* as parameter, is shown in Fig. 16.12.

The approximate shape of the shock polar for a specified value of V_1/c^* may easily be sketched by using Eq. 16.9 in conjunction with the construction of Fig. 16.11a, especially when it is realized that the second term on the right hand side of Eq. 16.9 is usually small compared to the first term.

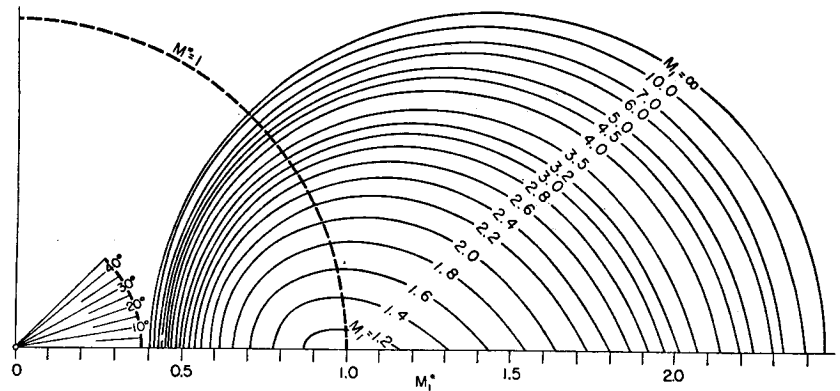


FIG. 16.12. Family of hodograph shock polars ($k = 1.4$).

EQUATION OF SHOCK POLAR. To obtain the equation of the shock polar in u -, v -coordinates, we find from the geometry of Fig. 16.11a that

$$V_{n1} = u_1 \sin \sigma; \quad V_t = u_1 \cos \sigma$$

$$V_{n2} = V_{n1} - \sqrt{v_2^2 + (u_1 - u_2)^2} = u_1 \sin \sigma - \sqrt{v_2^2 + (u_1 - u_2)^2}$$

Substituting these into the Prandtl relation, Eq. 16.9, we get

$$u_1^2 \sin^2 \sigma - u_1 \sin \sigma \sqrt{v_2^2 + (u_1 - u_2)^2} = c^{*2} - \frac{k-1}{k+1} u_1^2 \cos^2 \sigma$$

Then, eliminating σ with the additional relation obtained from Fig. 16.11, namely,

$$\tan \sigma = \frac{u_1 - u_2}{v_2}$$

we finally obtain after considerable algebraic rearrangement,

$$\left(\frac{v_2}{c^*} \right)^2 = \left[\frac{u_1}{c^*} - \left(\frac{u_1}{c^*} \right)^2 \right]^2 \frac{\frac{u_1 u_2}{c^* c^*} - 1}{\frac{2}{k+1} \left(\frac{u_1}{c^*} \right)^2 - \frac{u_1 u_2}{c^* c^*} + 1} \quad (16.18)$$

This formula allows us to plot v_2/c^* versus u_2/c^* for any specified value of the parameter u_1/c^* .

The Pressure-Turning Angle Shock Polar. Later we shall see that surfaces of discontinuity are usually formed when two shocks interact with each other, or when a shock interacts with a continuous wave.

These surfaces of discontinuity, usually called *slip lines*, or *vortex sheets*, are also streamlines, and divide two regions having equal pressures and flow directions but different velocities. For problems of this nature it is convenient to represent the oblique shock relations by a shock polar for which the coordinates are turning angle and pressure ratio.

For any given initial Mach Number, the formulas of Art. 16.2 allow us to find the pressure ratio, p_2/p_1 , as a function of turning angle, δ . Plotting these as in Fig. 16.13, we get the family of δ - p shock polars with M_1 as parameter. Convenient large-scale representations of these shock polars are given in Reference 15.

FIG. 16.13. Pressure-deflection shock polars.

16.5. Some Special Aspects of Oblique Shocks

Strong Versus Weak Shocks. A curious fact revealed by the graphical representations of Figs. 16.4, 16.5, 16.6, 16.13, and 16.14 is that for a given initial Mach Number M_1 and a given turning angle δ there are either two solutions to the oblique shock relations, or none at all. Let us consider specifically a uniform flow of Mach Number M_1 approaching a wedge of half-angle δ or approaching a concave corner of turning angle δ (Fig. 16.14). From the shock polars, we see that if a solution exists there may be either (i) a *strong shock* (2s), with a relatively large shock angle, a relatively large pressure ratio, and with the downstream state usually subsonic, or (ii) a *weak shock* (2w), with a relatively small shock angle, a relatively small pressure ratio, and with the downstream state usually supersonic. Which of these two solutions will occur in practice? Unfortunately, there is no simple and clear-cut answer to this question, but certain general considerations serve as a guide.

ONE-DIMENSIONAL CASE. As a start toward understanding this problem, let us consider the special case of one-dimensional, supersonic flow

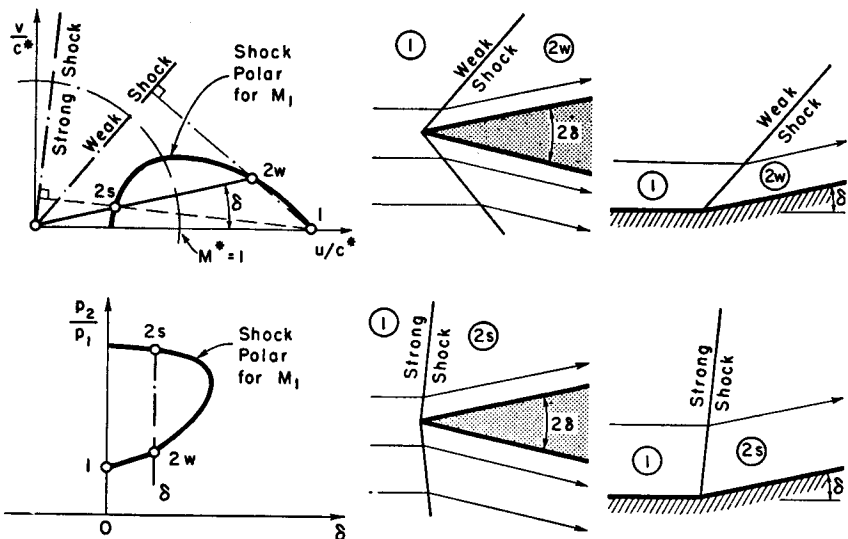


FIG. 16.14. Illustrates strong and weak shocks.

in a duct of constant area. For this case the turning angle δ is zero, and the strong solution on the shock polar of Fig. 16.15 is a normal shock, while the weak solution is an infinitesimal wave of zero pressure rise. From our previous discussions of one-dimensional flow in ducts, it is clear that the solution which occurs in practice depends on the boundary conditions, in particular on the ratio of downstream pressure to upstream pressure. If the downstream pressure is sufficiently low, the weak solution occurs, which is to say that there are no shocks at all.

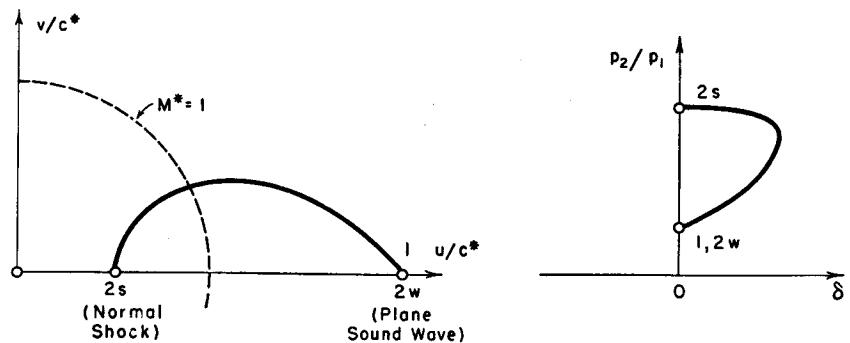


FIG. 16.15. Strong and weak shocks for $\delta = 0$.

If the downstream pressure is sufficiently high, a normal shock stands in the duct, which is to say that the strong solution occurs.

TWO-DIMENSIONAL CASE. Returning now to the general case of oblique shocks, we may generalize the argument of the preceding para-

graph by stating that whether the oblique shock is strong or weak depends, at least in part, on the boundary conditions as to pressure. If the downstream pressure for the two-dimensional flow, Fig. 16.16a, is sufficiently small, a weak shock will occur at corner *A* and the flow approaching corner *B* will usually be supersonic. If the back pressure is sufficiently high, on the other hand, the shock emanating from corner

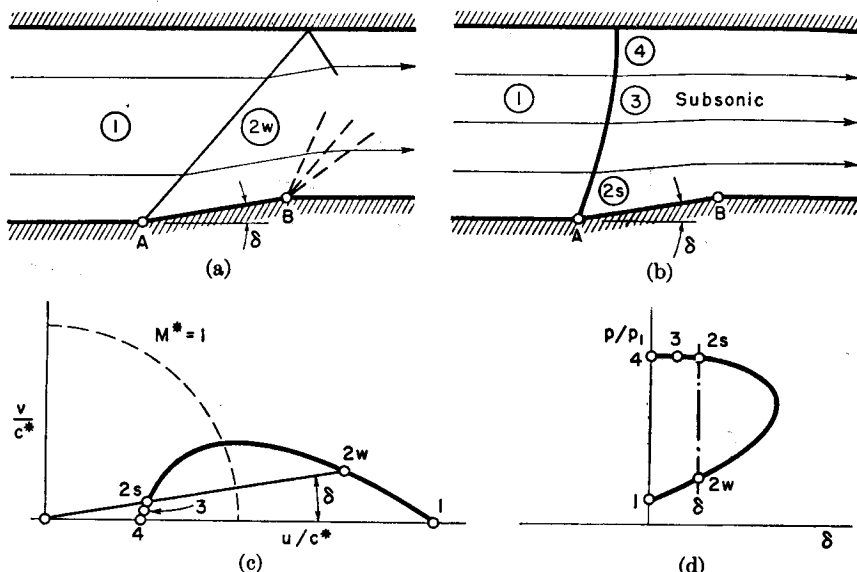


FIG. 16.16. Effect of back pressure on shock form.

- (a) Weak shock (low back pressure).
- (b) Strong curved shock (high back pressure).
- (c) Hodograph shock polar.
- (d) Pressure-deflection shock polar.

A will be of the strong type, and the flow approaching corner *B* will usually be subsonic.

As will be seen later, however, an oblique strong shock cannot extend to a wall, but rather curves as shown in Fig. 16.16b until it is a normal shock at the upper wall. Each streamline therefore passes through a shock of different strength, and each point on the shock line is represented by a corresponding point on the segments between $2s$ and 4 of the shock polars of Figs. 16.16c and 16.16d. The flow behind the shock is subsonic, the streamlines are curved, and there is vorticity or rotation in the flow downstream of the shock because of entropy variations from streamline to streamline.

When a symmetrical wedge of half-angle δ is moved through the atmosphere at supersonic speed, only the weak shock is observed in practice. This may be rationalized in the following way. Suppose that

the upper wall of Fig. 16.16a is moved infinitely far upward. Then in the limit, we obtain the upper half of the flow pattern for the wedge moving at supersonic speed. In the atmosphere, however, the pressures far downstream of the wedge can differ from those far upstream by only infinitesimal amounts, and hence the boundary conditions are such that the weak shock occurs. Thus, with supersonic aircraft, the oblique shocks seem to be invariably of the weak type, except under conditions described below where the geometry of the aircraft does not allow of attached shocks.

The schlieren photographs of Fig. 16.17 support the view that the boundary conditions determine whether the weak or strong shock appears in practice. All three photographs show the flow near the entrance



FIG. 16.17. Schlieren photographs showing influence of back pressure on type of shock. All three photographs are for the internal flow geometry (two-dimensional) of the right-hand photograph (after Busemann, NACA).

of a two-dimensional, supersonic inlet diffuser which has a symmetrical two-dimensional wedge as a core. In the left-hand photograph the back pressure for the internal flow is comparatively high, and strong shocks are attached to the nose of the wedge. In the right-hand photograph, corresponding to a comparatively low back pressure, the customary weak shocks are attached to the nose of the wedge, but suddenly change into strong shocks at some distance from the nose. In the center photograph, corresponding to an intermediate back pressure, the flow is unsymmetrical, with a weak shock on one side and a strong shock on the other side of the wedge.

Another factor which may influence the occurrence of strong or weak shocks is that concerning stability. It often seems possible in fluid dynamics to have two or more solutions which satisfy given boundary conditions. In such cases the solution which occurs in practice may depend on the direction from which the existing boundary conditions are approached and on disturbances which may be present in the steady-state flow. This situation is analogous to the hysteresis cycles which supersonic diffusers may exhibit under conditions of variable Mach Number, variable area ratio, or variable pressure ratio. This aspect of

the weak-versus-strong shock question has not as yet been explored sufficiently.

Detached Shocks. The various graphical representations of Figs. 16.4, 16.5, 16.6, 16.12, and 16.13 show that for a specified initial Mach number, M_1 , there is a maximum value of the turning angle, δ_{\max} , for which there exists an oblique shock solution. Or, conversely, for a specified turning angle, δ , there is a minimum initial Mach Number, $M_{1,\min}$, for which there is an oblique shock solution. From Figs. 16.18a and 16.18b

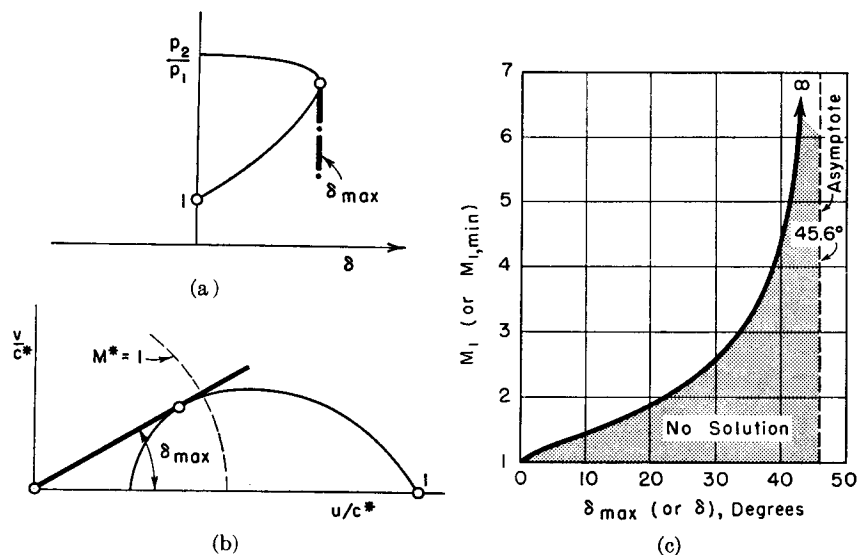


FIG. 16.18. Maximum turning angle for a given initial Mach Number.

- (a) Pressure-deflection shock polar.
- (b) Hodograph shock polar.
- (c) Chart for $k = 1.4$.

it is evident that at this limiting condition the weak and strong oblique shocks become identical. The relation between M_1 and δ_{\max} , or between $M_{1,\min}$ and δ , is shown in Fig. 16.18c. No solutions may be obtained in the shaded area below the curve in the graph. (See Problem 16.11a.)

Consider the case of uniform, parallel flow at Mach Number M_1 past a wedge of half-angle δ . If δ is less than δ_{\max} , the shock is attached to the wedge (Figs. 16.19a and 14.8). However, if δ is greater than δ_{\max} , the shock cannot be attached to the wedge, for this would require the streamline approaching the point of the wedge to turn through an angle greater than δ_{\max} . Under these circumstances, we observe in practice that the shock is detached from the wedge (Figs. 16.19b and d). Similarly, a detached shock always stands in front of a blunt body (Fig. 16.19c).

When the shock is detached, it is invariably curved. If the body of Fig. 16.19c represents the leading edge of the wing of a supersonic aircraft, we can see intuitively that the curved shock which begins at A

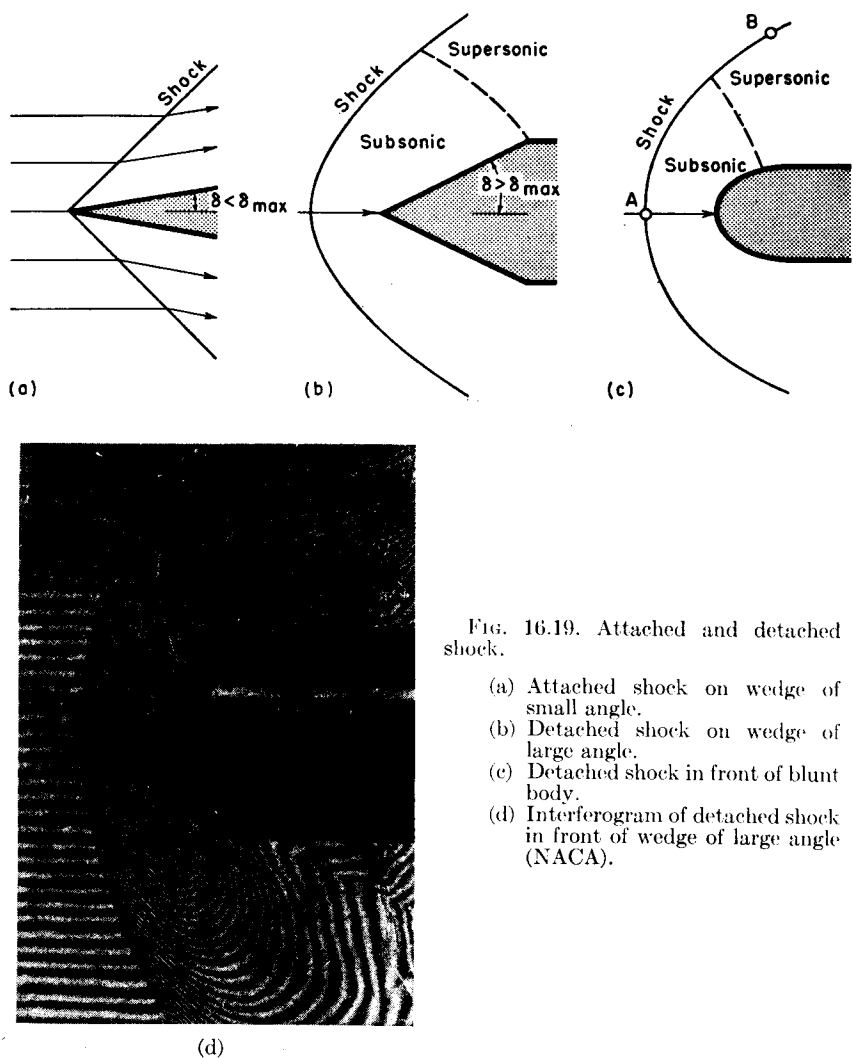


FIG. 16.19. Attached and detached shock.

- (a) Attached shock on wedge of small angle.
- (b) Detached shock on wedge of large angle.
- (c) Detached shock in front of blunt body.
- (d) Interferogram of detached shock in front of wedge of large angle (NACA).

as a normal shock must gradually weaken until at B, which is at a great distance from the body, it is of vanishing strength, i.e., it is a Mach wave. If this were not so, the air passing the wing would undergo an infinite change of entropy and this would result in infinite drag. With a curved detached shock as in Fig. 16.19c, therefore, there is a segment of the shock to correspond to every point on the shock polar curve pertaining

to the given M_1 . Behind the detached shock the flow is in part supersonic and in part subsonic, leading to great difficulties in analysis because of the radically different properties of the differential equations for subsonic and supersonic flow.

Similar considerations apply to the flow past a concave corner in a duct (Fig. 16.20).

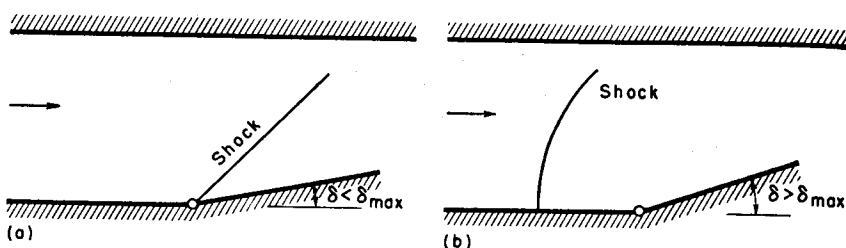


FIG. 16.20. Attached and detached shocks at concave corner in duct.

If the abscissa of Fig. 16.18c is regarded as the actual half-angle of the wedge or the actual turning angle of the concave corner, the region above the curve represents attached shocks, and the region below represents detached shocks.

Sonic Flow After Shock. As shown in Fig. 16.21, for each value of M_1 there is a certain turning angle, δ^* , for which the flow downstream of the shock is exactly sonic. The relation between δ^* and δ_{\max} is as illustrated in Fig. 16.21, that is, δ^* is always less than δ_{\max} . However, for $k = 1.4$, δ^* does not differ from δ_{\max} by as much as 0.5° over the

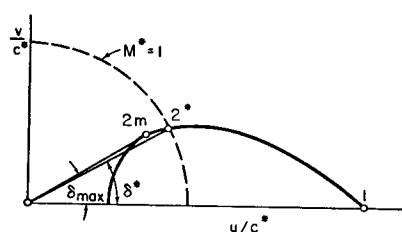


FIG. 16.21. Relation between δ_{\max} and δ^* .

entire range of Mach Numbers from unity to infinity. This means that, except in a very narrow range, *the flow behind a weak shock is supersonic and the flow behind a strong shock is subsonic*. (See Problem 16.11b.)

Nearly Normal Shocks. From the geometry of the hodograph shock polar, Fig. 16.11b, it may be seen that a strong shock of small turning angle will have a shock angle σ of nearly 90° . From the δ - p shock polar of Fig. 16.13, it may be seen furthermore that the pressure rise across such a shock is substantially the same as that across a normal shock.

Thus we have the approximate rule that strong shocks of small turning angle are nearly equivalent to normal shocks.

16.6. Very Weak Shocks

In practical design problems, an approximate treatment of weak shocks may often be used with advantage to simplify the calculations.

Shock Strength. We shall specify the shock strength in terms of the pressure ratio, p_2/p_1 , across the shock. The Rankine-Hugoniot relation, Eq. 16.8, then shows that the density ratio, ρ_2/ρ_1 , may also be used as a measure of shock strength. Inspection of Eq. 16.14 further reveals that $M_1 \sin \sigma$ is a direct measure of shock strength. Since the entropy change depends only on the pressure ratio and density ratio, the entropy change is also a unique measure of shock strength. Finally, the stagnation pressure ratio, p_{02}/p_{01} is a direct measure of shock strength because it is determined uniquely by the entropy change in an adiabatic process through the relation

$$s_2 - s_1 = -R \ln (p_{02}/p_{01})$$

Mach Wave as the Limit of a Shock Wave. By means of algebraic rearrangement, Eq. 16.8 may be written in the form

$$\frac{p_2 - p_1}{p_1} = \frac{2k}{k-1} \left(\frac{\rho_2 - \rho_1}{\rho_1} \right) / \left[\frac{2}{k-1} - \left(\frac{\rho_2 - \rho_1}{\rho_1} \right) \right]$$

From this we see that as $\Delta\rho$ goes to zero, Δp also goes to zero. The limiting relation between Δp and $\Delta\rho$, however, as $\Delta\rho/\rho_1$ goes to zero, is evidently

$$\Delta p/\Delta\rho = kp_1/\rho_1 = c_1^2$$

Thus we see that for weak shocks, $\Delta p/\Delta\rho = c_1^2$. But, since $c^2 = (\partial p/\partial\rho)_s$, it follows that the changes in pressure and density in a very weak shock are connected in the limit through the isentropic relation (see Fig. 16.3).

Combining this result with Eq. 16.7, and noting that, for very weak shocks, Eqs. 16.1 and 16.3 predict that V_{n2} approaches V_{n1} , we get

$$\frac{p_2 - p_1}{p_2 - p_1} \rightarrow c^2; \quad V_{n2}V_{n1} \rightarrow V_n^2; \quad \therefore \quad V_n \rightarrow c$$

In other words, the component of velocity normal to the wave becomes equal to the sound velocity. Therefore,

$$\tan \sigma \rightarrow (c/V) = \tan \alpha$$

so that in the limit the shock angle σ becomes identical with the Mach angle α . We have thus shown that in all respects an oblique shock wave

of vanishing strength is identical with a Mach wave. For a given initial Mach Number M_1 , the strength of the shock goes to zero as the turning angle δ goes to zero. If, in the geometric construction of Fig. 16.11b we allow point 2 to approach point 1, we obtain in the limit the construction of Fig. 16.22, where the direction of the Mach wave is given by the normal to the shock polar at point 1.

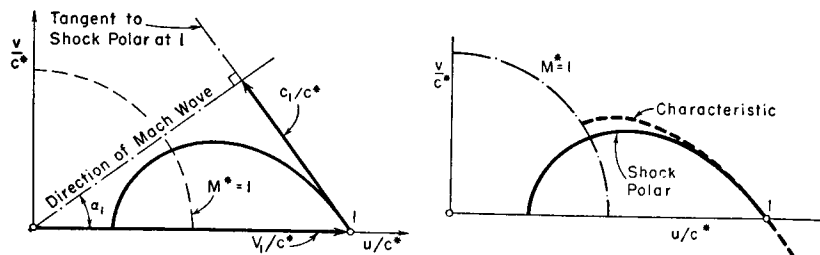


FIG. 16.22. Normal to hodograph shock polar at 1 has same direction as Mach line.

FIG. 16.23. Hodograph shock polar and hodograph characteristic passing through point 1 have equal slopes and radii of curvature.

Entropy Change Across Weak Shock. In Chapter 5 we found that the entropy change across a shock could be expressed in terms of shock strength through the series expansion

$$\frac{s_2 - s_1}{R} = \frac{k+1}{12k^2} \left(\frac{p_2 - p_1}{p_1} \right)^3 + \dots \quad (16.19)$$

thus demonstrating that the entropy change is of third order in shock strength and is extremely small for shocks of small pressure rise. In the light of our previous discussion, the entropy change is also of third order in such quantities as $M_1 \sin \sigma$ or $(p_{02} - p_{01})/p_{01}$ (Problem 16.12).

Since the isentropic relation and the Rankine-Hugoniot relation are identical up to and including terms of second order in shock strength, the curves of Fig. 16.3 are not only tangent as $p_2/p_1 \rightarrow 1$, but have the same radius of curvature as well.

Although $M_1 \sin \sigma$ is a unique measure of shock strength, in practical problems we are more likely to be interested in M_1 and δ as primary variables. There is no simple relation giving shock strength in terms of M_1 and δ . However, the curves of Fig. 16.6 show this relation graphically, and Fig. 16.6b demonstrates clearly that the entropy changes across shocks of small turning angle are extremely small.

Approximate Treatment of Flows Containing Weak Shocks. Remembering that the normal to the hodograph characteristic gives the direction of the Mach line (Fig. 15.13), it is evident from Fig. 16.22 that for a given initial state the shock polar and characteristic curves in the

hodograph plane are tangent to each other. Furthermore, since the shock relations and isentropic relations differ only in terms of third order of shock strength, it may be shown that the shock polar and characteristic curves have the same radius of curvature at point 1. Thus, as illustrated by Fig. 16.23, the shock polar and characteristic curves are very nearly identical for small angles of turn.

The preceding considerations suggest a greatly simplified procedure when dealing with two-dimensional flows involving weak shocks. Rather than use the exact oblique shock relations, we may with little loss of accuracy ignore the entropy change across the shock and treat the latter as a reversible compression wave. This is equivalent to using the hodograph characteristic curve rather than the hodograph shock polar. Assuming that there are no strong shocks present, the entire two-dimensional flow may then be treated by the characteristics methods of Chapter 15, without the need for changing the calculation procedure as weak shocks appear. This is an especially important simplification when it is recalled that shocks usually produce rotation in the flow, because if this rotation were taken into account the simple methods of Arts. 15.3 and 15.4 would have to be replaced by the complex methods of Art. 15.12.

In using the characteristics theory with the field method, continuous changes in stream properties were lumped into fictitious discontinuities which were assumed to be concentrated on certain discrete Mach lines. This is essentially the approximate procedure outlined above for weak shocks. However, there is a basic difference which should be kept clearly in mind. The analysis of continuous changes by the field method may be made as exact as we please merely by increasing the number of fields (or increasing the fineness of the Mach net), whereas no such improvement in accuracy is possible in the approximate treatment of shocks because the salient feature of shocks is their discontinuous nature.

Finally, it is interesting to note that the method of characteristics, the analysis for oblique shocks, and the linearized supersonic theory all give identical results for the limiting case where a supersonic stream is turned through a vanishingly small angle.

16.7. Reflection and Interaction of Shocks

In practical problems, oblique shock waves are often incident on solid boundaries or on free boundaries of jets; sometimes waves of opposite family cross each other; and, as demonstrated in Art. 16.3, two oblique shocks of the same family always tend to intersect. We shall now discuss the analytical treatment of such processes. The reader will find it instructive to compare the exact methods described here with the approximate methods of the linearized theory (Art. 14.7).

Reflection of Shock from Free Boundary. Shock A (Fig. 16.24b) is incident on the constant-pressure boundary of a two-dimensional

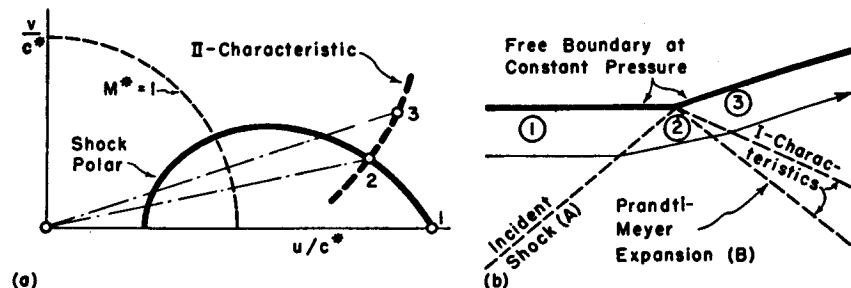


FIG. 16.24. Reflection of shock from constant-pressure boundary (see also Fig. 14.21).

- (a) Hodograph diagram.
(b) Streamlines and waves.

stream. Since the pressure in region 2 downstream of the shock is greater than that of the free boundary, it is evident that an expansion wave B must be reflected where wave A is incident on the free boundary.

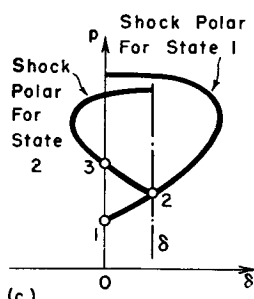
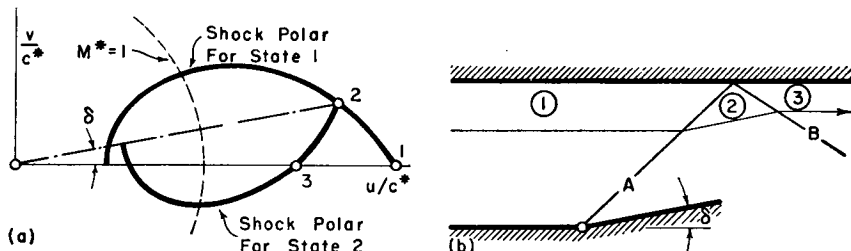


FIG. 16.25. Reflection of shock from solid boundary.

- (a) Hodograph diagram.
(b) Streamlines and shock lines.
(c) Pressure-deflection diagram.

Furthermore, rarefaction wave B must be a centered Prandtl-Meyer wave so that, at the free boundary, the sudden rise in pressure from p_1 to p_2 may be instantly canceled by the sudden drop in pressure from p_2 to p_3 . The strength of the simple wave B is related to the strength of shock A through the requirement that $p_2 - p_1 = p_2 - p_3$.

Regular Reflection from Solid Boundary.

In Fig. 16.25b shock A is incident on a straight wall. Since the gas flow is assumed to follow the solid boundary, it is necessary for shock B to be reflected so that the stream in region 3 will have the same direction as in region 1. The strength of shock B is

related to that of shock A by the requirement that they have equal turning angles.

Fig. 16.25b shows how the problem may be solved graphically with the help of the hodograph shock polars, and Fig. 16.25c shows the solution with the help of the $\delta-p$ shock polars. In both these graphical constructions the shock polar corresponding to M_2 is displaced through an angle δ so as to correspond to the actual direction in region 2.

It is evident from this example that an oblique shock is reflected from a solid wall in like sense, i.e., it is reflected as an oblique shock.

In practice, the presence of a boundary layer near the upper wall makes the process of reflection much more complicated than the simple solution given here, as will be seen in Art. 16.12.

A study of Figs. 16.25a and 16.25c will show that for a given M_1 there is a maximum value of turning angle δ for which the type of reflection in Fig. 16.25b, known as *regular reflection*, is possible. If δ is too large, then it will exceed the value of δ_{\max} corresponding to M_2 (see Fig. 16.18). It may also be seen that for a given δ , there is a minimum value of M_1 below which regular reflection is impossible. Fig. 16.26 summarizes the ranges of M_1 and δ within which regular reflection may occur.

When regular reflection is impossible, a *Mach reflection*, described later, takes place.

Crossing of Shocks of Opposite Family. Referring to Fig. 16.27a, suppose that oblique shocks A and B of known strength are propagated into region 1 and ultimately meet. How will the shocks influence each other? Let C be the continuation of B , and D be the continuation of A . Now consider two nearly adjacent streamlines which pass on opposite sides of the junction point, one streamline passing through A and C , and the other through B and D . After these streamlines have passed through the shock system, they must have the *same pressure and direction*. As they have passed through shocks of different strength, however, they have incurred different entropy increases, and hence they have different speeds. A surface of discontinuity (*slip line*) which is also a streamline, therefore emanates from the junction point. Regions $4'$ and $4''$ have the same direction and pressure, but different speeds. The slip line is therefore a very thin region of concentrated vorticity, and is sometimes called a *vortex sheet*.

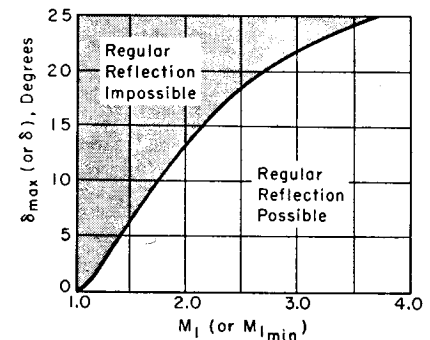


FIG. 16.26. Limiting values of M_1 and δ for regular reflection ($k = 1.4$).

The graphical solution to this problem with the aid of the shock polar diagrams is shown in Fig. 16.27b and 16.27c. The latter diagram is especially convenient for this type of problem.

Since fields $4'$ and $4''$ have the same pressure and same stagnation temperature, the adiabatic and isentropic relations require that the field with the lower stagnation pressure (higher entropy) have the lower

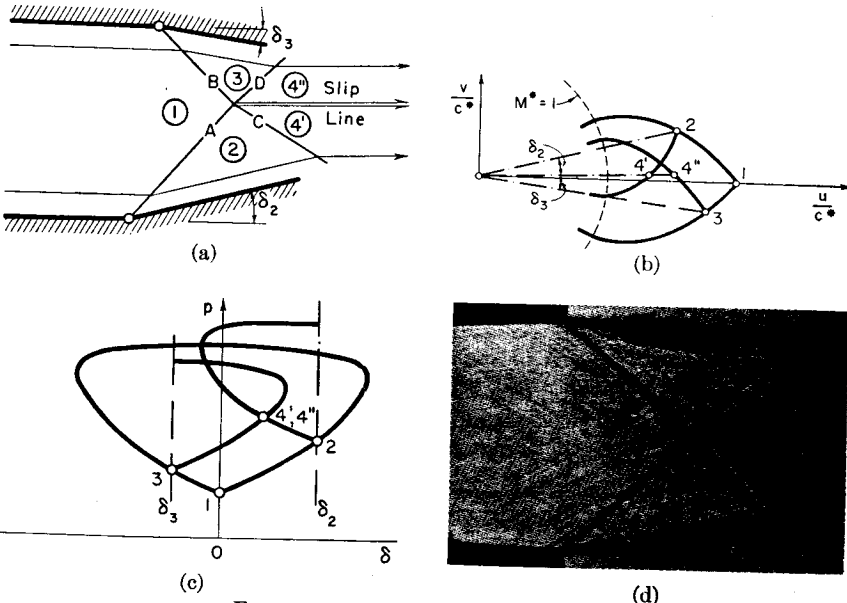


FIG. 16.27. Crossing of shock waves.

- (a) Streamlines, shock lines, and slip line.
- (b) Hodograph diagram.
- (c) Pressure-deflection diagram.
- (d) Schlieren photograph showing refraction of two shocks of equal strength; may also be interpreted as reflection of shock from straight boundary. (Reproduced by permission of The Macmillan Co. from *Elements of Aerodynamics of Supersonic Flows*, by A. Ferri, 1949.)

velocity. In this case shocks A and C are stronger than B and D , hence the gas speed is larger in field $4''$ than in field $4'$. This same rule may be applied whenever vorticity appears in an adiabatic flow.

If shocks A and B are of equal strength, i.e., if $\delta_2 = \delta_3$, then the shock configuration will be symmetrical, and no slip line will appear (Fig. 16.27d). The streamline passing through the junction point will undergo no change in direction, and the entire process will therefore be equivalent to that of Fig. 16.25, that is, to shock reflection from a plane wall.

The type of regular interaction shown in Fig. 16.27 may prove to be impossible if M_1 is too small or if δ_2 and δ_3 are too large, for the same reasons that regular reflection may be impossible with the incident wave pattern of Fig. 16.25. A *Mach reflection* then occurs.

Mach Reflection. When M_1 is so small or δ is so large as to preclude the possibility of regular reflection in Fig. 16.25, a *Mach reflection* (Fig. 16.28) occurs. Near the upper wall the shock must necessarily be normal, for this is the only way in which a shock can occur without a change in direction. Shock C , of opposite family to shock A , emanates from

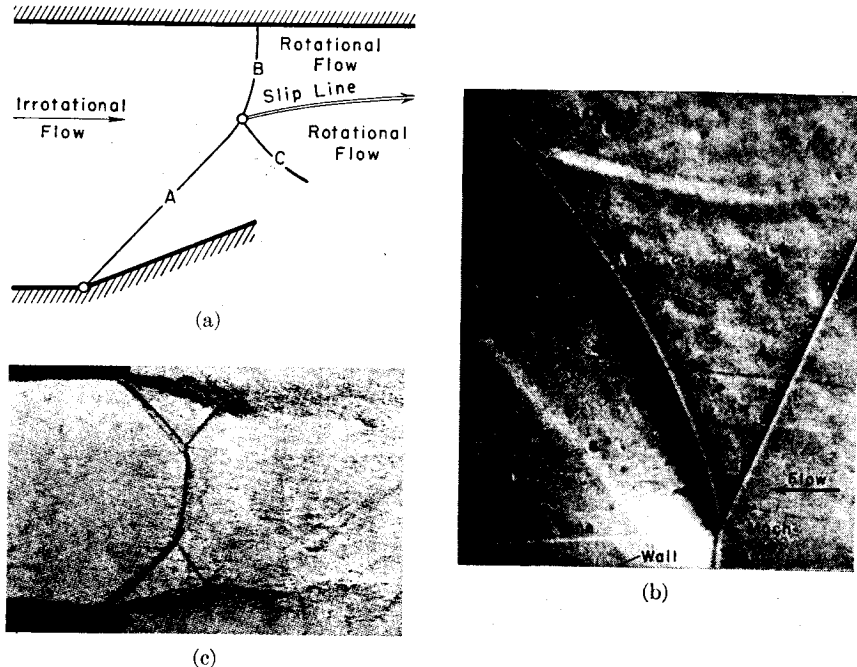


FIG. 16.28. Mach reflection.

- (a) Explanatory diagram.
- (b) Schlieren photograph of Mach reflection from wall, obtained with a moving wave system in a fluid at rest, thus obviating distortions due to boundary layer (after Bleakney and Taub).
- (c) Schlieren photograph of Mach reflection of two intersecting shocks, flow from right to left (reproduced by permission of The Macmillan Co. from *Elements of Aerodynamics of Supersonic Flows*, by A. Ferri, 1949).

the juncture of incident shock A and normal shock B . However, shocks A , B , and C cannot be straight to the point of mutual intersection, for the same reason that regular reflection of A was impossible to begin with. It is observed in practice that legs A , B , and C are curved near the junction point. A slip line emanates from the junction, and the flow behind all the shocks is rotational because of the curvature of the shocks. The curvature of the shocks also gives rise to a continuous wave system. Thus, the flow pattern is exceedingly complicated, and at present our knowledge is limited to the qualitative aspects of Mach reflection.

When regular crossing of waves *A* and *B* in Fig. 16.27 is impossible, a Mach reflection occurs (Fig. 16.28c). Waves *A* and *B* of Fig. 16.27a do not meet, but are bridged rather by a nearly normal shock.

Intersection of Shocks of Same Family. Referring to Fig. 16.29a, suppose that M_1 , θ_2 , and θ_3 are given, thus defining the angles and

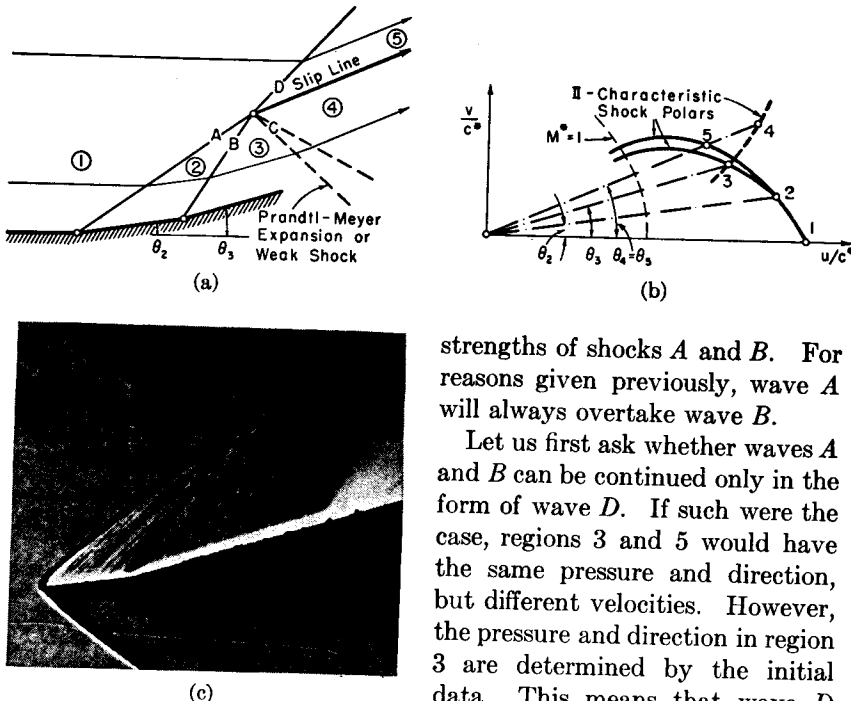


Fig. 16.29. Intersection of two left-running shock waves.

- (a) Physical plane.
- (b) Hodograph diagram.
- (c) Schlieren photograph of flow corresponding to (a). Note Mach lines generated from roughened surface and their interactions with both shocks. See Fig. 16.10 (after Johannesen).

exceptional circumstances, the pressure in region 5 will not match that in region 3.

These arguments serve to prove that something more than wave *D* is required. One way of resolving the difficulty is to suppose that wave *C*, which may be either a Prandtl-Meyer expansion or an oblique shock, also emanates from the junction point. Then, by suitably adjusting the strengths of waves *C* and *D* it is possible to obtain a solution for which

$p_5 = p_4$ and $\theta_4 = \theta_5$. Of course a slip line divides regions 4 and 5. The hodograph solution, with wave *C* shown as a rarefaction, is illustrated in Fig. 16.29b.

16.8. Curved Shocks

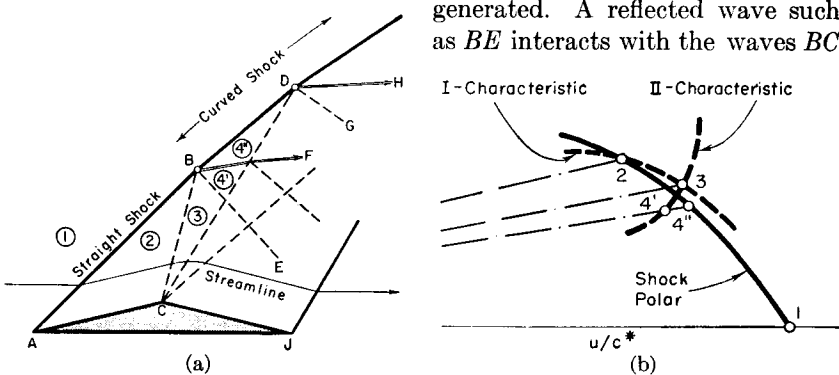
Applicability of Shock Equations. In most practical problems curved shocks appear either because the shock is necessarily detached (as in Figs. 16.19c and 16.20b), or because an initially straight shock interacts with a continuous wave.

Are the shock equations of Art. 16.2 valid for shock surfaces which are curved in two or three dimensions? The answer is yes, since the analysis of Art. 16.2 may be applied to two streamlines which in the limit approach each other. The shock relations are, therefore, applicable to each individual streamline, provided that the shock angle σ is measured between the streamline entering the shock surface and the tangent to the shock surface at the point of entry, in the plane containing the approach streamline and the normal to the tangent plane.

Interaction of Shocks with Continuous Waves. There are four possible types of such interactions, depending on whether the continuous wave is a compression or rarefaction, and on whether the continuous wave is of the same or opposite family to the shock wave.

As an illustration of the method of analysis, let us consider the flow past the triangular airfoil profile of Fig. 16.30a, in which the oblique shock generated at point *A* interacts with the continuous Prandtl-Meyer rarefaction wave of the same family originating at point *C*. From the profile geometry and initial Mach Number, and with the help of the shock relations, we may find conditions in zones 1 and 2. Then, employing the field method of calculation, we may split the centered rarefaction wave into several zones, the first of which is zone 3. Applying the characteristics theory to the expansion between 2 and 3, we may find the stream properties in zone 3 and the direction of the first rarefaction wave *CB*. Thus, point *B*, representing the beginning of the interaction process, may be located. Now consider the two streamlines immediately above and below *B*. Because of the pressure drop from 2 to 3, the shock above *B* will not be as strong as that below *B*, and the two streamlines referred to will undergo different entropy changes. In order to have equal pressures and flow directions in fields 4' and 4'', a small rarefaction wave *BE* must be reflected at point *B*. Since the speeds are different in fields 4' and 4'', a slip line *BF* emanates from point *B*. The strength of the shock between *B* and *D* and the strength of the reflected rarefaction *BE* are determined by the two simultaneous conditions that the pressures and flow directions must be the same in zones 4' and 4'', as illustrated in Fig. 16.30b.

The calculation procedure is continued by similar methods. Where the second rarefaction CD strikes the shock BD , the shock again changes strength and direction, and a slip line DH and reflected wave DG are generated. A reflected wave such as BE interacts with the waves BC



and CD , and this interaction may be computed by the method of characteristics. It should be noted also that when a wavelet such as CD crosses the slip line BF , the wavelet is in part transmitted with changed strength, and is in part reflected; this follows from the requirements that the pressures and flow directions must be the same for the adjacent streamlines forming the slip plane.

In the limit, if the stepwise procedure outlined above is made ever finer, it may be seen that the region of interaction extends between the first reflected wave BE and the portion of the shock downstream of point B . The shock is straight from A to B , and is continually curved downstream of B . In the limiting continuous solution, furthermore, no individual slip lines appear as such, but the entire region bounded by the streamline BF and by the curved shock downstream of B has vorticity. The slip lines are merely artifices of the stepwise solution which allow us to lump a continuously distributed vorticity into discrete discontinuities for convenience in calculation.

The method of characteristics for isentropic flow (Arts. 15.3 and 15.4) may not be applied to the region where vorticity exists, except as an approximation, because this region is not isentropic. However, it turns

Art. 16.9 EXPLICIT SOLUTIONS BY SERIES EXPANSIONS

out that this approximation very often gives acceptable results. In essence, the approximate method ignores the variations in entropy change across different parts of the oblique shock, and, therefore, the slip lines and the waves reflected from the shock do not appear. Fig. 16.30c shows the simplification in wave pattern afforded by this approximation.

In the region of vorticity where continuous waves are present, the entropy represents an additional variable. The method of characteristics may be worked out formally in this case, as in Art. 15.12.

Without formally working out the method of characteristics for non-isentropic flow, however, we may make calculations for the region of rotational flow by extending the ideas already presented. In isentropic flow the pressure is a unique function of velocity, whereas in nonisentropic flow this is not true. This difference explains why the hodograph characteristics are fixed for two-dimensional, isentropic flow but are not fixed for nonisentropic flow. These remarks suggest further that we apply the method of characteristics stepwise to the rotational flow patterns, using not the hodograph characteristics diagram, but rather working out the physical characteristics in terms of the relations between pressure change and direction change for each individual wavelet, taking note of the actual pressures, velocities, and Mach Numbers in each field. This method is in essence equivalent to the more formal mathematical methods.

SHOCKS CROSSING SLIP LINES. When a shock enters a region of parallel flow with varying speed, it is refracted and suffers partial reflection. This problem is discussed in Reference 14 (see Problem 16.36), and, more generally, in Reference 18.

16.9. Explicit Solutions by Series Expansions

The shock relations are so complex algebraically that it is seldom possible to get analytical solutions even for such simple cases as the flow over a flat-plate airfoil at an angle of attack. In Chapter 14 simple analytical results were achieved by means of the linearized theory. The formulas of the linear theory may be thought of as the first term of a series solution, thus suggesting that more accurate analytical results might be found by taking terms of higher order than the first.

Series Solution for Continuous Waves. Returning for the moment to isentropic waves of one family, the characteristic relations of Chapter 15 are

$$\pm\theta = \sqrt{\frac{k+1}{k-1}} \operatorname{arc tan} \sqrt{\frac{k-1}{k+1}} (M^2 - 1) - \operatorname{arc tan} \sqrt{M^2 - 1} + \text{constant}$$

For isentropic flow, moreover,

$$\frac{p_0}{p} = \left(1 + \frac{k-1}{2} M^2\right)^{\frac{k}{k-1}}$$

Eliminating M from this pair of equations, and then expanding $p - p_\infty$ in terms of M_∞ and $\Delta\theta$, where p_∞ is the initial pressure, M_∞ is the initial Mach Number, and $\Delta\theta$ is the turning angle of the streamline from the original direction, there is obtained after tedious calculations⁽¹⁰⁾

$$\frac{p - p_\infty}{\frac{1}{2} k p_\infty M_\infty^2} = \pm C_1(\Delta\theta) + C_2(\Delta\theta)^2 \pm C_3(\Delta\theta)^3 + \dots \quad (16.20)$$

where $\Delta\theta$ is positive when counterclockwise. The upper and lower signs refer respectively to left-running and right-running Mach waves, and the coefficients are as follows:

$$C_1 = 2/\sqrt{M_\infty^2 - 1} \quad (16.21a)$$

$$C_2 = [(M_\infty^2 - 2)^2 + kM_\infty^4]/2(M_\infty^2 - 1)^2 \quad (16.21b)$$

$$C_3 = \frac{M_\infty^4}{(M_\infty^2 - 1)^{7/2}} \left[\frac{k+1}{6} \left(M_\infty^2 - \frac{5+7k-2k^2}{2(k+1)} \right)^2 + \frac{-4k^4 + 28k^3 + 11k^2 - 8k - 3}{24(k+1)} \right] + \frac{3(M_\infty^2 - 4/3)^2}{4(M_\infty^2 - 1)^{7/2}} \quad (16.21c)$$

It will be noted that the first term of Eq. 16.20 represents the linearized solution.

Series Solution for Oblique Shock. If the shock relations of Art. 16.2 are expanded in a similar way, letting subscript 1 refer to conditions upstream of the shock, we find^(11,20) that the first two terms are the same as for isentropic waves of one family, with the difference between the two types of flow appearing initially in the third term:

$$\frac{p - p_\infty}{\frac{1}{2} k p_\infty M_\infty^2} = \pm C_1(\Delta\theta) + C_2(\Delta\theta)^2 \pm (C_3 - D)(\Delta\theta)^3 + \dots \quad (16.22)$$

where

$$D = \frac{(k+1)}{48} \frac{M_\infty^4}{(M_\infty^2 - 1)^{7/2}} [(5 - 3k) M_\infty^4 - (12 - 4k) M_\infty^2 + 8] \quad (16.23)$$

Although the coefficients C_1 , C_2 , C_3 , and D appear complex, they depend only on M_∞ and k , and need be computed only once. The coefficients C_1 and C_2 are tabulated in Table B.8 and are plotted in Fig. 16.41.

Equations 16.20 and 16.22 may then be used for obtaining analytical results, provided of course that waves of opposite family do not cross each other. Examples are given later.

If only terms up to second order in $\Delta\theta$ are employed, it is clear from these equations that the oblique shock theory and the continuous wave theory give identical results.

16.10. Examples of Two-Dimensional Flows Containing Shocks

Most supersonic flows include both shocks and regions of continuous waves. A number of illustrative problems will now be discussed in the light of the characteristics theory of Chapter 15 and of the oblique shock theory of this chapter.

Formation of Shock from Continuous Wave. When a pointed body with a profile such as $A-B-C-D-E-F$ in Fig. 16.31a is placed in a supersonic stream, compression wavelets are generated at each point on the concave surface. These wavelets converge and ultimately form the beginning of an envelope at G , at which point an oblique compression shock begins. As additional compression wavelets starting at C , D , etc., reach the initial wave at H , J , etc., they merge with the compression shock and strengthen the latter. Finally all the compression wavelets are coalesced into a single oblique shock beginning at point L .

Consider (Fig. 16.31b) the merging of the first two wavelets at point G . The pressures, velocities, and flow directions in fields 2 and 3 are found by applying the characteristics theory to waves AG and BG . The subsequent wave pattern near G is determined by the requirements that the streamline passing through the shock immediately above G end with the same pressure and flow direction (in field 4'') as the streamline passing through the two compression wavelets immediately below G (field 4'). In general, these conditions can be met only if a weak reflected wavelet GM is generated; furthermore, since field 4' has a higher stagnation pressure than field 4'', but the same static pressure, the gas speed in field 4' will be larger than that in 4'' and a slip line will divide fields 4' and 4''. (See Problem 16.13.)

If the calculation procedure of the preceding paragraph is continued, it is found that the shock $GHJKL$ is curved; that there is a weak system of reflected waves, GM , HN , etc.; and that slip lines GS , etc., cover the region downstream of GL , thus making this region one of vorticity. Furthermore each wavelet crossing a slip line suffers a partial reflection. To avoid complicating the figure, these very weak reflections are not shown.

Unless the shock is quite strong, the reflected waves GM , HN , etc., are extremely weak and the velocity difference across the slip lines is

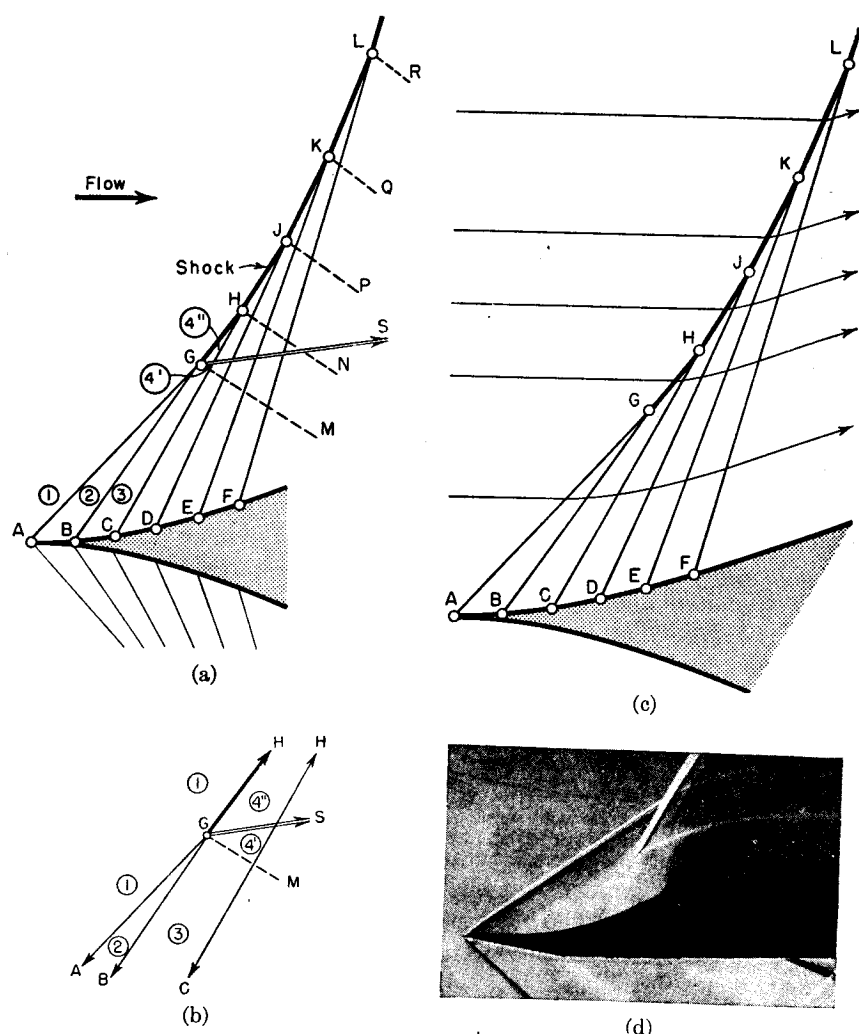


FIG. 16.31. Formation of shock from continuous compression wave.

- (a) Exact solution, taking account of vorticity behind curved shock. Slip lines emanating from H, J, K, L are omitted. Reflected wavelets generated on GS are also omitted.
- (b) Details of pattern near G .
- (c) Approximate solution, ignoring vorticity.
- (d) Schlieren photograph of shock formed from continuous wave generated at circular-arc surface. Turbulent boundary layer. Note vortex sheets (after Johannessen).

very small, thus suggesting the simplified solution of Fig. 16.31c in which the entropy changes across the shock are ignored. In many practical problems, the simple construction of Fig. 16.31c is quite adequate. Sometimes it is desirable to use the simple construction of Fig. 16.31c for the weaker portions of the shock and the more rigorous solution of Fig. 16.31a for the stronger portions of the shock.

Overexpanded Jet from Nozzle. Consider a uniform, parallel, super-

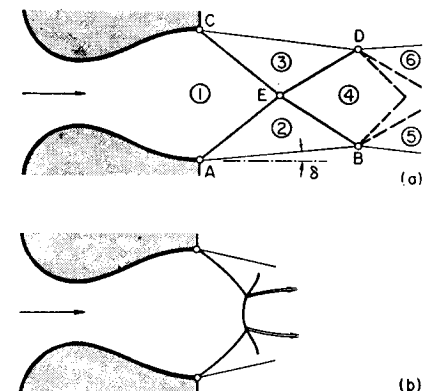


FIG. 16.32. Jet leaving overexpanded nozzle.

- (a) Regular reflection of shocks.
- (b) Mach reflection of shocks.

The pressure of the jet boundaries must be equal to that of the exhaust region. Accordingly, oblique compression waves AE and CE are generated and the jet boundaries are turned through an angle δ such that p_2 and p_3 are equal to the exhaust pressure.

Because of symmetry conditions, the interaction of oblique shock waves AE and CE is equivalent to the reflection of a shock from a plane wall. The strengths of waves ED and EB are determined by the condition that the stream has the same directions in fields 1 and 4.

The pressure in field 4 is greater than the exhaust pressure. In order for the jet boundary to remain at constant pressure, shock waves ED and EB must be reflected as centered Prandtl-Meyer rarefaction waves where the former strike the jet boundaries at D and B . The strengths of the rarefaction waves are determined by setting $p_5 = p_6 = p_2 = p_3$. The turning of the jet boundary at B and D is, approximately, 2δ , as given by the linear theory.

At section BD there is a uniform, parallel flow at a pressure greater than the exhaust pressure. Beginning with this section, therefore, the situation is equivalent to that of an underexpanded jet leaving a nozzle. All further reflections at the boundary are either centered rarefactions or centered compressions, and the jet goes through a series of repeated cyclic variations (Fig. 15.23a). Schlieren photographs (Figs. 5.24c and 16.27d) confirm the flow pattern constructed here except for the effects of viscous mixing at the boundaries.

Although both overexpanded and underexpanded jets exhibit a repeated pattern of cyclic variations, the first half-cycle of the overexpanded jet (the region between sections *AC* and *BD*) is never repeated.

These results may be compared with the approximate solutions based on the linearized theory (Fig. 14.23).

If the exhaust pressure is too much larger than the pressure in the exit plane, regular reflection is impossible, and the Mach type of reflection is observed (Figs. 16.32b and 16.28c). The subsequent flow pattern is very difficult to analyze because it consists of mixed subsonic and supersonic flow and contains regions of vorticity.

Jet Leaving Turbine Nozzle. The exit plane of a turbine nozzle is usually cut off at an angle to the direction of flow. Fig. 16.33 shows the

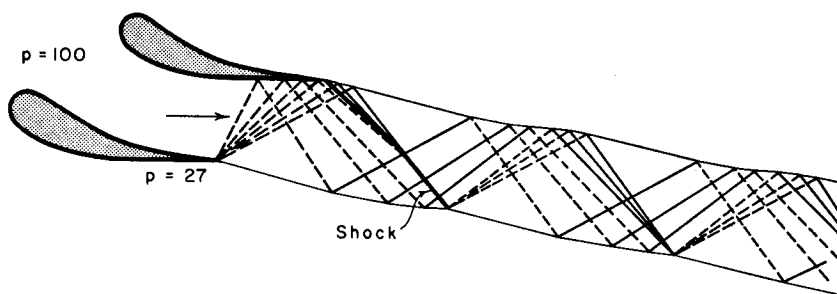


FIG. 16.33. Jet leaving converging turbine nozzle.

nature of the flow pattern for such a jet when the nozzle is of the converging type and the flow is underexpanded. The supply pressure is assumed to be 100 psia, and the exhaust region pressure 27 psia. Hence sonic flow exists at the throat with a pressure of 53 psia. The wave pattern is worked out for a 2° turning angle across each wave, except for the shock. Entropy increases across the latter are ignored. Expansion wavelets are shown by dashed lines, and compression wavelets by solid lines.

An important result demonstrated by Fig. 16.33 is that the average jet direction differs significantly from the nozzle direction because of the general bending of the jet. This bending effect reduces the work available from the turbine wheel.

Oblique-Shock Diffuser. Fig. 16.34 shows an oblique-shock diffuser, the upper boundary of which could be considered either as a streamline of symmetry or as a solid wall.

The oblique shock originating at the bend (point *A*) is reflected from each of the walls in turn. Each reflected shock has the same turning angle as the original shock *AB*. Because of the deceleration through each shock, a point is reached, depending on the initial Mach Number

and turning angle, beyond which regular reflection is impossible. The last shock, *DE*, is, therefore, curved, and reduces virtually the entire stream to subsonic speeds.

The potential advantage of such a diffuser is that the supersonic deceleration occurs across several oblique shocks of small turning angle. Calculations indicate that this leads to comparatively small losses in stagnation pressure. The normal, or nearly normal, shocks *DE* and *FG* appear only after the Mach Number has been reduced to nearly unity.

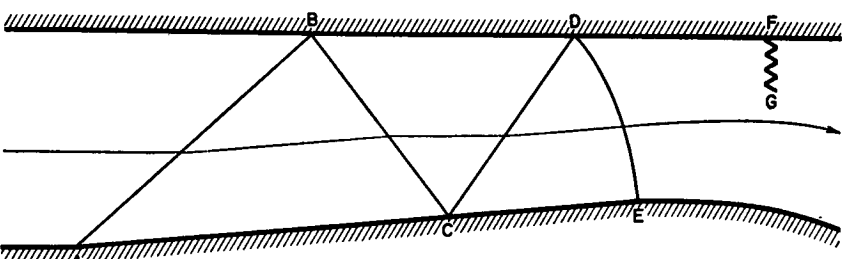


FIG. 16.34. Oblique-shock diffuser.

In practice the inviscid flow pattern of Fig. 16.34 is seriously modified by the interaction between the shock waves and the boundary layers on the walls.

16.11. Two-Dimensional Profiles

Shock-Characteristic Analysis for Two-Dimensional Profiles. The "exact" solution for the lift, drag, and moment produced by a supersonic stream on a two-dimensional profile is obtained by combining the shock analysis with the method of characteristics, on the assumption that viscous effects can be ignored.

Consider, for example, the flow past a symmetrical double-wedge profile at an angle of attack. The boundary conditions at the profile are satisfied by the wave pattern of Fig. 16.35. Each of the four faces of the diamond profile has a constant pressure over its surface. The wave between regions 1 and 2 is an oblique shock for small angles of attack, and a centered Prandtl-Meyer rarefaction wave for large angles of attack. For the case illustrated there is a shock between fields 1 and 2. The values of p_2 and M_2 may accordingly be found with the help of the oblique-shock theory from p_∞ , M_∞ , and the turning angle between 1 and 2. Next, the values of p_4 and M_4 may be found by applying the method of characteristics to the Prandtl-Meyer flow originating at point *B*, using the known turning angle between 2 and 4 and the previously found values of p_2 and M_2 . Similar calculations yield the pressures and Mach Numbers in fields 3 and 5.

Having found the pressure distribution over the profile, the resulting forces and moments may be calculated, leading finally to the lift, drag, and moment coefficients. Although the "exact" theory as given here is more accurate than the linear and second-order theories, it has the disadvantage that a separate set of numerical calculations is required for each combination of profile shape, angle of attack, and Mach Number, and that it is not possible to arrive at simple analytic formulas showing the effects of these variables.

Eggers and Syvertson⁽¹⁹⁾ have formulated a comparatively simple approximation to the shock-expansion method for thin profiles, which,

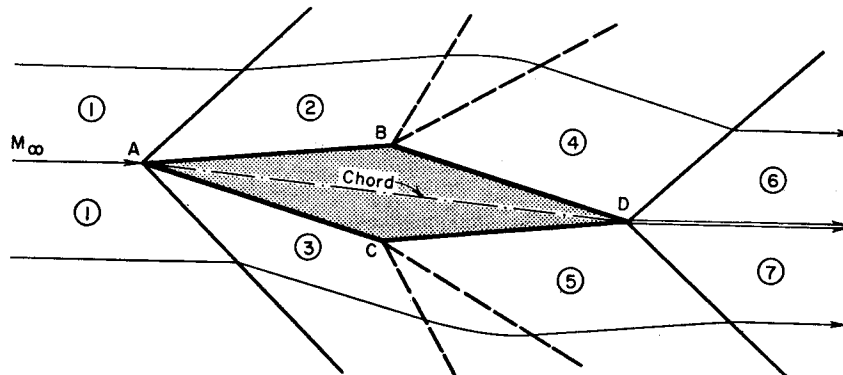


FIG. 16.35. Double-wedge profile.

for Mach Numbers greater than 3 and flow deflection angles less than 25°, yields pressure distributions in error by less than 10%.

In order to determine the nature of the wake immediately behind the profile, we note that the two shocks emanating from D must be of such strengths that the pressures and flow directions in regions 6 and 7 are the same. The two boundary streamlines passing through D have passed through shocks of different strength, and, consequently, have different stagnation pressures. Accordingly, the double streamline trailing from point D is a slip line, or vortex sheet. The common flow direction of fields 6 and 7 is in general different from that in region 1, and, furthermore, the common pressure in these fields differs from that of region 1. These differences, however, are usually minute.

The "exact" calculation is very much more difficult if the waves generated at the profile interfere with each other so near the profile that the reflected waves reach the profile further downstream, as is the case with the circular-arc profile of Fig. 16.36. Consider the flow over the upper surface (Fig. 16.36a). An oblique shock is generated at the nose in accordance with the turning angle associated with the tangent at the nose. Because of the continuous curvature of the profile, however,

expansion wavelets are continually generated. These intersect and weaken the shock. At the intersection of each wavelet with the shock there are generated a reflected wave and a slip line. Some of the reflected waves reach the profile and thereby modify the surface pressure distribution. The computations are evidently much complicated by the vorticity in the fluid downstream of the shock.

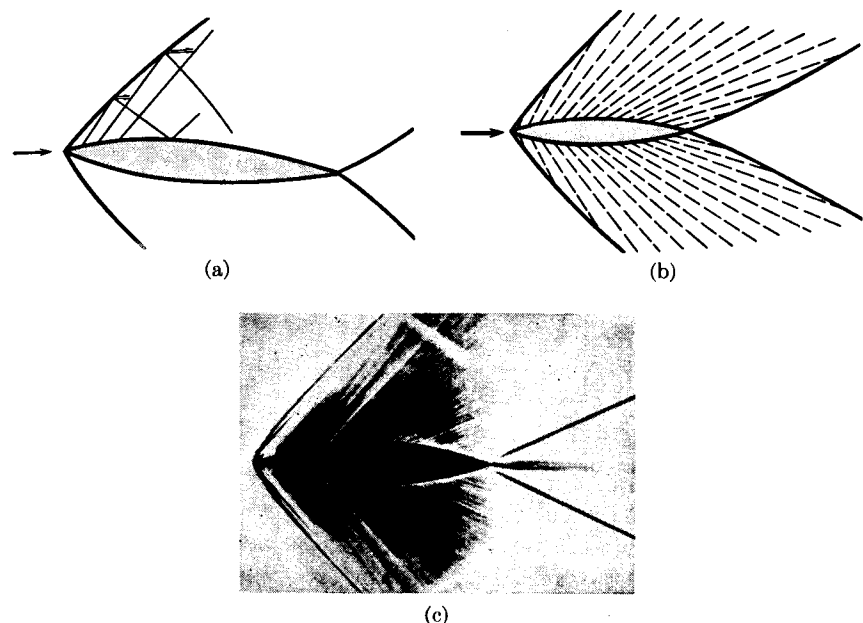


FIG. 16.36. Biconvex profile.

- (a) Some details of exact wave pattern, showing that wavelets reflected at curved shock influence surface pressure distribution.
- (b) Approximate wave pattern, ignoring vorticity behind shock.
- (c) Schlieren photograph for flow of (b) (after Ackeret).

As pointed out previously, however, it is often acceptable to ignore the variation in entropy change over a fairly large region. If this is done, there are no reflected wavelets to deal with, and we get the easily calculated flow pattern of Fig. 16.36b. On the upper and lower surfaces the flow is of simple wave type, and the curvatures of the shocks do not enter into the calculation of the lift, drag, and moment. Schlieren photographs (Fig. 16.36c) show wave patterns in good agreement with the approximate pattern of Fig. 16.36b, and the calculations of Reference 19 further confirm that there is little loss in accuracy incurred by ignoring the entropy variations.

Relation Between Wave Drag and Shock Losses. In Chapter 14 we saw from the linearized analysis that the pressure drag of supersonic

profiles is associated with the thickness of the profile and with the production of lift. We shall now look at the matter from another point of view.

Fig. 16.37 shows a control surface all the boundaries of which are at great distances from the profile. Although the flow pattern near the profile is marked by large variations in pressure and direction, the wave systems ultimately interact with each other and tend to wipe out non-uniformities. As described in more detail later, the net effect of the wave interactions is that at very great distances from the profile the flow is uniform and parallel and differs from the original direction and pressure

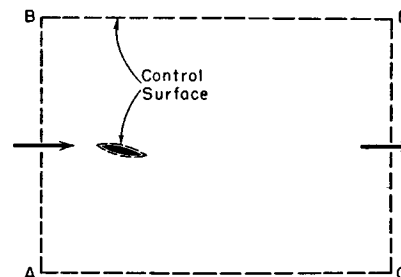


FIG. 16.37. Control surface for momentum analysis.

by only infinitesimal amounts. The approach flow is uniform and parallel over section AB , and, from the foregoing considerations, the stream pressure and direction over sections CD , BD , and AC are the same as over AB . Hence the drag force on the profile is equal to the momentum flux through AB minus the momentum fluxes through CD , BD , and AC . Within the control surface the streamlines suffer losses of stagnation pressure (or increases of entropy) wherever they cross shocks. In general, therefore, the stagnation pressure along AB is greater than that along CD , BD , and AC . But, since the pressures on these planes are equal, the velocities are smaller along CD , BD , and AC than along AB . Consequently there is a drag on the profile, a drag which is directly related to the losses in stagnation pressure through the shock system.

Translated into practical terms, these considerations show why supersonic profiles have sharp leading edges, for a rounded leading edge produces detached shocks which are nearly normal and hence have large losses in stagnation pressure. Furthermore, it is plain that with thin sections the leading edge shocks are relatively weak and produce relatively small losses in stagnation pressure; hence thin sections have relatively small drag. In order to obtain large lift coefficients it is necessary to have large angles of attack. The latter, however, are accompanied by relatively strong shocks which in turn give rise to a relatively large pressure drag. In supersonic two-dimensional flow, therefore, the production of lift is always accompanied by the production of drag.

The importance of a sharp leading edge for supersonic flow is illustrated strikingly by experimental data (Fig. 16.38) for the flow past a strut formed of a cylinder and a fairing.⁽¹²⁾ The lift-drag polars show clearly that in supersonic flow it is better to make the sharp end of the strut the leading edge and the rounded end the trailing edge. This is exactly the opposite of what is desirable for subsonic flow! In supersonic flow a blunt leading edge produces enormous increases in drag because of the strong detached shock wave in the flow field. Although

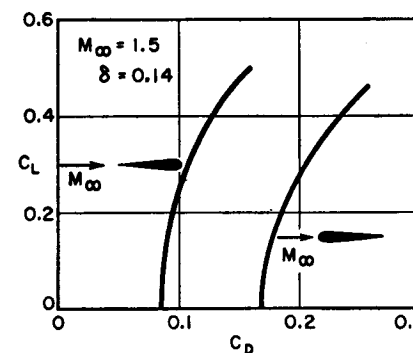


FIG. 16.38. Experimental drag polars for strut (after Busemann and Walchner).

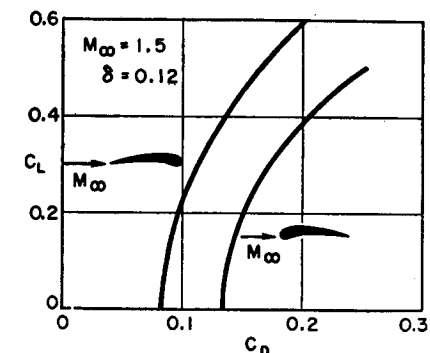


FIG. 16.39. Experimental drag polars for subsonic profile (after Busemann and Walchner).

it is desirable to have both the leading and trailing edges sharp, it is more important to avoid a blunt leading edge than a blunt trailing edge.

This point is demonstrated again in the experimental data⁽¹²⁾ of Fig. 16.39 for a conventional subsonic profile. In supersonic flow the profile is more efficient when the leading and trailing edges are reversed.

Second-Order Theory for Two-Dimensional Profiles. To obtain analytical results somewhat more accurate than the formulas of the linear theory (Chapter 14), we may employ the series expansions of Eqs. 16.20 and 16.22.

If third-order terms are taken into account, the calculations become so involved that it is easier to use the exact shock-characteristics theory. Hence, since simplicity is one of the chief aims of an approximate analysis, we shall consider only terms up to the second order in Eqs. 16.20 and 16.22. Since these two series expansions are identical up to second-order terms, the second-order theory takes no account of the entropy changes which accompany oblique shocks in the flow pattern.

We refer a system of axes to the profile (Fig. 16.40), with the ξ -axis passing through the sharp leading and trailing edges. The upper surface of the profile has the ordinate η_U , taken positive when above the

chord line; similarly the ordinate η_L of the lower surface is taken positive when *below* the chord line. The angle of attack, α , is positive when directed as shown in the sketch.

The method of analysis is similar to that of the linearized theory (Art. 14.6), but the second-order terms of Eqs. 16.20 and 16.22 are

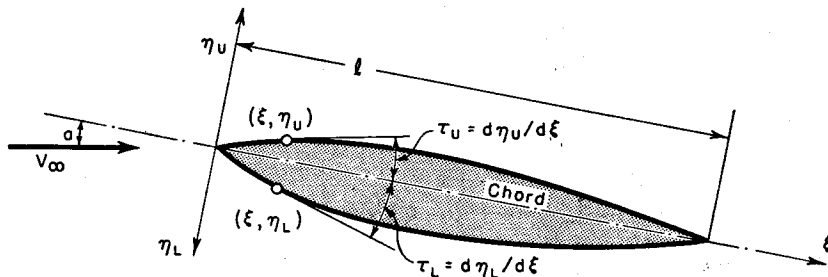


FIG. 16.40. Nomenclature for second-order thin profile theory.

taken into account. During the course of the calculations several integrals appear which depend only on the geometry of the profile. These are

$$J_1 = \int_0^1 \tau^2 d(\xi/l) \quad (16.24a)$$

$$J_2 = \int_0^1 \tau^3 d(\xi/l) \quad (16.24b)$$

$$J_3 = \int_0^1 \tau(\xi/l) d(\xi/l) \quad (16.24c)$$

$$J_4 = \int_0^1 \tau^2(\xi/l) d(\xi/l) \quad (16.24d)$$

Each of these definite integrals must be evaluated separately for the upper and lower surfaces. The corresponding values are denoted by J_{1U} , J_{1L} , etc.

The force and moment coefficients which result from the analysis are^(1,6)

$$C_L = 2C_1a + C_2(J_{1L} - J_{1U}) \quad (16.25)$$

$$C_D = 2C_1a^2 + C_1(J_{1L} + J_{1U}) + 3C_2(J_{1L} - J_{1U})a + C_2(J_{2L} + J_{2U}) \quad (16.26)$$

$$C_M = C_1a + C_1(J_{3L} - J_{3U}) + 2C_2(J_{3L} + J_{3U})a + C_2(J_{4L} - J_{4U}) \quad (16.27)$$

Only pressure drag is included in the drag coefficient given above. The skin-friction drag coefficient must therefore be added to the right-hand side of Eq. 16.26 in order to get the total drag coefficient.

The moment coefficient of Eq. 16.27 is reckoned about the leading edge, and is taken to be positive when the moment acting on the profile

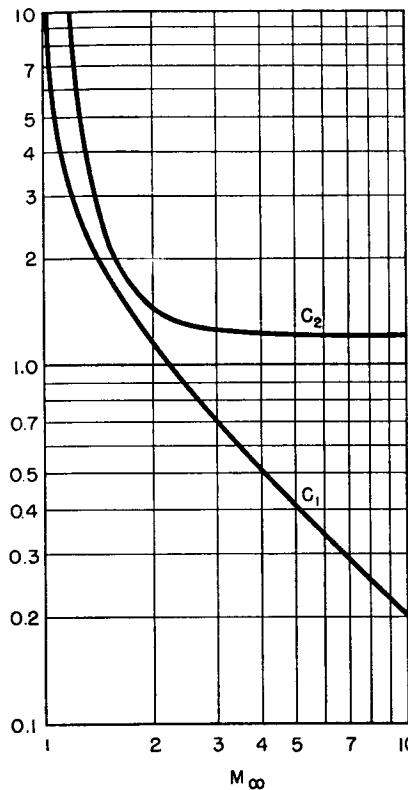


FIG. 16.41. Coefficients of the second-order theory ($k = 1.4$).

is counterclockwise, with the direction of flow from left to right as in Fig. 16.40.

By setting C_2 equal to zero in Eqs. 16.25, 16.26, and 16.27, the second-order theory is reduced to the first-order, or linear, theory, and the results are then identical with those previously found in Chapter 14.

The orders of magnitude of the coefficients C_1 and C_2 are shown in Fig. 16.41. These coefficients are always positive.

All the J -integrals are zero for a flat plate, and Eqs. 16.25, 16.26, and 16.27 then show that the first-order and second-order theories are identical for a flat plate because only terms in C_1 remain. We may therefore

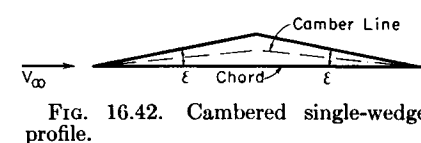


FIG. 16.42. Cambered single-wedge profile.

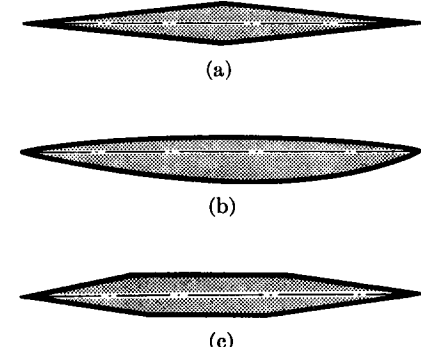


FIG. 16.43. Typical supersonic profiles.

state the general rule that the results of the second-order and linear theories approach each other as the profile shape approaches a flat plate.

TRIANGULAR PROFILE. To illustrate the difference between the second-order and linear theories, consider the triangular profile of Fig. 16.42 at zero angle of attack. The various J -integrals are

$$J_{1L} = J_{2L} = J_{3L} = J_{4L} = 0$$

$$J_{1U} = \epsilon^2; \quad J_{2U} = 0; \quad J_{3U} = -\epsilon/4; \quad J_{4U} = \epsilon^2/2$$

For the force coefficients we then obtain

$$C_L = -C_2\epsilon^2; \quad C_D = C_1\epsilon^2; \quad C_{\mathfrak{M}} = C_1(\epsilon/4) - C_2(\epsilon^2/2)$$

The first-order theory predicts zero lift, but the second-order theory predicts a negative lift. The latter fact is especially interesting in that it shows still another surprising difference between subsonic and supersonic flow. In subsonic flow at zero angle of attack with a positive camber as in Fig. 16.42, the lift is also positive; in supersonic flow the lift for the same profile is negative.

At zero angle of attack, the thickness drag for this profile is the same for both the first-order and second-order theories.

If $l_{c.p.}$ is the distance from the leading edge to the center of pressure, we may show by taking moments that

$$\frac{l_{c.p.}}{l} = \frac{C_{\mathfrak{M}}}{C_L} + \frac{C_D \epsilon}{C_L 4} = \frac{1}{2} - \frac{C_1}{4C_2} \left(\frac{1}{\epsilon} + \epsilon \right)$$

Thus, the second-order theory predicts that the c.p. is a finite distance forward of the mid-chord point, whereas the linear theory predicts it to be infinitely forward. As a general rule the most significant improvement of the second-order theory over the linear theory lies in a more accurate prediction of the center of pressure.

COMPLETELY SYMMETRICAL PROFILE. If the profile is symmetrical both laterally and longitudinally, we may set $J_L = J_U$ and we may also set $J_2 = 0$. We then obtain

$$C_L = 2C_1a \quad (16.28a)$$

$$C_D = 2C_1a^2 + 2C_1J_{1U} \quad (16.28b)$$

$$C_{\mathfrak{M}} = C_1a + 4C_2J_{3U}a \quad (16.28c)$$

No second-order terms appear in the expressions for C_L and C_D . We may write, for the location of the center of pressure,

$$\frac{l_{c.p.}}{l} \cong \frac{C_{\mathfrak{M}}}{C_L} = \frac{1}{2} + 2 \frac{C_2}{C_1} J_{3U} \quad (16.28d)$$

Now J_{3U} is equal to $(-S_U/l^2)$, where S_U is the cross-sectional area between the chord line and the upper surface of the profile. Therefore J_{3U} is always negative for such a symmetrical profile. Eq. 16.28d shows that the center of pressure is forward of the mid-chord, and, within the approximations of the second-order theory, it is independent of the angle of attack.

Some Types of Two-Dimensional, Thin Profiles for Supersonic Flow.

The common forms of supersonic profiles are modifications or combinations of two basic forms: (1) a profile formed of straight lines (Fig. 16.43a), and (2) a profile formed of circular arcs (Fig. 16.43b).

Many practical considerations may enter into the choice of a profile: drag at low and high angles of attack; stability of the center of pressure location over a wide range of angle of attack and Mach Number; performance at subsonic speeds; maximum stresses; maximum deflections; thermal stresses; vibrations; and weight and volume.

To avoid high drag, the thickness ratio must not be large, and the turning angles for shocks must not be large. For a given thickness ratio the symmetrical double wedge (Fig. 16.43a) has the smallest turning angles for shocks. It may in fact be demonstrated ⁽¹⁾ from the second-order theory, with the help of the calculus of variations, that (i) for a given thickness ratio, the profile of minimum drag is diamond-shaped, i.e., it is formed of four straight lines, (ii) for a given thickness ratio and minimum thickness drag, the diamond-shaped profile is symmetrical about the chord, but has its position of maximum thickness slightly aft of the mid-chord point, and (iii) for a given thickness ratio and maximum lift-drag ratio, the diamond-shaped profile has a slight positive camber and the position of maximum thickness is slightly aft of the mid-chord point.

From a practical point of view, it may be stated generally that an aerodynamically optimum profile shape seldom differs significantly from the symmetrical double wedge, and that slight variations in profile from this shape do not produce significant changes in aerodynamic characteristics. The actual choice of profile in any given instance will, therefore, depend heavily on the other factors listed above.

Comparison of Theoretical with Experimental Results for Thin Profiles. Figs. 16.44 and 16.45 show a comparison of typical experimental data ⁽¹³⁾ with the results of the linear, second-order, and exact theories. These same data were previously compared with the linear theory in a somewhat different way (Figs. 14.15 and 14.16).

From Fig. 16.44 we see that the second-order theory is a great improvement over the first-order theory in predicting the pressure distribution, and is almost as accurate as the "exact" theory. In comparing the latter with the experimental data, it should be noted that the "exact"

theory was applied only approximately, in that the type of solution of Fig. 16.36b, rather than that of Fig. 16.36a, was employed. At about 60% of chord, the measured pressure distribution on the lower surface departs markedly from the theoretical. This is the result of an interaction between the trailing-edge shock and the boundary layer, as will be discussed more fully later (Art. 16.12).

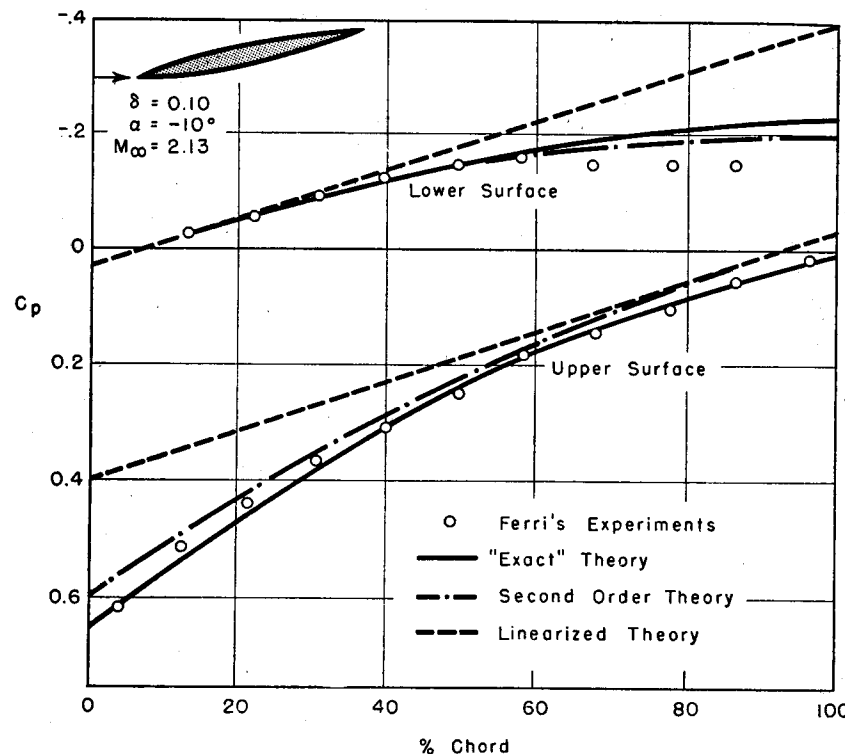


FIG. 16.44. Comparison of experimental pressure distribution with results of exact, second-order, and linear theories (after Ferri).

Fig. 16.45 shows that the second-order and exact theories give virtually identical results for lift and drag up to angles of attack of the order of 10° . Both provide a significant improvement over the linear theory, and compare very well with the experimental data. The agreement with the moment data is only fair. It is at first surprising that the actual drag is slightly less than the theoretical pressure drag of the exact theory, since the latter does not include skin friction. This effect is associated with the shock-boundary layer interaction near the trailing edge (Art. 16.12).

Downwash from Thin Profile. The flow aft of a profile is of interest if other bodies should have to be placed in the wake. For instance,

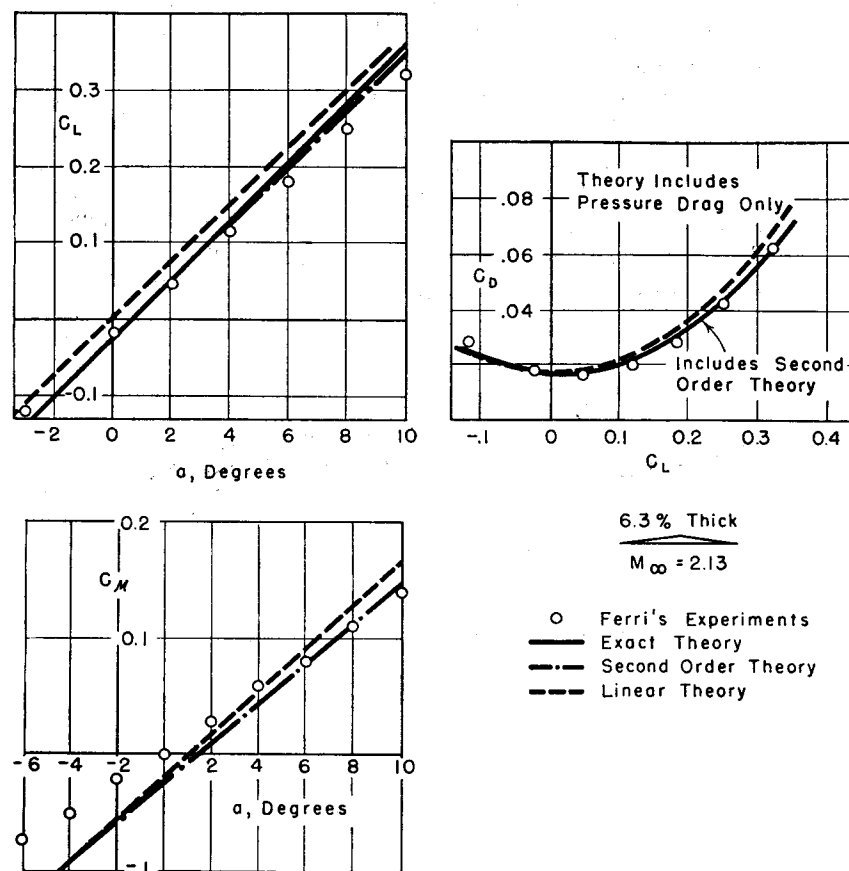


FIG. 16.45. Comparison of experimental force coefficients with results of exact, second-order, and linear theories (after Ferri).

control surfaces usually are in the wake of the main lifting surface of an aircraft.

If not for entropy increases across the shock waves (Fig. 16.46), there would be no slip line between zones 4 and 5 and the upwash angle β would be zero. It is therefore necessary to include terms of third order in Eqs. 16.20 and 16.22 in an investigation of the upwash angle. Such an analysis⁽¹⁰⁾ yields the following results for a flat-plate airfoil when $k = 1.4$:

M_∞	1.1	1.2	1.3	1.4	1.5	2.0	3.0	4.0	5.0	10.0
β/a^4	-332	-10.1	0.37	1.32	1.37	1.31	2.17	3.94	6.75	44.8

These results were found to check within 1% of the exact theory for $\alpha = 10^\circ$ and $M_1 = 5$. The magnitude of β is generally small, being always less than 0.06° for $\alpha = 5.7^\circ$ over the range of M_∞ from 1.2 to 5.0.

A surprising feature is that, except for M_∞ less than about 1.3, there is an upwash behind the wing, rather than a downwash as would be expected for subsonic flow. Of course momentum considerations require that a lift on the profile must be accompanied by a net downward change of momentum flux of all the air influenced by the profile; hence if the part of the airstream near the profile suffers an upwash, other parts of the airstream must acquire a downwash.

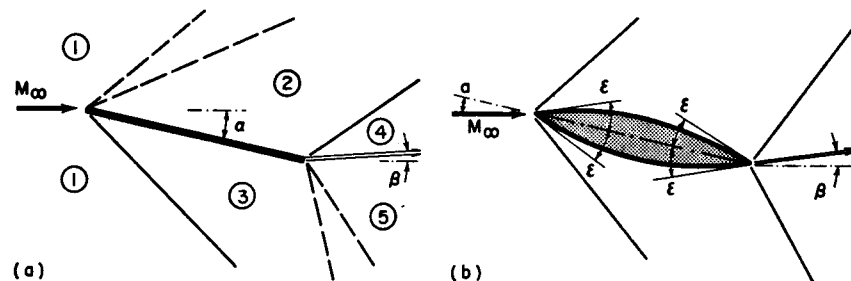


FIG. 16.46. Nomenclature for upwash relations.

(a) Flat-plate profile.
(b) Doubly symmetric profile.

When (i) the profile has thickness, (ii) there are four oblique shocks at the nose and tail (Fig. 16.46b), and (iii) the airfoil is completely symmetrical, it may be shown⁽¹⁰⁾ that

$$\beta = \left[\left(\frac{\epsilon}{a} + 1 \right)^4 - \left(\frac{\epsilon}{a} - 1 \right)^4 \right] \beta_{\text{flat plate}}$$

This formula indicates that the flow deflection for a profile with thickness is considerably larger than for a flat plate. For example, when $\epsilon = a$, the ratio between the two is 16.

Wave System in Wake. Let us consider the wake of a flat-plate profile at an angle of attack (Fig. 16.47). In the immediate neighborhood of the profile, owing to oblique shocks and Prandtl-Meyer waves, there are large variations in pressure and flow direction. However, the compression and expansion waves merge and thereby are mutually weakened. Vorticity is generated as a result of the curvature of the shocks. In the discrete wave pattern this phenomenon is represented by slip lines. Wavelets striking slip lines are in part transmitted and part reflected. Thus, more and more waves appear in the flow field, the net result being to distribute nonuniformities on an ever finer scale. At

very large distances from the profile the flow is, for all practical purposes, again uniform and parallel, with only infinitesimal deviations from the free-stream condition and with all waves at the free-stream Mach angle. A large part of the wave system for the lower side of the profile is omitted from Fig. 16.47 so as not to confuse the pattern unnecessarily.

It is this type of reasoning which justifies the analysis accompanying Fig. 16.37.

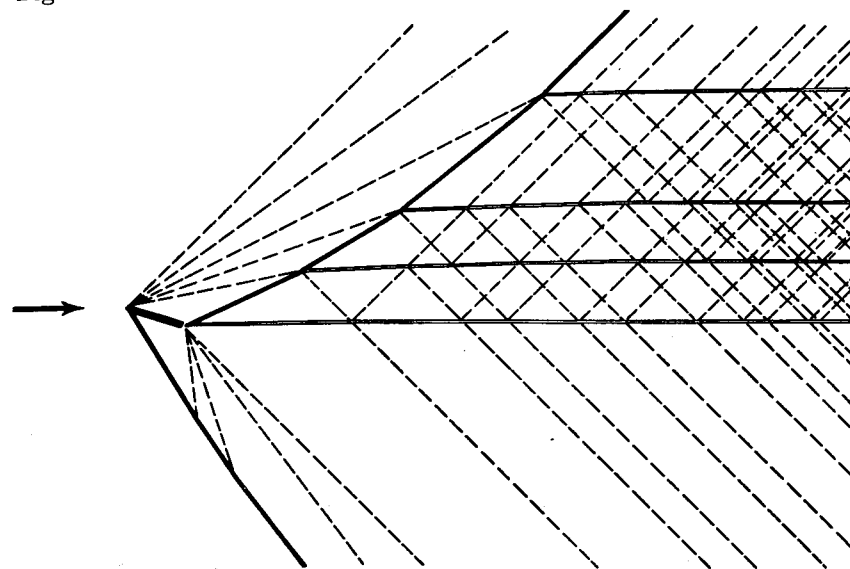


FIG. 16.47. Wave pattern downstream of flat-plate airfoil. Most of the wave system on the underside is omitted in the interest of clarity.

Supersonic Biplane. We have seen that in supersonic flow profiles must be very thin if large drags are to be avoided. This imposes severe practical difficulties in construction and makes it all but impossible to put propulsion plants inside the wings of supersonic aircraft.

An arrangement for avoiding these difficulties is the Busemann biplane (Fig. 16.48). The contours *ACE* and *BDF* are so shaped that, at zero angle of attack, the entering flow at section *AB* is decelerated reversibly to section *CD*, and is then reversibly accelerated to the initial Mach Number at section *EF*. Since there are no shock waves, there is no drag, and hence we see that the scheme permits a wing section of finite thickness without any accompanying thickness drag. If the biplane were inclined, the drag owing to angle of attack would be approximately the same as for a conventional supersonic profile, so that the advantage of the biplane (not taking into account the increased skin friction for the biplane) is in the range of low angles of attack.

The contours may be designed by the method of characteristics. Since the forward half of the biplane is a supersonic diffuser, care must be taken in adjusting the area ratio CD to AB , for otherwise the diffuser will not start, but rather a detached bow wave will stand ahead of the entrance and subsonic flow will prevail in the passage. From these considerations, it is clear that the allowable thickness of each half of the biplane increases with Mach Number.

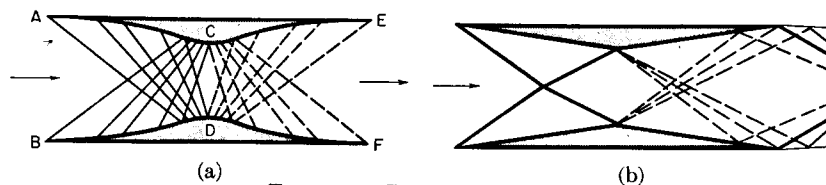


FIG. 16.48. Busemann biplane.

- (a) Zero thickness drag.
(b) Small thickness drag.

Even when shocks are present, as in the biplane design of Fig. 16.48b, they are confined to the space between the profiles and hence produce only a fraction of the drag which they would otherwise produce if allowed to propagate out to great distances from the profile.

16.12. Interaction of Shock Waves with Boundary Layer

We have thus far ignored the effects of viscosity on the nature of the flow pattern, but it is particularly important not to lose sight of viscous effects when shocks are present.

One of the great inventions in modern fluid mechanics is Prandtl's concept of the boundary layer. The underlying idea is that viscous stresses in a fluid of low viscosity are everywhere small compared with other terms in the momentum equation except in comparatively thin layers near solid boundaries where large velocity gradients, and hence appreciable viscous stresses, must necessarily exist. Viscous effects are therefore assumed to be important only in "boundary layers" adjacent to solid surfaces, and the exterior flow is assumed to be frictionless.

This approach is clearly a great simplification when the boundary layer flow does not significantly affect the external flow, for then the two regions of flow may be calculated separately, assuming for a first approximation that the boundary of the frictionless flow coincides with the solid boundary. Such is often the case for problems of subsonic flow, especially when the boundary layer is relatively thin compared with other significant length dimensions, e.g., the thickness of a profile or the diameter of a duct. The presence of the boundary layer then has only a second-order effect on the exterior flow.

When separation of the boundary layer occurs, however, due to adverse pressure gradients, as in the stalling of a wing profile, the boundary layer thickens to such an extent that it materially affects the exterior flow, and it is no longer possible to assume that the boundary of the exterior flow coincides approximately with the solid boundary. When this occurs the simplicity of the boundary-layer concept breaks down, for the boundary layer then affects the exterior flow in a manner which is by no means negligible.

When shock waves occur near solid bodies, the interaction between the shock waves and the boundary layer usually produces first-order effects on both flows. The extraordinary pressure gradients in the neighborhood of the shock wave violently distort the boundary-layer flow. These distortions, which are propagated both upstream and downstream in the subsonic part of the boundary layer, in turn influence the conditions outside the boundary layer by means of expansion and compression waves generated by the disturbed boundary layer. Thus there is a mutual interaction between a shock wave and a boundary layer, an interaction which may lead to a flow pattern radically different from what might be anticipated if no boundary layer were present. A more complete discussion than is given here is presented in Volume II, Chapter 28.

Oblique Shock Wave Incident on Flat Plate. In Fig. 16.49a the oblique shock AB is incident on a flat plate on which there is a boundary layer. If the boundary layer were not present, the incident shock would be reflected as an oblique shock of equal turning angle, as in Fig. 16.25b.

When a boundary layer is present this simple type of reflection cannot occur because (i) the shock bends as it enters the region of changing velocity in the boundary layer, and must terminate at the sonic line in the boundary layer, and (ii) the effects of the shock can be propagated upstream in the subsonic boundary layer.

As a result of the latter effect, the pressure in the boundary layer begins to rise before the point of incidence of shock AB . With this pressure rise goes a velocity decrease and hence a thickening of the boundary layer along DB . Oblique compression wavelets are generated along DB as a result of the turning of the streamlines. These wavelets coalesce into the shock EF , which may be thought of as part of the reflected shock system.

As the original shock AB enters the boundary layer, it is refracted along BC because it is in a region of changing Mach Number. As a result of this refraction, wavelets are generated along BC ; some of these are rarefaction wavelets, but often they are compression wavelets which coalesce into the shock MN .

The pressure at F is often greater than that at G because the stream at F has passed through a shock of comparatively great strength. Such

a pressure gradient, if present, causes the streamlines to turn back toward the wall. This streamline curvature in turn produces expansion waves in the supersonic flow.

If the pressure difference between F and G is quite large the flow may be turned toward the wall. The latter, however, constrains the flow in

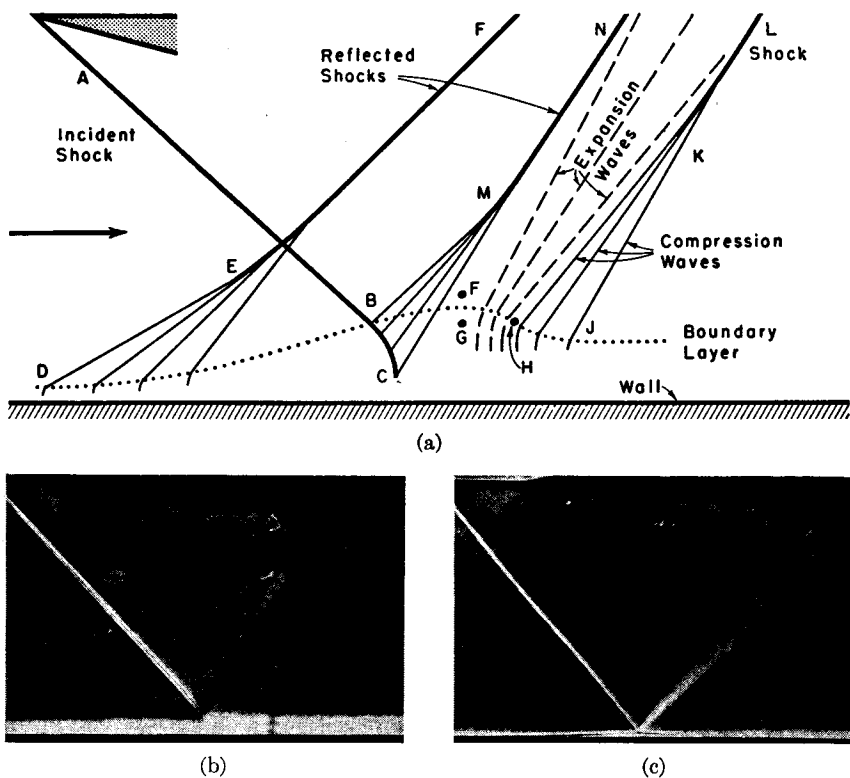


FIG. 16.49. Reflection of oblique shock from boundary layer on flat plate.

- (a) Schematic representation.
- (b) Schlieren photograph for turbulent boundary layer (after Liepmann, NACA).
- (c) Schlieren photograph for laminar boundary layer (after Liepmann, NACA).

such a way that compression wavelets are generated along the concave part of the boundary layer HJ . These wavelets coalesce into the shock KL .

Experimental observations are in qualitative accord with the foregoing rationalization of the wave pattern. The nature of the interaction depends upon Mach Number, shock strength, velocity profile in the boundary layer, and especially on whether the boundary layer is laminar or turbulent. In all cases observed, however, the flow patterns contain in greater or lesser degree all or part of the elements shown in Fig. 16.49a (see also Chapter 28 of Volume II).

"Normal" Shocks in Ducts. When discussing one-dimensional supersonic flows in ducts (Chapter 5) we often speak of a normal shock standing in the duct when the back pressure is high. In practice it is observed that the pressure rise through the shock occurs over an axial distance of several duct diameters, and schlieren photographs show patterns like those of Fig. 16.50. This pattern may be rationalized by noting that the

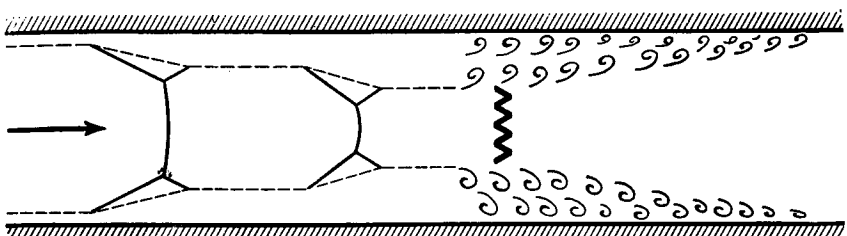


FIG. 16.50. "Normal" shock in duct.

normal shock could not possibly extend to the wall when a boundary layer is present and that the rapid thickening of the boundary layer upstream of the shock gives rise to an oblique shock. The reflected shock at the juncture of the normal and oblique shocks is necessary as a result of continuity requirements. Thus, a series of forked normal shocks appears, with the length of the normal shock becoming progressively smaller as the boundary layer thickens. Finally the sonic velocity is reached and the stream then decelerates subsonically as it refills the passage. In place of a normal shock, therefore, the stream contracts by means of a combination of normal and oblique shocks to Mach Number unity and then diverges to subsonic speeds.

Shock Propagated at a Bend.

When no boundary layer is present a shock is propagated in a straight line from a sharp concave bend, as in Fig. 16.1c.

The corresponding pattern for supersonic flow past a sharp concave corner with a boundary layer present is shown in Fig. 16.51.

The large pressure rise near the corner propagates upstream through the subsonic boundary layer. As the boundary layer decelerates, it also thickens, and thus continuously propagates compression wavelets into the supersonic flow. These wavelets merge and ultimately form a shock across which the turning of the stream occurs.

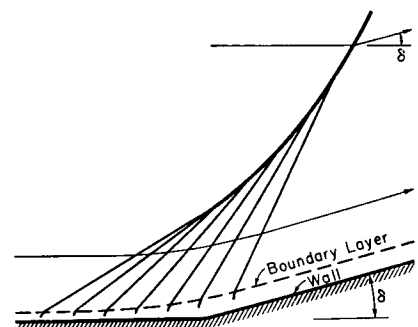


FIG. 16.51. Generation of shock in concave corner with boundary layer present.

Flow Near Trailing Edge of Supersonic Profile. The concepts of the preceding paragraph help to explain the flow near the trailing edge of a supersonic profile at an angle of attack.

Without a boundary layer, the wave pattern, flow pattern, and pressure distribution on the upper surface near the trailing edge are as shown in Fig. 16.52a.

With a boundary layer, the situation is much like that of Fig. 16.51, and the resulting wave pattern, flow pattern, and pressure distribution

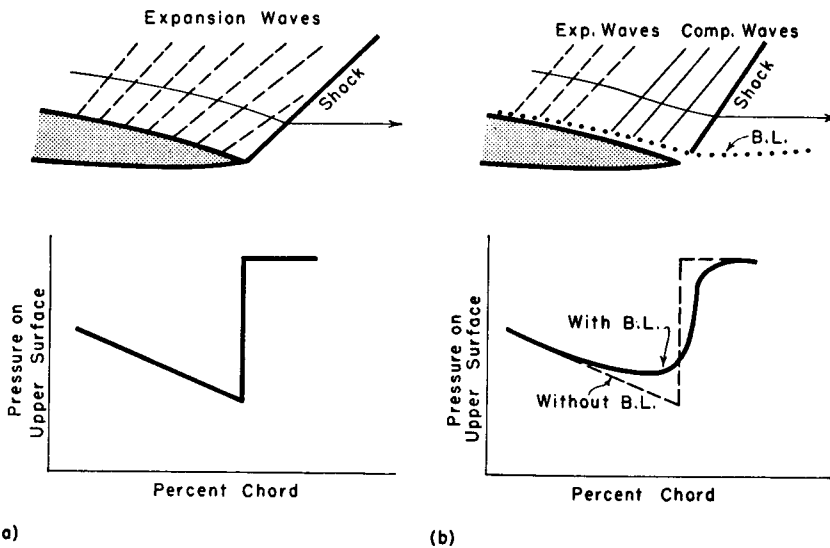


FIG. 16.52. Flow near trailing edge of supersonic profile.

- (a) Boundary layer absent.
- (b) Boundary layer present.

are as shown in Fig. 16.52b. The difference in flow patterns between Fig. 16.52a and Fig. 16.52b is the result of the rapid thickening of the boundary layer as it approaches the trailing edge.

The pressures on the upper surface near the trailing edge are higher than those which might be expected if viscosity were neglected. This conclusion is clearly confirmed by the typical experimental results of Fig. 16.44. Over the rearward half of the profile the measured pressures on the lower surface are markedly higher than those computed by the inviscid theory.

From a comparison of the pressure distributions of Figs. 16.52a and 16.52b it may be concluded that the effect of the shock boundary-layer interaction is to reduce the lift coefficient, and, surprisingly, to reduce the drag coefficient also. This latter effect explains why in Fig. 16.45 the measured drag is less than the calculated drag even though the latter does not include skin-friction drag.

REFERENCES AND SELECTED BIBLIOGRAPHY

1. FERRI, A. *Elements of Aerodynamics of Supersonic Flows*. New York: The Macmillan Co., 1949.
2. COURANT, R., and FRIEDRICH, K. O. *Supersonic Flow and Shock Waves*. New York: Interscience Publishers, Inc., 1948.
3. SAUER, R. *Introduction to Theoretical Gas Dynamics*. Translated by F. K. HILL and R. A. ALPHER, Ann Arbor: J. W. Edwards, 1947.
4. DAILEY, C. L., and WOOD, F. C. *Computation Curves for Compressible Fluid Problems*. New York: John Wiley & Sons, Inc., 1949.
5. NEICE, M. M. Tables and Charts of Flow Parameters Across Oblique Shocks, *NACA Tech. Note*, No. 1673 (1948).
6. AMES AERONAUTICAL LABORATORY. Notes and Tables for Use in the Analysis of Supersonic Flow, *NACA Tech. Note*, No. 1428 (1947).
7. ISENBERG, J. S. The Method of Characteristics in Compressible Flow, Part IA: Tables and Charts, *Air Materiel Command Report*, No. F-TR-1173B-ND (1947).
8. KEENAN, J. H., and KAYE, J. *Gas Tables*. New York: John Wiley & Sons, Inc., 1948.
9. ISENBERG, J. S., and LIN, C. C. The Method of Characteristics in Compressible Flow, Part I: Steady Supersonic Flow, *Air Materiel Command Report*, No. F-TR-1173A-ND (1947).
10. KAHANE, A., and LEES, L. The Flow at the Rear of a Two-Dimensional Supersonic Airfoil, *Jour. Aero. Sci.*, Vol. 15, No. 3 (1948), p. 167.
11. LAITONE, E. V. Exact and Approximate Solutions of Two-Dimensional Oblique Shock Flow, *Jour. Aero. Sci.*, Vol. 14, No. 1 (1947), p. 25.
12. BUSEMANN, A., and WALCHNER, O. Profileigenschaften bei Ueberschallgeschwindigkeit, *Forschung aus dem Gebiet des Ingenieur-Wesens*, Vol. 4 (1933), p. 87.
13. FERRI, A. Experimental Results with Airfoils Tested in the High-Speed Wind Tunnel at Guidonia, *NACA Tech. Memo.*, No. 946 (1940).
14. BUHLER, R. D. Reflection and Refraction of Oblique Shock Waves at Contact Discontinuities (Vortex Sheets), Report No. AL-944, North American Aviation, Inc. (1949).
15. ROCKETT, J. A., and HAYES, W. D. Monograph II: The Method of Characteristics in Compressible Flow, Part IC: Two-Dimensional Flow with Large Entropy Changes, *Air Materiel Command Report*, No. 102-AC49/6-100 (1949).
16. IVEY, H. R., STICKLE, G. W., and SCHUETTLER, A. Charts for Determining the Characteristics of Sharp-Nose Airfoils in Two-Dimensional Flow at Supersonic Speeds, *NACA Tech. Note*, No. 1143 (1947).
17. MOECKEL, W. E., and CONNORS, J. F. Charts for the Determination of Supersonic Air Flow Against Inclined Planes and Axially Symmetric Cones, *NACA Tech. Note*, No. 1373 (1947).
18. MOECKEL, W. E. Interaction of Oblique Shock Waves with Regions of Variable Pressure, Entropy, and Energy, *NACA Tech. Note*, No. 2725 (1952).
19. EGGLERS, A. J., JR., and SYVERTSON, C. A. Inviscid Flow About Airfoils at High Supersonic Speeds, *NACA Tech. Note*, No. 2646 (1952).
20. JOHANNESEN, N. H. Experiments on Two-Dimensional Supersonic Flow in Corners and over Concave Surfaces, *Aero. Research Council*, F.M. 1669 (Jan. 1952).

PROBLEMS

- 16.1.** Derive the oblique shock relations of Art. 16.2 by a transformation of the normal shock relations as suggested in Art. 16.1.

- 16.2.** Derive the relation between temperature ratio and pressure ratio for oblique shocks.

16.3. Demonstrate that the pressure ratio and the density ratio across an oblique shock depend only on k and on $M_1 \sin \sigma$. Note that as a consequence the normal shock tables give directly the pressure and density ratios for oblique shocks if the inlet Mach Number M_2 of the normal shock is interpreted as the value of $M_1 \sin \sigma$ for the oblique shock.

16.4. Investigate the branches of the hodograph shock polar for values of u_2/c^* greater than u_1/c^* . What is the physical significance of these branches? Can they be used for the graphical solution of problems, and, if so, in what way? What are the maximum values of u_2/c^* and v_2/c^* on the right-hand branches, in terms of u_1/c^* ?

16.5. Demonstrate that the hodograph shock polar is a circle for an initial Mach Number of infinity.

16.6. (a) Investigate the branches of the δ - p shock polars for p_2/p_1 less than unity, and discuss the physical significance of these branches.

(b) Derive the equations of the δ - p shock polars.

16.7. Compare incompressible flow in a concave corner with supersonic flow in a concave corner.

16.8. By expanding p_2/p_1 as a function of $(\rho_2 - \rho_1)/\rho_1$ for both the Rankine-Hugoniot relation and for the isentropic relation, demonstrate that the two relations give identical results up to and including terms in the second order of shock strength.

16.9. Derive the oblique shock relations with the assumption that there is sufficient longitudinal heat conduction to produce equal temperatures on the two sides of the shock.

Compare the results for such an oblique shock in a general way with the corresponding results for an adiabatic oblique shock.

16.10. Demonstrate the following limiting relations for oblique shocks as the initial Mach Number M_1 becomes very large:

$$\frac{\tan \sigma}{\tan(\sigma - \delta)} \rightarrow \frac{k+1}{k-1}$$

$$M_2^2 \rightarrow \frac{k-1}{2k \sin^2(\sigma - \delta)}$$

$$\frac{p_2}{p_1} \rightarrow \frac{2k}{k+1} M_1^2 \sin^2 \sigma$$

16.11. (a) Show that the shock angle σ_{\max} corresponding to the maximum turning angle δ_{\max} is given explicitly in terms of M_1 by the following expression:

$$\sin^2 \sigma_{\max} = \frac{1}{kM_1^2} \left[\frac{k+1}{4} M_1^2 - 1 + \sqrt{(k+1) \left(1 + \frac{k-1}{2} M_1^2 + \frac{k+1}{16} M_1^4 \right)} \right]$$

(b) Show that the shock angle σ^* corresponding to the turning angle δ^* for which the downstream Mach Number is unity is given explicitly in terms of M_1

by the following expression:

$$\sin^2 \sigma^* = \frac{1}{kM_1^2} \left[\frac{k+1}{4} M_1^2 - \frac{3-k}{4} \right] + \sqrt{(k+1) \left(\frac{9+k}{16} - \frac{3-k}{8} M_1^2 + \frac{k+1}{16} M_1^4 \right)}$$

16.12. Demonstrate the following series relation for the stagnation-pressure ratio in terms of the initial Mach Number and the shock angle, a relation especially useful for weak shocks where the shock angle is slightly larger than the Mach angle:

$$\frac{p_{02}}{p_{01}} = 1 - \frac{2k}{3(k+1)^2} (M_1^2 \sin^2 \sigma - 1)^3 + \frac{2k^2}{(k+1)^3} (M_1^2 \sin^2 \sigma - 1)^4 - \dots$$

16.13. (a) Demonstrate that if two points in the flow have the same pressure and same stagnation temperature, but different stagnation pressures, the velocities are related as follows:

$$\left(\frac{V_b}{V_a} \right)^2 = 1 - \left[\left(\frac{p_{0a}}{p_{0b}} \right)^{\frac{k-1}{k}} - 1 \right] \frac{k-1}{2} M_a^2$$

(b) From the above result show with the help of momentum considerations that the pressure drag of a two-dimensional supersonic profile in an infinite medium is directly related to the entropy increases across the shock waves in the flow field.

(c) From the result in part (a) show that when a slip stream appears in an adiabatic flow, the Mach Number is higher on the side of the slip stream having the lower entropy.

(d) Show that if the oblique shocks produced by a supersonic, two-dimensional profile did not interact with rarefaction waves in such a way that the oblique shocks were ultimately weakened to become Mach waves, the drag of such a profile would be infinite.

16.14. A parallel stream with a pressure of 10 psia and a Mach Number of 2.0 approaches a sharp 10° corner (see sketch).



PROB. 16.14.

(a) Assuming that the shock is of the weak variety, calculate the following quantities: the final Mach Number, the final pressure, the change of entropy, and the ratio of the final flow per unit area to the initial flow per unit area.

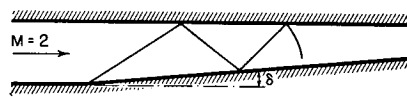
(b) Make a sketch to scale showing the streamlines, the shock line, and the Mach lines upstream and downstream of the shock.

(c) Compare the results of part (a) for final Mach Number and final pressure with the analogous result for a 10° -turn based on linearized theory, a 10° -turn based on the Prandtl-Meyer corner-type flow, and a 10° -turn based on the second-order theory.

16.15. Compare the linearized theory with the oblique-shock theory and the second-order theory by plotting curves of final Mach Number and of the fractional change in pressure ($\Delta p/p$) against the deflection angle, basing each curve on a constant initial Mach Number.

Use constant initial Mach Numbers of 1.5 and 2.5, and carry each curve from zero deflection to the maximum deflection angle.

16.16. Air flows in the passage shown in the sketch with an initial Mach Number of 2.0. Determine the maximum turning angle δ for which three regular reflections of the original shock are possible.

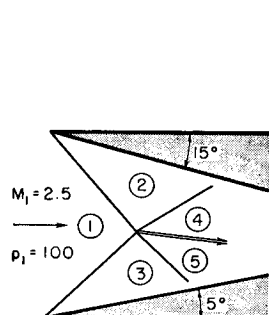


PROB. 16.16.

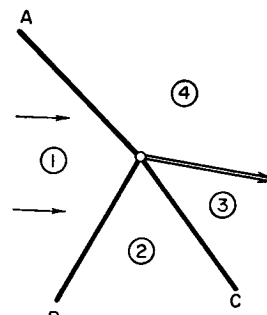
16.17. An initially uniform parallel flow undergoes a 10° -turn across shock *A* and a subsequent 10° -turn across shock *B* (see Fig. 16.29a). Assuming that $M_1 = 3.0$ and $p_1 = 100$, determine the values of M , θ , and p in fields 2, 3, 4, and 5.

16.18. The sketch shows the inlet of an unsymmetrical oblique-shock diffuser. Calculate the pressure and flow direction in fields 4 and 5 by

- The first-order theory
- The second-order theory
- The exact shock theory (in this case find also the value of $M_4^* - M_5^*$)



PROB. 16.18.



PROB. 16.19.

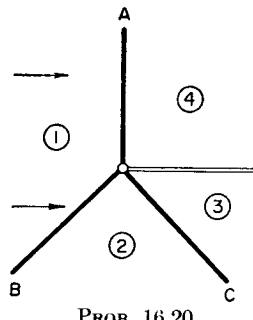
16.19. Consider a triple-shock configuration *A-B-C* as shown in the sketch. Find the values of M^* and flow direction θ in fields 2, 3, and 4 for $M_1^* = 1.50$ and $\theta_1 = 0$, if

- $\theta_2 = +4^\circ$ (Answer: $M_2^* = 1.421$; $M_3^* = 0.759$; $M_4^* = 0.679$; $\theta_3 = \theta_4 = -6^\circ$)
- $\theta_2 = +12^\circ$ (Answer: $M_2^* = 1.231$; $M_3^* = 0.823$; $M_4^* = 0.696$; $\theta_3 = \theta_4 = +9.2^\circ$)

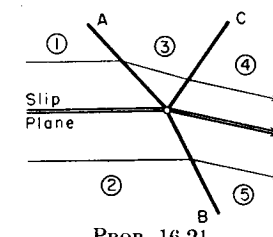
Sketch the shock directions to scale.

16.20. Consider a shock configuration *A-B-C* as shown in the sketch, where *A* is a normal shock. Find the dimensionless velocity ratio, M^* , and flow direction, θ , in fields 2, 3, and 4 if $M_1^* = 1.50$ and $\theta_1 = 0$. Sketch the shock directions to scale.

(Answer: $\theta_2 = 7.5^\circ$; $\theta_3 = \theta_4 = 0$; $M_2^* = 1.350$; $M_3^* = 0.788$; $M_4^* = 0.666$)



PROB. 16.20.



PROB. 16.21.

16.21. Consider an oblique shock *A* incident on a slip plane dividing regions 1 and 2 (see sketch). These regions have different Mach Numbers but the same pressures and stagnation temperatures.

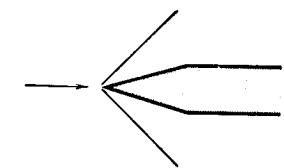
(a) Assuming that wave *A* is very weak and that the velocity difference between zones 1 and 2 is very small, show that the condition that there be no reflected wave *C* is that $M_1 \leq \sqrt{2}$.

(b) Assuming that $M_1 = 2.0$, $M_2 = 1.9$, $\delta_A = 10^\circ$, determine δ_B , δ_C , θ_5 , M_4 , and M_5 .

16.22. A wedge-shaped probe (see sketch) may be used for estimating the Mach Number of a supersonic wind tunnel.

(a) In a particular instance a wedge with a 10° included angle is used. Schlieren photographs show that the total included angle of the shock front is 98° . Estimate the Mach Number of the tunnel.

(b) What is the minimum Mach Number for which a 10° -probe can be used in this way as a Mach Number indicator?



PROB. 16.22.

16.23. Discuss the suitability of conventional subsonic profiles for supersonic speeds. Discuss the suitability of conventional supersonic profiles for subsonic speeds. Consider the design or invention of a profile which is to operate mainly at supersonic speeds but must be capable also of developing high lift at subsonic speeds.

16.24. Using the results of the second-order theory for thin profiles, determine an expression for the angle of zero lift, a_0 , in terms of shape integrals and Mach Number. Show from this result that a_0 must be positive for positive camber, and compare this conclusion with subsonic flow past thin profiles. Show that for a given profile the value of a_0 increases with M_∞ .

16.25. A flat-plate profile of chord l is to be tested at Mach Number 2.0 in a wind tunnel of rectangular cross section, the tunnel height being H . Determine the minimum ratio H/l required to avoid interference, for

- (a) Zero angle of attack
- (b) An angle of attack of 10°

16.26. Consider the flow past a symmetrical double-wedge profile of 10% thickness ratio at Mach Number 2.0, and determine the maximum angle of attack for which the leading-edge shock will be attached.

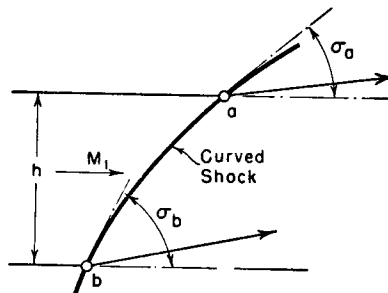
16.27. Consider the flow past a flat-plate profile at $M = \sqrt{2}$. Assuming a skin-friction coefficient of 0.005, determine the maximum lift-drag ratio and the corresponding angle of attack, using

- (a) The linearized theory
- (b) The second-order theory
- (c) The exact theory

16.28. Consider the flow past a symmetrical double-wedge profile of 10% thickness ratio, at Mach Number 2, and with an angle of attack of 5° . Calculate the lift, drag and moment coefficients for this profile by

- (a) The exact theory
- (b) The second-order theory
- (c) The linearized theory

16.29. Given the curved shock shown in the sketch with $M_1 = 2.0$. At points a and b , which are separated by the distance $h = 0.1$ ft, the shock angles are $\sigma_a = 35^\circ$ and $\sigma_b = 55^\circ$. The stagnation temperature is 530°R .



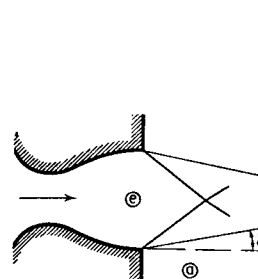
PROB. 16.29.

Determine approximately the rotation of the fluid downstream of the shock on a streamline midway between a and b , in seconds $^{-1}$.

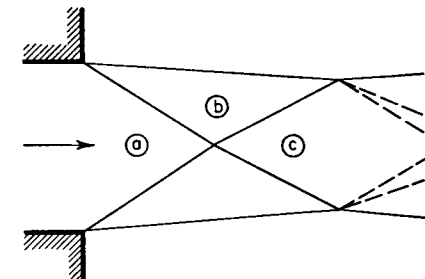
16.30. Design a practical supersonic biplane to operate at Mach Number 2.5 and zero angle of attack, taking note of starting problems, and with the aim of obtaining as large a cargo volume within the biplane wings as possible.

16.31. Consider a parallel, two-dimensional jet leaving a nozzle at e with $M_e = 2.0$. (a) Plot the deflection angle of the jet, δ , as a function of the pressure

ratio p_a/p_e , for values of the latter between unity and the value for which a normal shock stands in the exit plane. (b) Determine the range of pressure ratios, p_a/p_e , for which regular reflection of the oblique shock wave originating at the nozzle exit is not possible.



PROB. 16.31.



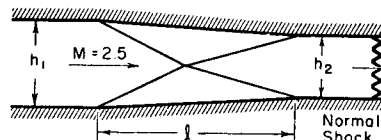
PROB. 16.32.

16.32. A supersonic stream leaves a nozzle in parallel flow (region a) with a Mach Number of 2.0 and a pressure of 10 psia. The pressure of the atmosphere into which the jet discharges is 15 psia.

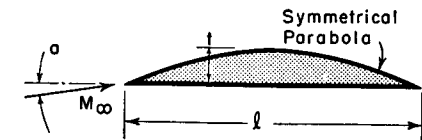
- (a) Calculate the pressures in regions b and c .
- (b) Make a sketch to scale showing streamlines and shock lines.
- (c) Assuming the pressure at the nozzle entrance to be maintained constant, what is the maximum atmospheric pressure for which this general type of flow configuration is possible? Describe the nature of the flow pattern when the exhaust-region pressure is raised above this limiting value.
- (d) Compare the results of part (a) with the results of calculations based on the first-order and second-order theories.

16.33. A two-dimensional supersonic diffuser is to be designed as shown in the sketch for a Mach Number of 2.5. The ratio h_2/h_1 is to be chosen so that the diffuser will barely swallow the initial shock, and the ratio l/h_1 is to be selected so as to obtain the wave pattern shown.

- (a) Determine h_2/h_1 and l/h_1 .
- (b) Neglecting friction, compare the over-all stagnation-pressure ratio of this diffuser with the stagnation-pressure ratio of a diffuser in which a normal shock occurs at Mach Number 2.5.
- (c) Compare the results of part (a) with the linearized theory.



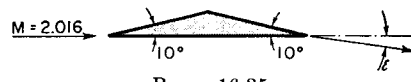
PROB. 16.33.



PROB. 16.34.

16.34. Using second-order theory, find C_L and C_D for the profile shown in the sketch in terms of M_∞ , t/l , and a .

16.35. A two-dimensional double-wedge profile (see sketch) is at zero angle



PROB. 16.35.

of attack in an air stream of Mach Number 2.016. Ignoring friction, and using exact methods,

- Calculate the lift coefficient.
- Calculate the drag coefficient.
- Calculate the ratio $l_{c.p.}/l$ where $l_{c.p.}$ is distance aft of the leading edge to the center of pressure, and l is the chord.
- Estimate the downwash angle, ϵ , immediately downstream of the trailing edge.
- Sketch the wave system at great distances from the profile.
- Compare the results obtained above with similar results based on the second-order theory.

16.36. (a) Demonstrate the following relation between turning angle, initial Mach Number, and shock strength expressed in terms of the fractional pressure rise $(p_2 - p_1)/p_1$:

$$\tan \delta = \pm \frac{1}{k} \frac{p_2 - p_1}{p_1} \frac{\sqrt{M_1^2 - \left(1 + \frac{k+1}{2k} \frac{p_2 - p_1}{p_1}\right)}}{\left(M_1^2 - \frac{1}{k} \frac{p_2 - p_1}{p_1}\right) \sqrt{1 + \frac{k+1}{2k} \frac{p_2 - p_1}{p_1}}}$$

(b) From this show that, if an oblique shock crosses a slip line which divides parallel flows having Mach Numbers M_{1A} and M_{1B} , the condition that the shock be transmitted without any reflection whatsoever is that

$$M_{1B}^2 = \frac{M_{1A}^2 \left(1 + \frac{k+1}{2k} \frac{p_2 - p_1}{p_1}\right) - \frac{p_2 - p_1}{kp_1} \left(2 + \frac{p_2 - p_1}{p_1}\right)}{M_{1A}^2 - \left(1 + \frac{k+1}{2k} \frac{p_2 - p_1}{p_1}\right)}$$

(c) Show from part (a) that for a fixed pressure ratio across the shock, there is a maximum turning angle, $\delta_{\max(p)}$, which occurs at a Mach Number given by

$$(M_1^2)_{\text{for } \delta_{\max(p)}} = 2 + \frac{p_2 - p_1}{p_1}$$

and that the corresponding value of maximum turning angle is given by

$$\tan \delta_{\max(p)} = \frac{\frac{1}{k} \frac{p_2 - p_1}{p_1}}{2 \sqrt{1 + \frac{k+1}{2k} \frac{p_2 - p_1}{p_1}} \sqrt{1 + \frac{k-1}{2k} \frac{p_2 - p_1}{p_1}}}$$

(d) From part (c) show that if an oblique shock crosses a weak slip line dividing parallel flows of nearly the same Mach Number, the condition that there shall be no reflection at the slip line is approximately

$$M_1^2 \cong 2 + \frac{p_2 - p_1}{p_1}$$

APPENDIX

Appendix A

THEORY OF CHARACTERISTICS

A.1. Introductory Remarks

The differential equations describing the motion of compressible fluids in two or three dimensions are, with the exceptions of a few simple cases or under greatly simplifying assumptions, not easily soluble by analytical methods. Fortunately, there is a class of problems for which solutions may be rather easily obtained by means of numerical or graphical procedures. Such is the case when the motion is described by a partial differential equation of hyperbolic type. We shall see that the possibility of constructing solutions arises from the special properties of certain *characteristic curves* which satisfy second-order, partial differential equations of *hyperbolic type* with two independent variables.

The purpose of this Appendix is to outline, for those readers not already familiar with the subject, the mathematical theory underlying the method of characteristics. Particular attention will be given to those aspects of the theory which are relevant to problems of compressible flow (readers are referred to Reference 1 for a more complete treatment than is given here).

NOMENCLATURE

A, B, C, D	functions of x, y, φ_x , and	φ	velocity potential
	φ_y		
c	speed of sound	$()_{\text{char}}$	signifies conditions along characteristic curve
k	ratio of specific heats	$()_I$	signifies conditions along characteristic of family I .
r	radius in cylindrical and polar coordinates	$()_{II}$	signifies conditions along characteristic of family II .
R	radius in spherical coordinates		
t	time		
u, v	velocity components		
x, y	Cartesian coordinates		

Some of the important physical problems which are easily handled by the method of characteristics may be summarized as follows (it is assumed throughout that we are dealing with a perfect gas having

neither viscosity nor thermal conductivity, and that there are no discontinuities in fluid properties such as occur in shock waves):

Two-Dimensional, Plane, Supersonic, Irrotational, Steady Flow (Chapter 15). Application of Euler's equation, the continuity equation, and the condition of irrotationality yields

$$(c^2 - \varphi_x^2)\varphi_{xx} - 2\varphi_x\varphi_y\varphi_{xy} + (c^2 - \varphi_y^2)\varphi_{yy} = 0 \quad (\text{A.1})$$

where φ is the velocity potential, x and y are the Cartesian space coordinates, c is the local sound velocity, and φ_{xx} denotes $\partial^2\varphi/\partial x^2$, etc. The velocity components u and v are given by

$$u = \frac{\partial \varphi}{\partial x} = \varphi_x; \quad v = \frac{\partial \varphi}{\partial y} = \varphi_y \quad (\text{A.2a})$$

The local sound velocity depends on φ_x and φ_y according to the energy equation,

$$c^2 = c_0^2 - \frac{k-1}{2}(\varphi_x^2 + \varphi_y^2) \quad (\text{A.2b})$$

where c_0 is the sound velocity at the stagnation temperature.

Axially Symmetric, Supersonic, Irrotational, Steady Flow (Volume II, Chapter 17). Application of Euler's equation, the continuity equation and the condition of irrotationality yields

$$(c^2 - \varphi_x^2)\varphi_{xx} - 2\varphi_x\varphi_r\varphi_{xr} + (c^2 - \varphi_r^2)\varphi_{rr} + \frac{c^2}{r}\varphi_r = 0 \quad (\text{A.3})$$

where φ is the velocity potential, x and r are cylindrical space coordinates (x being along the axis of symmetry and r normal to the axis of symmetry), and c is the local sound velocity. The velocity components u and v in the x - and r -directions, respectively, are given by

$$u = \varphi_x; \quad v = \varphi_r \quad (\text{A.4a})$$

The local sound velocity is, according to the energy equation, given by

$$c^2 = c_0^2 - \frac{k-1}{2}(\varphi_x^2 + \varphi_r^2) \quad (\text{A.4b})$$

where c_0 is the sound velocity at the stagnation temperature.

Non-steady, One-Dimensional Motion with Constant Cross-Sectional Area (Volume II, Chapter 24). Application of the Euler and continuity equations, together with the introduction of a velocity potential, yields

$$(c^2 - \varphi_x^2)\varphi_{xx} - 2\varphi_x\varphi_{xt} - \varphi_{tt} = 0 \quad (\text{A.5})$$

where x is the one-dimensional space coordinate measured along the direction of motion, t is the time coordinate, φ is the velocity potential,

and c is the local sound velocity. The fluid velocity in the x -direction is given by

$$u = \varphi_x \quad (\text{A.6a})$$

The local sound velocity is related to φ_x and φ_t through the equation

$$c^2 = c_0^2 - \frac{k-1}{2}\varphi_x^2 - (k-1)\varphi_t \quad (\text{A.6b})$$

where c_0 is the sound velocity at any arbitrary location and time.

Non-steady, Plane, Cylindrically Symmetrical Motion. Application of the Euler and continuity equations, together with the introduction of a velocity potential, yields

$$(c^2 - \varphi_r^2)\varphi_{rr} - 2\varphi_r\varphi_{rt} - \varphi_{tt} - \frac{c^2}{r}\varphi_r = 0 \quad (\text{A.7})$$

where r is the radius in polar coordinates, t is the time coordinate, φ is the velocity potential, and c is the local sound velocity. The fluid velocity in the r -direction is given by

$$u = \varphi_r \quad (\text{A.8})$$

The local sound velocity is related to φ_r and φ_t by an expression similar to Eq. A.6b, except that φ_x is replaced by φ_r .

Non-steady, Spherically Symmetrical Motion. Application of the Euler and continuity equations, together with the introduction of a velocity potential, yields

$$(c^2 - \varphi_R^2)\varphi_{RR} - 2\varphi_R\varphi_{RT} - \varphi_{tt} - 2\frac{c^2}{R}\varphi_R = 0 \quad (\text{A.9})$$

where R is the radius in spherical coordinates, t is the time coordinate, φ is the velocity potential, and c is the local sound velocity. The fluid velocity in the R -direction is given by

$$u = \varphi_R \quad (\text{A.10})$$

The local sound velocity is related to φ_R and φ_t by an expression similar to Eq. A.6b, except that φ_x is replaced by φ_R .

Quasi-linear Differential Equation of Second Order in Two Independent Variables. Eqs. A.1, A.3, A.5, A.7, and A.9 are all nonlinear partial differential equations of second order with two independent variables. They are sometimes called *quasi-linear* differential equations, as they are linear in the derivatives of highest order. All of them have the general form

$$A\varphi_{xx} + 2B\varphi_{xy} + C\varphi_{yy} = D \quad (\text{A.11})$$

where the coefficients A , B , C , and D are, in general, functions of x , y , φ_x , and φ_y .

The remainder of this Appendix is devoted to a study of certain properties of this differential equation, a study which leads to a convenient procedure for solving the practical problems mentioned previously.

Occasionally it will be helpful to think in terms of a physical analogue to the mathematical analysis. For this purpose we shall consider two-dimensional, supersonic flow (Eq. A.1) as a typical illustrative example. Then φ will be thought of as the velocity potential, φ_x will be the x -component of velocity (u), and φ_y will be the y -component of velocity (v). Since the φ_x, φ_y -plane is, for this case, usually called the *hodograph plane*, it will be convenient terminology to employ the same phrase as a generalization for the φ_x, φ_y -plane corresponding to Eq. A.11.

A.2. The Characteristic Curves

We consider here only regions of the flow where the fluid properties are continuous. This means that the derivatives φ_x and φ_y (the velocity components) are continuous functions of x and y . Hence, we may write, for arbitrary increments dx and dy ,

$$d\varphi_x = \frac{\partial \varphi_x}{\partial x} dx + \frac{\partial \varphi_x}{\partial y} dy = \varphi_{xx} dx + \varphi_{xy} dy \quad (\text{A.12})$$

$$d\varphi_y = \frac{\partial \varphi_y}{\partial x} dx + \frac{\partial \varphi_y}{\partial y} dy = \varphi_{yx} dx + \varphi_{yy} dy \quad (\text{A.13})$$

Integral Surfaces. Each solution to the differential equation (Eq. A.11) may be thought of as a three-dimensional surface in x, y, φ space, called an *integral surface*, and defined by a function $\varphi = \varphi(x, y)$ which satisfies Eq. A.11. We may imagine the integral surface to have drawn on it various space curves, each of which has a certain projection on the x, y -plane. A small step along one of these projected curves at a certain point determines corresponding values of $d\varphi_x$ and $d\varphi_y$ according to Eqs. A.12 and A.13.

Definition of Characteristics. We now ask: Is it possible that, on certain curves lying on an integral surface, the *derivatives* of φ_x and φ_y (e.g., the *derivatives* of the velocity components, and hence of all fluid properties) might be discontinuous? Such curves, when they exist, are called the *characteristic curves* of the solution, and their projections on the x, y -plane are called the *physical characteristics*.

Eq. A.11 is applicable at any point on the integral surface. Moreover, Eqs. A.12 and A.13 are applicable to the increments corresponding to an infinitesimal length of any curve lying in that surface. Since we are interested in possible indeterminacies of the derivatives $\varphi_{xx}, \varphi_{yy}$,

and φ_{xy} , we write these equations in the following manner:

$$\begin{aligned} A \varphi_{xx} + 2B \varphi_{xy} + C \varphi_{yy} &= D \\ dx \varphi_{xx} + dy \varphi_{xy} &= d\varphi_x \\ dx \varphi_{xy} + dy \varphi_{yy} &= d\varphi_y \end{aligned}$$

These may be regarded as simultaneous, linear, algebraic equations in the variables φ_{xx} , φ_{yy} , and φ_{xy} . Solving for φ_{xy} , we obtain, in determinant notation

$$\varphi_{xy} = \frac{\begin{vmatrix} A & D & C \\ dx & d\varphi_x & 0 \\ 0 & d\varphi_y & dy \end{vmatrix}}{\begin{vmatrix} A & 2B & C \\ dx & dy & 0 \\ 0 & dx & dy \end{vmatrix}} = \frac{A dy d\varphi_x - D dy dx + C dx d\varphi_y}{A dy^2 - 2B dx dy + C dx^2} \quad (\text{A.14})$$

At any point (x, y, φ) on the integral surface, the values of φ_x and φ_y are known from the shape of the surface. Consequently the coefficients A, B, C , and D are known at all points of the surface. In general, therefore, the value of φ_{xy} (and, by similar reasoning, the values of φ_{xx} and φ_{yy}) is determined by Eq. A.14, except when both the numerator and denominator of Eq. A.14 are equal to zero. The latter condition gives the answer to our original query, for when $\varphi_{xy}, \varphi_{xx}$, and φ_{yy} are indeterminate, they may be discontinuous.

Physical Characteristic Curves. By setting the denominator of Eq. A.14 equal to zero, we obtain the differential equation of the projections of the characteristic curves in the physical plane, namely,

$$A \left(\frac{dy}{dx} \right)_{\text{char}}^2 - 2B \left(\frac{dy}{dx} \right)_{\text{char}} + C = 0 \quad (\text{A.15a})$$

or, after solving the quadratic,

$$\left(\frac{dy}{dx} \right)_{\text{char}} = \frac{B \pm \sqrt{B^2 - AC}}{A} \quad (\text{A.15b})$$

Hodograph Characteristic Curves. By means of Eq. A.15b the slopes of the characteristics in the physical plane may be found. However, the coefficients A, B , and C , in terms of which the slopes $(dy/dx)_{\text{char}}$ are expressed, depend in part on φ_x and φ_y . In order to construct the characteristics in the physical plane, it is therefore necessary to determine how φ_x and φ_y vary along the characteristics. This is most easily done by finding the equation of the characteristics in the φ_x, φ_y -plane.

Since φ_{xy} is, in general, finite, it is necessary that the numerator as well as the denominator of Eq. A.14 vanish. Therefore we write

$$A d\varphi_x dy + C d\varphi_y dx = D dx dy$$

Solving for $d\varphi_y/d\varphi_x$, we obtain

$$\left(\frac{d\varphi_y}{d\varphi_x}\right)_{\text{char}} = -\frac{A}{C} \left(\frac{dy}{dx}\right)_{\text{char}} + \frac{D}{C} \left(\frac{dy}{d\varphi_x}\right)_{\text{char}}$$

which is further simplified by introducing Eq. A.15b, thus yielding

$$\left(\frac{d\varphi_y}{d\varphi_x}\right)_{\text{char}} = -\frac{B \pm \sqrt{B^2 - AC}}{C} + \frac{D}{C} \left(\frac{dy}{d\varphi_x}\right)_{\text{char}} \quad (\text{A.16})$$

Eq. A.16 gives the slopes of the characteristics in the φ_x , φ_y -plane in terms of φ_x , φ_y , x , and y . It may be recalled that Eq. A.15b gives the slopes of the characteristics in the x , y -plane also in terms of φ_x , φ_y , x , and y . Given suitable initial data, therefore, the characteristic curves in the physical and hodograph planes may simultaneously be constructed numerically or graphically in stepwise fashion. Since the physical data of interest (such as pressure, velocity, etc.) may be found from the values of φ_x and φ_y at each point, a solution of the problem is thereby determined. Before going into details, we shall discuss certain general features of the method.

Classification of Differential Equations. Examination of Eqs. A.15 and A.16 shows that the differential equation A.11 may be of three types, depending on the sign of $(B^2 - AC)$. These types are defined as follows:

Hyperbolic type. The value of $(B^2 - AC)$ is positive, so that Eqs. A.15 and A.16 each have two real roots. Two characteristic curves pass through every point of the physical and hodograph planes.

Parabolic type. The value of $(B^2 - AC)$ is zero, and there is one real root to Eqs. A.15 and A.16. This type is not of great practical significance.

Elliptic type. The value of $(B^2 - AC)$ is negative, so that Eqs. A.15 and A.16 have no real roots, and the characteristic curves are imaginary.

Applying these criteria to Eqs. A.1, A.3, A.5, A.7, and A.9, it is found that (i) for the two cases of steady motion the differential equation is hyperbolic for supersonic flow and elliptic for subsonic flow, whereas (ii) for the three cases of non-steady motion the differential equation is always of hyperbolic type. Hence real characteristics always exist for the non-steady motions, but exist for the steady motions only when the flow is supersonic.

Properties of Characteristic Curves. CHARACTERISTIC LINES VERSUS SHOCK LINES. The physical characteristics for two-dimensional, supersonic flow are the Mach lines (Chapter 15), and are inherently different from lines of shock discontinuities (Chapter 16). On a shock line the fluid properties (velocity, pressure, etc.) are discontinuous. On a characteristic curve, however, the fluid properties themselves are continuous, but their derivatives may be discontinuous.

CHARACTERISTIC CURVES AS SOLUTIONS TO THE DIFFERENTIAL EQUATION. Eqs. A.15b and A.16 satisfy the differential Eq. A.11. The latter may accordingly be solved by simultaneous solution of Eqs. A.15b and A.16. Although this simultaneous solution does not directly yield $\varphi = \varphi(x, y)$, it yields a result even more useful for practical purposes, namely, the velocity components at each point of the x , y -plane. Indeed, the possibility of arriving at solutions of Eq. A.11 merely by constructing the characteristic curves in the physical and hodograph planes constitutes the most important practical aspect of the theory of characteristics. The original task of solving a difficult nonlinear partial differential equation of second order (Eq. A.11) is thereby replaced by the comparatively easy task of simultaneously solving two pairs of ordinary differential equations of first order.

Thinking again of the solution to Eq. A.11 as a surface in φ , x , y -space, the shape of this surface may be approximated by a skeleton formed by a finite number of wires lying in the surface. If these wires follow the characteristic curves of the surface, then the physical characteristics (Eq. A.15b) are the projections of these wires in the x , y -plane, and the hodograph characteristics (Eq. A.16) are the representation of the slopes (φ_x and φ_y) of the wires. The physical and hodograph characteristics taken together may be used to construct the wire skeleton and thus to represent the solution of Eq. A.11.

CHARACTERISTIC CURVES AS LOCI OF POSSIBLE DISCONTINUITIES IN DERIVATIVES OF FLUID PROPERTIES. The characteristic curves are possible branch lines on an integral surface, in the sense that the second and higher derivatives of φ are indeterminate and may undergo discontinuities at points on these curves. Thus it follows that regions of flow of different types (i.e., described by expressions which are analytically different) may be joined, or "patched," on the characteristics. For this reason the characteristic curves are sometimes called *patching curves*. In two-dimensional, supersonic flow, for example, a region of uniform parallel flow can be joined to a region of nonuniform flow along a Mach line.

An extension of the foregoing reasoning leads to the conclusion that supersonic flows with prescribed initial conditions are inherently non-analytic in character. For example, if we are dealing with the super-

sonic flow past an arbitrary body or through an arbitrary duct, it is almost certain that no analytic expression exists which describes the entire flow pattern; at best analytical expressions may be found for describing certain limited regions of the flow (e.g., regions of *simple-wave flow*).

When the flows in two adjoining regions are described by expressions which are analytically different, the arguments given above lead to the conclusion that the two regions are necessarily adjoining along a characteristic curve. In two-dimensional, supersonic flow, for example, a region of uniform parallel flow can adjoin a region of nonuniform flow *only* on a characteristic curve.

Equations of the Characteristics for Certain Simplifying Conditions. There are two families of characteristics, corresponding to the plus and minus signs in Eqs. A.15b and A.16. We shall refer to them respectively as family *I* and family *II*. We may then summarize the equations of the characteristics as follows:

$$\left(\frac{dy}{dx}\right)_I = \frac{B + \sqrt{B^2 - AC}}{A}; \quad \left(\frac{dy}{dx}\right)_{II} = \frac{B - \sqrt{B^2 - AC}}{A} \quad (A.17a, b)$$

$$\left(\frac{d\varphi_y}{d\varphi_x}\right)_I = -\frac{B + \sqrt{B^2 - AC}}{C} + \frac{D}{C} \left(\frac{dy}{d\varphi_x}\right)_I \quad (A.18a)$$

$$\left(\frac{d\varphi_y}{d\varphi_x}\right)_{II} = -\frac{B - \sqrt{B^2 - AC}}{C} + \frac{D}{C} \left(\frac{dy}{d\varphi_x}\right)_{II} \quad (A.18b)$$

Substantial simplifications of procedure are possible under the three special sets of circumstances described below.

COEFFICIENTS *A*, *B*, *C* DEPEND ONLY ON *x* AND *y*. Under these conditions, it is evident from Eqs. A.17 that the characteristics in the physical plane are independent of the hodograph coordinates. That is, they may be found by direct integration of Eqs. A.17 without the need for simultaneously constructing the characteristics in the hodograph plane.

Important applications include (i) two-dimensional, supersonic, steady motion with small perturbations (Chapter 14), and (ii) one-dimensional, non-steady motion with small perturbations in a constant-area duct (Volume II, Chapter 23).

HOMOGENEOUS EQUATION. When the coefficient *D* is zero, the differential equation A.11 is homogeneous. It may then be shown from Eqs. A.15b and A.16 that

$$\left(\frac{dy}{dx}\right)_I \left(\frac{d\varphi_y}{d\varphi_x}\right)_{II} = -1; \quad \left(\frac{dy}{dx}\right)_{II} \left(\frac{d\varphi_y}{d\varphi_x}\right)_I = -1 \quad (A.19a, b)$$

These relations show (i) that the physical characteristic *I* is normal to the hodograph characteristic *II*, and (ii) that the physical characteristic *II* is normal to the hodograph characteristic *I*. This has obvious practical implications for the graphical construction of the characteristic nets.

HOMOGENEOUS EQUATION WITH *A*, *B*, *C* AS FUNCTIONS ONLY OF φ_x AND φ_y . Under these conditions, Eqs. A.18 indicate that the hodograph characteristics are completely independent of the physical coordinates. That is, they may be found by direct integration of Eqs. A.18 without the need for simultaneously constructing the physical characteristics. The hodograph characteristics may be found once for all from Eqs. A.18 and then may be used for all problems, irrespective of the nature of the flow in the physical plane. The physical characteristics are then found for each particular problem, starting with the given initial conditions, from Eqs. A.17. The construction is facilitated by the orthogonality relations of Eqs. A.19, especially inasmuch as the hodograph characteristic curves are known beforehand.

Important applications include (i) two-dimensional, steady, supersonic flow (Chapter 15), and (ii) non-steady motion in constant-area ducts (Volume II, Chapter 24).

A.3. Method of Constructing Characteristic Curves

Initial-Value Theorem. We shall now prove a theorem which is basic both to an understanding of the physical significance of the characteristics and to the method of employing the characteristics for practical computations. This theorem is related to the basic initial-value problem of hyperbolic differential equations. It states that *if the values of φ_x and φ_y are given at all points of a noncharacteristic curve 1-2 in the x, y -plane (Fig. A.1a), then the entire flow pattern is determined (and may be computed) within the quadrilateral formed by the characteristic curves passing through points 1 and 2*. By "noncharacteristic" is meant that the curve 1-2 is nowhere tangent to a characteristic curve. The demonstration of this theorem will at the same time illustrate a general method of stepwise computation which may be used for solving numerically any problems of the types under discussion.

General Numerical Solution. Along the noncharacteristic curve 1-2 in Fig. A.1a we suppose that we know the values of φ_x and φ_y (e.g., the velocity components) at each point. The image curve 1'-2' may therefore be constructed in the hodograph plane (Fig. A.1b).

The method of solution involves stepwise construction of a finite number of characteristic curves forming a characteristics *net* or *mesh*.

Accordingly, we select a number of discrete points along 1-2 as points through which these characteristics pass. For illustrative purposes we take four points, namely, 1, 2, 3, and 4. These in turn have four corresponding hodograph points, 1', 2', 3', and 4'.

The characteristics will form a network of the general form shown in Figs. A.1a and A.1b, where solid lines indicate characteristics of family I and dashed lines characteristics of family II. The problem is to determine this network, for, when this is done, the values of φ_x and φ_y are

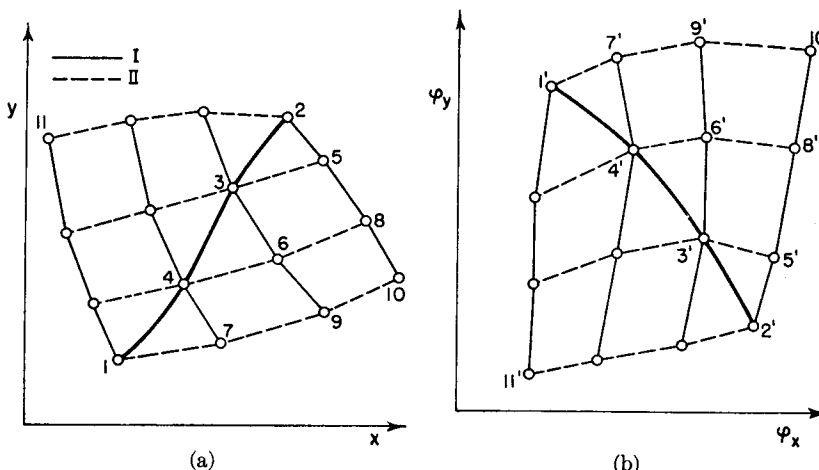


FIG. A.1. Characteristics net.

(a) Physical plane.
(b) Hodograph plane.

known at each point of the physical plane and consequently the entire flow pattern in terms of the velocity distribution is established. In the stepwise construction the curvilinear characteristics are replaced by straight-line segments connecting the lattice points of the network.

To establish a point such as 7 and its hodograph image 7', we proceed as follows:

(i) Using Eq. A.17a, the value of $(dy/dx)_I$ at point 4 is computed, using the values of A , B , and C corresponding to point 4. A line with the slope $(dy/dx)_I$ is tentatively passed through point 4.

(ii) Using Eq. A.17b, the value of $(dy/dx)_{II}$ at point 1 is computed, using the values of A , B and C corresponding to point 1. A line with the slope $(dy/dx)_{II}$ is tentatively passed through point 1. Its intersection with the line drawn in step (i) establishes, at least approximately, the location of point 7.

(iii) The value of $(d\varphi_y/d\varphi_x)_I$ at point 4' is computed from Eq. A.18a, and a line is tentatively drawn through 4' with the slope $(d\varphi_y/d\varphi_x)_I$.

In computing the value of $(dy/d\varphi_x)_I$ in Eq. A.18a, we use the approximate finite-difference form

$$\left(\frac{dy}{d\varphi_x} \right)_I \cong \frac{y_7 - y_4}{(\varphi_x)_{7'} - (\varphi_x)_{4'}}$$

The value of $y_7 - y_4$ is known approximately from step (ii), and the value of $(\varphi_x)_{7'}$ must, for the present, be estimated roughly and subsequently be improved as indicated later.

(iv) After a computation similar to that of step (iii), a line through point 1' is tentatively drawn with the value of the slope $(d\varphi_y/d\varphi_x)_{II}$ corresponding to 1'. The intersection of this line with that of step (iii) tentatively establishes point 7'.

(v) An iteration process is used to establish points 7 and 7' more accurately. Starting with the tentative locations found previously, the location of point 7 is found more accurately by drawing the lines through points 1 and 4 with slopes corresponding to the mean conditions between points 1 and 7, and between points 4 and 7, respectively. Likewise, point 7' is found more accurately by drawing the lines 1'-7' and 4'-7' with their respective mean slopes. The iteration is continued until satisfactory convergence has been attained.

To summarize, points 7 and 7' may be found from information concerning x , y , φ_x , and φ_y at points 1 and 4. Points 6 and 6' may be found in like manner from information at 3 and 4; and points 5 and 5' from 2 and 3. Proceeding in this way, points 8 and 9 are then found from 5, 6, and 7, and finally point 10 is found from 8 and 9. The entire flow pattern in the region 1-2-10 is thus established. It is evident that the flow pattern in the region 1-2-11 may also be calculated by a similar procedure.

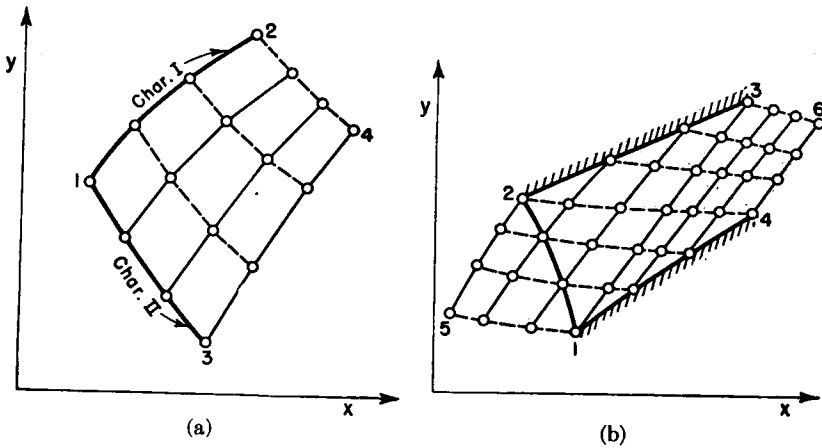
We have therefore proved that, given the values of φ_x and φ_y along the noncharacteristic curve 1-2, the entire flow pattern may be determined within the characteristic quadrilateral 1-10-2-11.

Other Types of Initial Data. If the initial-value curve 1-2 is at any point tangent to a characteristic, the construction described above will not yield results near the point of tangency. Hence the curve 1-2 must be noncharacteristic in order that the solution in the characteristic quadrilateral be completely determined by the data along 1-2.

In addition to the one shown in Fig. A.1 there are several other initial-value problems of practical importance for which the method of characteristics yields solutions in certain regions:

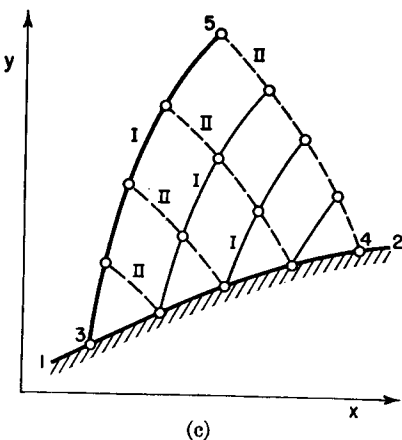
Fig. A.2a. If the values of φ_x and φ_y are given along two intersecting characteristics, 1-2 and 1-3, then the type of computation described previously leads to a solution within the characteristic quadrilateral 1-2-3-4.

Fig. A.2b. The values of φ_x and φ_y are given along the noncharacteristic curve 1-2, and either the magnitude or the direction of the velocity vector is given along the curves 1-4 and 2-3 (note that if curves 1-4 or 2-3 were solid boundaries, then the *direction* of the velocity would be



(a)

(b)



(c)

FIG. A.2. Various types of initial-value problems.

noncharacteristic boundary 1-2. By constructing the characteristics net, beginning with these initial data, the solution may be uniquely determined in the region 3-5-4.

A.4. Simple Waves

A degenerate type of flow known as a *simple-wave flow* plays a curiously important role in practical problems and occurs far more

frequently than one would superficially expect for a flow so special in nature. Simple waves occur only when the coefficient D in Eq. A.11 is zero and when A , B , and C depend only on φ_x and φ_y . These conditions will henceforth be assumed.

Definition of Simple-Wave Flow. We shall define a region of simple-wave flow as a region where φ_x and φ_y are not independent but are rather unique functions of each other. The implications of this are found by examining the differential equation A.11. In the light of the assumption that φ_x and φ_y depend only on each other, the derivatives in Eq. A.11 may be expressed as

$$\varphi_{xx} = \frac{\partial \varphi_x}{\partial x} = \frac{d\varphi_x}{d\varphi_y} \frac{\partial \varphi_y}{\partial x} \quad (A.20a)$$

$$\varphi_{xy} = \frac{\partial \varphi_x}{\partial y} = \frac{\partial \varphi_y}{\partial x} \quad (A.20b)$$

$$\varphi_{yy} = \frac{\partial \varphi_y}{\partial y} = \frac{d\varphi_y}{d\varphi_x} \frac{\partial \varphi_x}{\partial y} = \frac{d\varphi_y}{d\varphi_x} \frac{\partial \varphi_y}{\partial x} \quad (A.20c)$$

Substituting these into Eq. A.11, with $D = 0$, we find that

$$A \frac{d\varphi_x}{d\varphi_y} + 2B + C \frac{d\varphi_y}{d\varphi_x} = 0 \quad (A.21)$$

Multiplying through by $d\varphi_y/d\varphi_x$ and then solving the quadratic equation for the latter, we obtain two possible solutions:

$$\frac{d\varphi_y}{d\varphi_x} = \frac{-B \pm \sqrt{B^2 - AC}}{C}$$

Hodograph of Simple Wave. Comparing this with Eqs. A.18, we see that the relation between φ_x and φ_y in a simple-wave flow is the same as that on one of the fixed hodograph characteristics. The term "fixed" hodograph characteristics is used here because, as shown previously, the hodograph characteristics are immediately integrable when $D = 0$, irrespective of the particular physical problem. Consequently, a physical region of simple-wave flow is mapped in the hodograph plane as a single characteristic curve. Such a flow is *singly degenerate* inasmuch as a line on the physical plane maps as a point on the hodograph plane, and an area on the physical plane maps as a line on the hodograph plane.

Simple Wave in Physical Plane. Let us now investigate the nature of a line of constant φ_x in the physical plane. Since φ_x is related uniquely

to φ_y in a simple-wave flow, the line is one of constant φ_y as well as of constant φ_x , and therefore all fluid properties will be constant on such a line. The increment in φ_x may be written in the usual manner in terms of dx and dy ; employing Eqs. A.20 in addition, we obtain

$$d\varphi_x = \frac{\partial \varphi_x}{\partial x} dx + \frac{\partial \varphi_x}{\partial y} dy = \frac{d\varphi_x}{d\varphi_y} \frac{\partial \varphi_y}{\partial x} dx + \frac{\partial \varphi_y}{\partial x} dy$$

On a line where φ_x is constant, $d\varphi_x = 0$. On such a line, therefore, the foregoing equation yields

$$\left(\frac{dy}{dx}\right)_{\varphi_x, \varphi_y} = - \frac{1}{(d\varphi_y/d\varphi_x)}$$

Keeping in mind that $d\varphi_y/d\varphi_x$ is the slope of a hodograph characteristic, a comparison of this equation with Eqs. A.19 leads to the conclusion that the lines of constant fluid properties in the physical plane are identical with one family of physical characteristics. Examination of Eqs. A.17 shows that the physical characteristics under consideration are straight lines; this follows because A , B , and C depend only on φ_x and φ_y , and the latter in turn are constant on the physical characteristics.

To sum up, a special type of flow is possible when $D = 0$ and when A , B , and C depend only on φ_x and φ_y . In this simple-wave flow one family of physical characteristics consists of straight lines, with uniform fluid properties on each such characteristic. Each of the physical characteristics maps as a point on the hodograph plane. The locus of these points is the hodograph characteristic of opposite family.

Auxiliary Theorem. An important theorem⁽¹⁾ which follows from the foregoing results states that *if a region of constant state (i.e., uniform properties throughout) adjoins a region of nonuniform flow, then the latter must be a simple-wave flow*. This may be proved by noting that the two regions must be joined on a physical characteristic, and that a physical characteristic in a uniform flow must be a straight line. The significance of this theorem lies in the fact that regions of uniform flow are almost always present in practical applications.

In two-dimensional, supersonic, simple-wave flow one family of Mach lines is straight and the fluid properties are uniform on each such Mach line. If the Mach lines of family *II* are straight, then the entire flow is mapped on a hodograph characteristic of family *I*, and vice versa. Such a flow is called a Prandtl-Meyer flow. A region of uniform, parallel flow can only be adjoined to a Prandtl-Meyer flow.

REFERENCES AND SELECTED BIBLIOGRAPHY

1. COURANT, R., and FRIEDRICH, K. O. *Supersonic Flow and Shock Waves*. New York: Interscience Publishers, Inc., 1948.
2. DALITZ, R. H. *Some Mathematical Aspects of Compressible Flow*. Report ACA-20 of the Australian Council for Aeronautics (1946).
3. ISENBERG, J. S., and LIN, C. C. The Method of Characteristics in Compressible Flow, Part I: Steady, Supersonic Flow, *Air Materiel Command Tech. Report*, No. F-TR-1173A-ND (1947).
4. ROBERTS, R. C., and LIN, C. C. The Method of Characteristics in Compressible Flow, Part II: Unsteady Flow, *Air Materiel Command Tech. Report*, No. F-TR-1173-ND (1947).

Appendix B

TABLES OF COMPRESSIBLE-FLOW FUNCTIONS

Collected in this Appendix are Tables B.1 to B.8 for facilitating numerical calculations.

Listed below are (i) an index to the tables, (ii) nomenclature for the tables, (iii) the sources of the tables, and (iv) a bibliography of additional tables and charts available in the literature.

INDEX TO TABLES

TABLE	PAGE
B.1. Properties of the Standard Atmosphere	612
B.2. Isentropic Flow, $k = 1.4$	614
B.3. Normal Shock, $k = 1.4$	621
B.4. Frictional, Adiabatic, Constant-Area Flow (Fanno Line), $k = 1.4$	626
B.5. Frictionless, Constant-Area Flow with T_0 -Change (Rayleigh Line), $k = 1.4$	628
B.6. Influence Coefficients, $k = 1.4$	630
B.7. Hodograph Characteristic Functions for Two-Dimensional, Isentropic, Supersonic Flow, $k = 1.4$	632
B.8. Coefficients for Second-Order Theory of Two-Dimensional, Supersonic Flow, $k = 1.4$	633

NOMENCLATURE FOR TABLES

- | | |
|---------------------------------|----------------------|
| B.1. See footnote to Table B.1. | B.5. See Chapter 7. |
| B.2. See Chapter 4. | B.6. See Chapter 8. |
| B.3. See Chapter 5. | B.7. See Chapter 15. |
| B.4. See Chapter 6. | B.8. See Chapter 16. |

SOURCES OF TABLES

- | | |
|--|--|
| B.1. THE STAFF OF THE AMES 1- BY 3-FOOT SUPERSONIC WIND TUNNEL SECTION. Notes and Tables for Use in the Analysis of Supersonic Flow, <i>NACA Tech. Note</i> , No. 1428 (1947). | |
| B.2 to B.6. SHAPIRO, A. H., HAWTHORNE, W. R., and EDELMAN, G. M. The Mechanics and Thermodynamics of Steady One-Dimensional Gas Flow with Tables for Numerical Solutions, <i>Meteor Report</i> , No. 14, Massachusetts Institute of Technology Guided Missiles Program, Cambridge, Mass. (1947). | |
| B.7. STAFF OF THE GAS TURBINE LABORATORY, Massachusetts Institute of Technology, Cambridge, Mass. (1948). | |
| B.8. Same source as for Table B.1. | |

BIBLIOGRAPHY OF PUBLISHED TABLES AND CHARTS

1. DAILEY, C. L., and WOOD, F. C. *Computation Curves for Compressible Fluid Problems*. New York: John Wiley & Sons, Inc., 1949.
2. EMMONS, H. W. *Gas Dynamics Tables for Air*. New York: Dover Publications, 1947.
3. KEENAN, J. H., and KAYE, J. *Gas Tables*. New York: John Wiley & Sons, Inc., 1948.
4. SHAPIRO, A. H., HAWTHORNE, W. R., and EDELMAN, G. The Mechanics and Thermodynamics of Steady One-Dimensional Gas Flow, in *Handbook of Supersonic Aerodynamics*, NAVORD Report 1488 (Vol. 1), Superintendent of Documents, U. S. Govt. Printing Office (1950). See also EDELMAN, G. M., and SHAPIRO, A. H. Tables for Numerical Solution of Problems in the Mechanics and Thermodynamics of Steady, One-Dimensional Gas Flow Without Discontinuities, *Jour. App. Mech.*, Vol. 14, No. 4 (1947), p. A-344.
5. KOPAL, Z. Table of Supersonic Flow Around Cones, *Tech. Rep.*, No. 1, M.I.T. Center of Analysis, Mass. Inst. of Tech., Cambridge (1947).
6. KOPAL, Z. Tables of Supersonic Flow Around Yawing Cones, *Tech. Rep.*, No. 3, M.I.T. Center of Analysis, Mass. Inst. of Tech., Cambridge (1947).
7. KOPAL, Z. Supersonic Flow Around Cones of Large Yaw, M.I.T. Center of Analysis, Mass. Inst. of Tech., Cambridge (1947).
8. ISENBERG, J. S. Monograph II: The Method of Characteristics in Compressible Flow; Part IA: Tables and Charts, *Air Materiel Command Report*, No. F-TR-1173-ND (Dec., 1947).
9. ROCKETT, J. A., and HAYES, W. D. Monograph II: The Method of Characteristics in Compressible Flow; Part IC: Two-dimensional flow with large entropy changes, *Air Materiel Command Report*, No. 102-AC49/6-100 (Dec., 1949).
10. NEICE, M. M. Tables and Charts of Flow Parameters Across Oblique Shocks, *NACA Tech. Note*, No. 1673 (1948).
11. HUCKEL, V. Tables of Hypergeometric Functions for Use in Compressible-Flow Theory, *NACA Tech. Note*, No. 1716 (1948).
12. BURCHER, M. A. Compressible Flow Tables for Air, *NACA Tech. Note*, No. 1592 (1948).
13. TURNER, L. R., ADDIE, A. N., and ZIMMERMAN, R. H. Charts for the Analysis of One-Dimensional Steady Compressible Flow, *NACA Tech. Note*, No. 1419 (1948).
14. AMES AERONAUTICAL LABORATORY. Notes and Tables for Use in the Analysis of Supersonic Flow, *NACA Tech. Note*, No. 1428 (1947).
15. IVEY, H. R., STICKLE, G. W., and SCHUETTLER, A. Charts for Determining the Characteristics of Sharp-Nose Airfoils in Two-Dimensional Flow at Supersonic Speeds, *NACA Tech. Note*, No. 1143 (1947).
16. MOECKEL, W. E., and CONNORS, J. F. Charts for the Determination of Supersonic Air Flow Against Inclined Planes and Axially Symmetric Cones, *NACA Tech. Note*, No. 1373 (1947).
17. ORDNANCE AEROPHYSICS LABORATORY. Compressible Flow Tables and Graphs, in *Handbook of Supersonic Aerodynamics*, NAVORD Report 1488 (Vol. 2), Superintendent of Documents, U. S. Govt. Printing Office (1950).
18. ROSENHEAD, L. (ed.). *Selection of Tables for Use in Calculations of Compressible Airflow*. New York: Oxford University Press, 1952.

TABLE B.1

PROPERTIES OF THE STANDARD ATMOSPHERE

<i>h</i>	<i>t</i>	<i>c</i>	<i>p</i>	<i>ρ</i>	$μ \times 10^7$	$ν \times 10^4$
0	59.00	1117	2116.2	0.002378	3.719	1.564
1,000	57.44	1113	2040.9	0.002310	3.699	1.602
2,000	51.87	1109	1967.7	0.002242	3.679	1.641
3,000	48.31	1105	1896.7	0.002177	3.659	1.681
4,000	44.74	1102	1827.7	0.002112	3.639	1.723
5,000	41.18	1098	1760.8	0.002049	3.618	1.766
6,000	37.62	1094	1696.0	0.001988	3.598	1.810
7,000	34.05	1090	1633.0	0.001928	3.577	1.855
8,000	30.49	1086	1571.9	0.001869	3.557	1.903
9,000	26.92	1082	1512.8	0.001812	3.536	1.951
10,000	23.36	1078	1455.4	0.001756	3.515	2.002
11,000	19.80	1074	1399.8	0.001702	3.495	2.054
12,000	16.23	1070	1345.9	0.001649	3.474	2.107
13,000	12.67	1066	1293.7	0.001597	3.453	2.163
14,000	9.10	1062	1243.2	0.001546	3.432	2.220
15,000	5.54	1058	1194.3	0.001497	3.411	2.280
16,000	1.98	1054	1147.0	0.001448	3.390	2.341
17,000	-1.59	1050	1101.1	0.001401	3.369	2.404
18,000	-5.15	1046	1056.9	0.001355	3.347	2.470
19,000	-8.72	1041	1014.0	0.001311	3.326	2.538
20,000	-12.28	1037	972.6	0.001267	3.305	2.608
21,000	-15.84	1033	932.5	0.001225	3.283	2.681
22,000	-19.41	1029	893.8	0.001183	3.262	2.757
23,000	-22.97	1025	856.4	0.001143	3.240	2.834
24,000	-26.54	1021	820.3	0.001104	3.218	2.915
25,000	-30.10	1017	785.3	0.001066	3.196	2.999
26,000	-33.66	1012	751.7	0.001029	3.174	3.087
27,000	-37.23	1008	719.2	0.000993	3.153	3.177
28,000	-40.79	1004	687.9	0.000957	3.130	3.270
29,000	-44.36	999	657.6	0.000923	3.108	3.367
30,000	-47.92	995	628.5	0.000890	3.086	3.469
31,000	-51.48	991	600.4	0.000858	3.064	3.573
32,000	-55.05	987	573.3	0.000826	3.041	3.682
33,000	-58.61	982	547.3	0.000796	3.019	3.795
34,000	-62.18	978	522.2	0.000766	2.997	3.913
35,000	-65.74	973	498.0	0.000737	2.974	4.036
35,332	-67.6	971	489.8	0.000727	2.961	4.073
36,000	-67.6	971	474.8	0.000709	2.961	4.176
37,000	-67.6	971	452.5	0.0006766	2.961	4.376
38,000	-67.6	971	431.2	0.0006448	2.961	4.592
39,000	-67.6	971	411.0	0.0006145	2.961	4.819
40,000	-67.6	971	391.8	0.0005857	2.961	5.055
41,000	-67.6	971	373.4	0.0005582	2.961	5.305
42,000	-67.6	971	355.8	0.0005320	2.961	5.566
43,000	-67.6	971	339.1	0.0005071	2.961	5.839
44,000	-67.6	971	323.2	0.0004833	2.961	6.127
45,000	-67.6	971	308.0	0.0004605	2.961	6.430

TABLE B.1. PROPERTIES OF THE STANDARD ATMOSPHERE (Continued)

<i>h</i>	<i>t</i>	<i>c</i>	<i>p</i>	<i>ρ</i>	$μ \times 10^7$	$ν \times 10^4$
46,000	-67.6	971	293.6	.0004390	2.961	6.745
47,000	-67.6	971	279.8	.0004184	2.961	7.077
48,000	-67.6	971	266.6	.0003987	2.961	7.427
49,000	-67.6	971	254.1	.0003800	2.961	7.792
50,000	-67.6	971	242.2	.0003622	2.961	8.175
60,000	-67.6	971	150.9	.0002240	2.961	13.219
70,000	-67.6	971	93.5	.0001389	2.961	21.317
80,000	-67.6	971	58.0	.0000861	2.961	34.390
90,000	-67.6	971	36.0	.0000535	2.961	55.346
100,000	-67.6	971	22.4	.0000331	2.961	89.456
104,987	-67.6	971	17.59	.0000261	2.961	113.4
110,000	-47.4	996	13.92	.0000197	3.090	157.2
120,000	-7.2	1043	9.026	.0000116	3.339	287.6
130,000	33.0	1089	6.071	.00000717	3.579	498.9
140,000	73.3	1132	4.213	.00000460	3.809	827.9
150,000	113.5	1174	3.003	.00000305	4.032	1322
160,000	153.7	1215	2.190	.00000208	4.247	2043
164,042	170.0	1231	1.938	.00000179	4.332	2417
170,000	170.0	1231	1.624	.00000150	4.332	2886
180,000	170.0	1231	1.206	.00000111	4.332	3885
190,000	170.0	1231	.8956	.00000083	4.332	5232
196,850	170.0	1231	.7305	.00000068	4.332	6412
200,000	159.4	1220	.6645	.00000062	4.277	6844
210,000	125.9	1187	.4869	.00000048	4.099	8467
220,000	92.4	1152	.3504	.00000037	3.916	10600
230,000	58.9	1117	.2470	.00000028	3.727	13400
240,000	25.3	1080	.1699	.00000020	3.533	17330
250,000	-8.2	1042	.1139	.00000015	3.333	22700
255,905	-28.0	1019	.0886	.00000012	3.212	26880
260,000	-28.0	1019	.0742	.00000010	3.212	32090

Symbols: *h* = height above sea level, ft*t* = temperature, degrees F*c* = speed of sound, ft/sec*p* = pressure, lbf/ft²*ρ* = mass density, slug/ft³*μ* = coefficient of viscosity, slug/ft sec*ν* = *μ/ρ*, kinematic viscosity, ft²/sec

TABLE B.2
ISENTROPIC FLOW
Perfect Gas, $k = 1.4$

M	M^*	p/p_0	ρ/ρ_0	T/T_0	A/A^*	F/F^*	$\frac{A}{A^*} \cdot \frac{p}{p_0}$
0	0	1.0000,0	1.0000,0	1.00000	∞	∞	∞
.01	.01096	.9999,3	.9999,5	.99998	5.7,874	4.5,650	5.7,870
.02	.02191	.9997,2	.9998,0	.99992	2.8,942	2.2,834	2.8,934
.03	.03286	.9993,7	.9995,5	.99982	1.9,300	15.,232	1.9,288
.04	.04381	.9988,8	.9992,0	.99968	14.,482	11.,435	14.,465
.05	.05476	.9982,5	.9987,5	.99950	11.5,915	9.,1584	11.,5712
.06	.06570	.9974,8	.9982,0	.99928	9.6,659	7.,6428	9.,6415
.07	.07664	.9965,8	.9975,5	.99902	8.2,915	6.5,620	8.2,631
.08	.08758	.9955,3	.9968,0	.99872	7.2,616	5.7,529	7.2,291
.09	.09851	.9943,5	.9959,6	.99838	6.4,613	5.1,249	6.4,248
.10	.10943	.9930,3	.9950,2	.99800	5.8,218	4.6,236	5.7,812
.11	.12035	.9915,7	.9939,8	.99758	5.2,992	4.2,146	5.2,546
.12	.13126	.9899,8	.9928,4	.99714	4.8,643	3.8,747	4.8,157
.13	.14216	.9882,6	.9916,0	.99664	4.4,968	3.58,80	4.4,440
.14	.15306	.9864,0	.9902,7	.99610	4.18,24	3.34,32	4.12,55
.15	.16395	.9844,1	.9888,4	.99552	3.91,03	3.13,17	3.84,93
.16	.17483	.9822,8	.9873,1	.99490	3.67,27	2.94,74	3.60,76
.17	.18569	.9800,3	.9856,9	.99425	3.46,35	2.78,55	3.39,43
.18	.19654	.9776,5	.9839,8	.99356	3.27,79	2.64,22	3.20,46
.19	.20738	.9751,4	.9821,7	.99283	3.11,22	2.51,46	3.03,48
.20	.21822	.9725,0	.9802,7	.99206	2.96,35	2.40,04	2.88,20
.21	.22904	.9697,3	.9782,8	.99125	2.82,93	2.29,76	2.74,37
.22	.23984	.9668,5	.9762,1	.99041	2.70,76	2.20,46	2.61,78
.23	.25063	.9638,3	.9740,3	.98953	2.59,68	2.12,03	2.50,29
.24	.26141	.9607,0	.9717,7	.98861	2.49,56	2.04,34	2.39,75
.25	.27216	.9574,5	.9694,2	.98765	2.40,27	1.97,32	2.30,05
.26	.28291	.9540,8	.9669,9	.98666	2.31,73	1.90,88	2.21,09
.27	.29364	.9506,0	.9644,6	.98563	2.23,85	1.84,96	2.12,79
.28	.30435	.9470,0	.9618,5	.98456	2.16,56	1.795,0	2.05,08
.29	.31504	.9432,9	.9591,6	.98346	2.09,79	1.744,6	1.97,89
.30	.32572	.9394,7	.9563,8	.98232	2.035,1	1.697,9	1.911,9
.31	.33638	.9355,4	.9535,2	.98114	1.976,5	1.654,6	1.849,1
.32	.34701	.9315,0	.9505,8	.97993	1.921,8	1.614,4	1.790,2
.33	.35762	.9273,6	.9475,6	.97868	1.870,7	1.576,9	1.734,8
.34	.36821	.9231,2	.9444,6	.97740	1.822,9	1.542,0	1.682,8
.35	.37879	.9187,7	.9412,8	.97608	1.778,0	1.509,4	1.633,6
.36	.38935	.9143,3	.9380,3	.97473	1.735,8	1.478,9	1.587,1
.37	.39988	.9097,9	.9347,0	.97335	1.696,1	1.450,3	1.543,1
.38	.41039	.9051,6	.9312,9	.97193	1.658,7	1.423,6	1.501,4
.39	.42087	.9004,4	.9278,2	.97048	1.623,4	1.398,5	1.461,8
.40	.43133	.8956,2	.9242,8	.96899	1.590,1	1.374,9	1.424,1
.41	.44177	.8907,1	.9206,6	.96747	1.558,7	1.352,7	1.388,3
.42	.45218	.8857,2	.9169,7	.96592	1.528,9	1.331,8	1.354,2
.43	.46256	.8806,5	.9132,2	.96434	1.500,7	1.312,2	1.321,6
.44	.47292	.8755,0	.9094,0	.96272	1.474,0	1.293,7	1.290,5

Notes: (1) For values of M from 0 to 5.00, all digits to the left of the comma are valid for linear interpolation. Where no comma is indicated in this region, all digits are valid for linear interpolation.

(2) The notation .0429 signifies .000429. The notation 5370₄ signifies 5,370,000.

TABLE B.2. ISENTROPIC FLOW (Continued)
Perfect Gas, $k = 1.4$

M	M^*	p/p_0	ρ/ρ_0	T/T_0	A/A^*	F/F^*	$\frac{A}{A^*} \cdot \frac{p}{p_0}$
.45	.48326	.8702,7	.9055,2	.96108	1.448,7	1.276,3	1.260,7
.46	.49357	.8649,6	.9015,7	.95940	1.424,6	1.259,8	1.232,2
.47	.50385	.8595,8	.8975,6	.95769	1.401,8	1.244,3	1.205,0
.48	.51410	.8541,3	.8934,9	.95595	1.380,1	1.229,6	1.178,8
.49	.52432	.8486,1	.8893,6	.95418	1.359,4	1.215,8	1.153,7
.50	.53452	.8430,2	.8851,7	.95238	1.339,8	1.202,7	1.129,51
.51	.54469	.8373,7	.8809,2	.95055	1.321,2	1.190,3	1.106,31
.52	.55482	.8316,6	.8766,2	.94869	1.303,4	1.178,6	1.083,97
.53	.56493	.8258,9	.8722,7	.94681	1.286,4	1.167,5	1.062,45
.54	.57501	.8200,5	.8678,8	.94489	1.270,3	1.157,1	1.041,73
.55	.58506	.8141,6	.86342	.94295	1.255,0	1.147,2	1.021,74
.56	.59508	.8082,2	.85892	.94098	1.240,3	1.137,8	1.002,44
.57	.60506	.8022,4	.85437	.93898	1.226,3	1.128,9	.983,81
.58	.61500	.7962,1	.84977	.93696	1.213,0	1.120,5	.965,81
.59	.62491	.7901,2	.84513	.93491	1.200,3	1.112,6	.948,39
.60	.63480	.78400	.84045	.93284	1.188,2	1.1050,4	.931,55
.61	.64466	.77784	.83573	.93074	1.176,6	1.0979,3	.915,25
.62	.65448	.77164	.83096	.92861	1.165,6	1.0912,0	.899,46
.63	.66427	.76540	.82616	.92646	1.155,1	1.0848,5	.884,16
.64	.67402	.75913	.82132	.92428	1.145,1	1.0788,3	.869,32
.65	.68374	.75283	.81644	.92208	1.1356	1.0731,4	.8549,3
.66	.69342	.74650	.81153	.91986	1.1265	1.0677,7	.8409,6
.67	.70307	.74014	.80659	.91762	1.1178	1.0627,1	.8274,0
.68	.71268	.73376	.80162	.91535	1.1096	1.0579,2	.8142,1
.69	.72225	.72735	.79662	.91306	1.1018	1.0534,0	.8014,1
.70	.73179	.72092	.79158	.91075	1.0943,7	1.0491,5	.7889,6
.71	.74129	.71448	.78652	.90842	1.0872,9	1.0451,4	.7768,5
.72	.75076	.70802	.78143	.90606	1.0805,7	1.0413,7	.7650,7
.73	.76019	.70155	.77632	.90368	1.0741,9	1.0378,3	.7536,0
.74	.76958	.69507	.77119	.90129	1.0681,4	1.0345,0	.7424,3
.75	.77893	.68857	.76603	.89888	1.0624,2	1.0313,7	.7315,5
.76	.78825	.68207	.76086	.89644	1.0570,0	1.0284,4	.7209,5
.77	.79753	.67556	.75567	.89399	1.0518,8	1.0257,0	.7106,2
.78	.80677	.66905	.75046	.89152	1.0470,5	1.0231,4	.7005,4
.79	.81597	.66254	.74524	.88903	1.0425,0	1.0207,5	.6907,0
.80	.82514	.65602	.74000	.88652	1.0382,3	1.0185,3	.6811,0
.81	.83426	.64951	.73474	.88400	1.0342,2	1.0164,6	.6717,3
.82	.84334	.64300	.72947	.88146	1.0304,6	1.0145,5	.6625,9
.83	.85239	.63650	.72419	.87890	1.0269,6	1.0127,8	.6536,6
.84	.86140	.63000	.71890	.87633	1.0237,0	1.0111,5	.6449,3
.85	.87037	.62351	.71361	.87374	1.0206,7	1.0096,6	.6364,0
.86	.87929	.61703	.70831	.87114	1.0178,7	1.0082,9	.6280,6
.87	.88817	.61057	.70300	.86852	1.0153,0	1.0070,4	.6199,1
.88	.89702	.60412	.69769	.86589	1.0129,4	1.0059,1	.6119,3
.89	.90583	.59768	.69237	.86324	1.0108,0	1.0049,0	.6041,3
.90	.91460	.59126	.68704	.86058	1.0088,6	1.0039,9	.5965,0
.91	.92333	.58486	.68171	.85791	1.0071,3	1.0031,8	.5890,3
.92	.93201	.57848	.67639	.85523	1.0056,0	1.0024,8	.5817,1
.93	.94065	.57212	.67107	.85253	1.0042,6	1.0018,8	.5745,4
.94	.94925	.56578	.66575	.84982	1.0031,1	1.0013,6	.5675,4

See Notes at beginning of this table.

TABLE B.2. ISENTROPIC FLOW (Continued)
Perfect Gas, $k = 1.4$

M	M^*	p/p_0	ρ/ρ_0	T/T_0	A/A^*	F/F^*	$\frac{A}{A^*} \cdot \frac{p}{p_0}$
.95	.95781	.55946	.66044	.84710	1.0021,4	1.0009,3	.5606,6
.96	.96633	.55317	.65513	.84437	1.0013,6	1.0005,9	.5539,2
.97	.97481	.54691	.64982	.84162	1.0007,6	1.0003,3	.5473,2
.98	.98325	.54067	.64452	.83887	1.0003,3	1.0001,4	.5408,5
.99	.99165	.53446	.63923	.83611	1.0000,8	1.0000,3	.5345,0
1.00	1.00000	.52828	.63394	.83333	1.0000,0	1.0000,0	.5282,8
1.01	1.00831	.52213	.62866	.83055	1.0000,8	1.0000,3	.5221,8
1.02	1.01658	.51602	.62339	.82776	1.0003,3	1.0001,3	.5161,9
1.03	1.02481	.50994	.61813	.82496	1.0007,4	1.0003,0	.5103,1
1.04	1.03300	.50389	.61288	.82215	1.0013,0	1.0005,3	.5045,4
1.05	1.04114	.49787	.60765	.81933	1.0020,2	1.0008,2	.4988,8
1.06	1.04924	.49189	.60243	.81651	1.0029,0	1.0011,6	.4933,2
1.07	1.05730	.48595	.59722	.81368	1.0039,4	1.0015,5	.4878,7
1.08	1.06532	.48005	.59203	.81084	1.0051,2	1.0020,0	.4825,1
1.09	1.07330	.47418	.58685	.80800	1.0064,5	1.0025,0	.4772,4
1.10	1.08124	.46835	.58169	.80515	1.0079,3	1.00305	.4720,6
1.11	1.08914	.46256	.57655	.80230	1.0095,5	1.00365	.4669,8
1.12	1.09699	.45682	.57143	.79944	1.0113,1	1.00429	.4619,9
1.13	1.10480	.45112	.56632	.79657	1.0132,2	1.00497	.4570,8
1.14	1.11256	.44545	.56123	.79370	1.0152,7	1.00569	.4522,5
1.15	1.1203	.43983	.55616	.79083	1.0174,6	1.00646	.4475,1
1.16	1.1280	.43425	.55112	.78795	1.0197,8	1.00726	.4428,4
1.17	1.1356	.42872	.54609	.78507	1.0222,4	1.00810	.4382,5
1.18	1.1432	.42323	.54108	.78218	1.0248,4	1.00897	.4337,4
1.19	1.1508	.41778	.53610	.77929	1.0275,7	1.00988	.4293,0
1.20	1.1583	.4123,8	.53114	.77640	1.0304,4	1.01082	.4249,3
1.21	1.1658	.4070,2	.52620	.77350	1.0334,4	1.01178	.4206,3
1.22	1.1732	.4017,1	.52129	.77061	1.0365,7	1.01278	.4164,0
1.23	1.1806	.3964,5	.51640	.76771	1.0398,3	1.01381	.4122,4
1.24	1.1879	.3912,3	.51154	.76481	1.0432,3	1.01486	.4081,4
1.25	1.1952	.3860,6	.50670	.76190	1.0467,6	1.01594	.4041,1
1.26	1.2025	.3809,4	.50189	.75900	1.0504,1	1.01705	.4001,4
1.27	1.2097	.3758,6	.49710	.75610	1.0541,9	1.01818	.3962,2
1.28	1.2169	.3708,3	.49234	.75319	1.0581,0	1.01933	.3923,7
1.29	1.2240	.3658,5	.48761	.75029	1.0621,4	1.02050	.3885,8
1.30	1.2311	.3609,2	.48291	.74738	1.0663,1	1.02170	.3848,4
1.31	1.2382	.3560,3	.47823	.74448	1.0706,0	1.02292	.3811,6
1.32	1.2452	.3511,9	.47358	.74158	1.0750,2	1.02415	.3775,4
1.33	1.2522	.3464,0	.46895	.73867	1.0795,7	1.02540	.3739,7
1.34	1.2591	.3416,6	.46436	.73577	1.0842,4	1.02666	.3704,4
1.35	1.2660	.3369,7	.45980	.73287	1.0890,4	1.02794	.3669,7
1.36	1.2729	.3323,3	.45527	.72997	1.0939,7	1.02924	.3635,5
1.37	1.2797	.3277,4	.45076	.72707	1.0990,2	1.03056	.3601,8
1.38	1.2865	.3231,9	.44628	.72418	1.1042,0	1.03189	.3568,6
1.39	1.2932	.3186,9	.44183	.72128	1.1095,0	1.03323	.3535,9
1.40	1.2999	.3142,4	.43742	.71839	1.1149	1.03458	.35036
1.41	1.3065	.3098,4	.43304	.71550	1.1205	1.03595	.34717
1.42	1.3131	.3054,9	.42869	.71261	1.1262	1.03733	.34403
1.43	1.3197	.3011,9	.42436	.70973	1.1320	1.03872	.34093
1.44	1.3262	.2969,3	.42007	.70685	1.1379	1.04012	.33787

TABLE B.2. ISENTROPIC FLOW (Continued)
Perfect Gas, $k = 1.4$

M	M^*	p/p_0	ρ/ρ_0	T/T_0	A/A^*	F/F^*	$\frac{A}{A^*} \cdot \frac{p}{p_0}$
1.45	1.3327	.2927,2	.41581	.70397	1.1440	1.04153	.33486
1.46	1.3392	.2885,6	.41158	.70110	1.1502	1.04295	.33189
1.47	1.3456	.2844,5	.40738	.69823	1.1565	1.04438	.32896
1.48	1.3520	.2803,9	.40322	.69537	1.1629	1.04581	.32607
1.49	1.3583	.2763,7	.39909	.69251	1.1695	1.04725	.32321
1.50	1.3646	.2724,0	.39498	.68965	1.1762	1.04870	.32039
1.51	1.3708	.2684,8	.39091	.68680	1.1830	1.05016	.31761
1.52	1.3770	.2646,1	.38687	.68396	1.1899	1.05162	.31487
1.53	1.3832	.2607,8	.38287	.68112	1.1970	1.05309	.31216
1.54	1.3894	.2570,0	.37890	.67828	1.2042	1.05456	.30948
1.55	1.3955	.2532,6	.37496	.67545	1.2115	1.05604	.30685
1.56	1.4016	.2495,7	.37105	.67262	1.2190	1.05752	.30424
1.57	1.4076	.2459,3	.36717	.66980	1.2266	1.05900	.30167
1.58	1.4135	.2423,3	.36332	.66699	1.2343	1.06049	.29913
1.59	1.4195	.2387,8	.35951	.66418	1.2422	1.06198	.29662
1.60	1.4254	.23527	.35573	.66138	1.2502	1.06348	.29414
1.61	1.4313	.23181	.35198	.65858	1.2583	1.06498	.29169
1.62	1.4371	.22839	.34826	.65579	1.2666	1.06648	.28928
1.63	1.4429	.22501	.34458	.65301	1.2750	1.06798	.28690
1.64	1.4487	.22168	.34093	.65023	1.2835	1.06948	.28454
1.65	1.4544	.21839	.33731	.64746	1.2922	1.07098	.28221
1.66	1.4601	.21515	.33372	.64470	1.3010	1.07249	.27991
1.67	1.4657	.21195	.33016	.64194	1.3099	1.07399	.27764
1.68	1.4713	.20879	.32664	.63919	1.3190	1.07550	.27540
1.69	1.4769	.20567	.32315	.63645	1.3282	1.07701	.27318
1.70	1.4825	.20259	.31969	.63372	1.3376	1.07851	.27099
1.71	1.4880	.19955	.31626	.63099	1.3471	1.08002	.26882
1.72	1.4935	.19656	.31286	.62827	1.3567	1.08152	.26668
1.73	1.4989	.19361	.30950	.62556	1.3665	1.08302	.26457
1.74	1.5043	.19070	.30617	.62286	1.3764	1.08453	.26248
1.75	1.5097	.18782	.30287	.62016	1.3865	1.08603	.26042
1.76	1.5150	.18499	.29959	.61747	1.3967	1.08753	.25838
1.77	1.5203	.18220	.29635	.61479	1.4071	1.08903	.25636
1.78	1.5256	.17944	.29314	.61211	1.4176	1.09053	.25436
1.79	1.5308	.17672	.28997	.60945	1.4282	1.09202	.25239
1.80	1.5360	.17404	.28682	.60680	1.4390	1.09352	.25044
1.81	1.5412	.17140	.28370	.60415	1.4499	1.09500	.24851
1.82	1.5463	.16879	.28061	.60151	1.4610	1.09649	.24660
1.83	1.5514	.16622	.27756	.59888	1.4723	1.09798	.24472
1.84	1.5564	.16369	.27453	.59626	1.4837	1.09946	.24286
1.85	1.5614	.16120	.27153	.59365	1.4952	1.1009	.24102
1.86	1.5664	.15874	.26857	.59105	1.5069	1.1024	.23919
1.87	1.5714	.15631	.26563	.58845	1.5188	1.1039	.23739
1.88	1.5763	.15392	.26272	.58586	1.5308	1.1054	.23561
1.89	1.5812	.15156	.25984	.58329	1.5429	1.1068	.23385
1.90	1.5861	.14924	.25699	.58072	1.5552	1.1083	.23211
1.91	1.5909	.14695	.25417	.57816	1.5677	1.1097	.23039
1.92	1.5957	.14469	.25138	.57561	1.5804	1.1112	.22868
1.93	1.6005	.14247	.24862	.57307	1.5932	1.1126	.22699
1.94	1.6052	.14028	.24588	.57054	1.6062	1.1141	.22532

See Notes at beginning of this table.

See Notes at beginning of this table.

TABLE B.2. ISENTROPIC FLOW (Continued)
Perfect Gas, $k = 1.4$

M	M^*	p/p_0	ρ/ρ_0	T/T_0	A/A^*	F/F^*	$\frac{A}{A^*} \cdot \frac{p}{p_0}$
1.95	1.6099	.13813	.24317	.56802	1.6193	1.1155	.22367
1.96	1.6146	.13600	.24049	.56551	1.6326	1.1170	.22204
1.97	1.6193	.13390	.23784	.56301	1.6461	1.1184	.22042
1.98	1.6239	.13184	.23522	.56051	1.6597	1.1198	.21882
1.99	1.6285	.12981	.23262	.55803	1.6735	1.1213	.21724
2.00	1.6330	.12780	.23005	.55556	1.6875	1.1227	.21567
2.01	1.6375	.12583	.22751	.55310	1.7017	1.1241	.21412
2.02	1.6420	.12389	.22499	.55064	1.7160	1.1255	.21259
2.03	1.6465	.12198	.22250	.54819	1.7305	1.1269	.21107
2.04	1.6509	.12009	.22004	.54576	1.7452	1.1283	.20957
2.05	1.6553	.11823	.21760	.54333	1.7600	1.1297	.20808
2.06	1.6597	.11640	.21519	.54091	1.7750	1.1311	.20661
2.07	1.6640	.11460	.21281	.53850	1.7902	1.1325	.20515
2.08	1.6683	.11282	.21045	.53611	1.8056	1.1339	.20371
2.09	1.6726	.11107	.20811	.53373	1.8212	1.1352	.20228
2.10	1.6769	.10935	.20580	.53135	1.8369	1.1366	.20087
2.11	1.6811	.10766	.20352	.52898	1.8529	1.1380	.19947
2.12	1.6853	.10599	.20126	.52663	1.8690	1.1393	.19809
2.13	1.6895	.10434	.19902	.52428	1.8853	1.1407	.19672
2.14	1.6936	.10272	.19681	.52194	1.9018	1.1420	.19537
2.15	1.6977	.10113	.19463	.51962	1.9185	1.1434	.19403
2.16	1.7018	.09956	.19247	.51730	1.9354	1.1447	.19270
2.17	1.7059	.09802	.19033	.51499	1.9525	1.1460	.19138
2.18	1.7099	.09650	.18821	.51269	1.9698	1.1474	.19008
2.19	1.7139	.09500	.18612	.51041	1.9873	1.1487	.18879
2.20	1.7179	.09352	.18405	.50813	2.0050	1.1500	.18751
2.21	1.7219	.09207	.18200	.50586	2.0229	1.1513	.18624
2.22	1.7258	.09064	.17998	.50361	2.0409	1.1526	.18499
2.23	1.7297	.08923	.17798	.50136	2.0592	1.1539	.18375
2.24	1.7336	.08784	.17600	.49912	2.0777	1.1552	.18252
2.25	1.7374	.08648	.17404	.49689	2.0964	1.1565	.18130
2.26	1.7412	.08514	.17211	.49468	2.1154	1.1578	.18009
2.27	1.7450	.08382	.17020	.49247	2.1345	1.1590	.17890
2.28	1.7488	.08252	.16830	.49027	2.1538	1.1603	.17772
2.29	1.7526	.08123	.16643	.48809	2.1734	1.1616	.17655
2.30	1.7563	.07997	.16458	.48591	2.1931	1.1629	.17539
2.31	1.7600	.07873	.16275	.48374	2.2131	1.1641	.17424
2.32	1.7637	.07751	.16095	.48158	2.2333	1.1653	.17310
2.33	1.7673	.07631	.15916	.47944	2.2537	1.1666	.17197
2.34	1.7709	.07513	.15739	.47730	2.2744	1.1678	.17085
2.35	1.7745	.07396	.15564	.47517	2.2953	1.1690	.16975
2.36	1.7781	.07281	.15391	.47305	2.3164	1.1703	.16866
2.37	1.7817	.07168	.15220	.47095	2.3377	1.1715	.16757
2.38	1.7852	.07057	.15052	.46885	2.3593	1.1727	.16649
2.39	1.7887	.06948	.14885	.46676	2.3811	1.1739	.16543
2.40	1.7922	.06840	.14720	.46468	2.4031	1.1751	.16437
2.41	1.7957	.06734	.14557	.46262	2.4254	1.1763	.16332
2.42	1.7991	.06630	.14395	.46056	2.4479	1.1775	.16229
2.43	1.8025	.06527	.14235	.45851	2.4706	1.1786	.16126
2.44	1.8059	.06426	.14078	.45647	2.4936	1.1798	.16024

See Notes at beginning of this table.

TABLE B.2. ISENTROPIC FLOW (Continued)
Perfect Gas, $k = 1.4$

M	M^*	p/p_0	ρ/ρ_0	T/T_0	A/A^*	F/F^*	$\frac{A}{A^*} \cdot \frac{p}{p_0}$
2.45	1.8093	.06327	.13922	.45444	2.5168	1.1810	.15923
2.46	1.8126	.06229	.13768	.45242	2.5403	1.1821	.15823
2.47	1.8159	.06133	.13616	.45041	2.5640	1.1833	.15724
2.48	1.8192	.06038	.13465	.44841	2.5880	1.1844	.15626
2.49	1.8225	.05945	.13316	.44642	2.6122	1.1856	.15528
2.50	1.8258	.05853	.13169	.44444	2.6367	1.1867	.15432
2.51	1.8290	.05763	.13023	.44247	2.6615	1.1879	.15337
2.52	1.8322	.05674	.12879	.44051	2.6865	1.1890	.15242
2.53	1.8354	.05586	.12737	.43856	2.7117	1.1901	.15148
2.54	1.8386	.05500	.12597	.43662	2.7372	1.1912	.15055
2.55	1.8417	.05415	.12458	.43469	2.7630	1.1923	.14963
2.56	1.8448	.05332	.12321	.43277	2.7891	1.1934	.14871
2.57	1.8479	.05250	.12185	.43085	2.8154	1.1945	.14780
2.58	1.8510	.05169	.12051	.42894	2.8420	1.1956	.14691
2.59	1.8541	.05090	.11918	.42705	2.8689	1.1967	.14601
2.60	1.8572	.05012	.11787	.42517	2.8960	1.1978	.14513
2.61	1.8602	.04935	.11658	.42330	2.9234	1.1989	.14426
2.62	1.8632	.04859	.11530	.42143	2.9511	1.2000	.14339
2.63	1.8662	.04784	.11403	.41957	2.9791	1.2011	.14253
2.64	1.8692	.04711	.11278	.41772	3.0074	1.2021	.14168
2.65	1.8721	.04639	.11154	.41589	3.0359	1.2031	.14083
2.66	1.8750	.04568	.11032	.41406	3.0647	1.2042	.13999
2.67	1.8779	.04498	.10911	.41224	3.0938	1.2052	.13916
2.68	1.8808	.04429	.10792	.41043	3.1233	1.2062	.13834
2.69	1.8837	.04361	.10674	.40863	3.1530	1.2073	.13752
2.70	1.8865	.04295	.10557	.40684	3.1830	1.2083	.13671
2.71	1.8894	.04230	.10442	.40505	3.2133	1.2093	.13591
2.72	1.8922	.04166	.10328	.40327	3.2440	1.2103	.13511
2.73	1.8950	.04102	.10215	.40151	3.2749	1.2113	.13432
2.74	1.8978	.04039	.10104	.39976	3.3061	1.2123	.13354
2.75	1.9005	.03977	.09994	.39801	3.3376	1.2133	.13276
2.76	1.9032	.03917	.09885	.39627	3.3695	1.2143	.13199
2.77	1.9060	.03858	.09777	.39454	3.4017	1.2153	.13123
2.78	1.9087	.03800	.09671	.39282	3.4342	1.2163	.13047
2.79	1.9114	.03742	.09566	.39111	3.4670	1.2173	.12972
2.80	1.9140	.03685	.09462	.38941	3.5001	1.2182	.12897
2.81	1.9167	.03629	.09360	.38771	3.5336	1.2192	.12823
2.82	1.9193	.03574	.09259	.38603	3.5674	1.2202	.12750
2.83	1.9220	.03520	.09158	.38435	3.6015	1.2211	.12678
2.84	1.9246	.03467	.09059	.38268	3.6359	1.2221	.12605
2.85	1.9271	.03415	.08962	.38102	3.6707	1.2230	.12534
2.86	1.9297	.03363	.08865	.37937	3.7058	1.2240	.12463
2.87	1.9322	.03312	.08769	.37773	3.7413	1.2249	.12393
2.88	1.9348	.03262	.08674	.37610	3.7771	1.2258	.12323
2.89	1.9373	.03213	.08581	.37448	3.8133	1.2268	.12254
2.90	1.9398	.03165	.08489	.37286	3.8498	1.2277	.12185
2.91	1.9423	.03118	.08398	.37125	3.8866	1.2286	.12117
2.92	1.9448	.03071	.08308	.36965	3.9238	1.2295	.12049
2.93	1.9472	.03025	.08218	.36806	3.9614	1.2304	.11982
2.94	1.9497	.02980	.08130	.36648	3.9993	1.2313	.11916

See Notes at beginning of this table.

TABLE B.2. ISENTROPIC FLOW (Concluded)
Perfect Gas, $k = 1.4$

M	M^*	p/p_0	ρ/ρ_0	T/T_0	A/A^*	F/F^*	$\frac{A}{A^*} \cdot \frac{p}{p_0}$
2.95	1.9521	.02935	.08043	.36490	4.0376	1.2322	.11850
2.96	1.9545	.02891	.07957	.36333	4.0763	1.2331	.11785
2.97	1.9569	.02848	.07872	.36177	4.1153	1.2340	.11720
2.98	1.9593	.02805	.07788	.36022	4.1547	1.2348	.11656
2.99	1.9616	.02764	.07705	.35868	4.1944	1.2357	.11591
3.00	1.964,0	.027,22	.076,23	.357,14	4.23,46	1.2366	.115,28
3.10	1.986,6	.023,45	.068,52	.342,23	4.65,73	1.2450	.109,21
3.20	2.007,9	.020,23	.061,65	.328,08	5.12,10	1.2530	.1035,9
3.30	2.027,9	.0174,8	.055,54	.314,66	5.6,287	1.2605	.0983,7
3.40	2.046,6	.0151,2	.050,09	.301,93	6.1,837	1.2676	.0935,3
3.50	2.064,2	.0131,1	.045,23	.289,86	6.7,896	1.2743	.0890,2
3.60	2.080,8	.0113,8	.040,89	.278,40	7.4,501	1.2807	.0848,2
3.70	2.096,4	.0099,0	.0370,2	.267,52	8.1,691	1.2867	.0809,0
3.80	2.111,1	.0086,3	.0335,5	.257,20	8.9,506	1.2924	.0772,3
3.90	2.125,0	.0075,3	.0304,4	.247,40	9.7,990	1.2978	.0738,0
4.00	2.138,1	.0065,8	.0276,6	.238,10	10.7,19	1.3029	.0705,9
4.10	2.150,5	.0057,7	.0251,6	.229,25	11.7,15	1.3077	.0675,8
4.20	2.162,2	.0050,6	.0229,2	.2208,5	12.7,92	1.3123	.0647,5
4.30	2.173,2	.0044,5	.0209,0	.2128,6	13.9,55	1.3167	.0620,9
4.40	2.183,7	.0039,2	.0190,9	.2052,5	15.2,10	1.3208	.0595,9
4.50	2.193,6	.0034,6	.0174,5	.1980,2	16.5,62	1.3247	.0572,3
4.60	2.203,0	.0030,5	.0159,7	.1911,3	18.0,18	1.3284	.0550,0
4.70	2.211,9	.0027,0	.0146,3	.1845,7	19.5,83	1.3320	.0528,9
4.80	2.220,4	.0024,0	.0134,3	.1783,2	21.2,64	1.3354	.0509,1
4.90	2.228,4	.0021,3	.0123,3	.1723,5	23.0,67	1.3386	.0490,4
5.00	2.2361	.00189	.01134	.16667	25.000	1.3416	.04725
6.00	2.2953	.03633	.00519	.12195	53.180	1.3655	.03368
7.00	2.3333	.03242	.00261	.09259	104.143	1.3810	.02516
8.00	2.3591	.03102	.00141	.07246	190.109	1.3915	.01947
9.00	2.3772	.04474	.03815	.05814	327.189	1.3989	.01550
10.00	2.3904	.04236	.03495	.04762	535.938	1.4044	.01263
∞	2.4495	0	0	0	∞	1.4289	0

See Notes at beginning of this table.

TABLE B.3
NORMAL SHOCK
Perfect Gas, $k = 1.4$

M_x	M_y	p_y/p_x	V_x/V_y and p_y/p_x	T_y/T_x	A_x/A_y and p_0y/p_0x	p_0y/p_x
1.00	1.0000,0	1.0000,0	1.0000,0	1.0000,0	1.00000	1.8929
1.01	.9901,3	1.0234,5	1.0166,9	1.0066,5	.99999	1.9152
1.02	.9805,2	1.0471,3	1.0334,4	1.01325	.99998	1.9379
1.03	.9711,5	1.0710,5	1.0502,4	1.01981	.99997	1.9610
1.04	.9620,2	1.0952,0	1.0670,9	1.02634	.99994	1.9845
1.05	.9531,2	1.1196	1.0839,8	1.03284	.99987	2.0083
1.06	.9444,4	1.1442	1.10092	1.03931	.99976	2.0325
1.07	.9359,8	1.1690	1.11790	1.04575	.99962	2.0570
1.08	.9277,2	1.1941	1.13492	1.05217	.9994,4	2.0819
1.09	.9196,5	1.2194	1.15199	1.05856	.9992,1	2.1072
1.10	.9117,7	1.2450	1.1691	1.06494	.9980,2	2.1328
1.11	.9040,8	1.2708	1.1862	1.07130	.9985,8	2.1588
1.12	.8965,6	1.2968	1.2034	1.07764	.9982,0	2.1851
1.13	.8892,2	1.3230	1.2206	1.08396	.9977,6	2.2118
1.14	.8820,4	1.3495	1.2378	1.09027	.9972,6	2.2388
1.15	.8750,2	1.3762	1.2550	1.09657	.9966,9	2.2661
1.16	.8681,6	1.4032	1.2723	1.10287	.9960,5	2.2937
1.17	.8614,5	1.4304	1.2896	1.10916	.9953,4	2.3217
1.18	.8548,8	1.4578	1.3069	1.11544	.9945,5	2.3499
1.19	.8484,6	1.4854	1.3243	1.12172	.9937,1	2.3786
1.20	.8421,7	1.5133	1.3416	1.1280	.9928,0	2.4075
1.21	.8360,1	1.5414	1.3590	1.1343	.9918,0	2.4367
1.22	.8299,8	1.5698	1.3764	1.1405	.9907,3	2.4662
1.23	.8240,8	1.5984	1.3938	1.1468	.9895,7	2.4961
1.24	.8183,0	1.6272	1.4112	1.1531	.9883,5	2.5263
1.25	.8126,4	1.6562	1.4286	1.1594	.9870,6	2.5568
1.26	.8070,9	1.6855	1.4460	1.1657	.9856,8	2.5876
1.27	.8016,5	1.7150	1.4634	1.1720	.9842,2	2.6187
1.28	.7963,1	1.7448	1.4808	1.1782	.9826,8	2.6500
1.29	.7910,8	1.7748	1.4983	1.1846	.9810,6	2.6816
1.30	.7859,6	1.8050	1.5157	1.1909	.9793,5	2.7135
1.31	.7809,3	1.8354	1.5331	1.1972	.9775,8	2.7457
1.32	.7760,0	1.8661	1.5505	1.2035	.9757,4	2.7783
1.33	.7711,6	1.8970	1.5680	1.2099	.9738,2	2.8112
1.34	.7664,1	1.9282	1.5854	1.2162	.9718,1	2.8444
1.35	.7617,5	1.9596	1.6028	1.2226	.9697,2	2.8778
1.36	.7571,8	1.9912	1.6202	1.2290	.9675,6	2.9115
1.37	.7526,9	2.0230	1.6376	1.2354	.9653,4	2.9455
1.38	.7482,8	2.0551	1.6550	1.2418	.9630,4	2.9798
1.39	.7439,6	2.0874	1.6723	1.2482	.9606,5	3.0144
1.40	.7397,1	2.1200	1.6896	1.2547	.9581,9	3.0493
1.41	.7355,4	2.1528	1.7070	1.2612	.9556,6	3.0844
1.42	.7314,4	2.1858	1.7243	1.2676	.9530,6	3.1198
1.43	.7274,1	2.2190	1.7416	1.2742	.9503,9	3.1555
1.44	.7234,5	2.2525	1.7589	1.2807	.9476,5	3.1915

Notes: (1) For values of M from 1.00 to 3.00, all digits to the left of the comma are valid for linear interpolation. Where no comma is indicated in this region, all digits are valid for linear interpolation.

TABLE B.3. NORMAL SHOCK (Continued)

Perfect Gas, $k = 1.4$

M_x	M_y	p_y/p_x	V_x/V_y and ρ_y/ρ_x	T_y/T_x	A_x^*/A_y^* and p_{0y}/p_{0x}	p_{0y}/p_x
1.45	.7195,6	2.2862	1.7761	1.2872	.9448,3	3.2278
1.46	.7157,4	2.3202	1.7934	1.2938	.9419,6	3.2643
1.47	.7119,8	2.3544	1.8106	1.3004	.9390,1	3.3011
1.48	.7082,9	2.3888	1.8278	1.3070	.9360,0	3.3382
1.49	.7046,6	2.4234	1.8449	1.3136	.9239,2	3.3756
1.50	.7010,9	2.4583	1.8621	1.3202	.9297,8	3.4133
1.51	.6975,8	2.4934	1.8792	1.3269	.9265,8	3.4512
1.52	.6941,3	2.5288	1.8962	1.3336	.9233,1	3.4894
1.53	.6907,3	2.5644	1.9133	1.3403	.9199,9	3.5279
1.54	.6873,9	2.6003	1.9303	1.3470	.9166,2	3.5667
1.55	.6841,0	2.6363	1.9473	1.3538	.9131,9	3.6058
1.56	.6808,6	2.6725	1.9643	1.3606	.9097,0	3.6451
1.57	.6776,8	2.7090	1.9812	1.3674	.9061,5	3.6847
1.58	.6745,5	2.7458	1.9981	1.3742	.9025,5	3.7245
1.59	.6714,7	2.7828	2.0149	1.3811	.8988,9	3.7645
1.60	.66844	2.8201	2.0317	1.3880	.8952,0	3.8049
1.61	.66545	2.8575	2.0485	1.3949	.8914,4	3.8456
1.62	.66251	2.8951	2.0652	1.4018	.8876,4	3.8866
1.63	.65962	2.9330	2.0820	1.4088	.8838,0	3.9278
1.64	.65677	2.9712	2.0986	1.4158	.8799,2	3.9693
1.65	.65396	3.0096	2.1152	1.4228	.87598	4.0111
1.66	.65119	3.0482	2.1318	1.4298	.87201	4.0531
1.67	.64847	3.0870	2.1484	1.4369	.86800	4.0954
1.68	.64579	3.1261	2.1649	1.4440	.86396	4.1379
1.69	.64315	3.1654	2.1813	1.4512	.85987	4.1807
1.70	.64055	3.2050	2.1977	1.4583	.85573	4.2238
1.71	.63798	3.2448	2.2141	1.4655	.85155	4.2672
1.72	.63545	3.2848	2.2304	1.4727	.84735	4.3108
1.73	.63296	3.3250	2.2467	1.4800	.84312	4.3547
1.74	.63051	3.3655	2.2629	1.4873	.83886	4.3989
1.75	.62809	3.4062	2.2791	1.4946	.83456	4.4433
1.76	.62570	3.4472	2.2952	1.5019	.83024	4.4880
1.77	.62335	3.4884	2.3113	1.5093	.82589	4.5330
1.78	.62104	3.5298	2.3273	1.5167	.82152	4.5783
1.79	.61875	3.5714	2.3433	1.5241	.81711	4.6238
1.80	.61650	3.6133	2.3592	1.5316	.81268	4.6695
1.81	.61428	3.6554	2.3751	1.5391	.80823	4.7155
1.82	.61209	3.6978	2.3909	1.5466	.80376	4.7618
1.83	.60993	3.7404	2.4067	1.5542	.79926	4.8083
1.84	.60780	3.7832	2.4224	1.5617	.79474	4.8551
1.85	.60570	3.8262	2.4381	1.5694	.79021	4.9022
1.86	.60363	3.8695	2.4537	1.5770	.78567	4.9498
1.87	.60159	3.9130	2.4693	1.5847	.78112	4.9974
1.88	.59957	3.9568	2.4848	1.5924	.77656	5.0453
1.89	.59758	4.0008	2.5003	1.6001	.77197	5.0934

See Notes at beginning of this table.

TABLE B.3. NORMAL SHOCK (Continued)

Perfect Gas, $k = 1.4$

M_x	M_y	p_y/p_x	V_x/V_y and ρ_y/ρ_x	T_y/T_x	A_x^*/A_y^* and p_{0y}/p_{0x}	p_{0y}/p_x
1.90	.59562	4.0450	2.5157	1.6079	.76735	5.1417
1.91	.59368	4.0894	2.5310	1.6157	.76273	5.1904
1.92	.59177	4.1341	2.5463	1.6236	.75812	5.2394
1.93	.58988	4.1790	2.5615	1.6314	.75347	5.2886
1.94	.58802	4.2242	2.5767	1.6394	.74883	5.3381
1.95	.58618	4.2696	2.5919	1.6473	.74418	5.3878
1.96	.58437	4.3152	2.6070	1.6553	.73954	5.4378
1.97	.58258	4.3610	2.6220	1.6633	.73487	5.4880
1.98	.58081	4.4071	2.6369	1.6713	.73021	5.5385
1.99	.57907	4.4534	2.6518	1.6794	.72554	5.5894
2.00	.57735	4.5000	2.6666	1.6875	.72088	5.6405
2.01	.57565	4.5468	2.6814	1.6956	.71619	5.6918
2.02	.57397	4.5938	2.6962	1.7038	.71152	5.7434
2.03	.57231	4.6411	2.7109	1.7120	.70686	5.7952
2.04	.57068	4.6886	2.7255	1.7203	.70218	5.8473
2.05	.56907	4.7363	2.7400	1.7286	.69752	5.8997
2.06	.56747	4.7842	2.7545	1.7369	.69284	5.9523
2.07	.56589	4.8324	2.7690	1.7452	.68817	6.0052
2.08	.56433	4.8808	2.7834	1.7536	.68351	6.0584
2.09	.56280	4.9295	2.7977	1.7620	.67886	6.1118
2.10	.56128	4.9784	2.8119	1.7704	.67422	6.1655
2.11	.55978	5.0275	2.8261	1.7789	.66957	6.2194
2.12	.55830	5.0768	2.8402	1.7874	.66492	6.2736
2.13	.55683	5.1264	2.8543	1.7960	.66029	6.3280
2.14	.55538	5.1762	2.8683	1.8046	.65567	6.3827
2.15	.55395	5.2262	2.8823	1.8132	.65105	6.4377
2.16	.55254	5.2765	2.8962	1.8219	.64644	6.4929
2.17	.55114	5.3270	2.9100	1.8306	.64185	6.5484
2.18	.54976	5.3778	2.9238	1.8393	.63728	6.6042
2.19	.54841	5.4288	2.9376	1.8481	.63270	6.6602
2.20	.54706	5.4800	2.9512	1.8569	.62812	6.7163
2.21	.54572	5.5314	2.9648	1.8657	.62358	6.7730
2.22	.54440	5.5831	2.9783	1.8746	.61905	6.8299
2.23	.54310	5.6350	2.9918	1.8835	.61453	6.8869
2.24	.54182	5.6872	3.0052	1.8924	.61002	6.9442
2.25	.54055	5.7396	3.0186	1.9014	.60554	7.0018
2.26	.53929	5.7922	3.0319	1.9104	.60106	7.0597
2.27	.53805	5.8451	3.0452	1.9194	.59659	7.1178
2.28	.53683	5.8982	3.0584	1.9285	.59214	7.1762
2.29	.53561	5.9515	3.0715	1.9376	.58772	7.2348
2.30	.53441	6.0050	3.0846	1.9468	.58331	7.2937
2.31	.53322	6.0588	3.0976	1.9560	.57891	7.3529
2.32	.53205	6.1128	3.1105	1.9652	.57452	7.4123
2.33	.53089	6.1670	3.1234	1.9745	.57015	7.4720
2.34	.52974	6.2215	3.1362	1.9838	.56580	7.5319

See Notes at beginning of this table.

TABLE B.3. NORMAL SHOCK (Continued)

Perfect Gas, $k = 1.4$

M_x	M_y	p_y/p_x	V_x/V_y and ρ_y/ρ_x	T_y/T_x	A_x^*/A_y^* and p_{0y}/p_{0x}	p_{0y}/p_x
2.35	.52861	6.2762	3.1490	1.9931	.56148	7.5920
2.36	.52749	6.3312	3.1617	2.0025	.55717	7.6524
2.37	.52638	6.3864	3.1743	2.0119	.55288	7.7131
2.38	.52528	6.4418	3.1869	2.0213	.54862	7.7741
2.39	.52419	6.4974	3.1994	2.0308	.54438	7.8354
2.40	.52312	6.5533	3.2119	2.0403	.54015	7.8969
2.41	.52206	6.6094	3.2243	2.0499	.53594	7.9587
2.42	.52100	6.6658	3.2366	2.0595	.53175	8.0207
2.43	.51996	6.7224	3.2489	2.0691	.52758	8.0830
2.44	.51894	6.7792	3.2611	2.0788	.52344	8.1455
2.45	.51792	6.8362	3.2733	2.0885	.51932	8.2083
2.46	.51691	6.8935	3.2854	2.0982	.51521	8.2714
2.47	.51592	6.9510	3.2975	2.1080	.51112	8.3347
2.48	.51493	7.0088	3.3095	2.1178	.50706	8.3983
2.49	.51395	7.0668	3.3214	2.1276	.50303	8.4622
2.50	.51299	7.1250	3.3333	2.1375	.49902	8.5262
2.51	.51204	7.1834	3.3451	2.1474	.49502	8.5904
2.52	.51109	7.2421	3.3569	2.1574	.49104	8.6549
2.53	.51015	7.3010	3.3686	2.1674	.48709	8.7198
2.54	.50923	7.3602	3.3802	2.1774	.48317	8.7850
2.55	.50831	7.4196	3.3918	2.1875	.47927	8.8505
2.56	.50740	7.4792	3.4034	2.1976	.47540	8.9162
2.57	.50651	7.5391	3.4149	2.2077	.47155	8.9821
2.58	.50562	7.5992	3.4263	2.2179	.46772	9.0482
2.59	.50474	7.6595	3.4376	2.2281	.46391	9.1146
2.60	.50387	7.7200	3.4489	2.2383	.46012	9.1813
2.61	.50301	7.7808	3.4602	2.2486	.45636	9.2481
2.62	.50216	7.8418	3.4714	2.2589	.45262	9.3154
2.63	.50132	7.9030	3.4825	2.2693	.44891	9.3829
2.64	.50048	7.9645	3.4936	2.2797	.44522	9.4507
2.65	.49965	8.0262	3.5047	2.2901	.44155	9.5187
2.66	.49883	8.0882	3.5157	2.3006	.43791	9.5869
2.67	.49802	8.1504	3.5266	2.3111	.43429	9.6553
2.68	.49722	8.2128	3.5374	2.3217	.43070	9.7241
2.69	.49642	8.2754	3.5482	2.3323	.42713	9.7932
2.70	.49563	8.3383	3.5590	2.3429	.42359	9.8625
2.71	.49485	8.4014	3.5697	2.3536	.42007	9.9320
2.72	.49408	8.4648	3.5803	2.3643	.41657	10.0017
2.73	.49332	8.5284	3.5909	2.3750	.41310	10.0718
2.74	.49256	8.5922	3.6014	2.3858	.40965	10.1421
2.75	.49181	8.6562	3.6119	2.3966	.40622	10.212
2.76	.49107	8.7205	3.6224	2.4074	.40282	10.283
2.77	.49033	8.7850	3.6328	2.4183	.39945	10.354
2.78	.48960	8.8497	3.6431	2.4292	.39610	10.426
2.79	.48888	8.9147	3.6533	2.4402	.39276	10.498

TABLE B.3. NORMAL SHOCK (Concluded)

Perfect Gas, $k = 1.4$

M_x	M_y	p_y/p_x	V_x/V_y and ρ_y/ρ_x	T_y/T_x	A_x^*/A_y^* and p_{0y}/p_{0x}	p_{0y}/p_x
2.80	.48817	8.9800	3.6635	2.4512	.38946	10.569
2.81	.48746	9.0454	3.6737	2.4622	.38618	10.641
2.82	.48676	9.1111	3.6838	2.4733	.38293	10.714
2.83	.48607	9.1770	3.6939	2.4844	.37970	10.787
2.84	.48538	9.2432	3.7039	2.4955	.37649	10.860
2.85	.48470	9.3096	3.7139	2.5067	.37330	10.933
2.86	.48402	9.3762	3.7238	2.5179	.37013	11.006
2.87	.48334	9.4431	3.7336	2.5292	.36700	11.080
2.88	.48268	9.5102	3.7434	2.5405	.36389	11.154
2.89	.48203	9.5775	3.7532	2.5518	.36080	11.228
2.90	.48138	9.6450	3.7629	2.5632	.35773	11.302
2.91	.48074	9.7127	3.7725	2.5746	.35469	11.377
2.92	.48010	9.7808	3.7821	2.5860	.35167	11.452
2.93	.47946	9.8491	3.7917	2.5975	.34867	11.527
2.94	.47883	9.9176	3.8012	2.6090	.34570	11.603
2.95	.47821	9.9863	3.8106	2.6206	.34275	11.679
2.96	.47760	10.055	3.8200	2.6322	.33982	11.755
2.97	.47699	10.124	3.8294	2.6438	.33692	11.831
2.98	.47638	10.194	3.8387	2.6555	.33404	11.907
2.99	.47578	10.263	3.8479	2.6672	.33118	11.984
3.00	.47519	10.333	3.8571	2.6790	.32834	12.061
3.50	.45115	14.125	4.2608	3.3150	.21295	16.242
4.00	.43496	18.500	4.5714	4.0469	.13876	21.068
4.50	.42355	23.458	4.8119	4.8751	.09170	26.539
5.00	.41523	29.000	5.0000	5.8000	.06172	32.654
6.00	.40416	41.833	5.2683	7.9406	.02965	46.815
7.00	.39736	57.000	5.4444	10.469	.01535	63.552
8.00	.39289	74.500	5.5652	13.387	.00849	82.865
9.00	.38980	94.333	5.6512	16.693	.00496	104.753
10.00	.38757	116.500	5.7143	20.388	.00304	129.217
∞	.37796	∞	6.0000	∞	0	∞

See Notes at beginning of this table.

See Notes at beginning of this table.

TABLE B.4

FRictional, Adiabatic, Constant-Area Flow (FANNO Line)
Perfect Gas, $k = 1.4$

M	T/T^*	p/p^*	p_0/p_0^*	V/V^* and ρ^*/ρ	F/F^*	$4fL_{\max}/D$
0.00	1.2000	∞	∞	0.00000	∞	∞
.05	1.1994	21.903	11.5914	.05476	9.1584	280.02
.10	1.1976	10.9435	5.8218	.10943	4.6236	66.922
.15	1.1946	7.2866	3.9103	.16395	3.1317	27.932
.20	1.1905	5.4555	2.9635	.21822	2.4004	14.533
.25	1.1852	4.3546	2.4027	.27217	1.9732	8.4834
.30	1.1788	3.6190	2.0351	.32572	1.6979	5.2992
.35	1.1713	3.0922	1.7780	.37880	1.5094	3.4825
.40	1.1628	2.6958	1.5901	.43133	1.3749	2.3085
.45	1.1533	2.3865	1.4486	.48326	1.2763	1.5664
.50	1.1429	2.1381	1.3399	.53453	1.2027	1.06908
.55	1.1315	1.9341	1.2549	.58506	1.1472	.72805
.60	1.1194	1.7634	1.1882	.63481	1.10504	.49081
.65	1.10650	1.6183	1.1356	.68374	1.07314	.32460
.70	1.09290	1.4934	1.09436	.73179	1.04915	.20814
.75	1.07856	1.3848	1.06242	.77893	1.03137	.12728
.80	1.06383	1.2892	1.03823	.82514	1.01853	.07229
.85	1.04849	1.2047	1.02067	.87037	1.00966	.03632
.90	1.03270	1.12913	1.00887	.91459	1.00399	.014513
.95	1.01652	1.06129	1.00215	.95782	1.00093	.003280
1.00	1.00000	1.00000	1.00000	1.00000	1.00000	0
1.05	.98320	.94435	1.00203	1.04115	1.00082	.002712
1.10	.96618	.89359	1.00793	1.08124	1.00305	.009933
1.15	.94899	.84710	1.01746	1.1203	1.00646	.02053
1.20	.93168	.80436	1.03044	1.1583	1.01082	.03364
1.25	.91429	.76495	1.04676	1.1952	1.01594	.04858
1.30	.89686	.72848	1.06630	1.2311	1.02169	.06483
1.35	.87944	.69466	1.08904	1.2660	1.02794	.08199
1.40	.86207	.66320	1.1149	1.2999	1.03458	.09974
1.45	.84477	.63387	1.1440	1.3327	1.04153	.11782
1.50	.82759	.60648	1.1762	1.3646	1.04870	.13605
1.55	.81054	.58084	1.2116	1.3955	1.05604	.15427
1.60	.79365	.55679	1.2502	1.4254	1.06348	.17236
1.65	.77695	.53421	1.2922	1.4544	1.07098	.19022
1.70	.76046	.51297	1.3376	1.4825	1.07851	.20780
1.75	.74419	.49295	1.3865	1.5097	1.08603	.22504
1.80	.72816	.47407	1.4390	1.5360	1.09352	.24189
1.85	.71238	.45623	1.4952	1.5614	1.1009	.25832
1.90	.69686	.43936	1.5552	1.5861	1.1083	.27433
1.95	.68162	.42339	1.6193	1.6099	1.1155	.28989
2.00	.66667	.40825	1.6875	1.6330	1.1227	.30499
2.05	.65200	.39389	1.7600	1.6553	1.1297	.31965
2.10	.63762	.38024	1.8369	1.6769	1.1366	.33385
2.15	.62354	.36728	1.9185	1.6977	1.1434	.34760
2.20	.60976	.35494	2.0050	1.7179	1.1500	.36091

TABLE B.4. FRICTIONAL, ADIABATIC, CONSTANT-AREA FLOW (FANNO LINE)
(Concluded)

M	T/T^*	p/p^*	p_0/p_0^*	V/V^* and ρ^*/ρ	F/F^*	$4fL_{\max}/D$
2.25	.59627	.34319	2.0964	1.7374	1.1565	.37378
2.30	.58309	.33200	2.1931	1.7563	1.1629	.38623
2.35	.57021	.32133	2.2953	1.7745	1.1690	.39826
2.40	.55762	.31114	2.4031	1.7922	1.1751	.40989
2.45	.54533	.30141	2.5168	1.8092	1.1810	.42113
2.50	.53333	.29212	2.6367	1.8257	1.1867	.43197
2.55	.52163	.28323	2.7630	1.8417	1.1923	.44247
2.60	.51020	.27473	2.8960	1.8571	1.1978	.45259
2.65	.49906	.26658	3.0359	1.8721	1.2031	.46237
2.70	.48820	.25878	3.1830	1.8865	1.2083	.47182
2.75	.47761	.25131	3.3376	1.9005	1.2133	.48095
2.80	.46729	.24414	3.5001	1.9140	1.2182	.48976
2.85	.45723	.23726	3.6707	1.9271	1.2230	.49828
2.90	.44743	.23066	3.8498	1.9398	1.2277	.50651
2.95	.43788	.22431	4.0376	1.9521	1.2322	.51447
3.00	.42857	.21822	4.2346	1.9640	1.2366	.52216
3.50	.34783	.16850	6.7896	2.0642	1.2743	.58643
4.00	.28571	.13363	10.719	2.1381	1.3029	.63306
4.50	.23762	.10833	16.562	2.1936	1.3247	.66764
5.00	.20000	.08944	25.000	2.2361	1.3416	.69381
6.00	.14634	.06376	53.180	2.2953	1.3655	.72987
7.00	.11111	.04762	104.14	2.3333	1.3810	.75281
8.00	.08696	.03686	190.11	2.3591	1.3915	.76820
9.00	.06977	.02935	327.19	2.3772	1.3989	.77898
10.00	.05714	.02390	535.94	2.3905	1.4044	.78683
∞	0	0	∞	2.4495	1.4289	.82153

TABLE B.5

FRICTIONLESS, CONSTANT-AREA FLOW WITH CHANGE IN STAGNATION TEMPERATURE
(RAYLEIGH LINE)Perfect Gas, $k = 1.4$

M	T_0/T_0^*	T/T^*	p/p^*	p_0/p_0^*	ρ^*/ρ and V/V^*
0.00	0.00000	0.00000	2.4000	1.2679	0.00000
.05	.01192	.01430	2.3916	1.2657	.00598
.10	.04678	.05602	2.3669	1.2591	.02367
.15	.10196	.12181	2.3267	1.2486	.05235
.20	.17355	.20661	2.2727	1.2346	.09091
.25	.25684	.30440	2.2069	1.2177	.13793
.30	.34686	.40887	2.1314	1.1985	.19183
.35	.43894	.51413	2.0487	1.1779	.25096
.40	.52903	.61515	1.9608	1.1566	.31372
.45	.61393	.70803	1.8699	1.1351	.37865
.50	.69136	.79012	1.7778	1.1140	.44445
.55	.75991	.85987	1.6860	1.09397	.51001
.60	.81892	.91670	1.5957	1.07525	.57447
.65	.86833	.96081	1.5080	1.05820	.63713
.70	.90850	.99289	1.4235	1.04310	.69751
.75	.94009	1.01403	1.3427	1.03010	.75525
.80	.96394	1.02548	1.2658	1.01934	.81012
.85	.98097	1.02854	1.1931	1.01091	.86204
.90	.99207	1.02451	1.1246	1.00485	.91097
.95	.99814	1.01463	1.06030	1.00121	.95692
1.00	1.00000	1.00000	1.00000	1.00000	1.00000
1.05	.99838	.98161	.94358	1.00121	1.04030
1.10	.99392	.96031	.89086	1.00486	1.07795
1.15	.98721	.93685	.84166	1.01092	1.1131
1.20	.97872	.91185	.79576	1.01941	1.1459
1.25	.96886	.88581	.75294	1.03032	1.1764
1.30	.95798	.85917	.71301	1.04365	1.2050
1.35	.94636	.83227	.67577	1.05943	1.2316
1.40	.93425	.80540	.64102	1.07765	1.2564
1.45	.92184	.77875	.60860	1.0983	1.2796
1.50	.90928	.75250	.57831	1.1215	1.3012
1.55	.89669	.72680	.55002	1.1473	1.3214
1.60	.88419	.70173	.52356	1.1756	1.3403
1.65	.87184	.67738	.49881	1.2066	1.3580
1.70	.85970	.65377	.47563	1.2402	1.3745
1.75	.84785	.63096	.45390	1.2767	1.3901
1.80	.83628	.60894	.43353	1.3159	1.4046
1.85	.82504	.58773	.41440	1.3581	1.4183
1.90	.81414	.56734	.39643	1.4033	1.4311
1.95	.80359	.54774	.37954	1.4516	1.4432
2.00	.79339	.52893	.36364	1.5031	1.4545
2.05	.78355	.51087	.34866	1.5579	1.4652
2.10	.77406	.49356	.33454	1.6161	1.4753
2.15	.76493	.47696	.32122	1.6780	1.4849
2.20	.75614	.46106	.30864	1.7434	1.4939

TABLE B.5. FRICTIONLESS, CONSTANT-AREA FLOW WITH CHANGE IN STAGNATION
TEMPERATURE (RAYLEIGH LINE) (Concluded)Perfect Gas, $k = 1.4$

M	T_0/T_0^*	T/T^*	p/p^*	p_0/p_0^*	ρ^*/ρ and V/V^*
2.25	.74767	.44582	.29675	1.8128	1.5024
2.30	.73954	.43122	.28551	1.8860	1.5104
2.35	.73173	.41724	.27487	1.9634	1.5180
2.40	.72421	.40383	.26478	2.0450	1.5252
2.45	.71700	.39100	.25523	2.1311	1.5320
2.50	.71005	.37870	.24616	2.2218	1.5385
2.55	.70340	.36691	.23754	2.3173	1.5446
2.60	.69699	.35561	.22936	2.4177	1.5505
2.65	.69084	.34478	.22158	2.5233	1.5560
2.70	.68494	.33439	.21417	2.6342	1.5613
2.75	.67926	.32442	.20712	2.7508	1.5663
2.80	.67380	.31486	.20040	2.8731	1.5711
2.85	.66855	.30568	.19399	3.0013	1.5757
2.90	.66350	.29687	.18788	3.1358	1.5801
2.95	.65865	.28841	.18205	3.2768	1.5843
3.00	.65398	.28028	.17647	3.4244	1.5882
3.50	.61580	.21419	.13223	5.3280	1.6198
4.00	.58909	.16831	.10256	8.2268	1.6410
4.50	.56983	.13540	.08177	12.502	1.6559
5.00	.55555	.11111	.06667	18.634	1.6667
6.00	.53633	.07849	.04669	38.946	1.6809
7.00	.52437	.05826	.03448	75.414	1.6896
8.00	.51646	.04491	.02649	136.62	1.6954
9.00	.51098	.03565	.02098	233.88	1.6993
10.00	.50702	.02897	.01702	381.62	1.7021
∞	.48980	0	0	∞	1.7143

TABLE B.6
INFLUENCE COEFFICIENTS

k = 1.4

<i>M</i>	<i>M</i> ²	1 - <i>M</i> ²	<i>F</i> _A	<i>F</i> _f	<i>F</i> _{T₀} and <i>F</i> _{w/2}	<i>F</i> _Q and - <i>F</i> _w
0	0	1.0000	0	0	0	0
.05	.0025	.9975	-.00501	.05878	.00251	.00252
.10	.0100	.9900	-.02024	.03142	.01026	.01024
.15	.0225	.9775	-.04624	.03728	.02385	.02374
.20	.0400	.9600	-.08400	.00235	.04435	.04400
.25	.0625	.9375	-.13500	.00590	.07341	.07250
.30	.0900	.9100	-.20136	.01268	.11336	.11136
.35	.1225	.8775	-.28603	.02453	.16755	.16354
.40	.1600	.8400	-.39314	.04403	.24060	.23314
.45	.2025	.7975	-.52840	.07490	.33910	.32590
.50	.2500	.7500	-.70000	.12250	.47250	.45000
.55	.3025	.6975	-.91986	.19478	.65471	.61736
.60	.3600	.6400	-.1.2060	.30391	.90691	.84600
.65	.4225	.5775	-.1.5868	.46931	1.2627	1.1643
.70	.4900	.5100	-.2.1099	.72369	1.7787	1.6198
.75	.5625	.4375	-.2.8607	1.1264	2.5568	2.2982
.80	.6400	.3600	-.4.0107	1.7968	3.8021	3.3707
.85	.7225	.2775	-.5.9596	3.0141	5.9939	5.2371
.90	.8100	.1900	-.9.9076	5.6176	10.571	9.0976
.95	.9025	.0975	-.21.854	13.806	24.734	20.952
1.00	1.0000	0	∞	∞	∞	∞
1.05	1.1025	-.1025	26.256	-.20.263	-.33.391	-.27.358
1.10	1.2100	-.2100	14.312	-.12.1228	-.19.279	-.15.523
1.15	1.3225	-.3225	10.3708	-.9.6008	-.14.786	-.11.6934
1.20	1.4400	-.4400	8.4905	-.8.4980	-.12.713	-.9.8706
1.25	1.5625	-.5625	7.2917	-.7.9752	-.11.621	-.8.8542
1.30	1.6900	-.6900	6.5543	-.7.7537	-.11.031	-.8.2443
1.35	1.8225	-.8225	6.0469	-.7.7144	-.10.738	-.7.8694
1.40	1.9600	-.9600	5.6840	-.7.7984	-.10.640	-.7.6440
1.45	2.1025	-.1.1025	5.4179	-.7.9738	-.10.683	-.7.5204
1.50	2.2500	-.1.2500	5.2200	-.8.2215	-.10.832	-.7.4700
1.55	2.4025	-.1.4025	5.0722	-.8.5302	-.11.066	-.7.4748
1.60	2.5600	-.1.5600	4.9625	-.8.8927	-.11.374	-.7.5225
1.65	2.7225	-.1.7225	4.8823	-.9.3045	-.11.746	-.7.6048
1.70	2.8900	-.1.8900	4.8258	-.9.7627	-.12.175	-.7.7158
1.75	3.0625	-.2.0625	4.7886	-.10.266	-.12.660	-.7.8511
1.80	3.2400	-.2.2400	4.7674	-.10.812	-.13.196	-.8.0074
1.85	3.4225	-.2.4225	4.7597	-.11.403	-.13.783	-.8.1822
1.90	3.6100	-.2.6100	4.7635	-.12.038	-.14.419	-.8.3735
1.95	3.8025	-.2.8025	4.7774	-.12.716	-.15.105	-.8.5799
2.00	4.0000	-.3.0000	4.8000	-.13.440	-.15.840	-.8.8000
2.05	4.2025	-.3.2025	4.8305	-.14.210	-.16.625	-.9.0329
2.10	4.4100	-.3.4100	4.8678	-.15.027	-.17.461	-.9.2778
2.15	4.6225	-.3.6225	4.9115	-.15.892	-.18.348	-.9.5340
2.20	4.8400	-.3.8400	4.9610	-.16.808	-.19.288	-.9.8010

The notation .03429 signifies 0.000429. The notation 5370₄ signifies 5,370,000.

TABLE B.6. INFLUENCE COEFFICIENTS (Concluded)

k = 1.4

<i>M</i>	<i>M</i> ²	1 - <i>M</i> ²	<i>F</i> _A	<i>F</i> _f	<i>F</i> _{T₀} and <i>F</i> _{w/2}	<i>F</i> _Q and - <i>F</i> _w
2.25	5.0625	-.4.0625	5.0158	-.17.775	-.20.282	-.10.078
2.30	5.2900	-.4.2900	5.0754	-.18.794	-.21.332	-.10.365
2.35	5.5225	-.4.5225	5.1397	-.19.868	-.22.439	-.10.662
2.40	5.7600	-.4.7600	5.2082	-.21.000	-.23.604	-.10.968
2.45	6.0025	-.5.0025	5.2807	-.22.188	-.24.829	-.11.283
2.50	6.2500	-.5.2500	5.3571	-.23.438	-.26.116	-.11.607
2.55	6.5025	-.5.5025	5.4372	-.24.748	-.27.467	-.11.940
2.60	6.7600	-.5.7600	5.5207	-.26.124	-.28.884	-.12.281
2.65	7.0225	-.6.0225	5.6075	-.27.565	-.30.369	-.12.630
2.70	7.2900	-.6.2900	5.6975	-.29.075	-.31.924	-.12.987
2.75	7.5625	-.6.5625	5.7907	-.30.655	-.33.550	-.13.353
2.80	7.8400	-.6.8400	5.8869	-.32.308	-.35.250	-.13.727
2.85	8.1225	-.7.1225	5.9859	-.34.035	-.37.028	-.14.108
2.90	8.4100	-.7.4100	6.0879	-.35.839	-.38.884	-.14.498
2.95	8.7025	-.7.7025	6.1926	-.37.723	-.40.820	-.14.895
3.00	9.00	-.8.00	6.3000	-.39.690	-.42.840	-.15.300
3.50	12.25	-.11.25	7.5133	-.64.427	-.68.184	-.19.763
4.00	16.00	-.15.00	8.9600	-.100.352	-.104.832	-.24.960
4.50	20.25	-.19.25	10.6247	-.150.605	-.155.918	-.30.875
5.00	25.00	-.24.00	12.5000	-.218.750	-.225.000	-.37.500
6.00	36.00	-.35.00	16.869	-.425.09	-.433.52	-.52.869
7.00	49.00	-.48.00	22.050	-.756.32	-.767.34	-.71.050
8.00	64.00	-.63.00	28.038	-.1256.11	-.1270.13	-.92.038
9.00	81.00	-.80.00	34.830	-.1974.86	-.1992.28	-.115.830
10.00	100.00	-.99.00	42.424	-.2969.69	-.2990.91	-.142.424
	∞	∞	$-\infty$	∞	$-\infty$	$-\infty$

TABLE B.7

HODOGRAPH CHARACTERISTIC FUNCTIONS FOR TWO-DIMENSIONAL, ISENTROPIC, SUPersonic FLOW, $k = 1.4$
(ω and α are in degrees)

ω	α	$\alpha - \omega$	M	ω	α	$\alpha - \omega$	M
0.0	90.0000	90.0000	1.0000	45.0	21.2068	-23.7932	2.7644
1.0	67.5741	66.5741	1.0818	46.0	20.8297	-25.1703	2.8122
2.0	61.9969	59.9969	1.1326	47.0	20.4594	-26.5406	2.8609
3.0	58.1805	55.1805	1.1769	48.0	20.0956	-27.9044	2.9105
4.0	55.2048	51.2048	1.2177	49.0	19.7380	-29.2620	2.9610
5.0	52.7383	47.7383	1.2565	50.0	19.3865	-30.6135	3.0126
6.0	50.6186	44.6186	1.2938	51.0	19.0408	-31.9592	3.0652
7.0	48.7528	41.7528	1.3300	52.0	18.7005	-33.2995	3.1189
8.0	47.0818	39.0818	1.3655	53.0	18.3657	-34.6343	3.1738
9.0	45.5660	36.5660	1.4004	54.0	18.0360	-35.9640	3.2298
10.0	44.1770	34.1770	1.4349	55.0	17.7112	-37.2888	3.2871
11.0	42.8940	31.8940	1.4692	56.0	17.3911	-38.6089	3.3457
12.0	41.7007	29.7007	1.5032	57.0	17.0757	-39.9243	3.4056
13.0	40.5849	27.5849	1.5371	58.0	16.7646	-41.2354	3.4669
14.0	39.5366	25.5366	1.5709	59.0	16.4579	-42.5421	3.5297
15.0	38.5474	23.5474	1.6047	60.0	16.1552	-43.8448	3.5940
16.0	37.6108	21.6108	1.6385	61.0	15.8564	-45.1436	3.6600
17.0	36.7212	19.7212	1.6725	62.0	15.5615	-46.4385	3.7276
18.0	35.8739	17.8739	1.7065	63.0	15.2703	-47.7297	3.7969
19.0	35.0648	16.0648	1.7406	64.0	14.9826	-49.0174	3.8681
20.0	34.2904	14.2904	1.7750	65.0	14.6983	-50.3017	3.9412
21.0	33.5479	12.5479	1.8095	66.0	14.4174	-51.5826	4.0163
22.0	32.8344	10.8344	1.8443	67.0	14.1396	-52.8604	4.0936
23.0	32.1478	9.1478	1.8793	68.0	13.8650	-54.1350	4.1730
24.0	31.4859	7.4859	1.9146	69.0	13.5934	-55.4066	4.2548
25.0	30.8469	5.8469	1.9503	70.0	13.3247	-56.6753	4.3390
26.0	30.2293	4.2293	1.9862	71.0	13.0587	-57.9413	4.4258
27.0	29.6316	2.6316	2.0226	72.0	12.7955	-59.2045	4.5152
28.0	29.0524	1.0524	2.0593	73.0	12.5349	-60.4651	4.6076
29.0	28.4906	-0.5094	2.0964	74.0	12.2768	-61.7232	4.7029
30.0	27.9451	-2.0549	2.1339	75.0	12.0212	-62.9788	4.8014
31.0	27.4149	-3.5851	2.1718	76.0	11.7680	-64.2320	4.9032
32.0	26.8991	-5.1009	2.2103	77.0	11.5170	-65.4830	5.0085
33.0	26.3970	-6.6030	2.2492	78.0	11.2683	-66.7317	5.1176
34.0	25.9076	-8.0924	2.2887	79.0	11.0217	-67.9783	5.2306
35.0	25.4304	-9.5696	2.3287	80.0	10.7772	-69.2228	5.3479
36.0	24.9648	-11.0352	2.3693	85.0	9.5837	-75.4163	6.0064
37.0	24.5101	-12.4899	2.4105	90.0	8.4328	-81.5672	6.8190
38.0	24.0657	-13.9343	2.4523	95.0	7.3178	-87.6822	7.8509
39.0	23.6313	-15.3687	2.4947	100.0	6.2330	-93.7670	9.2105
40.0	23.2061	-16.7939	2.5378	105.0	5.1730	-99.8270	11.091
41.0	22.7900	-18.2100	2.5816	110.0	4.1331	-105.8669	13.874
42.0	22.3824	-19.6176	2.6261	115.0	3.1090	-111.8910	18.438
43.0	21.9828	-21.0172	2.6714	120.0	2.0965	-117.9035	27.335
44.0	21.5911	-22.4089	2.7176	125.0	1.0916	-123.9084	52.491
				130.0	.0908	-129.9092	631.03

TABLE B.8

COEFFICIENTS FOR SECOND-ORDER THEORY OF TWO-DIMENSIONAL, SUPersonic FLOW, $k = 1.4$

M_∞	C_1	C_2	M_∞	C_1	C_2	M_∞	C_1	C_2
1.02	9.950	746.293	2.02	1.140	1.456	3.02	.702	1.268
1.04	7.001	186.333	2.04	1.125	1.447	3.04	.697	1.266
1.06	5.689	82.987	2.06	1.110	1.437	3.06	.692	1.265
1.08	4.903	46.943	2.08	1.097	1.429	3.08	.687	1.264
1.10	4.364	30.315	2.10	1.083	1.420	3.10	.682	1.263
1.12	3.965	21.313	2.12	1.070	1.413	3.12	.677	1.262
1.14	3.654	15.905	2.14	1.057	1.405	3.14	.672	1.260
1.16	3.402	12.404	2.16	1.045	1.398	3.16	.667	1.259
1.18	3.193	10.013	2.18	1.032	1.392	3.18	.663	1.258
1.20	3.015	8.307	2.20	1.021	1.386	3.20	.658	1.257
1.22	2.862	7.050	2.22	1.009	1.380	3.22	.653	1.256
1.24	2.728	6.096	2.24	.998	1.374	3.24	.649	1.256
1.26	2.609	5.356	2.26	.987	1.369	3.26	.645	1.255
1.28	2.503	4.771	2.28	.976	1.363	3.28	.640	1.254
1.30	2.408	4.300	2.30	.966	1.358	3.30	.636	1.253
1.32	2.321	3.916	2.32	.955	1.354	3.32	.632	1.252
1.34	2.242	3.598	2.34	.945	1.349	3.34	.628	1.251
1.36	2.170	3.333	2.36	.936	1.345	3.36	.623	1.250
1.38	2.103	3.109	2.38	.926	1.341	3.38	.619	1.249
1.40	2.041	2.919	2.40	.917	1.337	3.40	.615	1.249
1.42	1.984	2.755	2.42	.908	1.333	3.42	.612	1.248
1.44	1.930	2.614	2.44	.899	1.330	3.44	.608	1.247
1.46	1.880	2.491	2.46	.890	1.326	3.46	.604	1.246
1.48	1.833	2.383	2.48	.881	1.323	3.48	.600	1.246
1.50	1.789	2.288	2.50	.873	1.320	3.50	.596	1.245
1.52	1.747	2.204	2.52	.865	1.317	3.60	.578	1.242
1.54	1.708	2.129	2.54	.857	1.314	3.70	.561	1.239
1.56	1.670	2.063	2.56	.849	1.311	3.80	.546	1.236
1.58	1.635	2.003	2.58	.841	1.308	3.90	.531	1.234
1.60	1.601	1.949	2.60	.833	1.306	4.00	.516	1.232
1.62	1.569	1.901	2.62	.826	1.303	4.10	.503	1.230
1.64	1.539	1.858	2.64	.819	1.301	4.20	.490	1.228
1.66	1.509	1.817	2.66	.811	1.298	4.30	.478	1.227
1.68	1.481	1.781	2.68	.804	1.296	4.40	.467	1.225
1.70	1.455	1.748	2.70	.797	1.294	4.50	.456	1.224
1.72	1.429	1.717	2.72	.791	1.292	4.60	.445	1.223
1.74	1.405	1.689	2.74	.784	1.290	4.70	.436	1.222
1.76	1.381	1.663	2.76	.777	1.288	4.80	.426	1.221
1.78	1.358	1.640	2.78	.771	1.286	4.90	.417	1.220
1.80	1.336	1.618	2.80	.765	1.284	5.00	.408	1.219
1.82	1.315	1.597	2.82	.759	1.282	6.00	.338	1.212
1.84	1.295	1.579	2.84	.752	1.281	7.00	.289	1.209
1.86	1.275	1.561	2.86	.746	1.279	8.00	.252	1.207
1.88	1.253	1.545	2.88	.741	1.277	9.00	.224	1.205
1.90	1.238	1.529	2.90	.735	1.276	10.00	.201	1.204
1.92	1.220	1.515	2.92	.729	1.274	15.00	.134	1.202
1.94	1.203	1.502	2.94	.723	1.273	20.00	.100	1.201
1.96	1.186	1.489	2.96	.718	1.271	100.00	.020	1.200
1.98	1.170	1.478	2.98	.712	1.270			
2.00	1.155	1.467	3.00	.707	1.269			

INDEX

(References are to pages of Vol. I only.)

- Absolute temperature scale, 32
Accelerating flows, 507
Acoustics, 48
Action, zone of, 500
Adiabatic ellipse, 58-59
Adiabatic flow
 critical velocity for, 79-81
 dimensionless velocity M^* of, 81-82
 energy equation of, 80-81
 flow per unit area of, 82
 maximum velocity for, 79-81
 one-dimensional, 160-178
 of perfect gas, 78-82
 at constant area, 162-73
 stagnation-temperature ratio for, 80
 Adiabatic process, definition of, 29
 entropy change for, 34
Adiabatic wall temperature, 211-12
Affine transformation, 319
Air, properties of, 612
Airfoils; *see also* Wings
 biconvex, 568
 completely symmetrical, 574
 double-wedge, 568
 lift-drag polars of, 571
 shock-characteristic theory of, 566
 subsonic
 pressure distributions for, 379-81
 at supersonic speeds, 571
 thickness of, 384-87
 in wind tunnel, 378
 without stagnation points; *see* Bump
 supersonic
 aerodynamically optimum, 575
 biplane, 579
 center of pressure of, 444, 446, 574
 downwash of, 576
 drag of, 442, 446, 572
 experimental data for, 447-48
 flow past, 501
 induced drag of, 442
 lift of, 441, 445, 472
 lift-drag polar of, 446
 lift-drag ratio of, 443
 linearized theory of, 440-49
 of minimum thickness drag, 575
 moment of, 444, 572
 performance of, 445
 pressure drag of, 442
 second-order theory of, 571-78
 shape of, 571
 skin-friction drag of, 443
 theory vs. experiment, 575
 thickness drag of, 443
 trailing-edge flow of, 584
 two-dimensional, 567-80
 types of, 575
 wake of, 578
 wave drag of, 443
 thin, supersonic flow for, 427
 triangular profile, 574
 two-dimensional, 567-80
Analogue techniques, 289
Angular velocity, 269
Area change, flow with, 219-55
Area change and friction, flow with, 241-42
Area ratio, for isentropic flow, 85-86
Aspect ratio, effect on compressibility, 400, 411-15
 generalized correlation of, 422
Atmosphere, properties of, 612
Atomic explosion, 211
Axially symmetric flow, 291, 294-95, 299, 596
Ballistics, 49
Barotropic fluid, 278
Bend, concave, 583
Bernoulli constant, 276
Bernoulli's equation, 276, 278
Biconvex airfoil, 568
Biplane, supersonic, 455, 579
Body, free, 11
Body, isolated, 11
Body forces, 18
Body of revolution; *see* Revolution, body of
Bomb, drag of, 408
Borda re-entrant orifice, 111
Boundary layer, 10, 265-66, 282, 379
 displacement thickness of, 266
 and interaction with shocks, 135-37, 266, 381-82, 580-84
 and pressure distribution, 308
 separation of, 379, 380, 415
Boundary of system, 11
Bump, flow past, 350, 372-74
Burning, slow, 207-11
Camber, in subsonic flow, 384-87
Cancellation of waves, 450, 452, 493
Cauchy-Riemann equations, 351
Cavitation, 475
Center of pressure, of supersonic airfoils, 446, 572

Centered waves, 474; *see also* Corner flow; Prandtl-Meyer wave
streamlines of, 525
Chapman-Jouguet rule, 210-11
Characteristic coordinates, 478
Characteristic curves, 482-86, 598; *see also* Method of characteristics
equations of, 602
hodograph, 599
initial-value theorem of, 603-6
method of constructing, 603-6
orthogonality relation for, 485, 603
physical, 599
properties of, 601
and shocks, 601
as solutions, 601
Characteristic function
series expression of, 561
table of, 632
Characteristic quadrilateral, 498, 499
Characteristics; *see also* Hodograph characteristic; Method of characteristics
hodograph, 467-68, 478, 485
table of, 468
working chart of, 467
method of, 462-523; *see also* Characteristic curves; Method of characteristics
illustrative example of, 479, 486-89
rules for using, 478
unit processes for, 492-94
physical, 484
physical significance of, 499
theory of, 482-91, 595-608
Chemical reaction, flow with, 206-11, 219-55; *see also* Simple T_0 -Change
Choking, 234-36, 257
due to heating, 192-93, 201-3, 205
due to Simple T_0 -Change, 192-93, 201-3, 205
in explosion wave, 210-11
frictional, 162, 170-78
for isentropic flow, 89-94
for isothermal flow, 183
rules of, 235-36
thermal, 192-93, 201-3, 205
Circular-arc profile, in subsonic flow, 375
Circular cylinder
in subsonic flow, 367
in free jet, 368
in wind tunnel, 357-58, 367
Circulation, 267-69, 278-80, 284
Clausius, inequality of, 32
Coefficient
of discharge; *see* Discharge coefficient
of friction; *see* Friction coefficient
of heat transfer, 212-13
influence; *see* Influence coefficients
pressure; *see* Pressure coefficient
Combustion
choking in, 198, 201-2
example of, 197-98
flow with, 206-11; *see also* Simple T_0 -Change
Combustion chamber, 219

Compressibility bubble, 326, 384
effect of aspect ratio on, 400
Compressibility of liquid, 69
Compressible flow
classification of, 58-59
hypersonic, 59
subsonic, 59
supersonic, 59
transonic, 59
Compression shock; *see* Shocks
Compression wave, steepening of, 127-31
Compressor, interference in, 315
Compressor cascades, 427, 462
supersonic, 505
Concave bend, 583
Condensation
flow with, 219-55
moisture, flow with; *see* Simple T_0 -Change
Condensation shock, moisture, 203-5
Conduction of heat, Fourier law of, 36
Conductivity, thermal, definition of, 36
Conservation of mass; *see also* Continuity equation
principle of, 12
for control volume, 13
Continuity equation, 14, 283-84; *see also* Conservation of mass
in cylindrical coordinates, 290
in spherical coordinates, 299
in steady flow, 15
Continuum
concept of, 4, 23
domain of, 56-58
Euler's description of, 11
Lagrange's description of, 11
limitations of, 56-58
mathematical description of, 10
properties of, 5, 35
Control surface, 12
Control volume, 12
First Law of thermodynamics for, 39
Second Law of thermodynamics for, 40
Converging nozzle
discharge coefficient of, 93
as flow meter, 93
as flow regulator, 93
with varying pressure ratio, 91-93
Converging-diverging nozzle
operating characteristics of, 139-43
with varying pressure ratio, 93-94
Cooling, flow with; *see* Simple T_0 -Change
Corner flow, supersonic, 463-64; *see also* Prandtl-Meyer wave; Simple-wave; Centered waves
Critical Mach Number; *see* Lower critical Mach Number
Critical point, 258
Critical pressure ratio, 76
Critical speed, 79-81
Critical state, 83
Critical velocity, in adiabatic flow, 79-81
Crocco's theorem, 281-82
Crossing of waves; *see* Intersection of waves

Curved shocks, 549, 559-61; *see also* Shocks
Curved wall, supersonic flow past, 464
Curves, characteristic, 598; *see also* Characteristic curves; Method of characteristics
Cycle, 24
First Law for a, 28
d'Alembert Paradox, 449
d'Arcy's formula, 189
Decelerating flows, 507
Deflagration, 207-11
Dependence, domain of, 499
Detached shocks, 548
Detonation, 207-11
Detonation wave, 219
Diffuser
isentropic flow in, 73
oblique-shock, 566
supersonic; *see also* Inlet, supersonic
of air-breathing engines, 147-51
allowable contraction for, 144-51
devices for starting of, 147
efficiency of, 151-52
of fixed geometry, 143-52
friction in, 147
limiting contraction ratio of, 149
one-dimensional, 143-52
operating conditions of, 146-47
overspeeding of, 150
special problems of, 143-44
starting of, 144-51
of variable geometry, 147-52
for wind tunnels, 144-47
Dimensional analysis, 315
of inviscid flow, 308-9
Dimensions, of dynamical quantities, 20
Direction index, 450
Discharge coefficient
of Borda orifice, 111
of nozzle, 99-100
of orifice, 359
of sharp-edged orifice, 100
Discontinuity, surface of; *see* Slip line; Vortex sheets
Displacement thickness, 266
Distorted models, 315
Disturbances, propagation of, 499
Domain of dependence, 499
Domain of influence, 499
Double wedge
lift-drag ratio of, 446
supersonic flow past, 444, 568
Drag, 449; *see also* Airfoils; Drag coefficient
and aspect ratio, 401
of bomb, 408
of flat plate normal to stream, 360
induced, 442
of wings, 412
internal, flow with, 219-55
and Mach Number, 383
and oblique shocks, 569
pressure, 442, 549
of spheres, 410
for subsonic flow, 386
of supersonic airfoils, 442, 446, 572
thickness, 443
wave, 443
Drag coefficient, 163, 379; *see also* Drag
Drag divergence, Mach Number of, 384-87
Duct
flow in
fed by converging nozzle, 173-75
fed by converging-diverging nozzle, 175-78
with friction, 159-86
isothermal, 178-83; *see also* Isothermal flow in ducts
with varying pressure ratio, 173-78
Efficiency
of nozzle, 98-99, 110
of supersonic diffuser, 151-52
thermal, of heat engines, 29
Ejector, 219
Elbow
for accelerated flow, 359-60
supersonic, 504
Ellipse, adiabatic, 58-59
Ellipsoid, subsonic flow past, 398-401
Ellipsoid of revolution
lower critical Mach Number of, 407
subsonic flow past, 405
Elliptic cylinder
lift of, 376
lower critical Mach Number of, 407
subsonic flow past, 354-56, 358, 369
Elliptic differential equation, 429, 600
Energy
internal, 27
for perfect gas, 41
 U , for pure substance, 35
kinetic, 36
flux of, 39
potential, 36
Energy effects, flow with; *see* Simple T_0 -Change
Energy equation
in kinematic form, 80-81
for steady flow, 39-40
Engines, heat, 29
Enthalpy
definition of, 36
flux of, 39
of perfect gas, 41, 43
stagnation, 75
Entropy
definition of, 33
evaluation of, 34
increase of
principle of, 34
in shock, 119-20
in weak shock, 125
of perfect gas, 43
Equality of temperature, 24
Equal-temperature process, 25

Equation of continuity; *see* Continuity equation

Equations of motion, 265–97

Euler's, 273–78; *see also* Euler's equations

linearized, 428

Equipotential lines

for flow past circular cylinder, 297

and streamlines, 295–97

Euler, method of, 11

Euler's equations

in Cartesian coordinates, 273–75

integration of

for irrotational flow, 277–78

along a streamline, 275–77

in streamline coordinates, 281

Evaporation, flow with, 219–55; *see also* Simple T_0 -Change

Exchanger, heat; *see* Heat exchanger

Expansion wave, spreading of, 128–31

Explosion

atomic, 211

hydrocarbon, 206–7

Explosion waves, 206–11

Fanno line, 114–15, 160–61, 192, 240

equation of, 155

table of, 626

Field method, 491

Fields in supersonic flow, 477

Film coefficient of heat transfer, 212–13

First Law of thermodynamics, 26

for control volume, 37–39

for a cycle, 28

Flame front, 219

propagation speed of, 207, 209–11

Flat plate

normal to subsonic stream, 360

subsonic flow past, 448

supersonic flow past, 444, 448

lift-drag ratio of, 446

Fliegner's formula, 85

Flow; *see also* One-dimensional flow

accelerating, 507

adiabatic; *see* Adiabatic flow

decelerating, 507

irrotational; *see* Irrotational motion

isentropic; *see* Isentropic flow

mass rate of, 14

one-dimensional

adiabatic, 160–78; *see also* Friction, one-dimensional flow with, adiabatic

with friction, 159–86; *see also* Friction, one-dimensional flow with potential; *see* Potential flow

rotational; *see* Rotation; Rotational flow

Flow coefficient, of nozzle, 99–100

Flow per unit area

isentropic, 84–85

maximum, 85

Flow with friction; *see* Friction, one-dimensional flow with

Flow with waves of one family; *see* Corner flow; Prandtl-Meyer flow; Simple waves

Fluid

barotropic, 278

definition of, 3

homogeneous, 278

inviscid, 10

Newtonian, 10

perfect, 10

Fluid curve, 269

Fluid line, 269

Fluid rotation, 269–73

Flux

of enthalpy, 39

of kinetic energy, 39

of mass, 14

of moment of momentum, 20

of momentum, 17

Force, units of, 20–21

Force break, 383–84

Force-divergence Mach Number, 384–87

Forces

body, 18

surface, 18

types of, 18

Fourier law of heat conduction, 36

Friction

one-dimensional flow with

adiabatic, 159–86, 219–55

choking effects in, 170–78

curves for, 169

example of, 169–70

formulas for, 166–69

isothermal, 178–83; *see also* Isothermal flow in ducts

laminar, 189

limiting duct length for, 170–71

in long ducts, 173–78

of perfect gas, 162–73

tables for, 169, 626

simple, 159–78; *see also* Friction, one-dimensional flow with

Friction and area change, flow with, 241–42

Friction and heat transfer, flow with, 242–55

Friction coefficient, definition of, 163

experimental, 184–86

for subsonic flow, 184–85

for supersonic flow, 185–86

Friction factor; *see* Friction coefficient

Frictional effects on gas flow; *see* Friction, one-dimensional flow with

Frictional flow, table of, 626

Frictional heating, 211–12

Frictionless flow, dimensional analysis of, 308–9

Gas, perfect; *see* Perfect gas

Gas constant, definition of, 41

and molecular weight, 41

universal, 41

Gas constants, relations among, 42

Gas dynamics, 49

Generation of wave, 449, 463, 493

Gladstone-Dale equation, 63

Gothert's rule, 316–21, 336

for bodies of revolution, 402–5

for one-dimensional flow, 331–32

for spheres, 409

for sweptback wings, 416

for three-dimensional flow, 394–99

for two-dimensional passages, 330–32

for wind tunnels, 327–30

for wings, 410

Green's theorem, 268–69

Heat, definition of, 27

mechanical equivalent of, 28

in reversible processes, 33

specific, 36

of perfect gas, 42

Heat conduction, Fourier law of, 36

Heat engines, 29

thermal efficiency of, 29

Heat exchanger, 214–55; *see also* Heat transfer

approximate method for low Mach Numbers, 249–51

with constant heat flux, 246–47, 251–52

with constant wall temperature, 243–51

graphical integration for, 244–48

in nuclear reactor, 252–55

numerical integration for, 244–48

Heat transfer; *see also* Heat exchanger

coefficient of, 212–13

experimental correlation of, 213

flow with, 219–55; *see also* Simple T_0 -Change

Heat transfer and friction, flow with, 242–55

Heating

flow with; *see* Simple T_0 -Change

frictional, 211–12

Hodograph characteristic, 468, 478, 485

related to shock polar, 552

Hodograph characteristic curves, 599

Hodograph characteristic function, 467

chart of, 467

table of, 468, 632

Hodograph coordinates, 338

Hodograph equations, 338–41

Hodograph method, 288, 336

Hodograph plane, 336, 465

equation of stream function in, 341

Hodograph shock polars, 542, 552

Hodograph streamlines, 336–37

and physical streamlines, 336–37, 341

Homogeneous fluid, 278

Hyperbolic differential equation, 429, 600

Hypersonic flow, 59

Impulse function

definition of, 86

for isentropic flow, 86–87

Impulse turbine blade, 504

Incompressible flow

Bernoulli's equation for, 278

similarity law for, 321–22

square network for, 297

velocity potential for, 289

Index of refraction, 63

Induced drag, 442

of wings, 412

Influence

domain of, 499

range of, 500

Influence coefficients, 226–31

table of, 228, 231, 237–38, 630

Initial-value theorem

for hyperbolic equations, 603–6

for supersonic flow, 497–500, 603–6

Injector, 219

Inlet, supersonic, 506; *see also* Diffuser, supersonic

of fixed geometry, 148–51

limiting contraction ratio for, 149

overspeeding of, 150

starting of, 147–51

of variable geometry, 150–51

Integral surface, 598

Interference in wind tunnel, 315, 335, 403

Interference pressure coefficient, 329

Interferogram

evaluation of, 62–65

fringe-displacement, 63–65

infinite-fringe, 61–63

Interferometer, 60–65

Internal energy, 27

of perfect gas, 41, 43

U, for pure substance, 35

Intersection of oblique shocks, 553–59

of same family, 558

Intersection of waves, 450, 453, 494

Inviscid flow, dimensional analysis of, 308–9

Inviscid fluid, definition of, 10

Irreversibility, 30

and perpetual motion, 31

and Second Law, 31

Irrotational flow; *see* Irrotational motion

Irrotational motion, 266, 267–273, 280, 282, 284, 286

in axially symmetric flow, 294

in cylindrical coordinates, 290

example of, 271–73

in spherical coordinates, 299

Isentropic flow

applications of, 73

charts for, 87

choking in, 89–94

of compressible liquid, 11

with deviations from perfect gas laws, 95–97

in diffuser, 73

formulas in powers of Mach Number, 95

general features of, 74–78

illustrative example of, 88

for low Mach Numbers, 94–95

Mach Number relations for, 83–86

Isentropic flow—Continued
 in nozzle, 73
 one-dimensional, 74–78, 239
 of perfect gas, 83–88
 in stream tube, 73
 tables for, 88, 614
 with van der Waals gas, 96–97
 with variable specific heat, 96–97
 Isentropic process
 enthalpy change in, 43
 of perfect gas, 43
 Isentropic stagnation pressure, 75
 Isentropic stagnation state, 83
 Isothermal flow in ducts, 178–83
 charts for, 181
 choking effects for, 183
 formulas for, 180–81
 at low Mach Number, 182–83
 variation of fluid properties for, 179–80
 Jet
 contraction ratio of, 358–59
 overexpanded, 454, 565
 turbine nozzle, 566
 underexpanded, 454, 479–81, 501
 Joukowski profile
 lift of, 370
 lower critical Mach Number of, 370
 in subsonic flow, 369
 Joule's constant, 28
 Karman-Tsien coordinate correction formula, 353
 Karman-Tsien method, 344–51
 for flow with circulation, 357
 with polygonal approximation, 357
 profile correction for, 351–56
 Karman-Tsien pressure correction formula, 323, 327, 341; *see also* Karman-Tsien rule
 Karman-Tsien rule, 370, 374, 375
 accuracy of, 349–50
 chart for, 348
 comparison with experiment, 350
 comparison with Prandtl-Glauert rule, 349
 Kelvin temperature scale, 32
 Kelvin's theorem, 278–80, 282
 Kinetic energy, 36
 flux of, 39
 Lagrange, method of, 11
 Laitone's modification of Prandtl-Glauert rule, 324–27
 Lambda shock, 381
 Laplace's equation, 289, 294, 297
 Lattice-point method, 491
 Layer, boundary; *see* Boundary layer
 Length, units of, 20–21
 Lift, of supersonic airfoils, 445, 572; *see also* Airfoils; Lift coefficient
 Lift coefficient; *see also* Airfoils; Lift of circular-arc profile, 375
 Gothert's rule for, 321

and Mach Number, 315, 326, 376, 383
 Prandtl-Glauert rule for, 322–23
 for subsonic flow, 385
 of supersonic airfoils, 441
 Lift-curve slope, effect of Mach Number on, 326
 Lift-divergence Mach Number, 384–87
 Lift-drag polar
 of subsonic profiles in supersonic flow, 571
 of supersonic profile, 446
 Lift-drag ratio, of supersonic airfoil, 443
 Limit line, 540
 Linear differential equation, 288, 289
 Linearized theory
 assumptions of, 308
 pressure coefficient in, 309–10
 and second-order theory, 561–63
 subsonic, 303
 supersonic, 426–56
 compared with experiment, 447–48
 general solution for, 429
 geometrical interpretation of, 434–37
 modified, 463, 477
 and shock theory, 553
 for three-dimensional subsonic flow, 394–99
 Liquid
 change in wave shape for, 131
 shock wave in, 155
 Lower critical Mach Number, 348, 349
 of bump, 372–74
 of circular-arc profile, 375
 of circular cylinder, 367
 of circular cylinder in wind tunnel, 358, 368
 of ellipsoid, 398–400
 of ellipsoid of revolution, 407
 of elliptic cylinder, 358, 369, 407
 of Joukowski profile, 370
 of profile, 387
 of sphere, 409
 and sweepback, 418
 Mach angle, 54, 432
 Mach cone, 51–54
 Mach line, 463, 484, 499; *see also* Mach wave
 Mach Number
 constant, flow with, 241–42
 definition of, 54
 influence of independent variables on, 233
 lower critical; *see* Lower critical Mach Number
 relation to M^* , 81–82
 as similarity parameter, 56
 Mach quadrilateral, 477, 498
 Mach reflection, 555–57
 Mach wave, 601; *see also* Mach line; Pressure wave; Wave
 compared with oblique shock, 531
 four basic types of, 436
 interaction with oblique shock, 541

Mach wave
 left-running, 432
 as limit of oblique shock, 551
 pressure-deflection relation for, 435
 right-running, 433
 Mass
 conservation of; *see* Conservation of mass; Continuity equation
 flux of, 14
 units of, 20–21
 Mass flow parameter, for adiabatic flow, 82
 Mass rate of flow, 14
 Maximum velocity, for adiabatic flow, 79–81
 Mechanical equivalent of heat, 28
 Method of characteristics, 462–528; *see also* Characteristics, method of; Characteristic curves
 compared with experiment, 514
 graphical, 494
 grid size vs. accuracy of, 497
 illustrative example of, 479, 486–89
 initial-value theorem of, 497–500, 603–6
 numerical, 494–97, 603
 for rotational flow, 516–23
 rules for using, 478
 and shock theory, 553
 theory of, 595–608
 unit processes for, 492–94, 495
 Mixing
 flow with, 239; *see also* Simple gas injection
 one-dimensional flow with, 219–55
 Models, distorted, 315
 Moisture condensation, flow with, 219–55; *see also* Simple T_0 -Change
 Moisture condensation shock, 203–5
 Moment of supersonic airfoils, 572; *see also* Airfoils; Moment coefficient
 Moment coefficient
 effect of Mach Number on, 315, 383
 Prandtl-Glauert rule for, 322–23
 of supersonic airfoils, 444
 Moment of momentum
 flux of, 20
 theorem of, 19
 Momentum, flux of, 17
 Momentum theorem, 16
 for moving reference frames, 18
 working form of, 17
 Motion
 equations of; *see* Equations of motion
 irrotational; *see* Irrotational motion
 perpetual, of second kind, 29
 Newtonian fluid, definition of, 10
 Newton's second law; *see* Euler's equations
 Nonlinear differential equation, 288
 Normal shock, 112–54, 199–200; *see also* Shocks; Wave
 curves for, 122
 development of, 125–32
 direction of, 120–21
 in ducts, 135–37, 583
 with energy effects, 203–11
 entropy increase in, 119–20
 example of, 123
 formation of, 125–31
 formulas for, 118–20
 governing equations of, 114–16
 impossibility of rarefaction, 120–21
 interaction with boundary layer, 135–37, 583
 in liquid, 155
 moving, 137–39
 in perfect gas, 116–22
 Prandtl's equation of, 118
 Rankine-Hugoniot equation of, 121–22
 stagnation-pressure loss in, 119
 strength of, 123–24
 tables for, 123, 621
 thickness of, 131–34
 transformed from oblique shock, 530
 of vanishing strength, 124
 velocity of, 124
 weak, 123–25
 Normal shock wave; *see* Normal shock; Wave
 Normal stresses, 18
 work done by, 38
 Nozzle; *see also* Isentropic flow
 converging
 discharge coefficient of, 93
 as flow meter, 93
 as flow regulator, 93
 with varying pressure ratio, 91–93
 converging-diverging
 operating characteristics of, 139–43
 with varying pressure ratio, 93–94
 discharge coefficient of, 99–100
 efficiency of, 98–99, 110
 isentropic flow in, 73
 overexpanded, 454, 565
 performance of, 98–100
 rocket, 219
 sharp-cornered, 512
 supersonic wind tunnel, 427, 507–16
 turbine, 566
 underexpanded, 454, 479–81, 501
 velocity coefficient of, 99
 wind tunnel, 502
 Nuclear reactor, 219
 heat transfer in, 252–55
 Nusselt Number, 213
 Oblique shocks, 529–84; *see also* Shocks
 approximate treatment of, 552
 charts for, 536–38
 compared with Mach waves, 531
 crossing of, 555
 crossing slip line, 561, 592
 curved, 549, 559–61
 detached, 548
 equations of, 532–39
 formation of, 540, 563
 formulas for, 535
 generation at concave bend, 583

Oblique shocks—Continued
 geometry of, 539–41
 impossibility of rarefaction, 539
 interaction with shocks, 541
 interaction with waves, 541, 559, 563
 intersection of, 553–59
 limit of as Mach wave, 551
 maximum deflection for, 548, 586
 minimum Mach Number for, 548
 nearly normal, 550
 Prandtl relation for, 534
 Rankine-Hugoniot law for, 533
 reflection of, 553–59
 from boundary layer, 582
 from free boundary, 554
 from wall, 554
 and Second Law of thermodynamics, 539
 series solution of, 562
 sonic flow after, 550, 586
 streamline turning in, 539
 strong, 544–48
 tables for, 536
 transformed from normal shock, 530
 and wave drag, 569
 weak, 544–48, 551–53, 587
 One-dimensional approximation, 73–74
 One-dimensional flow; *see also* Flow
 with area change, 219–55
 with chemical reaction, 219–55
 with evaporation or condensation, 219–55
 with friction, 159–86; *see also* Friction, flow with
 with friction and area change, 241–42
 with friction and heat transfer, 242–55; *see also* Heat exchanger
 general method of solution, 236–37
 Gothert's rule for, 331–32
 with heat transfer, 219–55; *see also* Simple T_0 -Change
 influence coefficients of, 237–38
 influence of independent variables on, 232–36
 with internal drag, 219–55
 with mixing, 219–55
 simple types of, 238–41
 table for, 239
 transition through sonic speed, 235–36
 unsteady, 596
 with wall friction, 219–55
 Optical methods, 59–68
 comparison of, 59–60
 Orifice, discharge coefficient of, 100, 359
 Orthogonal network of equipotential and streamlines, 296–97
 Overexpanded nozzle, 454, 565
 Parabolic differential equation, 600
 Patching curves, 482, 601
 Perfect fluid, definition of, 10
 Perfect gas
 adiabatic flow of, 78–82
 change in wave shape for, 131
 constants of, 42

definition of, 41
 enthalpy of, 41, 42
 entropy of, 43
 equation of state of, 41
 flow of, adiabatic constant-area, 162–73
 internal energy of, 41, 43
 isentropic flow of, 83–88
 isentropic process in, 43
 normal shock in, 116–22
 ratio of specific heats of, 42
 shock thickness in, 133–34
 specific heats of, 42
 velocity of sound in, 47
 Perpetual motion
 and irreversibility, 31
 of second kind, 29
 Perturbation potential, 305, 428
 Perturbation velocities, 305
 Perturbations, small, method of, 303; *see also* Linearized theory
 Physical characteristic curves, 484, 599
 Pipes, flow in; *see* Ducts, flow in
 Pitot tube
 subsonic, 94–95, 154
 supersonic, 153–54
 Plate, flat; *see* Flat plate
 Polars, shock; *see* Shock polars
 Potential, velocity; *see also* Velocity potential
 perturbation, 305, 426, 428
 Potential energy, 36
 Potential flow, 265–66
 Potential motion, 286
 Potential vortex, 271–73
 Pound of force, definition of, 20–21
 Pound of mass, definition of, 20–21
 Prandtl-Glauert method, 370–72
 Prandtl-Glauert rule, 321–24, 336, 370, 375, 376, 383, 400
 comparison with experiment, 326–27
 comparison with Karman-Tsien rule, 349
 and drag, 383
 Laitone's modification of, 324–26
 for wind tunnels, 327–30
 Prandtl-Meyer flow; *see* Centered waves; Corner flow; Prandtl-Meyer wave; Simple waves
 Prandtl-Meyer wave, 463–64, 539
 impossibility of, in concave corner, 540
 Prandtl number, as similarity parameter, 56
 Prandtl's equation
 for normal shock, 118
 for oblique shock, 534
 Pressure
 center of; *see* Center of pressure
 stagnation, 75
 total, 75
 Pressure coefficient, 107, 309
 dimensional analysis of, 308–9
 effect of Mach Number on, 309, 314–15, 327
 for elliptic cylinder, 369

Gothert's rule for, 320
 interference, 329
 Karman-Tsien rule for, 347
 lateral decay of, 314
 linearized, 309–10, 428
 Prandtl-Glauert rule for, 322–23
 for small perturbations, 428
 Pressure distribution
 and boundary layer, 308
 and Mach Number, 327
 on wing profiles, 379–81
 Pressure drag, 442
 and oblique shocks, 569
 Pressure index, 450
 Pressure ratio, critical, 76
 Pressure stresses, work done by, 38
 Pressure wave, 433, 463; *see also* Mach wave; Shock wave; Wave
 Process, adiabatic; *see* Adiabatic process
 definition of, 24
 equal-temperature, 25
 irreversible, 30
 reversible, 30
 Profiles; *see* Airfoils
 Prolate spheroid, subsonic flow past, 406
 Propagation of disturbances, 499
 Properties, thermodynamic, units of, 37
 Property
 specific value of, 35
 of a system, 24
 per unit mass, 35
 Pure substance, definition of, 34
 internal energy of, 35–36
 Quasi-linear equation, 597
 Ram jet, 219
 combustion in, 201–2
 Rankine-Hugoniot curve, 125
 Rankine-Hugoniot equation, 121–22, 533, 552
 Rankine temperature scale, 32
 Rarefaction wave, spreading of, 128–31
 Rayleigh line, 115–16, 191–93, 240
 equation of, 155
 table of, 628
 Rayleigh-Janzen method, 336, 365–67, 371
 for spheres, 409
 Rayleigh pitot-tube formula, 153–54
 Reactor, nuclear, 219
 Recovery factor, 211–13
 Reflection
 Mach, 555–57
 of oblique shock, 553–59
 from boundary layer, 582
 from free boundary, 493, 554
 from wall, 554
 regular, 555
 of wave
 from free boundary, 450, 452
 from surface of discontinuity, 461
 from wall, 450, 451, 493
 Refraction, index of, 63
 Regular reflection, 555

Relaxation method, 297, 336, 377–79
 Relief effect, three-dimensional, 399, 400, 414, 416
 Reversibility, 30
 Revolution
 body of
 disturbance of, 402
 drag of, 408
 experimental results for, 404, 407
 Gothert's rule for, 402–5
 pressure coefficient for, 402
 subsonic flow past, 401–10
 thin, 405–6
 ellipsoid of, subsonic flow past, 405
 Reynolds' analogy, 213, 243
 Reynolds Number
 of shock wave, 132–34
 as similarity parameter, 56
 of supersonic wind tunnel, 103–4
 Rocket motor, thrust of, 100–3
 Rocket nozzle, 219
 Rotation, 267, 269–71
 flow with; *see* Rotational flow
 in streamline coordinates, 280–81
 supersonic flow with, 516–23
 and thermodynamic properties, 280–82
 Rotational flow, 266, 271, 282, 516–23
 Saddle point; *see* Critical point
 Schlieren method, 59–60, 65–67
 analysis of, 66–67
 Second Law of thermodynamics, 30
 in analytical form, 34
 for control volume, 40
 corollaries of, 31
 and irreversibility, 31
 Second-order theory, 561–63, 571–78
 coefficients of, 562
 table of, 633
 compared with experiment, 575
 Separation of boundary layer, 379, 380, 415
 Shadowgraph, 59–60, 67–68
 Shaft work, 39
 Sharp-cornered nozzle, 512
 experiments on, 514
 Shear deformation, rate of, 270–71
 Shear stress, 18
 definition of, 9
 Shear stresses, work done by, 38
 Shear work, 38–39
 Shock-boundary layer interaction, 507, 576, 580–84
 Shock-characteristic theory, 575
 Shock polars, 542–44
 hodograph, 542, 552
 and characteristic curve, 552
 pressure-deflection, 544
 Shock wave; *see* Normal shock; Oblique shocks; Shocks; Wave
 normal; *see* Normal shock
 oblique; *see* Oblique shocks
 Shocks, 266; *see also* Normal shock; Oblique shocks; Wave
 and characteristics, 601

Shocks—Continued
 curved, 282, 549, 559–61
 detached, 548
 development of, 125–32
 direction of, 116
 as discontinuities, 112
 dissipative effects in, 131–32
 entropy increase of, 119–20
 for weak shock, 124–25
 explosion, 206–11
 formation of, 125–31
 impossibility of rarefaction, 120–21
 interaction of, with boundary layer, 135–37, 266, 381–82, 580–84
 lambda, 381
 moisture condensation, 203–5; *see also* Simple T_0 -Change
 moving, 137–39
 normal; *see* Normal shock
 oblique, 529–84; *see also* Oblique shocks
 Reynolds Number of, 132–34
 strength of, 123–24, 551
 swallowing of, 145–51
 thickness of, 112, 131–34
 in perfect gas, 133–34
 table for, 133–34
 for weak shocks, 133
 variation of fluid properties within, 134
 velocity of, 48
 and wave drag, 569
 Silence, zone of, 500
 Similarity laws, 303, 315–17; *see also* Gother's rule; Prandtl-Glauert rule
 for flow far from profile, 324
 for incompressible flow, 321–22
 subsonic, 303–32
 compared with experiment, 326–27
 for one-dimensional flow, 331–32
 for two-dimensional passages, 330–32
 for wind tunnels, 327–30, 335
 for two-dimensional subsonic flow, Gother's, 315–21
 Laitone's, 324–26
 Prandtl-Glauert, 321–24
 summary of, 323
 for wings, 410–15
 Similarity parameters, 54–56
 Simple area change; *see* Isentropic flow
 Simple friction; *see* Friction, one-dimensional flow with
 Simple gas injection, 239–41
 Simple heating; *see* Simple T_0 -Change
 Simple T_0 -Change, 190–211, 239
 chart for, 196
 choking due to, 192–93, 201–3
 example of, 197–98
 formulas for, 195–96
 of perfect gas, 193–203
 tables for, 196, 628
 variations of fluid properties in, 198–99
 Simple types of flow, 238–41
 table of, 239
 Simple wave flow; *see* Simple waves
 Simple waves, 431, 464, 489–91, 602,

606–8; *see also* Centered waves; Corner flow; Method of characteristics; Prandtl-Meyer wave
 calculation rules of, 467
 cavitation in, 475
 centered; *see* Centered waves
 complete, 474, 475
 exact solution for, 465–77
 example of, 468, 470
 features of, 471
 hodograph of, 607
 left-running, 472
 patching of, 608
 in physical plane, 607
 right-running, 473
 streamlines of, 475–77
 tables for, 468
 Skin-friction coefficient, 379
 Slender bodies, flow past; *see* Linearized theory
 Slip line, 519, 544, 555
 crossed by oblique shocks, 561, 592
 Slow burning, 207–11
 Slug, definition of, 20–21
 and pound force, 21
 and pound mass, 21
 Small perturbations; *see* Linearized theory
 Sonic point
 passage through, 258
 stability of, 260
 special conditions at, 255
 Sound, velocity of, 45–49; *see also* Velocity of sound
 in air, 48
 in incompressible fluid, 48
 in liquid, 69
 in perfect gas, 47
 transition through, 235–36
 Sources and sinks, method of, 401
 Specific heat
 definition of, 36
 of perfect gas, 42
 Speed, flame propagation, 207, 209–11
 Speed of sound; *see* Velocity of sound; Sound, velocity of
 Spheres
 drag of, 410
 subsonic flow past, 409–10
 Spherical coordinate system, 299
 Stagnation enthalpy, 75
 Stagnation pressure, 75
 loss of, in normal shock, 119
 Stagnation state, 83
 Stagnation temperature, 79
 Stagnation-temperature ratio, 80
 Stagnation velocity of sound, 79–81
 State, change of, 24
 equation of, for perfect gas, 41
 equilibrium, 40
 nonequilibrium, 40
 of a system, 24
 Steady flow
 continuity equation for, 15
 definition of, 11

energy equation of, 39–40
 one-dimensional, 15
 Stokes' theorem, 269
 Stream function, for axially symmetric flow, 294
 definition of, 291–92
 differential equations of, 291–92
 equation of
 for incompressible flow, 293
 in Cartesian coordinates, 292–94
 in cylindrical coordinates, 294–95
 in hodograph plane, 341
 physical meaning of, 292
 of plane source, 299
 and velocity potential, 295–97
 Stream tube, isentropic flow in, 73
 Streamline coordinates, 280
 Streamline curvature method, 387–91
 Streamlines
 and equipotential lines, 295–97
 for flow past circular cylinder, 297
 hodograph, 336–37, 341
 Strength of shock, 123–24, 551
 Stress, Mohr's circle of, 9
 normal, 18
 work done by, 38
 shear, 9, 18
 work done by, 38
 state of, 9
 hydrostatic, 9
 in inviscid fluid, 9
 in viscous fluid, 9
 surface, 18
 viscous, 18
 Subsonic flow, 59
 in accelerating elbow, 359–60
 for airfoil in wind tunnel, 378
 angle of attack in, 384
 for bodies of revolution, 401–10
 drag of, 408
 for bump, 372–74
 for circular arc profile, 375
 for circular cylinder, 367
 in free jet, 368
 in wind tunnel, 357–58, 367
 compared with supersonic, 76–78, 429, 448, 500
 effect of camber in, 384–87
 effect of Mach Number on flow far from profile, 324
 effect of thickness in, 384–87
 for ellipsoids, 398–401
 for elliptic cylinder, 354–56, 369
 at angle of attack, 358, 376
 experimental results for, 326–27, 350, 379–87
 for flat plate normal to stream, 360
 influence of compressibility in, 400
 for Joukowski profile, 369
 Karman-Tsien method for, 344–60
 lift coefficient for, 376
 pressure distributions in, 379–81
 similarity laws for, 303–32
 for spheres, 409–10
 for sweptback wings; *see* Sweptback wings
 for thin bodies of revolution, 405–6
 three-dimensional, 394–99
 wind tunnel corrections for, 327–30
 for wings, 410–15
 generalized correlation of, 422
 Subsonic pitot tube, 154
 Substance, pure
 definition of, 34
 internal energy of, 35–36
 Suction pressure, at nose of airfoil, 449
 Superposition of solutions, 289
 Supersaturation, 203
 Supersonic biplane, 579
 Supersonic diffuser; *see* Diffuser, supersonic
 Supersonic flow, 59
 compared with subsonic, 76–78, 429, 448, 500
 in duct with friction, 104–5
 Karman's rules of, 51
 linearized, 427–56
 general solution for, 429
 method of characteristics for, 482–91
 with rotation, 516–23
 with small perturbations, 427–56
 Supersonic inlet; *see* Diffuser, supersonic; Inlet, supersonic
 Supersonic nozzle, 426, 507–16; *see also* Supersonic flow
 Supersonic pitot tube, 153–54
 Supersonic wind tunnel, 459, 502
 Surface, control, 12
 integral, 598
 Surface forces, definition of, 18
 Surface of discontinuity; *see* Slip line; Vortex sheets
 Surface stresses, 18
 Surroundings, definition of, 11
 Sweepback; *see* Sweptback wings
 Sweptback wings
 compressibility effects for, 417
 drag of, 421
 experimental results for, 419–22
 generalized correlation of, 422
 Gother's rule for, 416
 lift of, 420, 421
 lower critical Mach Number of, 418
 subsonic flow past, 415–22
 System
 boundary of, 11
 definition of, 11
 property of, 24
 state of, 24
 Tangent gas, 336
 definition of, 342
 limitations of, 343–44
 polygonal extension of, 357
 properties of, 342–43
 Tangent-gas approximation, 341–44
 Temperature
 adiabatic wall, 211–12
 equality of, 24

Temperature—*Continued*
 ratio of stagnation to static, 80
 scale of, 24
 stagnation, 79
 total, 79

Temperature scale
 absolute, 32
 Kelvin, 32
 Rankine, 32

Temperature-entropy diagram, 34

Thermal conductivity, definition of, 36

Thermal efficiency of heat engines, 29

Thermodynamic properties, units of, 37

Thermodynamics
 First Law of, 26
 for a cycle, 28
 laws of
 for irrotational frictionless flow, 284
 of nonequilibrium states, 40
 Second Law of, 30
 in analytical form, 34
 for control volume, 40
 corollaries of, 31
 Zeroth law of, 25

Thickness
 displacement
 of boundary layer, 266
 effects of, in subsonic flow, 384–87

Thickness drag, 443

Thickness of normal shock, 112

Thin airfoil, supersonic flow past, 434; *see also* Linearized theory

Thin bodies, flow past; *see* Linearized theory

Thomson's theorem, 278–80, 282

Three-dimensional relief effect, 399, 400, 414, 416

Thrust of rocket motor, 100–3

Time, units of, 20–21

Total pressure, 75

Total temperature, 79

Transformation, affine, 319

Transition through speed of sound, 235–36

Transonic flow, 59, 378

Turbine, blade cascades of, 427
 impulse blade of, 504
 interference in, 315
 nozzle jet of, 566

Two-dimensional passages, subsonic similarity rule for, 330–32

Underexpanded jet, 454, 479–81, 501

Underexpanded nozzle, 454, 479–81, 501

Unit processes, for waves, 450, 492–94

Units of dynamic quantities, 20–21

Units of thermodynamic quantities, 37

Unsteady one-dimensional flow, 596

Upper critical Mach Number
 for bump, 372–74
 definition of, 372

Velocity
 critical, 79–81
 dimensionless, M^* , 81–82

flame propagation, 207, 209–11
 fluid, 6
 line integral of, 267
 maximum, for adiabatic flow, 79–81
 perturbation, 305
 of shock wave, 48
 of sound, 45–49
 in air, 48
 in incompressible fluid, 48
 in liquid, 69
 passage through, 258
 stability of, 260
 in perfect gas, 47
 special conditions at, 255
 stagnation, 79–81
 transition through, 235–36

Velocity plane, 465

Velocity potential, definition of, 285
 equation of, 284–91
 for axially symmetric flow, 291
 in Cartesian coordinates, 286–89
 in cylindrical coordinates, 289–91
 for incompressible flow, 289
 linearized, 304–8
 mathematical features of, 288
 in polar coordinates, 291
 solution of, 288
 for two-dimensional flow, 289
 of line vortex, 299

lines of; *see* Equipotential lines

perturbation, 305, 426, 428
 and stream function, 295–97

Viscosity
 coefficient of, 9
 effects of, in design, 506

Viscous stresses, 18

Volume, control, 12

Vortex, potential, 271–73

Vortex sheets, 519, 544, 555

Vorticity; *see* Rotation

Wake, wave system in, 578

Wake losses, effect of Mach Number on, 383

Wall
 curved, supersonic flow past, 464
 wave-shaped, flow past, 310–15

Wave; *see also* Mach wave; Pressure wave; Shocks
 cancellation of, 450, 452, 493
 centered; *see* Centered waves
 compression, steepening of, 127–31
 detonation, 219
 development of, 158
 analysis of, 128–31
 expansion, spreading of, 128–31
 explosion, 206–11
 generation of, 449, 463, 493
 interaction with oblique shocks, 559
 intersection with wave, 450, 453, 494
 left-running, 465
 lumped, 449
 Mach; *see* Mach wave
 normal shock, 112–54; *see also* Normal shock

Wind tunnel
 airfoil in, 378
 corrections for, 327–30
 interference in, 315, 335, 403
 supersonic, 459, 462, 502
 nozzles for, 507–16
 performance of, 152

Wings
 effect of aspect ratio on, 411–15
 experimental results for, 412–15
 of finite span
 lift-curve slope for, 411–12
 subsonic flow past, 410–15
 generalized correlation of, 422
 induced drag of, 412
 lift of, generalized correlation of, 422
 lift-curve slope of, 425
 supersonic; *see* Airfoils, supersonic sweptback; *see* Sweptback wings

Work
 definition of, 25
 done by normal stresses, 38
 done by shear stresses, 38
 measurement of, 26
 recognition of, 25
 shaft, 38–39
 shear, 38–39

Zeroth law of thermodynamics, 25

Zone of action, 500

Zone of silence, 500